AD A055518

SSI 7618-1

March 1978

THE SHOCK TUNNEL:
HISTORY AND RESULTS

Final Report

Contract No. DCP401-76-C-0311
Work Unit No. 1120A

SCIENTIFIC SERVICE, INC.

78 06 19

7618-1 Final Report   March 1978

THE SHOCK TUNNEL:
HISTORY AND RESULTS

by

C. Wilton, K. Kaplan, and B.L. Gabrielsen

Scientific Service, Inc.
1536 Maple Street
Redwood City, CA 94063

REPORT DOCUMENTATION PAGE	READ INSTRUCTIONS BEFORE COMPLETING FORM

1. REPORT NUMBER	2. GOVT ACCESSION NO	3. RECIPIENT'S CATALOG NUMBER

4. TITLE (and Subtitle)	5. TYPE OF REPORT & PERIOD COVERED
THE SHOCK TUNNEL: HISTORY AND RESULTS, Volumes I - V .	Final Report - July 1976 - February 1978
	6. PERFORMING ORG. REPORT NUMBER
	SSI-7618-1-2

7. AUTHOR(s)	8. CONTRACT OR GRANT NUMBER(s)
C. Wilton, K. Kaplan and B.L. Gabrielsen	DCPA01-76-C-0311

9. PERFORMING ORGANIZATION NAME AND ADDRESS	10. PROGRAM ELEMENT, PROJECT, TASK AREA & WORK UNIT NUMBERS
Scientific Service, Inc. 1536 Maple Street Redwood City, CA 94063	Work Unit No. 1123H

11. CONTROLLING OFFICE NAME AND ADDRESS	12. REPORT DATE
Defense Civil Preparedness Agency Washington, D.C. 20301	February 1978
	13. NUMBER OF PAGES
	438

14. MONITORING AGENCY NAME & ADDRESS(if different from Controlling Office)	15. SECURITY CLASS. (of this report)
	Unclassified
	15a. DECLASSIFICATION DOWNGRADING SCHEDULE

16. DISTRIBUTION STATEMENT (of this Report)

Approved for public release; distribution unlimited.

17. DISTRIBUTION STATEMENT (of the abstract entered in Block 20, if different from Report)

18. SUPPLEMENTARY NOTES

19. KEY WORDS (Continue on reverse side if necessary and identify by block number)

Shock Tunnel, Loading Studies, Wall Panel Analysis and Tests, Static Test Program, Prediction of Failure Pressures

20. ABSTRACT (Continue on reverse side if necessary and identify by block number)

This report summarizes the results of a program conducted by the Defense Civil Preparedness Agency to determine blast resistance of wall panels typically found in existing structures. The objective of this program was to determine the blast sheltering capability of structures in the National Fallout Shelter Survey inventory and to obtain information which could be used to upgrade these structures.

DD 1 JAN 73 1473   EDITION OF 1 NOV 55 IS OBSOLETE

Volume I describes the shock tunnel facility used for the experimental testing of full-scale wall panels. Included is a summary of the capabilities of the shock tunnel for dynamic loading and response studies and brief summaries of various experimental programs conducted in the shock tunnel which were not related to the wall panel test program.

Volume II of this report presents the results obtained from the experimental program conducted in the shock tunnel to determine the loadings which are received by wall panels mounted in the test section.

Volume III of this report is concerned with the dynamic response and failure of full-scale wall panels. Included are the development of theories of wall panel response and the results obtained from the testing of full-scale wall panels in the shock tunnel.

Volume IV of this report describes the static test program conducted to determine the physical properties of the wall panels and to assist in the development of failure theories and test predictions for wall panels.

Volume V summarizes the predicted failure pressures for wall panels based on the theoretical and experimental results.

7618-1 Summary Report   March 1978

THE SHOCK TUNNEL:

HISTORY AND RESULTS

Approved for public release;
distribution unlimited.

prepared for

by

C. Wilton, K. Kaplan, and B.L. Gabrielsen

Scientific Service, Inc.
1536 Maple Street
Redwood City, CA 94063

Summary Report
THE SHOCK TUNNEL:
HISTORY AND RESULTS

PURPOSE

This study summarizes a nine year program conducted for the Defense
Civil Preparedness Agency to determine the blast resistance of wall panels
typically found in existing structures. The objective was to determine
the blast sheltering capabilities of the structures in the National Shelter
Survey inventory and to obtain information which could be used to upgrade
these structures. The results of this study are presented in five volumes
(bound as one).

Volume 1 describes the shock tunnel facility used for the experimental
testing of full-scale wall panels. Included is a summary of the capabili-
ties of the shock tunnel for dynamic loading and response studies and brief
summaries of various experimental programs conducted in the shock tunnel
which were not related to the wall panel test program.

Volume 2 of this report presents the results obtained from the experi-
mental program conducted in the shock tunnel to determine the loadings which
are received by wall panels mounted in the test section.

Volume 3 is concerned with the dynamic response and failure of full-
scale wall panels. Included are the development of theories of wall panel
response and the results obtained from the testing of full-scale wall panels
in the shock tunnel.

Volume 4 describes the static test program conducted to determine the
physical properties of the wall panels and to assist in the development
of failure theories and test predictions for wall panels.

Volume 5 summarizes the predicted failure pressures for wall panels based on the theoretical and experimental results covered in Volume 3 and the static test data in Volume 4.

One of the most interesting results of this study was to summarize (in Volume 5) all the brick and concrete block wall panel results in a simple failure pressure chart. These are shown in Figs. 1 and 2 of this summary.
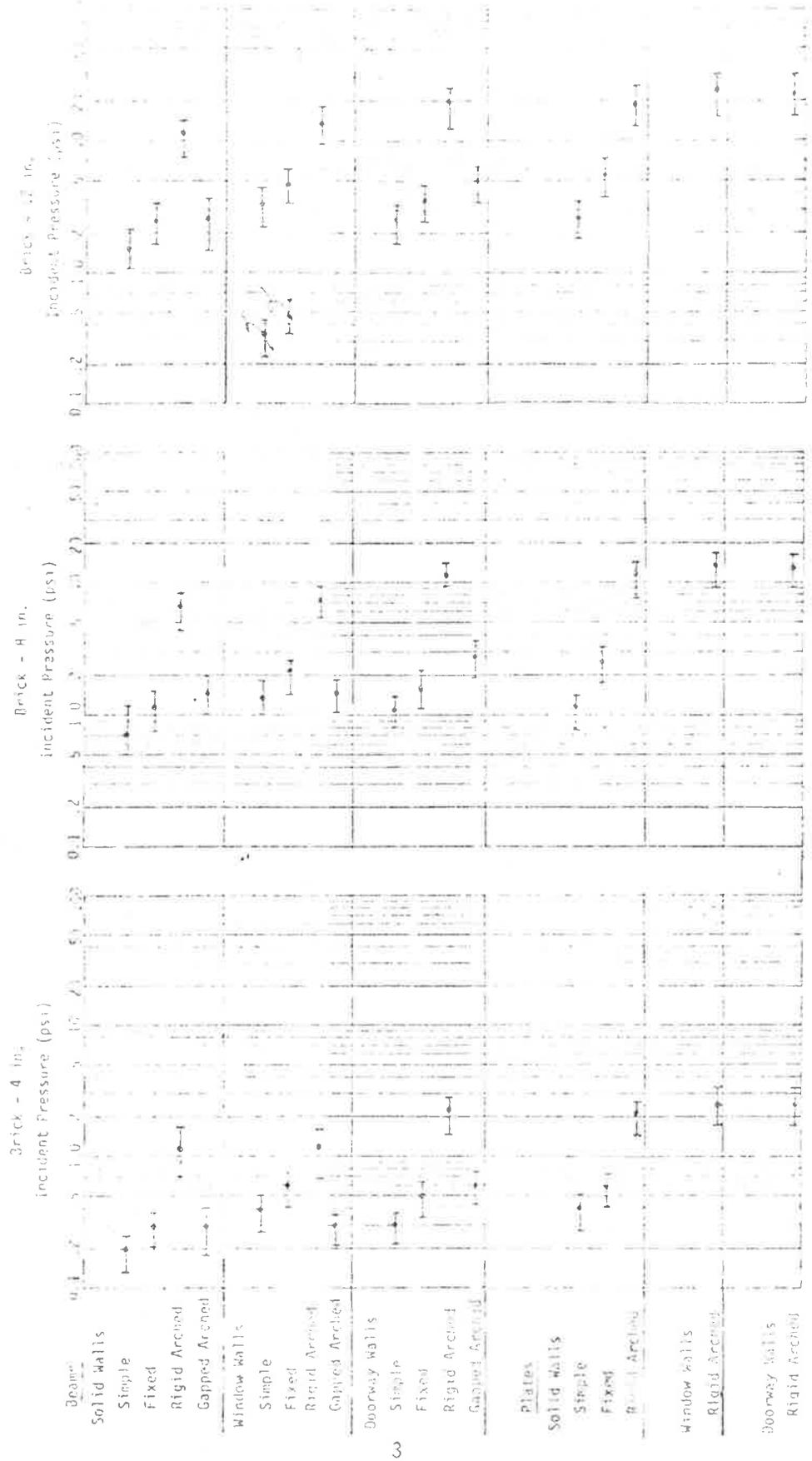
FAILURE PRESSURE CHART
Brick Walls

Fig. 1.

3

FAILURE PRESSURE CHART
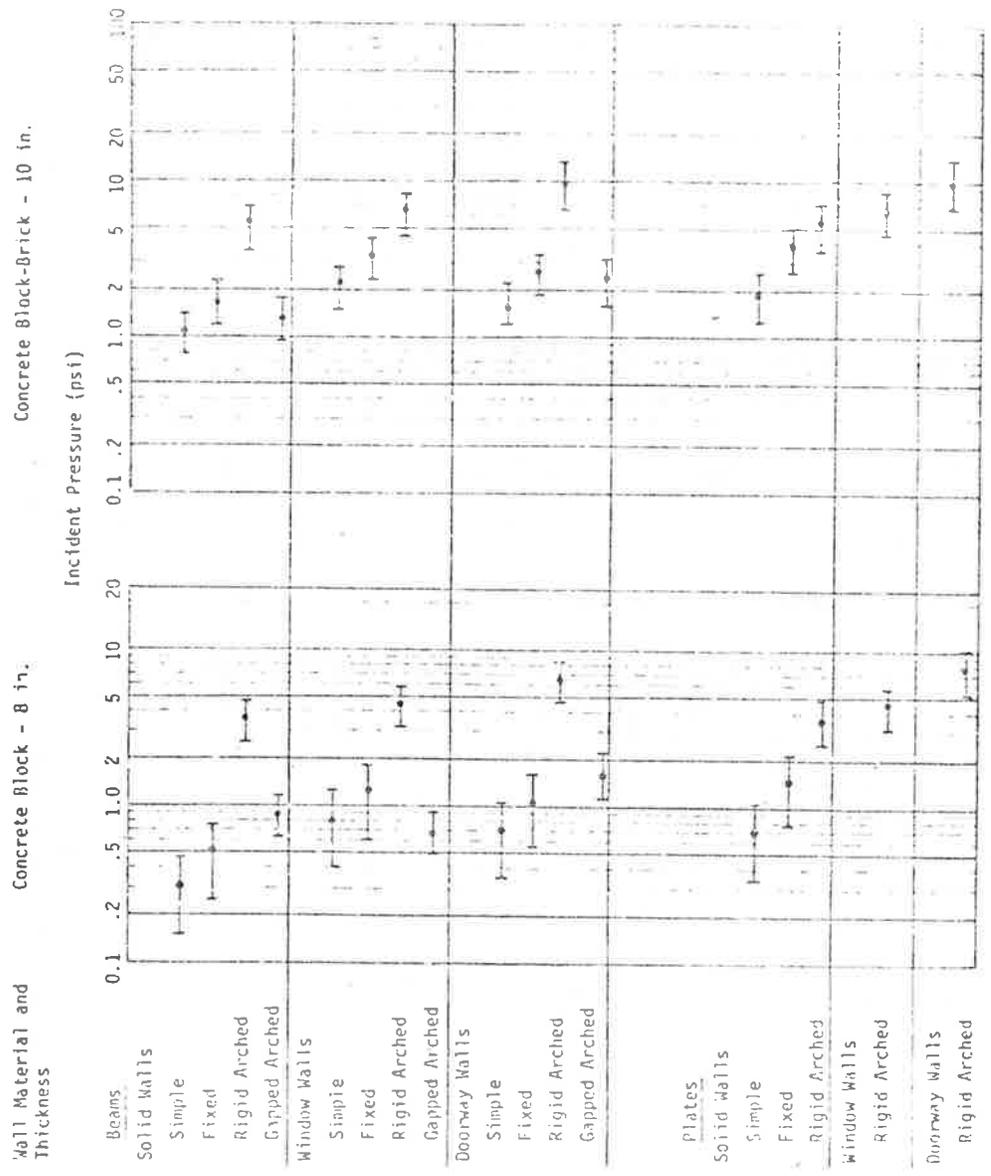
Concrete Block and Composite Brick-Concrete Block Walls

Fig. 2.

THE SHOCK TUNNEL:
HISTORY AND RESULTS
Volume I
THE FACILITY

PREFACE

I, 1921 Congress approved the construction of a coastal defense gun emplacement on the Marin Headlands at the entrance to San Francisco Bay. This emplacement containing two 16 in. guns was completed in 1940 and was named Battery Townsley in honor of Major General Clarence Page Townsley, who commanded the 30th Infantry Division during World War I.

Battery Townsley remained active until 1948 when it was closed and the guns removed. It remained unused until 1967 when it was suggested to the Office of Civil Defense (now the Defense Civil Preparedness Agency) that because of its massive, unique construction, it offered the opportunity for the development of an inexpensive test facility for full scale testing of the loading and response of structural elements and Civil Defense equipment.

Due to the persistence and farsightedness of Dr. M.A. Pachuta of DCPA, initial funding was obtained and the Shock Tunnel was put into operation. The Shock Tunnel remained in operation until November 1976 when Battery Townsley was turned over to the Golden Gate Recreation District of the National Park System; it will eventually become a museum or interpretive center.

Thus, in a sense, this report is an epitaph to a unique facility which contributed much to our knowledge of the blast resistance of structures and equipment. Many questions still remain unanswered and the loss of the facility will create a void in reliable full-scale experimental methodology. Its loss will be great in its impact on shock and dynamic analysis.

The purpose of this report which presents a review of the Shock Tunnel construction, operation, etc., however, is not to look back, but to look ahead and, as such, has two objectives. It seemed highly desirable to describe the more unique features of the construction and operation of the

facility to help the designers and operators of any new test facilities. Second, it is anticipated that the vast quantity of information developed in the Shock Tunnel may be used for many years and most likely for numerous purposes other than those which were originally intended. An understanding of the facility and its operation will allow the use and prevent the misuse of its data.

ABSTRACT

This is Volume 1 of a five volume report which summarizes the results of a program conducted by the Defense Civil Preparedness Agency to determine blast resistance of wall panels typically found in existing structures. The objective of this program was to determine the blast sheltering capability of structures in the National Fallout Shelter Survey inventory and to obtain information which could be used to upgrade these structures.

This volume describes the shock tunnel facility used for the experimental testing of full-scale wall panels. Included is a summary of the capabilities of the shock tunnel for dynamic loading and response studies and brief summaries of various experimental programs conducted in the shock tunnel which were not related to the wall panel test program.

Volume 2 of this report presents the results obtained from the experimental program conducted in the shock tunnel to determine the loadings which are received by wall panels mounted in the test section.

Volume 3 of this report is concerned with the dynamic response and failure of full-scale wall panels. Included are the development of theories of wall panel response and the results obtained from the testing of full-scale wall panels in the shock tunnel.

Volume 4 of this report describes the static test program conducted to determine the physical properties of the wall panels and to assist in the development of failure theories and test predictions for wall panels.

Volume 5 summarizes the predicted failure pressures for wall panels based on the theoretical and experimental results covered in Vol. 3 and the static test data in Vol. 4.

ACKNOWLEDGEMENTS

Table of Contents

Table of Contents (contd)

List of Figures

List of Figures (contd)

Section 1

INTRODUCTION

This volume describes the shock tunnel facility used for the experimental testing of full-scale wall panels. Section 2 reviews the design, construction, operation, and evaluation of this unique facility. Section 3 summarizes the capabilities of the shock tunnel and its application for a variety of dynamic loading and response studies. Section 4 summarizes various studies conducted in the shock tunnel which were not related to the wall panel test program, the basic subject of this overall report.

1

DEVELOPMENT OF THE SHOCK TUNNEL

DESCRIPTION OF SHOCK TUNNEL AREA OF THE COASTAL DEFENSE BATTERY

A cutaway view of the shock tunnel area of the Coastal Defense Battery is shown in Fig. 1 and a plan view in Fig. 2. The basic tunnel is 163-ft-long and includes a 63-ft-long section A, 8-ft-wide and 8.5-ft-high, used for the compression chamber; an 8-ft-long transition section B; and a 92-ft-long section C, 12-ft-wide and 8.5-ft-high, used for the expansion chamber. At the mouth of the tunnel is an 8-ft-long angled section D, which opens into the casemate E, 52-ft-wide, 36-ft-long and 15-ft-high.

There are eight side openings into the basic tunnel: five 6-ft-wide, 7-ft-high doorways, which lead to the two power rooms and to the storeroom; two 15-ft-wide, 8.5-ft-high openings to the shell rooms; and a 16-ft-wide, 13-ft-high opening at the rear of the casemate.

The wall thicknesses range from 8 to 12 ft on the west side of the tunnel and are typically 3-ft-thick on the east side. The ceiling is 7.5-ft-thick. All concrete is reinforced with 1/2-in.-thick square steel reinforcing bars typically 8-in. apart.

TUNNEL CONVERSION

To convert the basic tunnel into a shock tunnel required the following modifications:

> o Removal of shell-handling facilities.
> o Reinforcing and closing the end of the compression chamber area (Section A in Fig. 2).
> o Installation of closures for the openings in the east wall of the tunnel.
> o Installation of an instrumentation system.
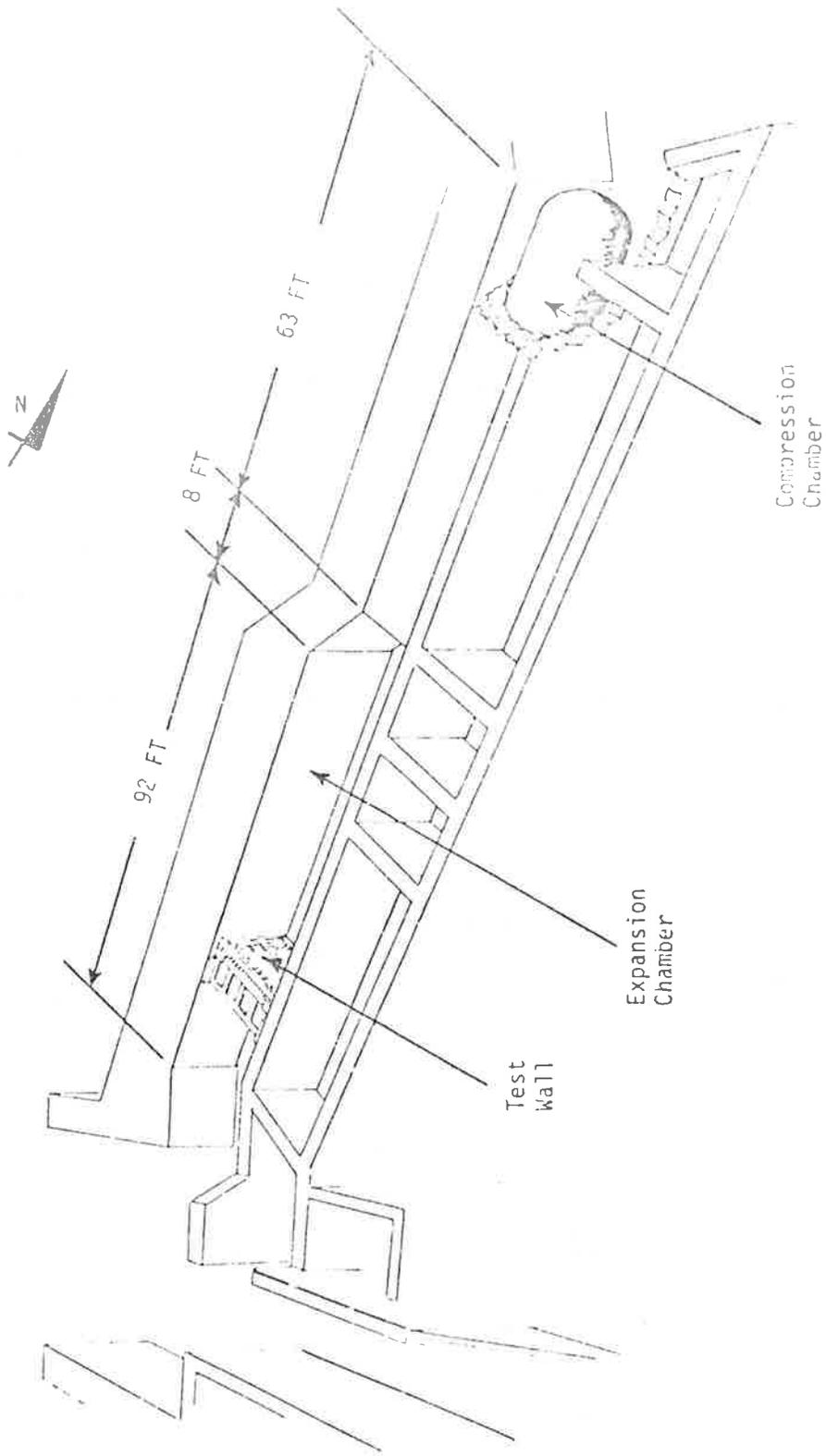
Fig. 1.   Cutaway View of Shock Tunnel Showing Wall in Place.

N

92 FT

63 FT

8 FT

Test Wall

Expansion Chamber

Compression Chamber

Fig. 2. Plan View of Shock Tunnel.

LEGEND
⬛ BLOCKED AREAS

CASEMATE

EXPANSION CHAMBER

COMPRESSION TUBE

POWDER ROOM

POWDER ROOM

SHELL ROOM

SHELL ROOM

STORE ROOM

163'

4
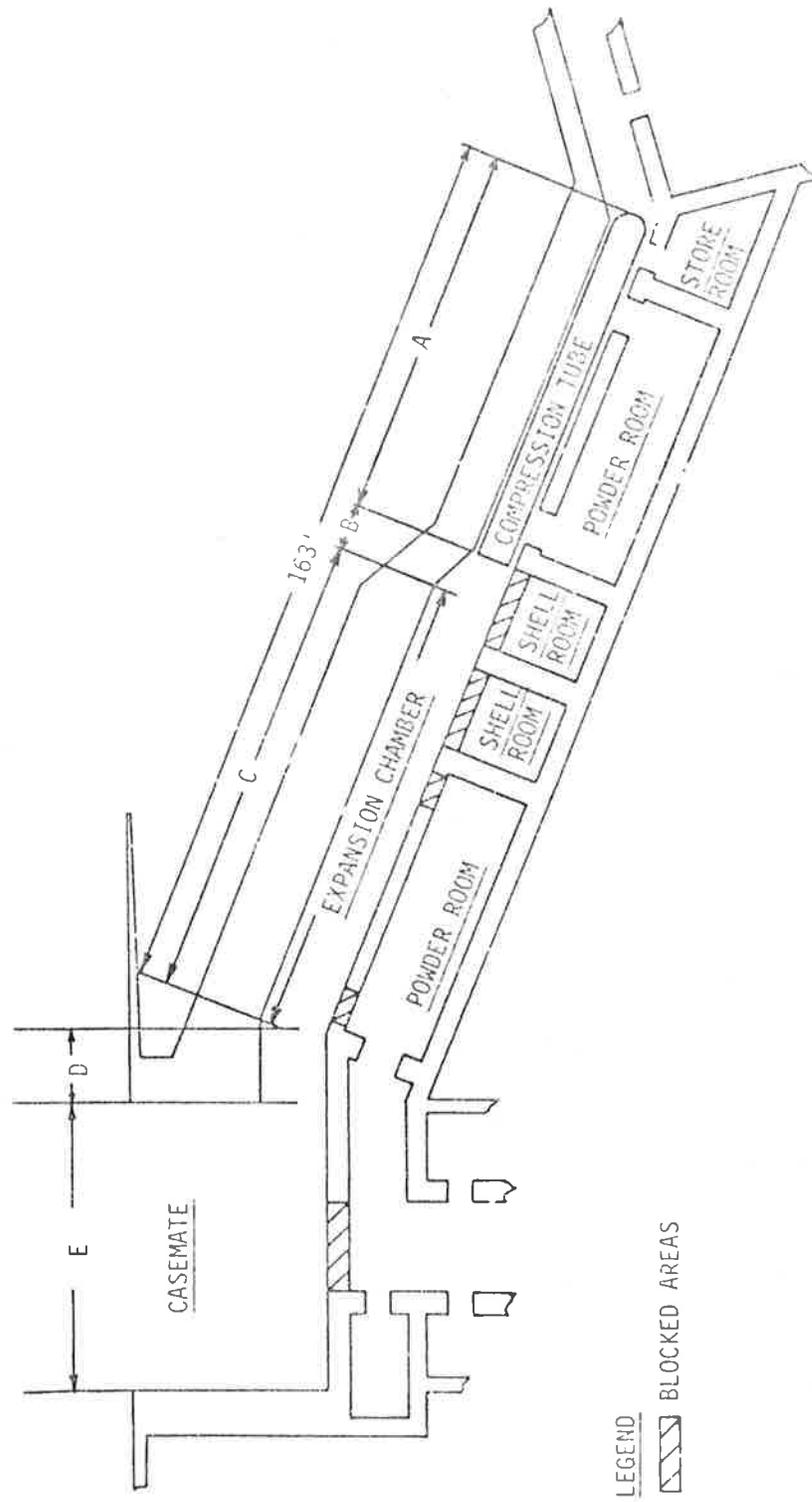
The reinforcing and closing of the compression chamber area was the most difficult part of the tunnel conversion. Preliminary calculations made at the start of the program had indicated that a peak incident shock overpressure of about 12 psi in the expansion chamber would be sufficient as an upper limit for the majority of tests of structural building panels. Based on work by previous investigators (Ref. 1) a peak incident shock overpressure of 12 psi would require approximately 50 psi in the compression chamber.

It was originally planned to use the compression chamber section of the tunnel essentially as it was, with the only modifications being the provision of an end closure and several side closures for doorways which opened onto this section of the tunnel and the reinforcement of the 3-ft-thick wall along one side of the tunnel. It soon became evident, however, that an extensive amount of work would be required to anchor the end closure and to reinforce the 3-ft-thick wall for the design load of 50 psi and that the simplest and most economical solution would be to install a steel liner in the compression chamber section of the tunnel. Accordingly, a 3/8 in.-thick, 7-ft, 8-in. diameter steel tube, 63 ft long with a 1/2 in.-thick domed end closure, was installed.

For the first proof tests, which were conducted at low pressure levels, the compression chamber tube was fastened to the tunnel by ceiling brackets, which were held in place by both epoxy cement and bolts (left after removal of a shell handling track) and by heavy steel channels, which were welded on the side of the tube and fit snugly into the two powder room doors on the east side of the tube. To prevent collapse of the compression tube on rebound, 12 screw jacks were installed in the tube. The jacks were installed in pairs, 90 degrees apart, and were spaced every 10 ft down the tube. The ends of the screw jacks pushed against 4- by 6- in. timbers running the full length of the tube. The space around the mouth of the tube - between the tube shell and the concrete walls, floor, and ceiling - was sealed with sandbags.

This method of fastening and sealing of the compression tube was

5

sufficient for the proof-testing and calibration series, but was not considered suitable for a continuing panel test program. The sandbag seal around the tube, for example, was largely destroyed during each test, was a source of dust, and took considerable time and manpower to replace. In addition, there was some concern that the ceiling brackets and steel channels might not be sufficient to hold the tube in place at the higher pressure levels required for some of the panel tests.

Accordingly, an investigation was conducted into various methods of restraining the tube, and a rather novel approach was selected which consisted of filling the space between the tube shell and the concrete walls of the tunnel with foamed-in-place rigid urethane foam. This method was very appealing in that it provided a continuous elastic support around and along the entire tube to prevent tube collapse. Also it supplied the necessary holddown strength and a large amount of damping on the tube to facilitate making pressure measurements on the walls of the tube. As a further side benefit, it reduced noise and vibration throughout the facility. Since this was a new application for this materi ', it was necessary to run a series of tests to determine if the foam would bond to the tube shell and to the concrete wall and if the foam would expand in the cold atmosphere of the shock tunnel facility. It had been determined from calculations that a bond strength of 10 psi tensile and 10 psi shear would be required. These tests showed that tensile bond strengths of 28-35 psi and shear bond strengths of 25-28 psi could be obtained if the tunnel and shell were washed with water and the tunnel and tube warmed to at least 70 degrees.

A number of small holes were cut in the tube shell to facilitate placement of the foam, the tube and tunnel walls were washed with a fire hose, and a series of heaters was placed in the tube shell. At an ambient temperature of 70 to 80 degrees in the tunnel, approximately 1200 lb of urethane foam were pumped through the holes in the tube shell. The resulting in-place density of the foam was approximately 2 lb/cu ft. A thin steel collar was installed around the mouth of the tube to protect the foam from air blast.

6

A 24 in. diameter access way with a blast door was installed in the domed end of the tube to allow access to the compression chamber for installing the explosive charges after the tunnel was blocked with a test specimen and to provide ventilation in the tunnel.

The installation of the compression tube eliminated three openings in the tunnel. The five remaining openings in the east wall; the two shell room openings, the two doorways to the powder rooms, and the opening to the casemate were closed by timber barricades. The two shell room openings and the powder room doors were provided with a front wall of 16-in.-thick timbers extending to the far wall of the powder and shell rooms. The casemate closure was constructed from 12-in. by 12-in. timbers set in a groove in the concrete floor and braced at the top by a steel frame. A 5-ft section of the closure was made into a sliding door to allow access to the casemate and tunnel areas from the panel storage area.

It is quite satisfying to note that the shock tunnel was in operation for over 7 years and that during this period ~ 1000 tests were run with no observable damage to any part of the basic facility. These included tests which generated shock waves with incident overpressures as high as 10-11 psi, subjecting the compression tube to thrusts of well over a million pounds.

TEST SECTION HARDWARE

A variety of test section hardware was developed for the various programs conducted in the shock tunnel. The major items included:

A - for the panel test program support hardware to permit simulation of the following mounting conditions:
1 - simple beam
2 - simple plate
3 - preloaded beams
4 - arched beams and plates

B - for evaluation of shock tunnel characteristics and loading studies:
  - a nonfailing wall with removable sections and pressure gauge
    instrumentation

C - for interior loadings and flow studies in rooms:
  - a second non-failing wall with removable sections which could be
    located from 4 to 15 ft behind the other non-failing wall.

Typical examples of this hardware are shown in Figs. 3, 4, and 5. Their detailed characteristics are discussed in the other volumes of this report in connection with the programs for which they were used.

SHOCK TUNNEL INSTRUMENTATION

The basic shock tunnel instrumentation included: air blast gauges mounted in the tunnel wall for monitoring the input loading wave; load cells for measuring the load transferred from a test specimen to its support frame during the loading cycle; strain gauge and air pressure instrumentation for the test specimens; and high-speed cameras in blast-protected mounts for recording the response of the test specimen and the effects of shock flows. Other instrumentation was added as needed for particular tests.

A block diagram of the basic instrumentation system is presented in Fig. 6. The locations of the air blast gauges in the tunnel walls are shown in Fig. 7.

OPERATING CONCEPT

The tunnel was operated as a shock tube by means of the volume detonation technique, with Primacord as the explosive material. In this mode of operation, the Primacord is distributed symmetrically throughout a section of the compression chamber portion of the tunnel. On detonation of the Primacord (which proceeds at a rate of about 20,000 ft/sec), a quasi-static pressure is built up very rapidly throughout the entire compression chamber. The expansion of this

8
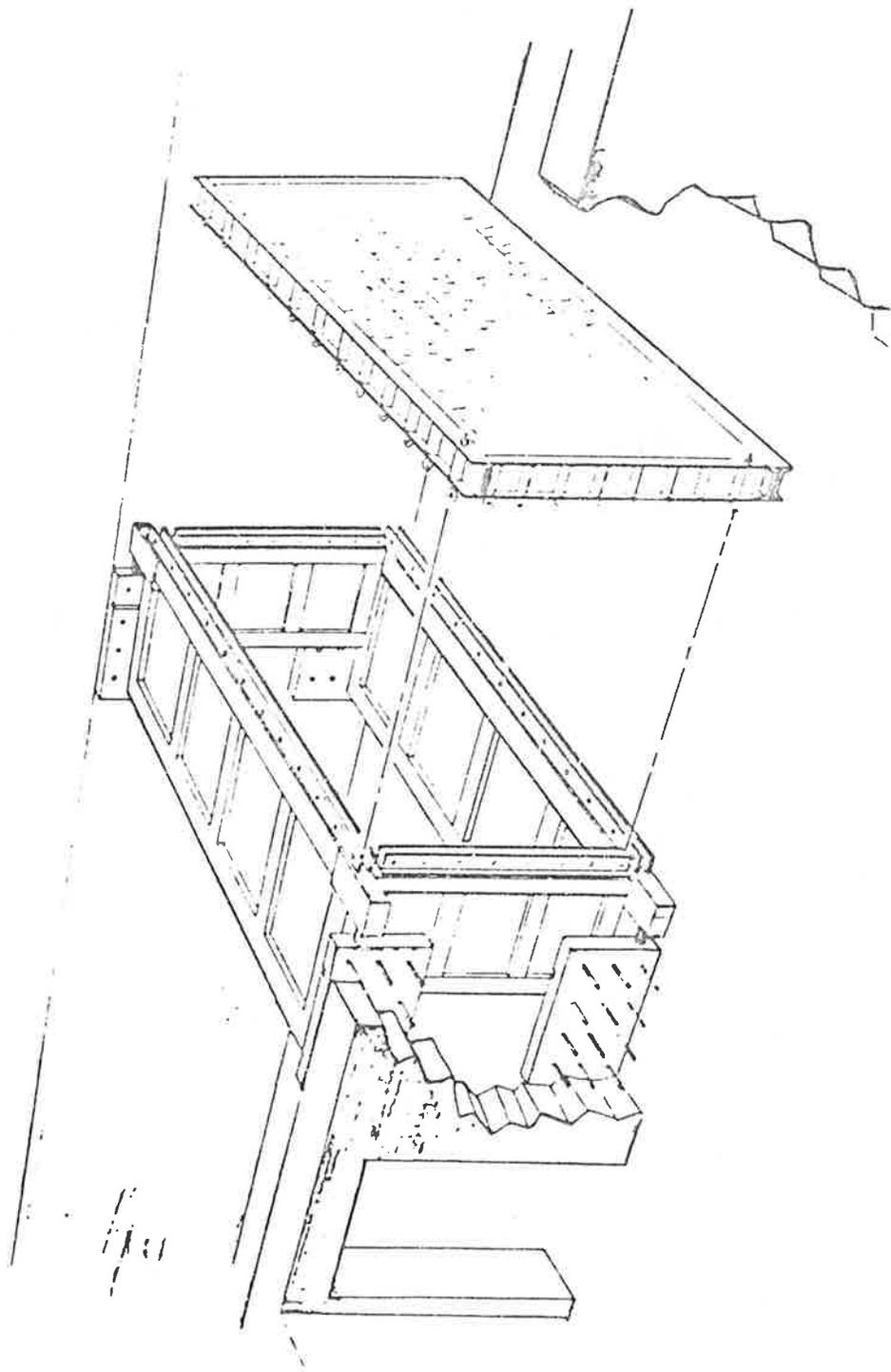
Fig. 3. Cutaway View of Shock Tunnel Showing Test Panel and Simple Plate Support Condition Hardware.

9
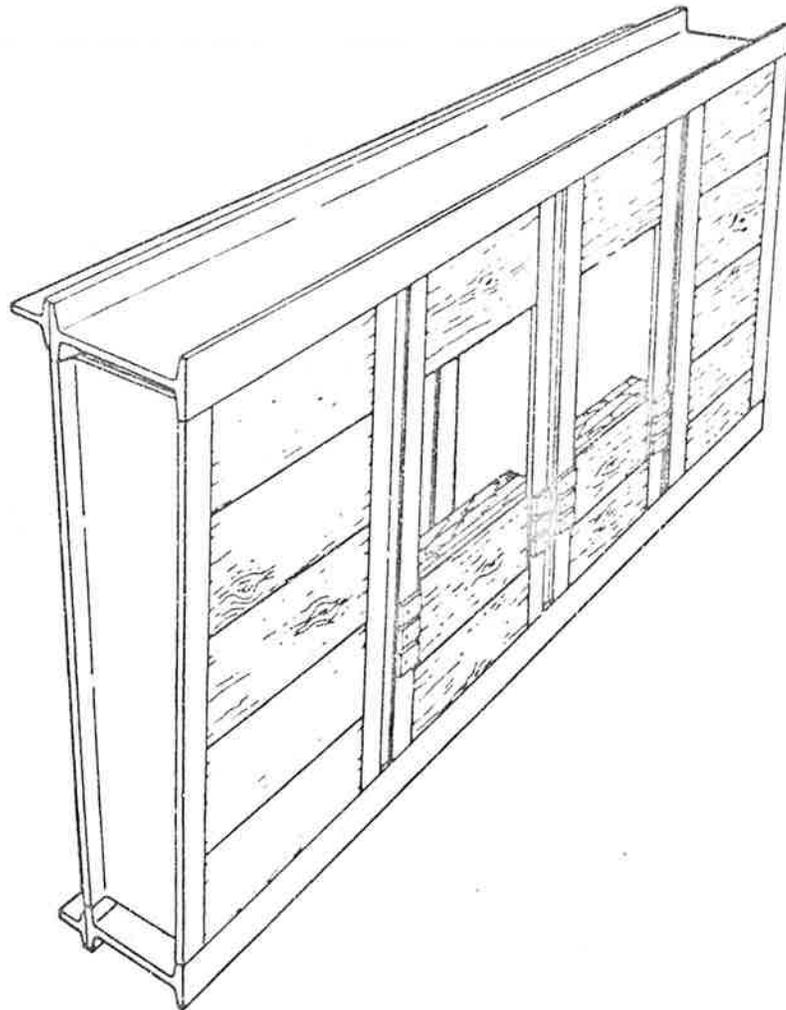
Fig. 4.   Sketch of Nonfailing Wall.

west

G

Station 7

E

F ⟵ SHOCK
WAVE
north

south B

BACK
WALL

FRONT
WALL

D

Station 6-0

A

H

east
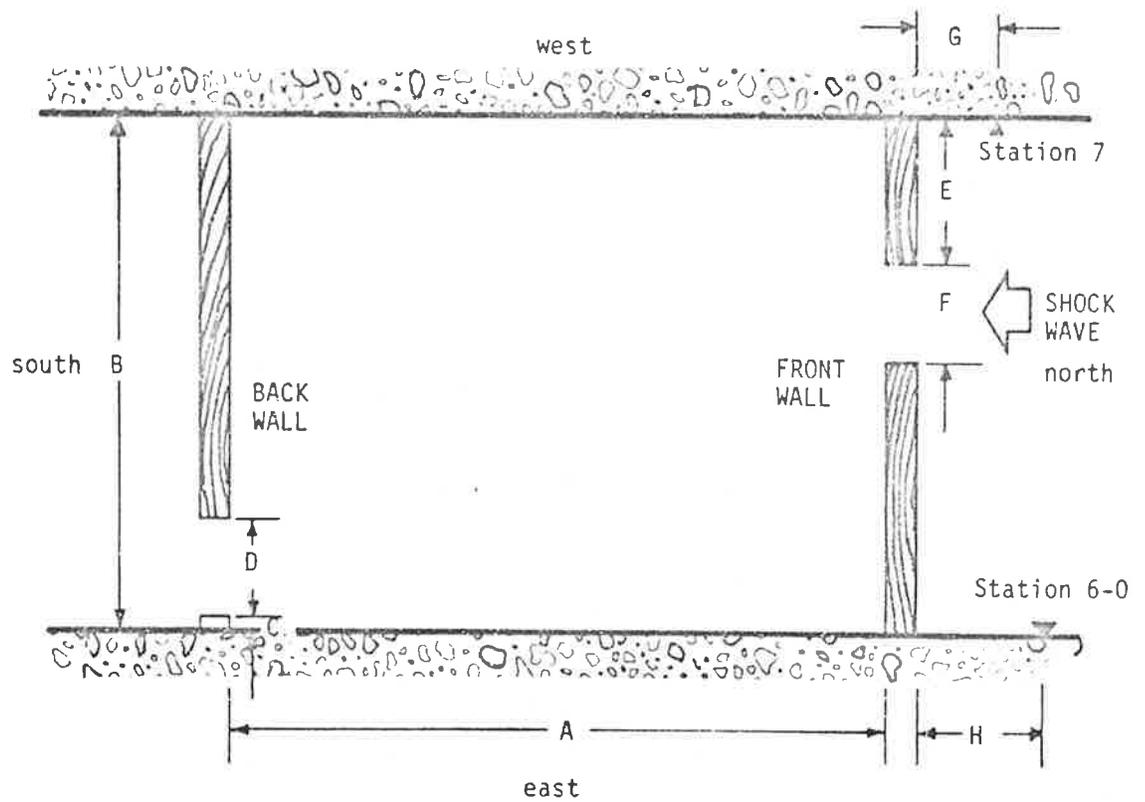
DIMENSIONS

A – 15 ft	E – 39-5/16 in.
B – 12 ft	F – 28-5/16 in.
C – 5-1/2 in.	G – 24 in.
D – 28-5/16 in.	H – 42 in.

Fig. 5. Plan View of Typical Test Room.
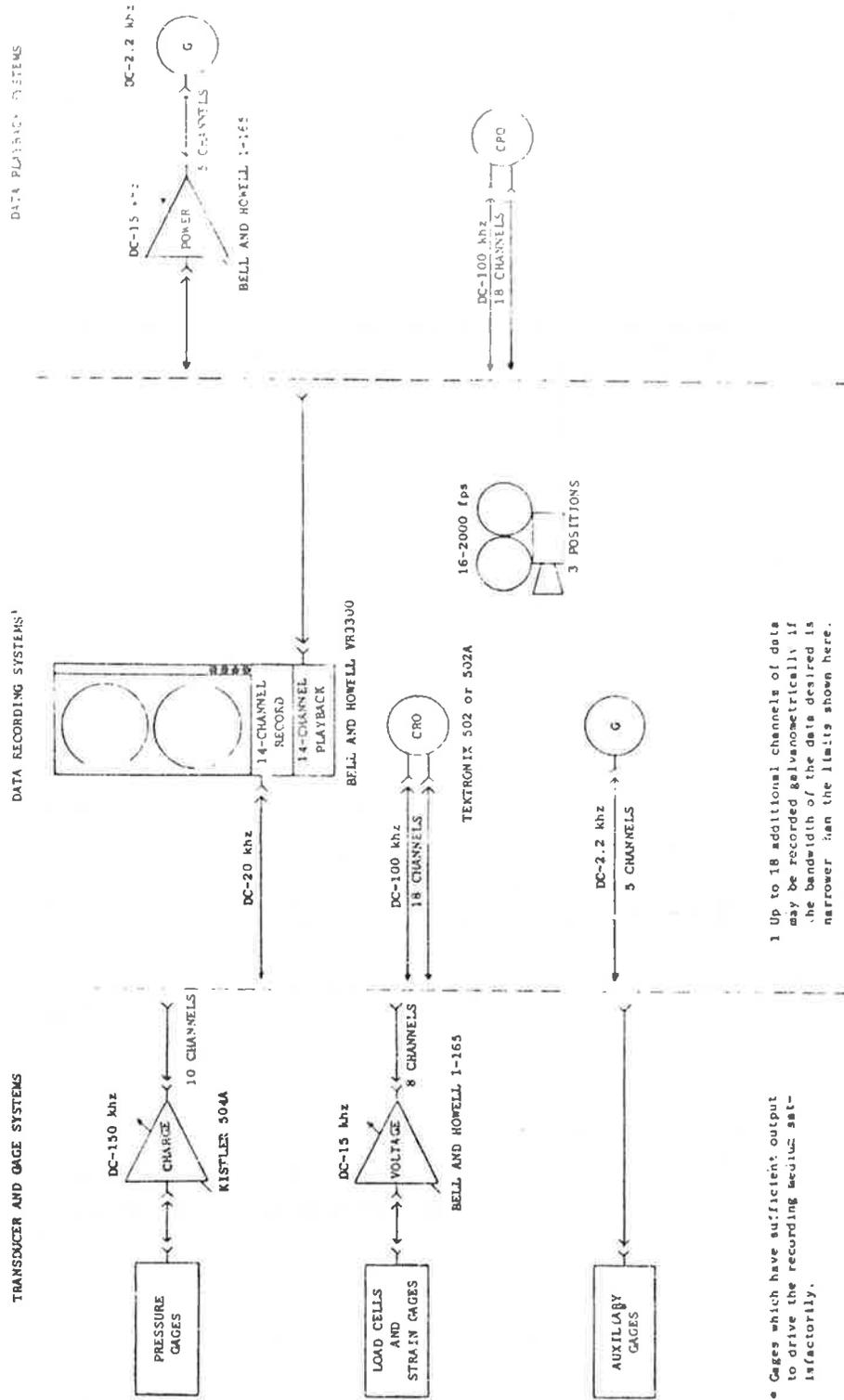
11

Fig. 6. Block Diagram of Data Recording and Playback Options.

Nominal Gauge Distances from
Mouth of Compression Tube

STATION	FT
1	49
2	53
3	57
4	61
5	65
6	69
7	73
8	74
9	76
10	81
11	71.5

N

63'

COMPRESSION TUBE

100'

GAUGE
STATIONS
1
2
3
4
5
6
7
9
10
8
11

TEST WALL

CAMERA LOCATION

CASEMATE

CAMERA LOCATION

Fig. 7.   Plan View of Shock Tunnel Facility.

13

high-pressure gas into the remaining part of the tunnel generates the desired shock wave. The charge density used ranged from one strand of Primacord, containing approximately 0.00625 lb explosive/ft, to eight strands of Primacord, containing approximately 0.05 lb of explosive/ft. The Primacord strands were mounted longitudinally in the compression chamber on a pipe "X" frame as shown in Fig. 8. In most of the tests, the Primacord was initiated at the closed end of the compression chamber, however, a few tests were conducted with initiation at other positions.

Unlike conventional compressed-gas shock tubes, it is not necessary to separate the compression chamber form the expansion chamber with a 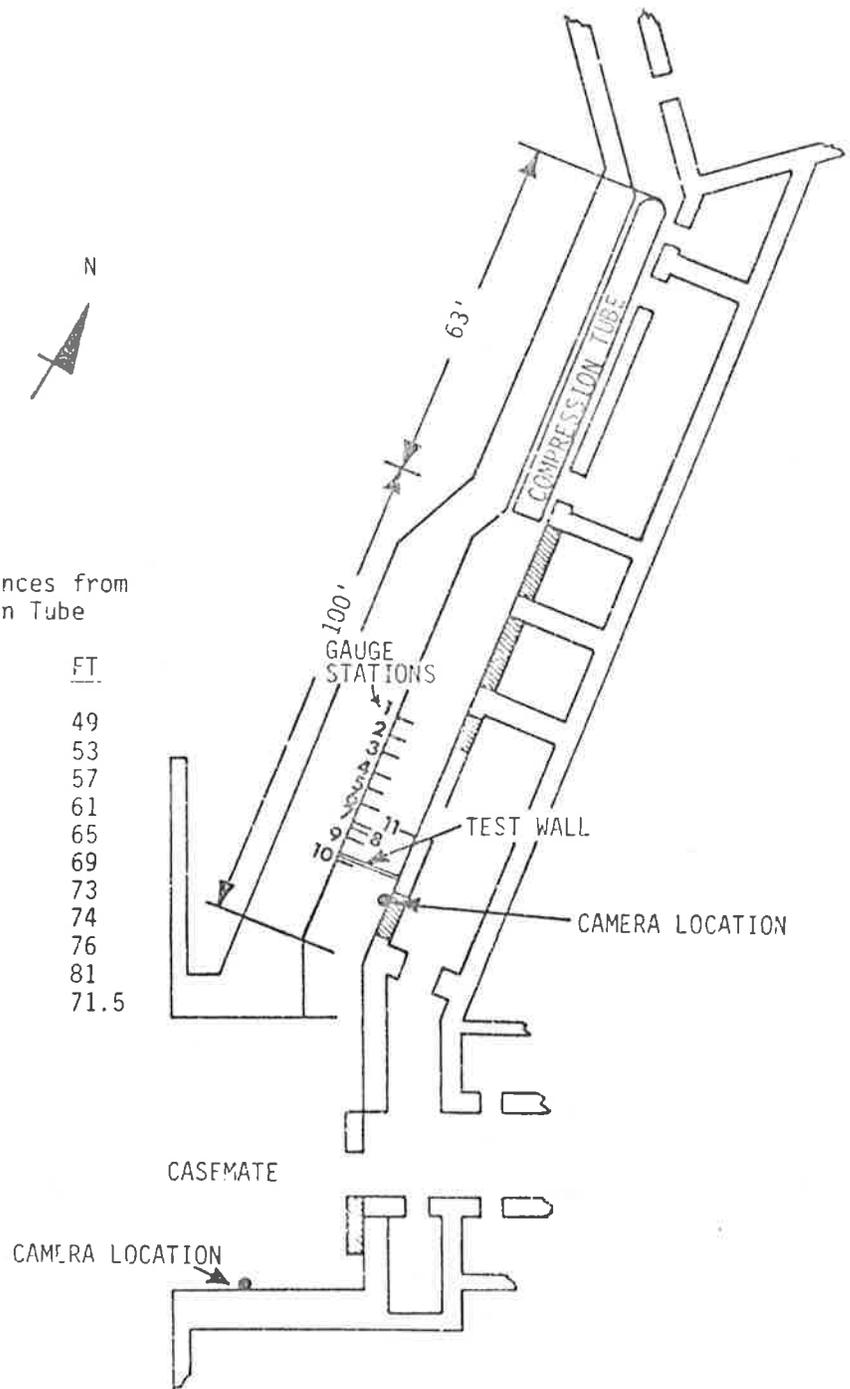frangible diaphragm. The detonation of the Primacord is sufficiently rapid that the pressure build up in the compression chamber is affected very little by the small amount of expansion of the gases out of the chamber during the build up process.

COMPARISON OF THE SHOCK TUNNEL DATA WITH SHOCK TUBE THEORY

To better understand the shock tunnel operation it is helpful to first consider the shock pulses which would be obtained if the tunnel operated as a simple, uniform-cross-section, cold-gas shock tube with a conventional diaphragm. On rupture of the diaphragm a uniform pressure shock wave would propagate down the expansion chamber and a rarefaction wave back towards the end of the compression chamber. Providing the expansion chamber is long enough a side-on pressure gauge downstream from the diaphragm would record a uniform pressure shock wave until the rarefaction wave reflects from the end of the compression chamber and returns to the gauge location and starts to reduce the pressure.

In the case of the shock tunnel, the expansion chamber is relatively short compared to the compression chamber so that the nature of the termination of the expansion chamber also has a major effect on the nature of the pulses recorded. With the tunnel end open the shock wave reflects at the open
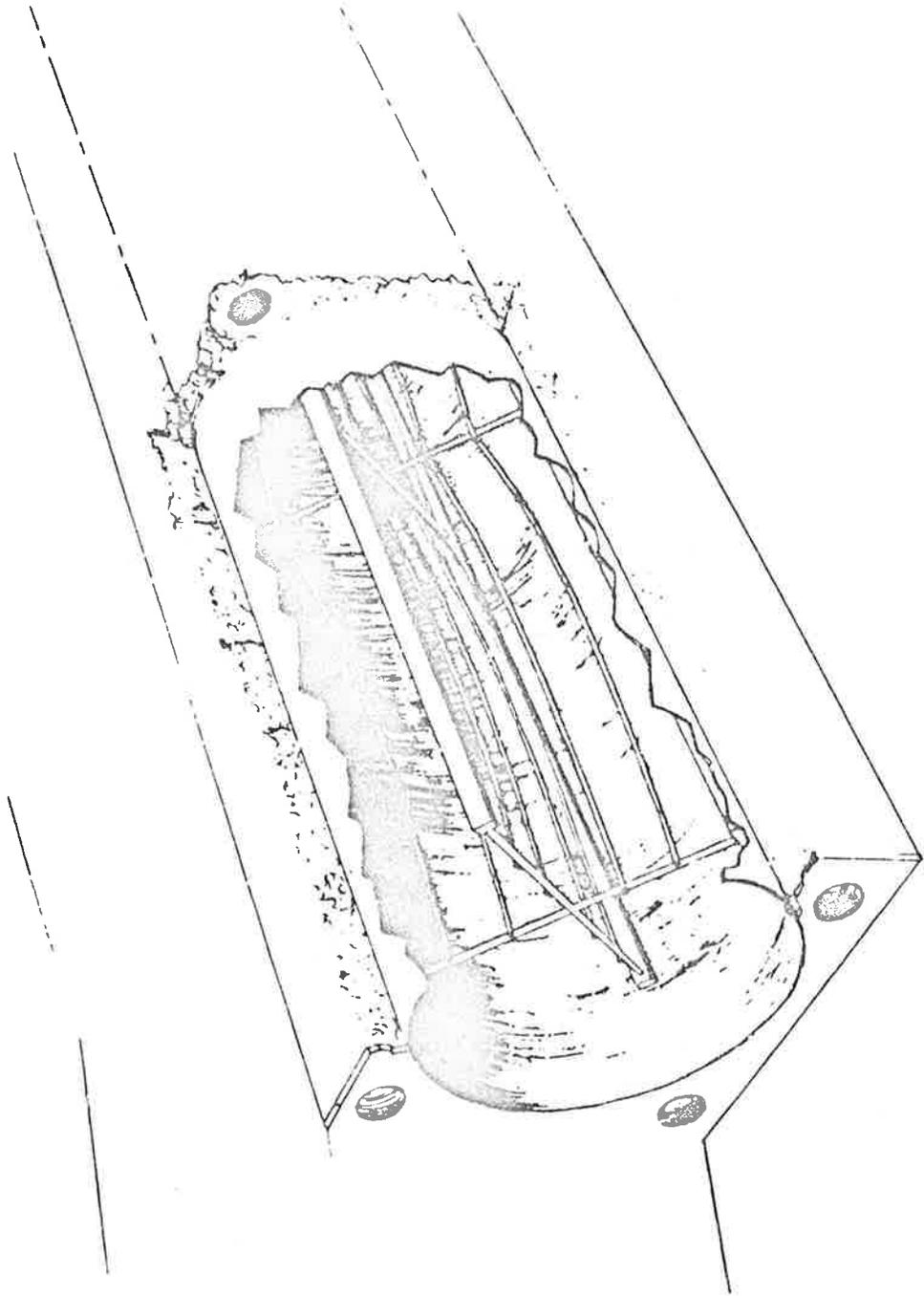
14

Fig. 8. Primacord Array.

15

end as a rarefaction and this rarefaction returns back up the expansion chamber. When it arrives at the gauge location it will start reducing the recorded pressure below the incident flat topped value. When the tunnel is completely closed by a non-failing wall, the side-on pressure gauges would measure the peak incident overpressure, followed after some time interval by reflected overpressure created by reflection of the shock wave by the non-failing wall. This time interval corresponds to the sum of the transit times for the shock wave from the gauge location to the wall, and the return of the reflected wave. When the tunnel is partially open, the reflected wave is weakened and an equilibrium value related to the flow through the opening is established. Idealized pressure traces corresponding to these conditions are shown in Fig. 9 for certain of the gauge locations indicated in Fig. 7.

The actual shock tunnel, however, has some important differences from the idealized case described above. It's cross section does not remain constant, but rather expands from the approximately 8-ft diameter circular cross section in the compression chamber to an 8-½ by 12-ft rectangular cross section of the expansion chamber in an 8-ft transition section. Also, the compression chamber pressure results from a volume detonation process using Primacord as a charge. Both of these differences can be expected to produce significant modifications in the idealized wave shapes. One of the major observations is a weak rarefaction wave starting from about 15 msec after the shock front, as illustrated in an idealized fashion in Fig. 10. As noted in this figure, the magnitude of the rarefaction relative to the peak value appears to decrease with increasing overpressure. The source of this rarefaction was not firmly identified, but seemed most likely to be due to the transition section or possibly to a significant time lag in reaching equilibrium in the driver section of the tunnel.

A second major difference between the actual pressure pulses and the idealized ones is the presence of high frequency oscillations on the shock tunnel records which have a period on the order of 2 msec and a magnitude on the order of 15% of the signal size. This phenomenon is illustrated in Fig. 11, pressure time pulses from Stations 7 and 9 for a four strand test. This noise is

16
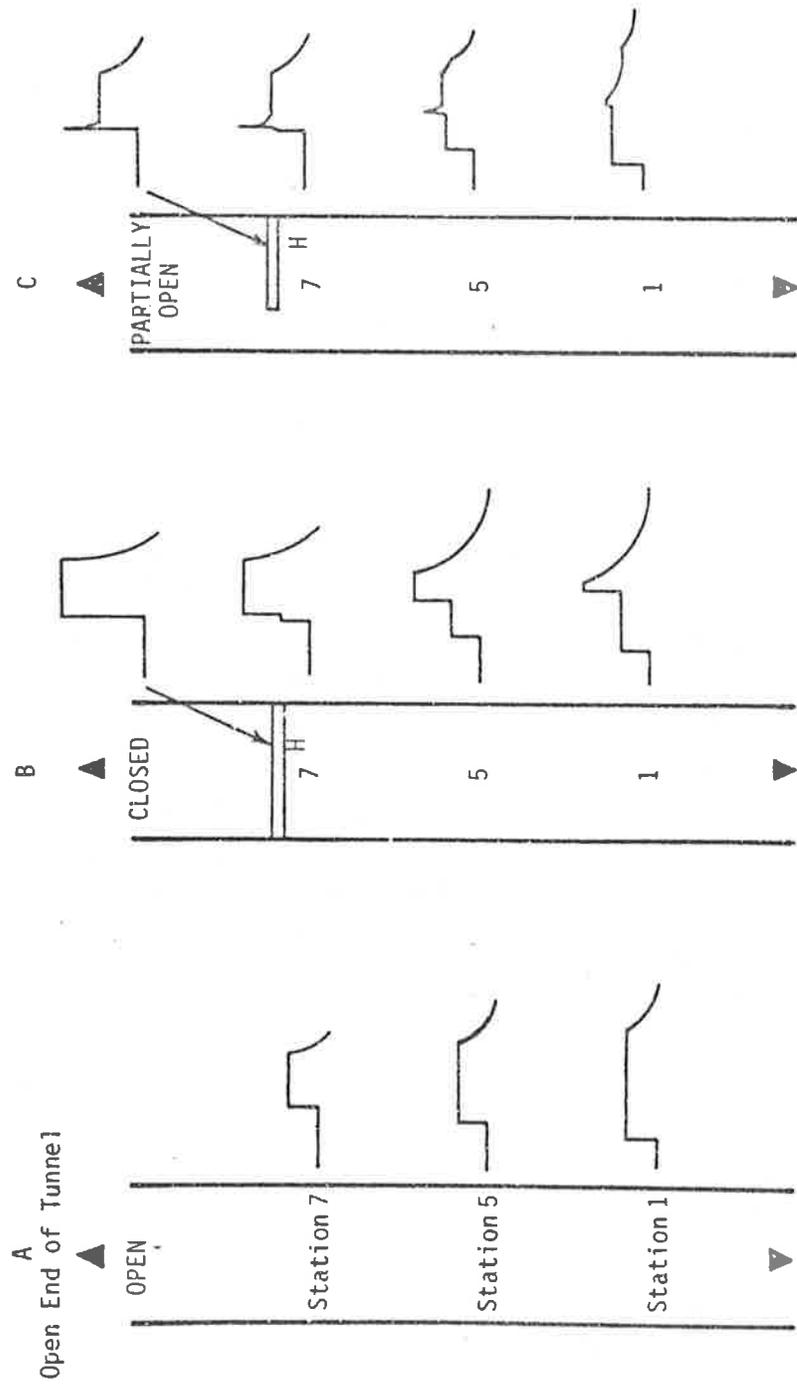
Fig. 9. Idealized Pressure Traces at Selected Locations in the Shock Tunnel.
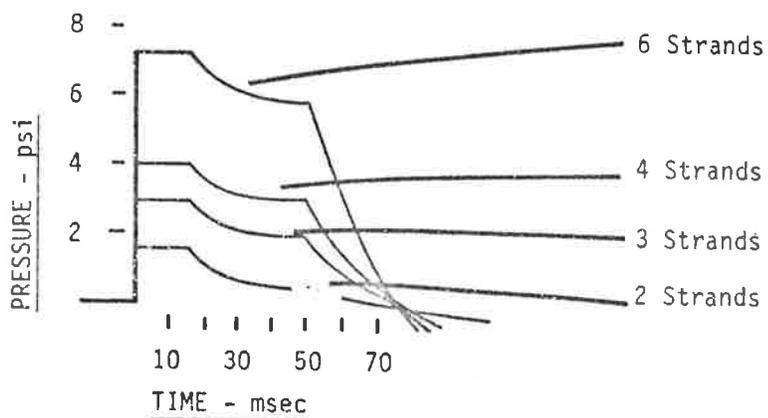
17

Fig. 10. Major Positive-Phase Pulse Shapes for a Range of Overpressure as
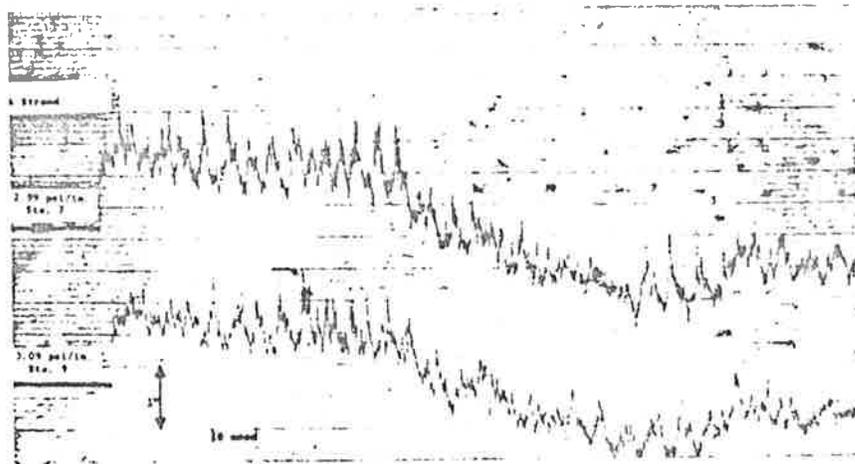Measured at Tunnel Wall Station 1

18

Fig. 11. Pressure-Time Pulses from Sta. 7 and 9 from a Four Strand Test.

attributed to the local shock waves that radiate from the Primacord line-charges and then interact with each other and the compression chamber walls. This high frequency oscillation had little effect on the response of the structural elements tested because it's period was much shorter than the response period of the elements.

Shock Tunnel Calibration

When first put into operation (in 1967), the shock tunnel performance was investigated by conducting approximately 50 tests in which variables of charge density, charge location, charge length, method of detonation, and tunnel geometry (both open and closed) were investigated (Ref. 2). These tests indicated that shock overpressures increase with increasing charge density and to some extent with increasing charge length and that the pulse shape varies with charge arrangement and length. For example, when a number of Primacord strands were placed together at the center of the tube, a somewhat classical peaked shock wave was obtained. When the strands were distributed throughout the cross section of the tube, as shown in Fig. 8, shapes that were essentially flat-topped are obtained. For the distributed charge arrangement, pulse durations increased with increase in charge length, with typical durations approximately 80 to 100 msec for a 60-ft charge. The duration of the flat-topped portion of the latter pulses ranged from 30 to 50 msec.

Based on these results a standard operating mode was selected which used the maximum length possible of the Primacord strands (60 ft), the distributed charge arrangement, and detonation at the closed end of the compression chamber. The relation between side-on or peak incident overpressure and the number of strands of Primacord used for this standard mode is shown in Fig. 12 and typical pulse shapes in Fig. 13. Statistical analysis of samples of calibration tests used in deriving Fig. 12 showed that the test to test standard deviation of incident pressure was about 10% for three strands of Primacord and about 15% for 2½ strands or less. This means that 95% of the time incident pressure should be within ± 20% of the mean value for 3 or more strands and ± 30% of the mean for for 2½ or less strands.
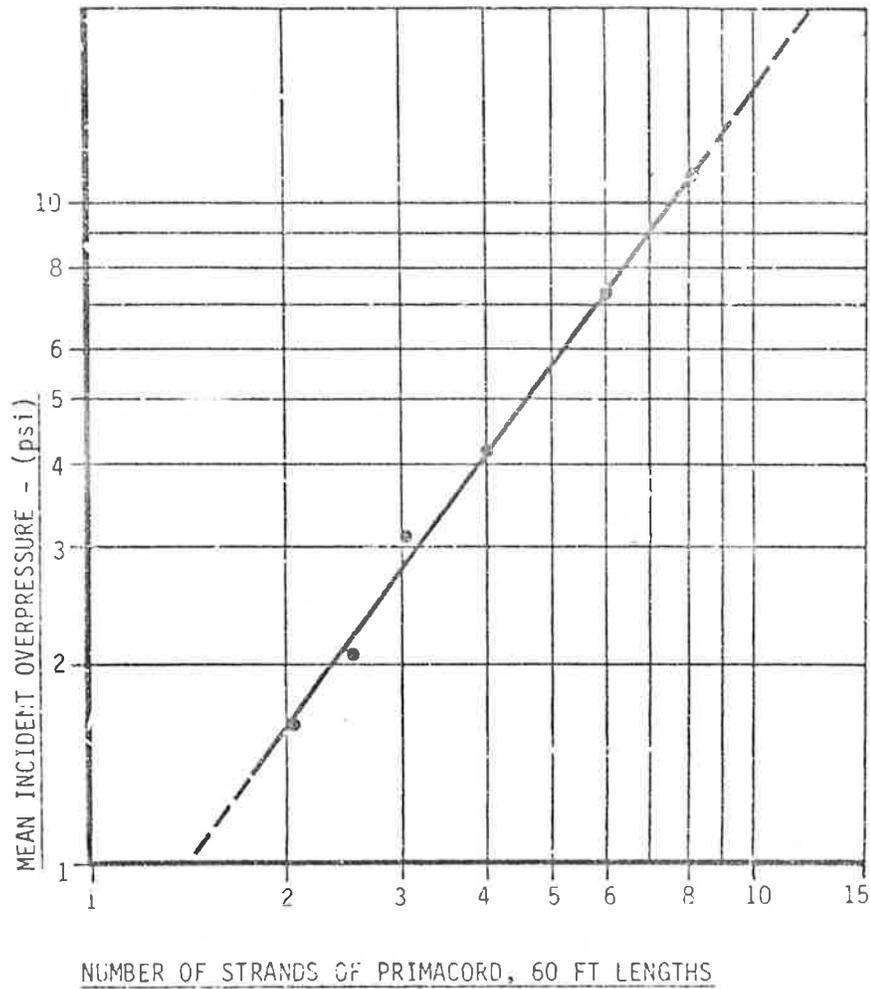
20

Fig. 12. Shock-Front Incident Overpressure as a Function of the Number of Parallel Strands of Primacord Detonated Simultaneously in the Compression Chamber.

21
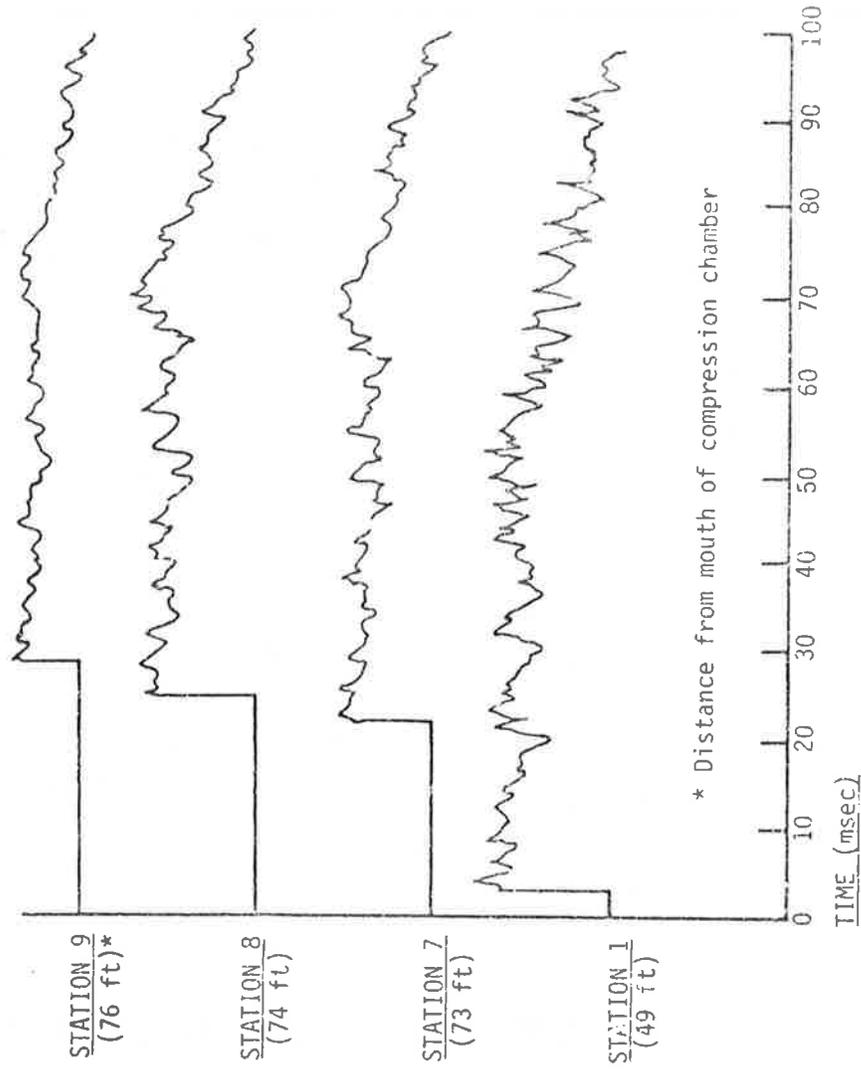
Fig. 13. Sample Data From Four-Strand Open-Tunnel Test.

* Distance from mouth of compression chamber

Similar analysis of the gauge to gauge variability in a given test showed a standard deviation of 5% or 95% limits of ± 10%.

Limited investigations were also made of the variability of the overpressures across the shock front near the test section (Ref. 3). Both the basic expansion process from the compression chamber to the expansion chamber and the non symmetrical nature of the expansion (see Fig. 2) suggested the likelihood of some nonuniformities. These results indicate that this variability was on the order of ± 10% from the mean value.

During late 1972 and 1973 after installation of improved instrumentation and data analysis systems another detailed evaluation of the shock tunnel air blast characteristics was carried out with a series of 18 tests with the tunnel end open configuration and 14 with the tunnel closed with the original non-failing wall (Ref. 4). The results for the tunnel end open are given in Fig. 14. These results are then compared with the earlier data in the Table given below.[*]

Number of Strands	Peak Overpressure		psi/Strand Primacord	
	1967	1973	1967	1973
1	-	1.0	-	1.0
2	1.64	2.0	0.82	1.0
3	3.00	3.5	1.00	1.17
4	4.15	4.9	1.04	1.22
5	-	6.0	-	1.20
6	7.30	7.2	1.22	1.20

It can be seen that the agreement is reasonably good but there is a clear tendency for the more recent data to be about 15% higher at the lower pressures. This difference is somewhat larger than would be expected from the statistical analysis of the first set of calibration data. It is believed that this difference was due to the fact that different lots of Primacord were used in the two test series since they were conducted some 6 years apart. In

---

[*] The 2½ strand data from the 1967 tests were not used because it was found that the ½ strength Primacord was unreliable.

23

Fig. 14. Shock-Front Incident Overpressure as a Function of the Number of Parallel Strands of Primacord Detonated Simultaneously in the Compression Chamber. Data from 1967 and 1973.
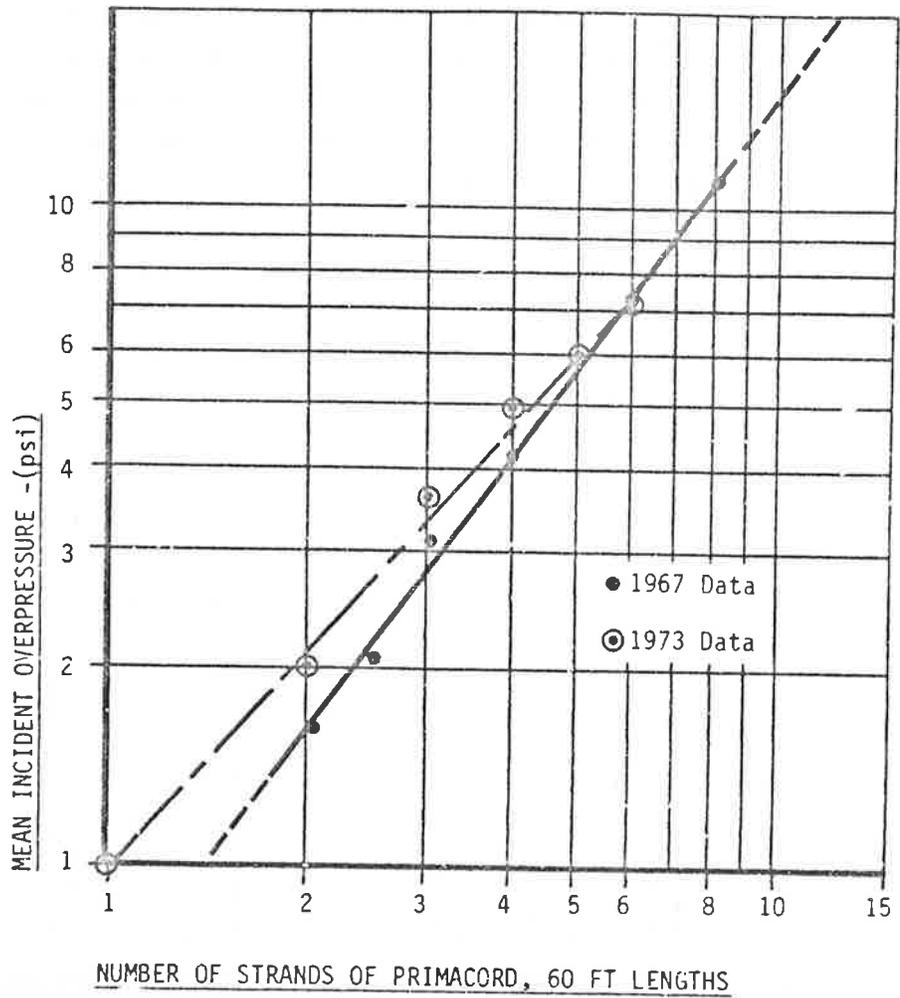
24

the production of Primacord the variable of interest is the velocity of deto-
nation and not the unit quantity of explosive.

The peak reflected overpressure data from the 14 closed tunnel tests are
given in Fig. 15 and compared with peak reflected overpressures calculated
from the peak incident values given in Fig. 14. The agreement is very good.

Sample pulse shapes for open end operation are given in Fig. 11. Sample
pulse shapes for closed end operation are given in Figs. 16-19 with Fig. 20
being a long time recording of a single gauge showing the multiple pulses
obtained as the decayed shock wave reflects back and forth in the shock
tunnel. In the closed end case the measurements were made at 4 positions in
the face of a nonfailing wall as shown in Fig. 21.

It can be seen that for the tunnel closed situation total pulse durations
(which provide the best measure of true loading duration because they are not
influenced by the return of the rarefaction from the open end of the tunnel)
are on the order of 100 msec with flat topped secions varying from about 50
to 80 msec.
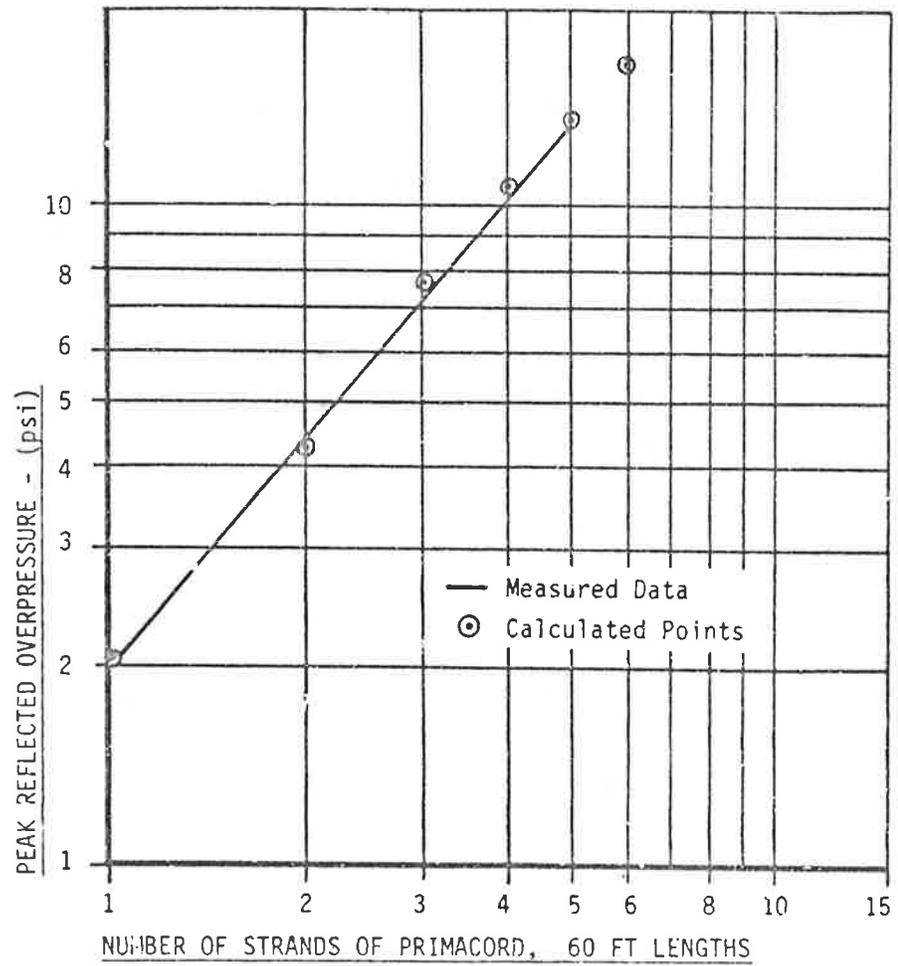
Fig. 15. Peak Reflected Overpressure as a Function of the Number of Parallel Strands of Primacord Detonated Simultaneously in the Compression Chamber.
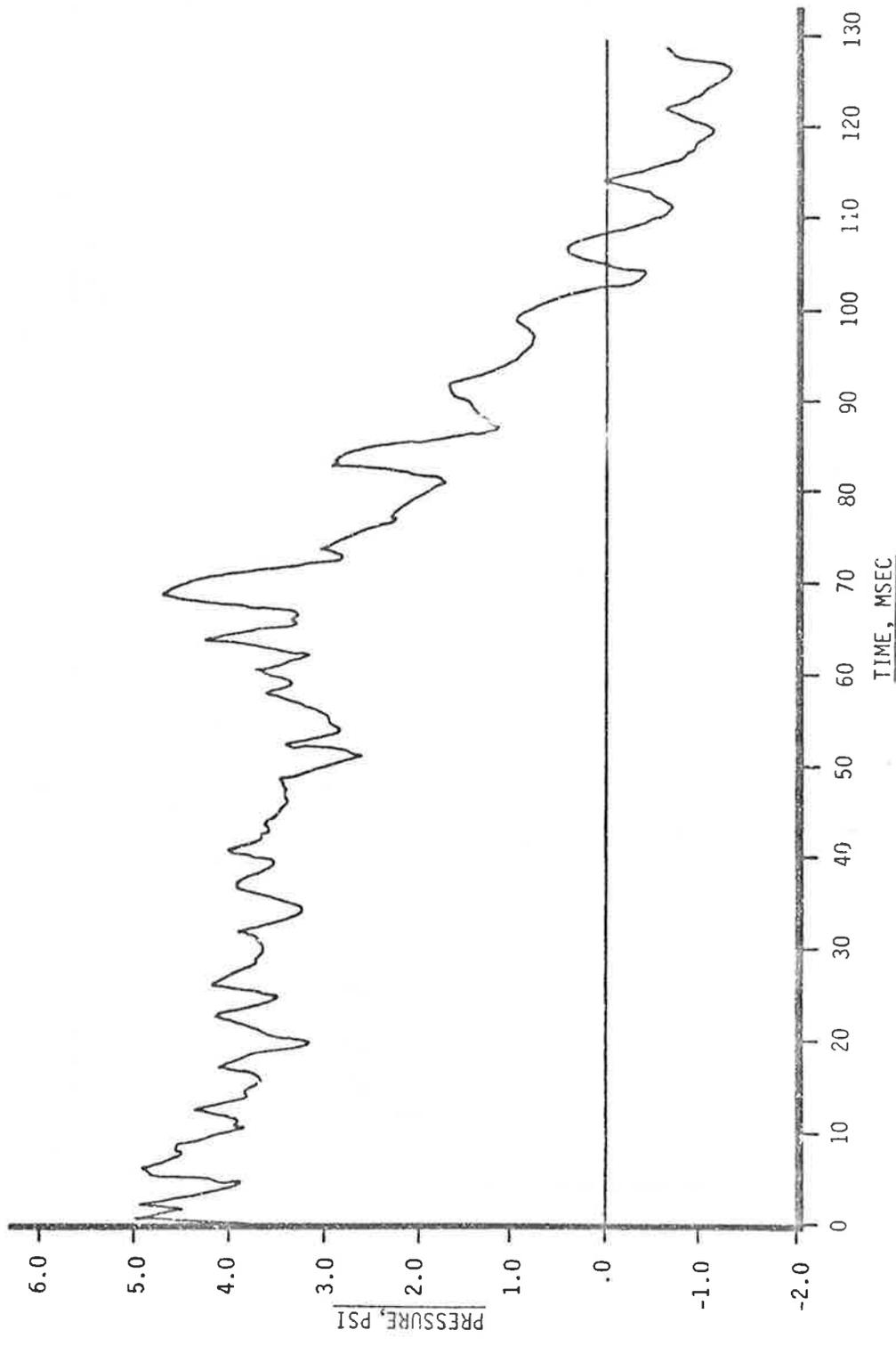
Fig. 16. Average Peak Overpressure vs Time for Two Strand Solid Wall Loading Study Tests 10-19-72-04, and 06; Gauges B-12, B-14, and B-15.

27

Fig. 17. Average Peak Overpressure vs Time for Three Strand Solid Wall Loading Study Tests 10-19-72-01, 02, and 03; Gauges B-12, B-13, B-14, and B-15.

28
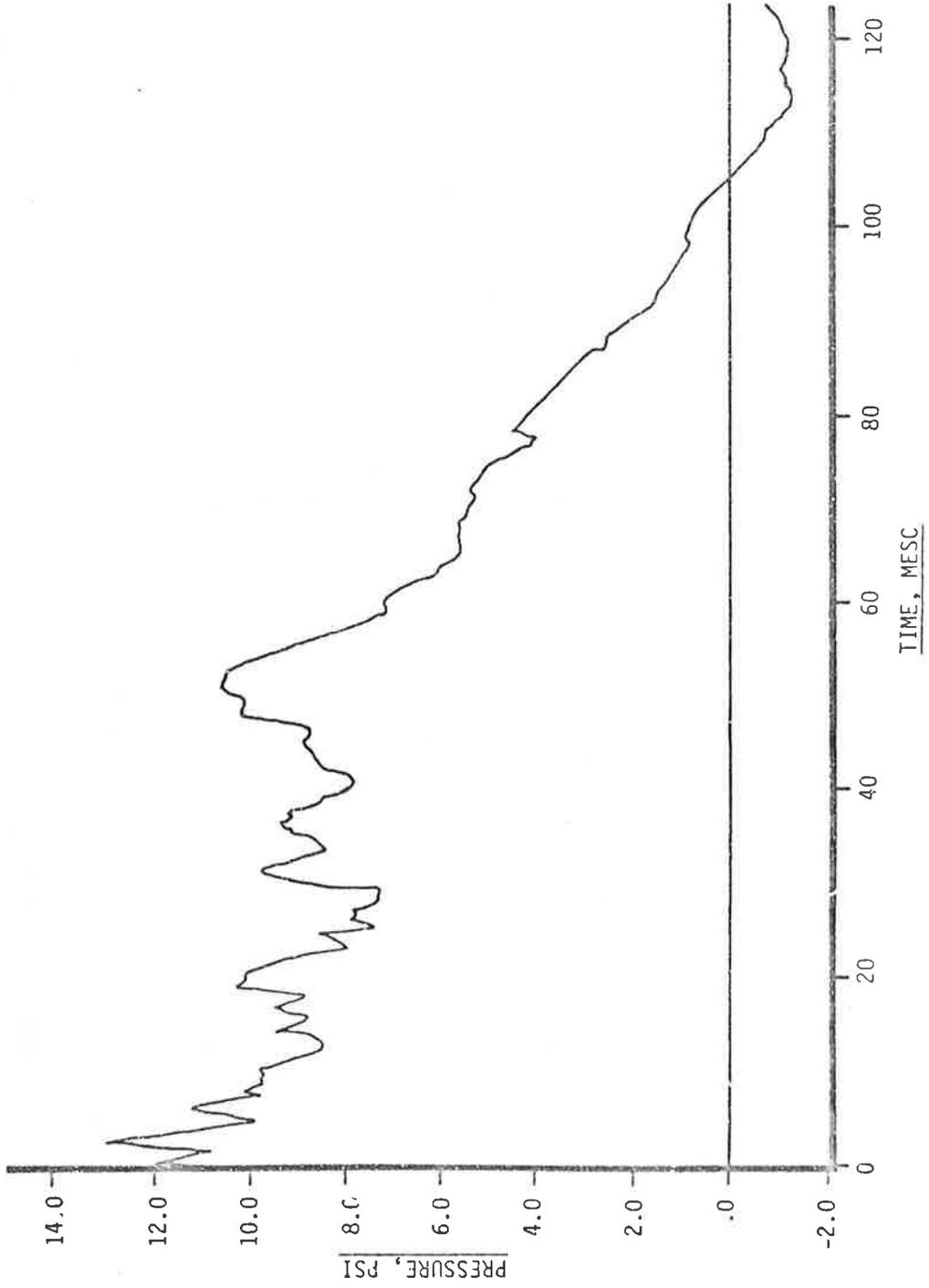
Fig. 18. Average Peak Overpressure vs Time for Four Strand Solid Wall Loading Study Tests 10-17-72-03, 10-17-72-04, and 10-18-72-01; Gauges B-12, B-13, B-14, and B-15.

29
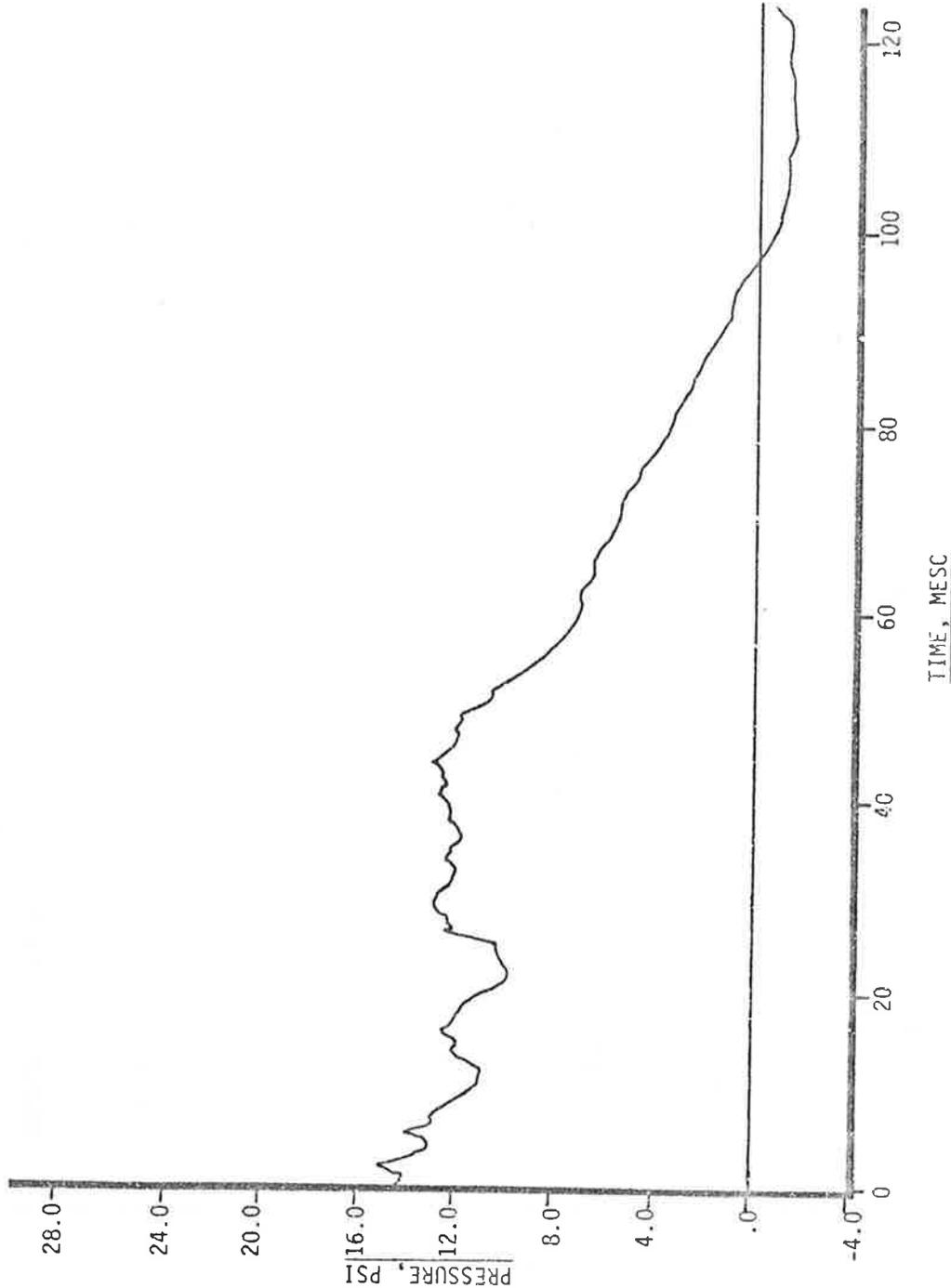
Fig. 19. Average Peak Overpressure vs Time for Five Strand Solid Wall Loading Study Tests 10-16-72-01, 10-17-72-01, and 02; Gauges B-12, B-13, B-14, and B-15.
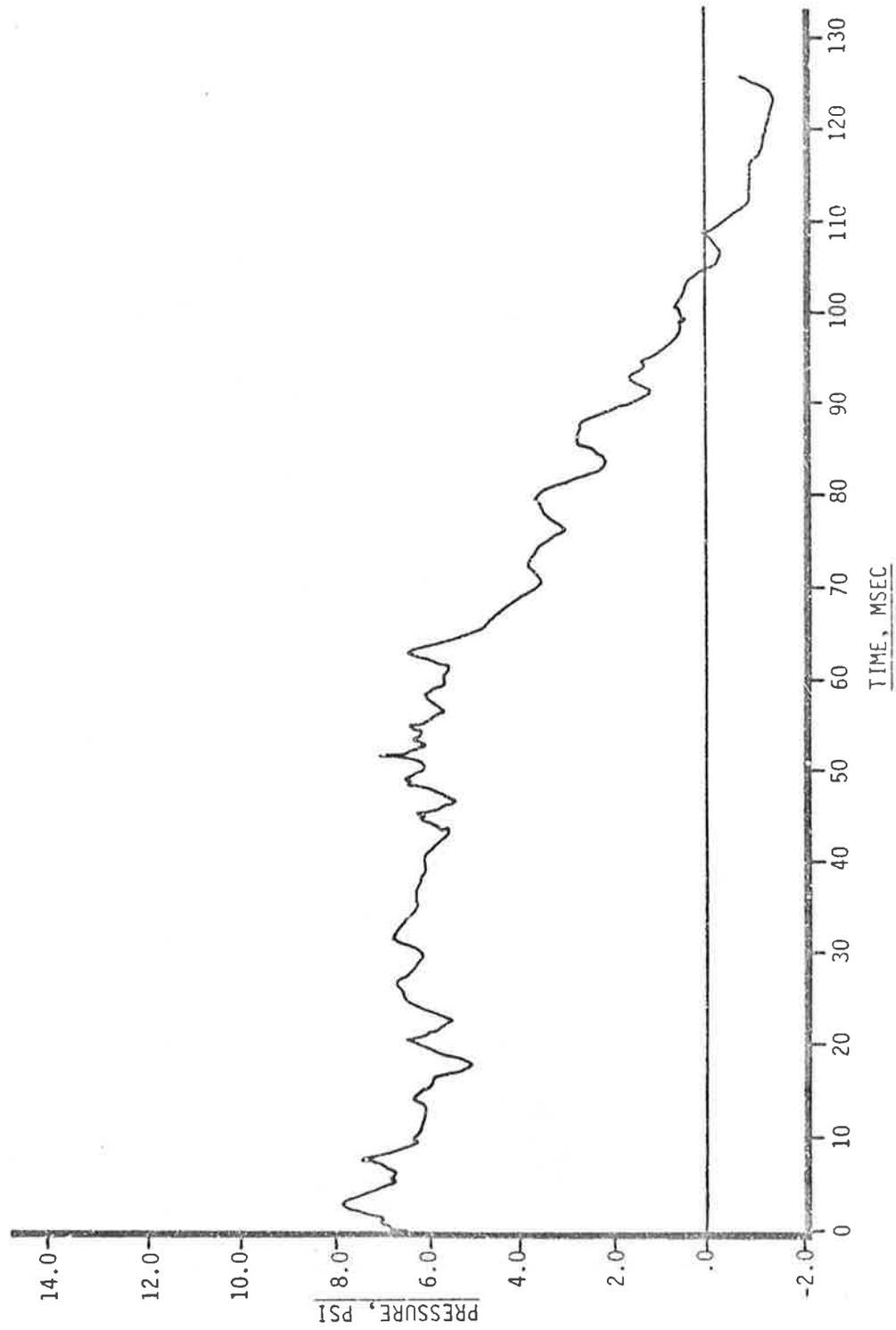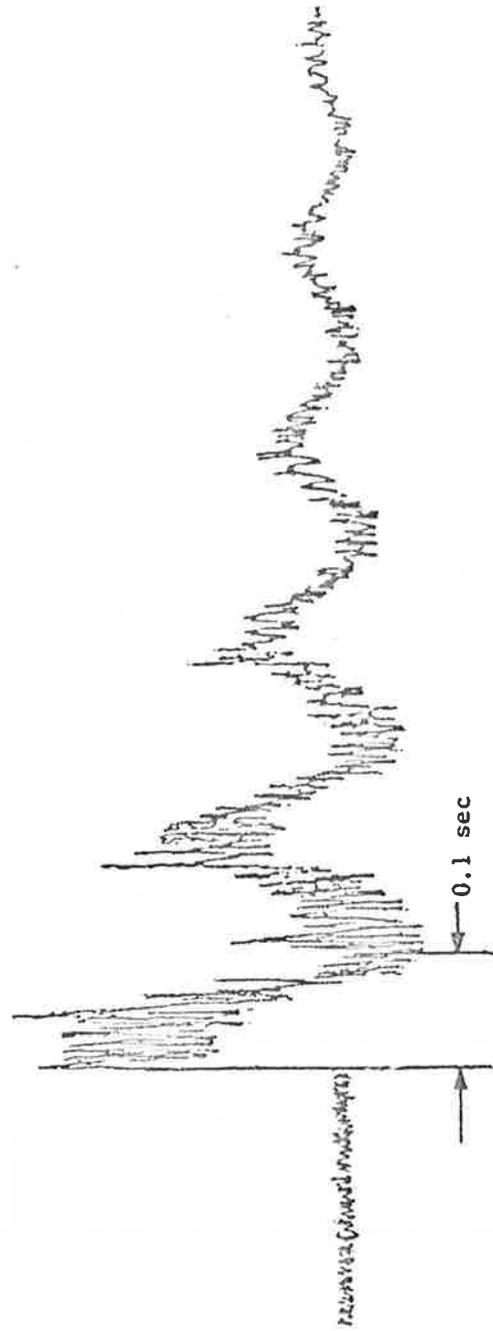
Fig. 20. Shock Tunnel Pressure Gauge Traces. Gauges Mounted in Nonfailing Wall (Peak reflected overpressure, first peak 5 psi).

0.1 sec

Non-failing wall

B15   B14   B13   B-12

↑

Blast
Wave

EAST   WEST
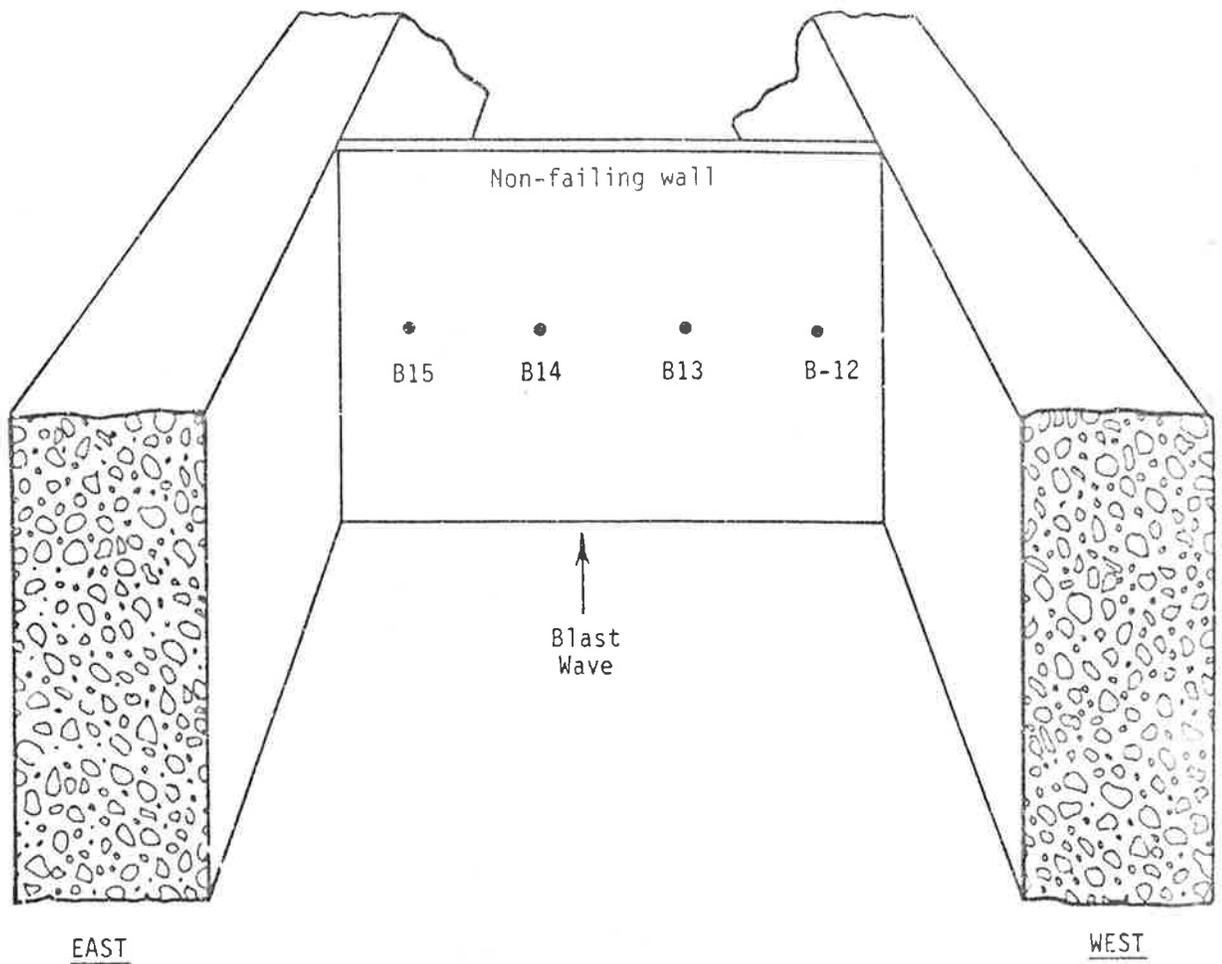
NONFAILING WALL GAUGES

GAUGE	DISTANCE FROM FLOOR	DISTANCE FROM WEST WALL OF TUNNEL
B-12	51"	$14-\frac{1}{4}$"
B-13	51"	47"
B-14	51"	$95-\frac{1}{4}$"
B-15	51"	$127-\frac{1}{2}$"

Fig. 21. Gauge Locations for Closed Tunnel Tests.

32

Section 3

SHOCK TUNNEL CAPABILITIES AND APPLICATIONS

CAPABILITIES

The shock tunnel capability of primary interest can be simply stated:

It provided controlled significant strength shock
wave loadings over a large rectangular cross
sectional area ($8\frac{1}{2}$ x 12 ft) and these loadings
simulated quite closely those from megaton
nuclear weapons for approximately 50-100 msec
of time.

The shock waves generated had total pulse durations varying from 90 to 110 msec with an initial approximately flat topped section of 50 to 80 msec. Peak incident overpressures up to 11 psi were used for open tunnel configurations and up to 8 psi for closed tunnel configurations. The latter provided peak reflected overpressures of 20 psi.

As would be expected because of the nature of Primacord driven shock tubes and the need to have an area expansion between the compression and expansion chambers in order to fit the shock tunnel into the existing tunnel complex, the shock waves had some variations from a classical shock tube wave. These variations included:

1. A sag in the tail of the flat topped section of the wave of less than 20% of the flat topped value.
2. A 2 msec period high frequency oscillation of the pulse of about 10% to 15% of the average value.
3. A shot to shot standard deviation in overpressure of 10% using the same lot of Primacord.
4. A cross sectional nonuniformity in pressure of about 10%.

The shot to shot variability was not of much concern since the shock over-pressures were measured on each test. The high frequency oscillations were

33

also generally not serious since their period was very short compared to the duration of the loading pulses and to the natural period of response of the structural elements of concern. Taking all factors into account, it was determined that the variations between shock tunnel blast waves and classical shock tube waves were unimportant.

APPLICABILITY OF THE SHOCK TUNNEL

The shock tunnel was applicable for a wide variety of blast loadings and response studies. These are summarized below.

Full-Scale Simulation Tests

The flat-topped portion of the shock wave closely approximated the initial portion of the blast wave from a megaton-range weapon. Thus a close simulation of actual field loading and response conditions was achieved in the shock tunnel for the following two general classes of target and loading conditions:

1. Targets whose natural periods are such that the times to maximum deflection (including failure) are less than the duration of the flat-topped portion of the wave.

2. Targets whose effective loading duration in a nuclear blast environment would be limited by the clearing times of the reflected pressure wave rather than by the actual free-field positive-phase duration. Examples of such targets could be structural elements on the front faces of structures. Typical front-face clearing times for structures with a minimum dimension (height or half-width) of 30 ft would be about 65 msec.

It should be noted that wall panels are one of the most important classes of targets which fit within both of these conditions.

For targets and loading conditions which did not satisfy either of the above two conditions, the use of the shock tunnel as a direct full-scale simulant was somewhat limited, since the maximum durations were less than those from a 1-kt weapon.

34

Scale-Model Tests

The general concepts discussed for the full-scale simulation tests also apply for scale-model tests; however, the pulse duration limitations were of even less concern. The natural period of scale-model objects and, thus the time to maximum deflection, is significantly shorter so that even a larger number of target-loading conditions were satisfied by one of the two criteria discussed earlier. Even when these criteria were not satisfied, the total pulse duration corresponded to that from a much larger weapon.

Response-Mechanism Tests

The basic purpose of this type of testing is to improve our understanding of the response mechanisms of various objects to the type of dynamic loading produced by blast waves. It was not necessary to be as specific about the loading requirements for this type of testing, since if the response mechanisms of a given element or system can be understood, for a given loading, then this understanding can be extended to the wider range of more complex loadings of a nuclear weapon environment. It is clear, however, that qualitatively, there were certain test capabilities which were very desirable.

One of the most important of these was the ability to handle full-scale, or at least large-scale, test objects. The response of most objects to dynamic loading is quite complicated, and there is always some uncertainty in working with a scale model as to whether the mode of response has been properly scaled; in fact, it almost requires knowledge of the behavior being investigated to be sure that such is the case. The degree of uncertainty, however, decreases the closer the model appr   es the full scale. The shock tunnel having such a large rectangular cross-sectional area well satisfied this requirement. Another capability is to have complete destruction of test samples without damage to the test facility.

Test Object Size Limitation

For any type of testing in the shock tunnel, one restriction, of course,

35

was that objects fit within the test section of the tunnel ($8\frac{1}{2}$ x 12 ft in cross section) and that by their presence they did not significantly disturb the blast wave. The size of the objects that could have been tested without disturbance depended on the method of mounting and exposing the objects. In the face-on orientation, the test panels were essentially the size of the tunnel cross section, since the entire section has to be blocked off in any case.

The biggest size limitation was on objects which it was desired to subject to all-around loading. Ideally, for this mode of loading, the object's cross-sectional area presented to the flow should be small compared to the total cross section. However, it has been shown that test objects having a cross-sectional area as large as 20-25% of the tube cross section do not create very much of a disturbance (Ref. 5). With this criterion the shock tunnel was capable of handling test objects having as much as 20 to 25 sq ft of cross section for all-around loading.

Cost

Probably one of the most important advantages of the shock tunnel was its capability of failure testing large, full-size test specimens at a minimum cost. Per test costs for such tests including as many as 12 channels of data, data reduction and analysis, theoretical and structural analysis, and reporting ranged from $1,000 to $2,000 during the seven years of operation.

36

Section 4

REVIEW OF OTHER SHOCK TUNNEL TEST PROGRAMS

As noted earlier, the prime motivation for development of the shock tunnel
was for the purpose of studying the loading and response, including debris pro-
duction, of wall panels. However, as discussed in Section 2 of this volume
the facility was useful for a wide range of applications and during the period
when it was operating a number of other blast related test programs were con-
ducted. These studies are listed below and in the following a brief summary
is given of the scope of each program including objectives, nature of tests
conducted, types of data obtained, and where feasible, significant results
and conclusions.

- o Air Blast Tests of OCD Ventilating Equipment
- o Air Blast Tests of OCD Shelter Supplies
- o Object Translation Experiments
- o Shock Tunnel Studies of Flow Fields in Enclosed Spaces
- o Effects of Air Blast on Urban Fires
- o The Ignition Hazard to Urban Interiors During Nuclear Attack
  Due to Burning Curtain Fragments Transported by Blast
- o Debris Generation Tests of Simply Supported Timber Stud Walls
- o Debris from Trees Subject to Blast
- o Shock Tunnel Tests of Aluminum Hull Panels
- o Shock Tunnel Ship Model Tests
- o Blast Loadings of Radomes

AIR BLAST TESTS OF OCD VENTILATING EQUIPMENT (Ref. 6, Appendix B)

This was a limited scope test series to investigate the effect of air blast
on Office of Civil Defense shelter ventilating equipment. The equipment tested
consisted of the Kearny Ventilator, A-Frame Ventilator, exhaust duct, and bicycle

ventilator. For this test series, two nonfailing walls were installed in the test section of the shock tunnel. This arrangement created a room 12 ft wide, 8½ ft high, and 15 ft deep. Sections of each nonfailing wall were removed to create doorways. One test was conducted for each item of equipment with a peak incident overpressure of ≃ 4 psi.

In the tests, all of the OCD shelter ventilation equipment was damaged beyond repair. In addition, a large number of potentially dangerous missiles were produced by the Kearny ventilator and the A-frame ventilator, and significant velocities were achieved by the doorway ventilator and the bicycle.

AIR BLAST TESTS OF OCD SHELTER SUPPLIES (Ref. 7)

This was a more extensive series of tests of OCD shelter supplies which included water and biscuit containers, radiation and sanitation kits, and ventilators both packaged and deployed. Again, two nonfailing walls were installed in the shock tunnel to create a room, the front wall of which had a doorway opening on one side, and the back wall of which was either made solid, to create dead-end conditions, or incorporated another doorway opening, to allow flow-through conditions in the room. Four tests were conducted, all at incident pressures of about 5 psi, with the supplies placed in various locations in the room.

As in the previous series, the deployed Kearny pump was virtually destroyed and served as a source of dangerous missiles. The pedal ventilator survived in "protected" location in the room. Most other supplies survived the tests, though some were moved and toppled when subject to high velocity flows.

The tests led to recommendations for re-design of the Kearny pump, and recommendations for placement of other supplies in shelters.

38

OBJECT TRANSLATION EXPERIMENTS (Ref. 3)

This was a test program conducted as part of an overall study for DCPA to analyze the effect of shelter opening on blast protection. Its basic purpose was to verify calculated values of the flow process and of the translation of sheltered objects (such as people) and to determine if the inclusion of sheltered objects significantly affected the flow process and thus the potential for translation of sheltered objects.

The tests were conducted using a room geometry with the front wall having a door and the rear wall solid. In some tests blocks representing shelterees were installed in the room with various densities. Measurements were made of the incident overpressures and of the pressures at various points on the walls of the room. High-speed photography of table-tennis balls was used for the flow evaluation.

The experimental results are presented in terms of pressure-time profiles at the various measuring positions, positions and velocities of the table-tennis balls at selected times, and the motions and posttest positions of the blocks. These results are discussed in light of existing flow theory and theoretically calculated values. It is shown that the calculated pressure-time profiles agree well with the measured ones and that the presence of the blocks does not alter significantly the pressure time profiles. It is also shown, however, that a high density of objects within the shelter can significantly disturb the flow field.

SHOCK TUNNEL STUDIES OF FLOW FIELDS IN ENCLOSED SPACES (Ref. 8)

This was a test program conducted in support of an overall study for DCPA to investigate the effects of air blast on urban fire response. The principal objectives were to gain insight into (1) flow fields generated in enclosed spaces by external blast loading and (2) the translational responses of representative room contents of urban structures.

A series of six tests was conducted with incident overpressures in the range of 3 to 4 psi. One test was conducted with the tunnel unobstructed, three with a single non-failing wall with a door (simulating a very long room), and two with a second non-failing wall having no openings located 10 ft downstream from the first wall (small room). Measurements made on the tests included wall overpressures, high-speed photography of the motions of the table-tennis balls and typical room contents, and posttest still photographs of the locations of the room contents.

The results for the simulated room tests are presented in the form of plots of positions of the table-tennis balls at various time increments up to 100 msec and in descriptions of the motions of the room contents. Some problems were encountered in photographing late time phenomena because of obscuration by smoke from the detonation of the Primacord.

EFFECTS OF AIR BLAST ON URBAN FIRES (Ref. 9)

This was a test program conducted as part of an overall study for DCPA to investigate the effects of air blast on urban fires. The objective was to determine the nature and magnitude of the effects of blast-fire interactions by experimentally exposing typical urban fuel arrangements to fire and then exposing the burning fuels to air blast. The tests were conducted using full-scale test rooms having a window in the wall facing the blast. Room furnishings simulated a typical living room, bedroom, and office. Incident over-pressures in the range from 1 to 5 psi were used. The fire-blast interactions were documented by conventional and high-speed motion picture photography and by post test photography and recorded observation.

It was found that the threshhold values of incident blast overpressure necessary to extinguish all flames in the test rooms occurred in the range between 1 psi and 2.5 psi. The debris of interior fuels that was capable of supporting smouldering combustion continued to smoulder, in most cases, after extinguishment of flame, and frequently rekindled into flaming combustion.

40

In Ref. 10, a limited series of somewhat similar tests were carried out with incident overpressures from 5 to 9 psi. In this case an open tunnel configuration was used, i.e., no rooms. The results were essentially the same as for the above study.

THE IGNITION HAZARD TO URBAN INTERIORS DURING NUCLEAR ATTACK DUE TO BURNING CURTAIN FRAGMENTS TRANSPORTED BY BLAST (Ref. 11)

This was a test program for DCPA conducted to investigate the propensity of burning curtains, carried into typical urban interiors by blast waves, to cause ignitions within the interiors capable of leading to flash-over.

The tests were conducted using a full-scale test room having a window in the wall facing the blast. Three different weights of curtain material, having different burning times, were used in the experiments. Curtains were ignited by propane gas jet manifolds arranged on the upstream side of the curtains with the jets directed toward the curtains. All tests were conducted at a nominal incident blast overpressure of 1 psi since it had been found that incident overpressures much higher than this invariably extinguish fire in burning curtains.

Seventeen tests were conducted. Severe hazard of room ignition resulted from 7 of the 17 experiments, while a small hazard of room ignition occurred in 4 cases. Tests resulting in severe hazard of room ignition corresponded closely to cases in which the blast wave arrived at an optimum stage in combustion of the curtains (when they were fully aflame but only partially consumed). In cases in which curtains were not fully ignited at blast arrival, the curtain fragments tended to smoulder, and to induce smouldering fires in the test room. Where curtains had passed the optimum stage of flaming combustion, charred remnants distributed throughout the test room lacked sufficient remaining fuel value to serve as efficient secondary ignition sources.

41

The hazard of secondary ignitions due to blast-transported burning curtain fragments appears to depend critically, in each case, on the burning time of the curtains relative to the time to blast arrival.

DEBRIS GENERATION TESTS OF SIMPLY SUPPORTED TIMBER STUD WALLS (Ref. 12)

This was a test program of limited scope designed to obtain information on the type and quantity of debris which would be generated from the breakup of a timber stud wall under blast loading. The results of these tests were required for the planning of the Bell Telephone Laboratories building fragmentation tests in Operation Prairie Flat at the Defense Research Establishment, Suffield, in August 1968.

Two tests were conducted at an incident overpressure of approximately 6 psi. Data obtained from these tests consisted of high-speed motion picture films, debris surveys, pre and posttest still photographs, and overpressure data. Cumulative debris distribution curves (frequency vs. weight) are given for each test. These show a normal distribution and good agreement between the two tests.

DEBRIS FROM TREES SUBJECTED TO BLAST (Ref. 13)

This was a test program conducted as part of an overall study for Bell Telephone Laboratories to examine the characteristics of debris from trees subjected to air blast. It consisted of 5 tests in which approximately 8-ft segments sawn from 30-40 ft high trees were exposed to incident overpressures of 10-11 psi. Both broad leaf and conifers were tested. Test data collected for each test included the incident overpressure, total load on the tree segment, high speed photographs of the tree motions, and a posttest debris survey.

The results are given in terms of a time sequenced description of the response of the tree segment, a description of the resultant debris including its mass distribution, and the measured loads.

42

SHOCK TUNNEL TESTS OF ALUMINUM HULL PANELS (Ref. 14)

This was a test program of the response of aluminum hull panels to blast loading conducted for the Naval Ship Research and Development Center, Bethesda, Maryland. Each of three types of panels was statically loaded, tested for natural period, then subjected to a blast wave with an incident overpressure of about 3 psi followed by one with an incident overpressure of about 5 psi. The panels were 7-ft, 6-in. high, 11-ft, 6-in. wide, and each was instrumented with eight strain gauges and a velocity sensor. Pressure transducers were mounted in the sidewall of the tunnel near each panel and, in two cases, on the panels themselves. Photographic coverage included two high-speed cameras and pre- and post-blast still photography.

None of the panels showed significant distress after the 3 psi test, but the Type I panel was virtually destroyed after the 5 psi test. Panel Types II and III fared better under the high pressure loading but both showed a permanent deflection of about 2 in. near the center of the panel.

SHOCK TUNNEL SHIP MODEL TESTS (Ref. 15)

This was a test program of the response of a model Surface Effects Ship (SES) to blast loading conducted for the Naval Ship Research And Development Center (NSRDC), Bethesda, Maryland. Its purpose was to acquire experimental data to compare with NSRDC predictions of ship motions due to blast waves with incident pressures of 1 to 2 psi. For the tests a pool, 15 in. deep, 25 ft long, and 12 ft wide was built into the shock tunnel. It was equipped with ramps at the leading and trailing edges to minimize turbulence from shock wave passage.

The model, 7 ft long, 3 ft wide, and 1 ft deep, was a 1/33 scale of a proposed 200-ton SES. It included an electric fan so it could hover at the surface of the water during the blast tests. It was instrumented with pressure transducers on the exterior surfaces, accelerometers in the structure and a roll, pitch, yaw meter. Pressure transducers were located in the side wall of

43

the tunnel near the model. Photographic coverage included two high-speed
cameras and pre- and post-blast still photography.

BLAST LOADINGS OF RADOMES

This was a test program of the response of a radome prototype to blast
loading conducted for ANCOM (the radome manufacturer).

Two 4.5-ft diameter prototypes were tested. Each was equipped with a
pressure transducer to monitor blast loading, and other pressure transducers
were mounted in the side walls of the tunnel. Photographic coverage included
two high-speed cameras and pre- and post-blast still photography.

The prototypes were exposed to blast waves with incident pressures of
1.5 and 4 psi. With the higher pressure, the first of the prototypes was
virtually destroyed. The simulated reflector motor came out of its mount,
and the face of the radome delaminated. The second prototype was a strength-
ened version of the first. The simulated motor was torn loose under the high
pressure loading, but the radome itself did not delaminate.

References

1. Willoughby, A.B., C. Wilton, B. Gabrielsen, "Development and Evaluation of a Shock Tunnel Facility for Conducting Full-Scale Tests of Loading, Response, and Debris Characteristics of Structural Elements", URS 680-2, URS Corporation, Burlingame, CA, December 1967.

2. Willoughby, A.B., C. Wilton, B.L. Gabrielsen, "A Study of Loading, Structural Response, and Debris Generation", URS 680-5, URS Research Company, Burlingame, CA, December 1968.

3. Melicahr, Jospeh F., "Analysis of the Effect of Shelter Openings on Blast Protection", URS 773-6, URS Research Company, San Mateo, CA, September 1970.

4. Gabrielsen, Bernard, C. Wilton, "Shock Tunnel Tests of Arched Wall Panels", URS 7030-19, URS Research Company, San Mateo, CA, prepared by Scientific Service, Inc., Redwood City, CA, December 1974.

5. C. Wilton, Gabrielsen, Bernard L., Willoughby, A.B., "Study of the Loading, Structural Response, and Debris Characteristics of Wall Panels, URS 680-3, URS Systems Corporation, Burlingame, CA, August 1968.

6. C. Wilton, Gabrielsen, B., Edmunds, J., Bechtel, S., "Loading and Structural Response of Wall Panels", URS 709-4, URS Research Company, Burlingame, CA, November 1969.

7. A.L. Kapil, "Blast Vulnerability of Shelter Supplies", GARD Final Report 1518, March 1972.

8. S.B. Martin, Ramstad, R.W., Goodale, T., Start, C.A., "Effects of Air Blast on Urban Fire Response", URS 705-5, URS Research Company, Burlingame, CA, May 1969.

9. Thomas Goodale, "Effects of Air Blast on Urban Fires, URS 7009-4, URS Research Company, San Mateo, CA, December 1970.

10. Thomas Goodale, "An Attempt to Explore the Effect of High Blast Overpressure on the Persistence of Smouldering Combustion in Debris", URS 7030-6, URS Research Company, San Mateo, CA, December 1971.

11. Thomas Goodale, "The Ignition Hazard to Urban Interiors During Nuclear Attack due to Burning Curtain Fragments Transported by Blast", URS 7030-5, URS Research Company, San Mateo, CA, December 1971.

12. C. Wilton, Zaccor, J., "Debris Generation Tests of Simply Supported Walls", URS 694-1, URS Systems Corporation, Burlingame, CA, April 1968.

References (cont.)

13. P.J. Morris, Wilton, C., "Debris From Trees Subjected to Blast", URS 794-1, URS Research Company, San Mateo, CA May 1970.

14. J. Boyes, Gabrielsen, B.L., Kaplan, K., "Shock Tunnel Tests of Aluminum Hull Panels", URS 7230, URS Research Company, San Mateo, CA, June 1973.

15. "Data Report Surface Effects Ship", URS 7510, URS Research Company, San Mateo, CA, prepared for Naval Research and Development Center, April 1975.

THE SHOCK TUNNEL:
HISTORY AND RESULTS:
Volume II
LOADING STUDIES

ABSTRACT

This is Volume 2 of a five volume report which summarizes the results of a program conducted by the Defense Civil Preparedness Agency to determine blast resistance of wall panels typically found in existing structures. The objective of this program was to determine the blast sheltering capability of structures in the National Fallout Shelter Survey inventory and to obtain information which could be used to upgrade these shelters.

This volume presents the results obtained from the experimental program conducted in the shock tunnel to determine the loadings which are received by wall panels mounted in the test section.

Volume 1 of this report describes the shock tunnel facility used for the experimental testing of full-scale wall panels. Included is a summary of the capabilities of the shock tunnel for dynamic loading and response studies and brief summaries of various experimental programs conducted in the shock tunnel which were not related to the wall panel test program.

Volume 3 of this report is concerned with the dynamic response and failure of full-scale wall panels. Included are the development of theories of wall panel response and the results obtained from the testing of full-scale wall panels in the shock tunnel.

Volume 4 of this report describes the static test program conducted to determine the physical properties of wall panels including estimates of their statistical distribution, and to assist in the development of failure theories and test predictions for wall panels.

Volume 5 summarizes the predicted failure pressures for wall panels based on the theoretical and experimental results covered in Vol. 3 and the static test data in Vol. 4.

Table of Contents

List of Figures

List of Figures (contd)

iv

List of Figures (contd)

List of Figures (contd)

Section 1
INTRODUCTION

This volume presents the results obtained from a series of tests conducted in the shock tunnel to determine the loadings which would be received by wall panels when they are mounted in the test facility. This information was needed for the correct design and evaluation of the wall panel test program described in Volume 3.

The general development, operation, and evaluation of the shock tunnel are described in Volume 1 of this series. In brief, the tunnel, shown in a cutaway drawing in Fig. 1-1, consisted of a 63-ft long, 8-ft diameter steel cylinder, closed on one end (the "compression chamber"); an 8-ft long transition section; and a 92-ft long rectangular tunnel section 8½ ft high and 12 ft wide (the "expansion chamber").

The tunnel was operated as a shock tube by means of the volume detonation technique with Primacord as the explosive material. In this mode of operation, Primacord is distributed symmetrically throughout a section of the compression chamber portion of the tunnel. On detonation of the Primacord (which proceeds at a rate of about 20,000 ft/sec), a quais-static pressure is built up rapidly throughout the entire compression chamber. The expansion of this high-pressure gas into the remaining part of the tunnel generates the desired shock wave. The strength of the shock wave was varied by varying the numbers of strands of Primacord from one to eight.

Section 2 of this volume briefly summarizes the blast wave characteristics obtained from the basic calibration tests of the shock tunnel without any test walls (open tunnel configuration). These results are presented in detail in Volume 1 and are summarized here for comparison purposes with results obtained from various closed tunnel configurations, i.e., those with walls mounted in the test section.

1

63 FT

8 FT

92 FT

Compression
Chamber

Expansion
Chamber

Test
Wall

Fig. 1-1.   Cutaway View of Shock Tunnel Showing Wall in Place.

2
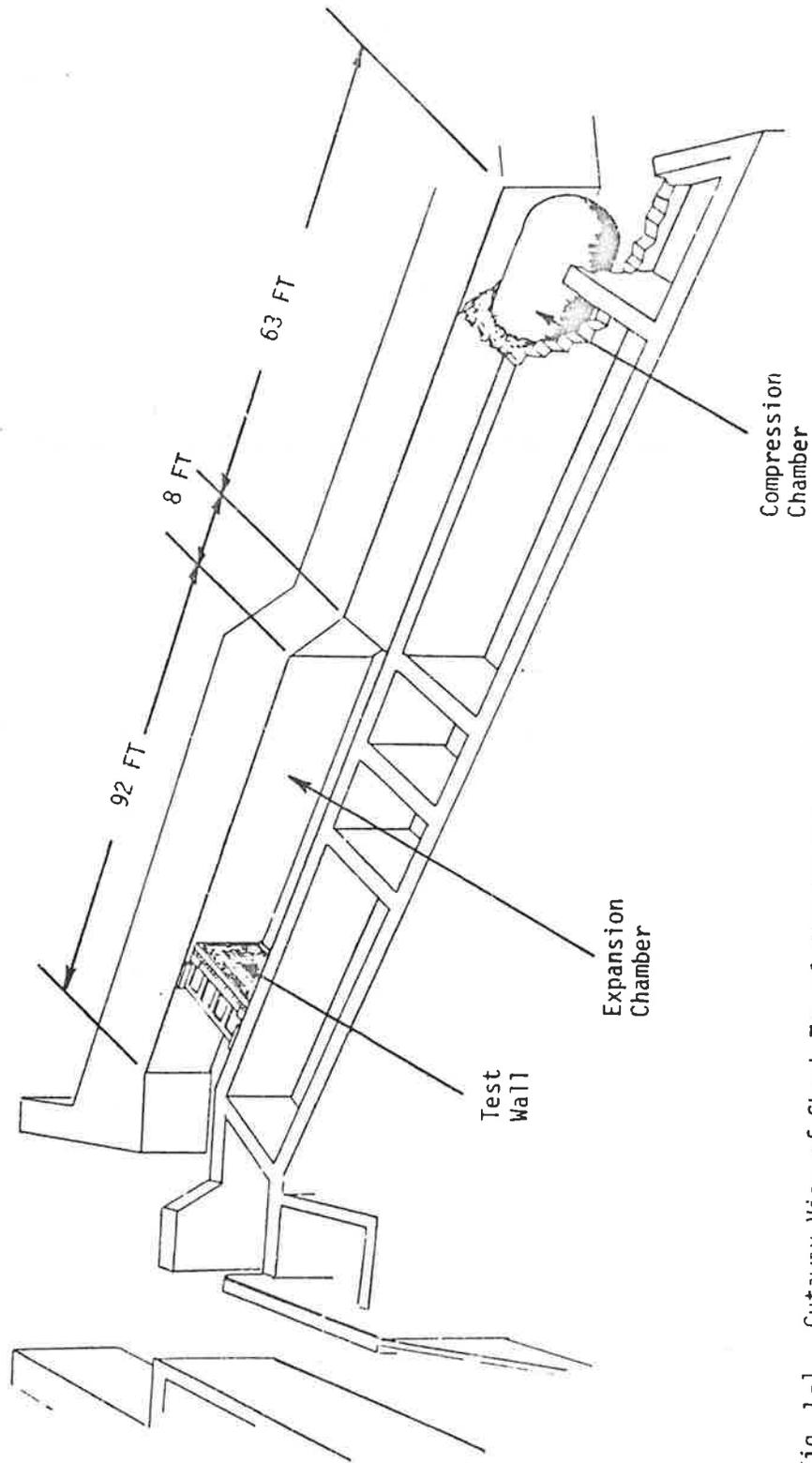
Section 3 of this volume presents the results for the loading on a solid non-failing test wall mounted in the test section of the tunnel.

Sections 4 and 5 cover loadings on non-failing walls with doorways and window openings respectively.

Section 6 covers the loading conditions for a room with a window in the upstream wall (facing the blast) and a solid wall on the downstream side.

Section 7 summarizes the application of the loading study to the overall program.

Section 2
OPEN TUNNEL TESTS

As described in Volume 1, at the time the shock tunnel was constructed and at intervals thereafter, open tunnel tests were conducted to document the type of pulses generated, and to calibrate the facility. Tests were conducted in which the length, number, and location of strands of Primacord were varied.

The standard operating mode used for the wall panel program was 60-ft strands of Primacord uniformly distributed throughout the compression chamber. The calibration tests for this mode showed that the shock waves generated had total pulse durations varying from 90 to 110 msec with an initial approximately flat topped section of 50 to 80 msec.

The incident overpressure in this approximately flat topped section varied with the number of strands used ($\sim$ 1 to 1.2 psi/strand) as shown by the data given in Fig. 2-1.*

As would be expected because of the nature of Primacord driven shock tubes and the need to have an area expansion between the compression and expansion chambers, in order to fit the shock tunnel into the existing tunnel complex, the shock waves had some variations from a classical shock tube wave. These variations included:

1. A sag in the tail of the flat topped section of the wave of less than 20% of the flat topped value.
2. A 2 msec period high frequency oscillation of the pulse of about 10% to 15% of the average value.
3. A shot to shot standard deviation in overpressure of 10% using the same lot of Primacord.
4. A cross sectional nonuniformity in pressure of about 10%.

---

* The differences between the two calibration curves conducted six years apart is attributed to the use of different lots of Primacord.

4
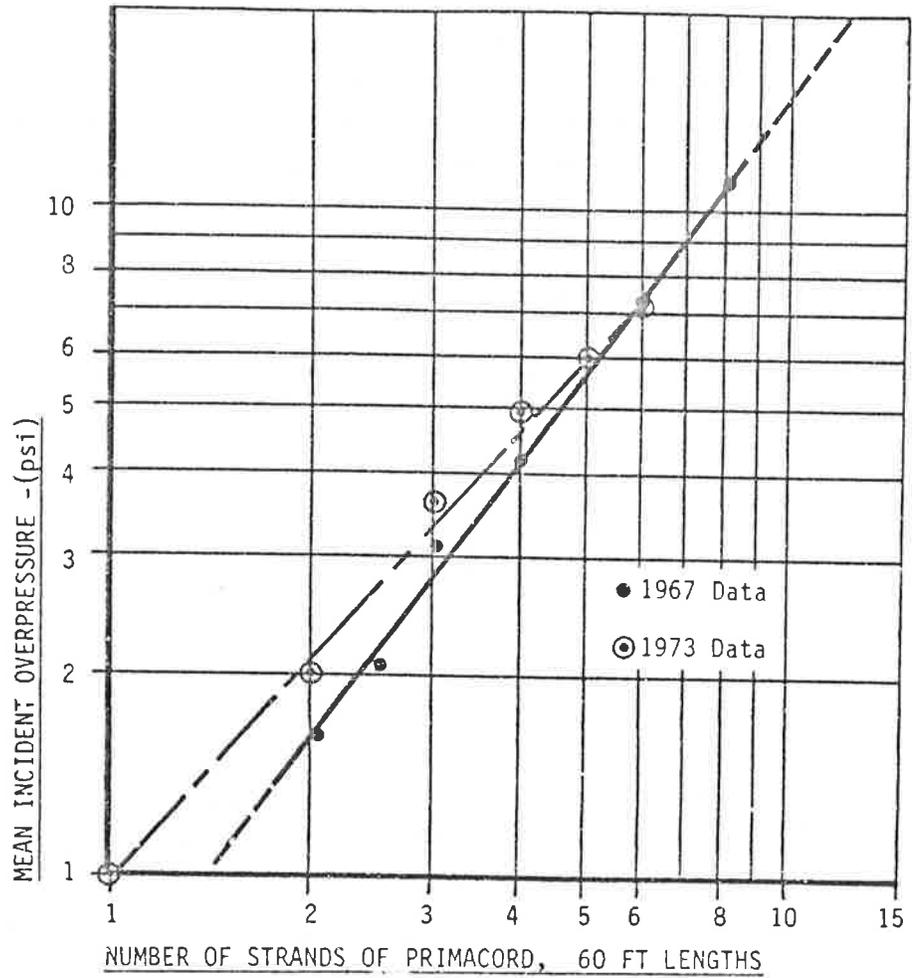
Fig. 2-1. Shock Front Incident Overpressure as a Function of the Number of Parallel Strands of Primacord Detonated Simultaneously in the Compression Chamber. Data from 1967 and 1973.

The shot to shot variability was not of much concern since the shock over-pressures were measured on each test. The high frequency oscillations were also not serious since their period was very short compared to the duration of the loading pulses and to the natural period of response of the structural elements of concern. Typical traces generated by explosions of two, four, and six strands of Primacord, are shown in Fig. 2-2; the location of the gauge stations from which the records were taken (7 & 9) are shown in Fig. 2-3.
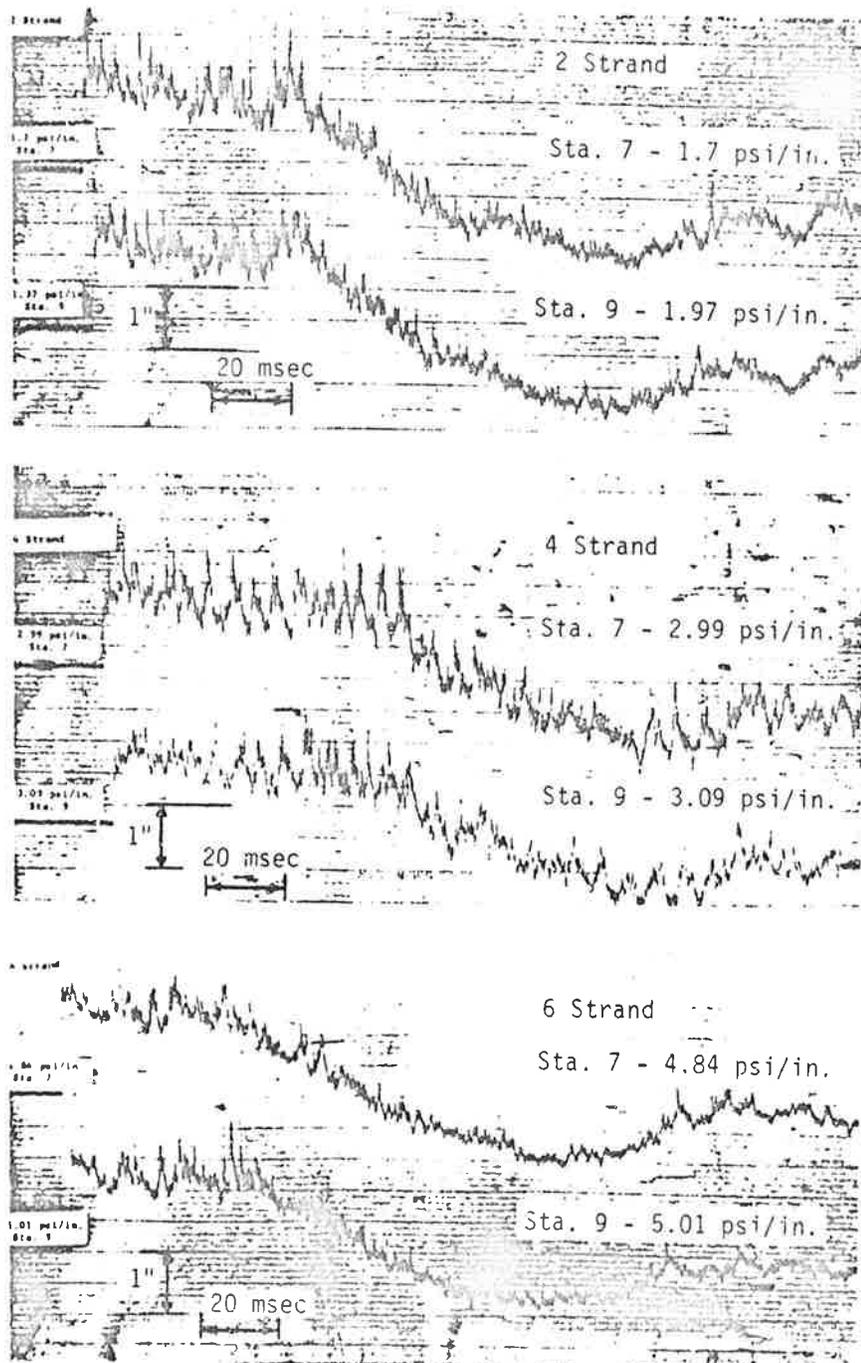
Fig. 2-2. Open Tunnel Pressure vs Time Traces from Testing Using Two, Four, and Six Strands of Primacord. Gauge Locations are shown in Fig. 2-3.

7

N

Nominal Gauge Distances from
Mouth of Compression Tube

STATION	FT
1	49
2	53
3	57
4	61
5	65
6	69
7	73
8	74
9	76
10	81
11	71.5

63'

100'

COMPRESSION TUBE

GAUGE
STATIONS

TEST WALL Location A

CAMERA LOCATION

Location B

CASEMATE

CAMERA LOCATION
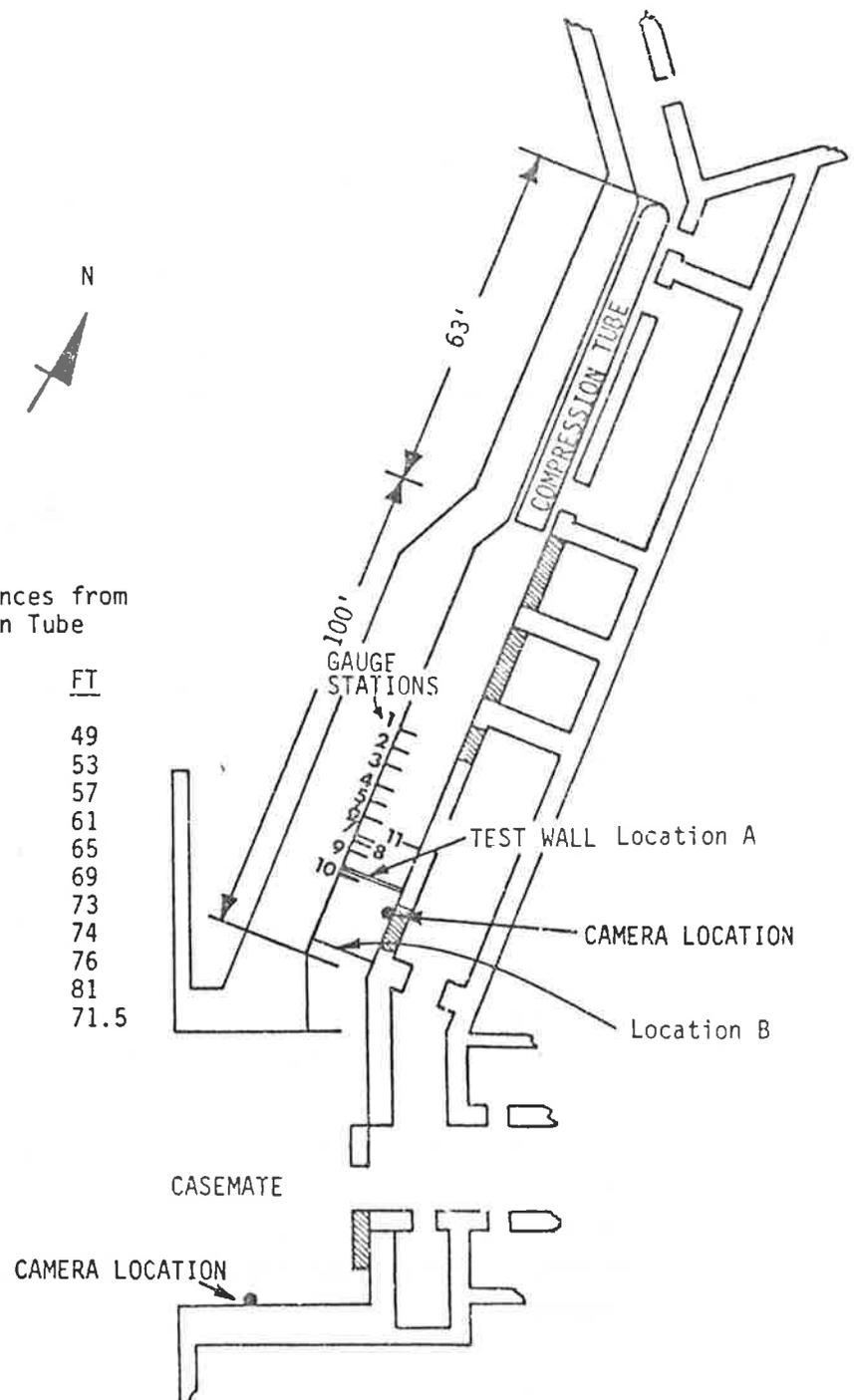
Fig. 2-3. Plan View of Shock Tunnel Facility.

8

Section 3
LOADING ON A NON-FAILING SOLID WALL

The basic purpose of these tests was to document the loadings that would be received by solid test walls completely blocking the test section of the shock tunnel. Theoretically, the loadings on such a wall can be computed from a knowledge of the incident shock wave characteristics and the theory of shock reflection. However, since there are some differences between the shock tunnel, shock waves, and ideal shock waves, it seemed best to experimentally determine the loading values. Furthermore, essentially the same test arrangement could be used for measuring loadings on non solid walls (having doorways or window openings) for which theoretical calculations of loading are very uncertain.

EXPERIMENTAL ARRANGEMENT

The loading tests were conducted using instrumented, non-failing walls. One of the two walls used during the program is shown in Fig. 3-1. It consists of a frame of four vertical and two horizontal steel I beams and 20 removable panels (termed modular panels) nominally 1½ ft high by 3 ft wide which fit between the vertical I beams. Each modular panel is made of 4½ in. thick plywood in a steel frame that can be mounted on either face of the wall with special fastening plates.

The modular panels are interchangeable, and any of them can be removed. Fig. 3-1 shows a configuration in which four panels have been removed to simulate a window opening. In another configuration, all panels between two of the vertical I beams were removed to simulate a wall with a doorway. (The tests with these two geometries are described in Sections 4 and 5.) The second non-failing wall was of similar construction except that the steel-framed, laminated plywood modular panels were replaced with 4 in. x 6 in. timbers.

The basic non-failing wall panel mounting system is shown in Fig. 3-2.

9

Fig. 3-1.   Non-failing Wall.

PLATE GIRDER

"U" MEMBER

LOAD CELL

NON-FAILING PANEL

WALL BLOCK

Fig. 3-2. Cutaway View of Shock Tunnel Showing a Non-failing Wall Panel, Supporting Plate Girders, Wall Blocks, and Load Cells.
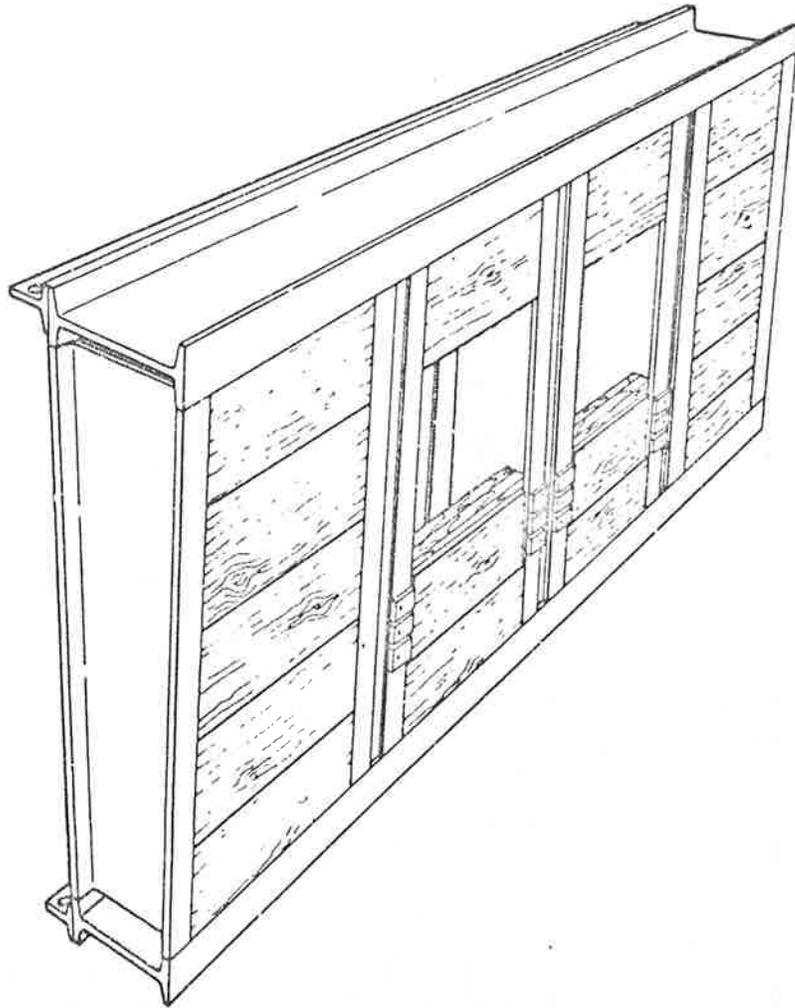
It consists of two massive steel plate girders, each 4½ in. thick, 4 ft deep, and 12 ft wide, weighing about 2600 lb and supported by wall blocks. Two complete sets of wall blocks and girders were fabricated. With one set of blocks mounted at Location A of Fig. 2-3, and the other set at Location B, the equivalent of a room up to 15 ft long could be created in the tunnel by mounting walls on girders at two locations. (Tests with this geometry are described in Section 6.)

The instrumentation used during the loading studies consisted of pressure transducers, mounted both on the removable modular panels of the non-failing walls and in tunnel walls themselves, and load cells between the girders and wall blocks.

The general test configuration and gauge locations employed in these tests are shown in Fig. 3-3. Two separate test series were run with slightly different wall locations. In Series A, the wall was mounted on the upstream edge of the plate girders on the wall blocks furthest from the compression chamber of the tunnel; in Series B, it was mounted on the downstream edge of these girders, about five feet further from the compression chamber. The tabular entries on the figure show the gauge locations for each test series.

12
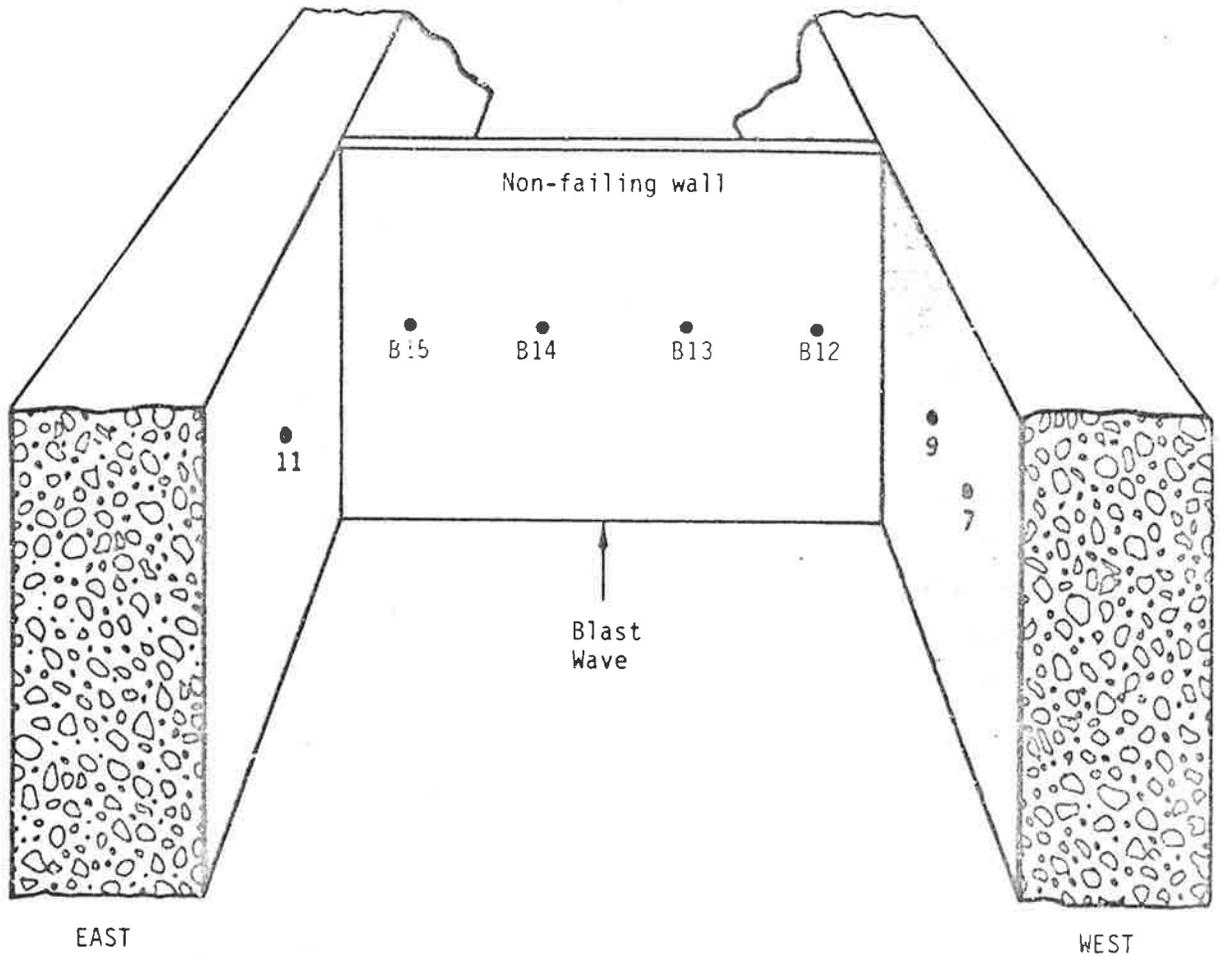
NON-FAILING WALL GAUGES			
GAUGE NO.	DISTANCE FROM FLOOR (in.)	DISTANCE FROM WEST WALL OF TUNNEL (in.)	
		Series A	Series B
B-12	51	14.3	14.3
B-13	51	47.0	47.0
B-14	51	75.3	95.3
B-15	51	132.5	127.5
TUNNEL WALL GAUGES			
GAUGE NO.	DISTANCE FROM FLOOR (in.)	DISTANCE FROM NON-FAILING WALL (in.)	
		Series A	Series B
Westwall-7	45	92.8	156
Westwall-9	45	52.3	116
Eastwall-11	49	110.4	174

Fig. 3-3. Solid Wall Test Configuration.

13

TEST RESULTS

Tests in these geometries were run using one, three, and five strands of Primacord, and typical pressure pulses recorded are shown in Fig. 3-4, from a Series A test using three strands of Primacord. The top two records of the figure are from gauges located in the tunnel side wall (Fig. 3-3) upstream from the non-failing wall. Clearly evident in these records is a period of constant pressure, the generally flat topped region about 14 ms long at Sta 7 and about 8 ms long at Sta 9 immediately behind the shock front of the incident pressure pulse. Thereafter, when the front of the shock wave that reflected upstream from the non-failing wall passed these two gauge stations, it caused a second step rise to a value something over twice the incident pressure step.

The lower three traces in Fig. 3-4 are from gauges located on the "test" wall head on to the blast wave. While the gauges in the side wall first experienced pressure from the incident wave, these gauges experienced the incident and reflected waves simultaneously. Thus, the traces exhibit only a single step, about the magnitude of the two steps of the traces from Sta 7 and Sta 9.* The remainder of the pulses until the time at which pressure decreases to ambient values are generally similar to those of Fig. 2-2.

While there are some differences among the lower three traces, they are generally similar. Analysis of many records indicated that pressure differences across the face of a wall vary no greater than 10%.

Because of this relative uniformity, average pressure on walls was derived from all gauges on the wall. Individual records such as those of Fig. 3-4 were digitized and computer plotted. The results of this process are given in Appendix A (Fig. A-1 through A-5).

---

* Of some interest in Fig. 3-4 is the sharp step on the right-hand side of the lower three traces about 225 ms after initial shock front arrival. This step marks the re-arrival of the pressure pulse which initially reflected (Footnote continued on bottom of page 16.)

14
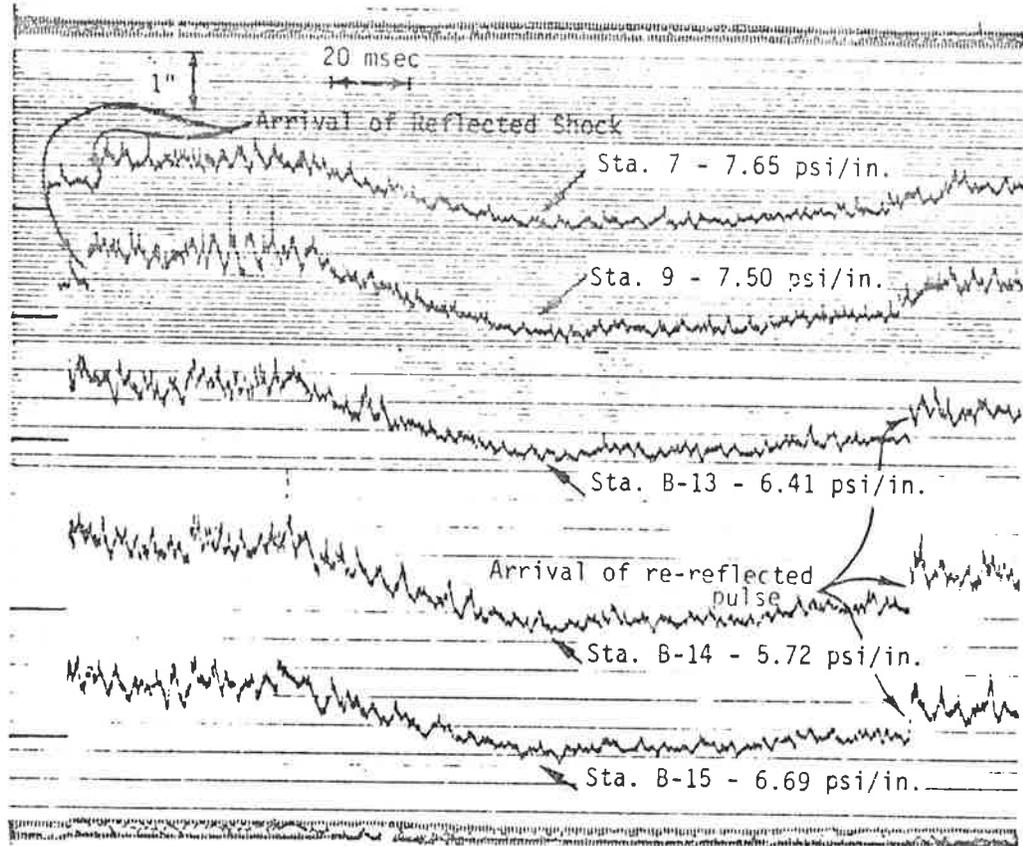
Fig. 3-4.   Solid Wall Pressure vs Time Traces from a Test Using Three Strands
of Primacord.   Sta 7 and 9 are in the Shock Tunnel Side Walls;
Sta B-13, 14, and 15 are on the Non-Failing Wall.   See Fig. 3-3.

Typical averaged traces from three and five strand tests are shown in Fig. 3-5 and for one strand tests, in Fig. 3-6. It can be seen that the wave shapes for the one strand tests are somewhat different than for the other cases. Most importantly the front of the wave does not exhibit a sharp rise -- it takes some 8 msec to reach peak value. This finite rise time has some effects on the response of the test walls as discussed in the next volume.

---

* (continued from page 14) from the non-failing wall, travelled upstream until it reflected frum the closed (rear) end uf the compression chamber, then travelled downstream until it arrived at the wall again. This process of reflecting and re-reflecting continued so that on records with a longer duration six (and more) reflections could be identified.

Fig. 3-5. Average Overpressure vs Time on a Solid Wall from Tests Using Three and Five Strands of Primacord.
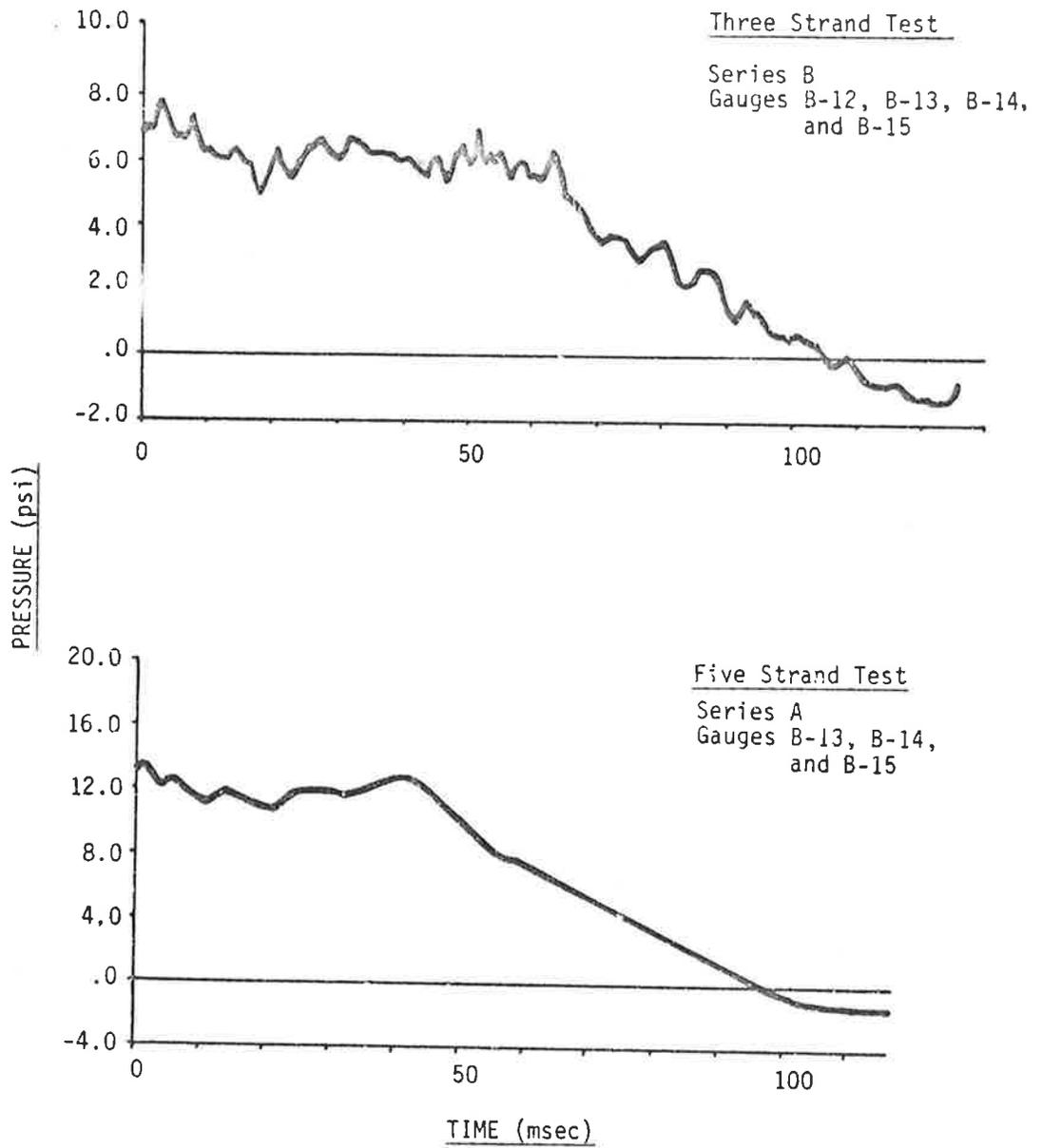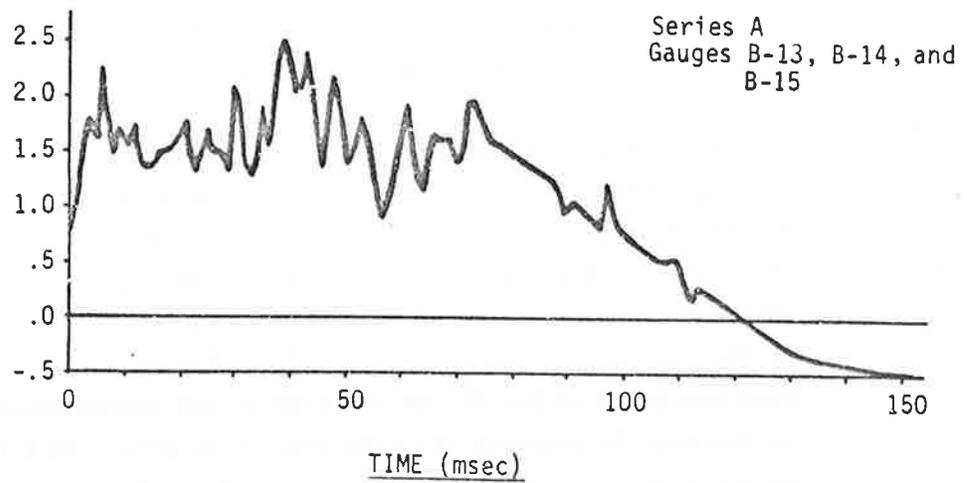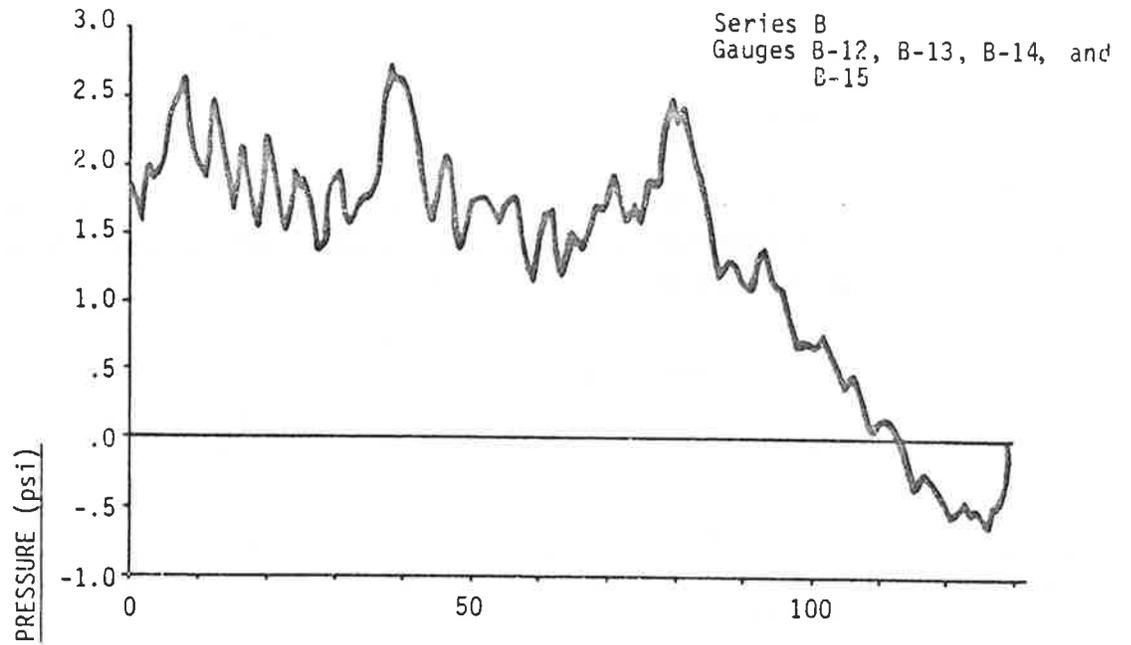
17

Fig. 3-6. Average Overpressure vs Time on a Solid Wall from Tests Using One Strand of Primacord.

18

Section 4
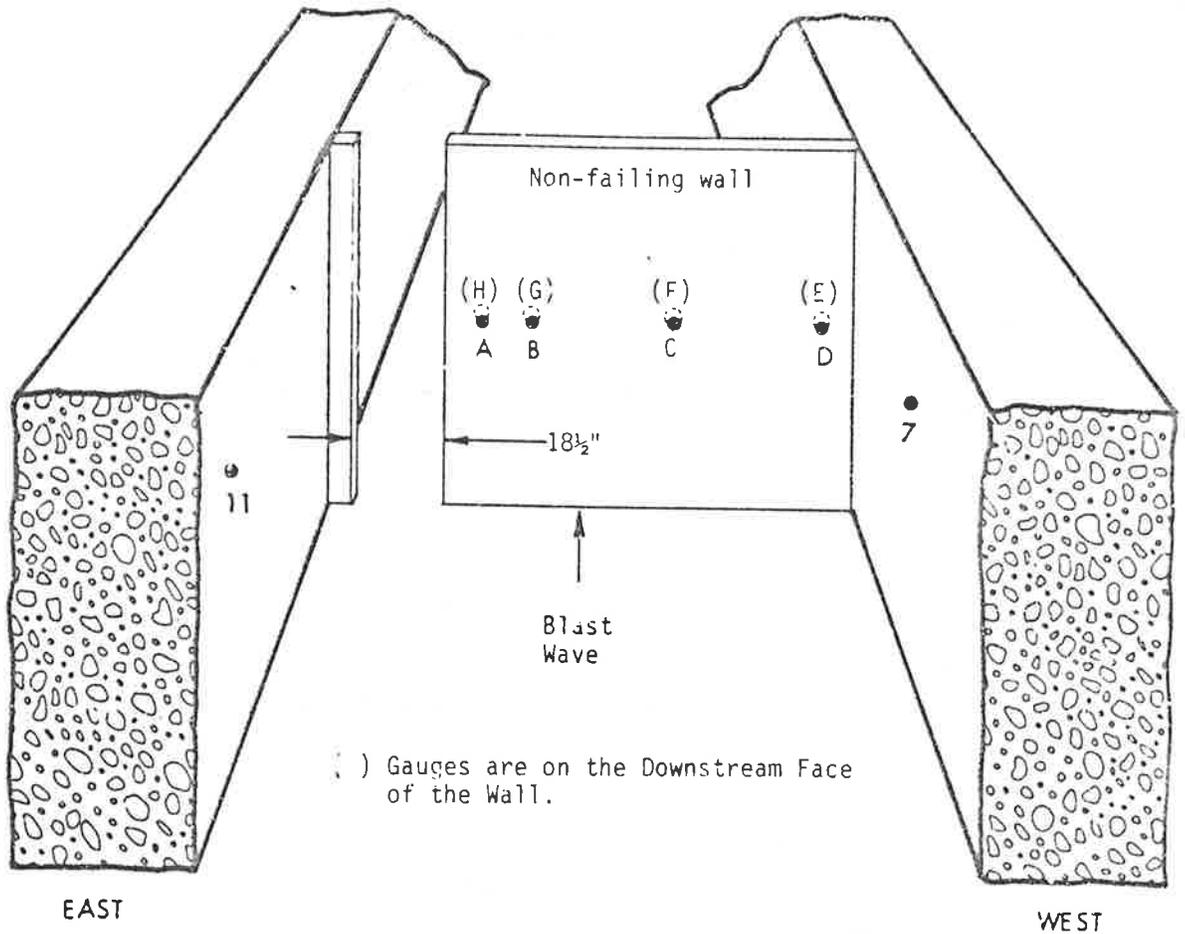## LOADING ON A WALL WITH A DOORWAY

GENERAL

Removing all the modular panels between two adjacent vertical I beams of the non-failing wall created a panel containing an 18½ in. wide doorway which occupied some 17.5% of the total area of the wall.

The open doorway provides a means for pressure to "leak" to the downstream side of such walls, thus reducing the net force tending to make the wall fail. To document the net loading on these walls, it was necessary to make measurements on both wall faces. This was done with paired gauges located near the horizontal centerline of the wall, as shown in Fig. 4-1. As in other loading studies, pressures were also monitored with gauges located in the tunnel side walls.

Tests were made with one, three, and five strands of Primacord, and a typical set of pressure traces at gauge stations identified in Fig. 4-1 are shown in Fig. 4-2 from a test employing three strands of Primacord.

As in Fig. 3-4 (from the solid wall tests), the first two traces are from gauges located in the tunnel side walls, which are closer to the wall than for the solid wall case. The effect of this can be seen immediately by comparing the Station 7 trace of Fig. 3-4 with that of Fig. 4-2. In the former case, incident pressure persisted for about 14 ms before the reflected shock arrived at the station; in the latter case it persisted for only about 3 ms. Note that the gauge of Sta 11, on the side of the tunnel nearest the doorway shows an increase in pressure starting about 6 ms after shock arrival, but because of its proximity to the opening it is not nearly as sharp fronted, nor as high as that from the gauges at Sta 7 in the opposite tunnel wall.

The remainder of the traces are from gauges on both the upstream and

19

Non-failing wall

(H) (G)   (F)   (E)

A B   C   D

←18½"

7

11

Blast
Wave

( ) Gauges are on the Downstream Face
of the Wall.

EAST

WEST

NON-FAILING WALL GAUGES		
GAUGE NO.	DISTANCE FROM FLOOR (in.)	DISTANCE FROM EDGE OF DOOR (in.)
A-H*	51	12
B-G*	51	24
C-F*	51	60
D-E*	51	108
* Gauges E through H are on Back of the Wall		
TUNNEL WALL GAUGES		
GAUGE NO.	DISTANCE FROM FLOOR (in.)	DISTANCE FROM WALL (in.)
Westwall-7	45	21
Eastwall-11	49	38

Fig. 4-1. Wall With a Doorway Test Configuration.

20

20 msec

1"

Sta. 7 - 3.58 psi/in.

Arrival of
Reflected Shock

Sta. 11 - 4.13 psi/in.

Sta. A - 3.05 psi/in.

Possible Vortex Effect

Sta. H - 2.95 psi/in.

Sta. B - 3.91 psi/in.

Sta. G - 2.16 psi/in.

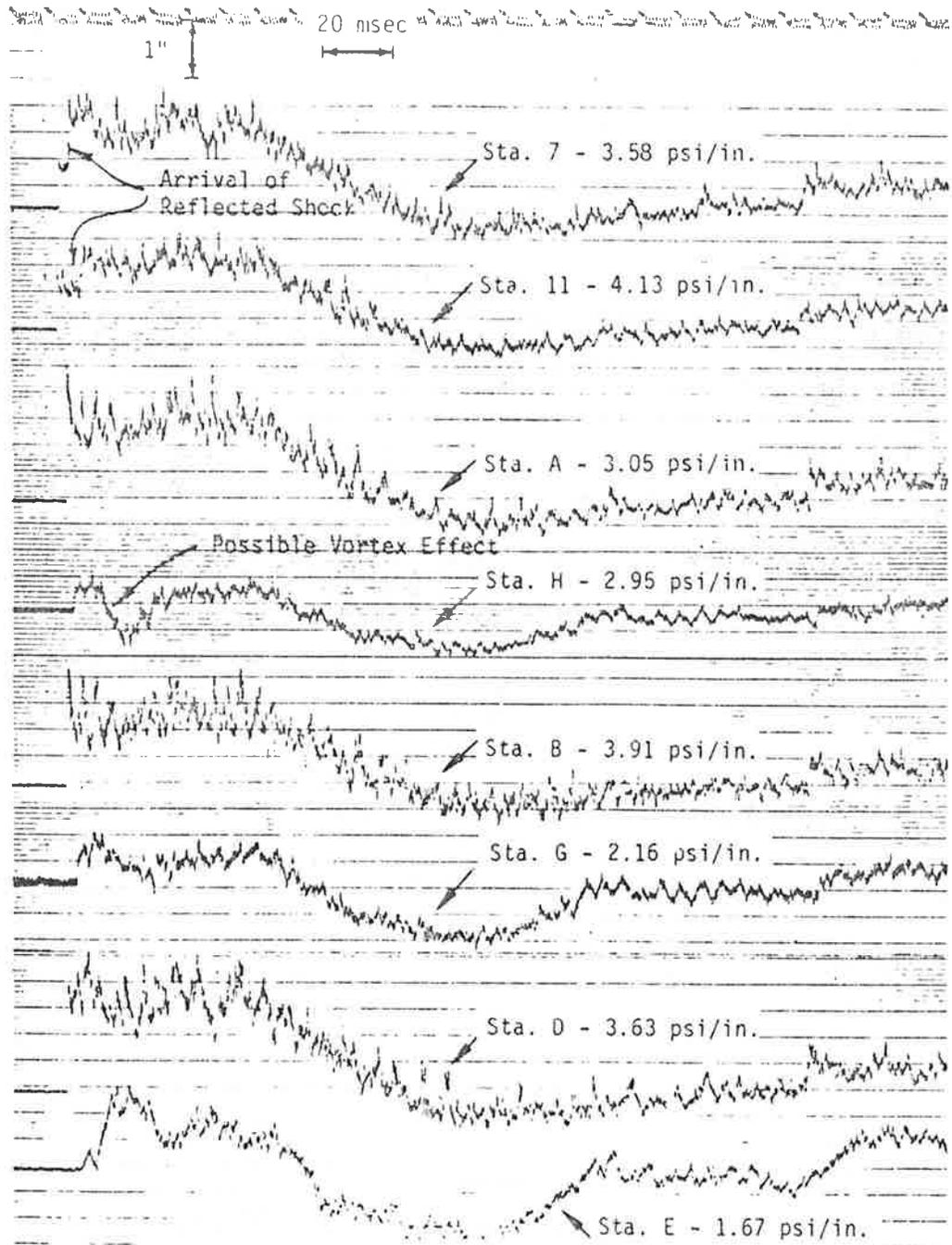Sta. D - 3.63 psi/in.

Sta. E - 1.67 psi/in.

Fig. 4-2 Wall with a Doorway Pressure vs Time Traces from a Test Using
Three Strands of Primacord. Sta 7 and 11 are on the Shock Tunnel
Side Walls; Sta A-H, B-G, and D-E are Paired Gauges on the Upstream
and Downstream Faces of the Doorway Wall. See Fig. 4-1.

21

downstream faces of the test wall. Refer first to the traces from Sta A and B, those closest to the doorway on the upstream face of the wall. These traces differ in two respects from those in similar locations on the solid wall. First, the early time pressure variations are larger; second, the average pressure at early times is about 75% of that on a solid wall.

Time variation of pressure on the downstream face of a wall with a doorway strongly influences the instantaneous net force at each point on the wall. The totality of integrated net forces at any time defines the net loading on the wall. Downstream face pressures can be complex as is illustrated by the trace from Sta H (nearest the doorway) of Fig. 4-2. Backface pressure (downstream) first rises slightly, later here than it does at its upstream counterpart Sta A, but then suddenly falls to below ambient pressure. Positive backface pressure reduces net force acting in the downstream direction; negative backface pressure increases net downstream force.

It is thought that the negative pressure observed on the downstream face is associated with a vortex which forms at the edge of the doorway, spreads out (thereby weakening) and propagates across the downstream face. This appears to be borne out by the record from Sta G, which also shows a pressure drop, but not as distinct a one as Sta H.

There is also a distinct pressure drop at Sta E, furthest from the doorway, which might be enhanced by reflection of the vortex-induced rarefaction from the tunnel wall.

LOCALIZED NET PRESSURE

Average localized net pressures were derived for each paired gauge loca-
tion (A-H, B-G, D-E). This was done by first digitizing the basic pressure
traces such as those given in Fig. 4-2. Then the digitized data were averaged
for each station from all repeat tests conducted with the same number of Prima-
cord strands. Finally, the average pulse from the downstream station of each
pair was subtracted from that from the upstream station (e.g., the pulse from
Sta H was subtracted from that from Sta A -- see Fig. 4-1). Net pressures
at the several measuring stations so determined for tests with one, three, and
five strands of Primacord are given in Appendix A (Figs. A-6 to A-8). The
pulse from tests with three strands are reproduced as Fig. 4-3.

For comparison purposes the average pressure loading from the solid wall
tests discussed in Section 2 is included on each graph. For the solid wall
case this average pressure loading is equivalent to the net pressure.

From this figure it can be seen that:

o The net pressure traces from the wall with a doorway show an
   initial pulse whose peak is essentially peak reflected pressure
   (pressure on solid wall), followed by a fall-off pressure essen-
   tially to incident values. The net pressure then rose again to
   values higher than incident, but generally lower than reflected.

o There is significant variability in the details of the pulse
   shapes from station to station on the wall with a doorway. For
   example, at the gauge locations furthest from the doorway net
   pressures remained at about peak reflected pressure for almost
   10 msec, while at the other gauge pairs net pressure was down to
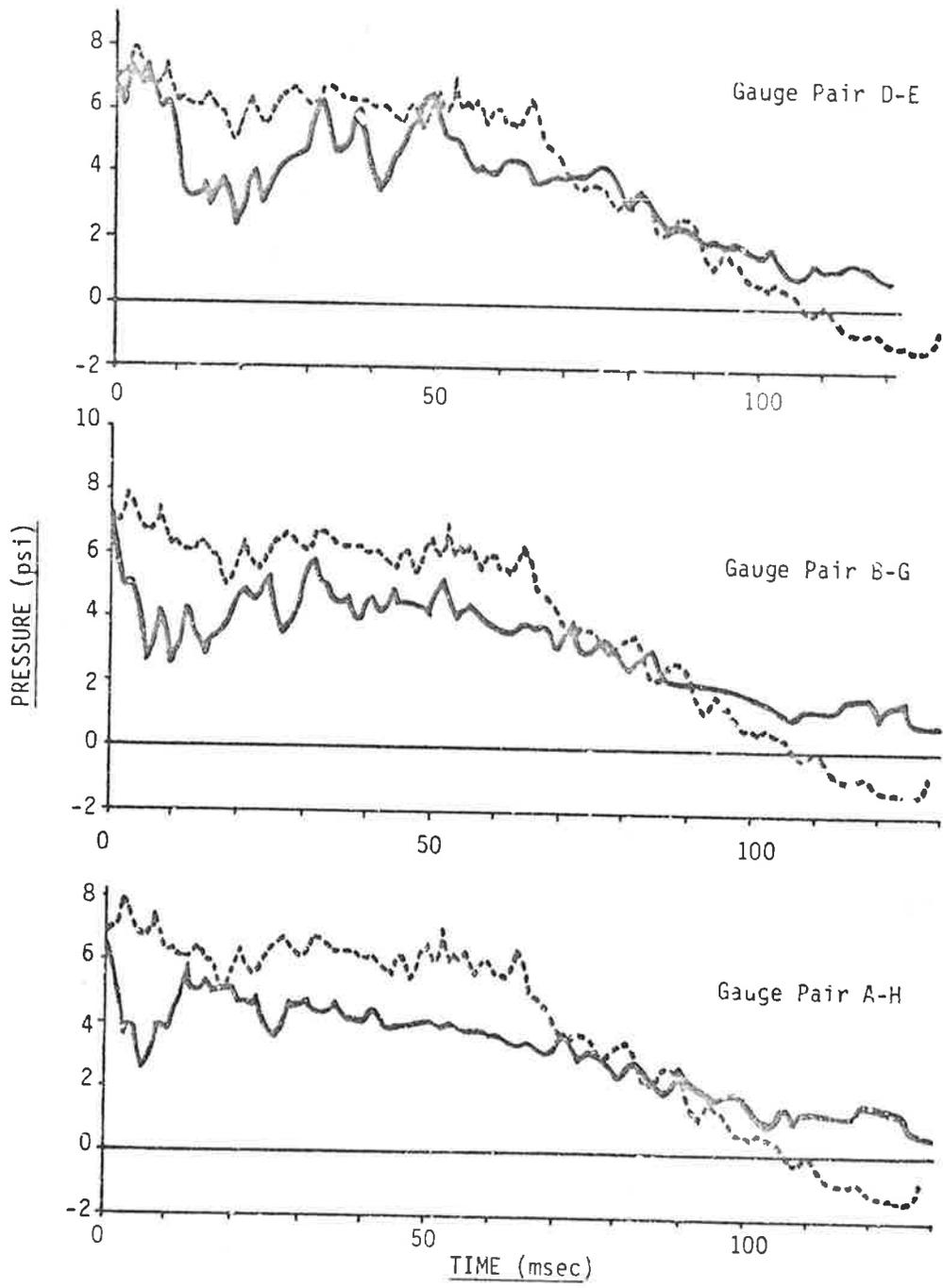   almost incident value in about 5 sec.

23

Fig. 4-3. Localizer Net Pressure vs Time from Paired Gauges from Tests Using Three Strands of Primacord. Solid Curves for Wall With a Doorway, Dashed Curves for Solid Wall. For Gauge Locations, See Fig. 4-1.

24

o The average net pressures throughout the first 50 msec are sig-
   nificantly lower for the wall with a doorway than for the solid
   wall.

NET IMPULSE

The early-time parts (up to 25 ms) of net pressure-time records, such as those of Fig. 4-3, were integrated to derive a net impulse as a function of time at the locations of the paired gauges. The results for one, three, and five-strand tests are shown in Fig. A-9, Appendix A; the plot from the three-strand test is reproduced as Fig. 4-4.

From Fig. 4-4 it can be seen that there are some variations in net impulse at early times as a function of distance from the doorway with the net impulse decreasing as the distance from the doorway decreases.
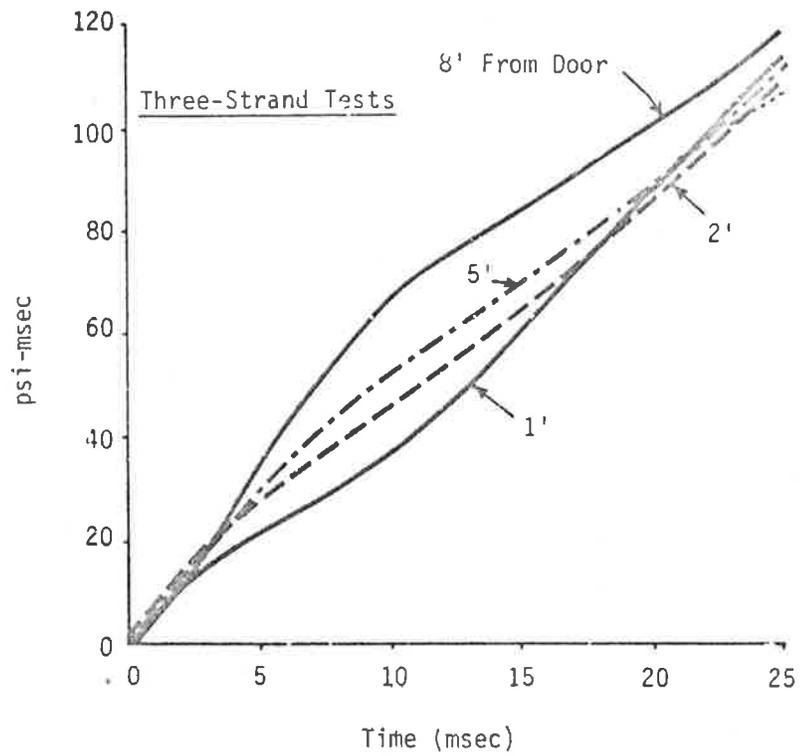
Fig. 4-4. Wall with a Doorway. Net Impulses vs Time at Various Distances from the Doorway from Tests Using Three Strands of Primacord.

27

Section 5
LOADING ON A WALL WITH A WINDOW OPENING

GENERAL

Two basic window sizes were used: the first, 38 in. high and 62 in. wide, occupied about 17% of the wall area; the second, 64 in. high and 62 in. wide, occupied about 27% of the wall area. The window configurations and locations of gauges used for the two cases are shown in Figs. 5-1 and 5-2, and typical traces from a test with the small window opening, in which three strands of Primacord were used, are shown in Fig. 5-3.

The traces from the gauges in the tunnel side walls (Sta 7 and 11) are the lowermost ones in Fig. 5-3. As with the previous tests with solid walls and walls with a doorway, the arrival at Sta 7 and 11 of the pulse reflected from the wall can readily be identified, and the remainder of the traces suggest that the wall experienced a complex net loading pattern. The traces from the upstream stations (A, C, and D) are relatively simple, generally resembling the open channel pulses at least until pressure in the pulse falls to ambient values. Average pressure values at Sta A and C are about 75% of peak reflected pressure, while the average at Sta D (nearest the floor) is close to peak reflected -- though it does show relatively wider pressure fluctuations.

The traces from the downstream stations (E, G, and H) are quite different, however. At Sta E, early-time pressures are positive (i.e., directed upstream) and relatively uniform, but they become strongly negative just after pressures on the side of the wall begin to drop off. The trace from Sta G shows a similar pattern, though pressure fluctuations are greater; with pressures becoming equal or close to ambient pressure a number of times. The trace from Sta H (the station nearest the floor) has much different characteristics. It drops below ambient values very early, as at Sta H in Fig. 4-3, but remains negative or close to ambient pressure for the remainder of the pulse. It is suspected that this trace is anomalous.

28

EAST

WEST
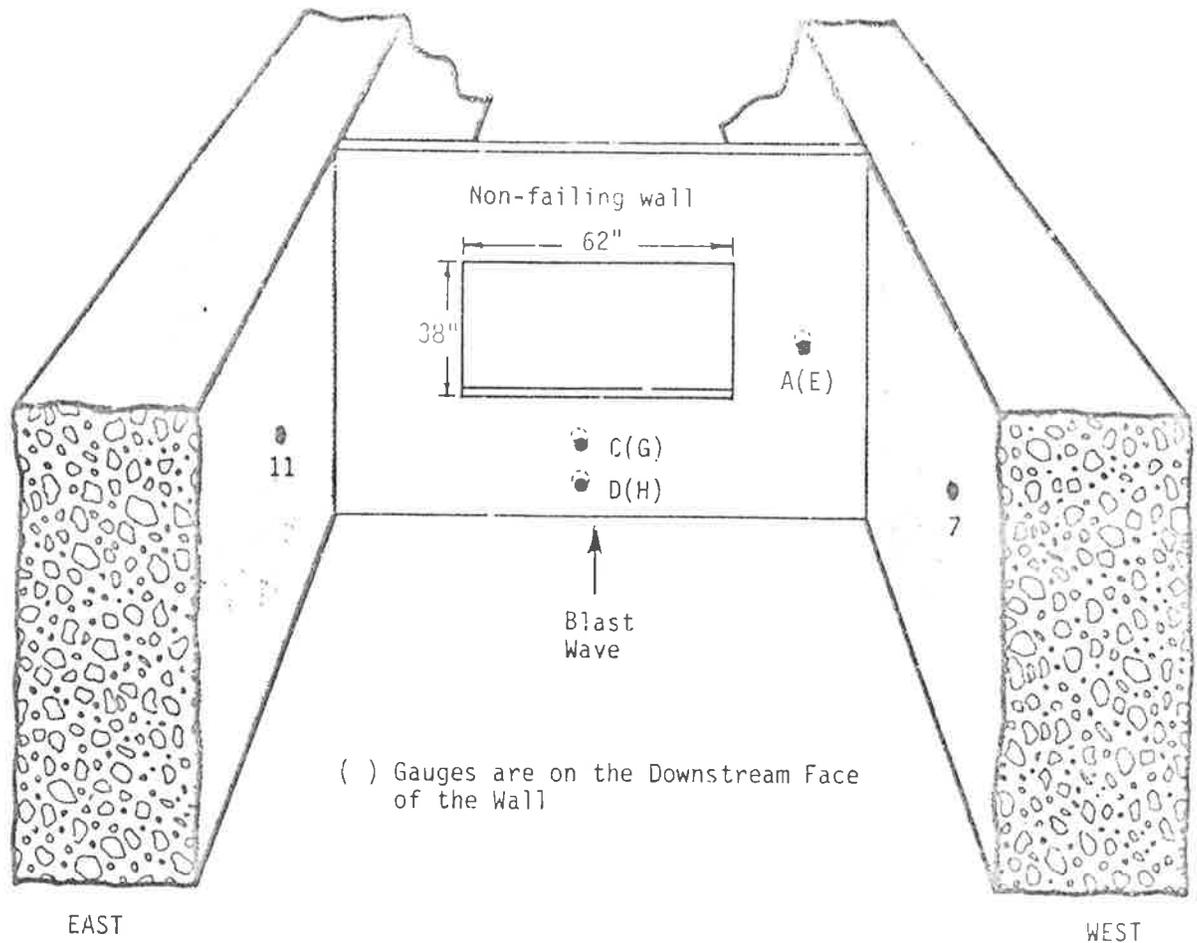
NON-FAILING WALL GAUGES		
GAUGE NO.	DISTANCE FROM FLOOR (in.)	DISTANCE FROM WINDOW (in.)
A-E*	51	24
C-G*	27-1/2	6-1/2
D-H*	14-1/2	19-1/2
* Gauges E, G and H are on the Back of the Wall.		
TUNNEL WALL GAUGES		
GAUGE NO.	DISTANCE FROM FLOOR (in.)	DISTANCE FROM WALL (in.)
7	45	21
11	49	38

Fig. 5-1. Configuration for Tests on a Wall with a 38-in. x 62-in. (17%) Window Opening.

EAST   WEST
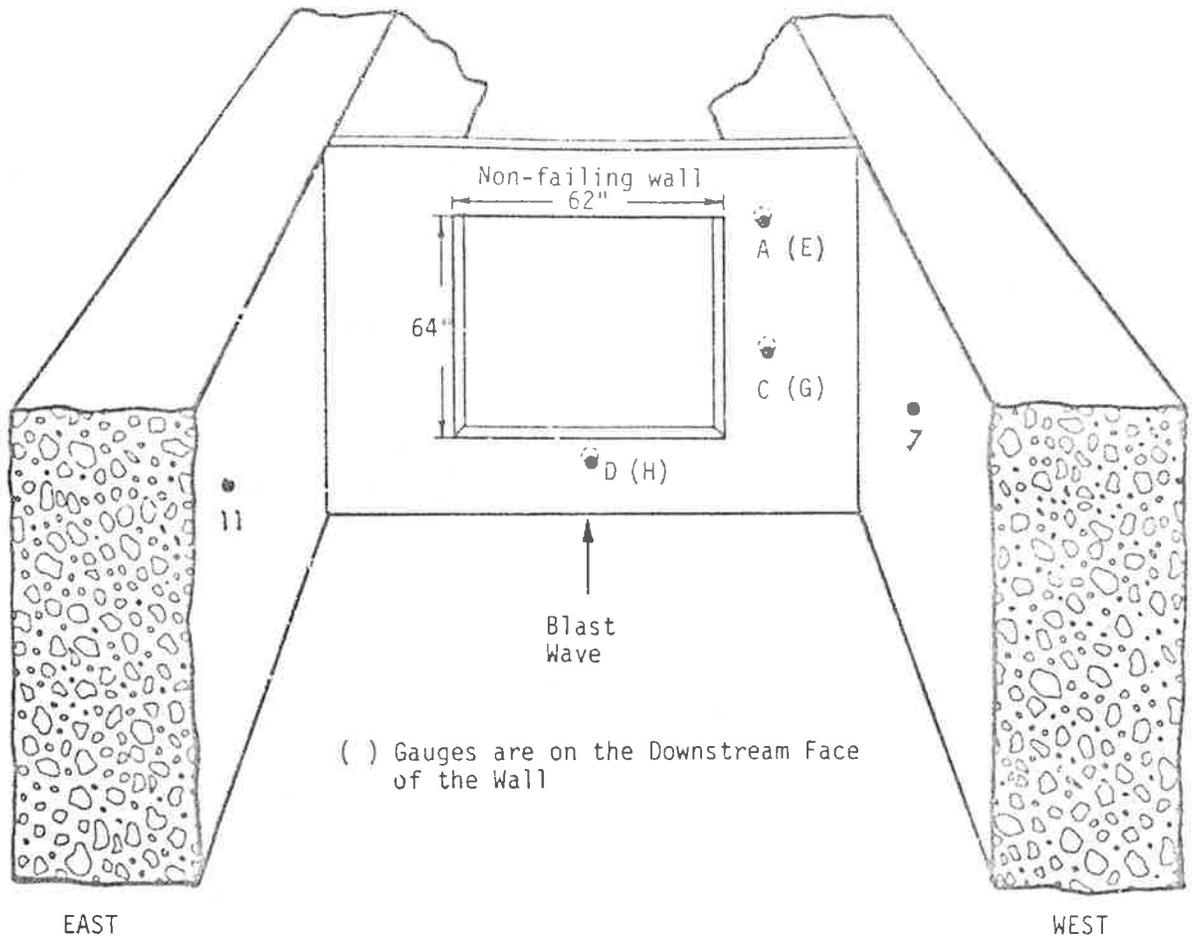
NON-FAILING WALL GAUGES		
GAUGE NO.	DISTANCE FROM FLOOR (in.)	DISTANCE FROM WINDOW (in.)
A-E*	89-1/2	12
C-G*	51	12
D-H*	14	7
* Gauges E, G and H are on Back of the Wall.		
TUNNEL WALL GAUGES		
GAUGE NO.	DISTANCE FROM FLOOR (in.)	DISTANCE FROM WALL (in.)
Westwall-7	45	21
Eastwall-11	49	38

Fig. 5-2.   Configuration for Tests on a Wall with a 64-in. x 62-in. (27%)
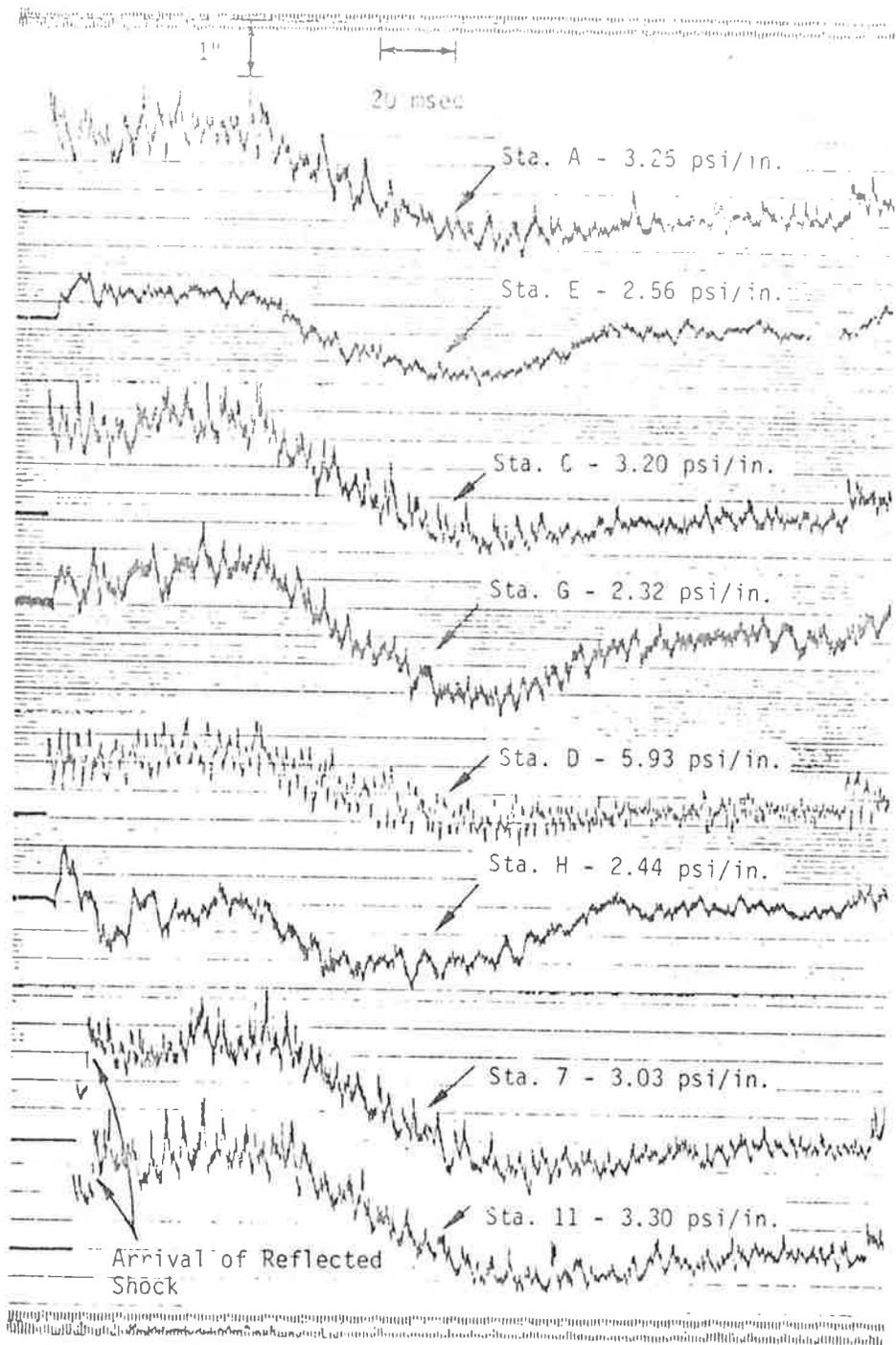Window Opening.

30

Fig. 5-3   Pressure vs Time Traces from a Test of a Wall with a 38-in. x 62-in.
(17%) Window Opening Using Three Strands of Primacord. Sta 7 & 11 are
on the Shock Tunnel Side Walls; Sta A-E, C-G, and E-H are Paired Gauges
on the Upstream and Downstream Faces of the Window Wall. See Fig. 5-2.

31

LOCALIZED NET PRESSURES

The net pressures, derived as before, from digitized records are given in Appendix A (Fig. A-10 through A-15), for tests using one, three, and five strands of Primacord.

Typical samples of these results are given in Fig. 5-4 which show the net pressure pulses for position C-G for both the small and large window openings for three strand tests. For comparison purposes a similar record obtained from the solid wall tests discussed in Section 2 is included on each graph. These results are typical of all other results for three and five strand loading with one exception.* Results from single-strand tests do not display an initial high peak, undoubtedly reflecting the rounded nature of the one-strand shock tube pulses generated in the shock tunnel as shown in Fig. 3-6 discussed earlier.

From Fig. 3-4 it can be seen that at the time of the shock wave arrival the pressure is approximately the peak reflected value but that the pressure drops within about 5 msec to some lower and roughly constant value for the first 50 msec of loading.

The effect of window size manifested itself mostly in the general net pressure level at times between 5 and 50 msec. With the small (17%) window opening, the net pressure level was about 55% of peak reflected pressure; with the large (27%) opening, the level was about 35% of peak reflected pressure. The lower average net loading value for the larger window reflects the fact that more of the incident shock wave can pass through the window to load the back (downstream) side of the wall, thus reducing net loadings on the wall.

---

* The one exception is from the three-strand test with a small window, traces from which are shown in Fig. 5-3. The record from gauge pair D-H follows the initial pattern of a rapid drop from peak reflected pressure but it then rises again to a value greater than initial peak reflected pressure. This shows the effects of the early negative pressures recorded at Sta H.
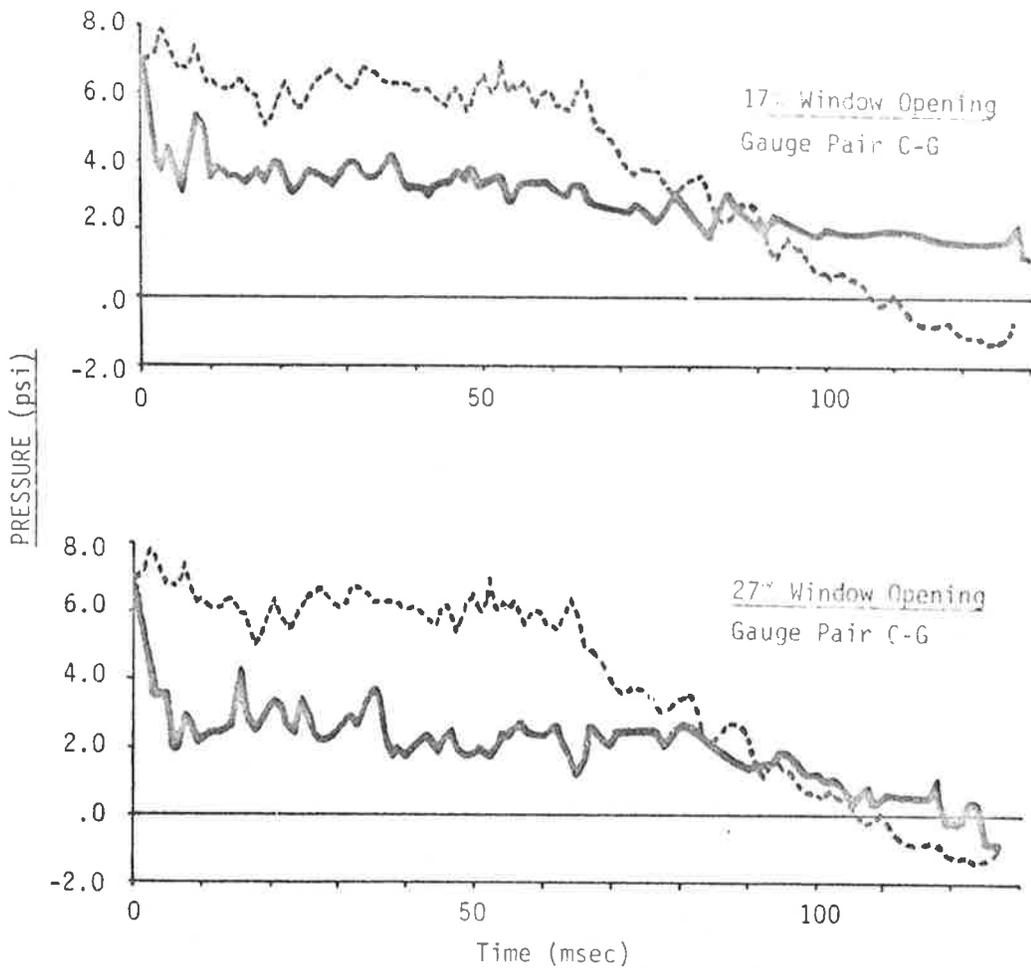
32

Fig. 5-4. Localized Net Pressure vs Time from Paired Gauges from Tests Using
Three Strands of Primacord. Solid Curves for Wall With Window,
Dashed Curves for Solid Wall. For gauge locations see Figs. 5-1
and 5-2.

33

Although the data are rather limited it is interesting to plot the
loading pressures (as a percent of peak reflected pressure) versus window area
(as a function of total wall area) on semi-log paper as shown in Fig. 5-5. It
can be seen that a simple exponential equation fits the data. The line in
Fig. 5-5 is dashed past the last data point to indicate lack of certainty
in the extrapolated values. Up to about 50 msec, Fig. 5-5 can be used to
estimate net pressure on a wall with a window as a percentage of peak reflect-
ed pressure. As noted before, the information would be useful for calculating
wall motions that are insensitive to short-time transients.

NET IMPULSE

As with the wall with a doorway, calculations were made of net impulses
at the locations of the front and back face pairs of stations around the window.
These are given in Figs. A-16 and A-17 of Appendix A, with the curves from the
three-strand tests being reproduced in Fig. 5-6. These data illustrate the
decrease in loading with increased window area and similarity of results
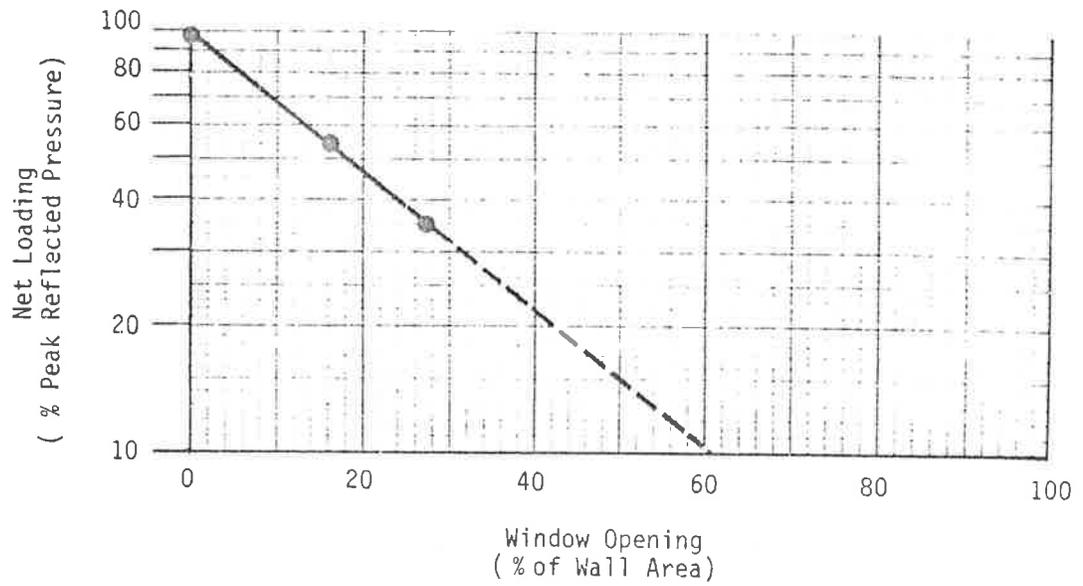between the various measuring positions for a given window area.

34

Fig. 5-5. Net Loading on a Wall with a Window as a Function of Window
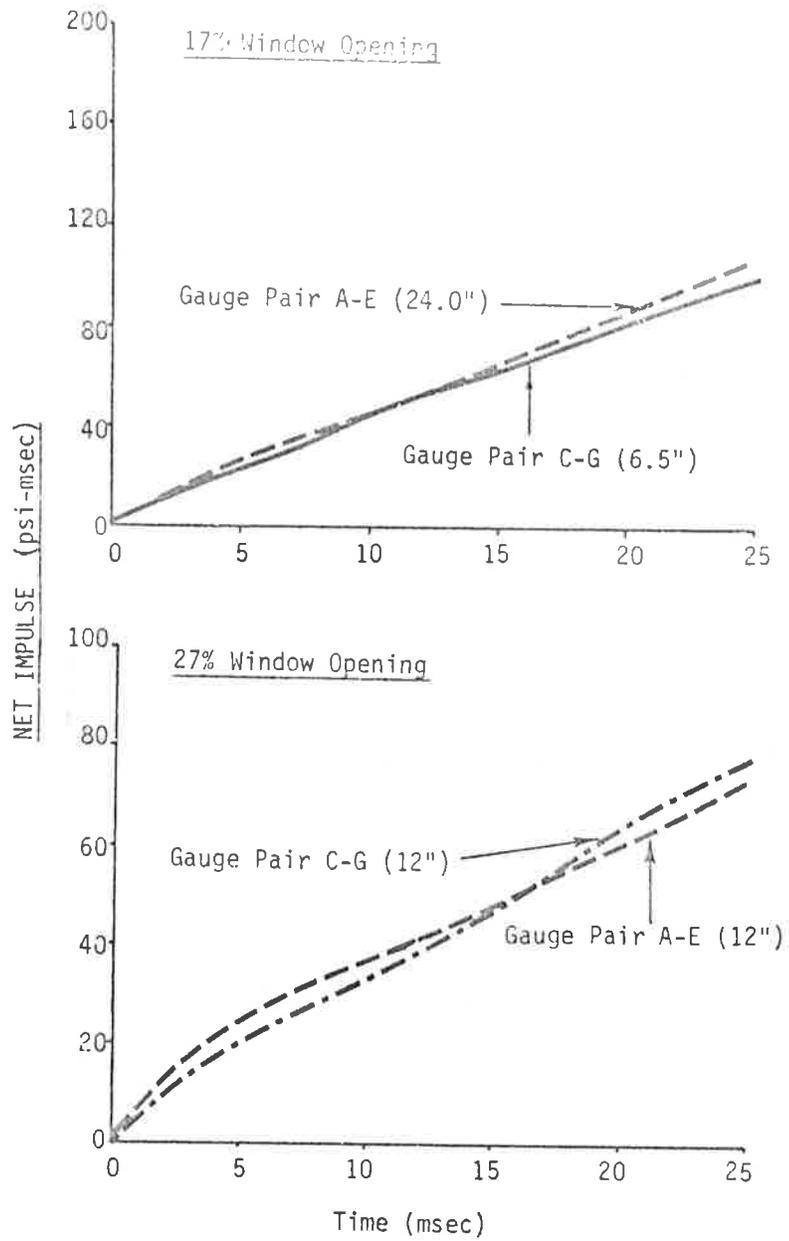Opening Area.

35

Fig. 5-6. Net Impulse for Walls with 17% and 27% Window Openings from Gauge Pairs for Tests with Three Strands of Primacord.

36

EFFECT OF GLASS IN WINDOW OPENINGS

In the loading study test series involving window openings a few tests were devoted to assessing the effect of the presence of glass in windows. Ordinary window glass was placed in the large window opening for one test with three strands of Primacord (peak incident pressure 3.3 psi, peak reflected pressure = ≈7 psi), and two tests with five strands (peak incident pressure ≈6 psi, peak reflected pressure ≈14 psi). The early-time (<12 msec) effect of the glass on the backface was truly impressive. Fig. 5-7 shows pressure-time records from gauge H (opposite gauge D, see Fig. 5-2) taken during tests involving five strands of Primacord. One curve presents data from the tests with glass in the windows, and one is from tests without glass. The first pressure peak with glass (∼1.5 psi) is almost a factor of three less than the pressure peak without glass (∼4.3 psi), and occurs about 5 msec later. Thus, initial net force on the wall (the difference between pressures on the upstream and downstream faces) could be 30 to 40% higher for a window opening with glass in place than for one without glass, even if pressure on the upstream face of the wall were identical in the two cases. Impulses would be similarly affected. The impulse calculated from Fig. 5-7 up to a time of 10 msec is 53% less with glass in the window than without glass. Up to 15 msec, the difference is 30%.
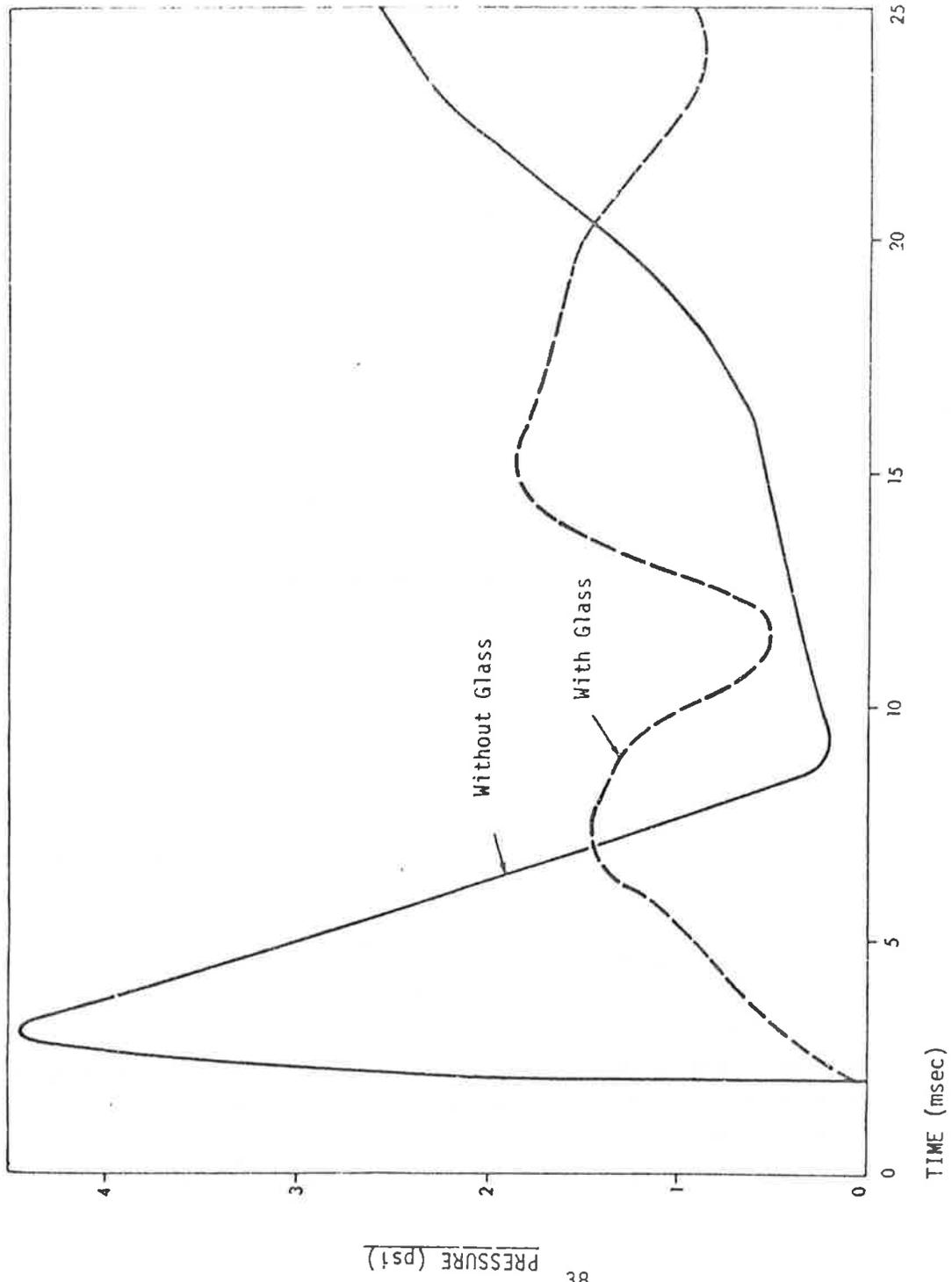
Fig. 5-7. Effect of Window Glass. Average Pressure vs Time From a Gauge on the Downstream (Back) Face of a Wall with a 64-in. x 62-in. (27%) Window Opening.

38

Section 6
LOADING ON WALLS OF A ROOM WITH A WINDOW

GENERAL

By placing two walls across the tunnel a 15-ft long room was created with a window opening facing the blast wave source. Two separate test series were conducted with this configuration, both of which used an upstream (front) wall with a window opening of about 20% of the wall area, and a solid downstream (rear) wall.

Details of the test arrangements are shown in Fig. 6-1. The rear wall gauge arrays on the two series were somethat different, though the location of gauge stations D-2 and D-3 of the first series were essentially the same as Stations W and Y of the second series. In addition, the second series incorporated two gauge pairs A-H and B-G on the upstream and downstream faces of the front (window) wall. Both series also included gauge Stations 7 and 11 in the tunnel side walls upstream from the front wall, and on the first series, gauge Station 10, in the tunnel side wall but within the room, was also used.

Typical traces from one of the second series of tests in which three strands of Primacord were used are shown in Fig. 6-2. The traces clearly reveal the effects of various reflecting surfaces. As before, the step rise near the front of the pulse from Sta 7 is due to the arrival of the wave reflected from the front wall at the station. The more gradual steps 25-30 msec after the first recorded pressures at Sta G and H are due to the arrival at the upstream face of the front wall of the wave reflected from the rear wall, and there is a hint of a third step in each trace representing a second arrival of a shock reflected from the rear wall. The gradual steps in the traces from Sta W, X, and Y are due to the re-arrival at the rear wall of the wave that first reflected from that wall then from the front wall. As might be expected, the time difference between the arrival of the incident
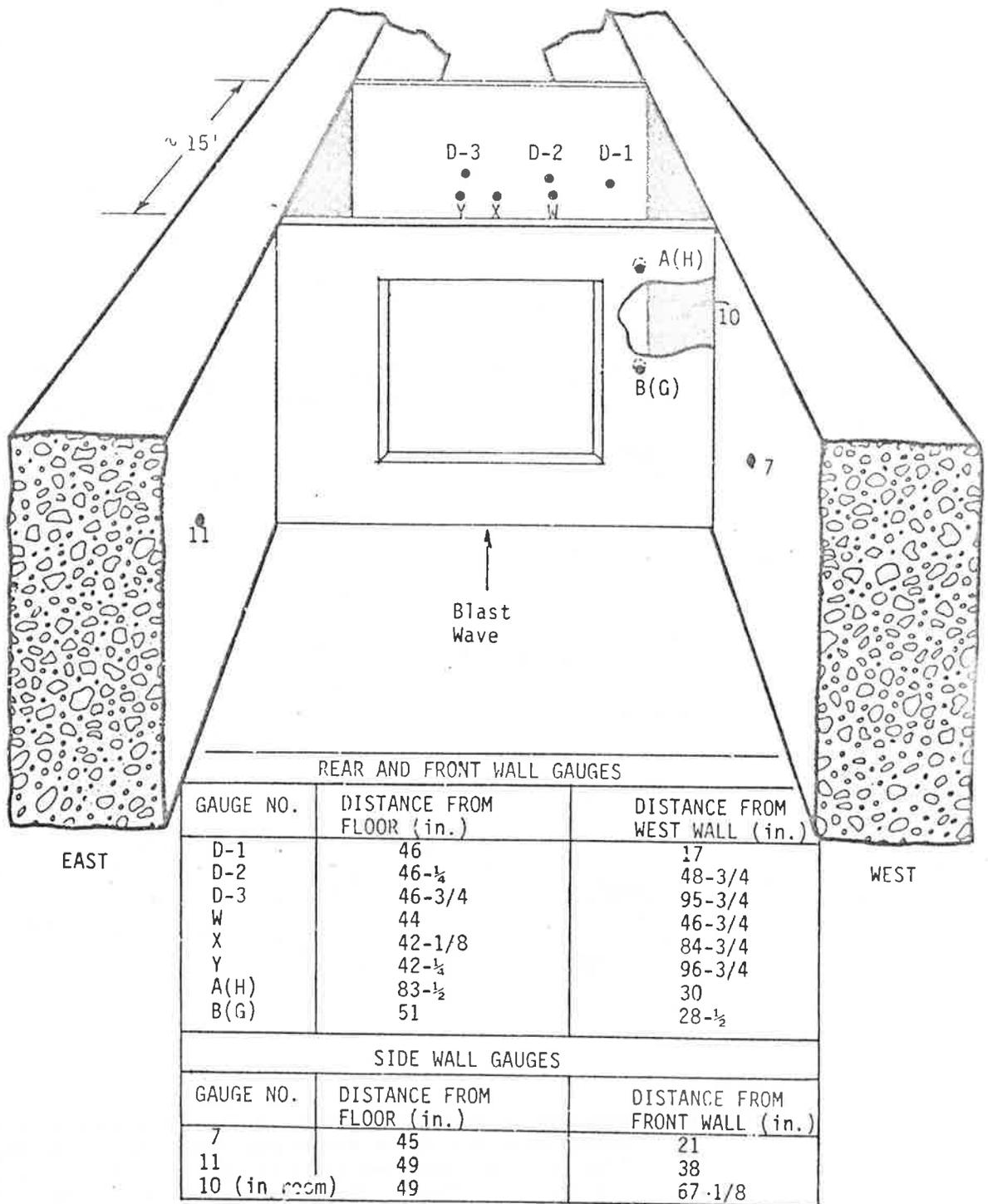
REAR AND FRONT WALL GAUGES		
GAUGE NO.	DISTANCE FROM FLOOR (in.)	DISTANCE FROM WEST WALL (in.)
D-1	46	17
D-2	46-¼	48-3/4
D-3	46-3/4	95-3/4
W	44	46-3/4
X	42-1/8	84-3/4
Y	42-¼	96-3/4
A(H)	83-½	30
B(G)	51	28-½
SIDE WALL GAUGES		
GAUGE NO.	DISTANCE FROM FLOOR (in.)	DISTANCE FROM FRONT WALL (in.)
7	45	21
11	49	38
10 (in room)	49	67·1/8

Fig. 6-1.   Room with a Window Test Configuration.

40

1"

20 msec

Arrival of Shock Reflected from Window Wall

Sta. 7 - 6.06 psi/in.

Sta. Y - 2.55 psi/in.

Sta. A - 5.38 psi/in.

Sta. H - 2.99 psi/in.

Sta. W - 2.56 psi/in.

Sta. X - 4.10 psi/in.

Sta. B - 3.90 psi/in.

Arrival of Shock Reflected
from Rear Wall

Sta. G - 5.54 psi/in.
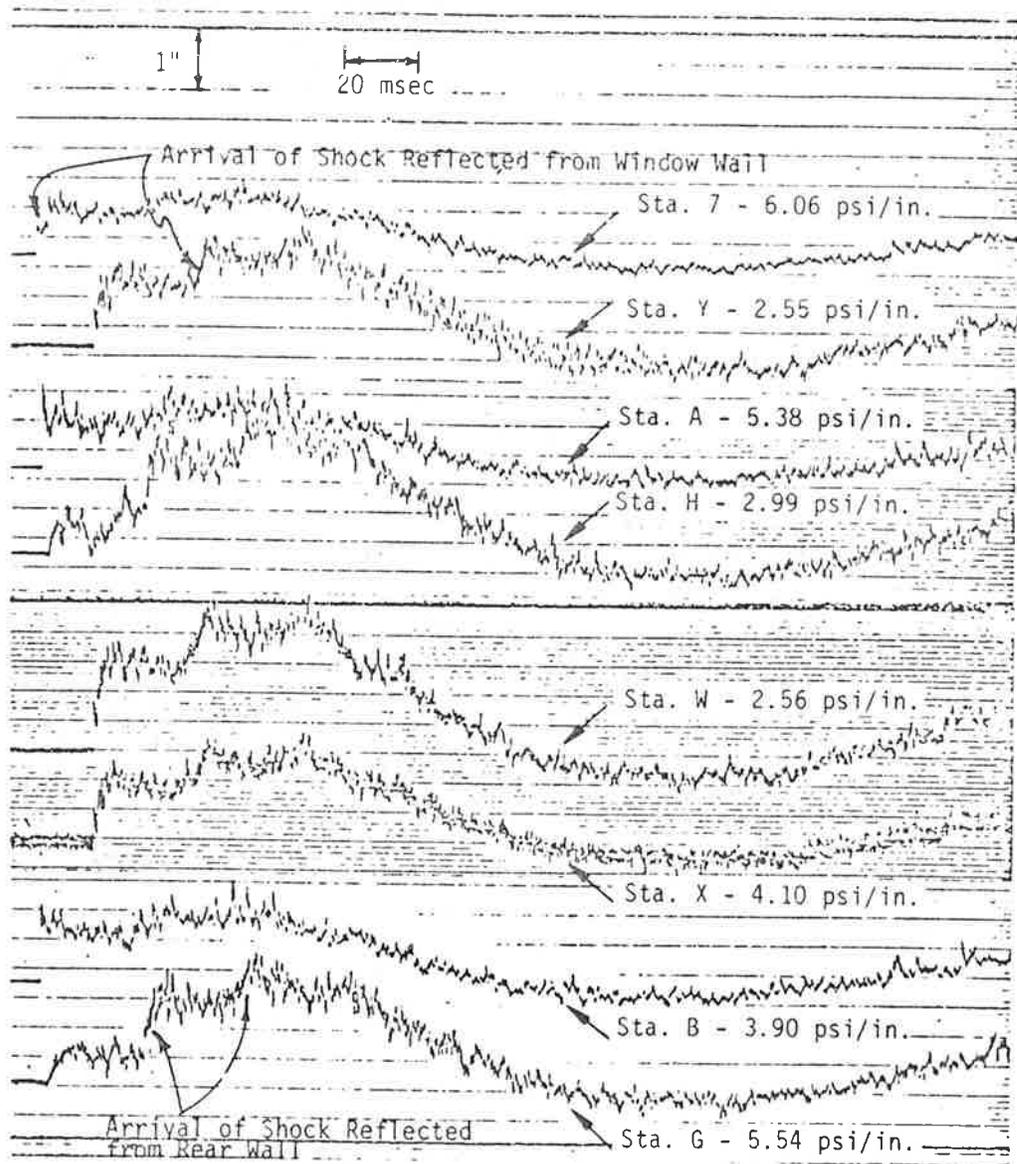
Fig. 6-2. Pressure vs Time Traces from a Test with a Room with a Window
Using Three Strands of Primacord. Sta 7 is in the Shock Tunnel
Side Wall Upstream from the Front (Window) Wall; Sta W, X, and Y
are on the Rear Wall; Sta A-H and B-G are Upstream and Downstream
Paired Gauges on the Front Wall. See Fig. 6-1.

41

shock wave at the front wall (Sta A and B) and at the rear wall (Sta W, X, and Y) -- about 13.5 ms -- is essentially one-half the time difference between the steps on the traces from Sta G and H (on the interior face of the front wall) and from Sta W, X, and Y (on the rear wall). The steps after the first in these last five traces represent the arrival of shock waves that have traversed the room twice.

The traces from Sta A, B, and 7 indicate that little shock wave energy propagated upstream from the window wall after the shock had traversed the room once. The traces from these stations are generally similar to those from the equivalent stations in tests which involved only a single wall with a window opening. (See traces from Sta A, C, D, and 7 in Fig. 5-3.)

NET PRESSURES

As with the other loading study series, the traces from tests involving a room with a window were digitized at 1 msec intervals and results from a number of tests and stations were averaged. The records from all rear wall stations indicted general uniformity, so that records from these stations taken during both test series were averaged.

Rear wall and side wall data from tests with one through five strands of Primacord are shown in Figs. A-18 through A-21 of Appendix A. Net loading information from the gauge pairs on the front wall, from tests with one, three, and four strands are shown in Figs. A-22 and A-23 of Appendix A. Results from tests with three strands of Primacord are reproduced in Figs. 6-3 and 6-4. For comparison purposes a similar record obtained from the solid wall tests is included on each graph.

The plots in Fig. 6-3, from gauges on the solid walls of the room, (that is, the rear and side walls) show effects of the shock wave spreading out after it passes through the window and reflecting from various interior surfaces. At the rear wall, initial pressures appear to be somewhat below incident, and they rise -- during the early part of the pulse -- to values between 35% and 50% higher than incident, well below the more than twice incident values that would be experienced by a solid wall exposed directly to a blast wave. Pressures then increase again when the wave within the room, first reflected from the rear wall and now reflected from the front wall, arrives at the rear wall.

The side wall gauge within the room (Fig. 6-3) first registers a very low pressure which then rises to a value some 35% below incident pressure. The pressure increases sharply as the shock reflected from the rear wall arrives at the station, after which the pulse appears to gradually increase at least until the pressure in the main loading wave decreases.

The importance of room geometry is perhaps most clearly apparent in the
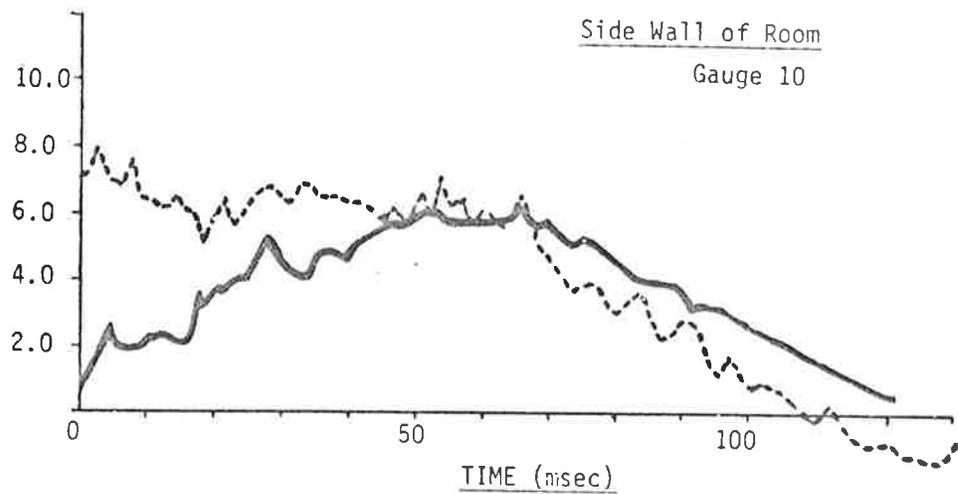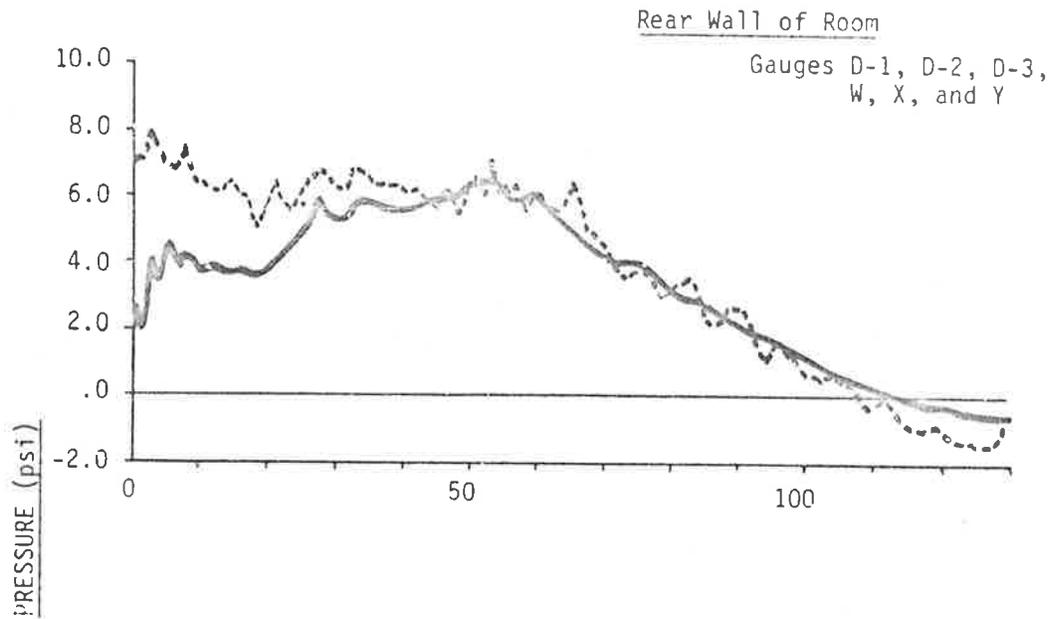
43

Fig. 6-3. Average Pressures from Gauges on Solid Walls Within the Room with a Window from Tests Using Three Strands of Primacord. Solid Curves for Room with a Window; Dashed Curves for Solid Wall. For Location of Gauges see Fig. 6-1.
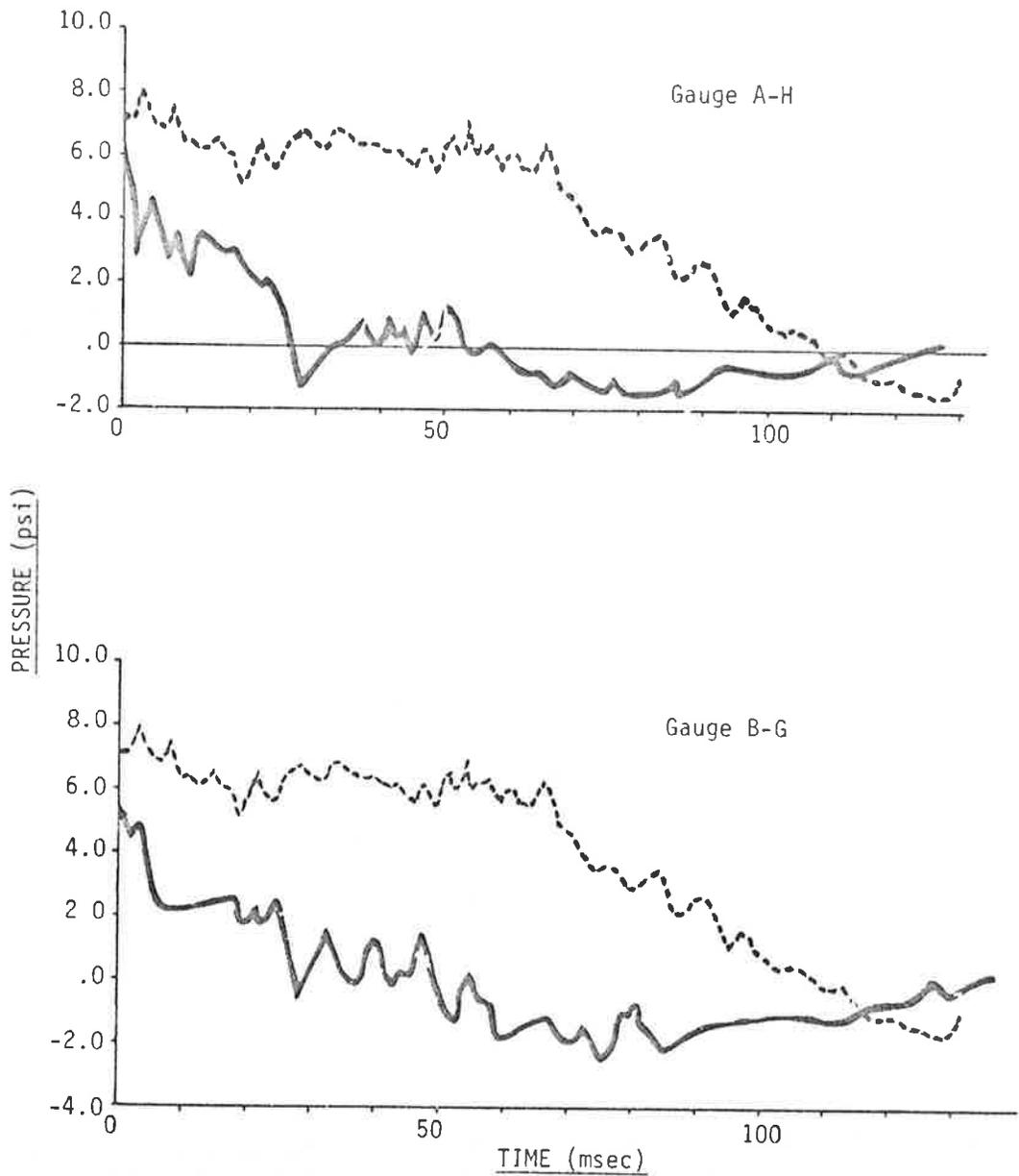
44

Fig. 6-4. Net Pressure Pulses from Paired Gauges on the Front (Upstream, or Window) Wall of the Room with a Window from Tests Using Three Strands of Primacord. Solid curves for Room with a Window; Dashed Curves for Solid Wall. For Location of Gauges, see Fig. 6-1.

45

net pressure pulses of gauge pairs (Fig. 6-4). Data from paired gauges in similar locations on the wall containing a similar window opening (Fig. 5-4) showed an initial sharp drop from zero-time peak reflected pressure to a value close to incident pressure at 10 ms. The net pressure then remained at about this value until the main loading wave started decreasing in pressure.

In contrast, the net loading on the window wall which is part of a room, shows not only the same initial sharp drop, but a continuing drop to zero and below (net force actually directed upstream) well before pressure in the incident main loading pulse begins to decrease. The cause is clearly the shock wave reflecting from the rear wall of the room, which -- as noted before -- changes the loading on the interior face of the window wall substantially, but has little effect on the exterior face.

Section 7
SUMMARY

The loading study series was important to the overall program in a number of ways.

Studies with an instrumented non-failing solid wall which blocked the shock tunnel confirmed the uniformity of the loading generated across the shock tunnel and furnished loading data which was used in the computer analysis of wall panel failure prediction and also was used in the design of the test program conducted with structural wall panels.

The test series with instrumented walls with window and doorway openings was probably the most important series in that it provided experimental data on net loadings, i.e., the actual load a wall with an opening will see, taking into account the frontface loading and the backface loading caused by blast leakage through the opening. This is one of the few sources of this data and was extremely valuable in the development of failure predictions for complex walls with opening geometries.

The room geometry tests were equally important to the program in that they supplied data on loading that would be experienced by interior walls in a typical room configuration.

When using this loading study data for purposes other than this program, it should be recalled that the loading pulses generated in the shock tunnel are only an adequate simulation of the early-time portion (50 msec) of the blast from a megaton-range nuclear weapon. This suggests that the loading study data has the greatest utility for:
1. Targets whose natural periods are such that the times to maximum deflection (including failure) are less than the duration of the flat topped portion of the wave.

2. Targets whose effective loading duration in a nuclear blast environment would be limited by the clearing times of the reflected pressure wave, rather than by the actual free-field positive-phase duration. Examples of such targets could be structural elements on the front faces of structures. (Typical frontface clearing times for structures with a minimum dimension height of half-width of 30 ft would be about 65 msec.)

It should be noted that wall panels are one of the most important classes of targets which fit within both of these conditions.

Appendix A

Included in Appendix A are the supplemental data plots which are called out in the text.
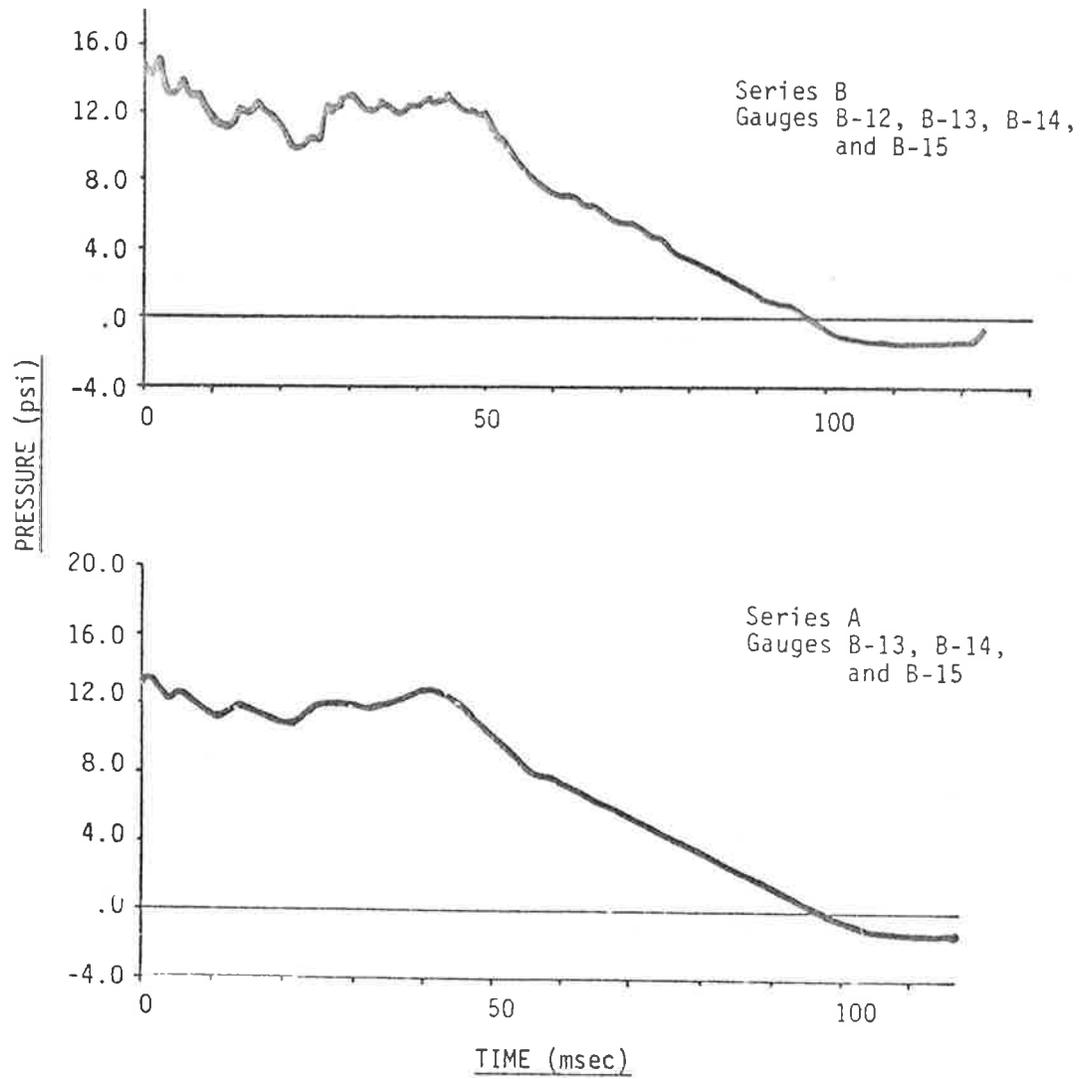
Fig. A-1. Average Overpressure vs Time on a Solid Wall from Tests Using Five Strands of Primacord.

A-1
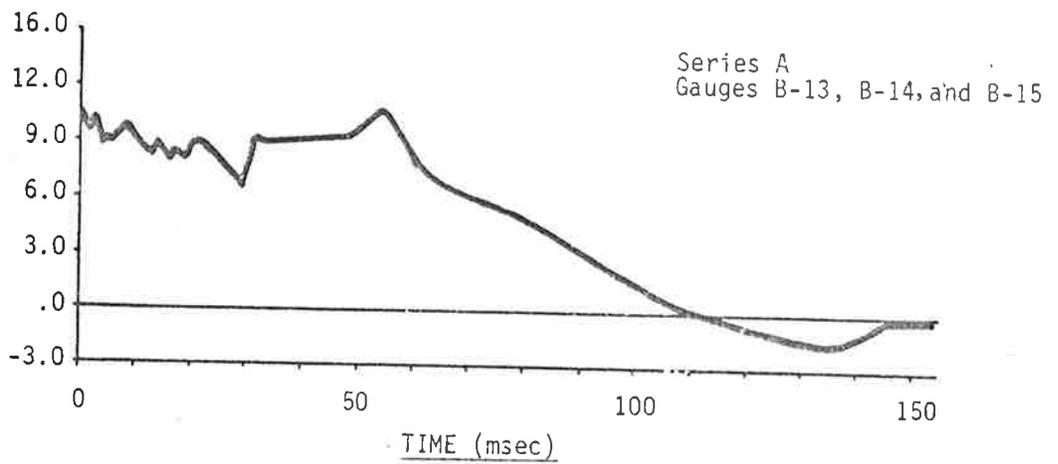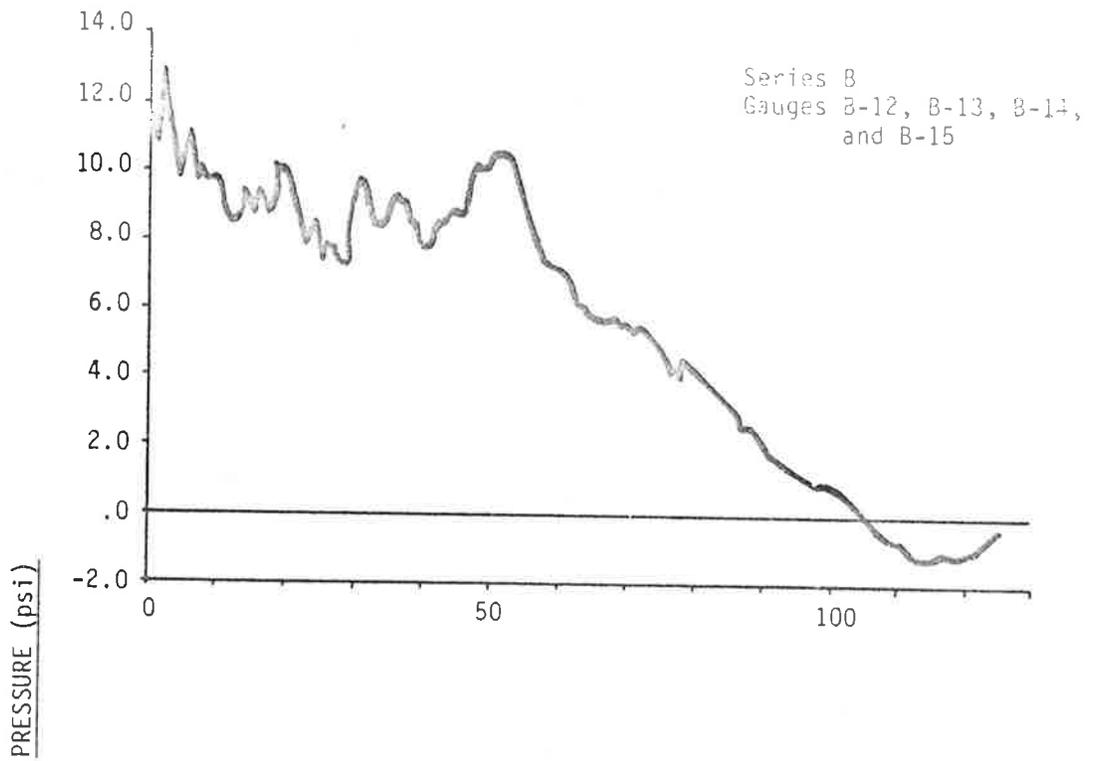
Fig. A-2.   Average Overpressure vs Time on a Solid Wall from Tests using four
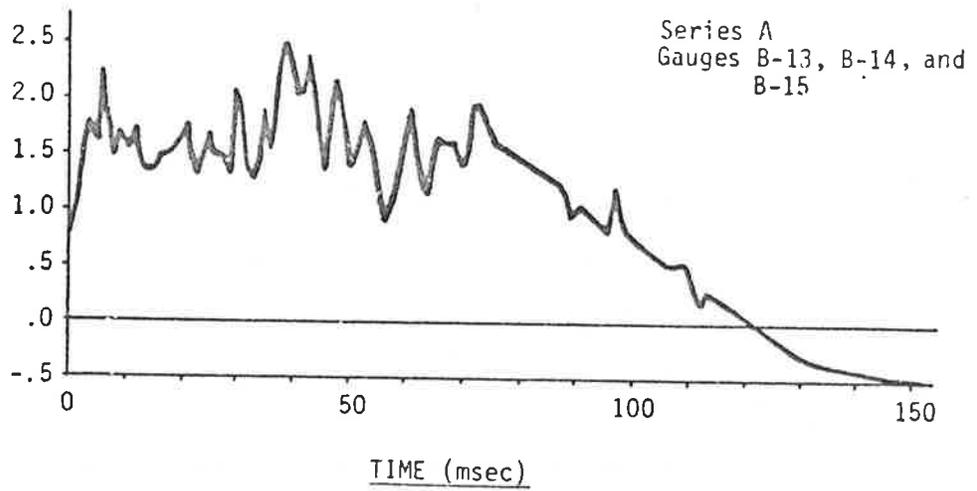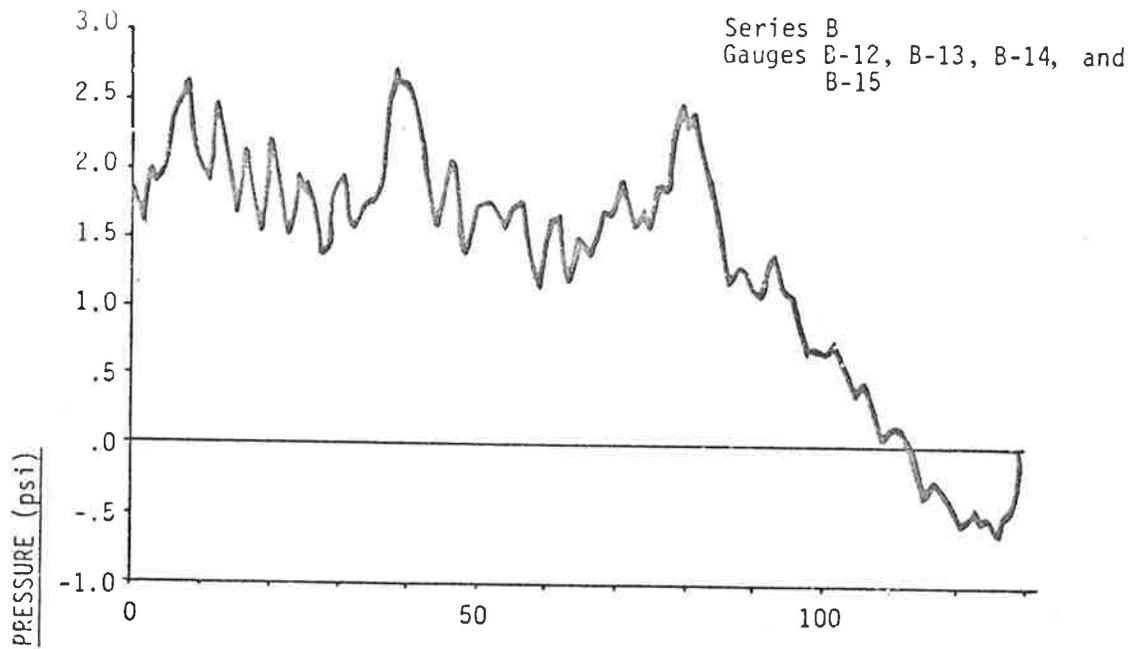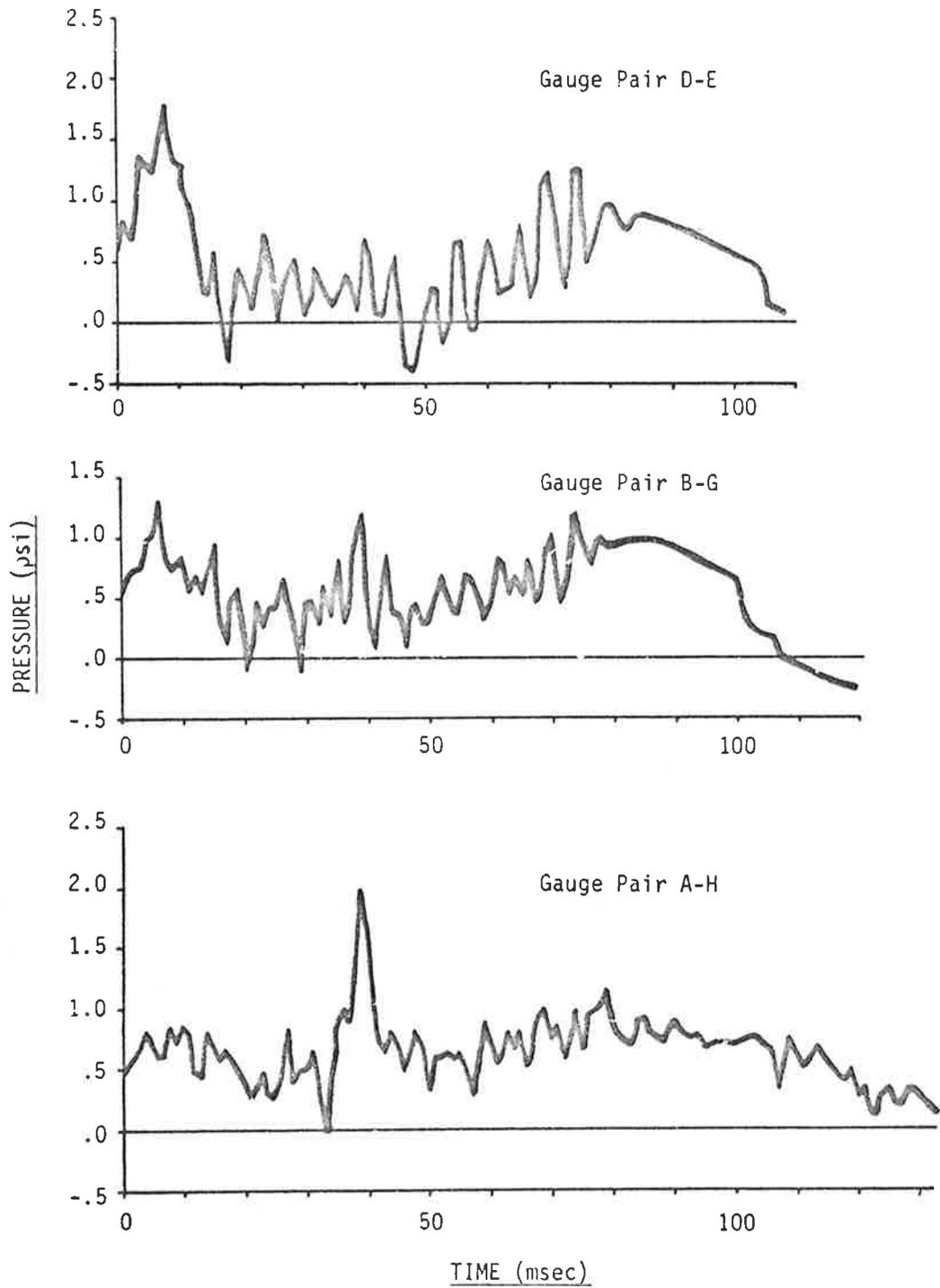Strands of Primacord.

A-2
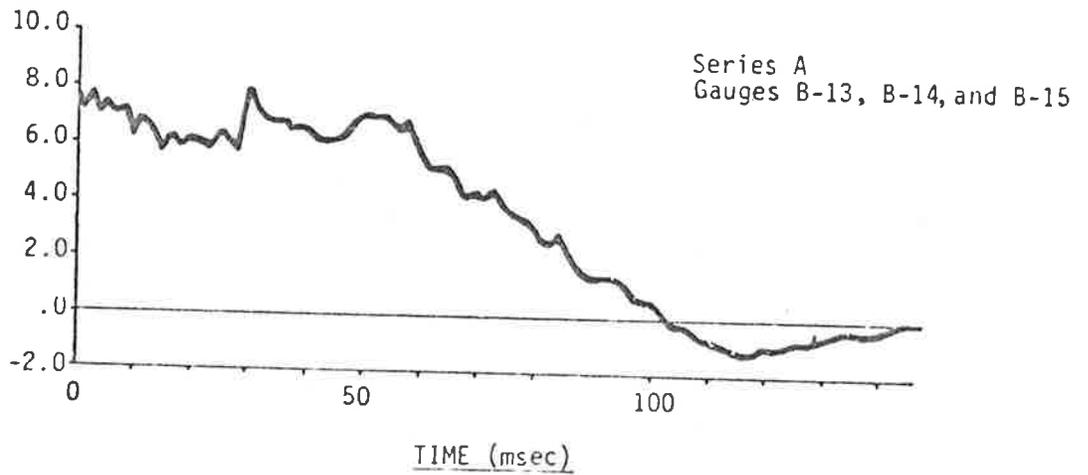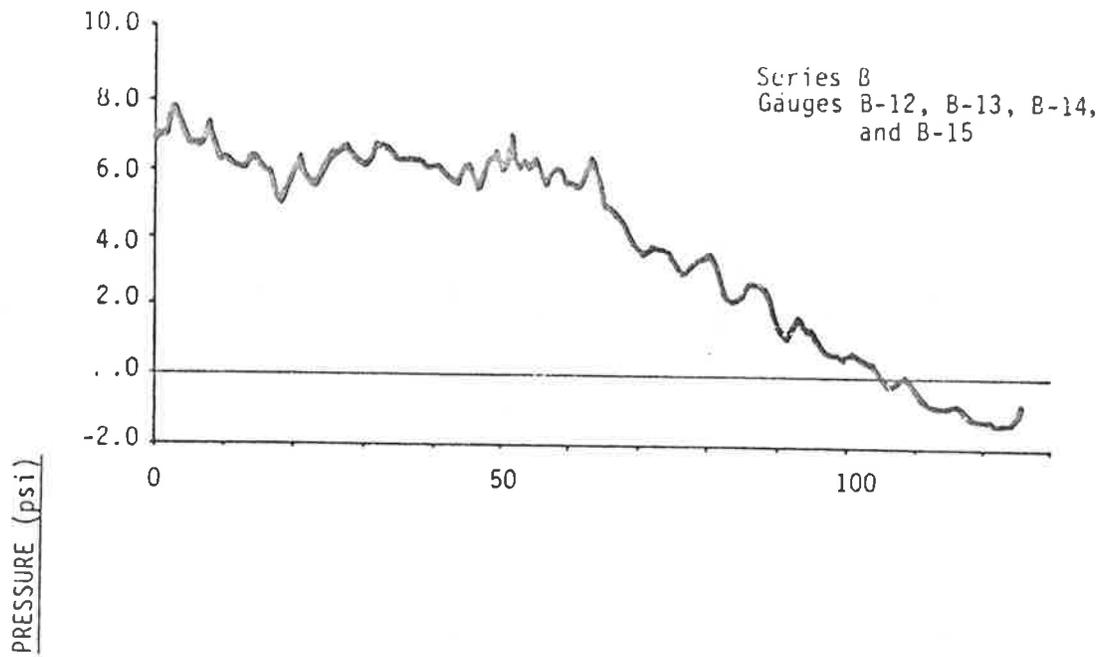
Fig. A-3. Average Overpressure vs Time on a Solid Wall from Tests Using Three Strands of Primacord.
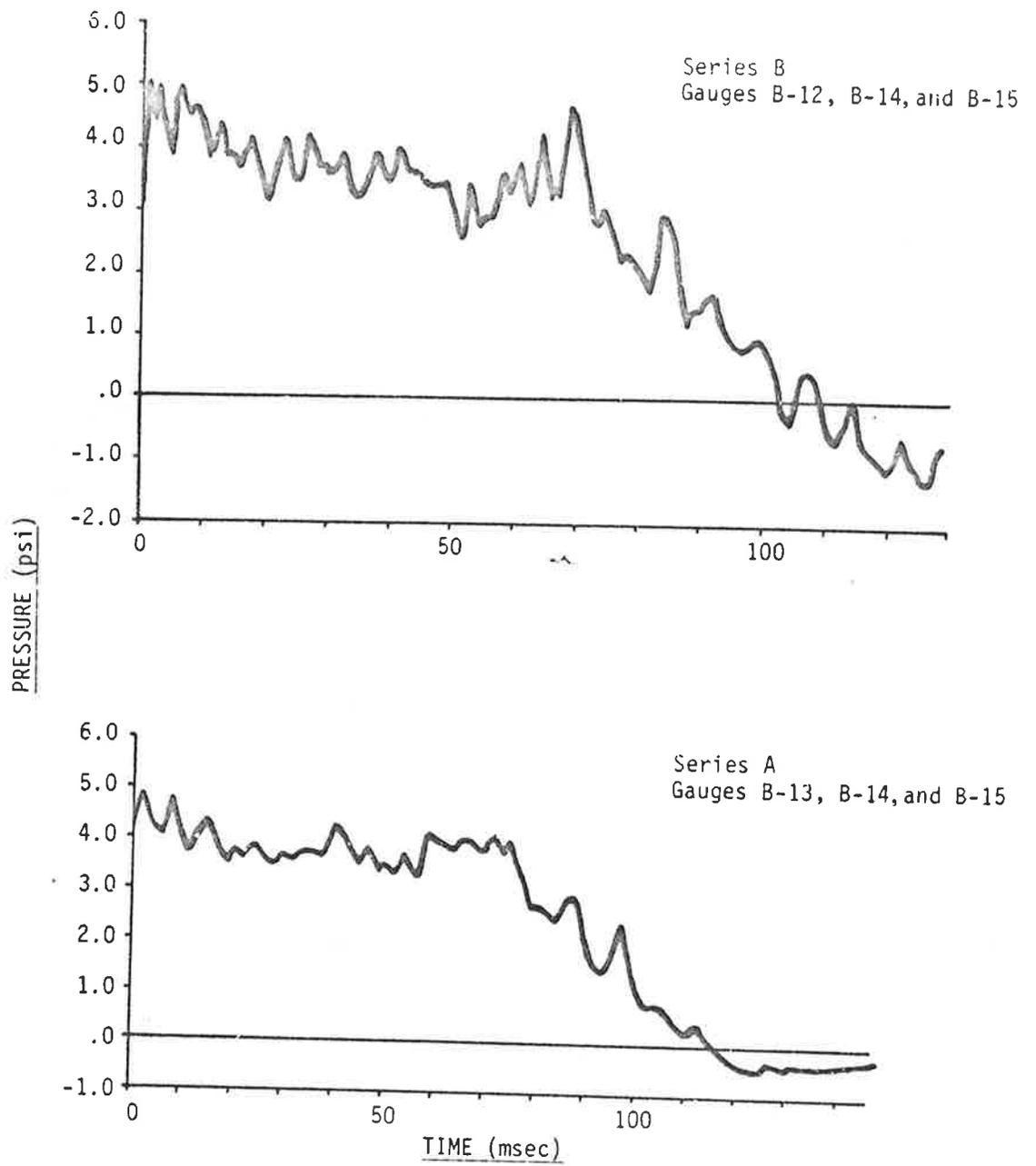
Fig. A-4. Average Overpressure vs Time on a Solid Wall from Tests Using Two Strands of Primacord.

A-4

Fig. A-5. Average Overpressure vs Time on a Solid Wall from Tests Using One Strand of Primacord.

Fig. A-6. Average Net Pressure vs Time from Paired Gauges on a Wall with a Doorway from Tests Using One Strand of Primacord.

A-6
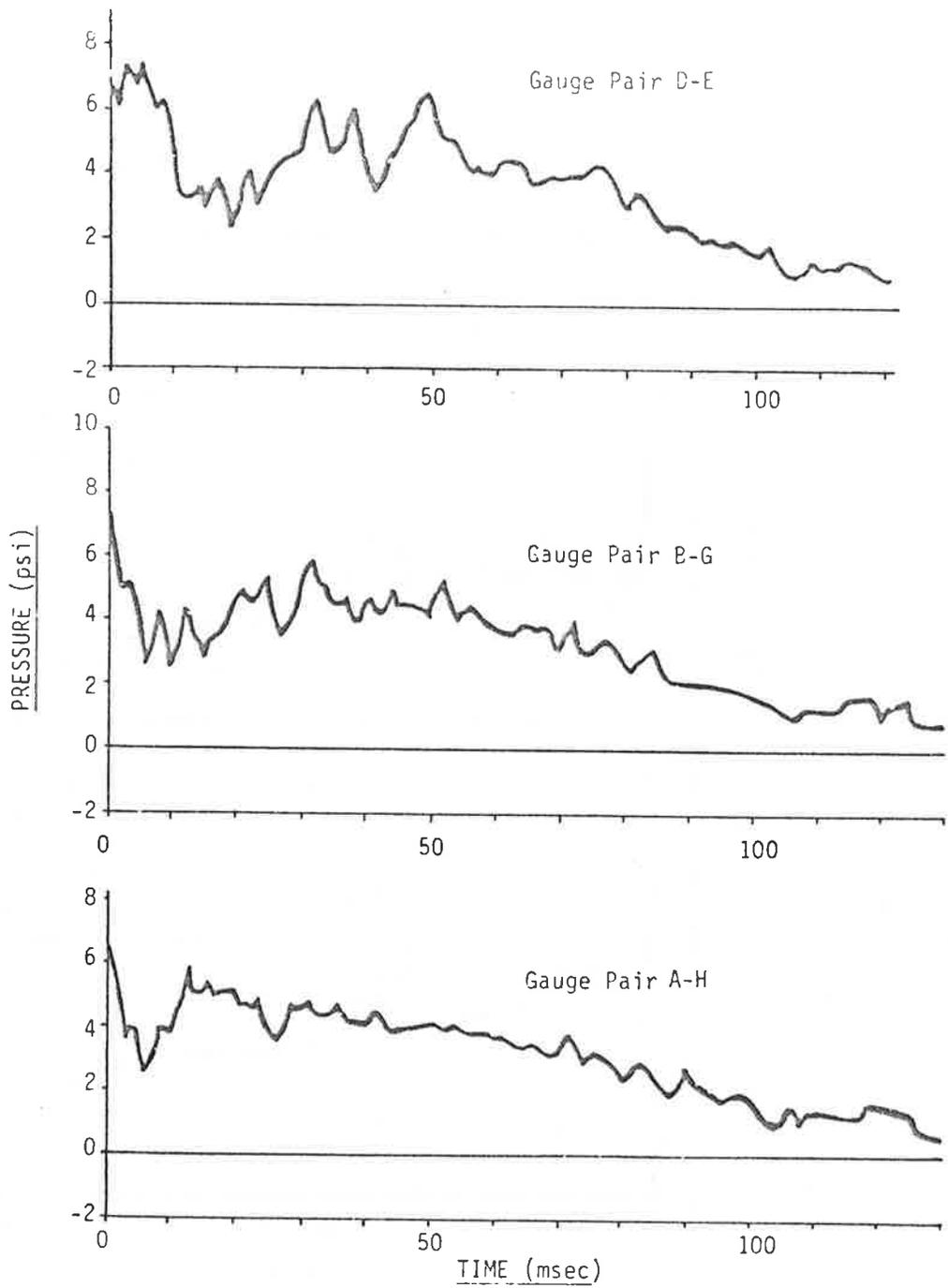
Fig. A-7. Average Net Pressure vs Time from Paired Gauges on a Wall with a Doorway from Tests Using Three Strands of Primacord.
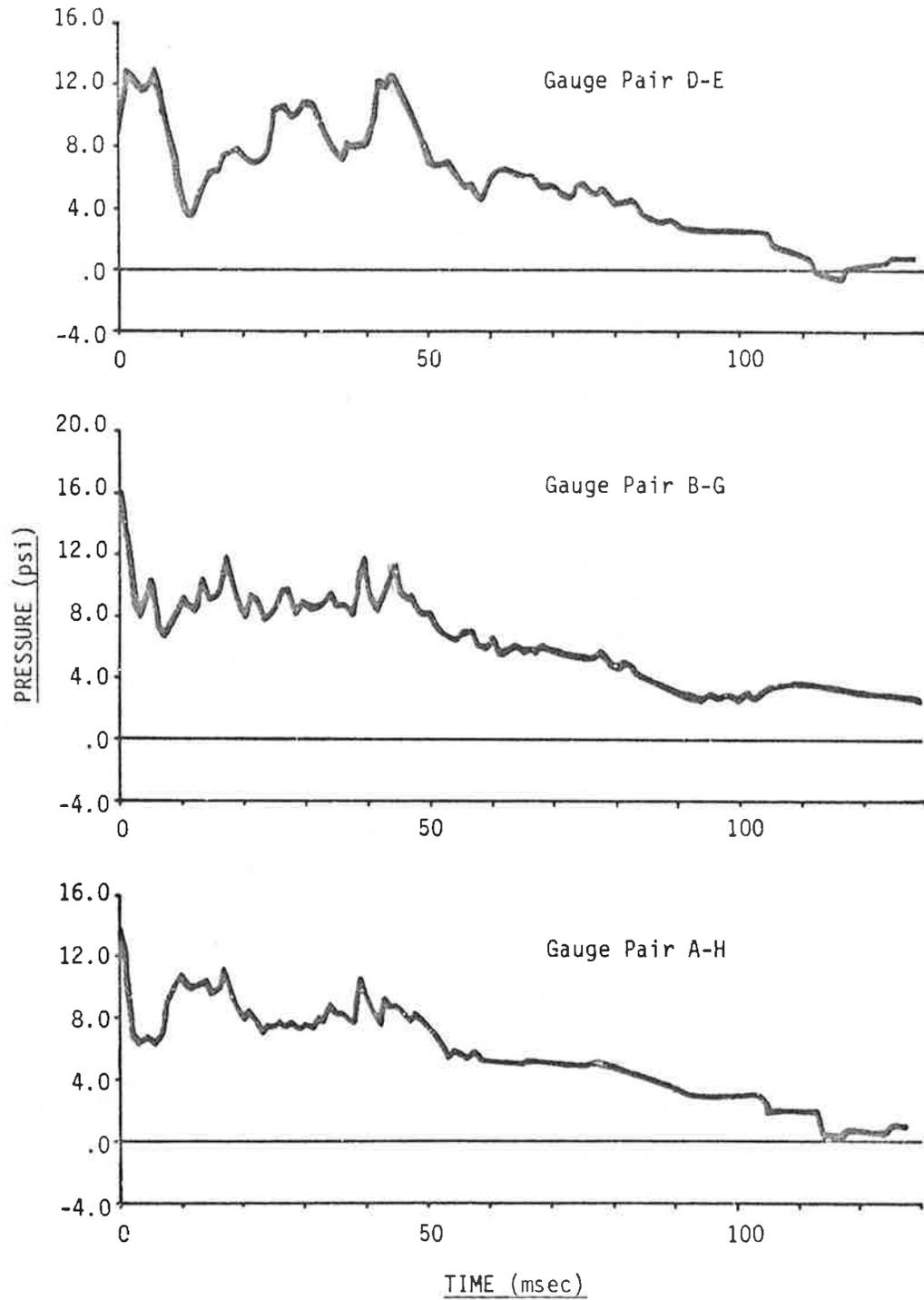
A-7

Fig. A-8. Average Net Pressure vs Time from Paired Gauges on a Wall with a Doorway from Tests Using Five Strands of Primacord.
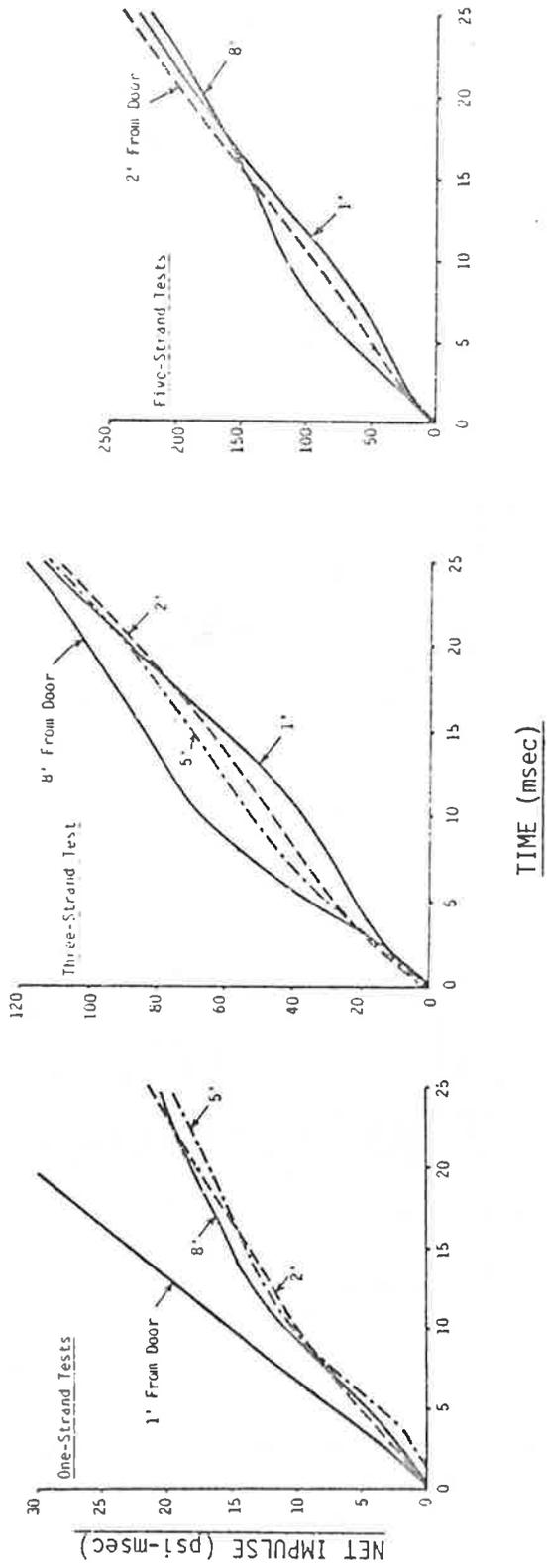
A-8

Fig. A-9. Net Impulses vs Time on a Wall with a Doorway at Various Distances from the Doorway from Tests with One, Three, and Five Strands of Primacord.
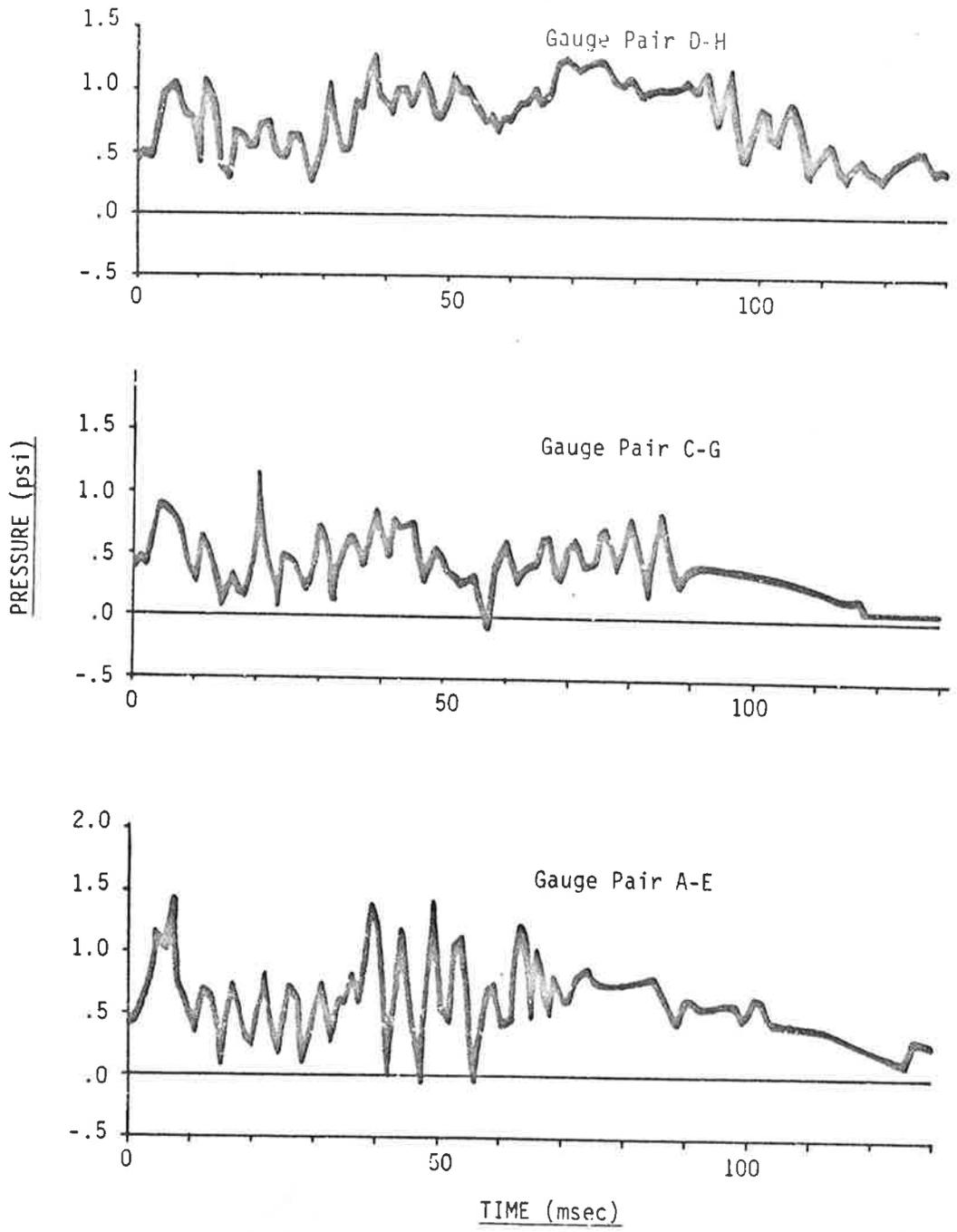
Fig. A-10. Average Net Pressure vs Time from Paired Gauges on a Wall with a 38-in. x 62-in. (17%) Window Opening from Tests Using One Strand of Primacord.
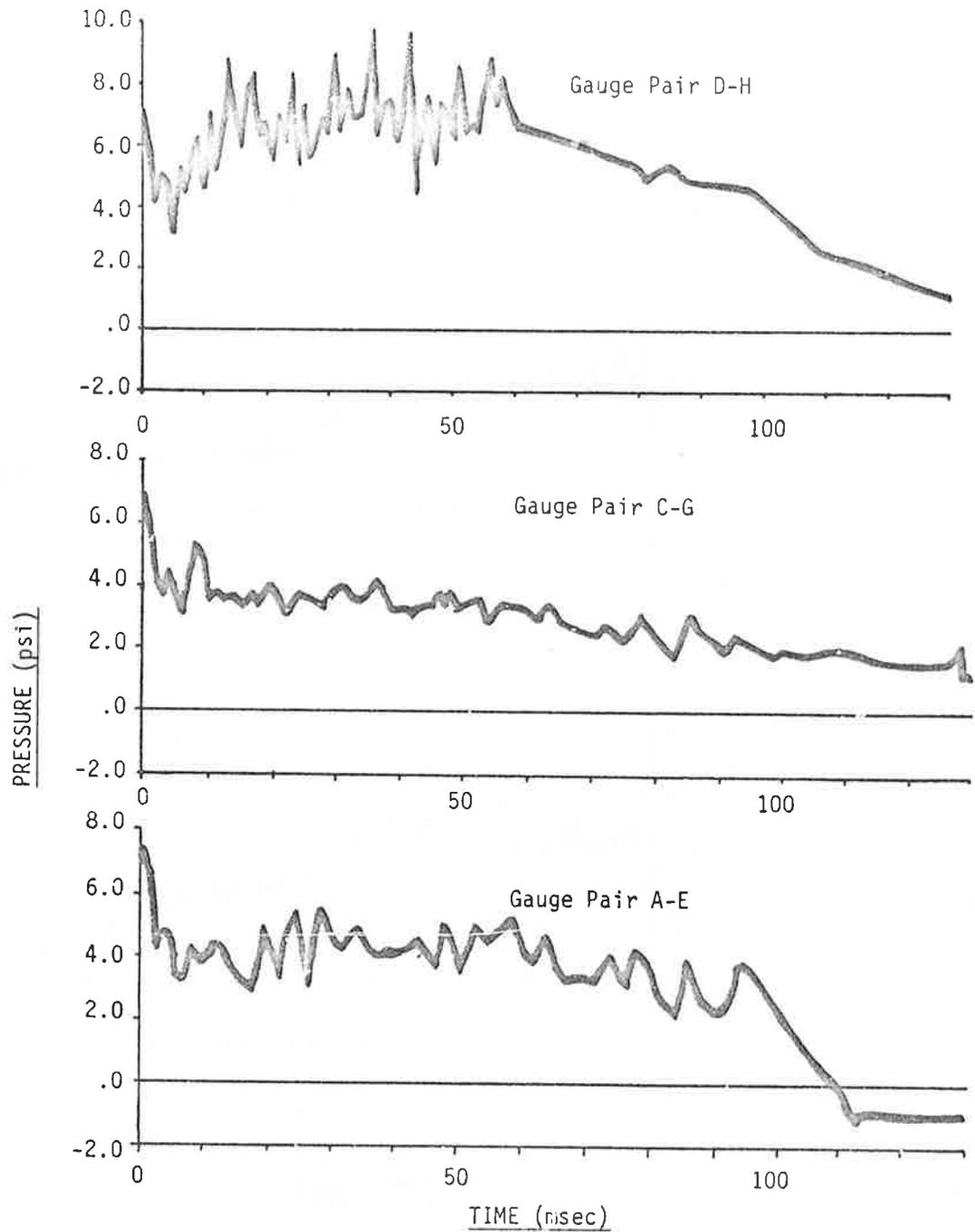
A-10

Fig. A-11. Average Net Pressure vs Time from Paired Gauges on a Wall with a 38-in. x 62-in. (17%) Window Opening from Tests Using Three Strands of Primacord.
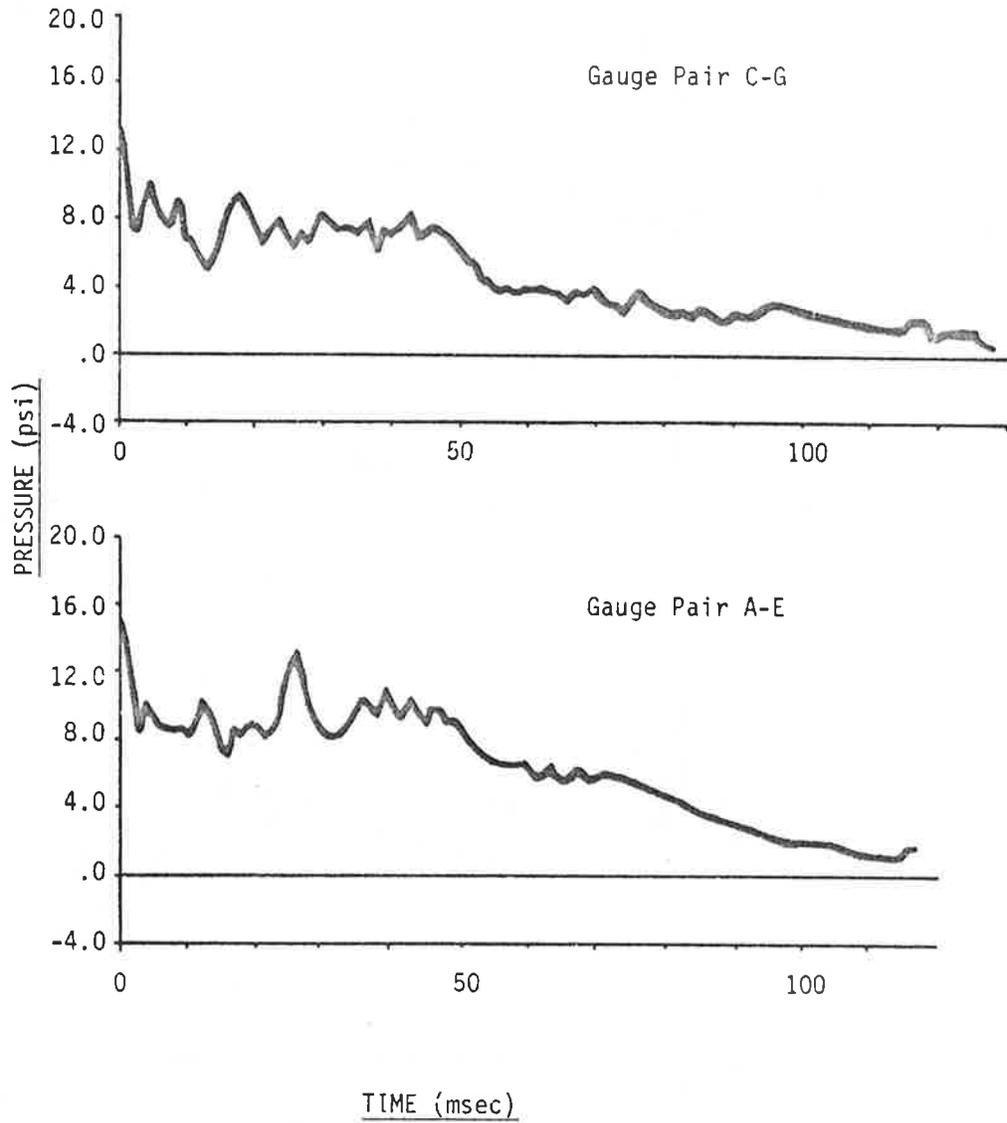
A-11

Fig. A-12. Average Net Pressure vs Time from Paired Gauges on a Wall with a 38-in. x 62-in. (17%) Window Opening from Tests Using Five Strands of Primacord.
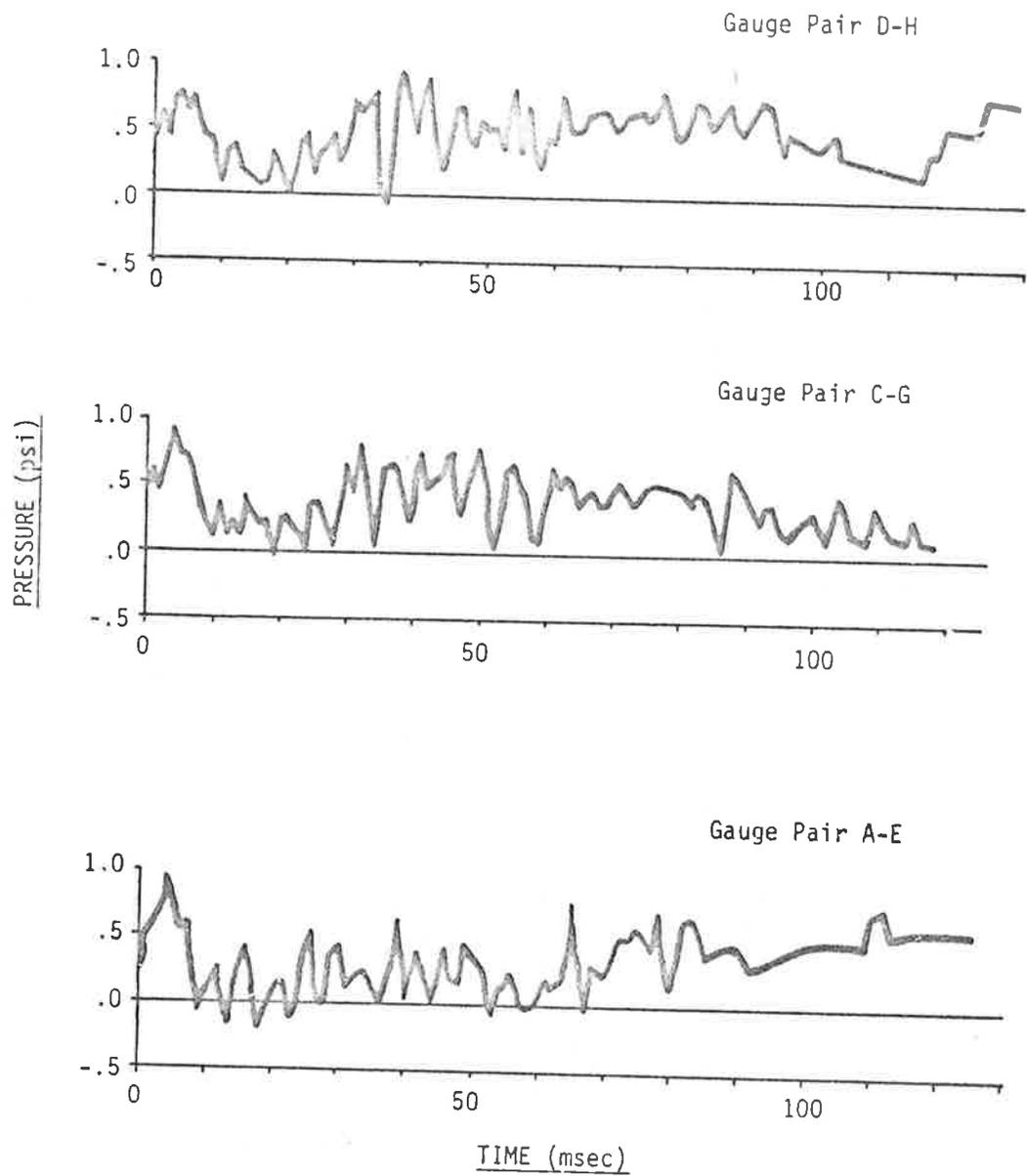
A-12

Fig. A-13. Average Net Pressure vs Time from Paired Gauges on a Wall with a 64-in. x 62-in. (27%) Window Opening from Tests Using One Strand of Primacord.

A-13

Fig. A-14. Average Net Pressure vs Time from Paired Gauges on a Wall with a 64-in. x 62-in. (27%) Window Opening from Tests Using Three Strands of Primacord.

A-14
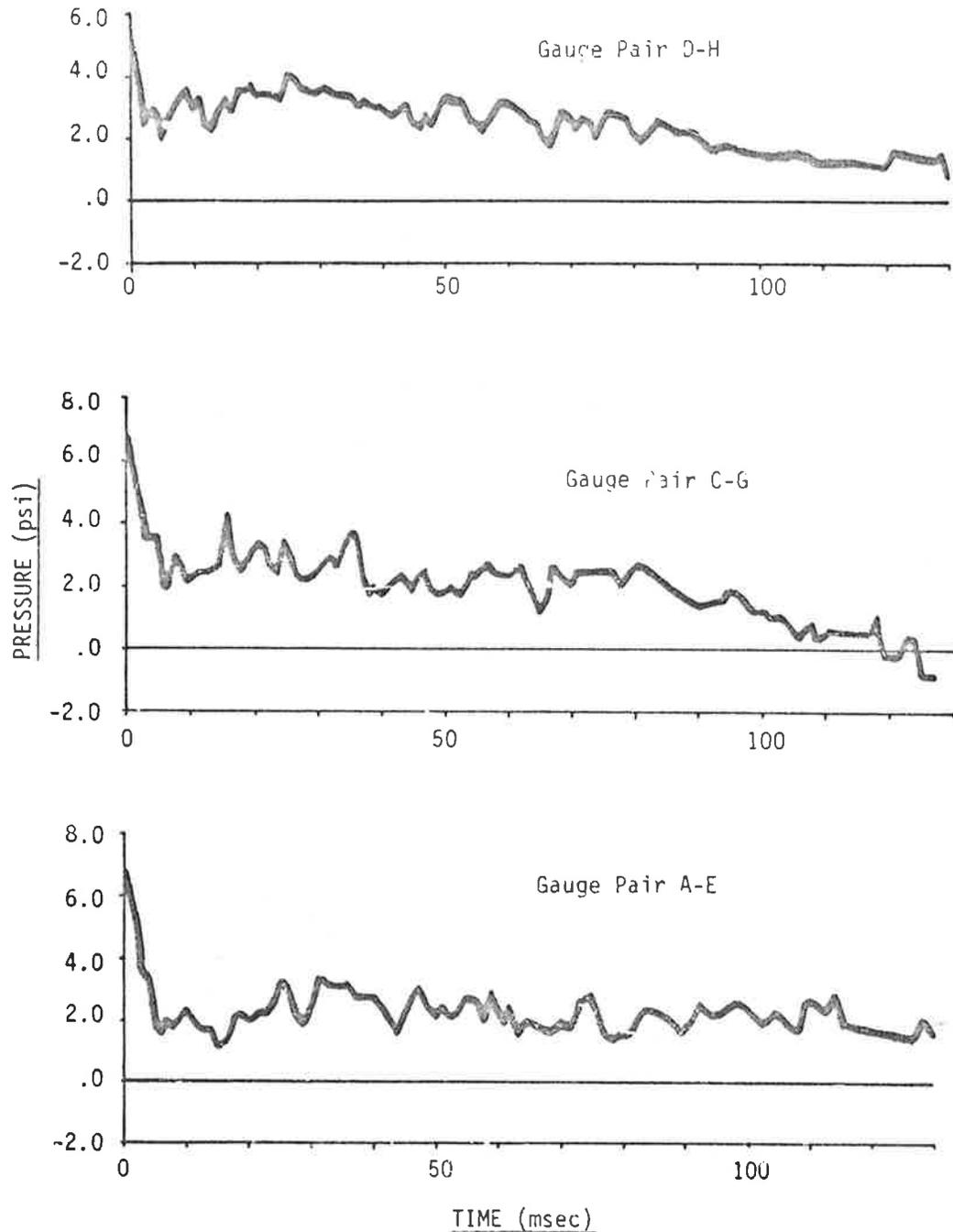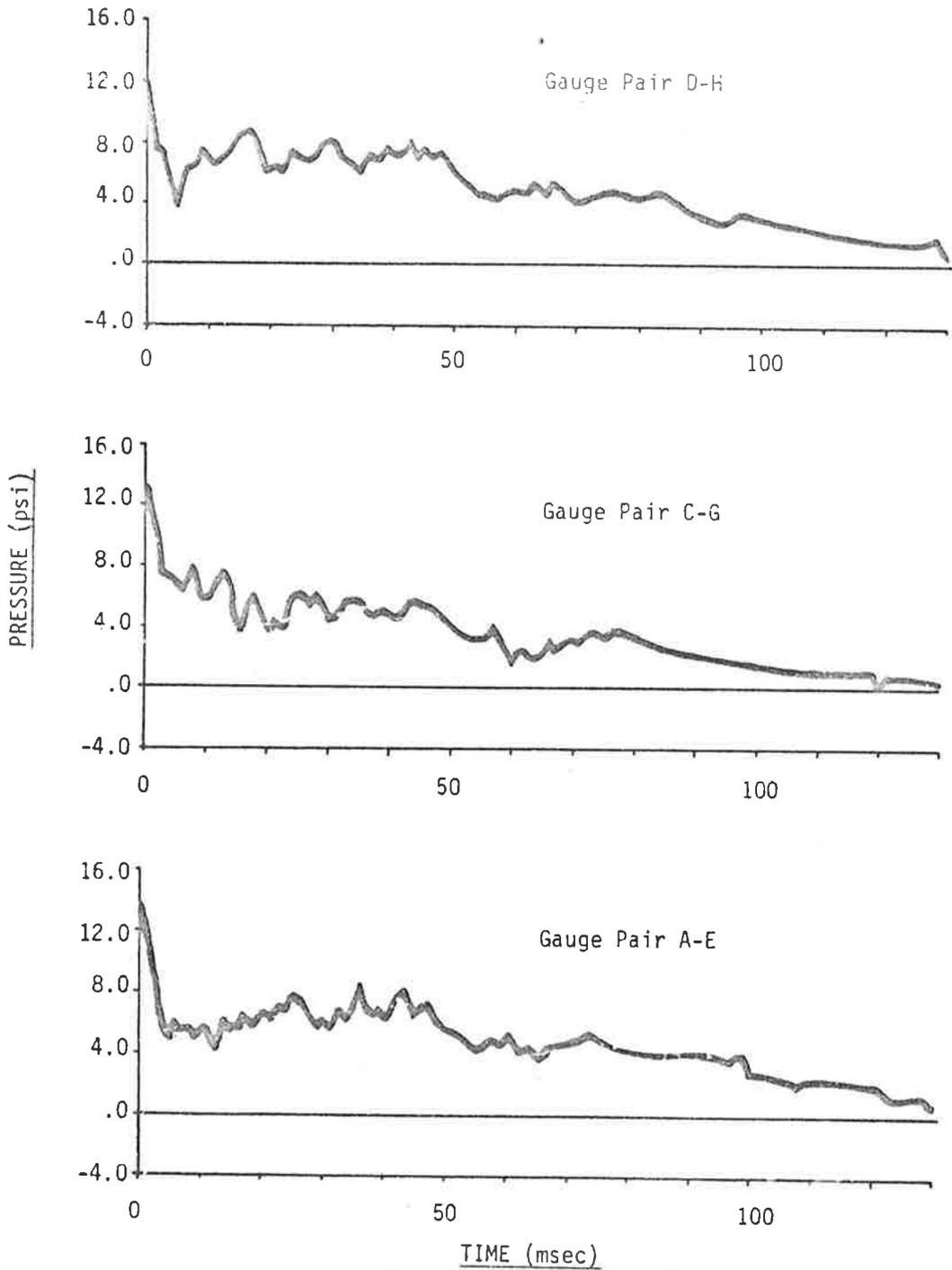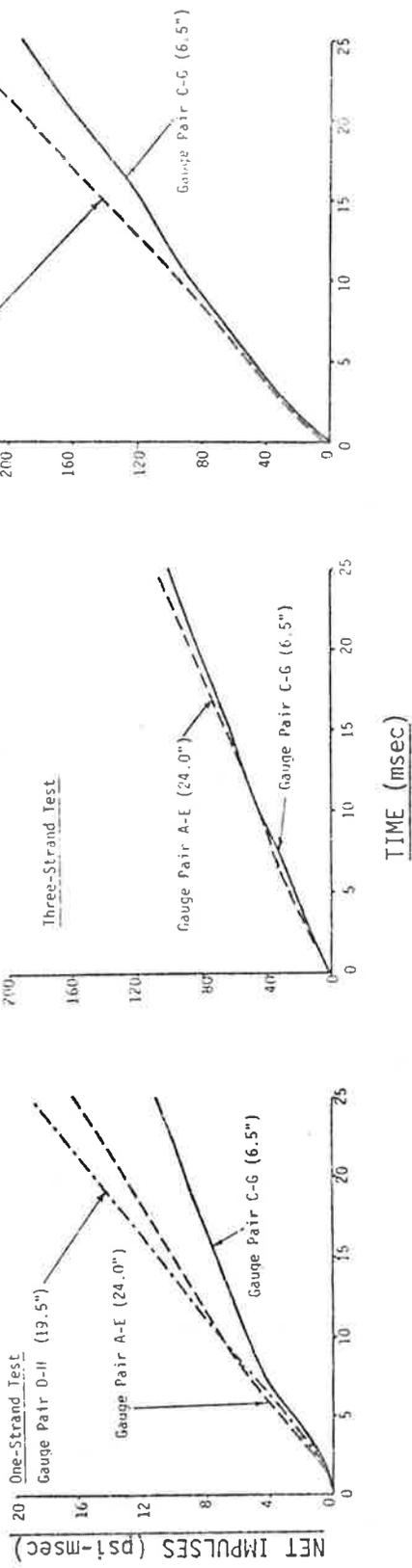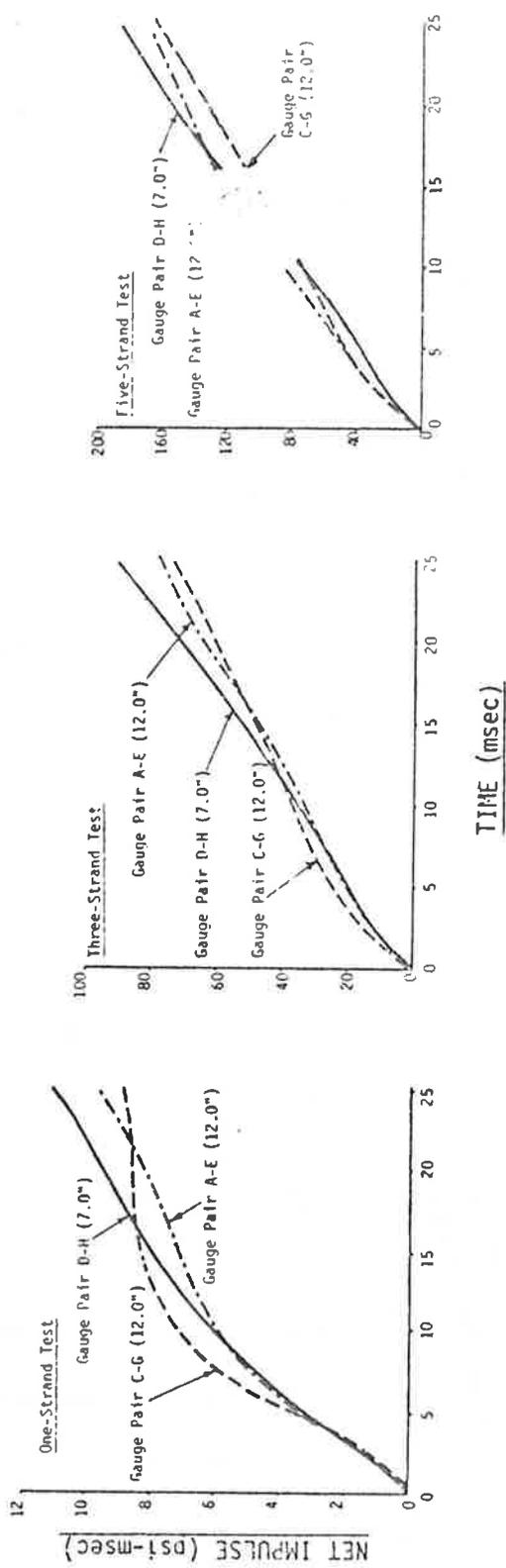
Fig. A-15. Average Net Pressure vs Time from Paired Gauges on a Wall with a 64-in. x 62-in. (27%) Window Opening from Tests Using Five Strands of Primacord.

A-15

Fig. A-16. Wall with a 38-in. x 62-in. (17%) Window Opening. Localized Net Impulses from Tests with One, Three, and Five Strands of Primacord. Numbers in Parenthesis Give Distances of Gauge Pairs from Windows (see Fig. 2-12).

A-16

Fig. A-17. Wall with a 64-in. x 62-in. (27%) Window Opening. Localized Net Impulses from Tests with One, Three, and Five Strands of Primacord. Numbers in Parenthesis Give Distances of Gauge Pairs from Windows (see Fig. 2-13).

A-17

Fig. A-18. Average Pressure vs Time on the Rear Wall of a Room with a "20%" Window from Tests with One, Two, and Three Strands of Primacord.

A-18
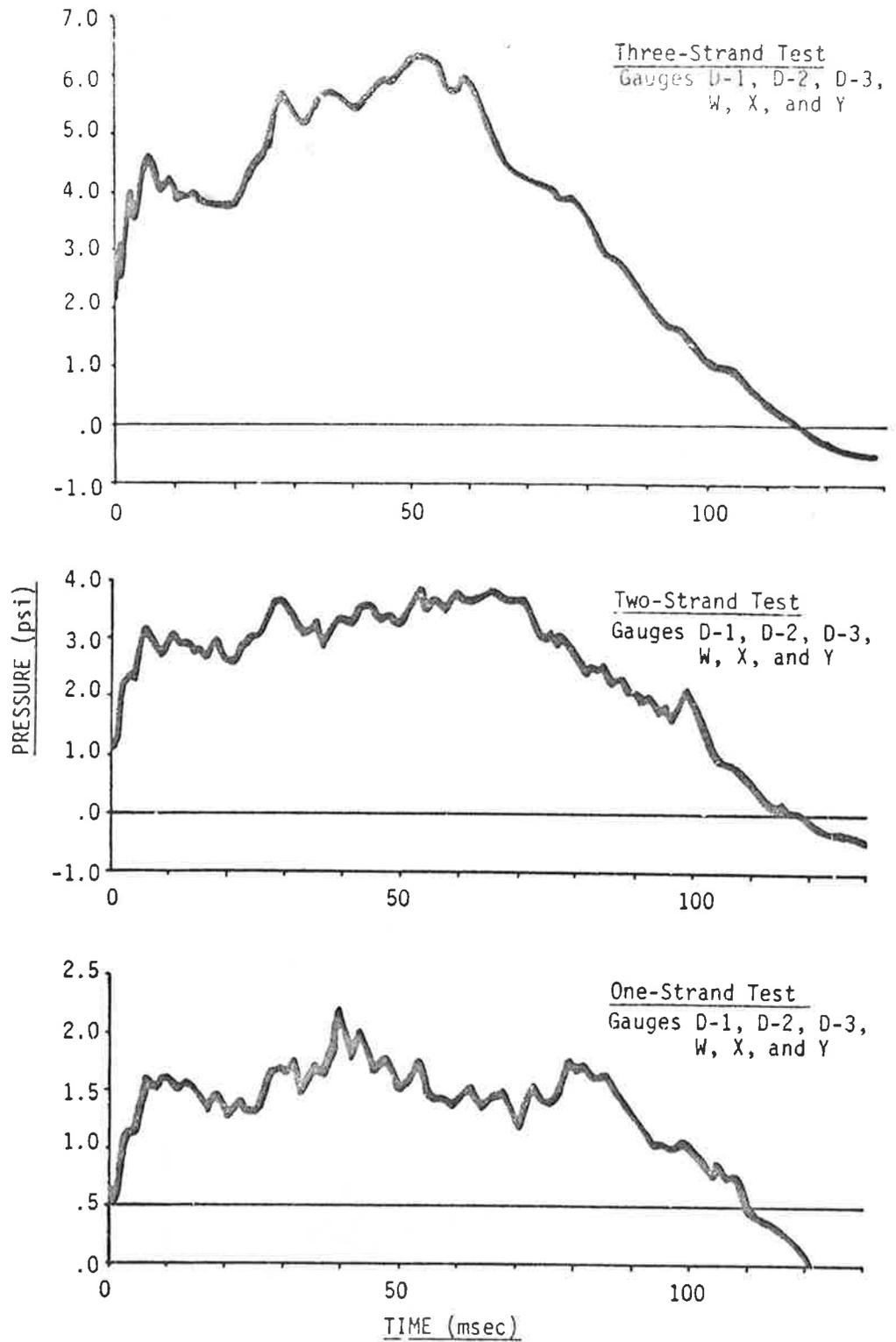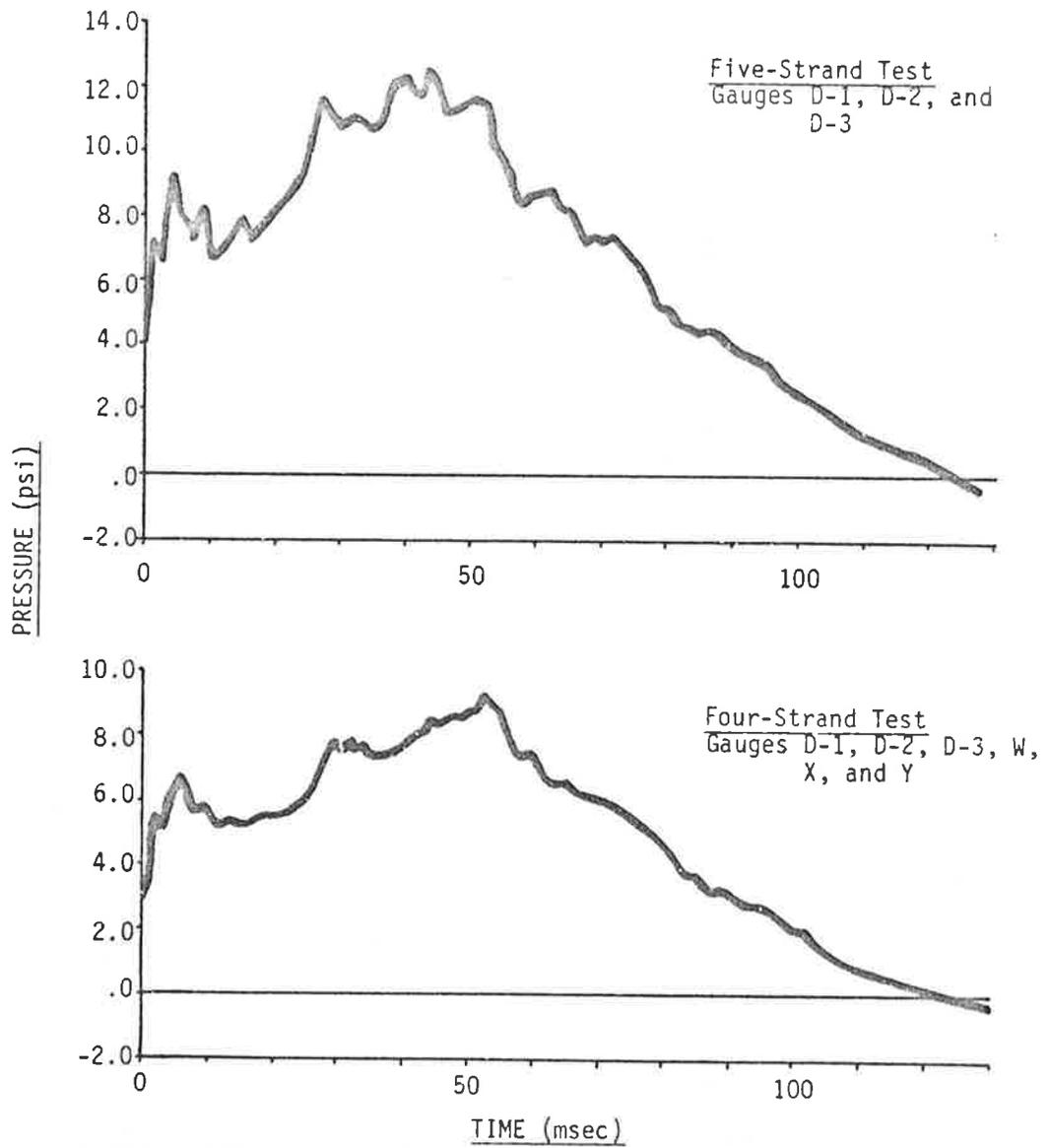
Fig. A-19. Average Pressure vs Time on the Rear Wall of a Room with a "20%" Window from Tests with Four and Five Strands of Primacord.
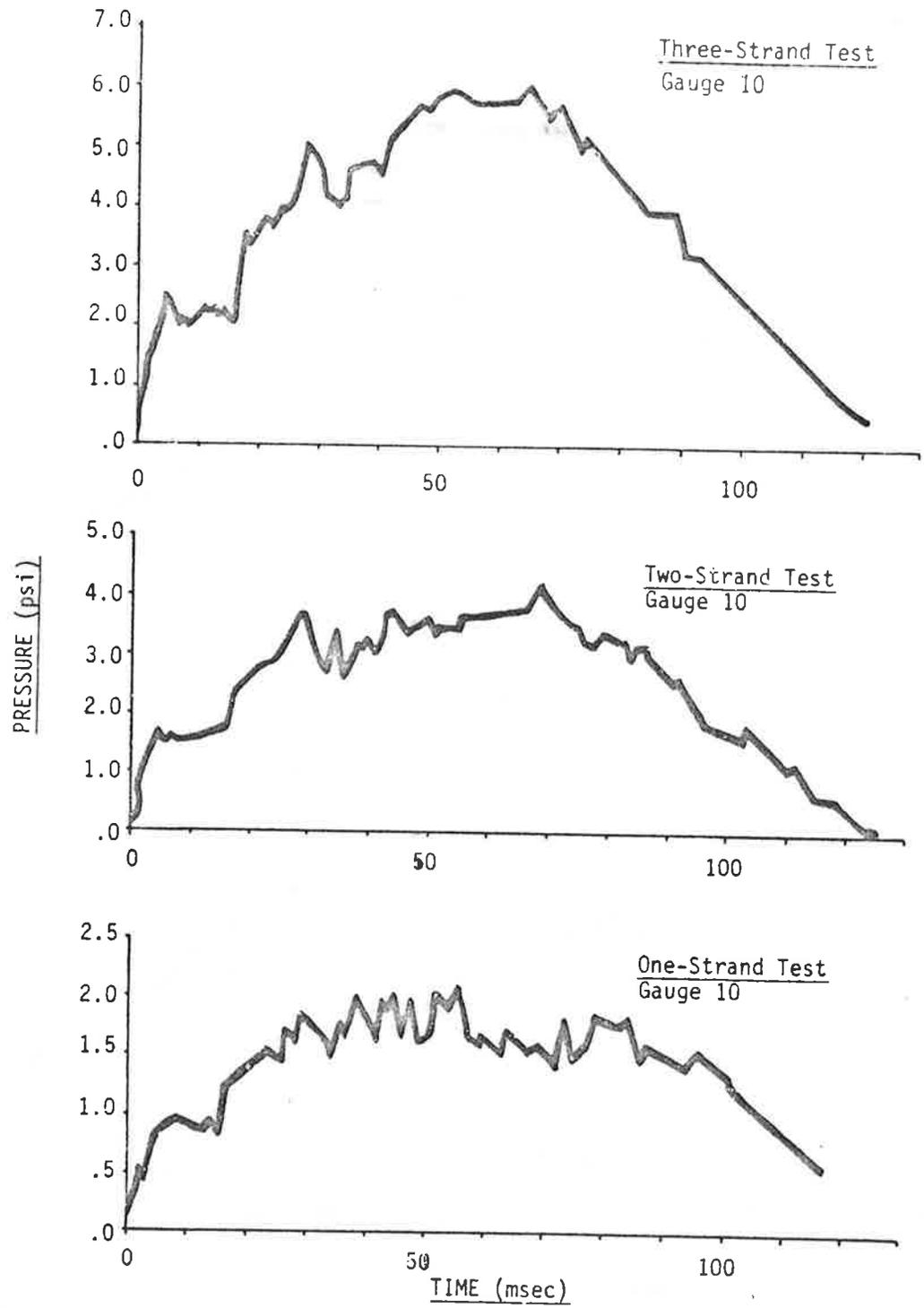
Fig. A-20. Average Pressure vs Time Inside a Room with a "20%" Window from Tests with One, Two, and Three Strands of Primacord.

A-20
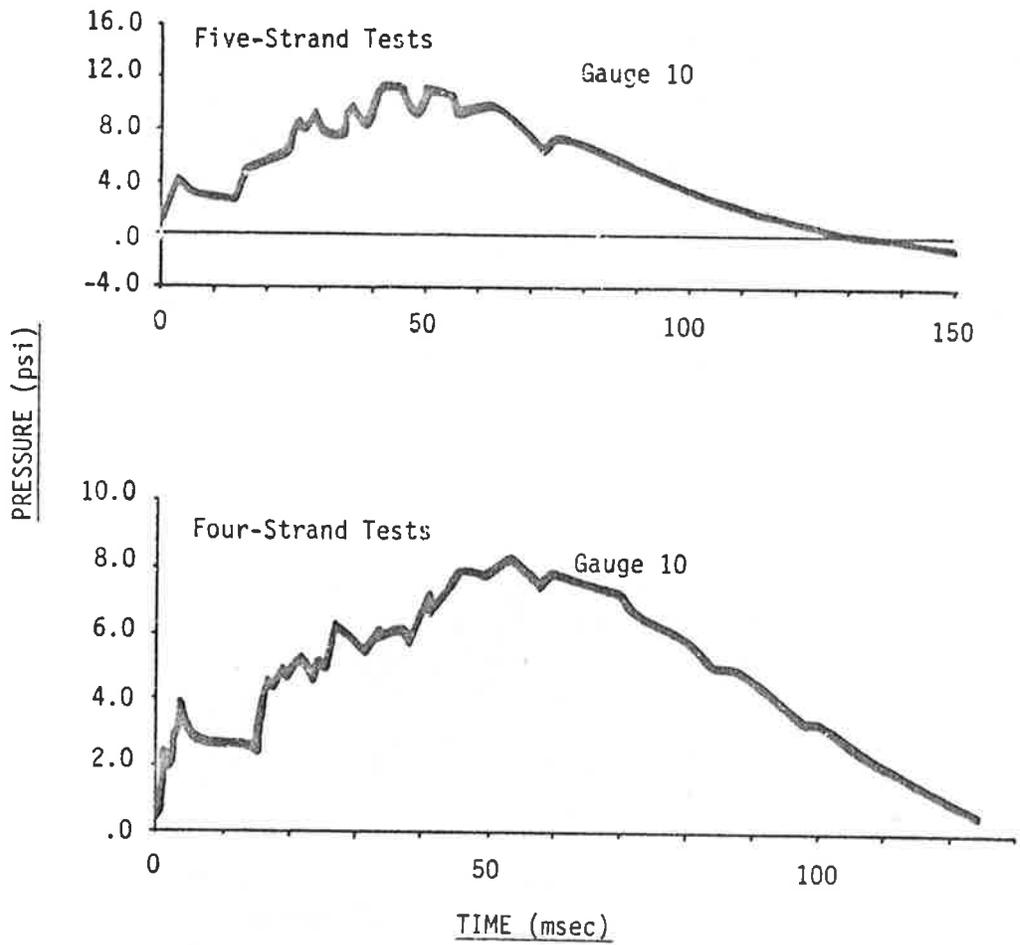
Fig. A-21. Average Pressure vs Time Inside a Room with a 20% Window from Tests with Four and Five Strands of Primacord.

Fig. A-22. Net Loading vs Time on the Front Wall of a Room with a "20%" Window from Tests with One, Three, and Four Strands of Primacord.
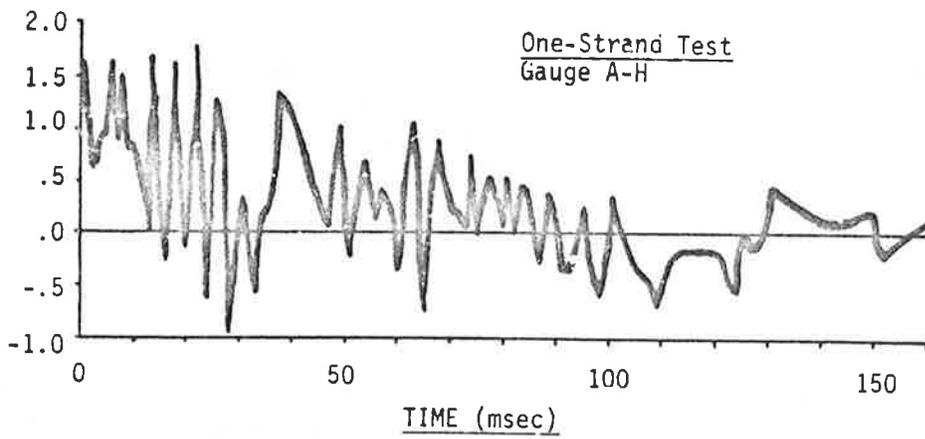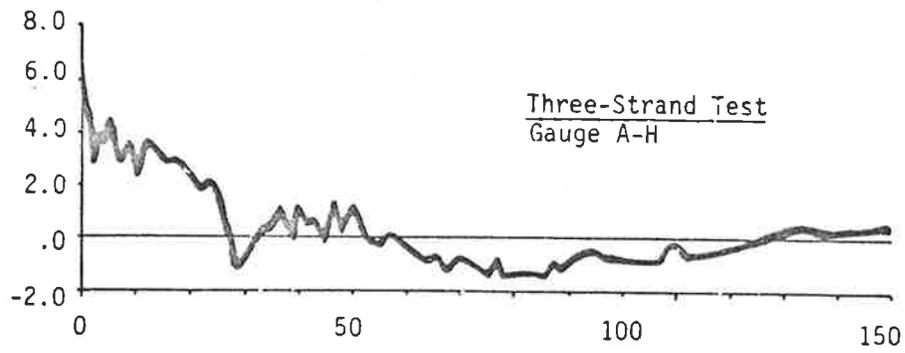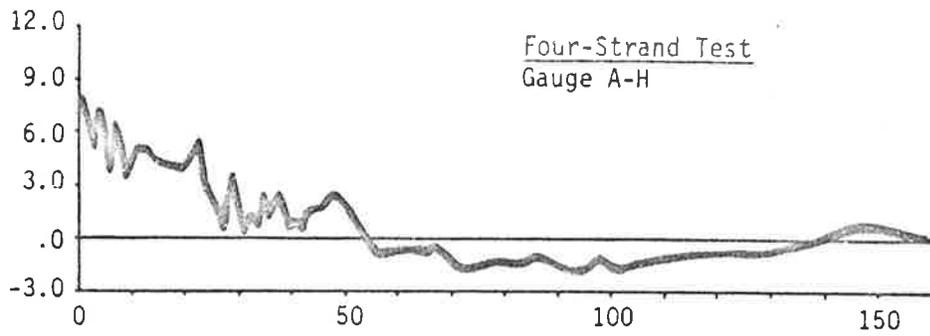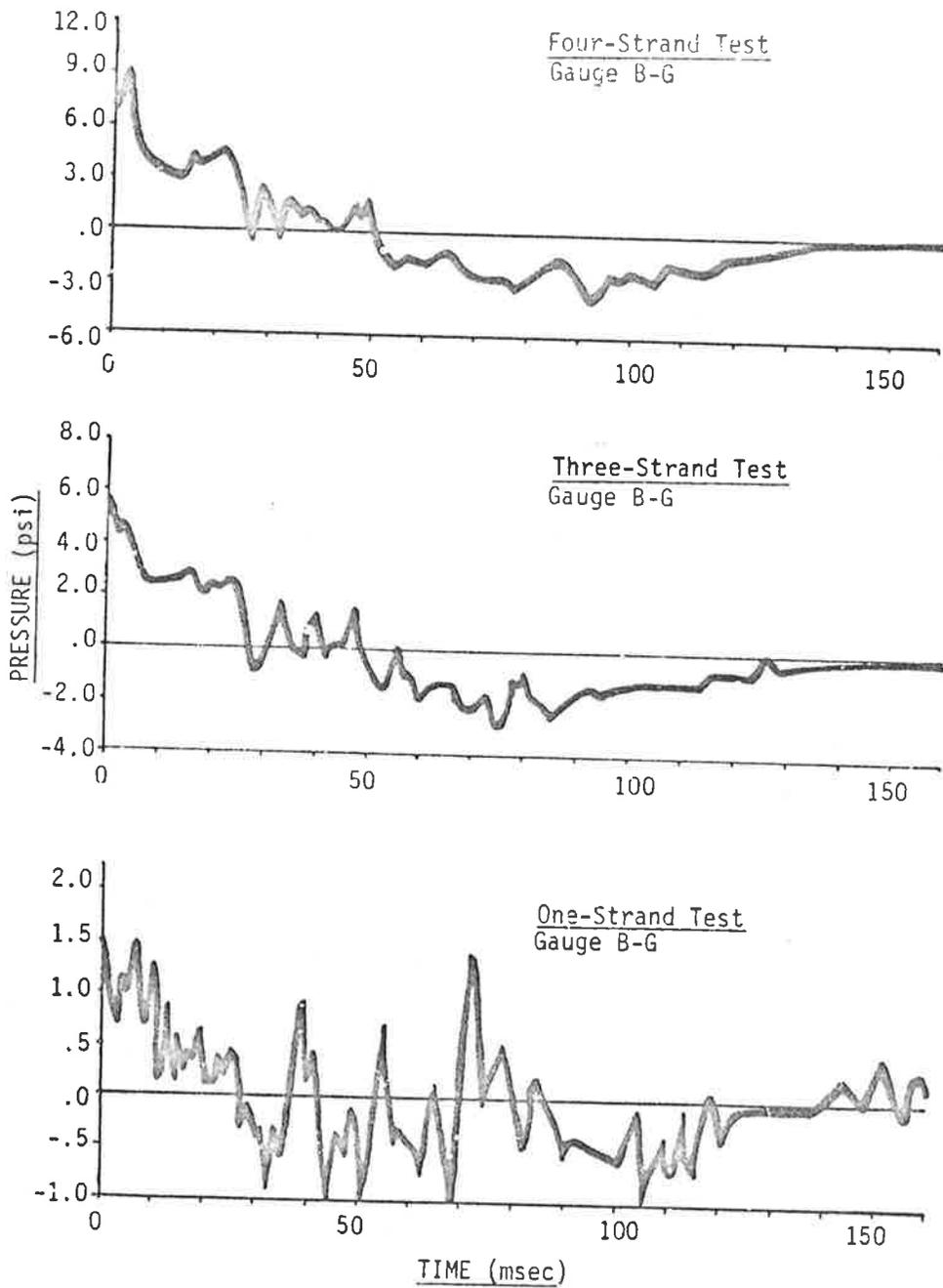
A-22

Fig. A-23. Net Loadings vs Time on the Front Wall of a Room with a "20%" Window from Tests with One, Three, and Four Strands of Primacord.

A-23

THE SHOCK TUNNEL:
HISTORY AND RESULTS
Volume III
WALL PANEL ANALYSIS AND TESTS

ABSTRACT

This is Volume 3 of a five volume report which summarizes the results
of a program conducted by the Defense Civil Preparedness Agency to determine
blast resistance of wall panels typically found in existing structures. Such
information was needed to determine the blast sheltering capability of struc-
tures in the National Fallout Shelter Survey inventory and to develop means
for upgrading these structures.

This volume is concerned with the dynamic response and failure of full-
scale wall panels. Included are the development of theories of wall panel
response and the results obtained from the testing of full-scale wall panels
in the shock tunnel.

Volume 1 of this report describes the shock tunnel facility used for the
experimental testing of full-scale wall panels. Included is a summary of the
capabilities of the shock tunnel for dynamic loading and response studies and
brief summaries of various experimental programs conducted in the shock tunnel
which were not related to the wall panel test program.

Volume 2 presents the results obtained from the experimental program
conducted in the shock tunnel to determine the loadings which are received
by wall panels mounted in the test section.

Volume 4 describes the static test program conducted to determine the
physical properties of the wall panels, and to assist in the development of
failure theories.

Volume 5 summarizes the predicted failure pressures for wall panels
based on the theoretical and experimental results covered in Volume 3 and
the static test data in Volume 4.

Table of Contents

Table of Contents (cont.)

References

List of Figures

List of Figures (contd)

vi

List of Figures (contd)

vii

List of Figures (contd)

List of Figures (contd)

ix

List of Figures (contd)

x

List of Figures (contd)

xi

List of Figures (contd)

List of Tables

Section 1
INTRODUCTION

This program, to investigate the dynamic response and failure of walls subjected to blast loadings, involved the development of theories of wall response and failure, and tests on full-scale walls to verify -- and provide information for -- the theories. The majority of the effort was devoted to walls of unreinforced masonry, because an analysis of the characteristics of buildings in the National Fallout Shelter Survey showed that the preponderance of shelter spaces were in buildings with such walls (Ref. 1).

Mounting and configuration of walls were varied. Represented among these were bearing walls, curtain walls, infill walls, solid walls and some containing window or doorway openings. Most effort was devoted to walls supported on two edges, thus resembling beams, though walls supported on four edges (plate-mounted) were also treated.

Two basic types of support conditions were investigated; mountings which permitted free rotation of the wall elements about the supports (termed "pinned" or "simple" supports); and mountings in which rotation about the support was restricted (termed "moment resisting" supports). For the latter an additional restriction was occasionally adopted, viz, that displacements of the supports in a direction parallel to the plane of a wall face were prohibited. This added constraint converts the moment resisting supports to so-called "rigid" supports.

Effort was concentrated on walls with pinned support conditions, because these are more common in real structures. In some cases, however, "rigid" support conditions can be closely approached in structures (as with infill wall in massive frames), so that special consideration of this condition was merited. Walls with "rigid" supports that prevent in-plane wall motion even after flexural cracking occurs (generally at the edges and center of the wall) are termed "arching walls", because fractured portions wedge themselves

1-1

between frame members and develop substantial resistance to out-of-plane forces (such as with blast loads).

The blast tests on full-scale walls were conducted in the shock tunnel, the general development and operation of which are detailed in Volume 1 of this series. In brief, the tunnel, shown in a cutaway drawing in Fig. 1-1, consisted of a 63-ft long, 8-ft diameter steel cylinder, closed at one end (termed the "compression chamber"); an 8-ft long transition section; and a 92-ft long rectangular, concrete-walled, tunnel section 8½ ft high and 12 ft wide (termed the "expansion chamber") near the end of which test walls were placed.

The tunnel was operated as a shock tube by means of the volume detonation technique with Primacord as the explosive material. In this mode of operation, Primacord is distributed symmetrically throughout a section of the compression chamber portion of the tunnel. On detonation of the Primacord (which proceeds at a rate of about 20,000 ft/sec), a quasi-static pressure is built up rapidly throughout the entire compression chamber. The expansion of this high-pressure gas into the remaining part of the tunnel generates the desired shock wave. The strength of the shock wave was varied by varying the numbers of strands of Primacord from one to eight. The loadings received on the test walls for the various test arrangements used are given in Volume 2.

Details of wall construction, transportation, and mounting techniques used for these tests are given in Appendix A. Instrumentation included pressure gauges for monitoring loading, load cells for measuring load transmitted from the panels to fixed supports, gauges for determining time of cracking of walls, displacement and velocity gauges for measuring wall motions, and high speed photography for monitoring overall response. The basic instrumentation system is described in Volume 1.

Three different computer codes were used to predict wall panel behavior under blast loading. All three used the so-called "Finite Element" method in which a continuous structure is modeled (mathematically) by an assemblage

Fig. 1-1. Cutaway View of Shock Tunnel Showing Wall in Place.

Compression Chamber

Expansion Chamber

Test Wall

63 FT

8 FT

92 FT

1-3
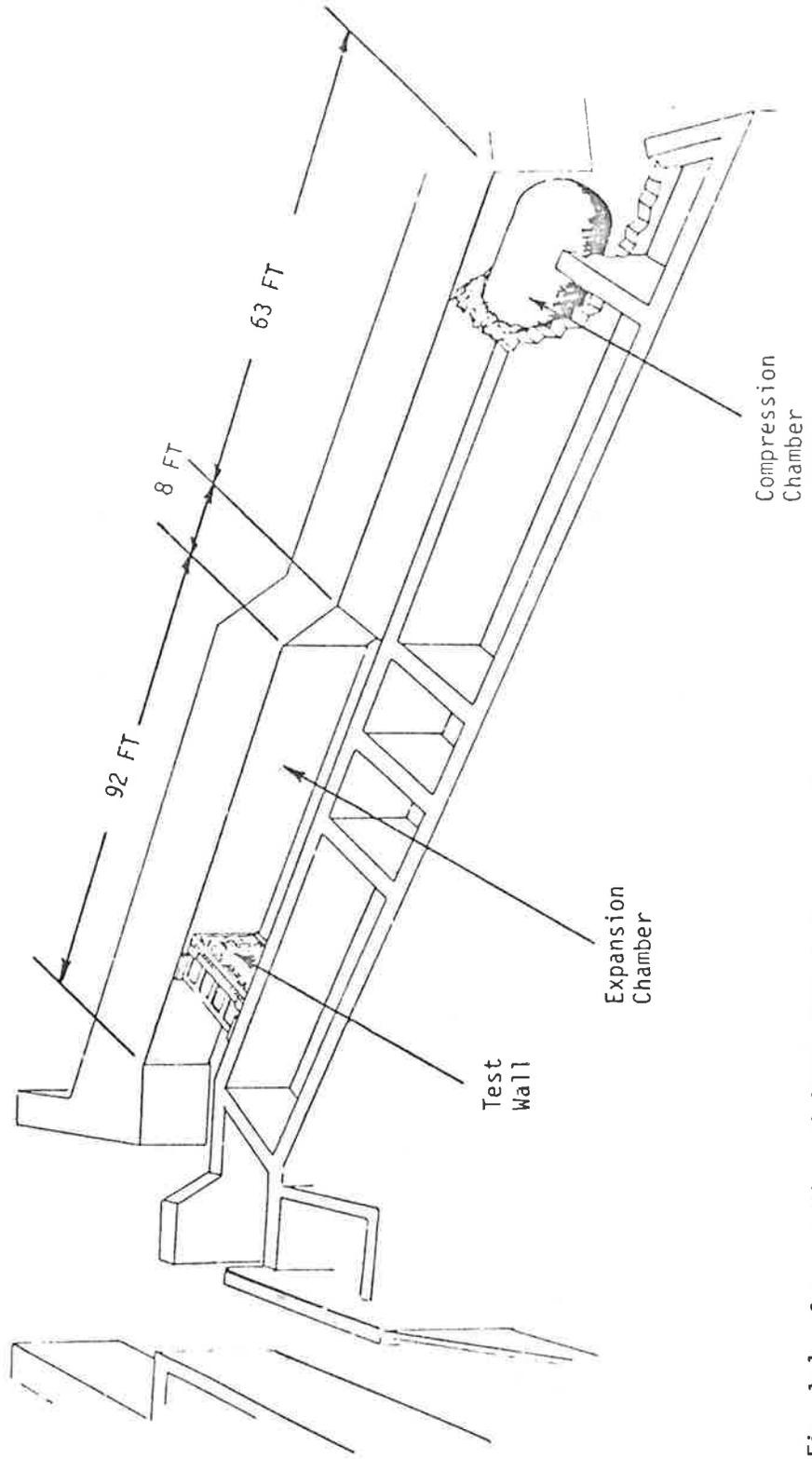
of individual elements of various shapes and sizes, interconnected at a finite number of points known as nodal points or nodes. Based on the material properties of the structural materials, matrices are then written to obtain element stresses and node displacements under the forces imposed on the structure.

With judicious selection of element size and node locations, the behavior of the model will closely approximate the behavior of the real structures under the applied loads, and within the limits of the theory used. In the analyses conducted for this program, only linear elastic theory was employed, thus information on panel behavior generated by the computer analyses was restricted to the linearly elastic domain.

The initial computer effort was directed toward developing dynamic response information on both beam- and plate-mounted, non-arching walls. That effort employed one of the pioneer finite element codes, SAMIS, the acronym for Structural Analysis and Matrix Interpretive System. SAMIS was developed by Philco Corporation, Western Development Laboratories, with R.J. Melosh serving as project engineer (Ref. 2).

Two different codes were used in the analysis of arching walls. The first -- the Mechanical Analysis of Continuously Elastic Systems (MACE), available on the Tymeshare System -- is of modest capability, and it only provides nodal displacements from static loads. It is very fast, however, (and thus economical) and was used to deveop analytic information to aid in the analysis of the first tests on arching wall panels.

The second code, STARDYNE, developed by the Mechanics Research Institute and accessible through Control Data Corporation on their CYBERNET service system, is a considerably more sophisticated code, with a much broader range than MACE. Only limited STARDYNE analyses were carried out, however.

Descriptions of the capabilities of the three codes, and of the mathematical models which they used are given in Appendix B.

Section 2 of this volume summarizes the work on solid walls supported as beams, and includes discussions of the blast resistance of preloaded wall panels; of the dynamics of wall behavior to the point of flexural failure; and of wall behavior after flexural failure (except for arching walls). It concludes with a description of the experimental results, and a comparison of these results with theory developed during the course of the program.

Section 3 deals with walls with windows and Section 4, with those with doorways. Both sections contain a discussion of dynamics of wall behavior up to the point of flexural failure, and a description of experimental results of tests on such walls.

Section 5 treats walls supported as plates. Calculations of wall behavior are presented for the same range of conditions treated for beams and comparisons are made with the experimental results for the one condition studied in the shock tunnel, a solid, pin-mounted wall.

Arching walls are discussed in Section 6, which includes a description of arching theory developed during the program, and a comparison of theoretical predictions with results of tests on wall panels specifically designed to arch.

The last section of this volume briefly summarizes work done on other wall types and mounting conditions to which limited effort was devoted during the program.

Note that, because of their large number, all figures in Sections 2 through 6 are put at the end of each section.

SOLID WALLS SUPPORTED AS BEAMS

GENERAL BEHAVIOR

A wall supported on two opposite edges (beam-mounted) may have one or both supports essentially fixed (as with a wall mortared to a floor), and capable of resisting moments; or pinned (as with a wall supporting a floor or roof structure, but not rigidly attached to it). It may also support only its own weight -- a non bearing wall -- or be preloaded by the weight of walls and other structural elements on top of it -- a bearing wall. (Effects of preload are discussed in the next part of this section and the special case of beam-mounted walls that permit arching is discussed in Section 6.)

In the case of uniform loading normal to a face, (as would occur when a blast wave strikes a wall head-on), a beam-mounted wall will bend. When the maximum tensile stress exceeds the wall material's tensile strength the wall will develop tensile cracks. For this case, the place on the wall at which maximum tensile stress occurs prior to flexural cracking depends on type of wall support and not on the magnitude of the load. With pinned supports, maximum tensile stress would occur halfway between supports. With either fixed-pin, or fixed-fixed supports, the maximum stress would occur at the supports. Immediately after flexural cracking occurs at a fixed support, however, it becomes essentially a pin support. Thus, both fixed-fixed, and fixed-pin supported walls can convert to pin-pin mounted walls, with subsequent flexural cracking occuring at the center of the walls.

After flexural cracking, the wall's motion is influenced by the fact that no tensile stress can be carried across a crack. If, for example, a wall had two pin-type supports and cracked in flexure at its center, it would subsequently behave as two distinct, though possibly touching, wall elements. Because of built up strains in the wall during its pre-cracking

2-1

stage, the individual elements might oscillate immediately after cracking, but for all practical purposes, the wall's resistance to blast thereafter would be provided by vertical in-plane forces, namely the weight of the wall elements, and any preload.

The general behavior of two walls of this type is illustrated in Fig. 2-1. The walls first bend (initial elastic phase), crack at the supports (secondary elastic phase), and finally crack at the center becoming two separate elements, touching at the center. (Bending is exaggerated in Fig. 2-1 for clarity.)

EFFECTS OF PRELOAD

The most general form of a wall is the preloaded wall, i.e., a wall that supports vertical load of upper walls, floors, and roof in addition to its own weight. (A non-bearing wall can be considered to be a special case of a preloaded wall, with preload equal to zero.) As is evident from Refs. 3 & 4, preloads can be applied at many different points between two faces of a wall. The maximum stabilizing effect of preload, however, occurs when it is applied to the downstream face of a wall.

The preload effect is most easily seen with a so-called curtain wall, in which individual stories of wall support only the weight of upper stories of the same wall.* A three story curtain wall is illustrated in Fig. 2-2. The first two stories of the walls in that figure are continuous both top and bottom, thus they may be visualized as walls with "fixed-fixed" type supports. The top story is continuous only at the bottom, and thus, it may be visualized as a wall with "fixed-pin" supports (essentially a propped cantilever).

Resistance to Statically Applied Loads

The important steps in the response of preloaded walls can be seen in Fig. 2-3 -- plots of resistance of two fixed-fixed walls to statically applied loads as a function of displacement at the centerlines of the walls. The curves are for walls with preloads of 2 w (the first story in Fig. 2-2), and of zero, and with flexural strengths, σ_r, of 150 psi. In each case, during the first two phases of motion, (i.e., prior to cracking at the center-line), the walls are still behaving elastically, and maximum displacement is

---

* In general, preloaded walls also support floor and roof loads, but the basic response of such walls can be masked by extraneous details such as the response of the various types of connections that may be used. Loads imparted by floors and roofs, however, are of the same order as those that will be considered. In heavy construction (e.g., concrete joist/floor) loads are on the order of 100 lbs per linear inch of wall width, which is equivalent to about the weight of two stories of 8-in. thick brick curtain walls. Lighter timber construction and roof systems impart preloads on the order of 25 lb/in., equivalent to about a half story brick curtain wall.

maximum bending of an elastic beam. After fracture at the centerline, maximum displacement can no longer be determined from elastic theory. Displacements during the two elastic phases are very small. They are shown in the figure in an inset with an expanded displacement scale.

Fig. 2-3 shows that wall resistance to cracking at the center was less than resistance to cracking at the base. For very weak walls, however, the opposite can occur; resistance to center cracking can be larger than resistance to base cracking. It was shown in Ref. 5, however, than even when this occurs, elastic strain energy stored in such a wall prior to its cracking at the base is frequently capable of causing a dynamic excursion adequate to crack the wall at its center with no additional load applied.

In Fig. 2-3, the effect of preload on resistance during the two elastic phases is slight, changing the resistance at which cracking occurs, either at the base or at the center, by less than 10%. This is principally because compressive stress created by the preload (about 14 psi) is relatively small compared with the wall tensile strength in flexure (σ_r = 150 psi) used to derive the figure.

Even a relatively small preload appears to have a substantial effect during the third, post-fracture phase, however. After the wall cracks at both the base and the centerline, only the preload and the weight of the wall resist blast loading. When the preload is applied at the downstream edge of the wall, it is twice as effective in generating resistance as the wall weight (concentrated at the wall center). The preload used in Fig. 2-3 is twice as large as the wall weight itself, and thus contributes substantially to wall resistance during this phase. In the figure, however, the post-fracture resistances of both preloaded and unpreloaded walls are far smaller than their elastic phase resistance. Thus a pulse whose pressure was adequate to crack these walls, would certainly cause their failure if its duration were long enough, failure being defined as movement of the wall centerline great enough to cause wall instability under gravity alone. For this to occur, the upstream edge of the centerline crack must move one wall thickness.

2-4

With weaker walls pre-fracture resistance can be smaller than post-fracture resistance. With σ_r = 50 psi, for example, a fixed-pin wall subject to a preload of w would crack at the base with p = 0.40 psi while its post-fracture resistance would be 0.56 psi.

Another facet of preloaded walls considered in the program (Refs. 5 & 6) is the failure of systems of bearing and/or curtain walls. The important conclusion of that study is that the strength of the system of walls can approach the strength of the weakest wall as a lower bound.

Resistance to Dynamically Applied Loads

A uniform loading applied suddenly to one face of a wall supported as a beam, will cause it to deflect further than it would under the same loading statically applied. The maximum fiber stress generated by these deflections will also be larger for suddenly applied loadings than for static loadings, and thus the resistance of a wall to a particular value of loading will be smaller.

The ratio between maximum deflections under dynamic and static loading is termed the dynamic load factor, or DLF. If a wall behaves as a simple un-damped elastic system, a step load -- that is, a constant load applied with a rise time of zero -- would cause a maximum deflection twice as large as that caused by a static load. For rise times between static and step load-ings, the DLF (as well as the time required to attain maximum deflection) depends on the magnitude of the rise time of the loading relative to the natural period of the wall, in the manner shown in Fig. 2-4 (from Ref. 7).

The maximum fiber stress generated by loadings applied to preloaded, beam-mounted walls with pin-pin supports is given by:

$$\sigma = \frac{pD\ell^2}{8zL} - \frac{P + W/2}{t\ell} \qquad (2-1)$$

where: p = loading pressure

D = dynamic load factor

2-5

ℓ = wall height

L = wall length

t = wall thickness

z = wall section modulus = $t^2/6$

P = preload per unit length of wall

W = wall weight per unit length of wall.

DYNAMICS OF WALL BEHAVIOR PRIOR TO FLEXURAL FAILURE

Appendix B contains a description of the computer program (SAMIS) used to develop predictions of the behavior of solid, beam-mounted walls under blast loading before they cracked in flexure. In the following material, some of the more important results of these calculations are presented. In all cases, the loading is a single step loading similar to that shown in Fig. B-1A, but with its maximum value normalized to 1 psi.

The results of SAMIS calculations for beam-mounted, solid walls are summarized in Figs 2-5 through 2-9. In each figure the "A" plot is for walls with pin-pin supports, and the "B" plot, for walls with fixed-fixed supports. The displacement and velocity vs time of a single node (360) near the centerline of the wall are shown first, followed by a comparison of displacements vs time of three nodes (10,160, and 310) along the horizontal centerline of the wall, and a contour display of the maximum downstream displacement of the entire wall. Stress* vs time at one triangular element (9) near both the edge of the wall and its horizontal centerline is then shown, followed by a contour plot of stress over the entire wall at the time of maximum downstream displacement.

Fig. 2-5A for a wall pinned at both top and bottom indicates that, under a 1 psi load, the maximum displacement of a node near the wall center is about 0.05 in. and occurs at a time of about 17 msec (when velocity at that point goes through zero and reverses direction). The differences in response caused by replacing the pinned supports with fixed supports can readily be seen by comparing Fig. 2-5B with Fig. 2-5A. The maximum displacement of the wall with fixed-fixed supports is less than one quarter that of the wall with pin-pin supports (about 0.012 in. vs 0.050in.), and it occurs in less than half the time (about 8 msec vs 17 msec). Clearly the fixed-fixed wall is far stiffer than the pin-pin wall, with a natural frequency about twice as great.

---

* Direction of the principal stress at element 9 can be found in Ref. 8.

The same basic patterns are seen in Fig. 2-6, plots of displacements at three different points on the wall. In addition, however, Fig. 2-6A shows that for a pin-pin wall, there is a high degree of uniformity of displacement as a function of time all along the horizontal centerline of the wall; for a node at the wall edge (10), one at quarter point (160), and one at the center (310), the displacement curves lie almost one atop the other. This is not quite the case for the fixed-fixed wall (Fig. 2-8B), in which the maximum displacement at the center of the wall is about 20% larger than the displacement at the wall edge.

The contours of maximum displacement in Fig. 2-7 show the differences in patterns of displacements at various points on the wall. Fig. 2-7A shows the substantial uniformity of maximum displacement with the pin-pin wall suggested by Fig. 2-6A. Except at the very edges of the wall near the centerline, the contours are very nearly parallel to each other. Fig. 2-7B indicates a greater relative variation in maximum displacement across the face of the fixed-fixed wall than across the face of the pin-pin wall (though the absolute value of maximum displacement is still only about one quarter as large)*. In addition, the greatest displacement occurs at the center of the fixed-fixed wall, but at the edges along the horizontal centerline of the pin-pin wall.

Stresses in the wall follow patterns similiar to those of wall displacements. As can be seen in Fig. 2-8, stress in an element of the fixed-fixed wall has about one quarter the maximum magnitude, and about twice the natural frequency as that in the same element of the pin-pin wall. Similarly, the maximum stress contours of Fig. 2-9 show a greater uniformity of stress across the face of the pin-pin wall, than across the face of the fixed-fixed wall.

For loading pressures other than 1 psi, at any time prior to the occurrence of flexural cracking, displacements can be found from Figs. 2-5 and 2-6, and stresses from Fig. 2-8 by multiplying the displacements and stresses

---

* Note that the slight "hollowing effect", i.e. greater displacement at the center than the edge is caused by the flexibility of the girder and the Poissons Ratio effect.

2-8

given on those figures by the actual step loading pressures in psi. In
addition, Fig. 2-8 can be used to determine at what time a particular wall
will begin to crack under a given loading if the flexural strength of the
wall is known. If , for example, a wall with pin-pin supports has a flexural
strength of 120 psi and is subject to a blast loading of 3 psi, it would be
expected to begin to crack at a time of about 5 msec, i.e., when the stress
from a 1 psi loading is 40 psi. At that time, the stress from a 3 psi load-
ing pulse would be 120 psi, the flexural strength of the wall.

Note that the loading that would just cause cracking to occur in this
wall is about 0.55 psi, (the loading that would lead to maximum stress in
Fig. 2-8A of 120 psi instead of about 220 psi). Thus, a 3 psi loading is
about 5.5 times that at which cracking would be initiated.

WALL BEHAVIOR AFTER FLEXURAL FAILURE

After a blast-loaded, beam-mounted wall with pinned supports cracks in flexure, the individual wall elements, still being accelerated by the blast load, continue their overall motion downstream.* (The response of walls with fixed supports after their flexural failure is discussed later in the arching wall section.) As long as the elements remain in contact with the wall supports and each other, their weight and any preload borne by the wall before blast loading modify the tendency of the blast load to overturn the elements or accelerate them downstream. To bound the problem, calculations of wall motion after flexural failure were made first for the case in which preload contributes to wall stability to the maximum extent possible (preload applied in the plane of the downstream face of the wall), and second, for the case in which it contributes most to wall instability (preload applied in the plane of the upstream face). A free-body diagram for the case in which preload adds to wall stability is shown in Fig. 2-10.

Assuming that the wall elements stay in contact with their supports immediately after they crack in flexure, the angular rotation θ, and the rotational velocity ω, as functions of time, t, for either half of the wall of Fig. 2-10 up to the point at which the centerline of the wall has moved one wall thickness can be written as:

$$\theta = 6 \; kt^2/2 \; m\ell^2 \qquad \text{and} \qquad \omega = 12 \; kt/m\ell^2 \qquad (2\text{-}2)$$

In these equations, for the walls preloaded in the plane of the tension face, $k = [(p\ell/2) - (P + W/2) \theta_0]$ and for walls preloaded in the plane of the compression face, $k = [(p\ell/2)]$ where ℓ, p, W and θ_0 are as given in Fig. 2-10, and m = the wall's mass per unit area.

_____

* The elastic strain energy stored up by the individual elements during the wall's bending (flexure) phase, manifests itself as oscillations of the elements, which may still be in contact with their supports, and thus transmitting loads to them. The nature and effects of these oscillations are discussed in Ref. 9.

For 8-in. thick brick walls and for blast loading pressures of 4 psi and above (incident blast pressure ≈ 2 psi) it was shown in Ref. 10 that the errors in angular velocity would be less than 10% if preload and wall weight were both neglected. Eqs. 2-2 then become

$$\theta = 3\ p\ell^2/4m\ell \qquad\qquad \text{and} \qquad\qquad \omega = 3\ pt/2m\ell \qquad\qquad (2\text{-}2a)$$

As was noted earlier, preloaded walls in the shock tunnel were both supported and preloaded halfway between tension and compression faces. Equations of wall motion for such walls, however, are identical to Eqs. 2-2.

After walls have failed completely (that is, after the wall centerline has moved one wall thickness, rendering the wall elements unstable under their own weight) the two halves of the wall can be considered to be free of their supports. While still rotating, they would be accelerated downstream by the blast wave (if the duration of the blast were long enough). It was shown in Ref. 10 that for incident blast waves of 2 psi and above, the total horizontal velocity imparted to the upper wall element whose thickness is "s"

$$v_x = [(3/4)^{\frac{1}{2}} + (1/3)^{\frac{1}{2}}]\ [(ps/m)^{\frac{1}{2}}] = 1.44\ (ps/m)^{\frac{1}{2}} \qquad\qquad (2\text{-}3)$$

in which $[(3/4)(ps/m)]^{\frac{1}{2}}$ is the velocity acquired by the wall element prior to wall failure (approximately the velocity of its center of mass from Eqs. 2-2a) and $[(1/3)(ps/m)]^{\frac{1}{2}}$ is the velocity acquired after wall failure.

EXPERIMENTAL RESULTS

A total of 23 solid, non-reinforced, masonry walls with simple beam supports were subjected to 32 separate tests in the shock tunnel. Nineteen of the walls were of brick, two of concrete block, and two of clay tile. A summary of the types of tests conducted, and of their general results is given in Table 2-1.

Massive Brick Walls

Three walls (50, 51, and 52) nominally 12 in. thick, were tested. Walls No. 50 and 51 were tested at peak loading pressures of 4.0 and 4.3 psi respectively, and failed.*

Wall No. 52, however, was subjected to a series of four tests, three at peak loading pressures of 1.5 psi. These tests were conducted to determine the wall's natural period and to look for possible presence of "low-level fatigue" effects, that is, effects of multiple loadings prior to wall failure. (See Ref. 11 for a discussion of low-level fatigue.) No signs of failure could be detected after any of these low pressure tests. On the fourth test a loading pressure of 4.2 psi was applied and the wall collapsed. The bottom half of the wall rotated until it struck the floor; the top half rotated approximately 90 degrees and landed on the bottom half. (Pre and posttest photographs of the wall are shown in Fig. 2-11.) A plot of displacement of the wall centerline as a function of time is given in Fig. 2-12.

---

* In discussing the shock tunnel test results in this volume, loading pressure -- that is, the pressure actually experienced by a wall -- is employed in place of incident pressure -- the pressure in a blast wave before it stikes a test wall. For a solid wall, the loading pressure is the same as reflected pressure. For walls with windows and doorways, only the initial loading pressure is reflected pressure. Actual differences between incident, reflected, and loading pressures for other cases are discussed as needed in the appropriate sections.

Table 2-1

Summary of Tests on Non-Reinforced Masonry Walls
Without Openings Supported as Simple Beams

Wall No.	Loading Pressure (psi)	Maximum Total Load (kip)	Natural Period (msec)	Crack Gauge Readings (msec)	Initial Preload (kip)	Wall Behavior
Massive Brick Walls (12-in. Thick)						
50	4 0			13		Failed
51	4.3			15		"
52a	1.5		38			No Sign of Failure
52b	1.5		38			"
52c	1.5		38			"
52d	4.2	74.0		12.5, 13.2		Failed
Interior Walls (8-in. Thick Concrete Block)						
58a				9, 15		Cracked
58b	1.5	11.6				Failed
59a			30-35			No Sign of Failure
59b	1.5	10.5		15.3, 19.3, 20.4		Failed
Interior Walls (6-in. Thick Hollow Clay Tile)						
62a			37			No Sign of Failure
62b	1.5	9.8				Failed
63a			-			No Sign of Failure
63b	1.5	12.2		18, 22.5, 23		Failed

2-13

Table 2-1 (cont.)

Summary of Tests on Non-Reinforced Masonry Walls
Without Openings Supported as Simple Beams

Wall No.	Loading Pressure (psi)	Maximum Total Load (kip)	Natural Period (msec)	Crack Gauge Readings (msec)	Initial Preload (kip)	Wall Behavior
Preloaded Walls (8-in. Thick Brick)						
64a	1.6	17.5		62,87,100	16.5	Cracked
64b	1.6	6.8		-	16.5	Failed
65	1.6	11.5		19,25,25	16.5	Failed
66	1.6	6.0		18,24,66	23.5	Cracked
67	6.1	64		8,8, 9.5	23.5	Failed
81	1.6	7.2		25,31,40	28.5	Cracked
82a	1.6	8.4		20,21,24	28.5	Cracked
82b	4.0			-		Failed
Debris Tests (8-in. Thick Brick)						
1	3.0					Failed
2	3.4					"
3	3.4					"
5	3.6					"
7	3.6					"
21	3.4					"
4	10.0					Failed
6	10.0					"
20	10.1					"
22	10.0					"

Interior Walls

Two walls of concrete block, and two of hollow clay tile were installed in the tunnel 15 ft downstream from a wall containing a window opening, 62 in. wide and 54 in. high (i.e., occupying about 23% of the wall area). The window wall was specially designed not to fail under blast loading. The general test arrangement is shown in Fig. 2-13.

Although a significant portion of the incident blast wave was reflected from the solid portion of the window wall, by the time the remainder of the wave reached the test wall it had a relatively sharp front (a rise time of about 8 msec), and the wall experienced an almost flat-topped loading pressure of 1.5 psi, essentially the same as the pressure that would have been experienced by a solid wall at the window wall's location. (Pressures at the test wall location resulting from stronger shocks incident on the window wall were significantly smaller than they would have been on a solid wall at the window wall's location. See Volume 2 for more information about the characteristics of loading pulses.)

All four walls were first exposed to the very weak blast wave from a short length of Primacord for the purpose of determining their natural periods. The two concrete block walls (designated Numbers 58 and 59) were tested first. On the first test of Wall No. 58, a 10-ft long strand of Primacord was used, and its blast wave damaged the wall, causing it to crack along its horizontal centerline. No usable information on natural period was obtained. On the first test of Wall No. 59, a 2-ft long strand of Primacord was used. The resultant blast wave caused no visible damage to the wall, but its intensity was so low that only an approximate value for natural period could be obtained.

As noted earlier, a second test with a loading pressure of about 1.5 psi was conducted on each wall. They both failed, scattering pieces as far as 30 ft from the walls' original location. Fig. 2-14 contains a pretest photograph of Wall No. 58 and a posttest photograph of the debris from that wall. (The debris from Wall No. 59 was scattered in similar fashion.) The non-

failing window wall can be seen in the posttest photograph. Fig. 2-15 gives the displacement of the centerlines of each wall as a function of time from blast arrival.

The two clay tile walls (designated Numbers 62 and 63) were subjected to similar tests, with similar results. The low level blasts from 2-ft long strands of Primacord were applied to find the walls' natural period (though none could be determined for Wall No. 63). When subjected to tests with loading pressures of 1.5 psi, both walls failed, scattering debris as far as 30 ft from the walls' original location. Fig. 2-16 shows the debris from Wall No. 62, and Fig. 2-17 shows the displacement of the two centerlines of each wall as a function of time. The displacements of the lower parts of the two curves suggest that the arrival time of one or the other is in error (by about 2.5 msec). Such a difference becomes negligible, of course, at times on the order of 50 msec and more, thus the two curves merge at these later times.

Preloaded Walls

Preloaded walls may be either interior or exterior. Using the mechanism described in Appendix A of this volume, six solid, 8-in. thick walls were subjected to preloads ranging from 16.5 to 28.5 kips, approximately the equivalent of the weight of two to three and one half test walls (i.e., 2W to 3.5W). Five of the walls (64, 65, 66, 81, and 82) were subjected to blast loads of about 1.6 psi. Of the five, Nos. 64 and 65 had initial preloads of about 2W, No. 66 about 3W and Nos. 81 and 82 about 3.5W.

Four of these walls (64, 66, 81, and 82) cracked, but did not collapse upon initial loading. Walls 64 and 82 were loaded a second time in order to obtain load and displacement data for theoretical analysis. Wall No. 64 was reloaded to the same level as the initial loading (1.6 psi) and collapsed. Wall No. 82 was reloaded to 4.0 psi and also collapsed. Wall No. 67 received an initial loading of 6.1 psi and collapsed in catastrophic fashion, with some debris coming to rest more than 40 ft downstream from its original location.

Centerline displacement gauges were employed on all the tests. In addition, on the tests with Walls 81 and 82, a load cell was placed at the bottom of the walls to monitor the actual preload imparted to the walls.

The general pretest layout and the type of debris formed when the walls failed are shown in the photographs of Figs. 2-18 and 2-19. Two of the debris photographs are of walls subjected to 1.6 psi blast loads (64 and 65); the third is of a wall subjected to a 4.0 psi loading. The debris from the three walls is very similar, it is characterized by very large pieces, with much of the material confined to the immediate vicinity of the walls' original location. Wall No. 67, loaded to 6.1 psi, did not appear to break up differently from Walls 64 and 65, but the debris was somewhat more widely scattered.

The recordings of displacement of the walls' centerlines as a function of time are given on Figs. 2-20 and 2-21. The four records from walls subjected to a loading of 1.6 psi are shown in Fig. 2-20, and the two records from walls subject to stronger loadings (6.1 psi, for Wall No. 67; 4.0 psi, for the second test with Wall No. 82) are shown on Fig. 2-21. As with the displacement records of interior walls, the large departures of the lower part of the curve for Wall No. 65 from the others on Fig. 2-20 suggest an error in arrival time, which virtually disappears at later times. In Fig. 2-21, the effect of the higher loading pressure on Wall No. 67 than on Wall No. 82 is clearly evident.

Debris Studies

In the early part of the program, attention was focused on the type, quantity, and distribution of debris produced by brick wall panels that failed under blast loading. As a result, on tests with 10 of the 19 walls, extensive surveys of the quantity (weight) and location of posttest debris were made, in addition to measurements of air blast pressures on the walls.

All ten "debris" walls were 8-in. thick brick with simple beam supports. Six of them were subject to blast loading pressures of between 3 and 3.6 psi, four to loading pressure of about 10 psi. All the panels failed under these

2-17

loadings with initial cracking occurring at or near the horizontal mid-line.

Virtually all debris from the low pressure tests came to rest within about 30 ft of the original wall locations, with the majority -- including some very large pieces that weighed as much as 2400 lb -- remaining very close to the walls' original location. The debris from the walls subject to the high loading pressures was scattered to a much greater degree. Individual pieces were generally smaller than pieces found on the low pressure tests, but some sizeable pieces remained intact.

A photograph of the debris from one of the low pressure tests, and a bar chart giving the distribution of debris by total weight and distance for another low pressure test are given in Fig. 2-22. A similar photograph and chart from two of the high pressure tests are shown in Fig. 2-23. Included within the bars on both charts are numbers showing the weight of the largest unbroken piece of wall found in the distance range covered by the bar.

The differences in debris distribution between the two types of tests are immediately apparent. On the low pressure tests, the lower half of the walls did little more than fall over and move a small distance downstream. The upper half was propelled a bit further downstream, but all debris remained within 30 ft, and much of it in very large pieces. As can be seen, with Wall No. 7, the largest piece weighed more than a ton; it contained some 300 bricks. Motion picture films indicated that some pieces were even larger when projected from the wall, final breakup occurring only after a piece struck the tunnel floor.

On the high pressure tests, debris was projected to far greater distances with little of it remaining in the vicinity of the wall. Relatively large pieces were projected to great distances. In the case of Wall No. 20, for example, the third largest piece found came to rest just under 80 ft from the wall's original location. In another case (Wall No. 22), a piece weighing more than 750 lb containing almost 100 bricks was the most distant piece of debris found on the test, about 70 ft from the wall's original

2-18

location. As with the low pressure tests, final breakup of some of the wall elements did not occur until they struck the tunnel floor.

COMPARISON OF EXPERIMENTAL RESULTS WITH THEORY

Massive Brick Walls

The tests on the three 12-in. thick walls (Nos. 50, 51, and 52) discussed earlier showed that

    o One wall exhibited no damage when subjected to three successive tests with a 1.5 psi loading pressure

    o This same wall and the other two walls all failed completely when subjected to loading pressures of 4.2, 4.0, and 4.3 psi respectively.

The SAMIS calculations (Fig. 2-8A) show that a loading pressure of 1 psi generates a maximum flexural stress of 220 psi for an 8-in. thick brick wall. For a 12-in. thick wall, the equivalent stress is 98 psi, i.e., 220 psi multiplied by $(8/12)^2$. The static test data for the statistical distribution of flexure strength of brick beams (discussed in Volume 4) are given in Fig. 2-24. These data show that the mean flexural strength is 176 psi and that ⌄80% of the results fall between ± 30% of this value.* Using these values and the 98 psi from SAMIS gives the mean expected loading pressure for failure as 1.8 psi with ⌄80% of the walls expected to fail between 1.3 psi and 2.3 psi.

Thus the fact that one wall survived tne 1.5 psi loading and that all three walls failed at a loading pressure of about 4 psi is consistent with the above predictions.

Another check between theory and experiment was made by comparing

---

* As discussed in Volume 4, these data correlate well using the distribution from extreme probability theory which, in contrast to a normal distribution, is heavily skewed to the lower side from the modal value. For the purpose of simplifying the presentation of the statistical scatter, a measure of the dispersion from minus one reduced variate to plus two reduced variates about the mode was selected. This included a range from 7 to 88% of the data, is generally symmetric about the mean, and -- for brick beams -- extends over a range of ± 30% about the mean.

predicted and measured centerline wall displacements for Wall No. 52. The predictions were made using Eq. 2-2a assuming that cracking occurred when the wall displacement was greater than 0.05 in. From this comparison, which is given in Fig. 2-25, it can be seen that the measured and predicted motions are in good agreement.

Interior Walls

The tests on the two 8-in. concrete block walls showed that:

o   A 1.5 psi loading pressure caused massive failure of both walls (No. 58 and No. 59)

o   A special test for determining natural frequency using 10 ft of Primacord caused cracking (but not failure) of one wall (No. 58)

The static test data (from Volume 4, Fig. 3-2) show a mean flexural strength of 130 psi, and 80% of the results fall between ± 50% of this value. Using these values and the failure theory, the mean expected failure loading is 0.6 psi with 80% of the walls expected to fail between 0.3 psi and 0.9 psi. These predictions are consistent with the massive failure of both walls at 1.5 psi loading. Relatively little can be said about the cracking caused by the 10 ft Primacord test since the loadings were not sufficiently well documented. However, since some walls would be expected to fail at 0.3 psi, that is, only one fifth of the loading pressure obtained from the 60-ft long strand of Primacord used to generate the 1.5 psi loading, the result is certainly not surprising.

Another check between theory and experiment was made by comparing predicted and measured centerline wall displacements for Wall No. 58 subjected to the 1.5 psi loading. The predictions were made using Eq 2-2a and, since the wall was already cracked, no additional assumptions were necessary about the displacement necessary for cracking. From this comparison, which is given in Fig. 2-26, it can be seen that the predicted values are somewhat higher than the measured ones, particularly at early times. It is believed that this difference is primarily due to the fact that the predicted loading

assumes a sharp-fronted loading pulse while the front of the actual loading pulse for the 1.5 psi loading is somewhat rounded (see Volume 2).

The experimental tests with the clay tile walls showed that both failed completely under 1.5 psi loadings, a not unexpected result because such walls are expected to be weaker than an equivalent concrete block wall.

Preloaded Walls

In the experimental program on preloaded walls, five walls with varying degrees of preload were subjected to 1.5 to 1.6 psi loadings and all cracked, however, only one of these failed (collapsed) on the first test.* The fact that four of the walls did not collapse is quite interesting when it is realized that the walls, if initially cracked, could only resist a maximum loading force of 0.9 psi. ** As shown by the following discussion of the time sequence of wall cracking, it is believed that, though the walls did not collapse, the loading was near the threshold value for collapse.

The measured period of the 8-in. thick brick walls was about 32 msec, a value that compares favorably with the predicted value from SAMIS (about 34 msec). It has already been noted, in Volume 2, that the 1.5 psi loading pulse, while essentially flat-topped, had a rise time of about 8 msec, i.e., about one quarter the natural period of the walls. With simple elastic systems this would result in a Dynamic Load Factor of about 1.9 (see Fig. 2-4). The lower plot of that figure indicates that the time to reach maximum deflection is about three times the ramp rise time t_r, which in this case is about T/4. Thus, if the walls behaved essentially as simple elastic systems, they would attain maximum deflection in a time of $3T/4 \simeq 24$ msec (in place of $T/2 \simeq 16$ msec, the time to attain maximum deflection from a step load).

---

* All preloaded wall were treated as a group since the calculated effect of preload using Eq 2-1 showed the maximum reduction in fiber stress from the least preload (2W) to the maximum preload (3.5W) was less than 4%.

** One wall, which cracked on first loading, but did not fail, was loaded a second time to 1.6 psi and failed completely.

With three of the four walls that cracked but did not fail, crack gauges recorded initial cracking on or before 18, 20, and 25 msec, which indicates that they cracked near the time they attained maximum deflection. This suggests a reason for their stability even under loadings that could have caused them to fail after cracking: namely, that the walls had already begun to move upstream on the second half of their initial elastic phase oscillation before their cracking was completed and they ceased behaving elastically. This clearly happened with two of the three walls on which the last crack gauges to register did so at 40 to 66 msec. The third wall's last crack gauge registered at 124 msec (its first gauge registered at 20 msec), which suggests that its stability was really borderline. Another wall exhibited a similar crack history (first and last gauges recording at 19 and 25 msec) and it did fail.

The last wall that remained stable had first and last cracks recorded at 62 and 100 msec. This can only mean that this wall did not crack during its first oscillation at or near a crack gauge, but during some later oscillation.

In interpreting these results, it should be recalled that after cracking, a steady state loading of 0.9 psi would be sufficient to collapse the walls. Thus, if the flat-topped loading in the shock tunnel had been significantly longer, it can be assumed that the walls would have collapsed. Clearly, the pulse durations from megaton range nuclear weapons are much longer than the shock tunnel pulses, although, in some cases,* the actual loading duration on a wall panel of a building exposed to such a pulse need not necessarily be longer.

Since it is impractical here to consider all such geometries, it was

---

* Loading duration depends on the location of the wall on the building and the size of the building. For example, the loading on a panel on the front face of a building would initially be the peak reflected pressure, however, the pressures would be reduced significantly by the time "clearing" of the reflected pressure on the front face occurred. Typical front face clearing times for structures with a minimum dimension -- height or half width -- of 30 ft would be about 55 msec.

conservatively assumed that the real durations would be much longer so that cracking of the walls implied that failure would occur under blast loads from megaton range weapons.

On this basis it can be said that the upper bound for the failure loading for the preloaded brick beams is 1.5 psi with the estimated mean value not much lower than this. A safe lower bound would be the 0.9 psi needed to fail a zero strength preloaded wall.

The calculated failure loading from SAMIS for unloaded walls is 0.8 ± 0.2 psi. Adjusting for the average effect of preload and the effect of the rounded nature of the wave front would increase the failure loading to 0.9 ± 0.3 psi. This calculated range, from 0.6 - 1.2 psi, although lower than the 0.9 - 1.5 psi range determined experimentally is not inconsistent since the ranges overlap significantly

Displacements of the centerline of the wall as a function of time (after the walls have cracked) predicted from Eq. 2-2a compare quite well with measured values. This is shown in Fig. 2-27 for the second tests on Walls No. 64 and No. 82, each of which cracked during its first test at 1.6 psi. Wall No. 64 was reloaded with a 1.6 psi pressure; Wall No. 82 was exposed the second time to a 4 psi loading pressure.

2-24

A. Fixed-Fixed Walls.

B. Fixed-Pin Walls.
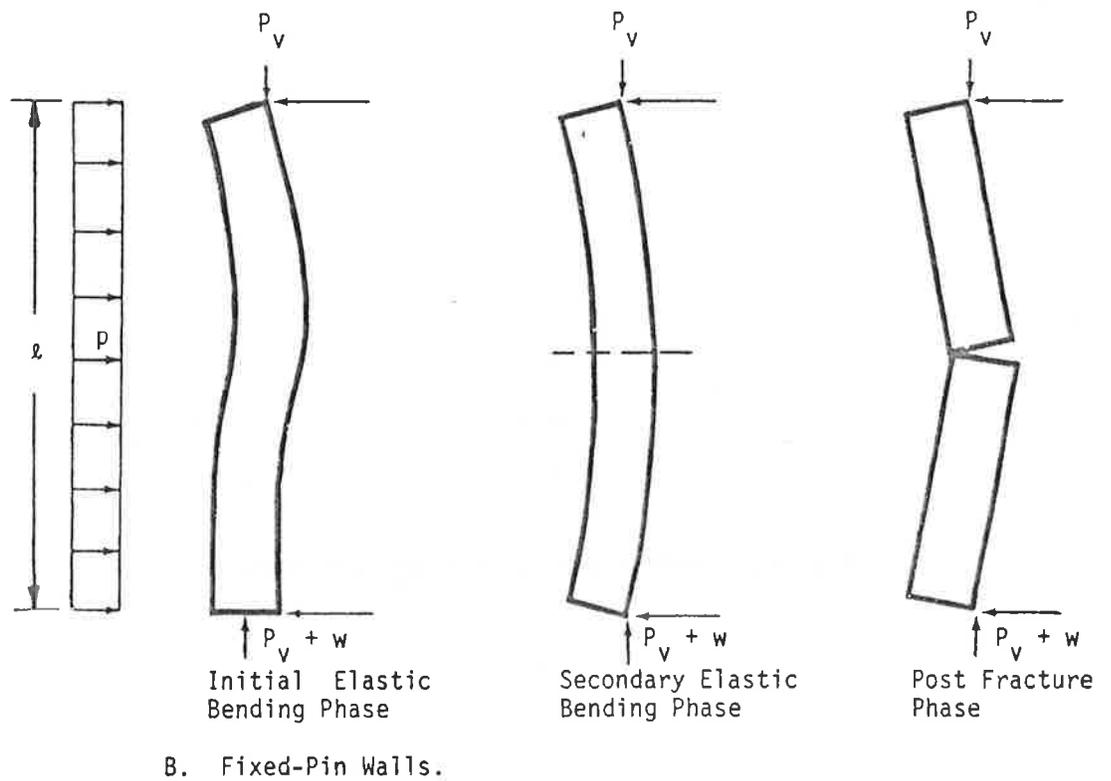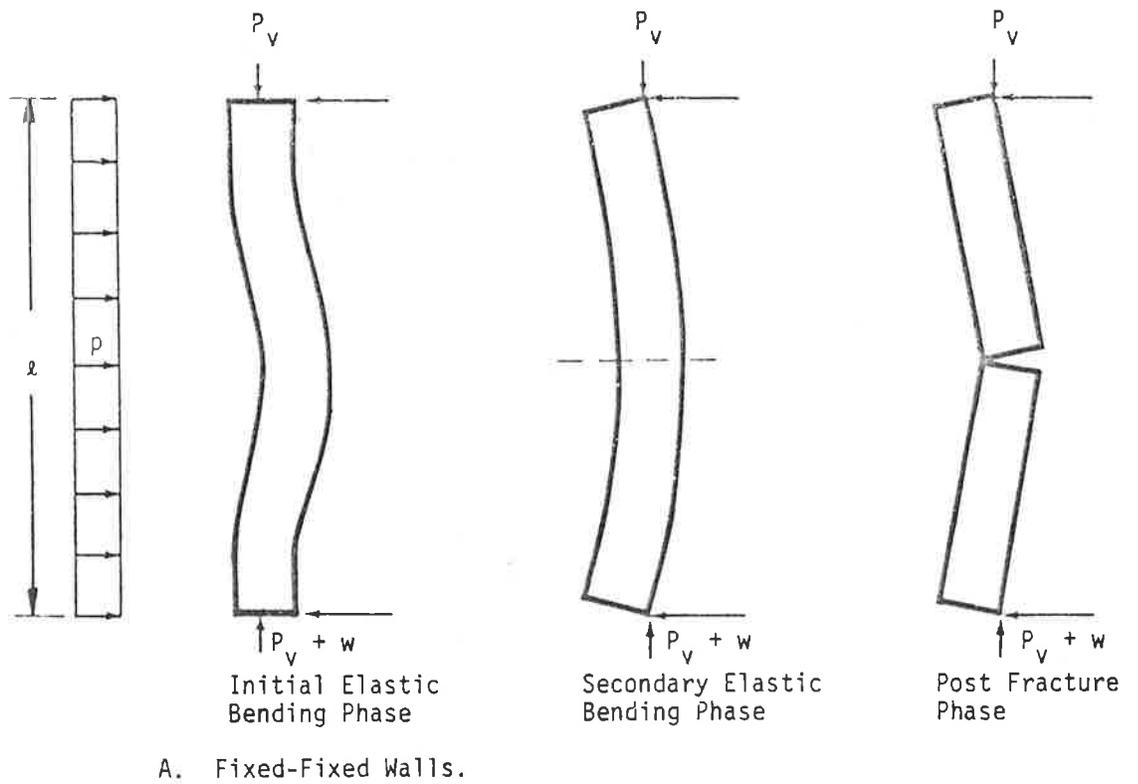
Fig. 2-1. Response of Beam-Mounted Walls to Blast. P_v = Preload, w = Wall Weight.

2-25
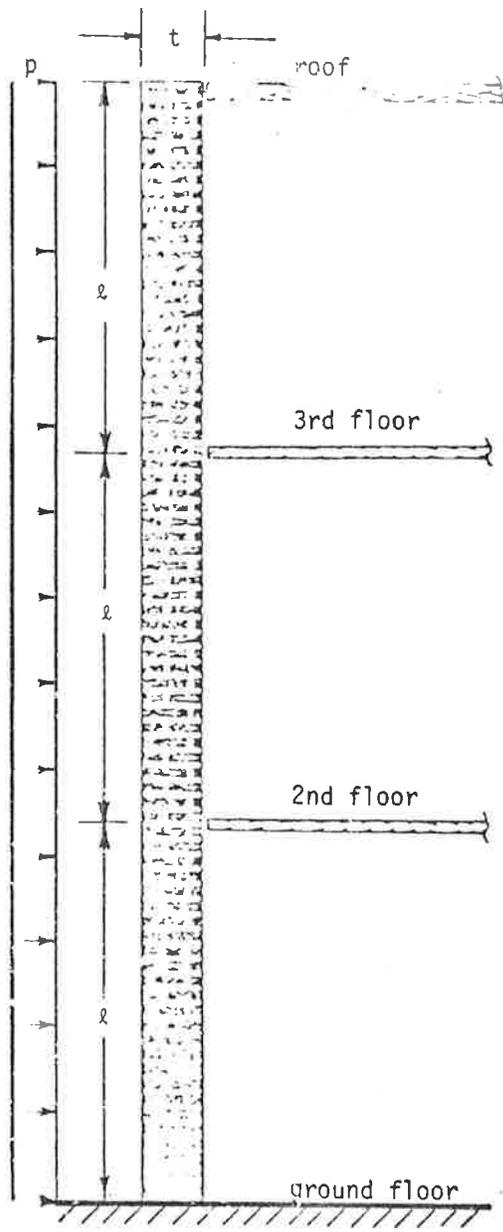
Fig. 2-2. Multistory Curtain Wall Structure.
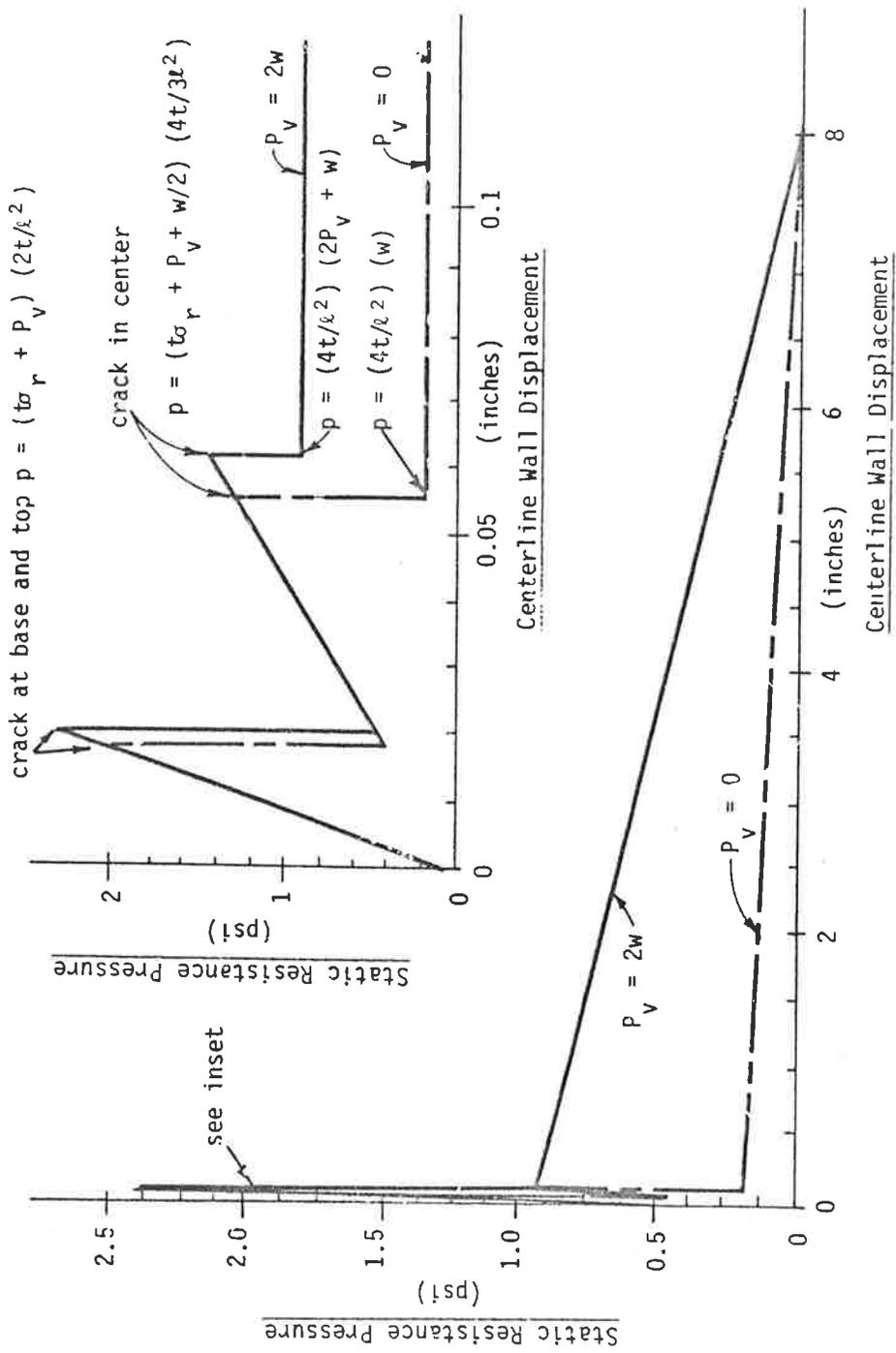
Fig. 2-3. Static Resistance of a Fixed-Fixed, Beam-Mounted Wall to Pressure Loading Normal to its Face. σ_r = Flexural Strength, t = Wall Thickness, ℓ = Wall Height, w = Wall Weight per Unit Length, P_v = Preload per Unit Length.

A. Dynamic Load Factor, DLF.

B. Time of Maximum Response, t_m.
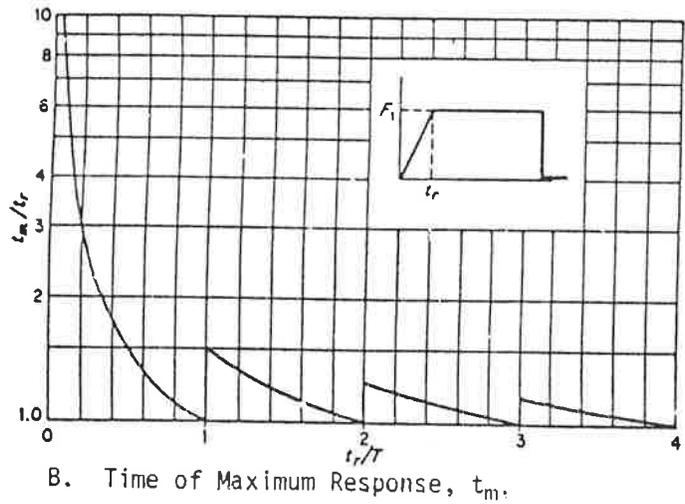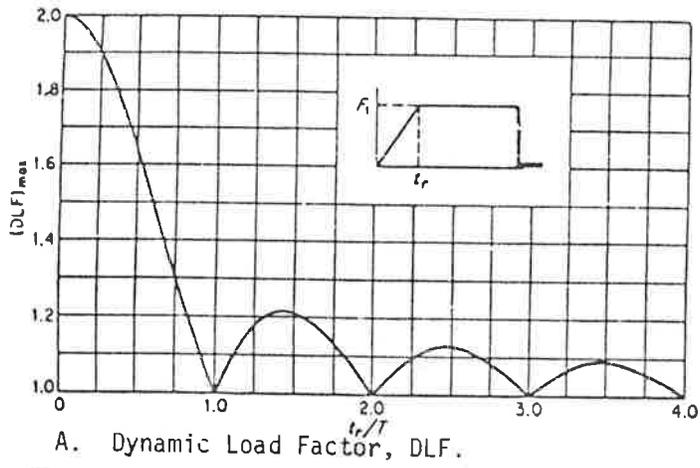
Fig. 2-4. Maximum Response of One-Degree Elastic Systems (undamped) Subjected to Constant Force with Finite Rise Time. T = Natural Period.

2-28
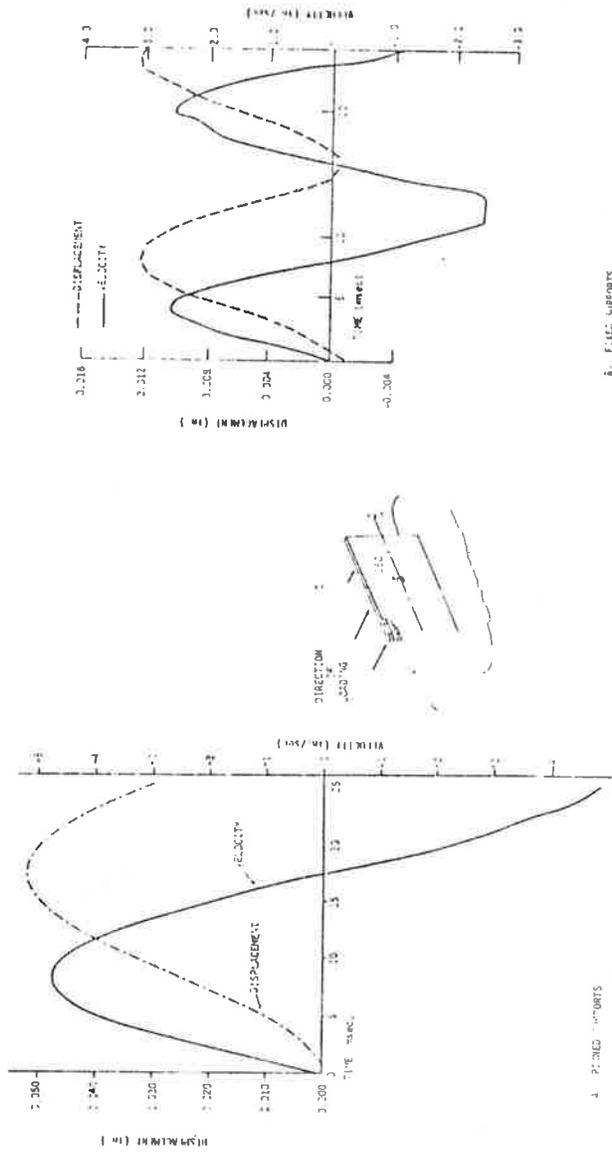
Fig. 2-5. Displacement and Velocity vs Time of Node 360 on a Solid Wall with Pinned and Fixed Supports Top and Bottom.
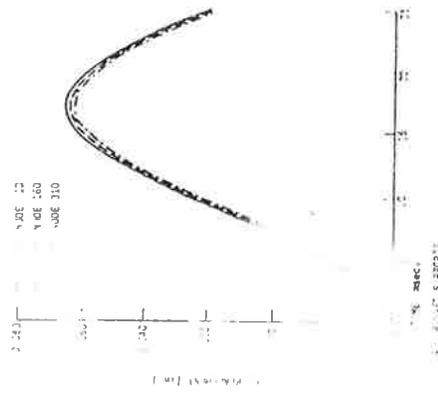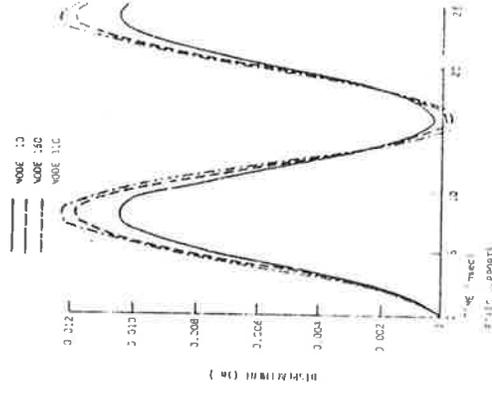
Fig. 2-6. Displacement vs Time for Nodes 10, 160, and 310 on a Solid Wall with Pinned Fixed Supports Top and Bottom.
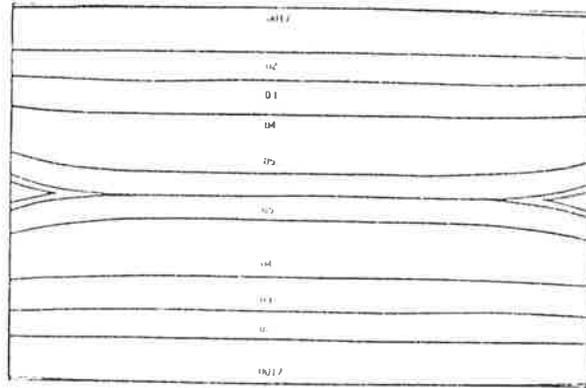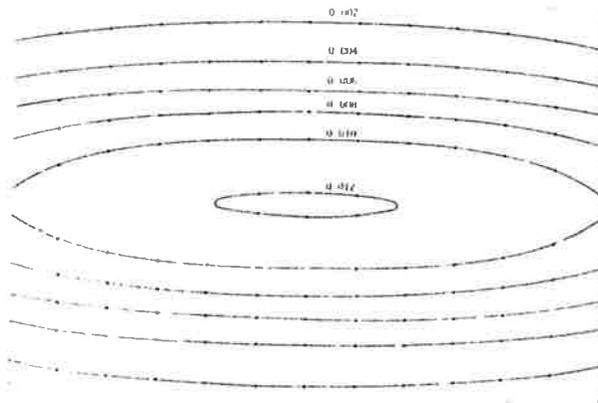
A. PINNED SUPPORTS.

B. FIXED SUPPORTS

Fig. 2-7. Contours of Maximum Displacement (in.) of the Surface of a Solid
Wall with Pinned and Fixed Supports Top and Bottom.

2-31
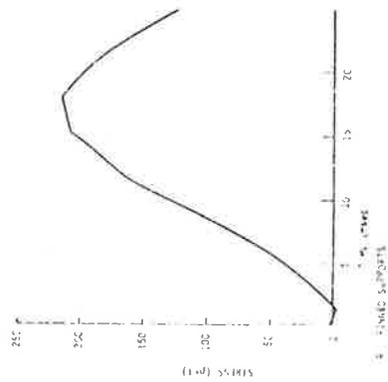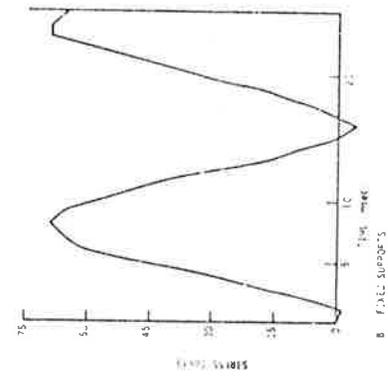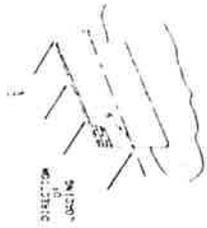
Fig. 2-8.   Stress vs Time for Element No. 9 on a Solid Wall with Pinned and Fixed Supports Top and Bottom. Note Element No. 9 is not the Maximum Stressed Element for the Fixed-Fixed Case – for Comparison Only.

2-32
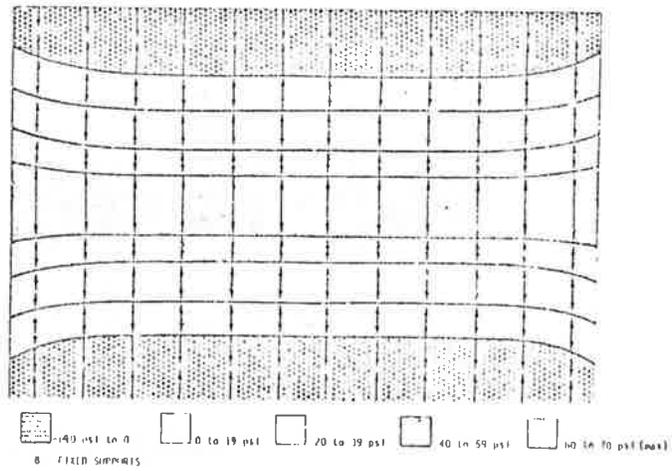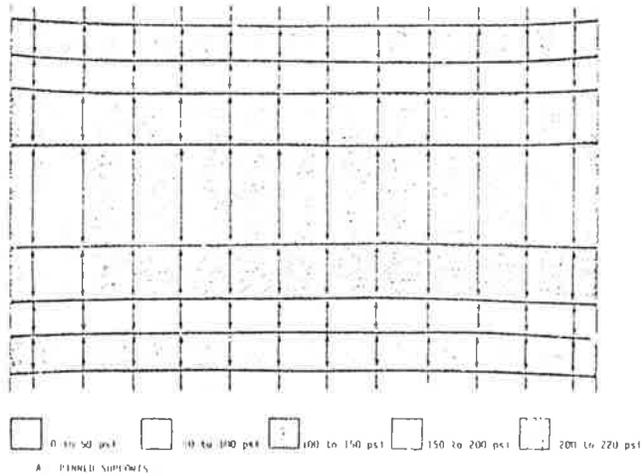
Fig. 2-9.   Stress Contours at Time of Maximum Displacement on the Downstream
           Face of a Solid Wall with Pinned and Fixed Supports Top and Bottom.
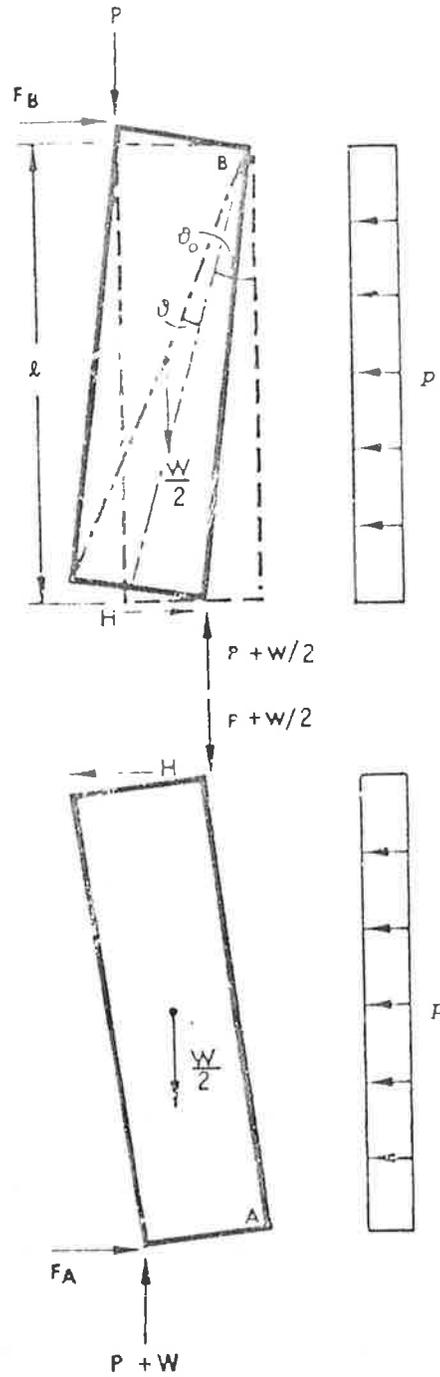
Fig. 2-10. Free-Body Diagram Showing Forces Acting on a Preload Wall, with Preload Applied in the Plane of the Downstream (Tension) Face of the Wall. For Small Values of θ and θ_0, $H = (W/4)(\theta_0 - \theta)$.
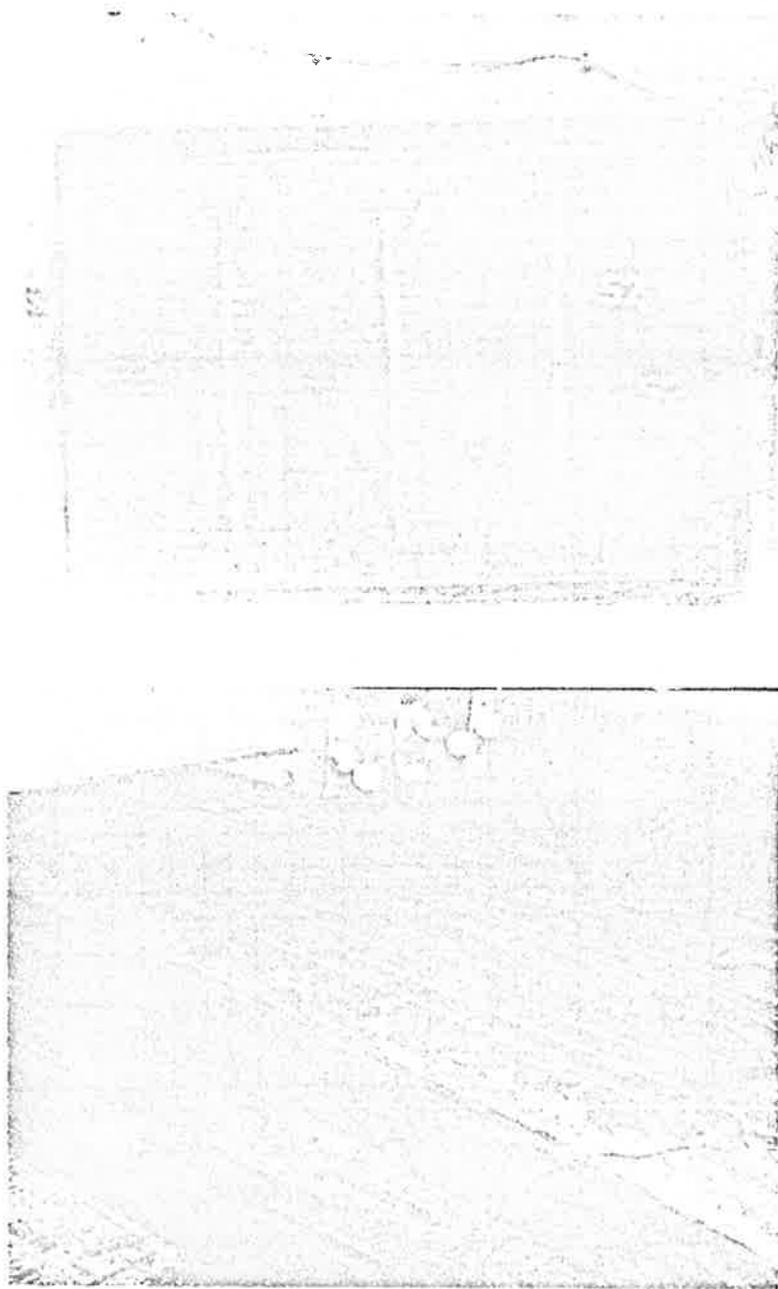
Fig. 2-11. Pre and Posttest Photograph of 12 in. Non-reinforced Brick Wall
No. 52. Peak Loading Pressure = 4.2 psi.
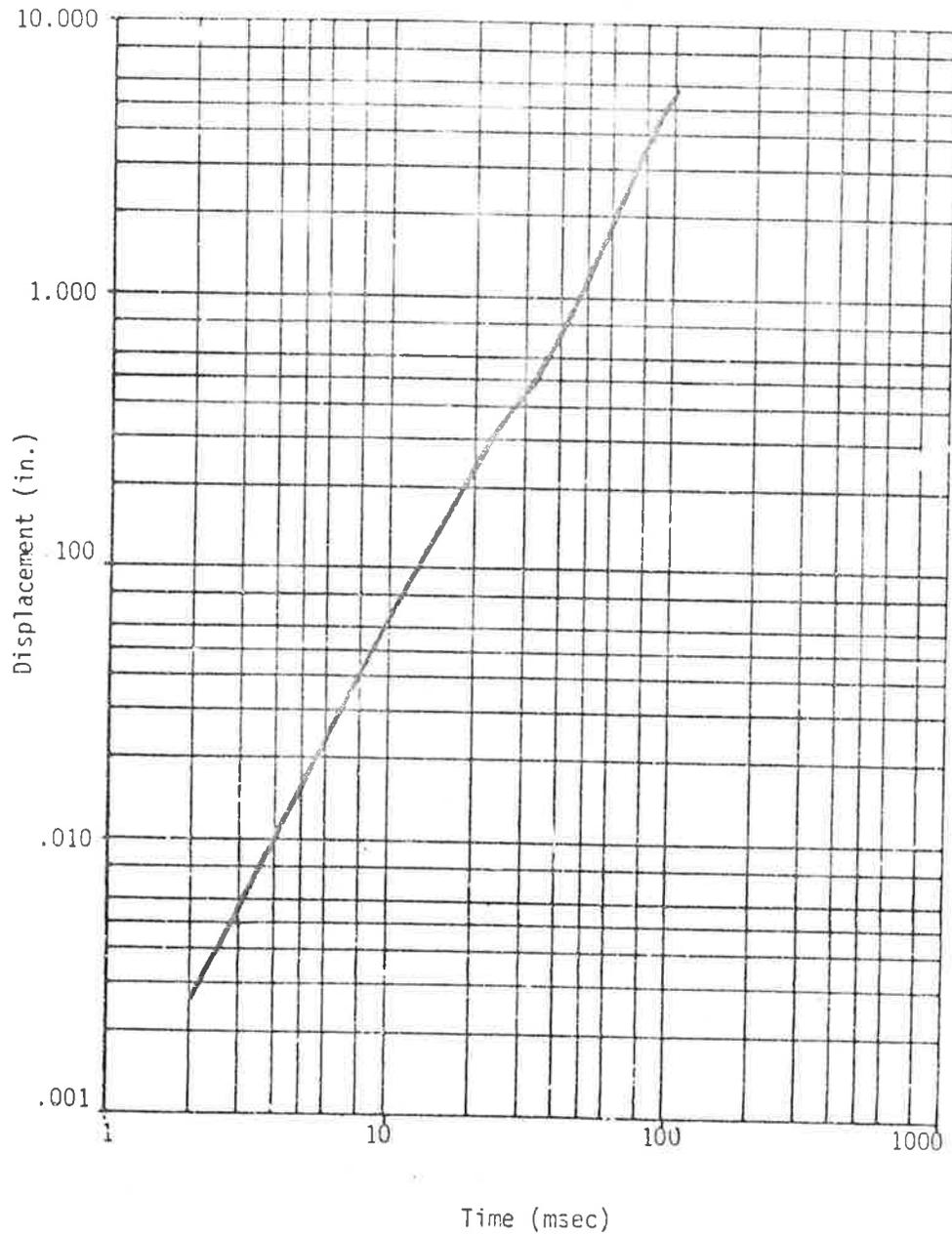
Fig. 2-12. Displacement as a Function of Time for 12 in. Non-reinforced Brick Wall No. 52. Peak Loading Pressure = 4.2 psi.

Test Wall

15'

Non-Failing
Wall

Direction
of
Loading

EAST

WEST
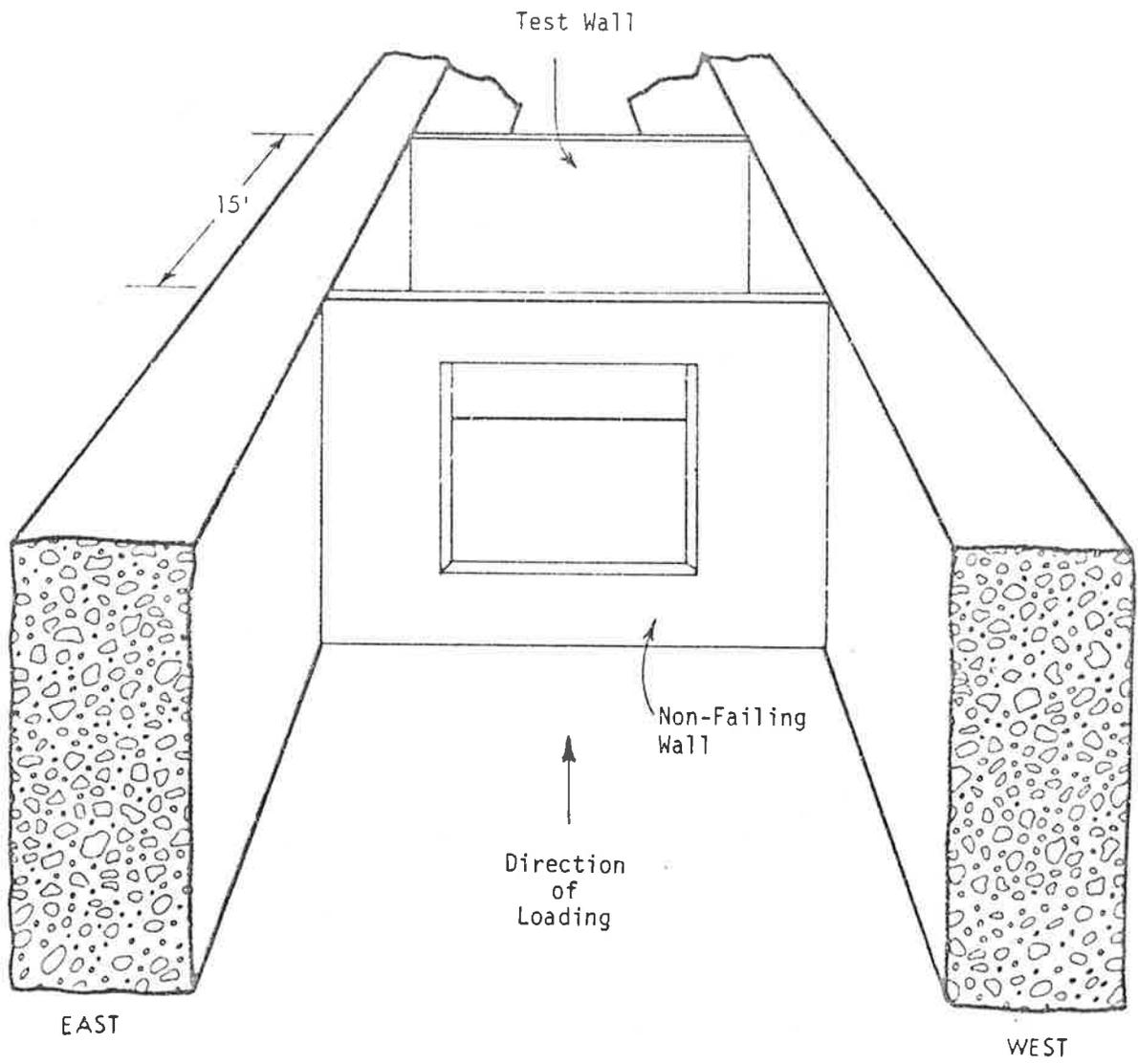
Fig. 2-13. Test Setup for Tests of Interior Walls.

2-37
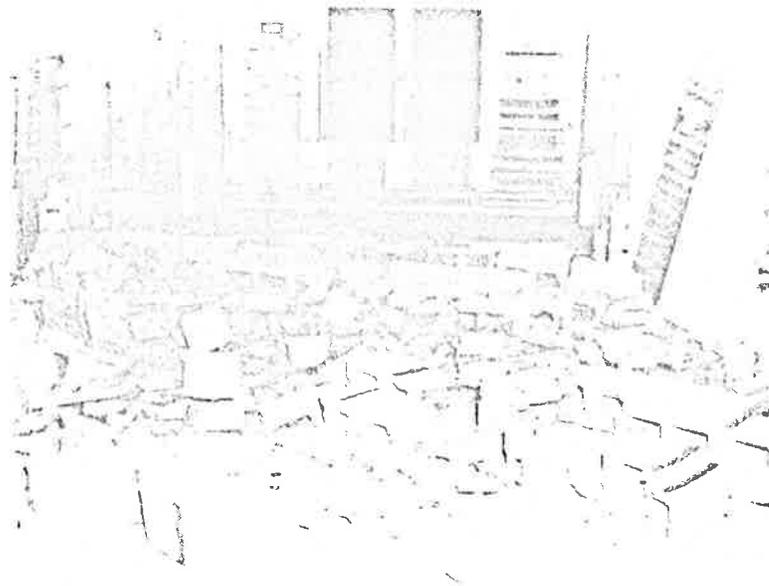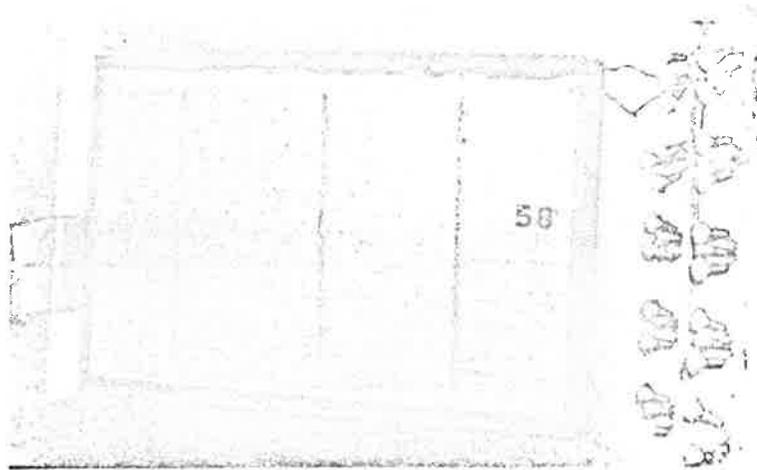
Fig. 2-14. Pre and Posttest Photographs of Wall No. 58. Non-reinforced
Concrete Block Interior Wall. Peak Loading Pressure = 1.5 psi.
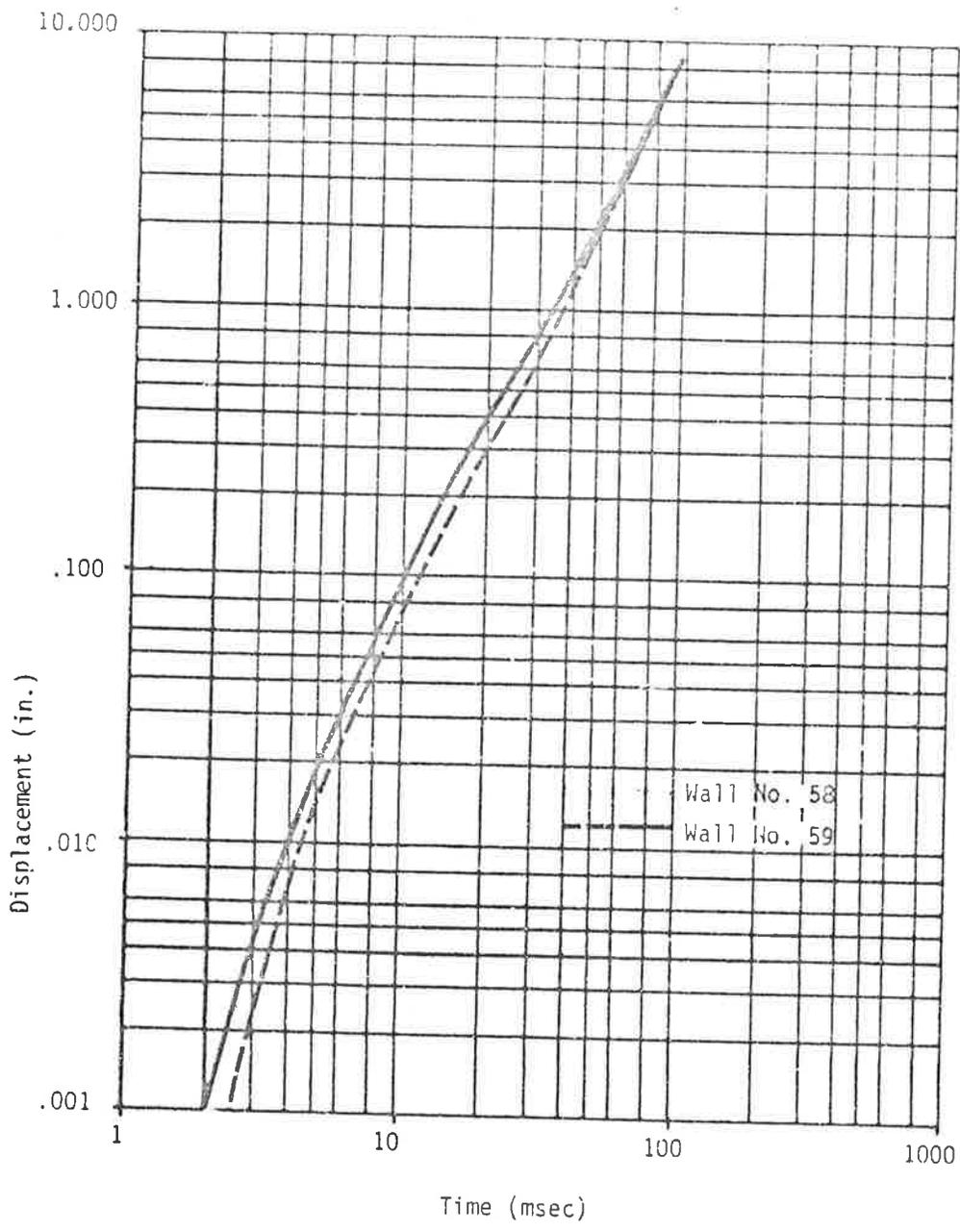
Fig. 2-15. Displacement as a Function of Time at the Centerlines of Walls
No. 58 and 59, (Non-reinforced Concrete Block Interior Walls).
Peak Loading Pressure ≈ 1.5 psi.
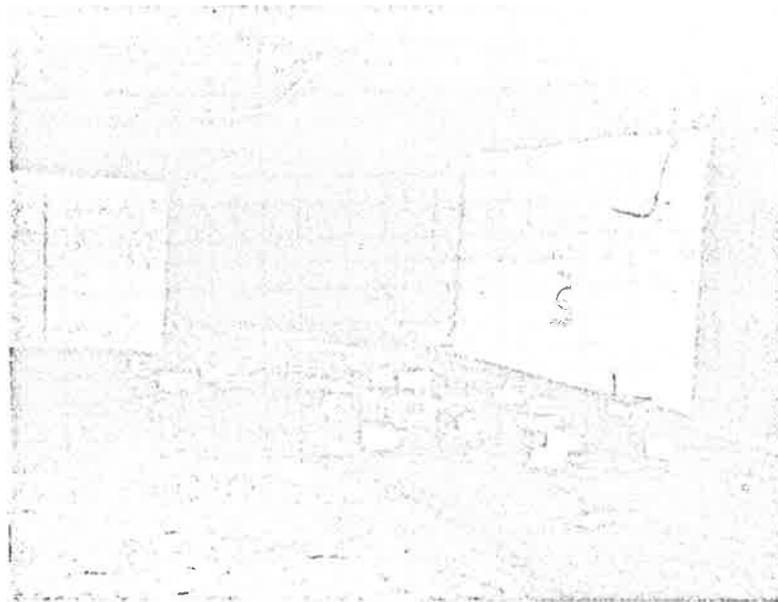
Fig. 2-16. Posttest Photographs, Wall No. 62, Non-reinforced Hollow Clay Tile
Interior Wall. Peak Loading Pressure ≈ 1.5 psi.
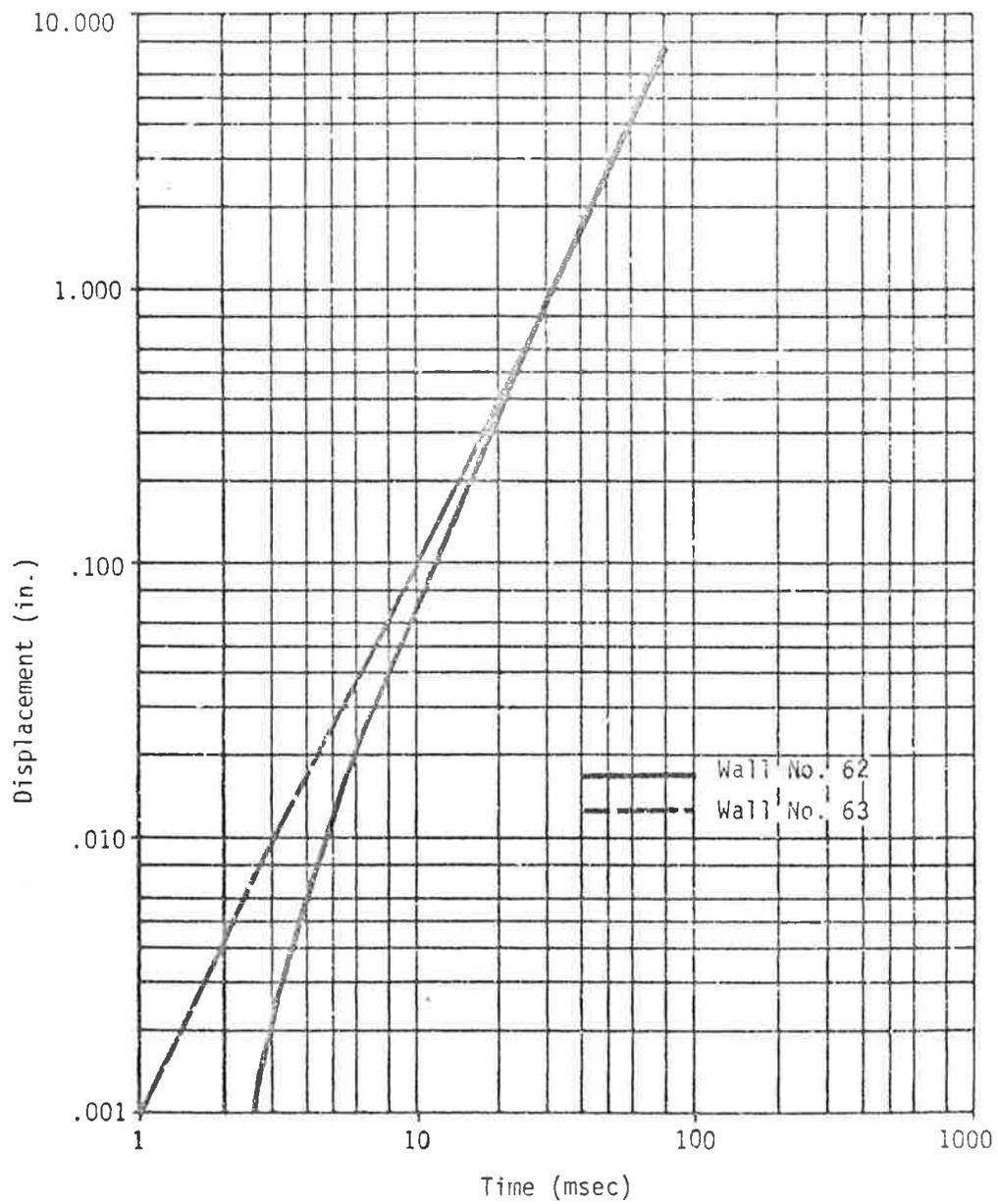
Fig. 2-17. Displacement as a Function of Time for Walls No. 62 and 63, Non-reinforced Hollow Clay Tile Interior Walls. Peak Loading Pressure = 1.5 psi.

2-41
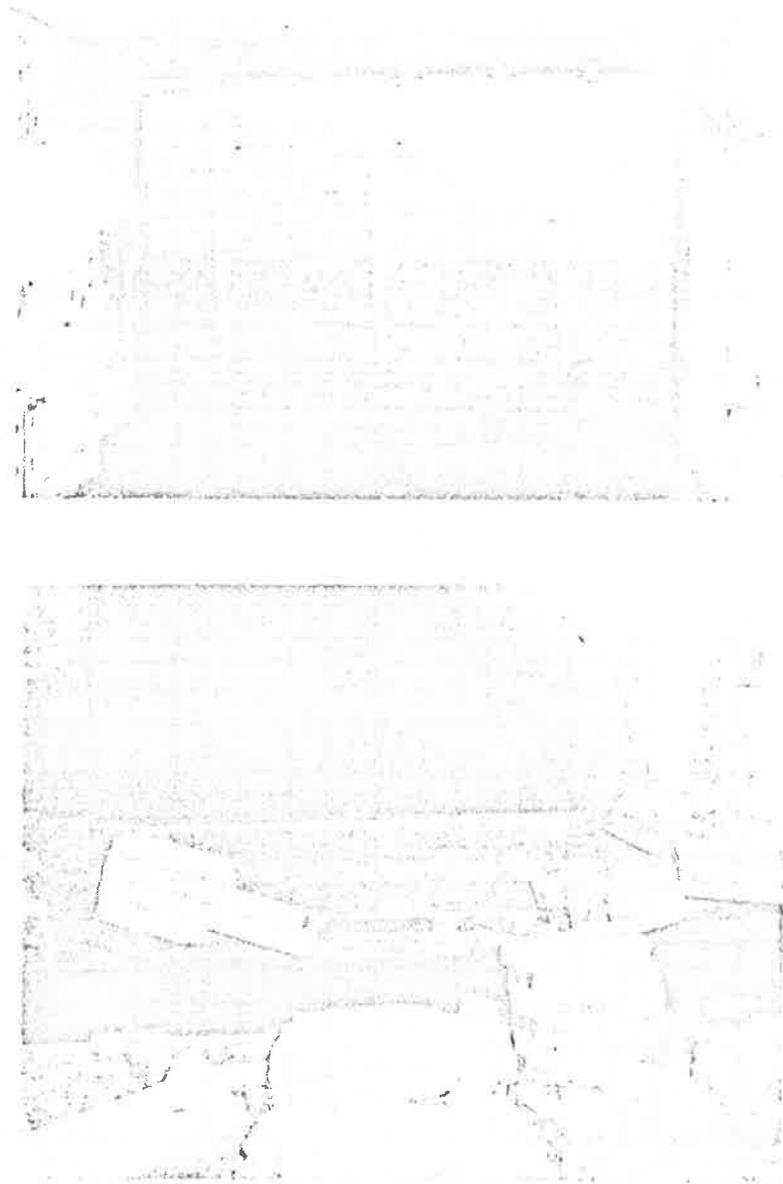
Fig. 2-18. Pre and Posttest Photographs of Wall No. 64, Preload was 2W;
Loading Pressure was 1.6 psi.

2-42

Wall No. 65.

Wall No. 82.

Fig. 2-19.   Posttest Photographs of Walls No. 65 and 82.   Preload on Wall
No. 65 was 2W; Loading Pressure was 1.6 psi.   Preload on Wall
No. 82 was 3.5W; Loading Pressure was 4.0 psi.

2-43
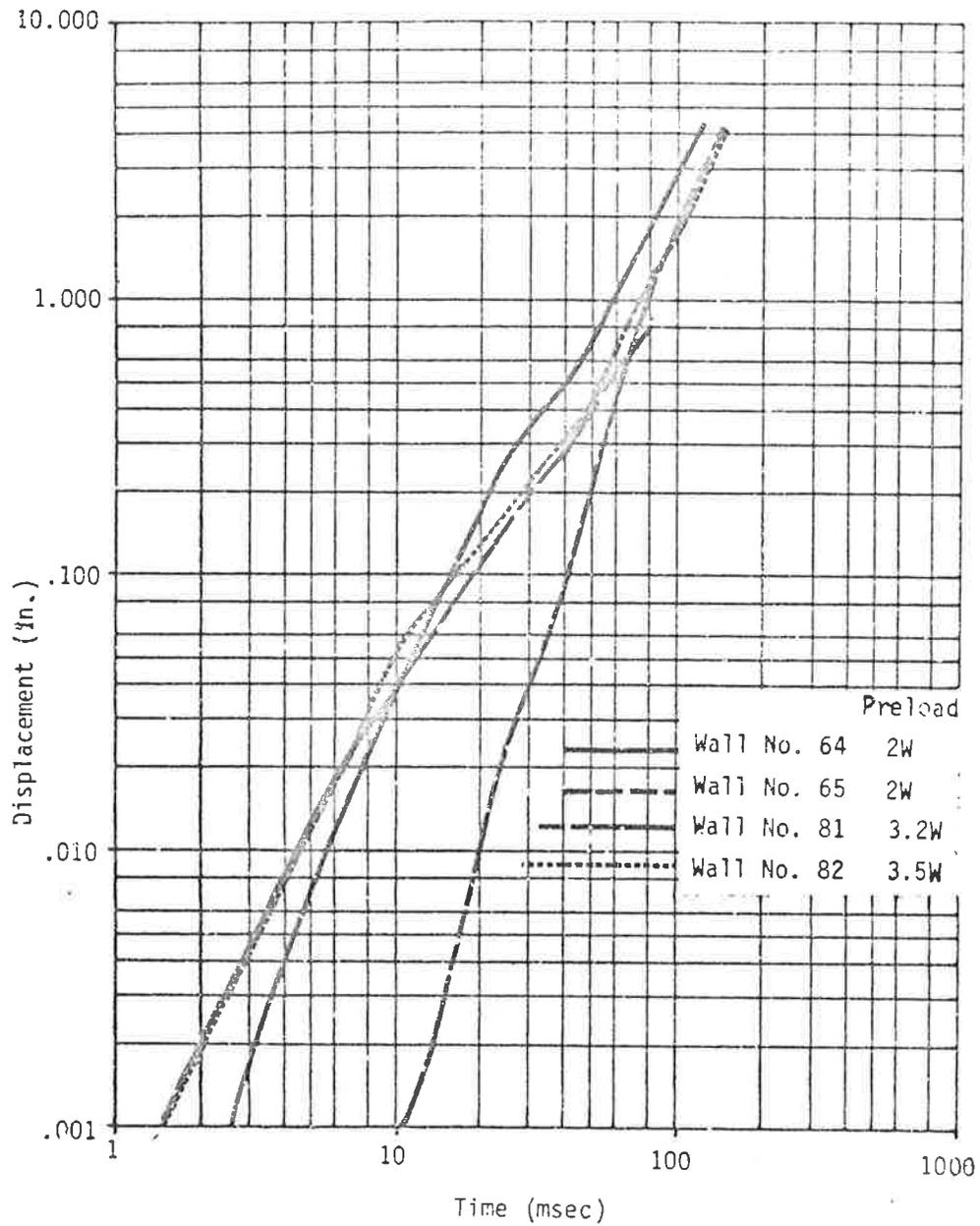
Fig. 2-20. Displacement as a Function of Time, Walls No. 64, 65, 81, and 82, Non-reinforced Preloaded Brick Walls. Loading Pressure = 1.6 psi.
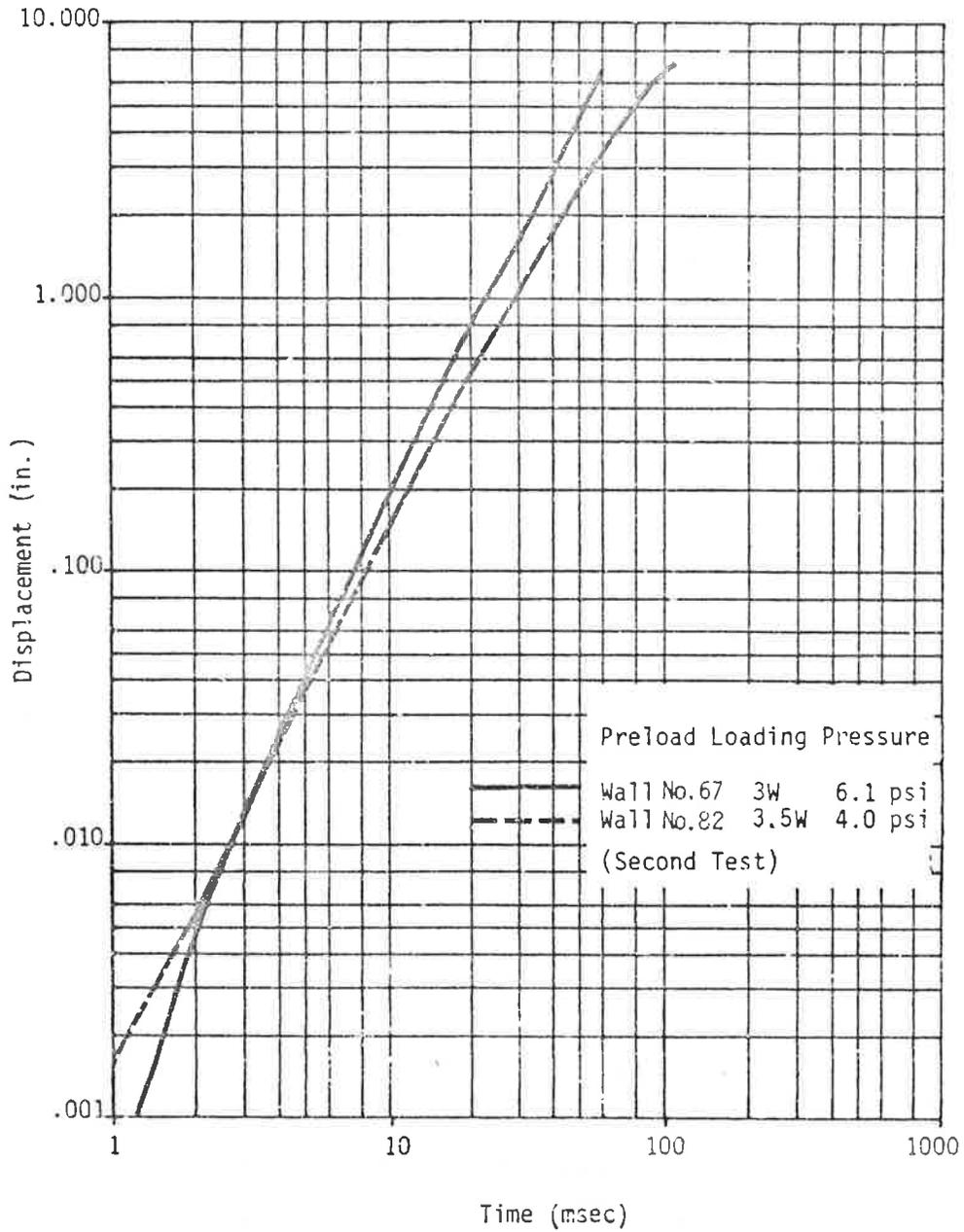
Fig. 2-21. Displacement as a Function of Time, Walls No. 67 and 82 (Second Test), Non-reinforced Preloaded Brick Walls.

A. Test Wall No. 2.
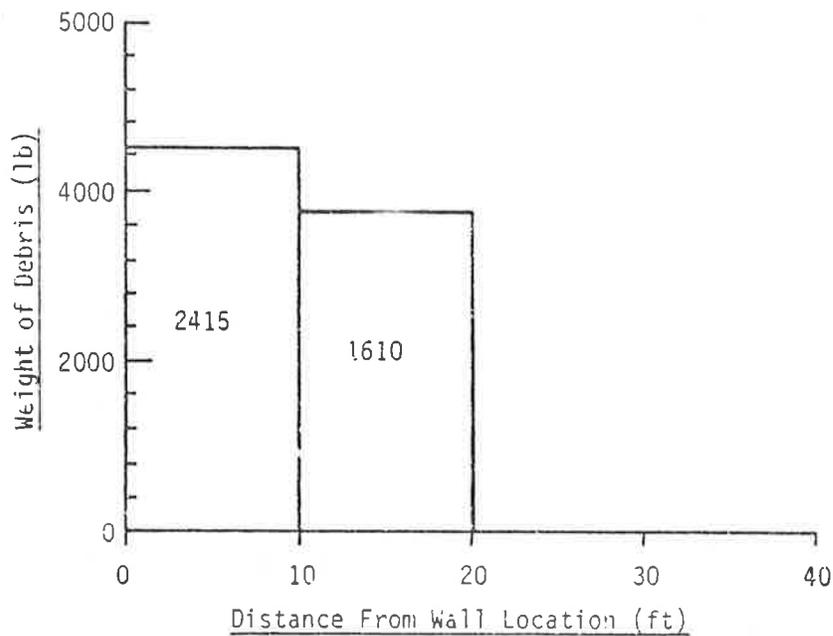
B. Test Wall No. 7.

Fig. 2-22. Photograph of Debris, and a Debris Distribution Chart from Tests on 8-in. Thick Brick Walls, Mounted as Simple Beams, and Subject to Blast Loading Pressures of 3.6 psi. The Numbers on the Charts Represent the Weight of the Largest Piece of Debris Found in the Distance Range in lb.

A. Test Wall No. 4.
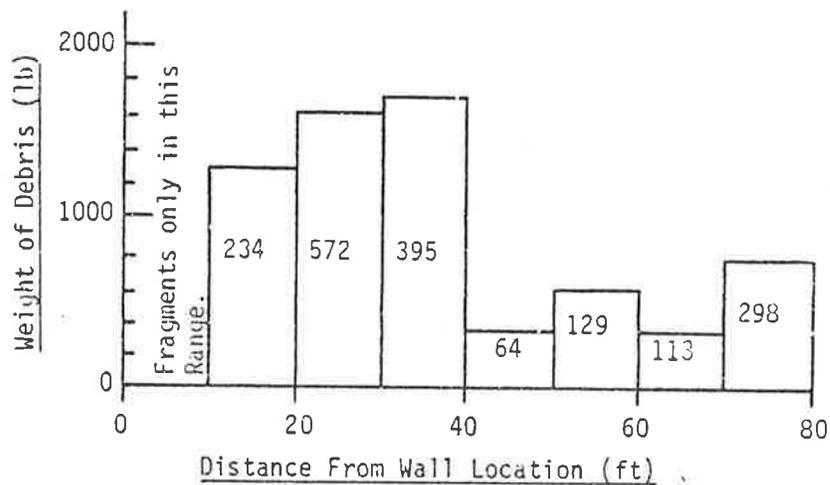
B. Test Wall No. 20.

Fig.2-23. Photograph of Debris, and a Debris Distribution Chart from Tests
on 8-in. Thick Brick Walls Mounted as Simple Beams and Subject
to Blast Loading Pressures of 10 psi. The Numbers in each Bar
of the Chart Represent the Weight of the Largest Piece of Debris
Found in the Distance Range in lb.

2-47
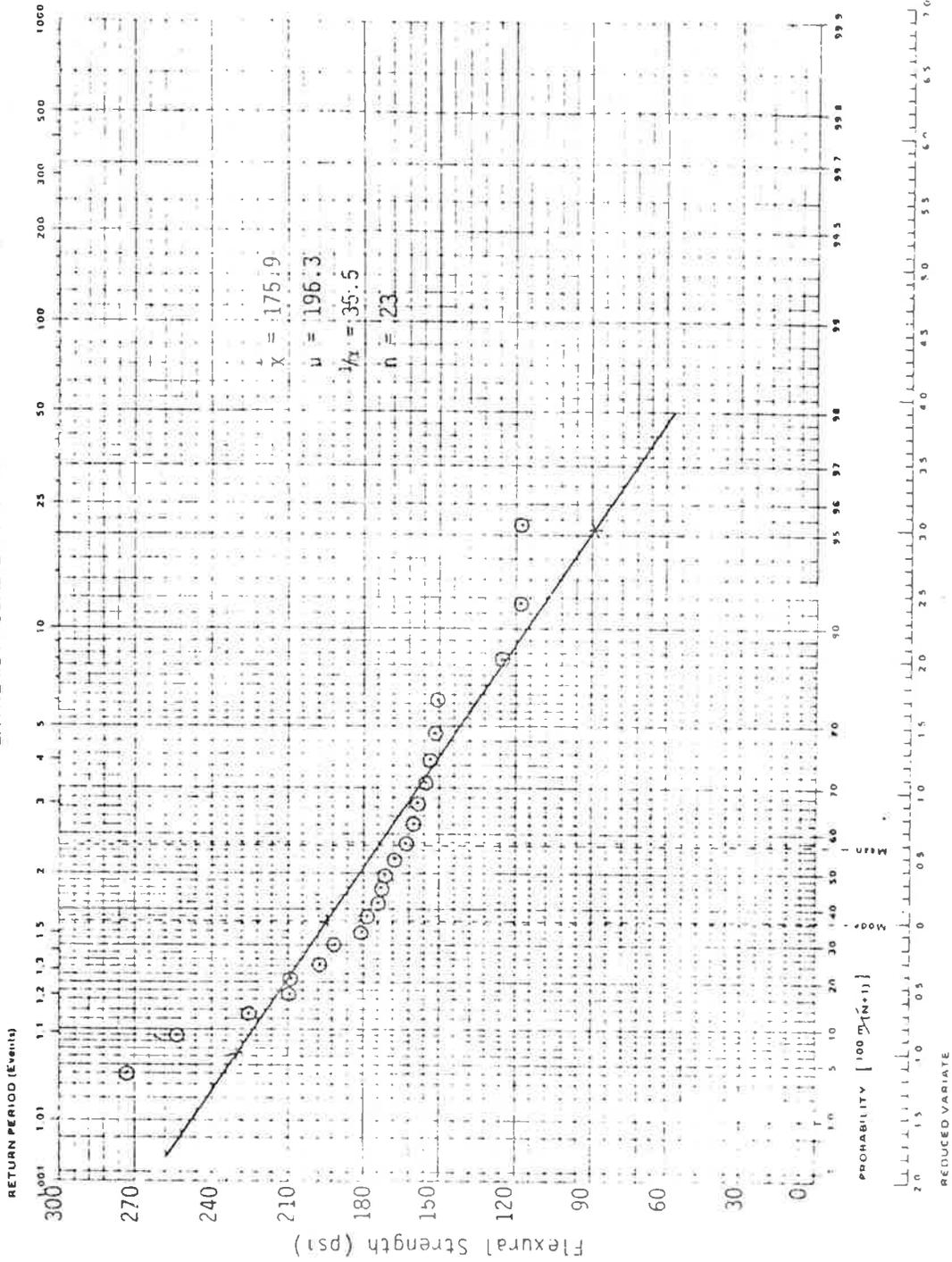
Fig. 2-24. Flexural Strength of Brick and Mortar Beams.
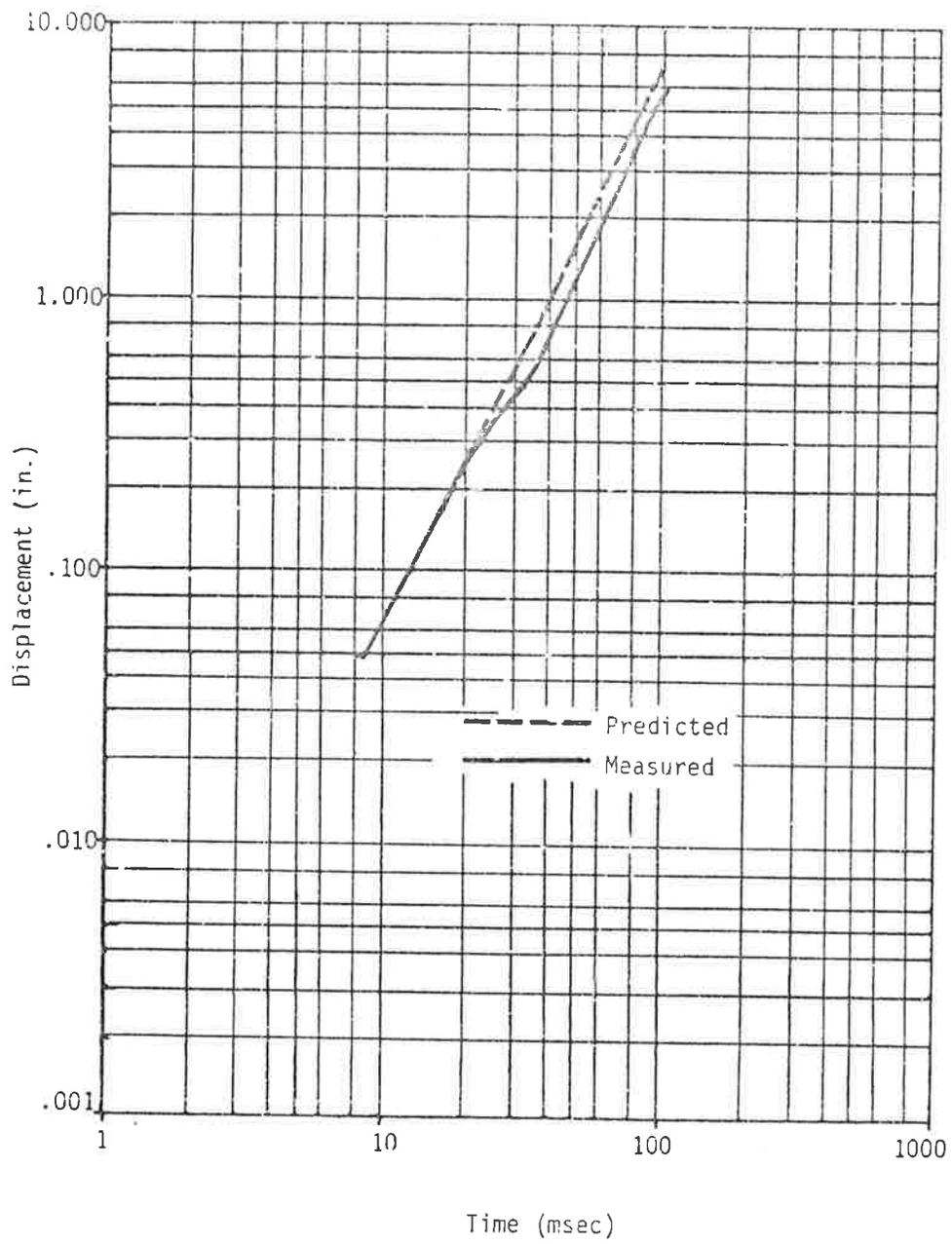
Fig. 2-25.   Predicted and Measured Displacement as a Function of Time for 12-in.
Non-reinforced Brick Wall No. 52.
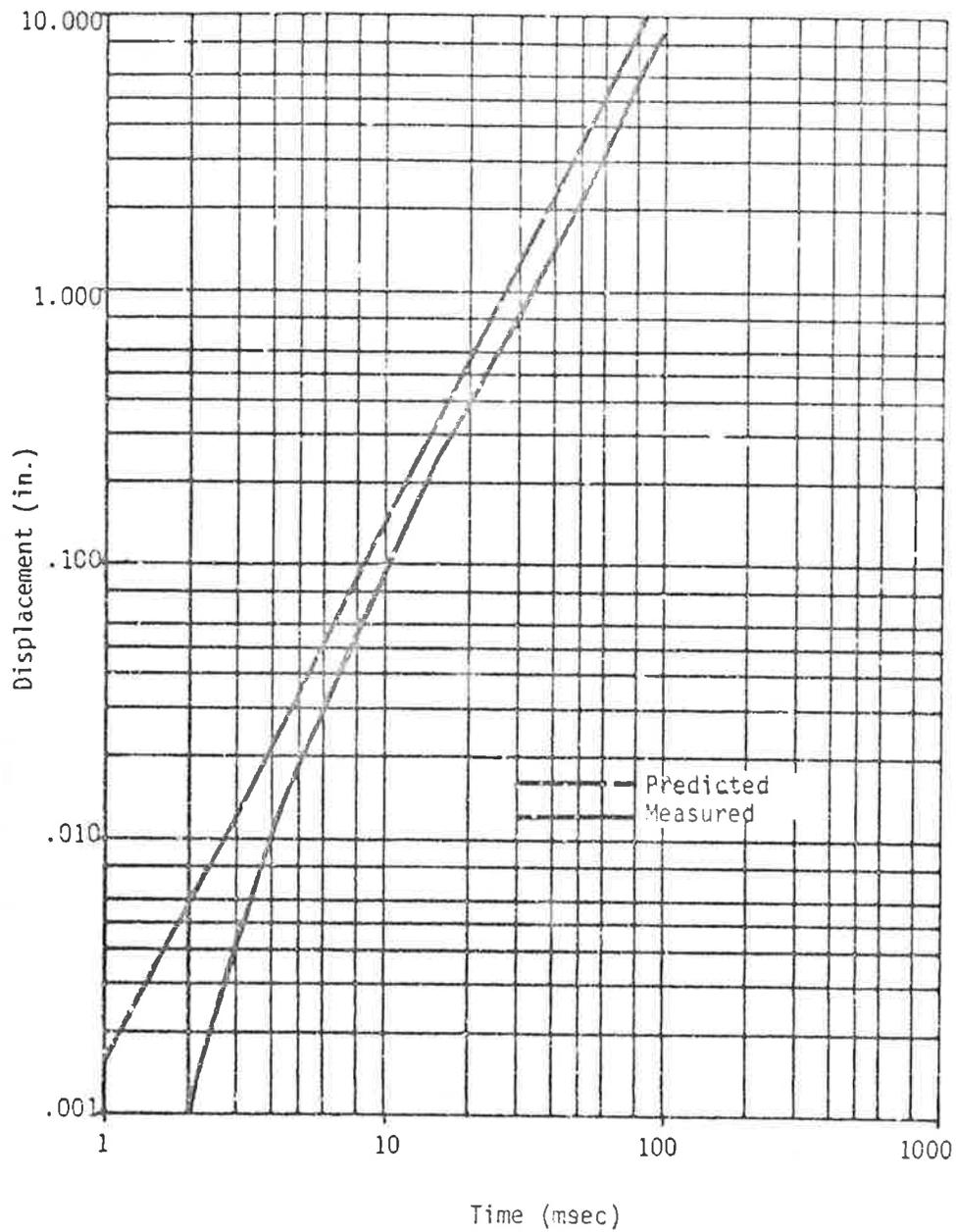
Fig. 2-26.   Comparison of Predicted and Measured Displacement as a Function of Time for Wall No. 58, Non-reinforced Concrete Block Interior Wall, Second Test, Loading Pressure ≈1.5 psi.
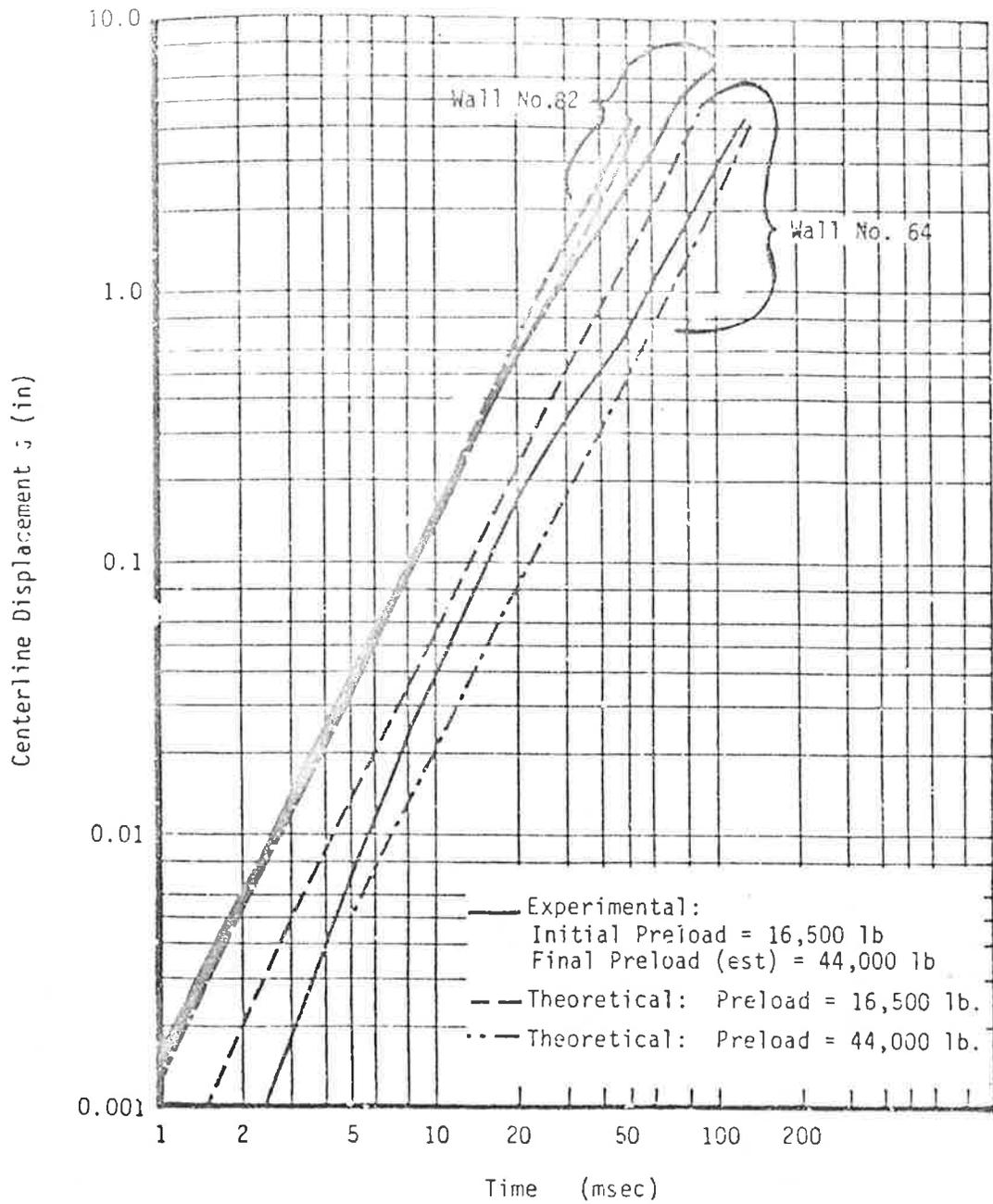
Fig. 2-27. Experimental and Theoretical Centerline Displacement vs Time for a Preloaded, 8-in. Thick, Brick Wall Responding to a 1.6 psi Blast-Load in the Shock Tunnel.

Section 3
WALLS WITH WINDOWS SUPPORTED AS BEAMS

GENERAL BEHAVIOR

The basic behavior of a beam-mounted wall with a window opening is similar to that of a similarly mounted solid wall. That is, with a uniform pressure pulse applied normal to its face, a wall will bend until, at some point dependent on the type of support (and in this case on the characteristics of the windows), a tensile stress will occur that exceeds the tensile strength of the walls. When this happens, the wall will crack, and if the continuing loading is large enough, it will fail.

The loading on the window wall is less than that on a solid wall for two reasons. First, as the blast wave passes through the window, rarefaction waves are generated which reduce the loading on the front surface of the wall. Second, the blast wave after passing through the window diffracts and applies a loading to the rear surface of the wall. The effective net loading on the wall is the difference between these two loadings. As shown in Volume 2 the net loading pulses on the window wall are characterized by a rapid rise to peak reflected pressure followed by a rather rapid drop to a constant value well below the initial value. (See Fig. B-1B.) In contrast, the solid wall pulse (Fig. A-1A) remains essentially at the peak reflected value for the duration of the flat-topped part of the blast wave.

As for the influence of the wall configuration itself, the rectangular window opening considered here tends to induce points of stress concentration at the corners of the windows. This causes a tendency for cracks to form at the window corners and propagate across the face of the wall. Thus, the windows in these walls introduce areas of weakness not present in solid walls.

The effects of preload on such walls are broadly similar to those on solid walls, that is, preload would increase the resistance of the walls to

3-1

flexural cracking. For the same value of preload, the actual increase in tensile strength in flexure at mid height of a wall with a centered window, will be larger than that of a solid wall with the same overall dimensions. (Preload places the walls in compression and the compressive stress due to the preload on the wall with a window opening will be greater because of the reduced cross section at mid height supporting the preload.) But as with a solid wall, the importance of preload in resisting blast loadings depends largely on the initial strength of the wall materials. If the walls were inherently strong (as with the brick walls built for test), the relative increase in strength due to preload would be small. If the walls were inherently weak (as with the concrete block or clay tile walls), the relative increases could be significant.

DYNAMICS OF WALL BEHAVIOR

As with the solid walls, the computer program SAMIS was used to make
predictions of the behavior of walls with window openings -- at least until
flexural cracking occurs. Some results of the SAMIS calculations are shown in
in Figs. 3-1 through 3-5, a set of figures similar to those for solid walls
(Figs. 2-5 through 2-9). The first three figures deal with wall deflections
(displacements); the last two with wall stresses. Each figure has two
parts; the "A" part being for a pin-pin wall; the "B" part for a fixed-fixed
wall.

Figs. 3-1 and 3-2 show that the fixed-fixed supports result in a much
higher frequency than the pin-pin supports, a phenomenon also observed with
solid walls. In addition, for a node on the horizontal centerline near the edge
of the wall, Fig. 3-1 shows that the displacement for the two types of mountings
are of the same order with window walls, where with solid walls, the displace-
ments differed by more than a factor of four (see Fig. 2-6). There is also
a strong displacement reversal of a node on the horizontal centerline of the
fixed-fixed wall with a window, while only downstream displacements occur with
a fixed-fixed solid wall.

Fig. 3-2 contains plots of predicted displacements of nodes at some distance
from the horizontal centerline. In the case of the pin-pin wall, displacements
of these nodes are smaller than those of nodes on the horizontal centerline,
(the maximum for a node on the vertical centerline being only about one half
as great) but they are otherwise similar. In the case of the fixed-fixed walls,
both the maximum nodal displacements and the patterns of the displacements differ.
The maximum of those away from the horizontal centerline are far smaller (only
about 20% as large) as those on the centerline.

The contours of displacement, at times near the maximum of the two preceding
figures are shown in Fig. 3-3. Displacements, in the case of the fixed-fixed

wall are less uniform and about one fourth as large as those of the pin-pin wall.

The patterns of stress vs time in Fig. 3-4, and stresses near the time of maximum deflection in Fig. 3-5 generally follow the displacement histories. A concentration of stress in the vicinity of the window corners is especially noticable in the pin-pin stress contour map shown in Fig. 3-5A.

SAMIS also produced information on directions of stress in the various elements. From this information it was possible to predict the probable direction which a crack would take from the corner of the window assuming that the brick-mortar assemblages were homogeneous). This prediction is shown in Fig. 3-6. Note that the crack extends almost horizontally from the window.

EXPERIMENTAL RESULTS

Shock tunnel tests were conducted on a total of eight non-arching non-reinforced masonry walls supported as pin-pin beams, and containing a window opening. Four of these were of brick and four of concrete block, all nominally 8-in. thick. Two of the brick, and two of the concrete block walls were provided a preload of 22,500 lb, the equivalent of about three stories of identical walls in the case of the brick walls and about six stories in the case of the concrete block walls. Fig. 3-7 contains pretest photographs (looking upstream) of typical brick and block walls in the shock tunnel. Both windows were nominally 38 in. high and 62 in. wide. Note that one of the crack gauges on each wall (the vertical strips on the wall faces) is located quite close to the window opening.

Most walls were subjected to more than one blast wave from either one or two strands of Primacord. In the cases of the two non-preloaded concrete block walls, the initial tests -- conducted to acquire information on the natural frequencies of the walls -- employed only 10-ft long strands of Primacord.

At the end of the series of tests run on each wall, in all but one case the wall had collapsed, with the largest amount of debris landing within 10 ft of the initial wall position, though with smaller pieces of debris being thrown as far as 30 ft. Photographs of debris from two of the test series are shown in Fig. 3-8. With all eight walls, cracking first took place at the corners of the windows, and progressed horizontally across the wall face.

Brick Walls

Walls 56 and 57 had no preload; Walls 69 and 70 were preloaded with 22,500 lb using the preload mechanism described in Appendix A. Wall No. 56 was exposed to a nominal peak reflected pressure ≈ 4.0 psi. It failed completely with the top portion landing atop the bottom portion. One window side panel

remained attached to the top until it impacted the floor.

Wall No. 57 was tested four times, the first three times using a nominal peak reflected pressure = 1.3 psi. The wall cracked on the first test, (with the first crack being recorded 19 msec after initial loading) and the cracks enlarged during the succeeding two tests. In the fourth test, a nominal peak reflected pressure of 4.1 psi was used and the wall collapsed in much the same manner as did Wall No. 56.

Both preloaded brick walls were subjected to two tests, the first using a nominal peak reflected pressure of 1.6 psi; the second using 4.3 psi. In both cases, the first tests caused no apparent damage. With Wall No. 69, the second test caused cracking at the top of the window opening (the earliest crack occurring 7 msec after the initial loading), but the wall did not fail. With Wall No. 70, the second test caused wall failure, as shown in Fig. 3-8A. A plot of displacement at the horizontal centerlines of Walls No. 56, 57, and 70 (the three walls that failed) is shown in Fig. 3-9.

Concrete Block Walls

The two wall panels without preload were Numbers 60 and 61; the two panels preloaded with 22,500 lb were Numbers 72 and 73. As already noted, the initial tests on Walls No. 60 and No. 61 used a single strand of Primacord only 10 ft long. The purpose of these low level tests was to establish a natural frequency for the walls, which appeared to be on the order of 30 msec, about one half that of brick walls as predicted by SAMIS.

Despite the low loading pressure, and the very short duration of the loading pulse, each wall cracked during its first test. Each wall was then subjected to a nominal peak reflected pressure of 1.5 psi, and Wall No. 60 collapsed. Wall No. 61 did not, though the cracks caused by the blast from the short length of Primacord enlarged. It was then loaded again at the same level, and this time, it too collapsed as shown in Fig. 3-8B. Fig. 3-10A shows displacement of the two walls (measured at the horizontal centerline) as a function of time during the tests which caused wall collapse.

3-6

The two preloaded walls first withstood a nominal peak reflected pressure of 1.6 psi, then collapsed on a second test when exposed to 4.3 psi. Fig. 3-10B shows the downstream displacements along the horizontal centerline as a function of time during the second tests of these two walls.

COMPARISON OF EXPERIMENTAL RESULTS WITH THEORY

The tests on the two brick walls without preload showed that:

o One wall did not collapse under three successive tests with a
   peak loading pressure of 1.3 psi although cracking occurred.

o This wall and the other failed completely for peak loading
   pressures of 4.0 and 3.8 psi respectively.

In applying the above information it is necessary again to consider the
significance of a crack without collapse. As discussed earlier for solid
preloaded walls, the occurrence of a crack (without wall collapse) was taken
as a measure of failure, since after cracking the wall was much weaker, and
if the pulse duration was much longer the wall would have collapsed. This
same argument does not hold for a window wall because of the different nature
of the loading. For the solid wall an essentially uniform loading equal to
 e peak reflected pressure is applied for the duration of the loading pulse.
For the window wall, however, (as discussed earlier) only the initial effective
net loading is the peak reflected value. This rapidly (in about ≈5 msec) de-
creases to a value significantly less than peak reflected. Since the window
wall does not experience peak reflected pressure loading after cracking, but
a significantly lower value, cracking was not taken to mean failure (collapse)
for window walls. Thus, 1.3 psi can be taken as the lower bound and 3.9 psi as
the upper bound for the experimentally determined peak loading pressure necessary
for failure.

The calculated failure loading pressure as given by SAMIS and the static
test data predict mean failure pressures of 1.6 ± 0.4 psi. As for previous
brick wall data the results are not inconsistent with each other, with the
calculated value tending to be lower than the experimental value.

The tests on the two brick walls with preload showed that:

o Neither wall showed damage for an incident peak loading of 1.6 psi.

o One wall failed and the other cracked for a peak loading pressure of 4.2 psi.

The SAMIS calculation predicts a mean failure pressure of 1.8 ± 0.6 psi (this includes a 17% correction for the effect of the preload in reducing wall stress). Again the experimental and calculated ranges overlap with the calculated values being lower.

The two tests on the concrete block walls without preload showed that:

o One wall collapsed with a peak loading pressure of 1.5 psi.

o A second wall survived one loading with a peak reflected pressure of 1.5 psi, but failed on a second similar loading.

These results indicate that 1.5 psi is a reasonable estimate of the loading for failure. The SAMIS calculation gives 1.2 ± 0.7. The experimental result is somewhat higher, but well within the uncertainty band.

The two tests on preloaded concrete block walls showed that:

o Both walls showed some damage, but did not fail with a peak loading pressure of 1.5 psi.

o Both walls failed under a peak loading pressure of 4.3 psi.

These results give bounds of 1.6 - 4.3 psi with the estimated value likely tending towards the lower limit. The SAMIS calculation gives a value of 1.4 ± 0.8 psi. Again there is overlap between the experimental and theoretical ranges with the theoretical values being lower.
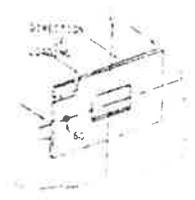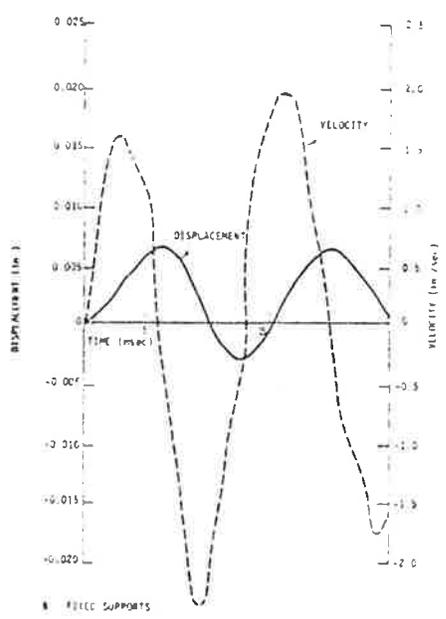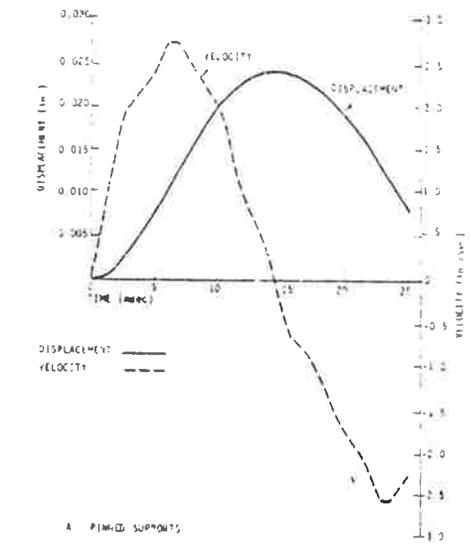
Fig. 3-1. Displacement and Velocity vs Time for Node 60 on a Wall with a
Window with Pinned and Fixed Supports Top and Bottom.
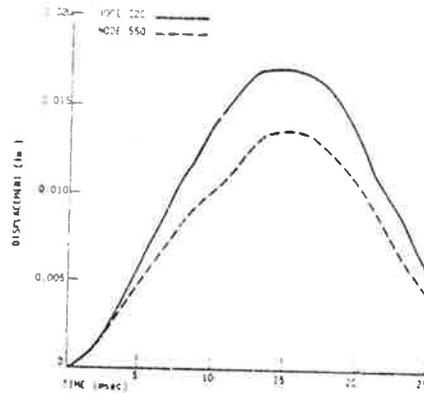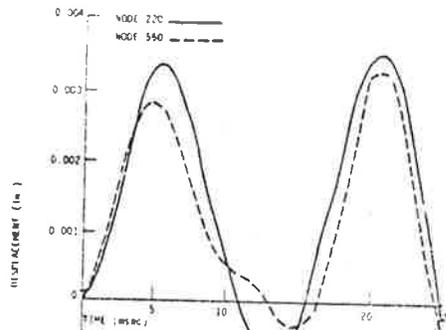
A   PINNED SUPPORTS
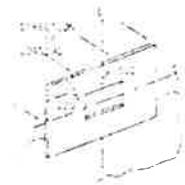
B   FIXED SUPPORTS

Fig. 3-2.   Displacement vs Time for Nodes 220 and 550 on a Wall with a
Window with Pinned and Fixed Supports Top and Bottom.

3-11

A PINNED SUPPORTS   TIME = 0.015 sec

B FIXED SUPPORTS   TIME = 0.016 sec
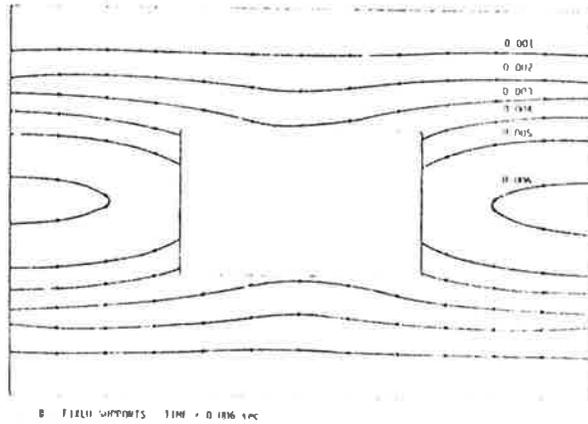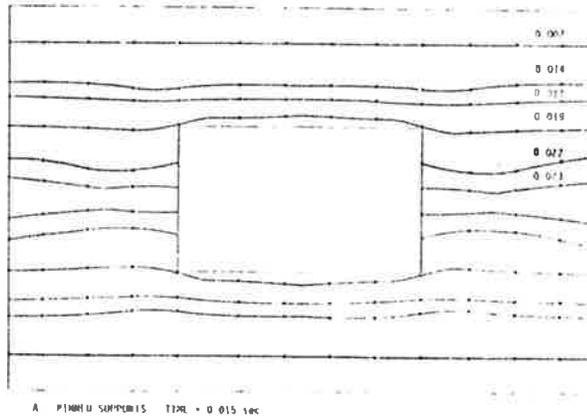
Fig. 3-3.   Deflection Contours (in.) at the Time of Maximum Deflection of a
Wall with a Window with Pinned and Fixed Supports Top and Bottom.

3-12
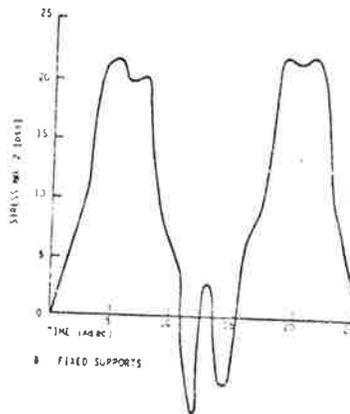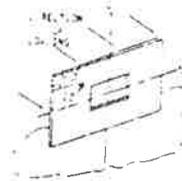
Fig. 3-4. Stress vs Time for Element No. 22 on a Wall with a Window with Pinned and Fixed Supports Top and Bottom. Note, Element No. 22 is not the Maximum Stressed Element for the Fixed-Fixed Case.

3-13

A PINNED SUPPORTS TIME = 0.015 sec

B FIXED SUPPORTS TIME = 0.006 sec

Fig. 3-5. Stress Contours for Downstream Face at Time of Maximum Deflection of a Wall with a Window with Pinned and Fixed Supports Top and Bottom.

3-14
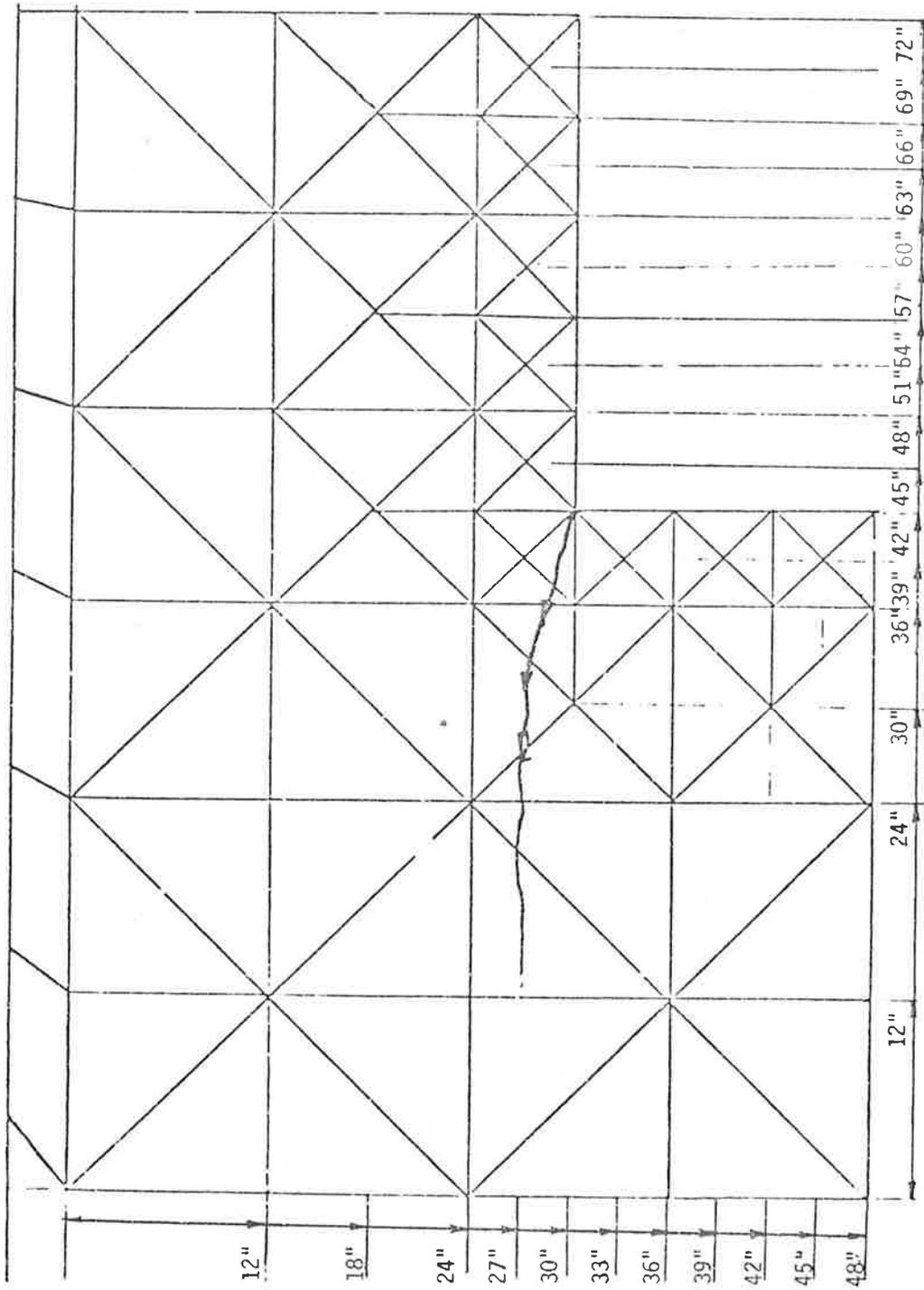
Fig. 3-6. Coordinates and Predicted Crack Trajectory on a Wall with a Window with Pinned Supports Top and Bottom.

3-15
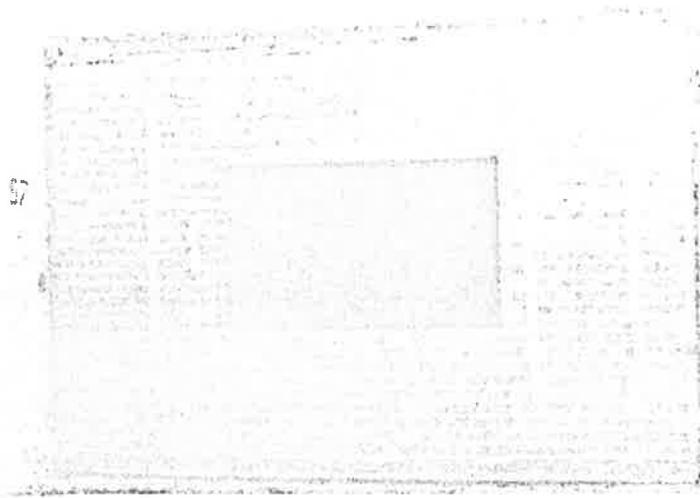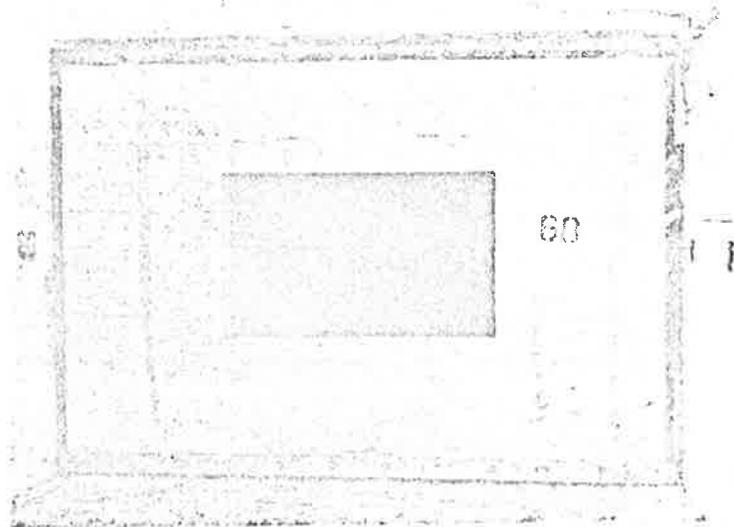
A. Brick.

B. Concrete Block.

Fig. 3-7. Pretest Photographs of 8-in. Thick, Non-reinforced Brick and Concrete Block Wall Panels with a Window Opening.

A. Brick Wall No. 70. Loading Pressure = 4.3 psi.

B. Concrete Block Wall. Second Test at Loading Pressure = 1.5 psi.

Fig. 3-8. Posttest Photographs of Brick and Concrete Block Walls with Windows.
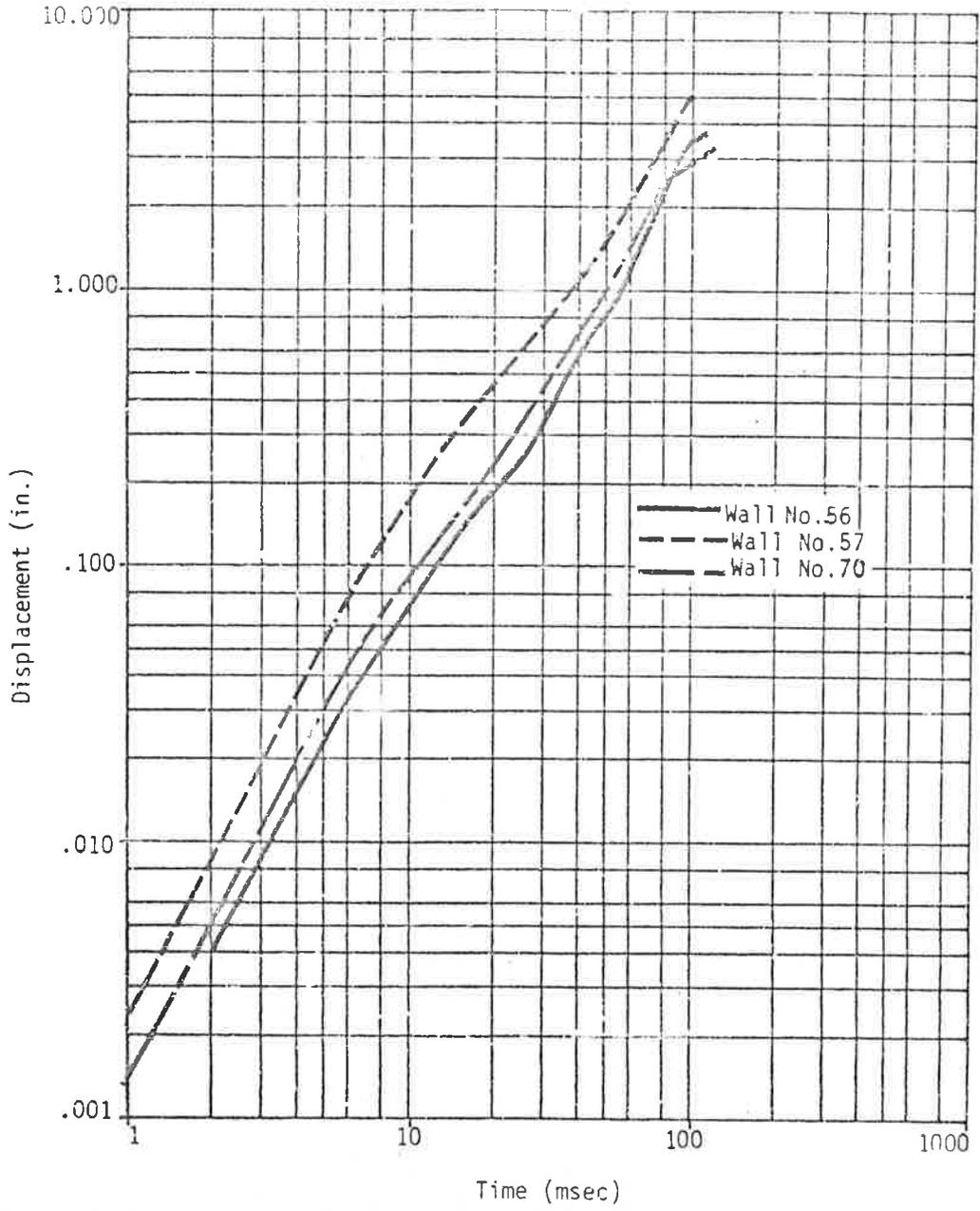
Fig. 3-9.   Displacement vs Time of Three 8-in. Thick Non-reinforced Brick
Walls with Window Openings, Loading Pressure ≈ 4 psi.
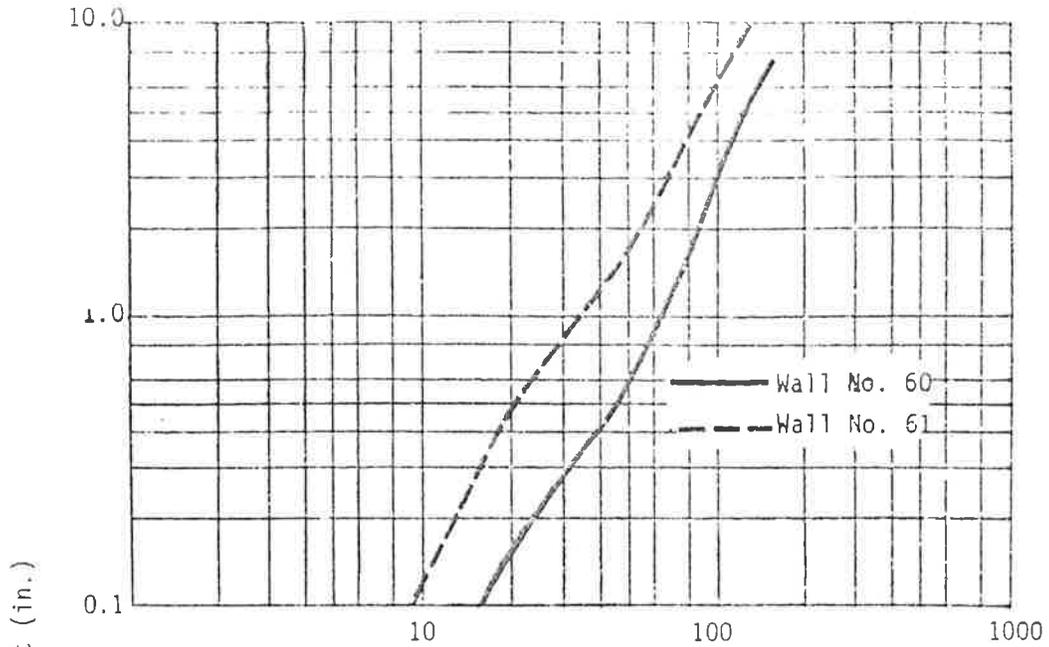
A. Without Preload. Loading Pressure ≈ 1.6 psi.
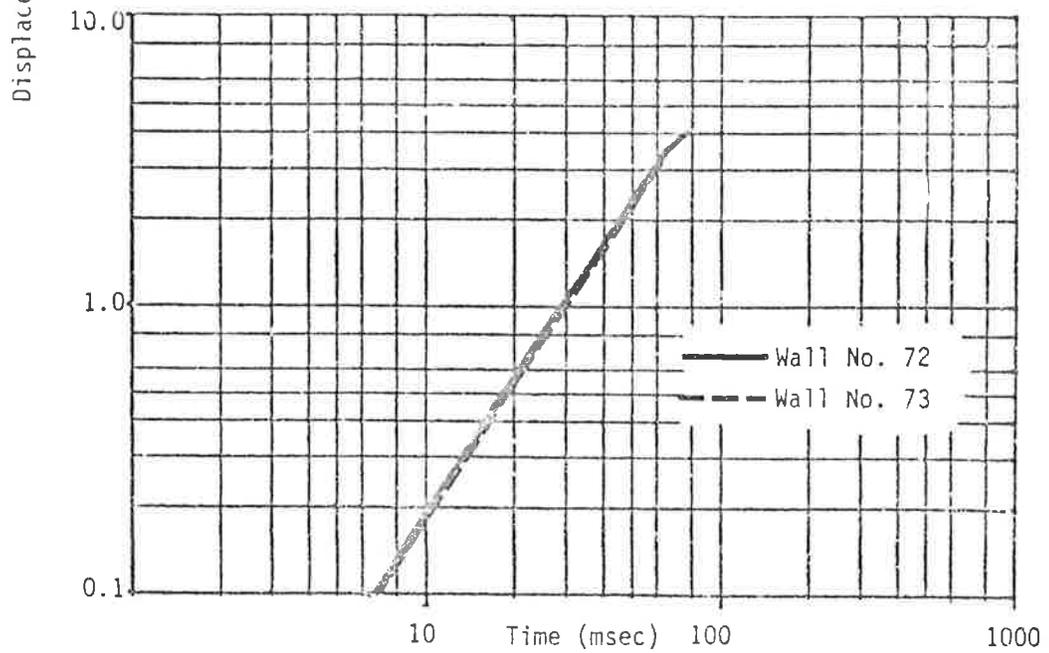
B. With Preload. Loading Pressure ≈ 4.3 psi.

Fig. 3-10. Centerline Displacement vs Time of Concrete Block Walls with and Without Preload.

3-19

Section 4

WALLS WITH A DOORWAY SUPPORTED AS BEAMS

GENERAL BEHAVIOR

The basic failure mode of a beam-mounted wall with a doorway that extends the full height of the wall, is similar to that of a solid wall, in that a uniform load applied to one face causes the highest stresses and greatest displacements to occur at the horizontal centerline of the wall. If these stresses exceed the tensile strength in flexure of the wall materials, failure at this centerline will occur.

Details of this behavior, however, differ in the two cases principally because the loading on the wall with a doorway is far more complex than that on a solid wall. On a solid wall, a flat-topped incident pressure pulse generates a uniform, flat-topped loading pressure on the wall equal to peak reflected pressure. On a wall with a doorway, this same flat-topped incident pulse results in a loading pattern that changes with time and with location on the wall.

As shown in Volume 2, shock and rarefaction waves propagating across both upstream and downstream faces of the wall cause the net loading pulse at a particular point to decrease from its initial peak reflected pressure at a time related to the distance of the point from the doorway. At a later time, the pulse again increases with the result that net loadings across the face of the wall become highly non-uniform. (See Fig. B-2.) The result of this non-uniform loading is a wall response which, while symmetrical in the verti- cal direction, is unsymmetrical in the horizontal direction.

The preload effects on a wall with a doorway should be similar to those on solid walls, being relatively unimportant for walls that are inherently strong (e.g., the brick walls built for test), but of possible significance for inherently weak walls (concrete block or clay tile walls).

4-1

DYNAMICS OF WALL BEHAVIOR

Predictions of the dynamic behavior in the elastic range (i.e., with no flexural cracking occurring) of a wall with a doorway were made using the computer program SAMIS. Some results of the SAMIS calculations are shown in Figs. 4-1 through 4-4 for walls with both pin-pin supports and fixed-fixed supports.

As with the solid wall, the fixed-fixed supports cause a much higher natural frequency but much lower displacement (Fig. 4-1) and stress (Fig. 4-3) than pin-pin supports. Maximum displacements and stresses with the fixed-fixed supports are only about one third as great as those with the pin-pin supports.

The effect of a non-uniform loading across the face of the wall is most apparent in Fig. 4-2, displacement contours drawn for the times when displacement at the doorway was near its maximum (= 17 msec for pin-pin walls; ≈ 7 msec for fixed-fixed walls. See Fig. 4-1). Both parts of Fig. 4-2 show a symmetry of displacement about the horizontal centerline, but an asymmetry about the vertical, a result quite consistent with the observed loading patterns. It is interesting to note that at the times of the two parts of the figure, the wall with pin-pin supports has its maximum displacement at the doorway, while the wall with fixed-fixed supports has its minimum displacement at the doorway.

Not apparent in Fig. 4-2 is the manner in which the changing loading across the face of the wall changes wall response as a function of time. This can be seen in Fig. 4-5, plots of displacement countours at three different times after loading. The changing loading is clearly causing a wave-like response, with the displacement maximum along the horizontal centerline shifting from one side of the wall to the other. At a time of 13 msec, the maximum is almost uniform across the entire wall face.

EXPERIMENTAL RESULTS AND COMPARISON WITH THEORY

Tests were made on four beam-mounted, pin-pin supported walls with a door-way, in the geometry sketched and photographed in Fig. 4-6. Wall No. 44 was subjected to the blast wave from four 60-ft strands of Primacord (peak reflected pressure ≈10 psi). It failed catastrophically, breaking into many pieces scattered well down the tunnel. Wall No. 46 was subjected to the blast wave from two strands of Primacord (peak reflected pressure ≈4 psi). It, too, failed, but the debris consisted of large pieces in the immediate vicinity of the initial position of the wall.

Walls No. 45 and No. 48 were tested more than once. With Wall No. 45, a single 12-ft long strand of Primacord was used to provide a low-level load with which the wall's natural period could be determined. This was measured as about 33 msec, consistent with the natural period which could be inferred from the SAMIS results (Fig. 4-1). No damage was observed. The wall was then exposed to a loading with a peak reflected pressure ≈4 psi. It collapsed, initially breaking into two pieces at the horizontal centerline. The lower half rotated until it struck the floor; the upper half rotated 90 degrees and landed directly atop the lower half.

Wall No. 48 was subjected to five separate tests. In the first with a 10-ft strand of Primacord, the wall's natural period was determined to be 33 msec, identical with that of Wall No. 47. The wall did not appear to be damaged. The next three tests were conducted at a nominal peak reflected pressure of about 1.7 psi. Again, no damage was observed from any of these tests.

On the fifth test, with peak reflected pressure ≈4 psi, the wall failed in a manner similiar to that of Wall No. 45. Fig. 4-7 shows the debris from the final tests on Walls No. 45 and No. 48. Fig. 4-8 is a plot of wall displacement at the horizontal centerline as a function of time, recorded during these last tests. The displacement-time plots are similar,

though it appears that Wall No. 48 slowed between 10 and 20 msec, while Wall No. 45 appears to have sped up a bit during the same period.

The experimental results showed that:

- o One wall survived three successive tests with a peak loading pressure of 1.5 psi and exhibited no damage.
- o This wall and two others failed with peak loading pressure of 3.5 to 3.7 psi.

The SAMIS calculations for this configuration predict the failure loading pressure as 1.3 ± 0.4 psi. Although there is overlap between the experimentally and theoretically determined ranges of failure pressure, the theoretical values again are lower.
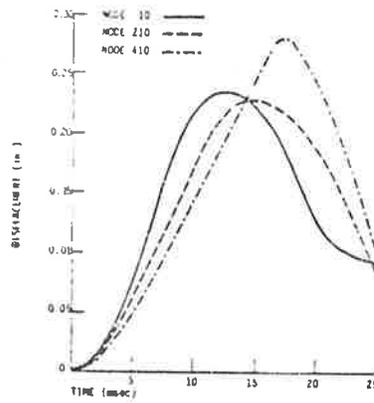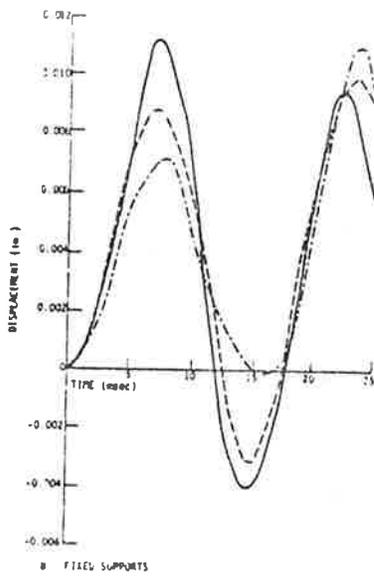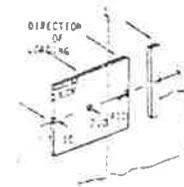
Fig. 4-1. Displacement vs Time for Nodes 10, 210, and 410 of a Wall with a Doorway with Pinned and Fixed Supports Top and Bottom of Wall.
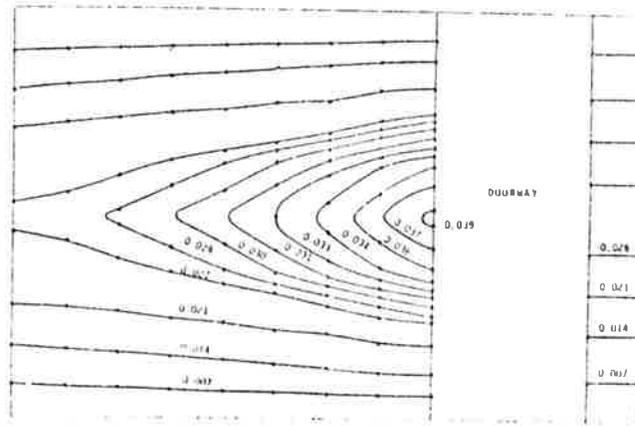
4-5
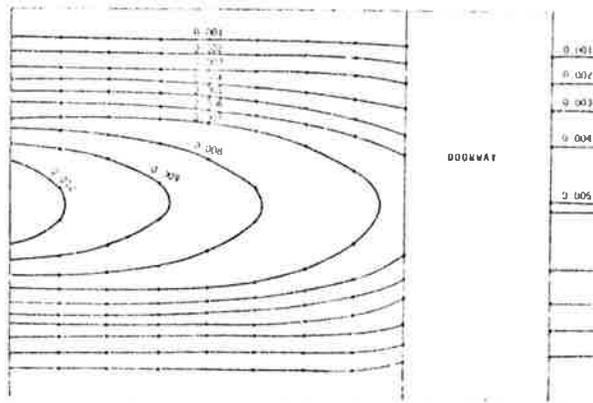
Fig. 4-2. Displacement Contours (in.) at Time of Maximum Deflection of a Wall with a Doorway with Pinned and Fixed Supports Top and Bottom.
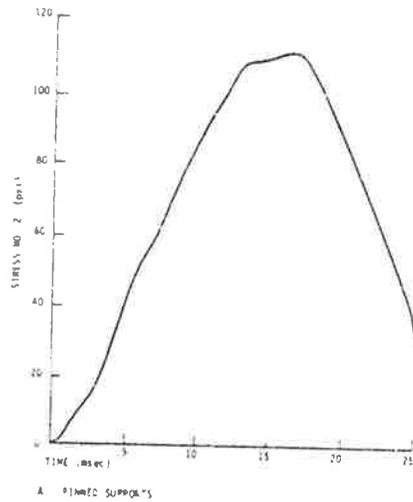
4-6
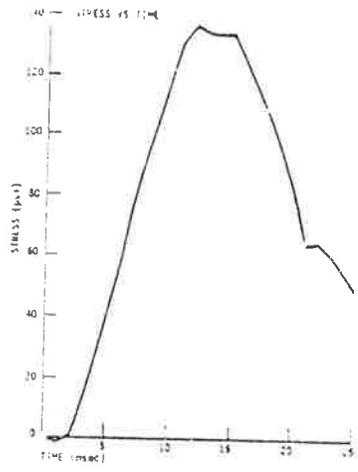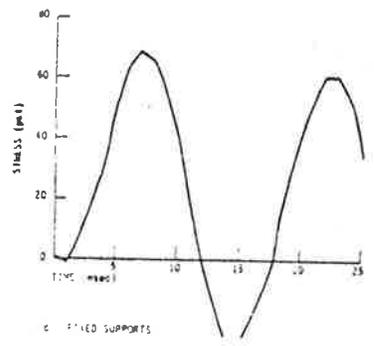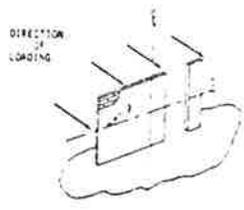
Fig. 4-3. Stress vs Time for Element No. 9 on a Wall with a Doorway with Pinned and Fixed Supports Top and Bottom. Note, Element No. 9 is not the Maximum Stressed Element for the Fixed-Fixed Case.
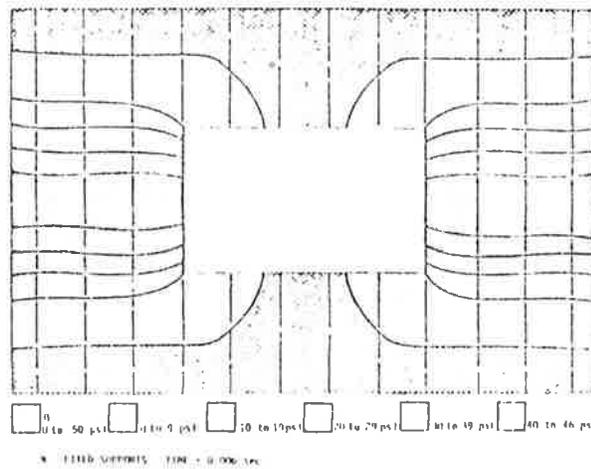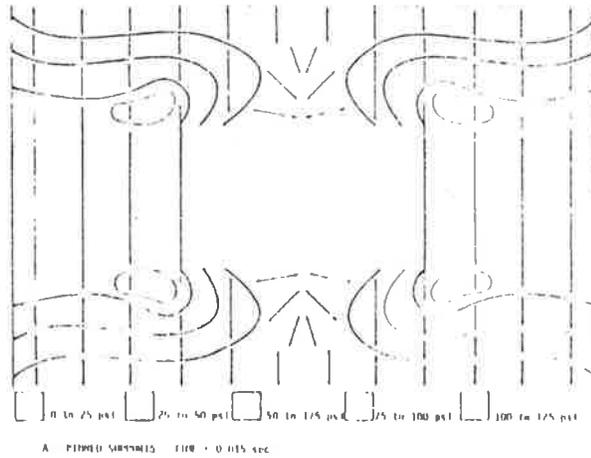
4-7
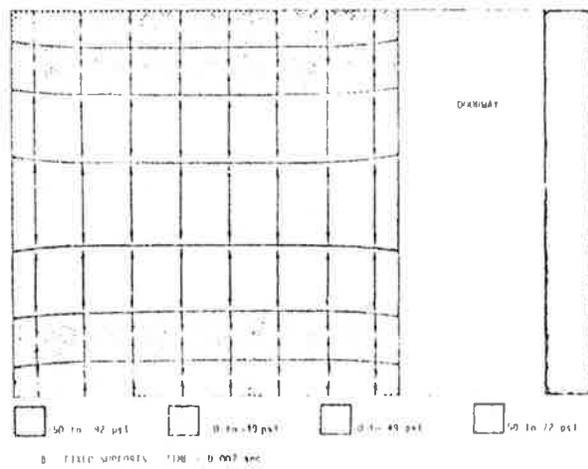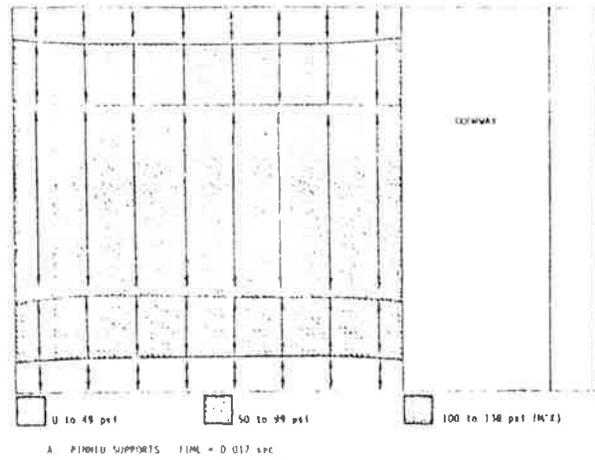
Fig. 4-4. Stress Contours on Downstream Face at Time of Maximum Deflection of a Wall with a Doorway with Pinned and Fixed Supports Top and Bottom.

A. TIME = 0.013 sec.

B. TIME = 0.014 sec.

C. TIME = 0.017 sec.
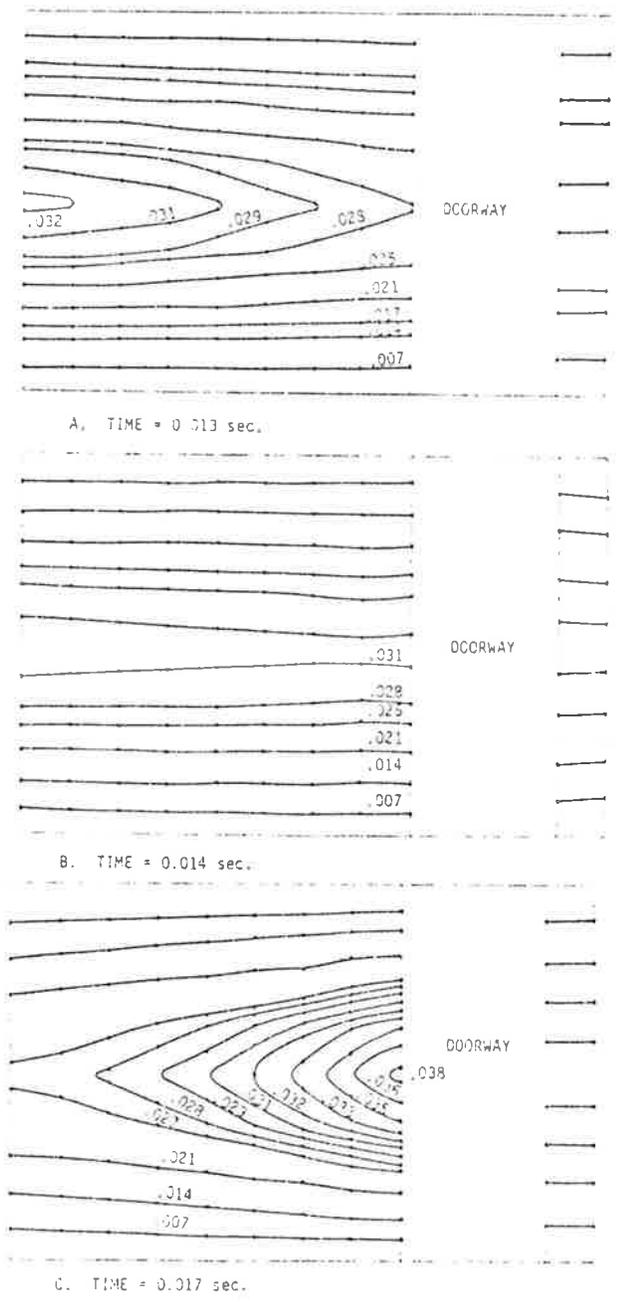
Fig. 4-5. Displacement Contours from SAMIS of a Wall with a Doorway with Pinned Supports Top and Bottom. Displacements are in inches.
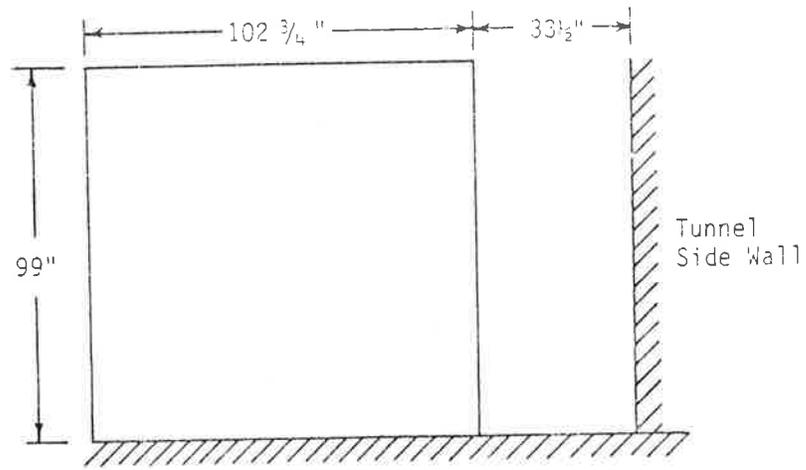
Fig. 4-6. Photograph and Sketch of Brick Wall with a Doorway.

A. Wall No. 48.

B. Wall No. 45.

Fig. 4-7. Posttest Photographs of Walls No. 45 and 48, 8-in. Non-reinforced Brick Walls with a Doorway. Loading Pressure for Both Walls = 4 psi.
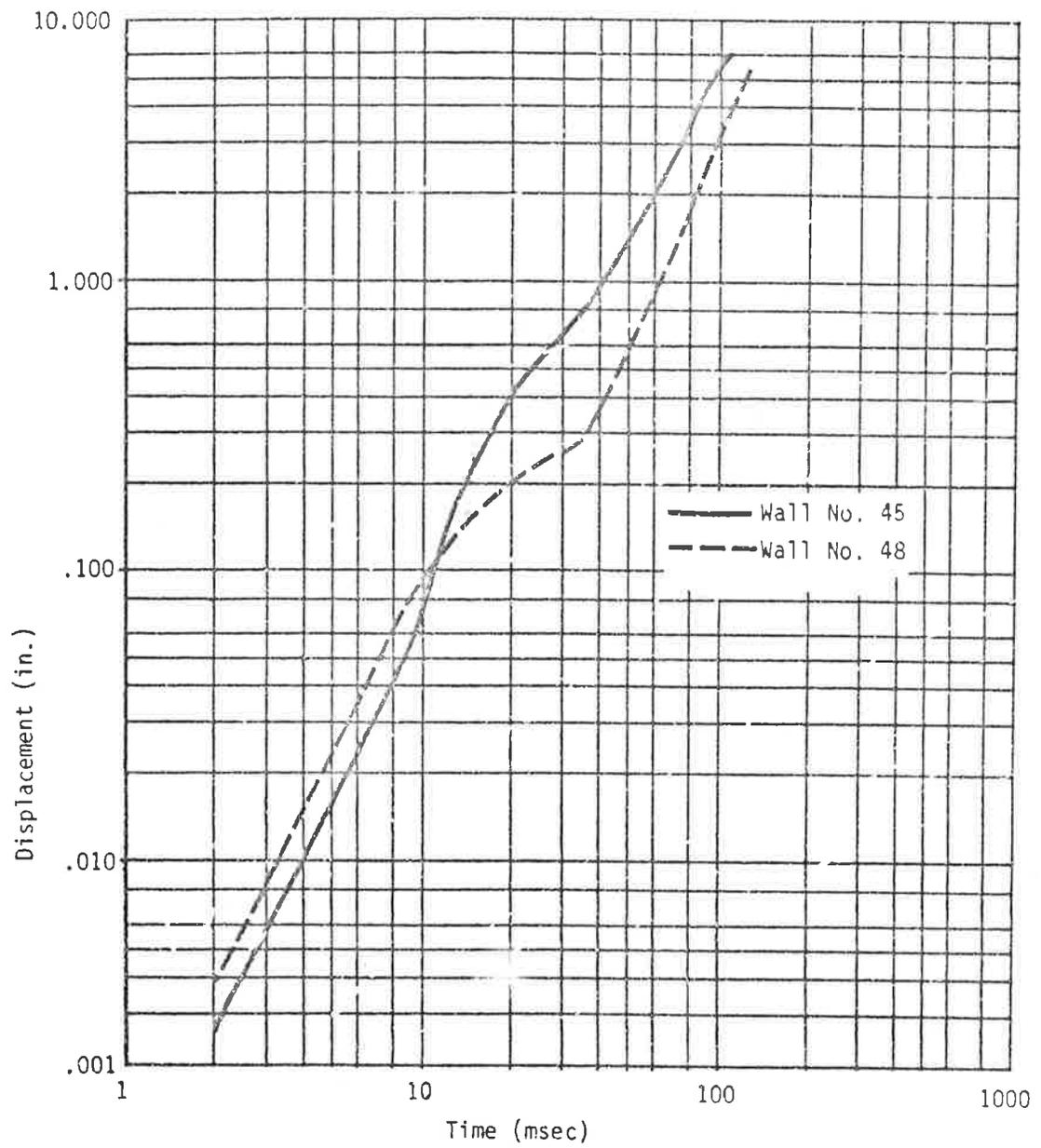
Fig. 4-8. Displacement as a Function of Time for Walls No. 45 and 48, 8-in. Non-reinforced Walls with a Doorway. Loading Pressure on Both Walls ≈ 4 psi.

Section 5

WALLS MOUNTED AS PLATES

The response to blast waves of walls supported on all four edges (plate type supports) is substantially different from that of walls supported on but two edges (beam type supports). Displacements and stresses at those edges of the walls which would have been free if the walls were mounted as beams, are reduced essentially to zero, and even maximum displacements and stresses (e.g., at the wall center in the case of a solid wall) are considerably reduced.

The computer program SAMIS was used to predict the behavior of the same six types of walls which have been previously discussed in their beam-mounted condition. (The three different wall geometries -- solid, with a window, and with a doorway -- were first assumed to have pinned supports, then to have fixed supports.) Only solid walls with pinned supports on all sides were subjected to blast waves in the shock tunnel.

SOLID WALLS

Predicted Behavior

Deflections of solid walls with both pinned and fixed supports on all sides are shown in Fig. 5-1, and stresses for the same types of walls in Fig. 5-2. Parts A and C of Fig. 5-1 show the deflections at three nodes as functions of time for the two support conditions, and Parts B and D are deflection contour, at a time close to that at which maximum deflections occur. Parts A and C of Fig. 5-2 show ress vs time on one wall element, and Parts B and D are stress contours a time close to that at which maximum deflections occur.

As before, the walls with fixed supports have shorter natural periods, smaller deflections and smaller stresses than the walls with pinned supports. The differences in behavior between beam-mounted and plate-mounted walls are

immediately apparent from the deflection plots (Fig. 5-1 for plate-mounted walls, Figs. 2-5, 2-6 for beam-mounted walls). In the beam-mounted condition, the plotted maximum deflections were all essentially the same for all three nodes. In the plate-mounted condition, however, node 10 nearest the wall edge has virtually zero deflection, and the deflection of node 160, halfway between the wall edge and its center, is much smaller than that of node 310 at the wall center. These differences are manifest in the two contour plots. In the beam-mounted condition, the wall bends uniformly about the two edge supports, with the maximum deflection occurring along the horizontal center-line, which is essentially a line about which deflections are symmetrical. The plate-mounted walls assume a dished shape with the maximum deflection occurring at the wall center, a point about which deflections are symmetrical.

The stress contour plots which are also symmetrical about the center of the wall, include arrows showing the directions of stresses at various places along the wall. With these stresses, the expected crack pattern on the down-stream face of a wall with pinned supports on all sides would be as shown in Fig. 5-3.

Experimental Information and Comparison With Predictions

Eleven plate-mounted solid walls with pinned supports that were free to rotate were subjected to blast waves in the shock tunnel. Measured peak load-ing pressures ranged from 3 psi to 19.3 psi. Six of the walls were tested under loadings in excess of 9 psi and collapsed immediately.

Four of the walls (24, 25, 27, and 29) which were exposed to measured peak loading pressures ranging from 3.2 psi to 4.0 psi, cracked as a result of the test, but did not collapse, though a 500-lb section of Wall No. 27 did fall out. The fifth wall (No. 28), subjected to a 4.0 psi loading did col-lapse. The crack patterns taken from high speed motion picture records of the downstream faces of these walls are shown in Fig. 5-4, and photographs of the cracks on the downstream face of Wall No. 24 are shown in Fig. 5-5.

The similarity between these crack patterns and those predicted by SAMIS

in Fig. 5-3 are apparent, clearly indicating that the walls responded as plates with pinned supports on all sides up to the time they cracked. If they had continued to do so after cracking, they would have failed under the blast loading. The mortar used in their construction, however, tended to bond the wall panels to the steel frame members in which they were constructed, and which were themselves pinned to the support girders (see Appendix A). With a wall deflection after fracture of more than a few tenths of an inch, these support members became a perimeter restraining ring, the bond of the wall to the frame at wall corners having the effect of making the perimeter continuous in nature instead of being free at each corner. This continuity provided thrust resistance and permitted a wall to go into an arching mode of response and be more resistant to ultimate failure than it would have been if it continued to have simple pinned supports. The phenomenon is illustrated in Fig. 5-6.

Walls 24 and 29 were subjected to second tests at peak loading pressures of 3.1 and 4.2 psi respectively. Wall No. 24 failed as a result of this second loading; Wall No. 29 lost about 350 bricks, but did not fail completely.

In view of the above discussion of arching, extensive cracking of the plate was taken as a measure of failure since in the absence of the perimeter restraining ring the walls would have been expected to have collapsed. Thus it can be concluded that 4.0 psi is an upper bound to the loading pressure necessary to collapse an 8-in. brick simple plate wall. No experimental data are available as a lower bound.

The SAMIS calculations give the predicted loading pressure for wall cracking as 1.4 ± 0.4 psi.

5-3

WALL WITH A DOORWAY

Predictions of deflections using SAMIS, of a plate-mounted wall with a
doorway, having both pinned and fixed supports on all sides and subjected to
a 1 psi step load are shown in Fig. 5-7. The stresses for the same conditions
are shown in Fig. 5-8. As before, the wall with fixed supports has a shorter
natural period than the wall with pinned supports. Its maximum deflection
is only about one fourth as great, and maximum stresses are about one third
as great. Because of the asymmetric nature of the loading pulse over these
walls, their response, while symmetric about the horizontal centerline, has
no symmetry about a vertical axis.

Comparing the maximum stresses for the pinned plate wall with the door-
way (Fig. 5-8) with those for the solid plate wall (Fig. 5-2B) shows that
the wall with a doorway is expected to require approximately 1.7 times the
solid wall loading to cause failure. It is interesting to note that for the
beam case the ratio was about the same, viz, 1.6.

WALL WITH A WINDOW OPENING

The SAMIS predictions for a plate-mounted wall with a window opening
are shown in Figs. 5-9 and 5-10. Walls with both fixed supports display
deflections and stresses which are symmetric about the wall center. The
natural period of the wall with fixed supports is about one half that of the
wall with pinned supports; its maximum deflections are one fourth to one third
as large, and its maximum stress approximately one half as large.

Comparing the maximum stresses for the plate wall with a window (Fig.
5-10B) with those for the solid plate wall (Fig. 5-2B) shows that the wall
with the window is expected to require about 1.9 times the solid wall loading
to cause failure. For the beam case the ratio was 2.2, again about the same.
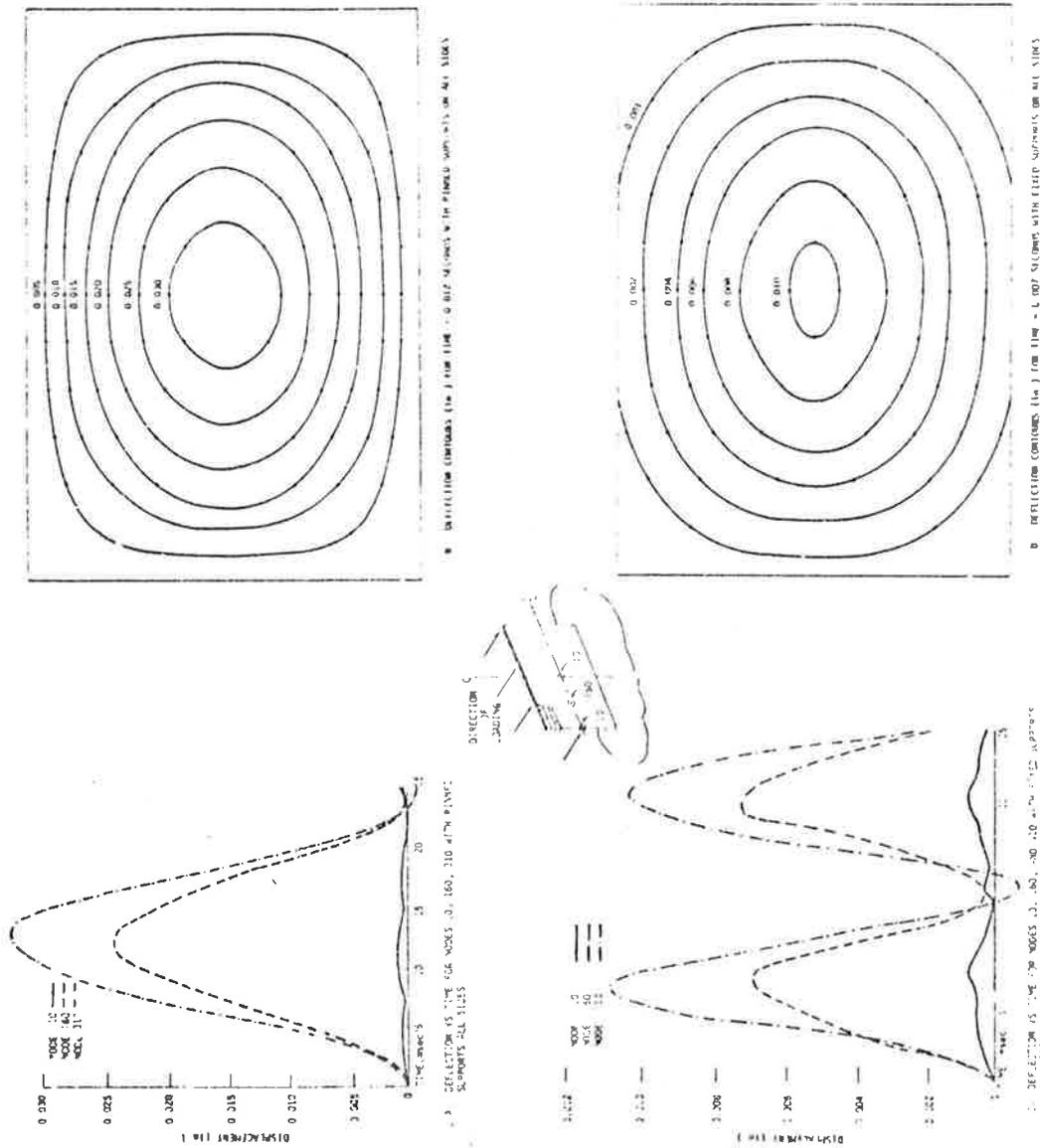
Fig. 5-1. Predicted Deflections for Plate-Mounted Solid Walls with Pinned and Fixed Supports.

5-6
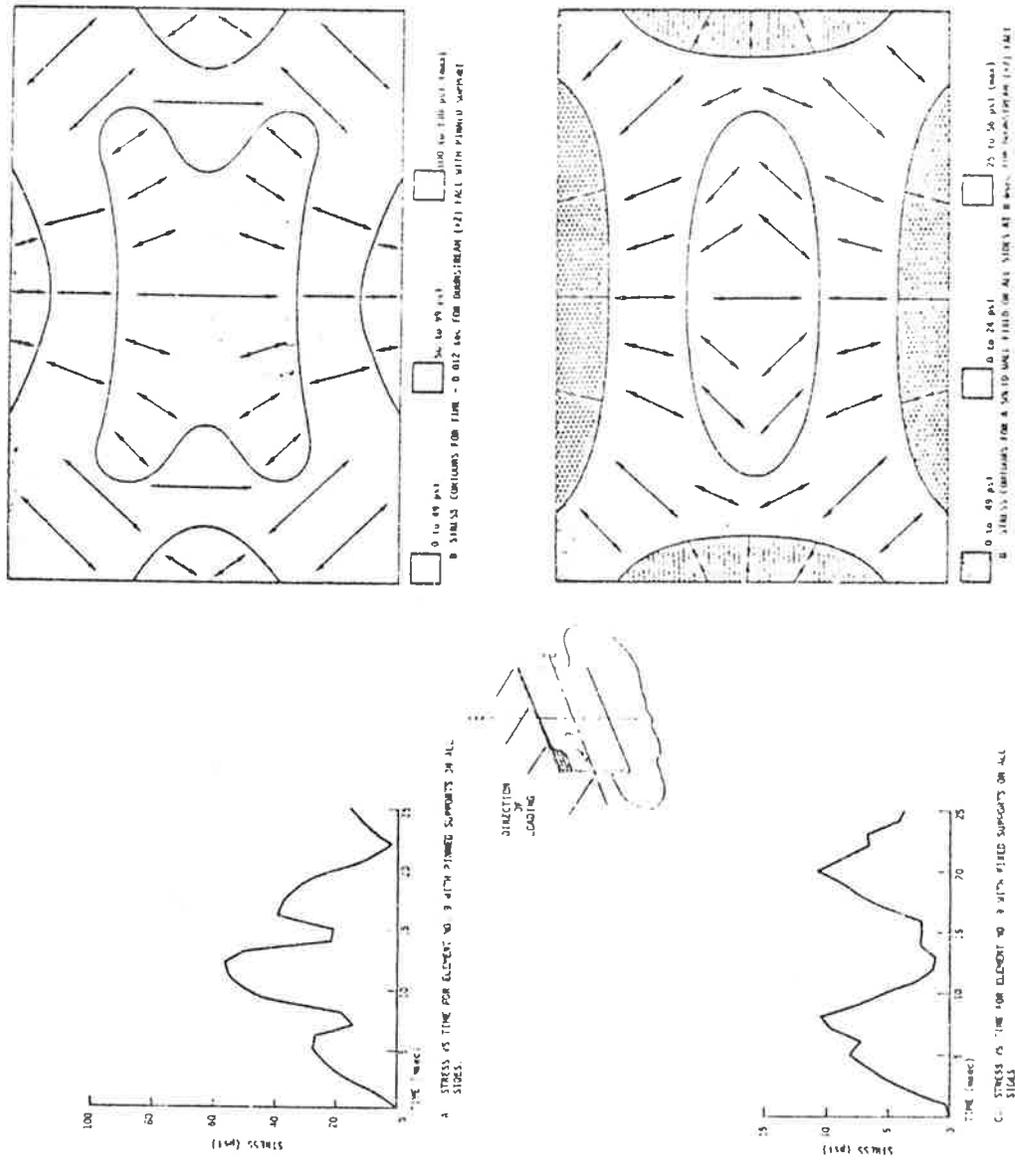
Fig. 5-2. Predicted Stresses for Plate-Mounted Solid Walls with Pinned and Fixed Supports. Note, Element No. 9 not Necessarily Maximum Stressed Element – for Comparison only.
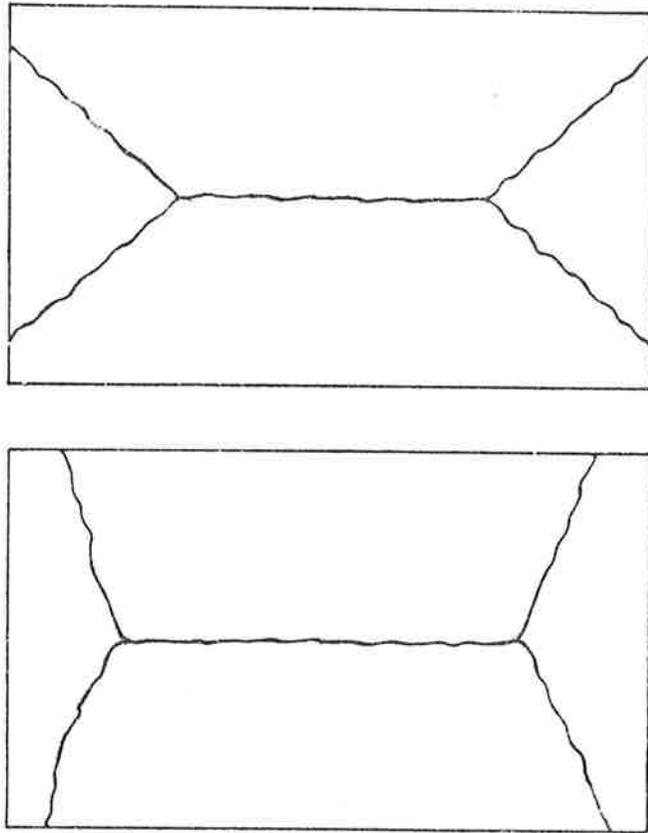
Fig. 5-3. Anticipated Downstream Face Crack Pattern (Form and Zone) for Plate-Mounted Solid Walls with Pinned Supports.
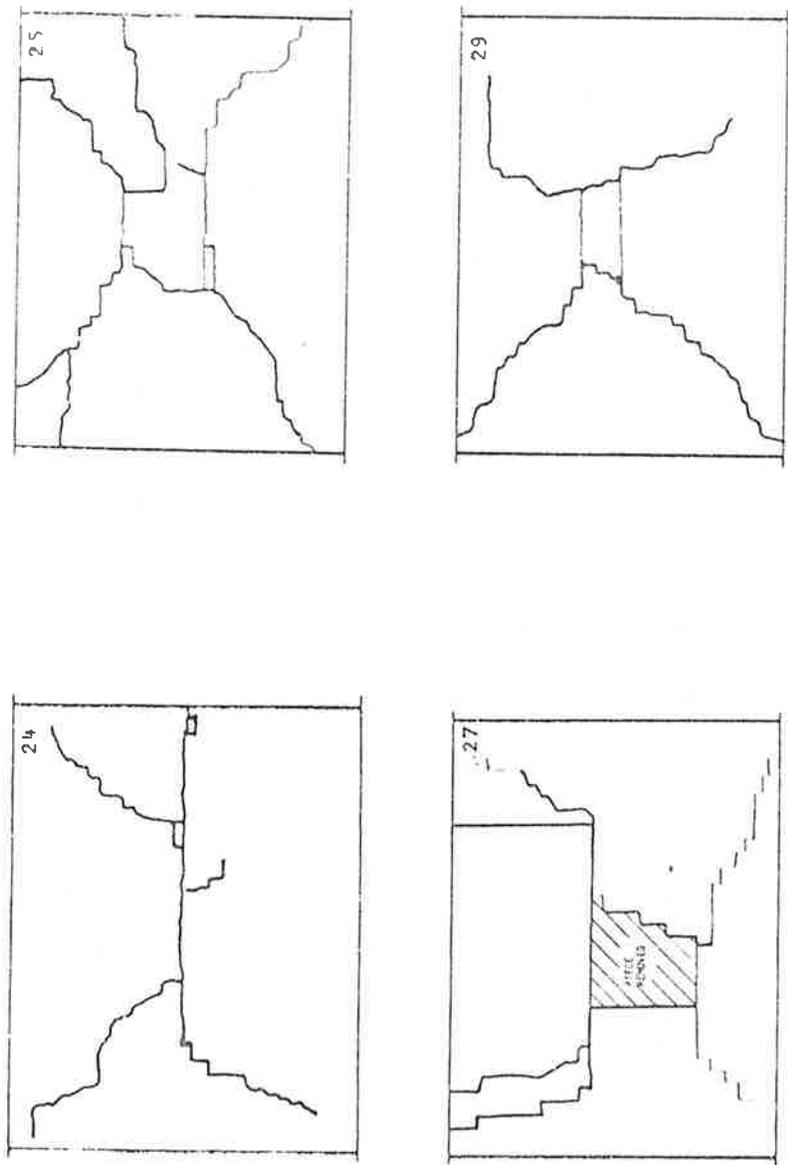
Fig. 5-4. Crack Patterns from Plate-Mounted Solid Walls, Peak Reflected Pressures = 3.2 to 3.8 psi. Walls No. 24, 25, 27, 29.
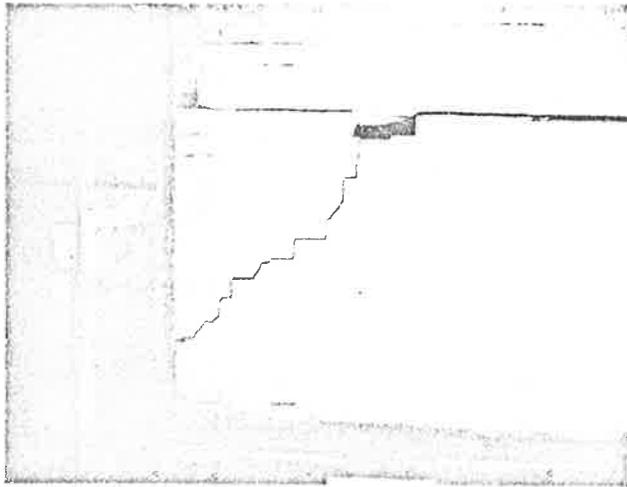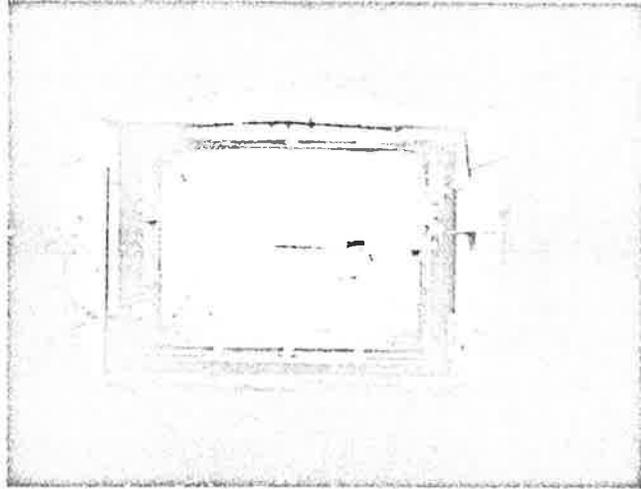
Fig. 5-5. Cracking on the Downstream Face of Wall No. 24.

STEEL PERIMETER MEMBERS

BONDING CORNERS

DOWNSTREAM

FRACTURE

LINES OF ARCHING THRUST
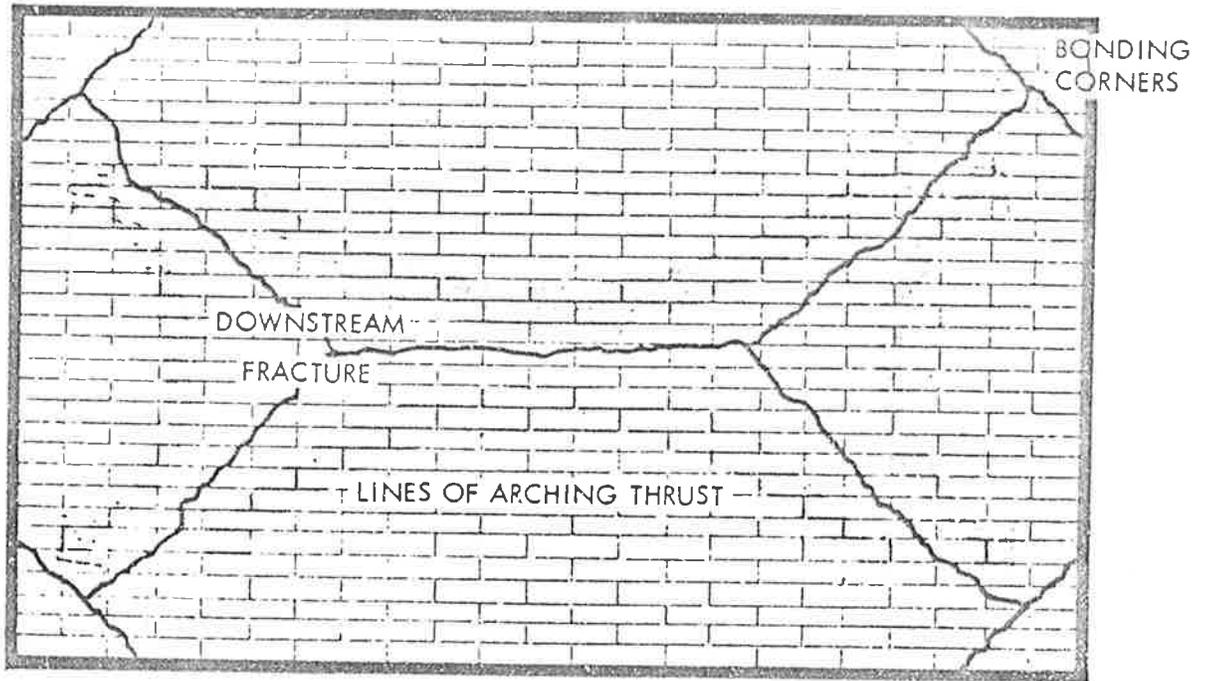
Fig. 5-6. Sketch Showing Effect of Steel Frame on Crack Pattern.
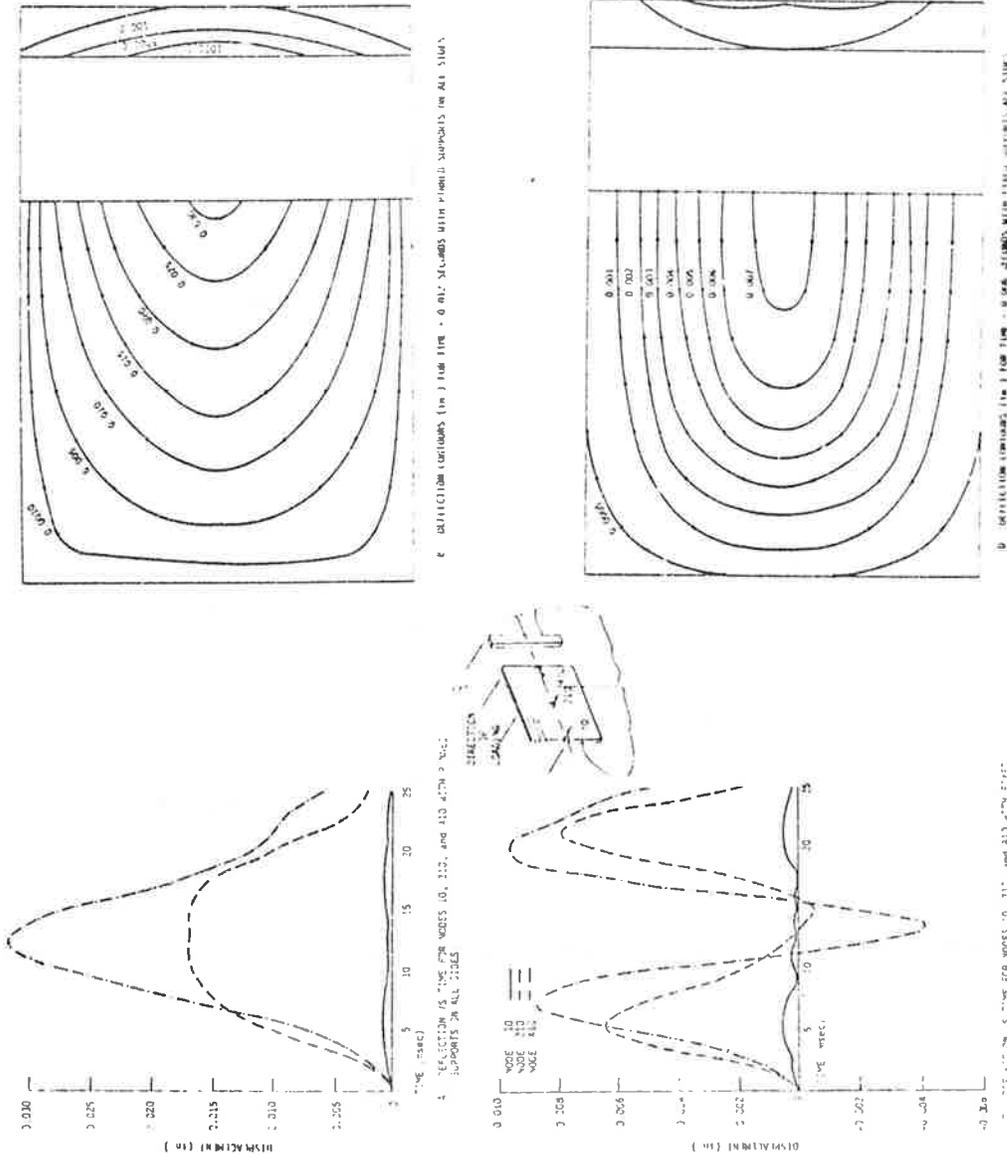
Fig. 5-7. Predicted Deflections for Wall with a Doorway with Pinned and Fixed Supports.
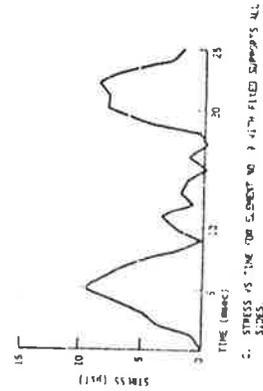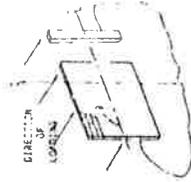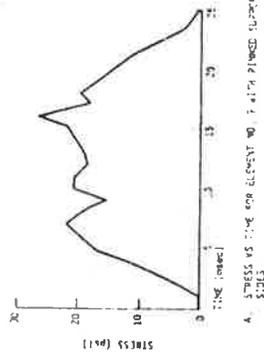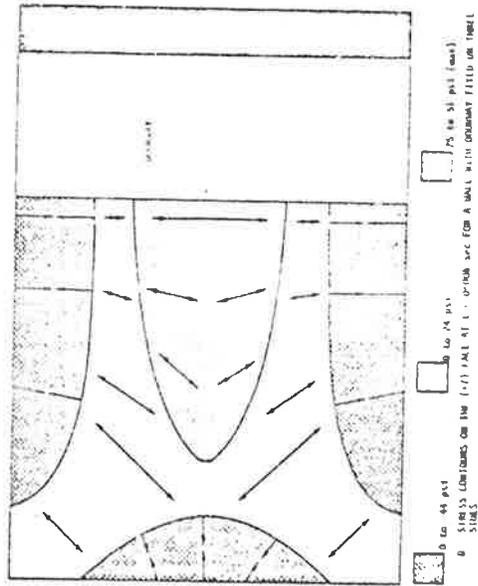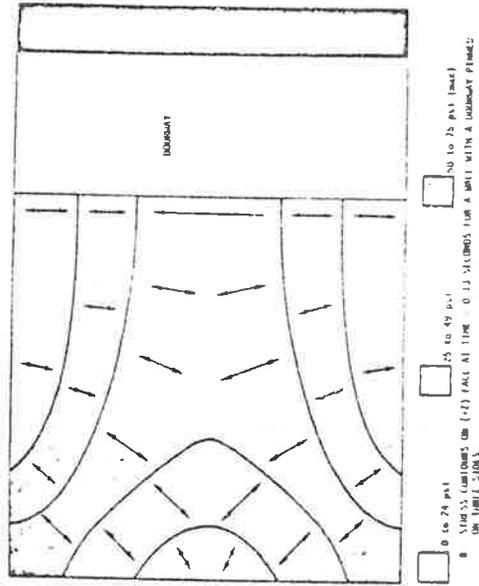
Fig. 5-8.   Predicted Stresses for Wall with a Doorway with Pinned and Fixed Supports. Note, Stresses in Element No. 9 not Necessarily Maximum.
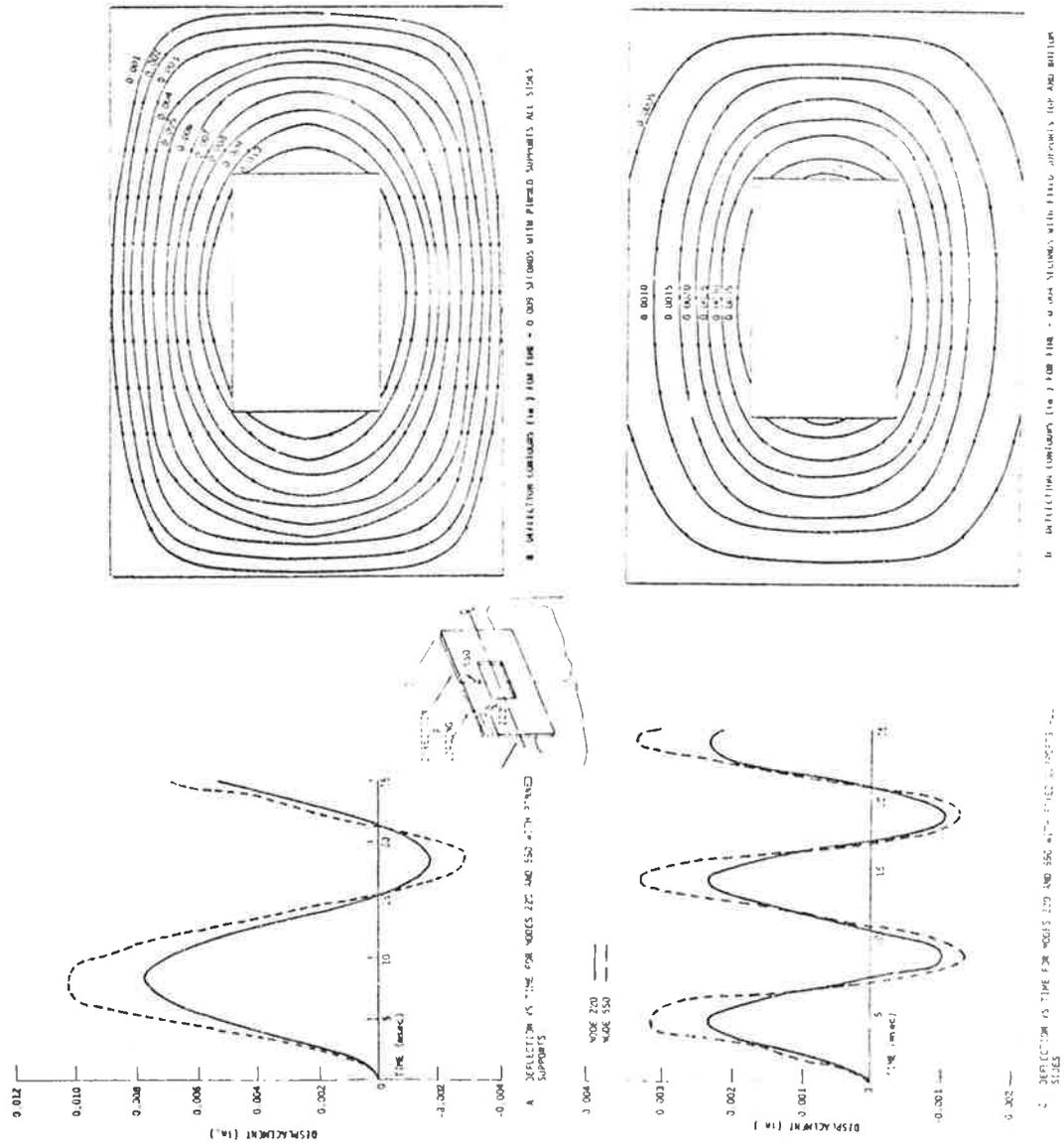
Fig. 5-9. Predicted Deflections for Wall with a Window Opening with Pinned and Fixed Supports.
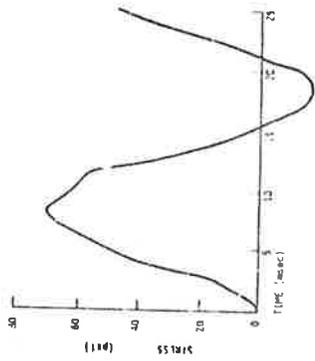
5-14
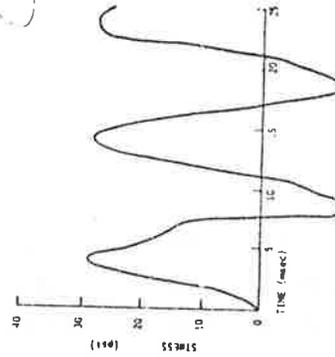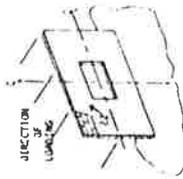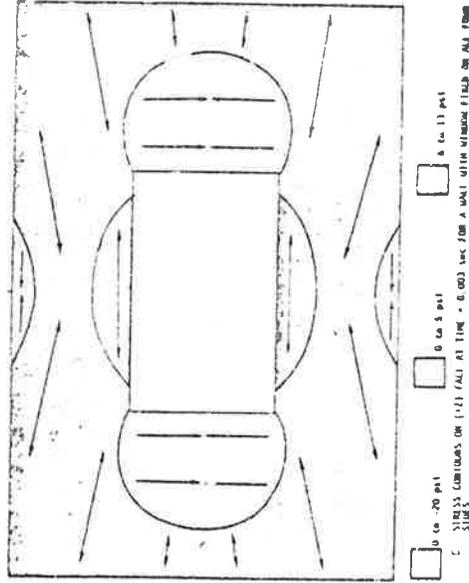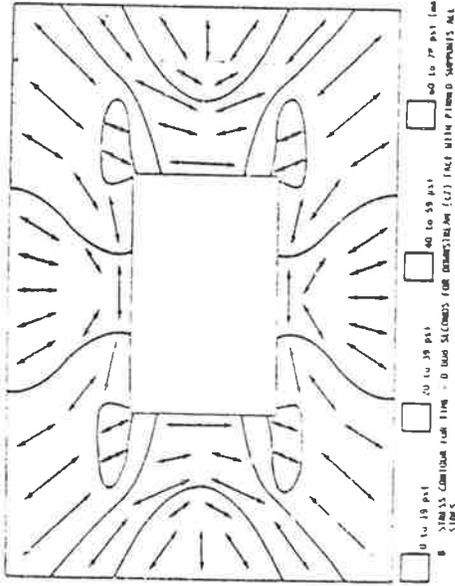
Fig. 5-10. Predicted Stresses for Wall with a Window Opening with Pinned and Fixed Supports. Note, Element No. 22 not Necessarily Maximum Stressed Element.

Section 6
ARCHING WALLS

INTRODUCTION

The ability of a masonry wall, confined within a rigid frame or structure so that in-plane motions and rotation about the wall's supports are prevented, to develop substantial resistance to out-of-plane forces such as those generated by blast waves has been recognized for many years. After flexural cracking occurs, the individual wall elements wedge themselves into the frame, and form a multi-hinged arch which will only fail after material crushing or spalling takes place at the hinge points. Theories of the behavior of such walls under out-of-plane blast loadings were developed about twenty years ago (Ref. 12,13).

During the course of this program the question arose whether a similar phenomenon could occur with walls which, though located within members that would prohibit in-plane motions, were separated from these members by a gap. The question had pertinence for two reasons: because some manuals of construction practice indicate that the inclusion of such a gap (or equivalent, a low-strength, flexible seal) between an infill wall and a frame is good building practice (it permits design frame action to occur); and because even where infill walls are carefully grouted into framing elements, mortar shrinkage is likely to cause the small gaps to form between wall and frame.

Analysis of this problem, subsequently supported by experiment, indicated that a form of arching could still occur where there was a small gap (as little as about 0.01 in.) between wall and frame ("gapped arching"). However, it was of a different kind than the arching that occurred where there was no gap ("rigid arching").

Fig. 6-1 illustrates, in exaggerated fashion, the differences in wall

6-1

motion in rigid and gapped arching.* Note that in rigid arching, a symmetrical three-hinged arch forms, with hinge points at the downstream top and bottom wall edges, and at the upstream edge of the crack in the center of the wall. In gapped arching, the three-hinged arch is unsymmetrical, the hinges being at the downstream bottom edge of the wall, at the upstream top edge of the wall, and at the upstream edge of the central crack.

Fig. 6-2 is a free-body diagram showing forces in rigid and gapped arching. Note that in rigid arching resultant forces at the top and bottom wall edges are directed into the wall, which should result in a crushing (largely compression) type of failure. In gapped arching, resultant forces at the top and center are directed away from the wall, which should result in a spalling (largely tensile) type of failure.

Special tests had to be devised to investigate material strengths under these types of failures (in which failure takes place along the edge of a crack, i.e., along a line). These tests are described in detail in Volume 4. Very broadly, it was found that the material strengths in the crushing type of failures such as those that occur with rigid arching are more than four times as great as the strengths in the tensile types of failures that occur with gapped arching.

Table 6-1 gives initial values of the forces at various points in Fig. 6-2, both in general terms and for a wall with dimensions similar to those tested in the tunnel, viz 8 ft high and 8 in. thick. It can be seen immediately that forces at the hinge points in gapped arching (R_A, R_B, and R_C) are almost twice as large as those in rigid arching. This, coupled with the fact that material strengths in gapped arching failures are smaller than those in rigid arching failures, strongly suggest that resistance to blast loadings

---

* The discussion concentrates on "one-way" arching, in which the wall is restrained on only two edges. Two-way (plate type) arching in which the wall is restrained on all four edges can also occur. Walls undergoing two-way arching can be considerably stronger than those undergoing one-way arching. A third form of arching occurred in the shock tunnel (see Section 5).

Table 6-1

Forces in Rigid and Gapped Arching

Force	General Formula		Values for ℓ = 96 in., t = 8 in. (lb/in.)	
	Rigid Arching	Gapped Arching	Rigid Arching	Gapped Arching
H	$p\ell^2/8t$	$p\ell^2/4t$	144p	288p
S_B	$p\ell/2$	$p\ell/4$	48p	24p
R_B	$(p\ell/8t)\sqrt{\ell^2 + (4t)^2}$	$(p\ell/4t)\sqrt{\ell^2 + t^2}$	152p	289p
S_C	-	$p\ell/4$	0	24p
R_C	$H = p\ell^2/8t$	$(p\ell/4t)\sqrt{\ell^2 + t^2}$	144p	289p
S_A	$p\ell/2$	$3p\ell/4$	48p	72p
R_A	$(p\ell/8t)\sqrt{\ell^2 + (4t)^2}$	$(p\ell/4t)\sqrt{\ell^2 + 3t^2}$	152p	297p

with gapped arching is much lower than those with rigid arching. (It is, however, greater than the blast resistance of ordinary beam-mounted walls after flexural failure takes place.)

ANALYSIS OF WALL BEHAVIOR

The behavior of arching walls depends strongly on the behavior of the wall materials under the line loads generated with arching. The small tilted static test samples used to determine material properties under forces generated by rigid arching behaved generally as shown below.

Behavior of 8.5 in. Thick Brick Samples Under Line Loading.
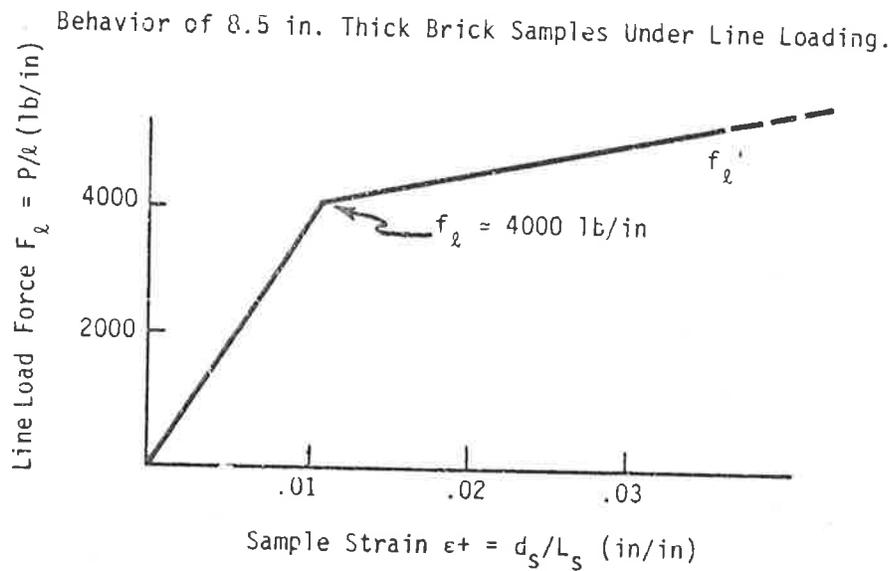
In this figure, the term ℓ refers to the length of the line, or sample edge, along which a load of P was applied; L_s is the height of the sample between the base platen and the loading head, and d_s is the loading head displacement.

In general, the samples exhibited an elasto-plastic form of behavior with displacement being a linear function of line load, F_ℓ (actual force P divided by the length of line over which the force is applied) up to a line

6-5

load "yield" strength, f_ℓ. At higher values of line load, crushing and spalling accelerated, and relatively little increase in load resulted in relatively large displacements until complete sample failure occurred at a yield strength of f'_ℓ. The slope $F_\ell/\epsilon^+ = F_\ell L_s/d_s$ of the first part of the line load vs strain plot has been termed E^+ because it plays a role similar to the modulus of elasticity E in ordinary compression testing (in which the sample is not tilted).

Information from data like that shown in the foregoing figure along with the displacements from the MACE computer program (see Appendix B) were used in Ref. 6 to derive static resistance functions for walls 8 in. thick and 8 ft high, i.e., similar to those tested in the shock tunnel. Since MACE only deals with displacements in the elastic range, a composite modulus of elasticity of 100,000 psi derived from the static test data was employed in the calculations until f_ℓ, the line load force at the wall center, equalled 4000 lb/in. (see foregoing figure) after which it was sharply reduced as F_ℓ approached the ultimate line load strength $f'_\ell = 5000$ lb/in. Resisting moments were determined by noting that the resisting moment arm (the horizontal distance between the point at the wall base around which the wall rotates, and the point at the centerline crack where the two wall elements touch -- see Fig. 6-1) decreases as the wall deflects. In the MACE analysis, these points were assumed to be 8 in. inboard of the wall face. Thus, the initial resisting moment arm was 6 in. long, see Fig. B-7.

The result of these calculations is shown by the solid line (labelled "mean") in Fig. 6-3A. The dashed lines from Ref. 8 were derived by using a 10% coefficient of variation for the f_ℓ value. They show the 68% (1σ) and 95% (2σ) bands on static resistances, assuming a normal distribution.

Similar methods of calculation were employed to derive the static resistance function in rigid arching for a wall 4 in. thick (Ref. 14), and in gapped arching for a wall 8 in. thick (Ref. 8). These are both shown in Fig. 6-3. There were two important differences in the gapped arching calculations.

First, the f_ℓ value used, taken from static test data, was 1000 psi instead of the 4000 psi used for the rigid arching case. Second, the displacement at which ultimate failure takes place, (where the static resistance goes to zero and the wall becomes unstable under gravitational forces alone) was much smaller in gapped arching than in the rigid arching. This decrease in the limiting displacement occurs because the depth of the arch itself in gapped arching is only about one half that in rigid arching (see Fig. 6-2). At any displacement of the centerline, therefore, the moment arm of the resisting moment in gapped arching is also about one half that in rigid arching. (This also accounts for the much higher initial forces at the hinge points of the arch as in gapped than in rigid arching, see Table 6-1.)

In Ref. 10, similar calculations were made for rigid arching of an 8.5 in. wall using a more rigorously correct physical failure model than the mathematical model employed with the MACE program. As already noted, in the MACE model, the fact that crushing occurred at the wall base and centerline crack (the hinge points) while the wall displaced was accounted for by moving the hinge points inboard one inch, see Fig. B-7. The new model employed a moving center of resistance to account for progressive crushing during wall centerline displacement. Crushing was observed to be about three times as extensive at the base of the wall than at the center crack, and the new model also took this into account.

A sketch of the model is shown in Fig. 6-4A, and the static resistance functions generated with it are shown in Fig. 6-4B. Two static resistance curves are shown. The one labelled "p vs δ" is a plot of static resistance pressure vs displacement of a point on the centerline. It indicates that an actual displacement of only about ½ in. generates the maximum resistance (i.e., when f_ℓ = 4000 psi). With models employing hinge points fixed in the wall, a displacement of about 2.5 inches was required to achieve maximum resistance (Fig. 6-3). The second curve of Fig. 6-4B, that labelled "p vs $(t_w - m)$", is much closer to that from the fixed hinge point model. It is a plot of static pressure resistance as a function of change of moment arm, that is, the change in the horizontal distance between the hinge point at the base of

6-7

the wall and that at the centerline crack. The fixed hinge point resistance function curve is also a plot of resistance vs change in moment arm, so it is not surprising that the shapes of the two curves are similar.

Fig. 6-4B was used in a dynamic analysis of wall behavior under a step blast loading in order to compare predictions of displacements of wall center-lines with measurements made in the shock tunnel. Not surprisingly it was found that walls which did not fail (i.e., walls in which the blast wave did not cause displacements great enough for the walls to be inherently unstable) behaved much like spring-mass systems, in that the wall oscillated. Its center-line moved back upsteam after its maximum downstream displacement was achieved, even though downstream directed blast forces were still being applied. Even when a wall did fail, its centerline displacement could be substantially slowed by the increasing resistance represented by the first (rising) part of the resistance vs displacement curve, Fig. 6-4B.

Whether a particular wall would fail or recover depended entirely on its strength relative to the stress generated by blast induced motion. Two ex-amples of typical predicted behavior are shown in Fig. 6-5. Fig. 6-5A shows the effect of different wall strengths for identical blast loads, and Fig. 6-5B, the effect of different blast loads for identical wall strengths. In Fig. 6-5A, early displacements are identical since the blast pressure causing the displacements are the same. The 13 psi loading, however, would generate a stress greater than the f_ℓ = 2700 lb/in. line load strength, so that this weak wall continues to displace downstream until it becomes unstable ($\delta > 8.5$ in.) while the stronger (f_ℓ = 4000 lb/in.) wall recovers. In Fig. 6-5B the wall centerline displaces more rapidly under the 20 psi blast load which would gen-erate a maximum line load stress greater that than the line load strength of f_ℓ = 4000 lb/in. The p = 13 psi blast wave would not generate a line load stress greater than f_ℓ = 4000 lb/in. so the wall rocks back upstream. (The recovery conditions in the two plots are the same, i.e., p = 13 psi, f_ℓ = 4000 lb/in.)

Analyses of arching behavior using STARDYNE, a powerful and sophisticated

6-8

finite element code, and mathematical models with far more detail (smaller elements, many more nodes, see Appendix B) were begun during the program. Results of the initial runs with STARDYNE which show local stress directions are given in Figs. B-8 and B-9.

As noted earlier in this section, little work, either analytical or experimental was done with two way arching. However, from an engineering standpoint, the approximation suggested in Ref. 15 of using the ACI (American Concrete Institute) 1963 code provision of two-way slabs, seems to be sound. This approach suggest that an 8-ft x 12-ft two-way, interior slab (arched wall in our case) would be 1.4 times as strong as a one-way slab (arched wall).

EXPERIMENTAL RESULTS AND COMPARISON WITH PREDICTIONS

Rigidly arching walls of both brick and concrete block were tested in
a number of different configurations. In one-way arching (i.e., with walls
supported as beams), brick walls that were solid (both 4-in. and 8-in. nominal
thickness), and that contained doorway and window openings were tested.
Concrete block walls and composite concrete block and brick walls were only
tested in a solid configuration.

One brick and two concrete block solid walls were also tested in a two-
way arching configuration. Five gapped arching walls were tested; four were
solid (2 brick, 2 concrete block). One, of brick, contained a doorway.
Table 6-2 summarizes the results of all arching wall tests.

The greatest number of tests were conducted with solid brick walls in
the one-way rigid arching mode. Since this wall type was the only one theo-
retically analyzed in any detail, its test results will be described first,
and they will be compared with predictions of behavior from the analytical
work.

One-Way Rigid Arching

Solid Brick Walls. The first arching wall tested in the shock tunnel
was only one wythe of brick thick (nominally four inches) and was fabricated
and cured in place in the shock tunnel. There is no doubt that arching occurred,
for the wall withstood a loading pressure of 1.5 psi, well above the pressure
that would have caused it to fail were it mounted as either a pinned or fixed
edge beam. It failed at a loading pressure of 3.6 psi, above the maximum
static resistance of about 1.9 psi given in Fig. 6-3B.

Most of the remainder of the tests were conducted with walls which were
two wythes (nominally 8 in.) thick. Two were fabricated and cured in the

Table 6-2

Summary of Arched Wall Tests

Test Number	Incident (and Reflected) Overpressure (psi)		Remarks
ONE-WAY RIGID ARCHING			
1. Solid		4-in. Brick	
68a	.75	(1.5)	Wall cracked
68b	1.7	(3.6)	Wall failed
		8-in. Brick	
71a	1.9	(4.1)	Test for natural period
71b	2.9	(6.4)	Wall cracked
71c	4.3	(9.7)	Cracks enlarged
71d	5.6	(12.9)	Wall failed
74	5.5	(12.7)	Wall failed
75	5.9	(13.9)	Wall failed
76	5.6	(12.9)	Wall failed
87a	5.7	(13.2)	Wall cracked
87b	6.3	(14.6)	Cracks enlarged
87c	8.2	(19.9)	Wall failed
88a	7.8	(18.7)	Wall cracked
88b	3.6	(8.0)	Cracks enlarged
94	7.8	(18.8)	Wall failed
96	6.7	(15.8)	Wall failed (pre-split)
		8-in. Concrete Block	
77	3.3	(7.4)	Wall cracked
77	2.0	(4.3)	No additional damage
77	3.4	(7.6)	Wall failed
78	4.5	(10.2)	Wall failed
		10-in. Composite Concrete Block-Brick	
79	5.6	(12.9)	Wall failed
92a	3.5	(7.8)	Wall cracked
92b	3.5	(7.8)	No additional damage
92c	5.0	(11.4)	Cracks enlarged
92d	5.7	(12.9)	Failed

Table 6-2 (cont.)

Summary of Arched Wall Tests

Test Number	Incident (and Reflected) Overpressure (psi)		Remarks
	ONE-WAY RIGID ARCHING		
2. Wall With Doorway		8-in. Brick	
86a	6.1	(14.2)	Wall cracked
86b	8.4	(20.5)	Cracks enlarged
3. Wall With Window		8-in. Brick	
80a	5.7	(13.2)	Wall cracked
80b	6.3	(14.7)	Wall failed
84a	6.4	(15.0)	Wall cracked
84b	7.8	(18.7)	Wall failed
85a	6.2	(14.5)	Wall cracked
85b	5.8	(14.1)	Cracks enlarged
85c	7.5	(18.0)	Slight additional cracking
85d	9.5	(23.8)	Wall failed
	8-in. Concrete Block		
91	3.5	(7.8)	Wall failed
92	3.5	(7.8)	Wall cracked
	TWO-WAY RIGID ARCHING		
1. Solid		4-in. Brick	
83a	2.2	(4.8)	Wall cracked
83b	2.1	(4.5)	Wall failed
	8-in. Concrete Block		
89	5.0	(11.4)	Wall failed
90	4.0	(8.9)	Wall failed
	ONE-WAY GAPPED ARCHING		
1. Solid		8-in. Brick	
97	2.3	(4.9)	Wall failed
98	1.9	(4.1)	Wall failed

Table 6-2 (cont.)

Summary of Arched Wall Tests

Test Number	Incident (and Reflected) Overpressure (psi)		Remarks
	ONE-WAY GAPPED ARCHING		
1. Solid (cont.)	8-in. Concrete Block		
115	4.1	(9.1)	Wall failed
116	1.7	(3.6)	Wall failed
2. Wall With Doorway	8-in. Brick		
95	8.6	(21.0)	Wall failed

tunnel, the remainder were constructed and cured in frames outside the tunnel, then were moved in and mounted in the manner described in Appendix A. No difference in behavior due to the differences of construction methods were found.

The data from the 8-in. solid one-way arched brick walls are summarized below. The lower bound is the highest loading pressure applied to the wall without causing failure and the upper bound is the lowest pressure which caused failure. The walls in Series No. 1 were fabricated and tested in 1972 and those for Series No. 2 in 1973.

Series	Wall No.	Lower Bound (psi)	Upper Bound (psi)
1	71	9.7	12.9
	74	-	12.7
	75	-	13.9
	76	-	12.9
		10	14
2	87	14.6	19.9
	88	18.7	-
	94	-	18.8
	96	-	15.8
		15	20

It is evident from this data that the Series No. 1 walls with failure pressure bounds of ≈ 10 to 14 psi were significantly weaker than the Series No. 2 walls, with bounds of 15 to 20 psi. All data can be included within bounds of 10 to 20 psi. Sample posttest photographs of the failed walls are shown in Fig. 6-6. Fig. 6-6A is for a wall which failed at 13.9 psi near the lower bound and Fig. 6-6B is for a wall which failed at 18.8 psi near the upper bound. In general the motions of the walls were consistent with the predicted behavior of rigidly arched walls from the dynamic analysis. In Fig. 6-7, the curves are for a single wall (87) tested three times at

6-14

increasing loading pressures. It did not fail at loadings of about 13 or 15 psi; it did fail at a loading of about 20 psi. As might be expected, as the load increased, displacements at various times after the onset of loading also increased. It can also be seen that the walls behaved as spring mass systems during the tests which did not result in failure. Two cycles of oscillations were recorded.

Fig. 6-8 compares predicted and measured values of displacements vs time for this same wall (87) whose line load strength must have been very close to the 4000 psi used in the calculations. Note that even the oscillations measured at loading pressures of about 13 psi and 15 psi, are very close to predicted values.

Fig. 6-9 illustrates the apparent effect of differences in line load strength. In Fig. 6-9A with an f_ℓ of 4000 psi, and a loading pressure of about 13 psi wall recovery was predicted. Wall No. 76, however, failed under that blast load. Shown as a dotted line is the predicted motion if f_ℓ were 2700 psi. It lies very close to the measured displacement curve. In Fig. 6-9B, with an f_ℓ of 4000 psi and a loading pressure of about 19 psi, wall failure was predicted, but Wall No. 88 recovered. Shown as a dotted line is the predicted motion if f_ℓ were 6000 psi, which would lead to a prediction of wall recovery.

Crushing and spalling of material at the base of the wall along its downstream edge and at the upstream edge of the centerline crack occurred as expected (see Fig. 6-10).

Solid Concrete Block Walls. Only two such walls were tested in the shock tunnel, and though both failed at blast loadings considerably below the lowest loading at which brick arching walls failed, their mode of failure makes it difficult to compare the behavior of walls of these different materials. With both concrete block walls a hole extending from top to bottom was blown in one side of the wall, but the remainder of the wall, while cracked, remained standing. In contrast, all the brick walls that failed cracked at

or near the centerline, and the entire wall was projected downstream. It is for this reason that the measurements of wall centerline displacement shown in Fig. 6-11 (which were made on a part of the walls that remained standing) suggest that wall recovery occurred. Note that Wall No. 77 was subjected to three tests (at blast loads of 7.4, 4.3, and 7.6 psi) and "failed" on the third. Plotted in Fig. 6-11 are the displacement measurements of the first and third tests on this wall. Wall No. 78 was tested only once at 10.2 psi and "failed" in a similar manner. Its measured displacements are shown in Fig. 6-11B. Photographs of the two failures are shown in Fig. 6-12.

Solid Composite Concrete Block-Brick Walls. Two of these walls, consisting of 6-in. concrete block with a 4-in. facing of brick were tested in the tunnel, the blast load being applied to the brick face (see Appendix A, Fig. A-13). They were apparently considerably stronger than the concrete block walls. One wall (No. 92) did not fail at loading pressures of 7.8 psi (twice) and 11.4 psi, but did fail at 12.9 psi. The other wall (No. 79) was loaded but once at about 13 psi and failed. The plot of measured centerline displacement vs time for this wall, shown in Fig. 6-13A suggests strongly that this was a threshold loading. Twice during its displacement history, the wall began to recover. The recovery of Wall No. 92, loaded successively at 7.8, 7.8, and 11.4 psi without failure occurring, is apparent in Fig. 6-13B. It can be seen in Fig. 6-14A that a portion of the wall near its base remained in place after Wall No. 79 failed. Fig. 6-14 B shows the type of spalling that occurred at the base of Wall 92.

Brick Wall With a Doorway. Wall No. 86 was installed so as to undergo rigid arching. It was tested twice at about 14 and 20 psi and cracked but did not fail. Its displacement vs time history is shown in Fig. 6-15A.

Walls With a Window Opening. Three brick and two concrete block walls, each with a window opening about 38 in. high and 60 in. wide (17% of the wall area) were tested in the shock tunnel. The first brick wall (No. 80 had

window glass installed prior to the first tests with an initial blast loading of 13.2 psi. The wall cracked but did not fail. The window glass was then replaced with a sheet of ¼ in. plywood, and the wall was subjected to an initial blast load of 14.7 psi. It failed.

Brick walls numbered 84 and 85 were first subjected to initial blast loads of about 15 psi, both cracked but did not fail. Wall No. 84 was then exposed to a 18.7 psi blast load and failed. The displacement vs time history of these tests is shown in Fig. 6-16A. After withstanding its initial loading, Wall No. 85 was then exposed to initial blast loads of 14.1 and 18.0 psi and though cracking increased, the wall remained upright. Finally it was subjected to a blast load of almost 24 psi, which caused failure. One side of the wall failed completely; the other side remained standing, though a portion of its downstream wythe of brick was broken off (see Fig. 6-16B). The walls appeared to be somewhat stronger than their solid counterparts undoubtedly because of the relief of downstream-directed loading due to the blast wave passing through the window opening.

The two concrete block walls were subjected to an initial loading pressure of about 8 psi. One failed (No. 91) in a manner similar to that of the brick wall (Fig. 6-17B), the other (No. 93) did not, though it exhibited extensive cracking. Displacement vs time histories of the two walls are shown in Fig. 6-17A. As can be seen in Fig. 6-17B, the displacement gauge used with Wall No. 91 was located on the side that did not fail.

Two-Way Rigid Arching

Only three two-way (plate) arching walls were tested in the tunnel. One, of 4-in. thick brick withstood a blast loading of almost 5 psi before failing under a second similar loading. It was clearly stronger than its one-way arching counterpart. The other two were of concrete block, 8 in. thick. They were subjected to loading pressures of 8.9 and 11.4 psi and failed.

One-Way Gapped Arching

8-in. Brick. Three such walls were tested; two were solid, and one had

6-17

a doorway. The two solid walls had gaps at the top of approximately 0.2 in. (No. 97) and 0.1 in. (No. 98). These two walls failed when subjected to loading pressures of 4.9 and 4.1 psi respectively. Clearly these walls were much weaker than their rigid arching counterparts which had failure boundaries from 10 to 20 psi.

The wall with a doorway (No. 95) was tested before the theory for gapped arching was developed. It was subjected to a blast load of about 21 psi and failed. Its displacement vs time history is shown in Fig. 6-15A, and a photograph of the debris created is given in Fig. 6-15B. Gapped arching theory suggests that this wall should be considerably weaker than its rigid arching counterpart. Both the displacement history and the photograph tend to bear this out.

8-in. Concrete Block. Two walls were tested having gaps of less than 1/8 in. at the top. Wall No. 115 was subjected to a 9.1 psi loading and failed; Wall No. 116 was subjected to a loading of 3.6 psi and failed.
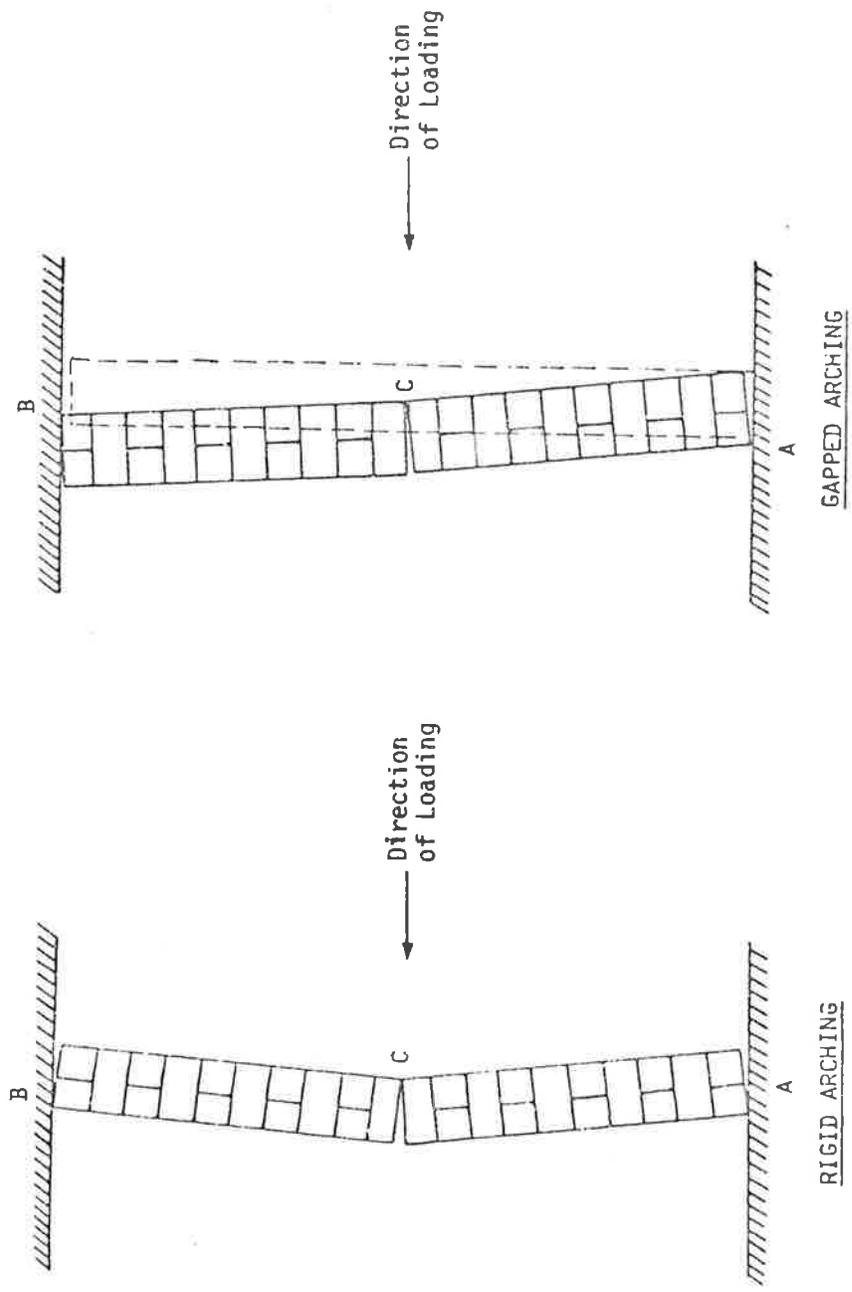
Fig. 6-1. Sketch Illustrating the Differences in Motion Between Rigid Arching and Gapped Arching.

6-19
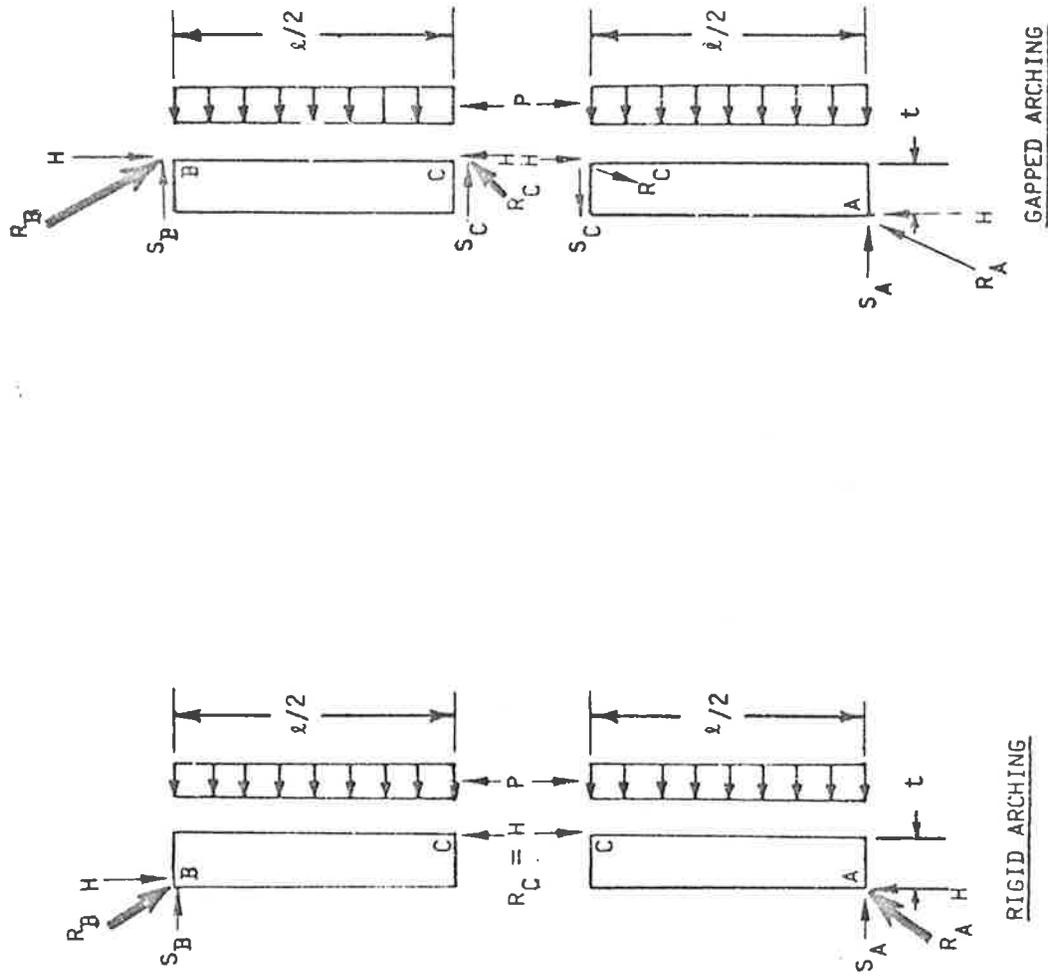
Fig. 6-2. Free Body Diagrams Showing Forces in Rigid and Gapped Arching. (See Table 6-1 for Force Values).

A   EIGHT-in. THICK WALL IN RIGID ARCHING (MACE MODEL)

B   EIGHT-in. THICK WALL IN RIGID AND GAPPED ARCHING, AND FOUR-in. THICK WALL IN RIGID ARCHING.
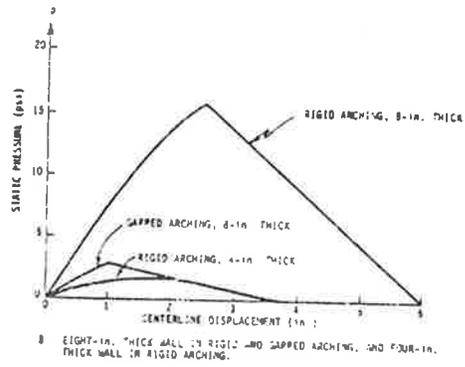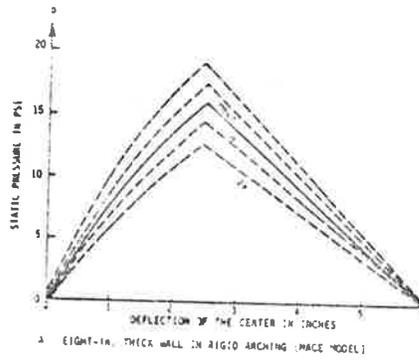
Fig. 6-3. Predicted Static Pressure Resistance vs Centerline Displacement for Brick Arched Walls.

6-21
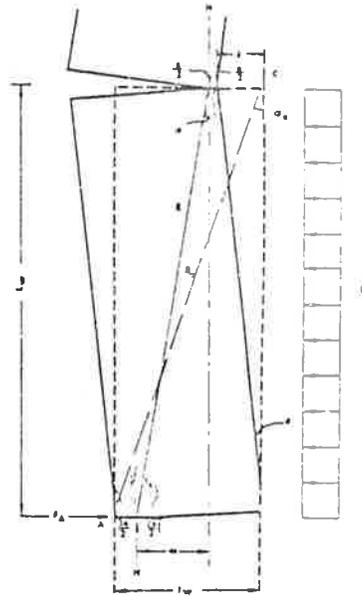
A. MODEL OF RIGID ARCHING WALL BEHAVIOR
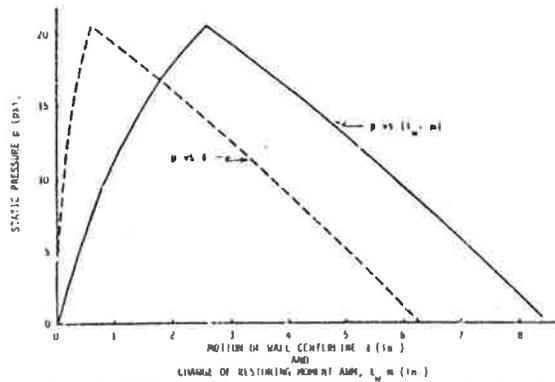
B. STATIC PRESSURE ON A RIGIDLY ARCHING WALL VS δ, THE MOTION OF THE WALL AT ITS CENTERLINE, AND t_w-m, THE CHANGE IN MOMENT ARM OF THE RESTORING FORCES.

Fig. 6-4. Model and Predicted Static Resistance for 8.5-in. Thick Wall in Rigid Arching.
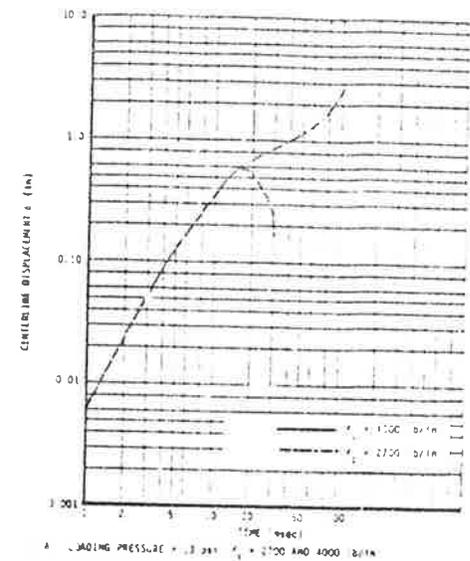
6-22
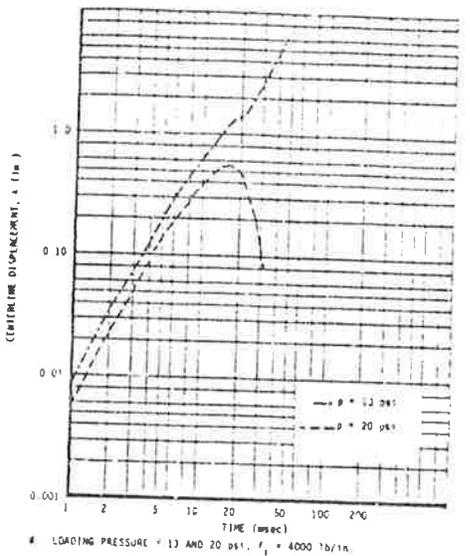
Fig. 6-5. Effect of Line Load Strength (f_ℓ) on the Predicted Behavior of 8.5-in. Thick, Brick Walls Undergoing Rigid Arching.
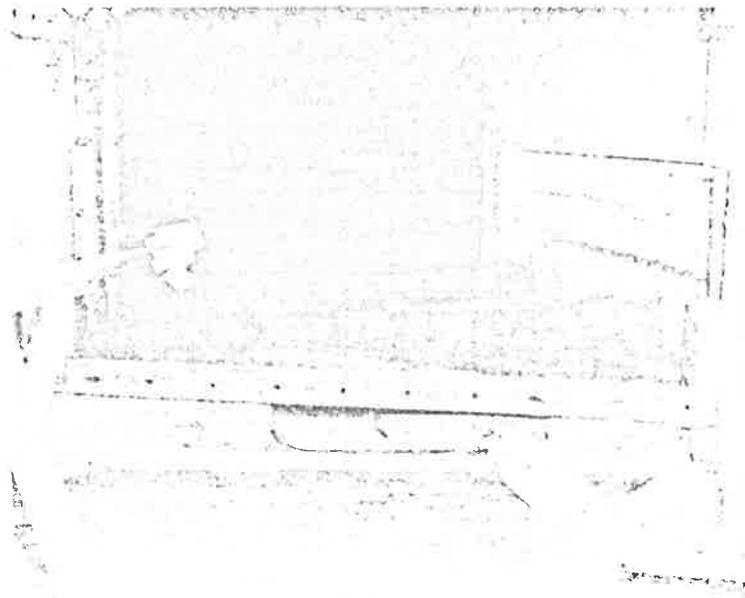
A. Wall No. 75. Loading Pressure ≈ 13.9 psi.
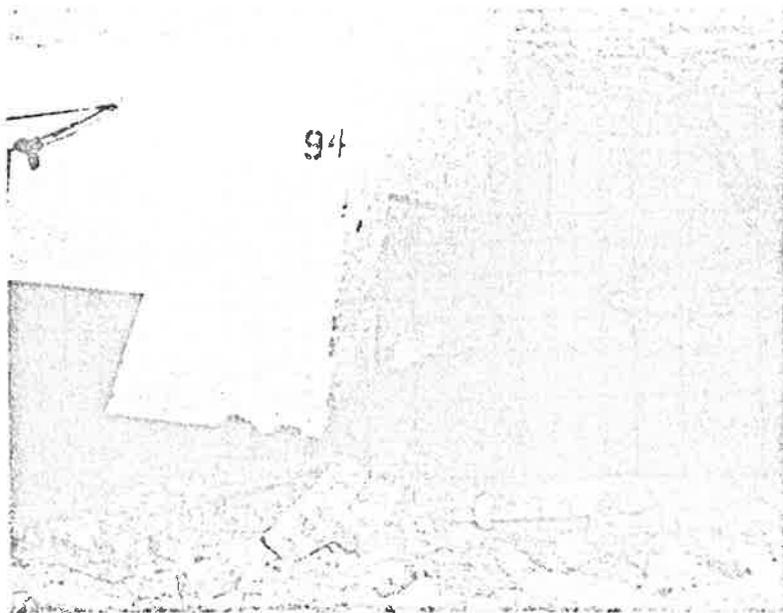
B. Wall No. 94. Loading Pressure ≈ 18.8 psi.

Fig. 6-6. Debris from Rigid Arching Walls that Failed Under Blast Loading.
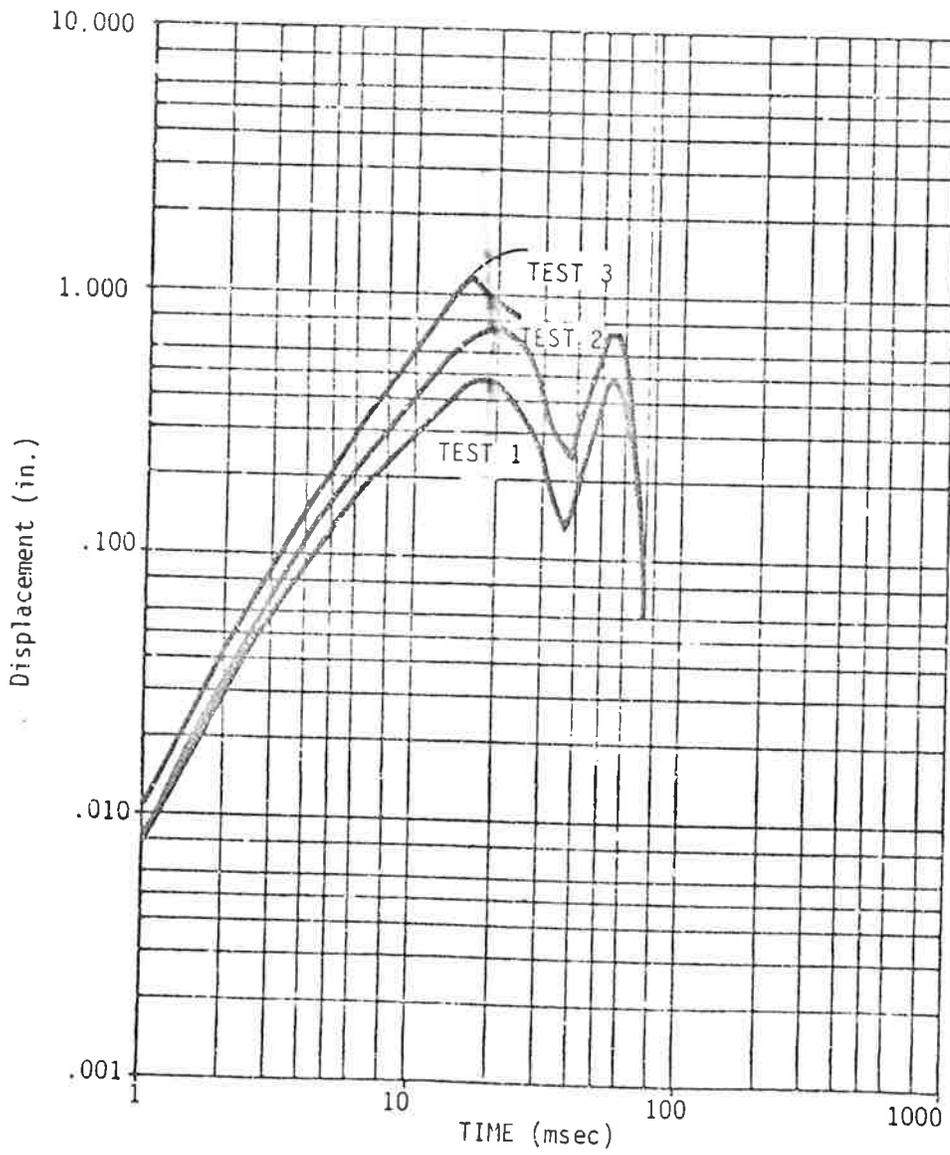
Fig. 6-7. Displacement as a Function of Time, Wall No. 87. Loading Pressures were 13 psi for Test 1, 15 psi for Test 2, and 20 psi for Test 3.
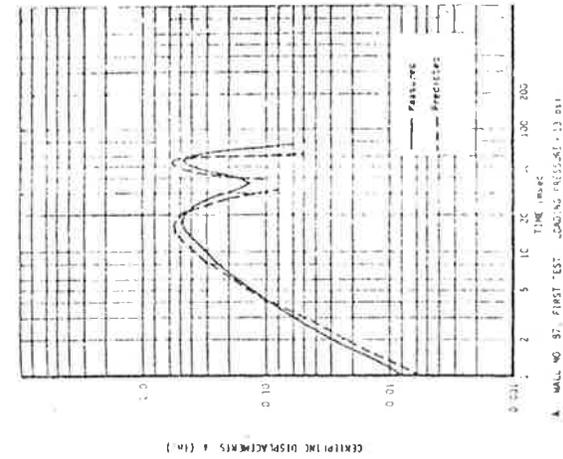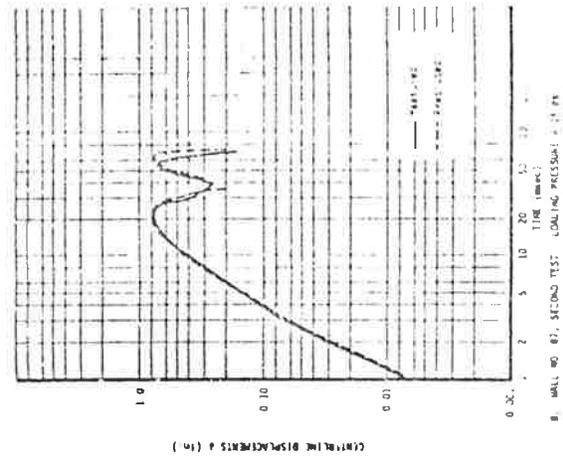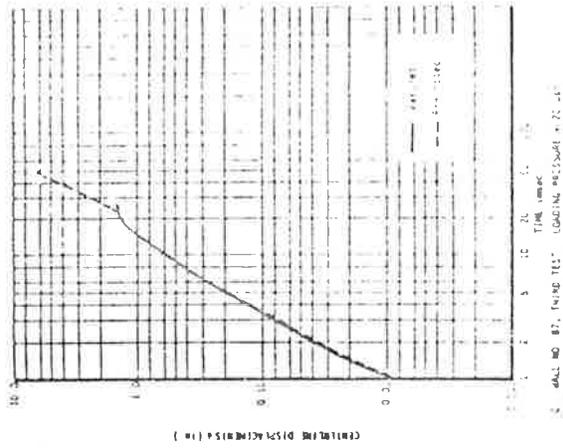
Fig. 6-8. Predicted and Measured Wall Centerline Displacements for Wall No. 87.
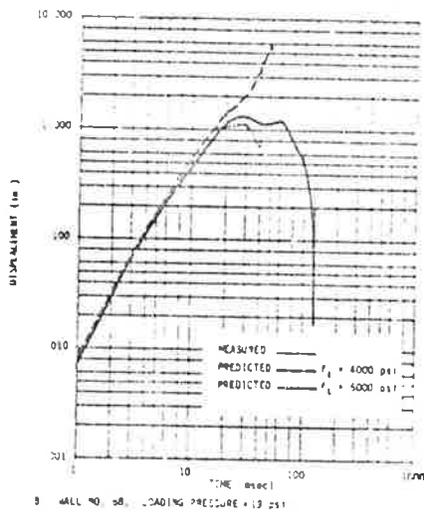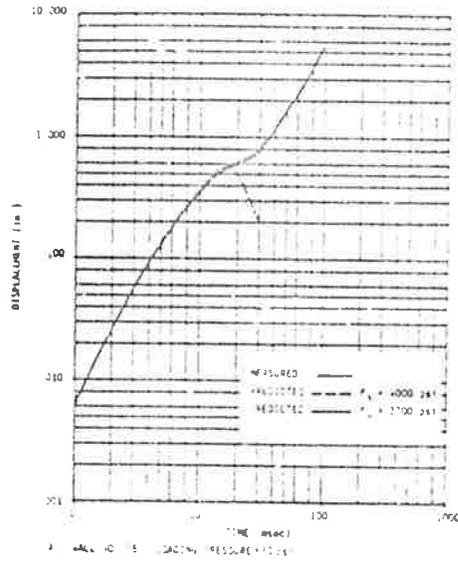
Fig. 6-9. Comparison of Measurements of Centerline Displacement of Rigid Arching Walls with Predictions Using Various Values of Line Load Strength (f_ℓ).
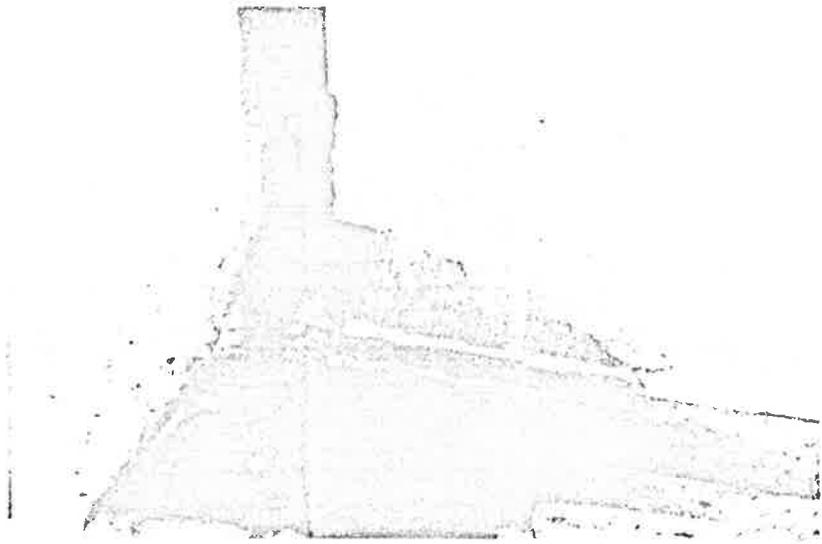
A. Crushing at the Base.

B. Crushing along the Centerline Crack.

Fig. 6-10. Posttest Photographs of Wall No. 98.
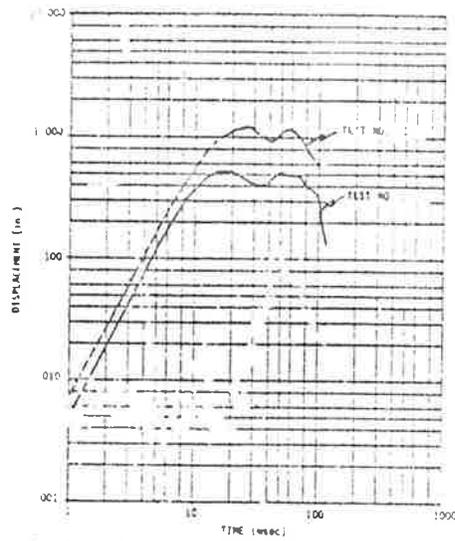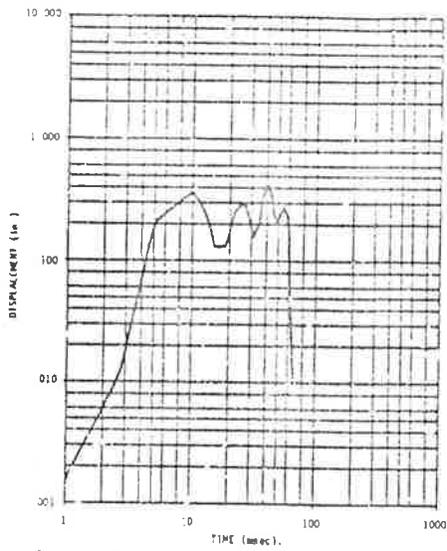
Fig. 6-11. Centerline Displacement vs Time for Concrete Block Walls
Undergoing Rigid Arching.
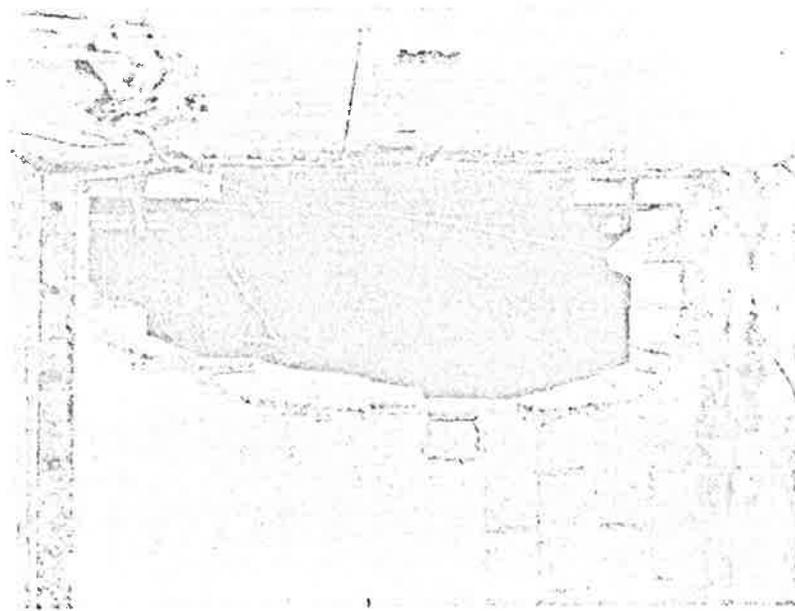
B. Wall No. 78.

A. Wall No. 77

Photographs of Rigid Arching Concrete Block Walls after Failure.

6-30
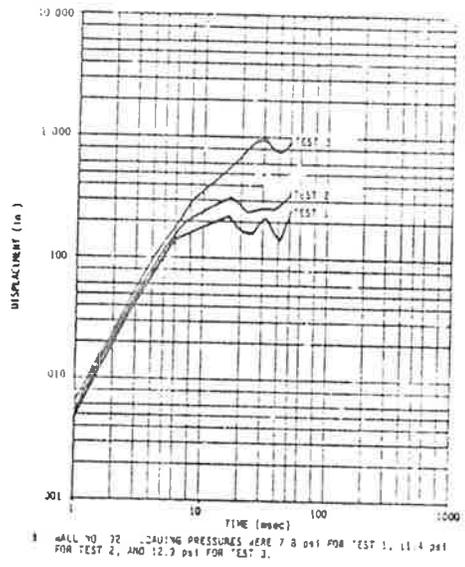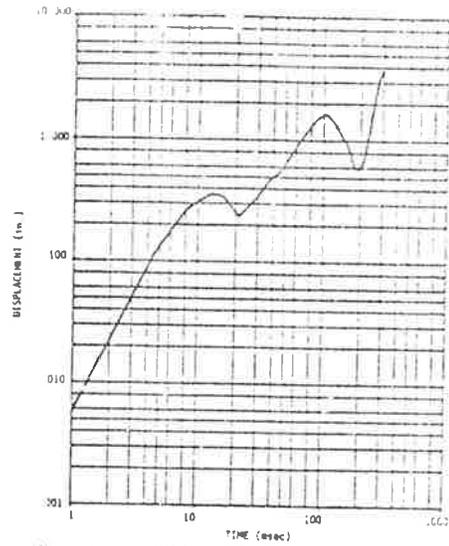
Fig. 6-13. Centerline Displacement vs Time for Concrete Block and Brick
Walls Undergoing Rigid Arching.

6-31
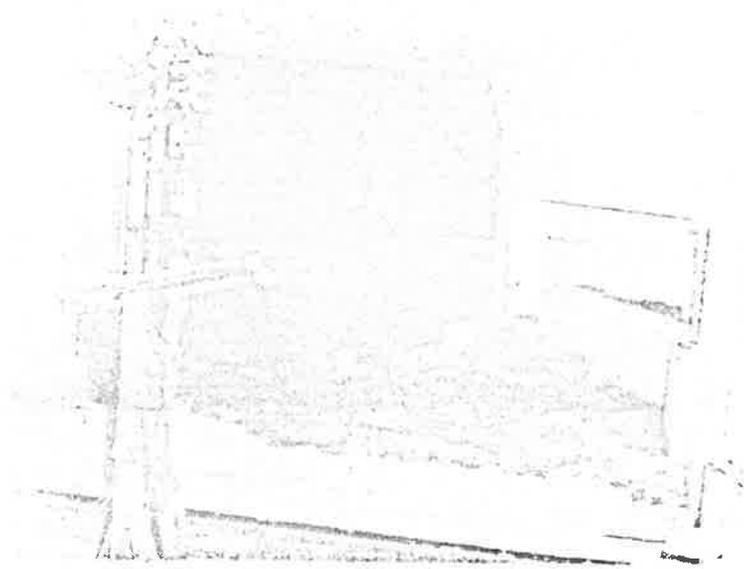
A. Wall No. 79. Loading Pressure ≈ 13 psi.

B. Wall No. 92. Loading Pressure ≈ 7.8 psi.

Fig. 6-14. Posttest Photographs of Rigid Arching Concrete Block and Brick Walls.
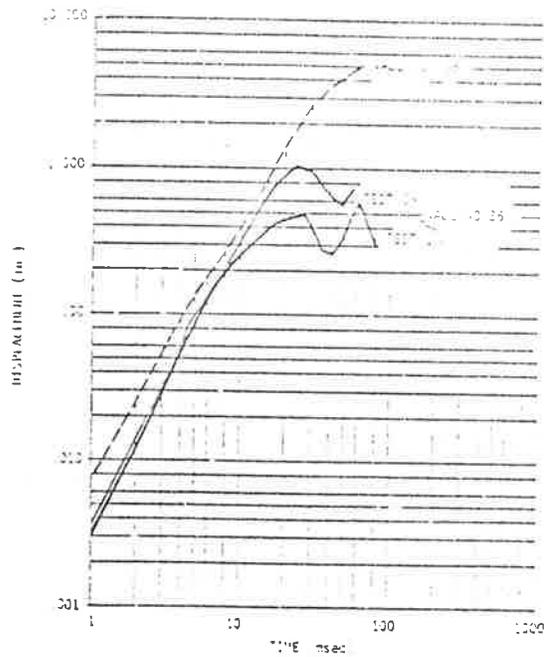
A. Loading Pressures were 14 psi for Test 1, 20 psi for Test 2, with Wall No. 86, and 21 psi for Wall No. 95.
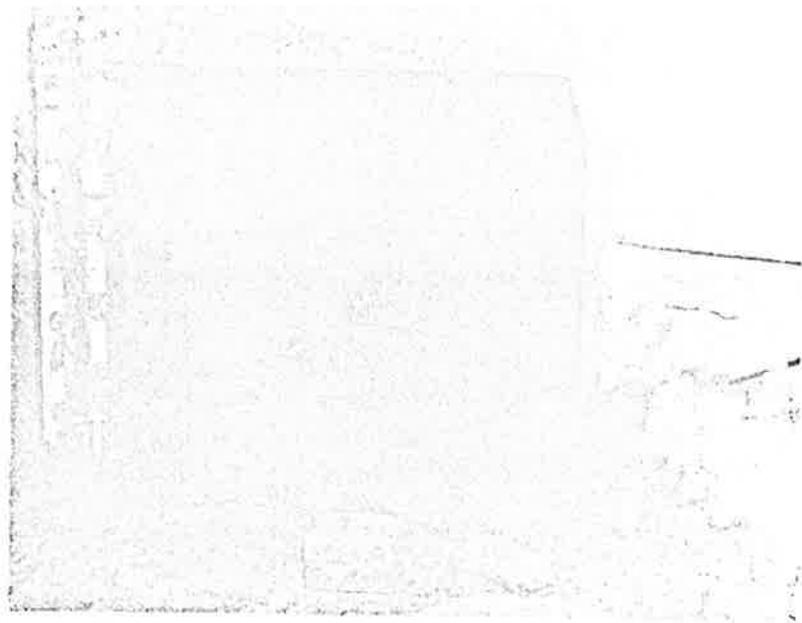
B. Posttest Photograph of Wall No. 95 (Gapped Arching) Looking Downstream.

Fig. 6-15. Displacement vs Time Record and Posttest Photograph of Debris from Arching Brick Walls (No. 86 and 95) with a Doorway.

6-33
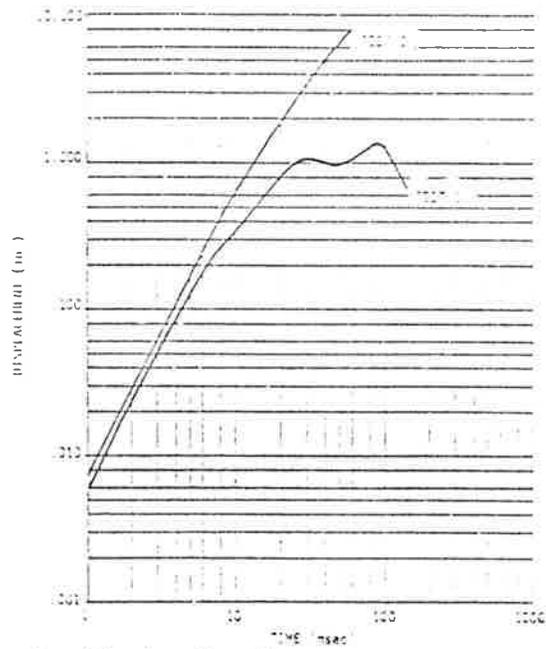
A. Wall No. 84. Loading Pressures were 15 psi for Test 1, 18.7 psi for Test 2.
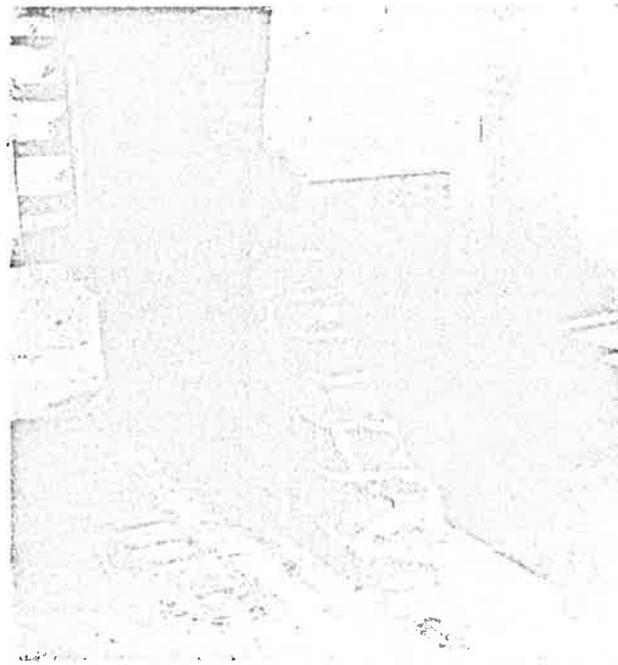
B. Posttest Photograph of Wall No. 85.

Fig. 6-16. Centerline Displacements vs Time and a Posttest Photograph of Rigid Arching Brick Walls with Windows.
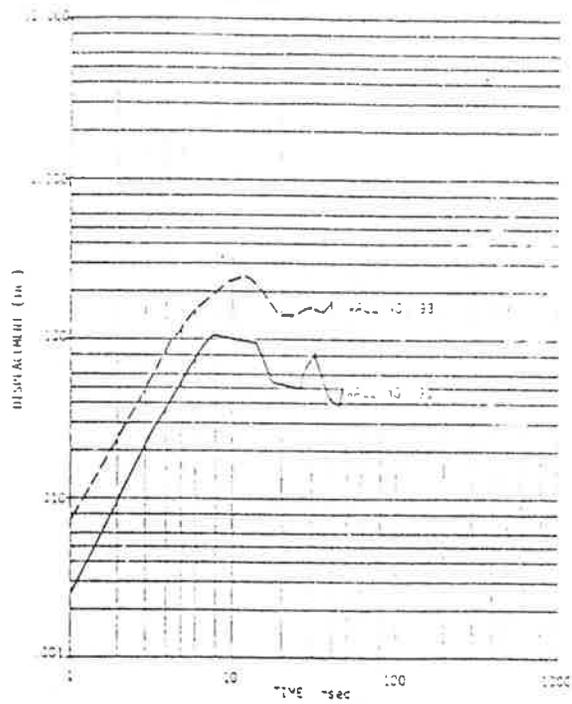
A. Walls No. 91 and 93. Loading Pressures were 8 psi for both Walls.
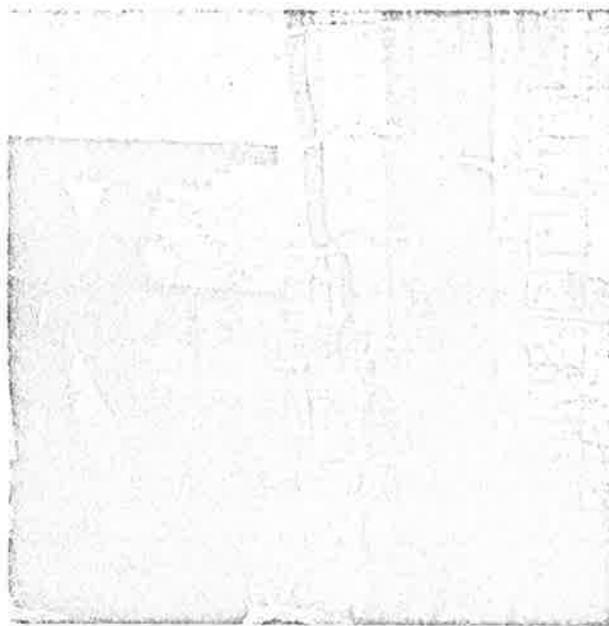
B. Posttest Photograph of Wall 91.

Fig. 6-17. Centerline Displacement vs Time and a Photograph of Rigid Arching Concrete Block Walls with Windows.

Section 7
MISCELLANEOUS WALLS

CANTILEVERED MASONRY AND PLATE-MOUNTED SHEETROCK INTERIOR WALLS

Three types of solid walls were tested as interior walls, that is, they formed the rear wall of a room with a front (upstream) wall containing a window opening. The window opening occupied about 27% of the front wall. Two of the wall types were of masonry (8-in. concrete block, and 6-in. clay tile) and cantilevered from the floor of the tunnel. The third type was of sheetrock with wood or metal studs, and was affixed to the tunnel walls, floor, and ceiling. Two interior wall types with doorways were also tested. One was of concrete block and was cantilevered from the floor; the other was of sheetrock and studs, the perimeter members of which were affixed to the tunnel. Loading pressures were well above those that would just cause failure.

Motion picture records were made of tests on these walls. In every case they showed that -- after failure -- very large pieces of the walls remained upright or had only a small rotational component, and moved downstream for considerable distances before striking the floor and breaking up into smaller pieces. An analysis of the effect of blast forces on the masonry cantilevered walls predicted that they would rupture about one third of the wall height above the floor (see Ref. 11). Failure of the plate-mounted sheetrock walls was expected to occur along their perimeters. In all tests, failure took place as expected.

Wall displacements were calculated in Ref. 10 and were compared with measured displacements from the high-speed motion picture records of each test. The comparison for the clay tile and concrete block cantilevered walls is shown in Fig. 7-1 in which the solid lines are experimental values (or delineate the range of experimental values if two or more tests were made with one wall type), and the dashed lines are predictions from Ref. 10.

7-1
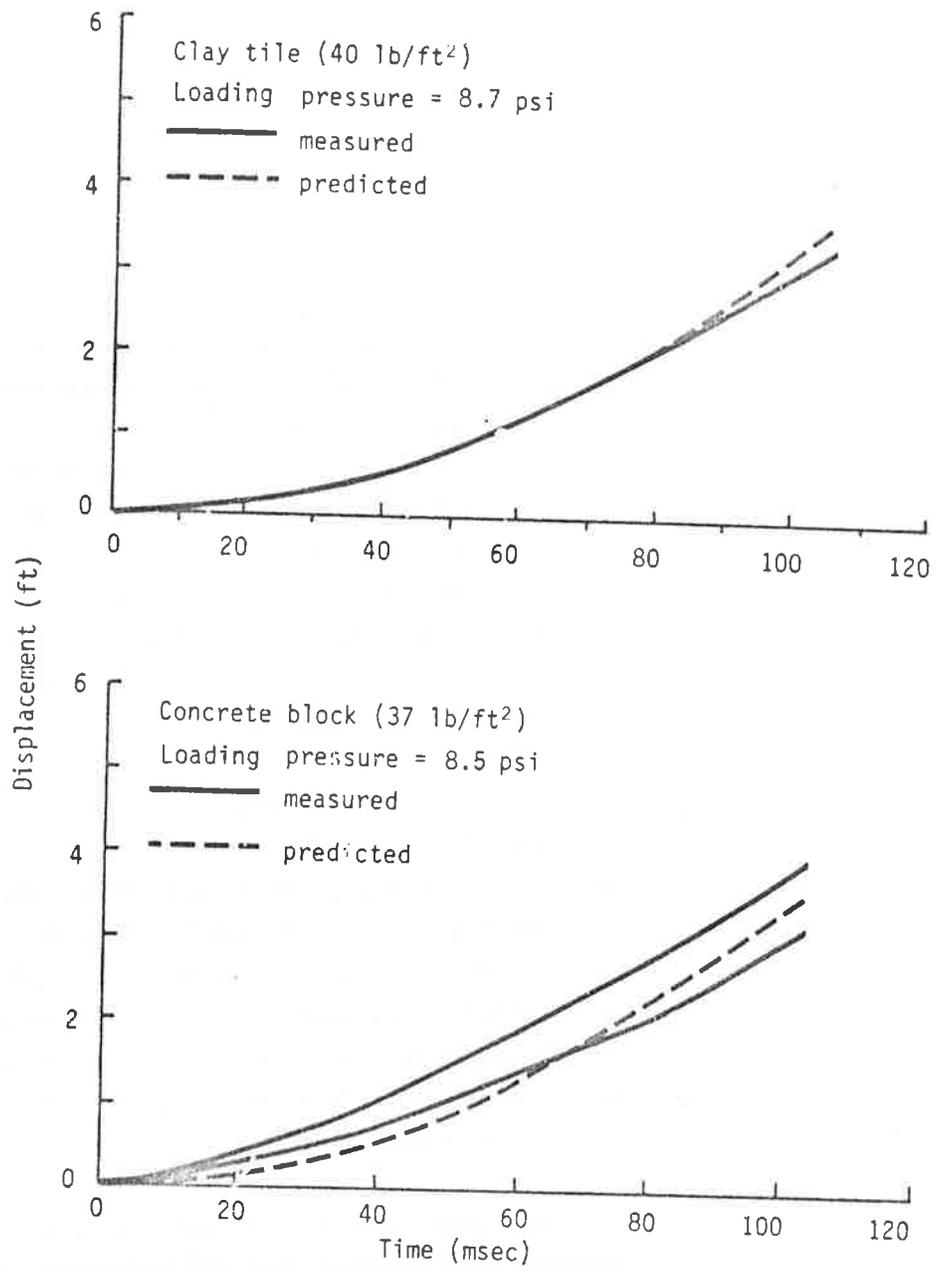
Fig. 7-1. Debris Displacement vs Time for Interior Clay Tile and Concrete Block Solid Walls.

Fig. 7-2 shows a similar plot for solid sheetrock walls at two different incident pressures, (note the change in the time scales) and Fig. 7-3 is a similar plot for the interior walls with doorway openings. In all cases, theoretical and measured values agree well.
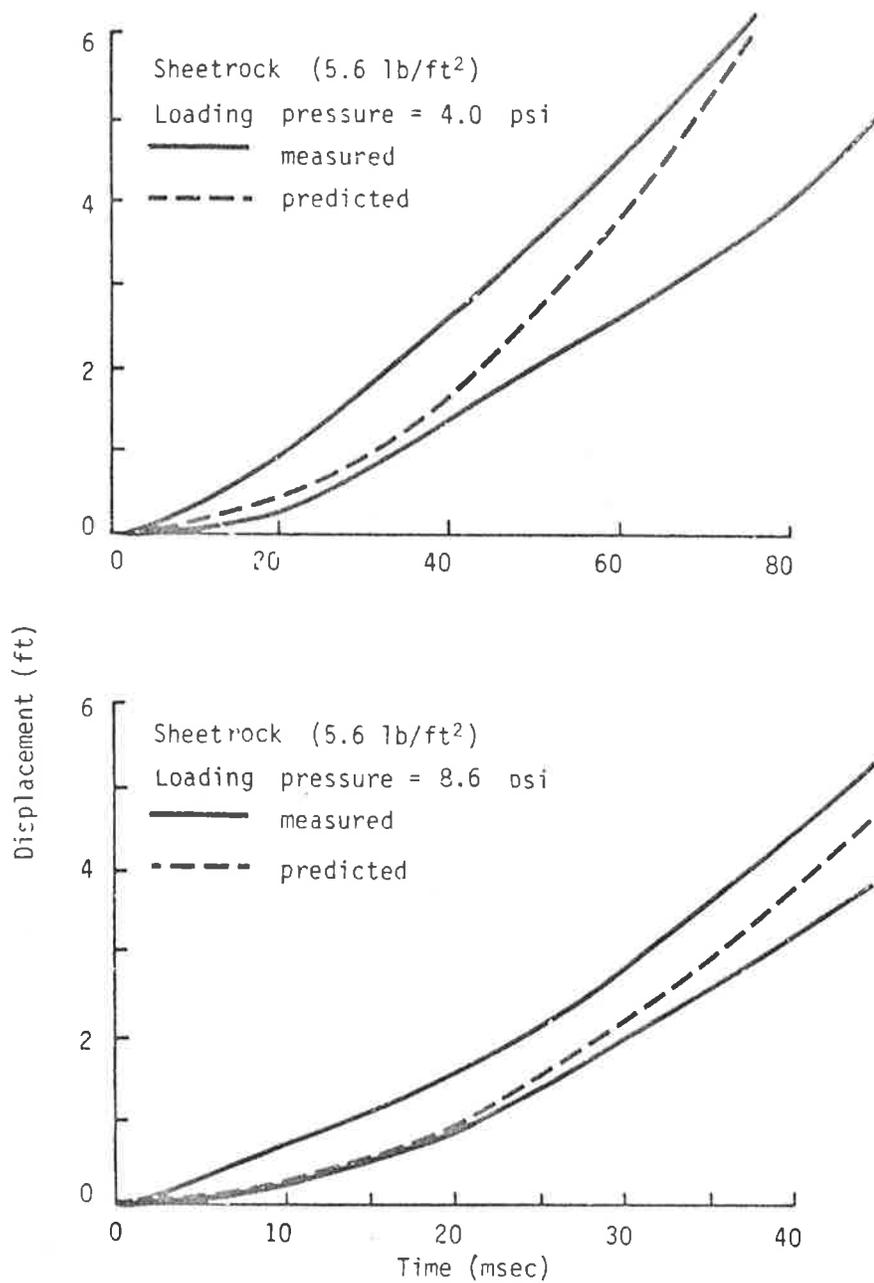
Fig. 7-2. Debris Displacement vs Time for Interior Sheetrock-Stud, Solid Walls.

7-4
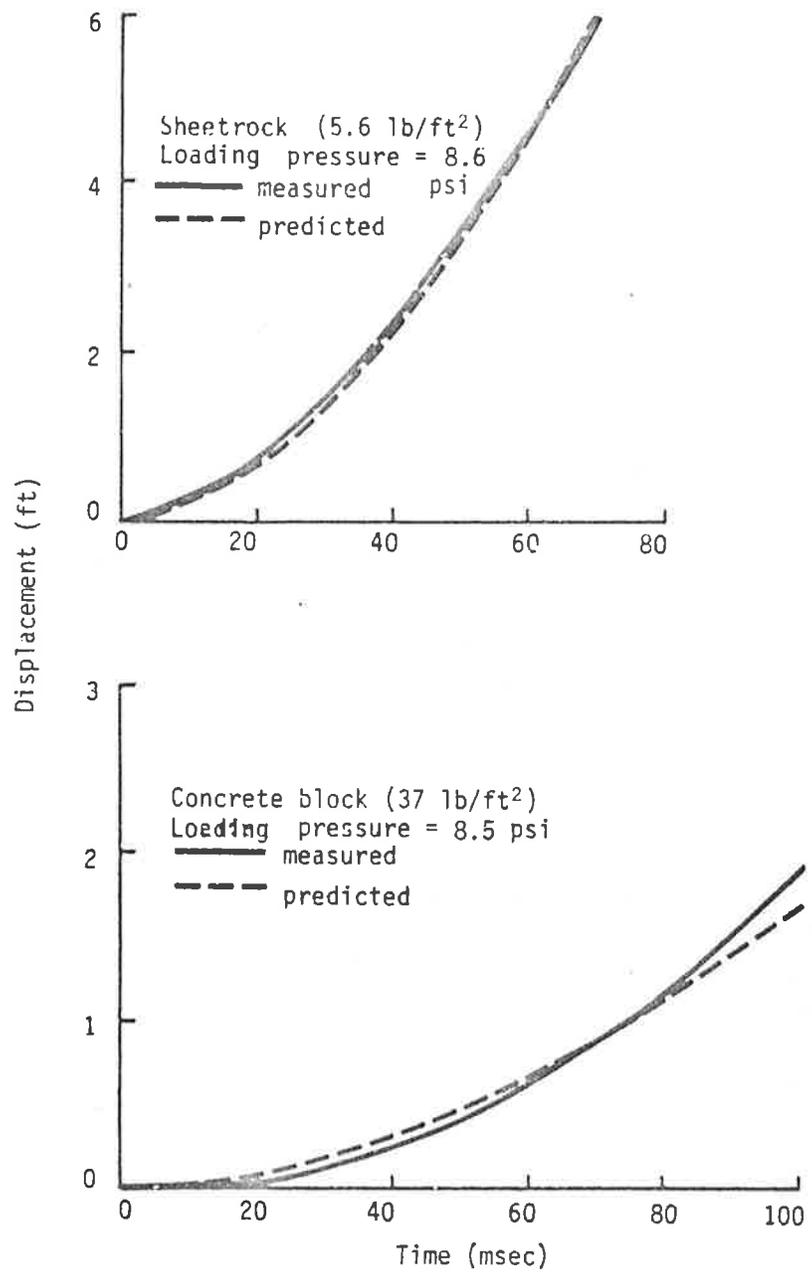
Fig. 7-3. Debris Displacement vs Time for Interior Sheetrock-Stud and Concrete Block Walls with Doorways.

APPENDIX A

WALL PANEL TEST PROGRAM HARDWARE

Appendix A
WALL PANEL TEST PROGRAM HARDWARE

WALL CONSTRUCTION AND TRANSPORT TECHNIQUES

Wall Construction

With a few exceptions, the masonry wall panels subjected to blast tests were constructed outside the tunnel and -- after being cured for a minimum of 28 days -- were moved into the tunnel and mounted for test. The walls were constructed in a steel frame designed to hold, support, and protect them during construction, storage, transportation, and test. Provided on this frame were the hardware required to create the edge connections necessary for the particular panel and test conditions, lifting eyes for transport of the panel, and the hardware necessary for fastening the panel into the test section of the tunnel. A version of the frame that was used on early tests is sketched in Fig. A-1 with a beam-mounted wall in place. (The wall was not mortared to the end channels, and the top and bottom members were mounted so that they were essentially free to rotate, providing the required pin-pin support conditions for a simple beam type of support.)

A critical element in the design of the frame was the bottom member which was required to support the panel in such a manner that when it was lifted for transporting into the tunnel, the panel would remain within the limits one might expect in a building frame. All frames used in the progam had a deflection to span ratio of 1/440 or less, which is less than the 1/360 typically used in building construction.

Most panels tested were of brick and mortar nominally 8 in. thick; used the "Common Flemish Bond" style of construction with every sixth row a bond course; and weighed about 80 lb/ft^2. A few 12-in. thick brick walls, as well as concrete block and hollow clay tile panels were also tested in the tunnel. The concrete block panels, nominally 8 in. thick, weighted about 36 lb/ft^2. The clay tile panels, about 7 in. thick, weighed about 40 lb/ft^2.

A-1
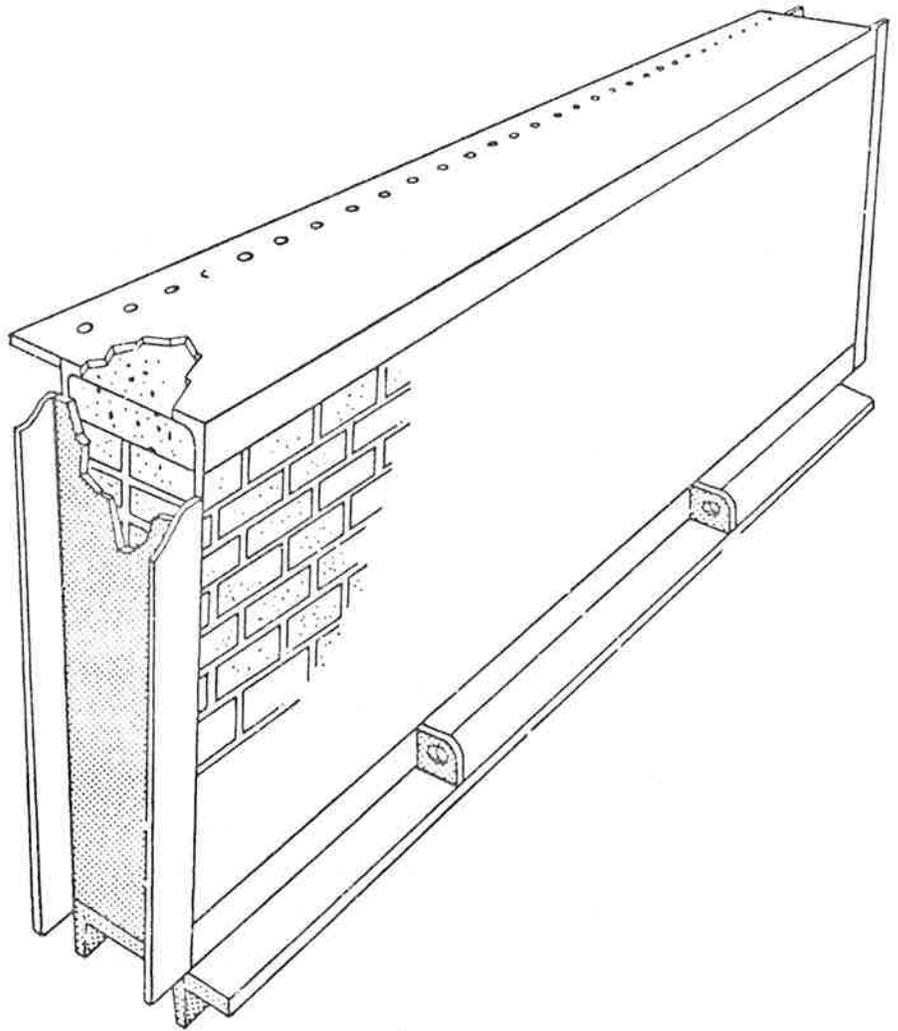
Fig. A-1. Sketch of Mounting and Transport Frame Showing Beam-Mounted Wall in Place.

To assure quality control in the construction of the panels and to determine their strength at the time they were tested, a static test program, described in detail in Volume 4, was established. At the time of construction of each panel, brick and mortar samples were taken and beams, columns, tensile bond test specimens, and shear bond test specimens were constructed. These specimens were stored along with the panels through the 28-day curing time and were then tested at about the same time as the panels.

The building bricks, concrete blocks, mortar, and construction details all conformed with applicable Uniform Building Code requirements. Local masons were employed to build the panels to assure that standard construction techniques were used.

Transport Hardware and Techniques

The transport hardware included panel transporter and panel roller assemblies. The panel transporter was a rubber-tired "tuning-fork"-shaped vehicle which supported a test panel as shown in Fig. A-2. Four roller chain and turnbuckle fasteners clamped onto the lifting eyes fastened to the bottom frame of the panel to be tested, and the panel was lifted by a hydraulic ram assembly. The panel transporter carried the panel from the storage area into the tunnel and placed the panel on rollers. The transporter was then removed from the panel which was rotated and positioned into place in the tunnel. This procedure for installing the panels allowed them to be just inches narrower than the tunnel itself.
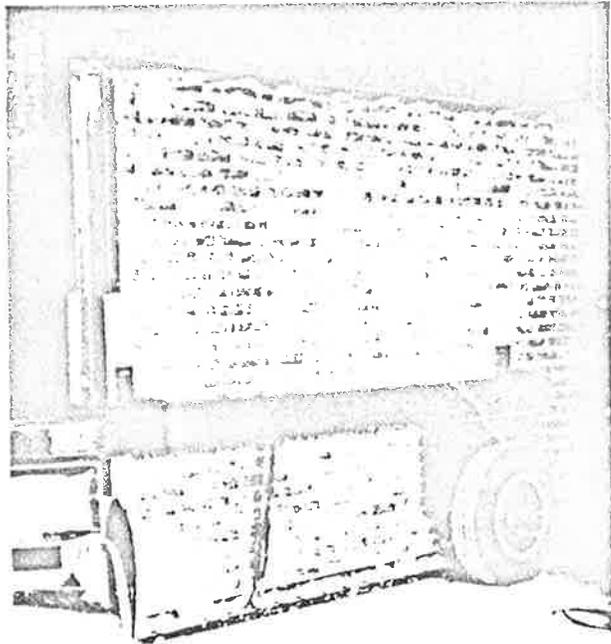
Fig. A-2. Panel Transporter.

PANEL MOUNTING DETAILS

All walls supported as simple beams and plates were mounted in the tunnel using specially designed hardware. Some of the walls were preloaded in the vertical direction, and other walls were mounted so as to have fixed end conditions permitting them to arch.

Basic Panel Mounting Hardware

All panels that used pinned supports (simple beams and plates) were affixed -- along the top and bottom edges in the case of the beams, and along all four edges in the case of plates -- to specially designed steel girders which spanned the tunnel. These in turn were supported by steel blocks bolted to the tunnel wall. The hardware for mounting a wall panel with plate support conditions is shown in Fig. A-3. The plate girders support a test pnael along its entire length with a minimum of deflection, while still permitting the panel edges to rotate, thus simulating the pinned support condition desired. They were of rather unique welded steel construction, with "box" flanges made of structural channels and channel stiffeners. The horizontal girders weighed about 2600 lb each, were 4½ in. thick, 4 ft deep, and had a span of 12 ft. The vertical girders, constructed in similar fashion, weighed about 1800 lb each and were about 8 ft long, spanning the distance between the horizontal girders. Load cells were placed between the wall blocks and the horizontal girders and preload was established between the girders and blocks to avoid high impact forces on the load cells.

Attachment hardware used to fasten the test panel frame to the girders consisted of a "U" shaped member welded to the girder, and mating elements attached to the test panel support frame. In early tests, plates drilled to match the holes in the "U" member, were attached to the top and bottom member of the test panel frame. These plates were inserted into the "U" shape and bolted on 6-in. centers. In later tests, the steel channels on the panel support frame were replaced with I beams. Sections of steel angle were fitted between the flanges of the outer channel-shaped portions of the I beams at

A-5
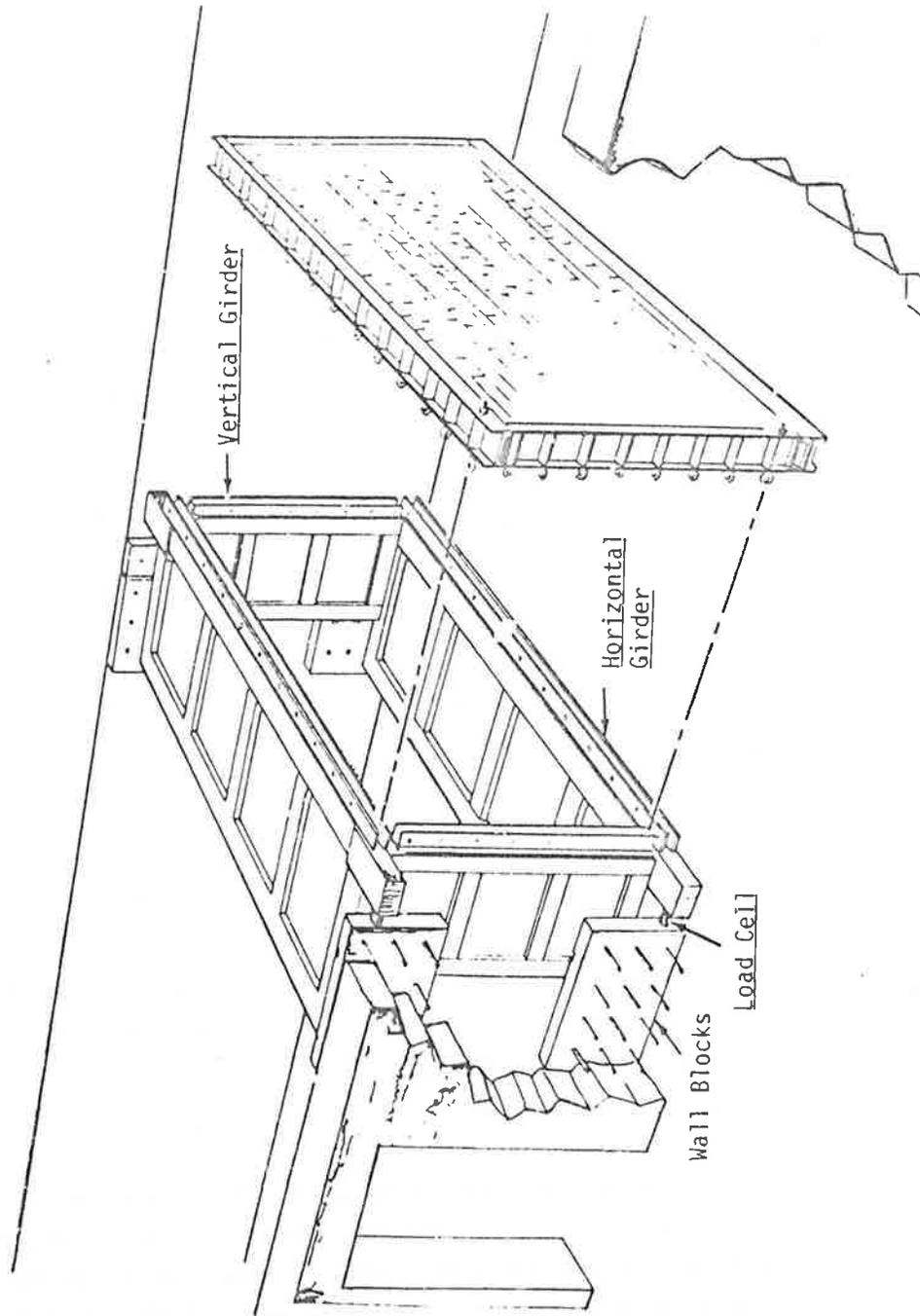
Fig. A-3. Cutaway View of Shock Tunnel Showing Test Panel and Location of Horizontal and Vertical Plate Girders, Wall Blocks, and Load Cells.

A-6

each bolt location (see Fig. A-3) and the panel tied to the girders with eye bolts. Both of these methods provided freedom of rotation. Fig. A-4 is a photograph showing the wall blocks and upper girder with a concrete block wall (containing a window opening) mounted downstream of the girder. (Wall panels could also be mounted on the upstream edges of the girders.) The element on the stand to the left of the window is a displacement vs time sensor.

Two complete sets of wall blocks and girders were fabricated, with the second set of blocks being installed downstream from the first set. By this means a "room" could be created in the tunnel with one wall mounted on the upstream set of blocks, and the other on the downstream set. The blocks were so located that walls could be separated by as much as 15 ft. Both sets of blocks can be seen in Fig. A-5, a posttest photograph looking upstream. The frame is still attached to the upstream set of blocks, with some concrete blocks still clinging to the top frame element. On the right-frontal side is a mounting standard containing photo flood lights used in making motion picture records of wall and debris motion. Just visible in the background is the round mouth of the compression chamber.

Preload Mechanism

A bearing wall is preloaded in the vertical direction by virtue of the vertical load of upper stories, roofs, floors, etc. After a preloaded wall cracks in flexure (at the top, bottom, and center) under blast loading, the preload's point of application tends to shift to the plane of the downstream face. This shift tends to increase the wall's resistance to the blast loading until the center of the wall has displaced an amount about equal to the wall's thickness, that is, until the wall has failed. Thus, it was determined that the mechanism used in the shock tunnel to simulate preloading in the field should be capable of providing a known resistance in a wall before blast wave arrival, and an increase in resistance after the blast arrived until the wall failed. (Detailed analysis and rationale may be found in Ref. 16.)

A-7
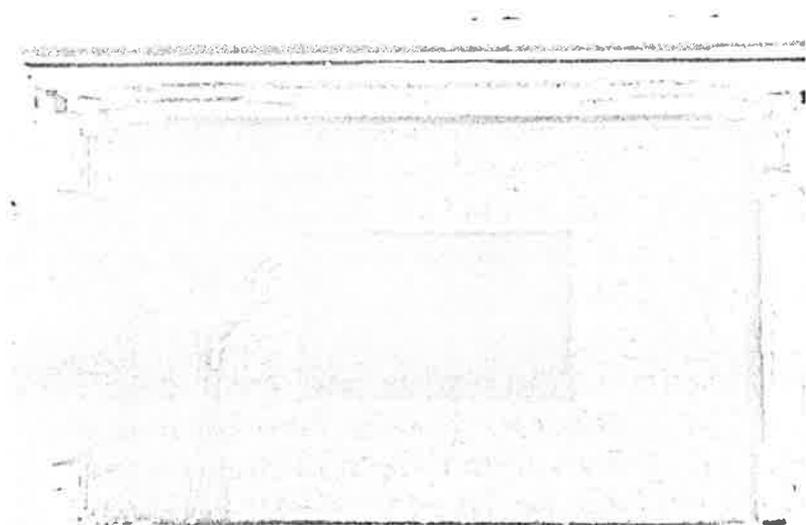
Fig. A-4. Wall Blocks, Top Girder, and Wall Mounted on the Downstream Edge of the Girder.
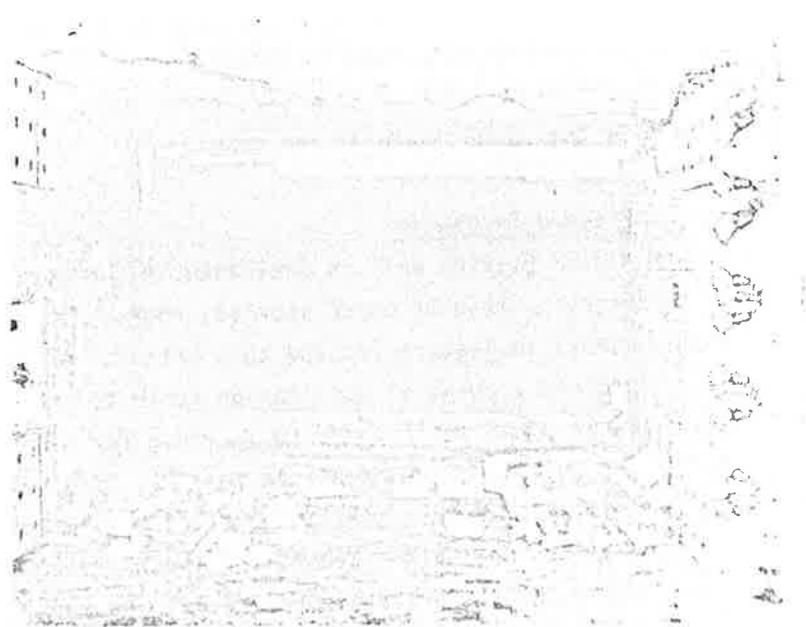
Fig. A-5. Posttest Photograph Showing Both Downstream (Foreground) and Upstream Sets of Wall Blocks, and the Remains of a Concrete Block Wall Still Attached to the Upstream Girder.

A-8

As discussed in Ref. 16, it was decided that the most suitable mechanism would apply load halfway between upstream and downstream faces of the walls. It would provide the desired increase in wall resistance by generating an increase in vertical load while a wall was responding to blast loads, but before the wall became unstable (i.e., before the center of the wall moved far enough that the wall would collapse even if the blast load were removed). It would have a plastic response to preclude serious extraneous oscillation.

A lever system was used, the basic design and operation of which is shown in Fig. A-6. A wall subject to a high enough blast load would first crack in flexure at the center, and then continue to deflect, driving the point of contact with the lever downward and increasing the force on the wall as the weight w was accelerated. The lever was modified by building into it a "yield point" or plastic hinge (a hole was drilled through the lever arm to force the lever to display plastic behavior). This served two purposes: it limited the overload (the load in excess of the static load due to w alone) on the wall; and it eliminated oscillating preload forces that the system would generate. (Actually if the lever could have behaved perfectly plastically, that is, deflecting at constant force, no increase in preload forces would have been generated by it at all; thus the preload would have remained at its initial value until the wall became unstable.)

Under blast loading, a test wall deflected rapidly enough that the motion of the preloading weight was small, and vertical loading imposed by the lever system during the time of interest was similar to the load that would have been imposed by a "real world" system. The load on a wall from such a system as a function of the vertical motion at the bottom of the wall can be derived from the curve of Fig. A-7 which shows the load from the static tests of the plastic hinge mechanism. A wall preloaded initially to some (arbitary) value P_{vo}, would experience a vertical load while it was deflecting given by the portion of the curve of Fig. A-7 above P_{vo}. Figs. A-8 and A-9 are photographs of the preload system as installed. In Fig. A-9, both the yield and the pivot points can be seen.

A-9

= Initial Position of Wall

= Position of Wall After
Blast Loading

W

δ

Δ

Yield Point
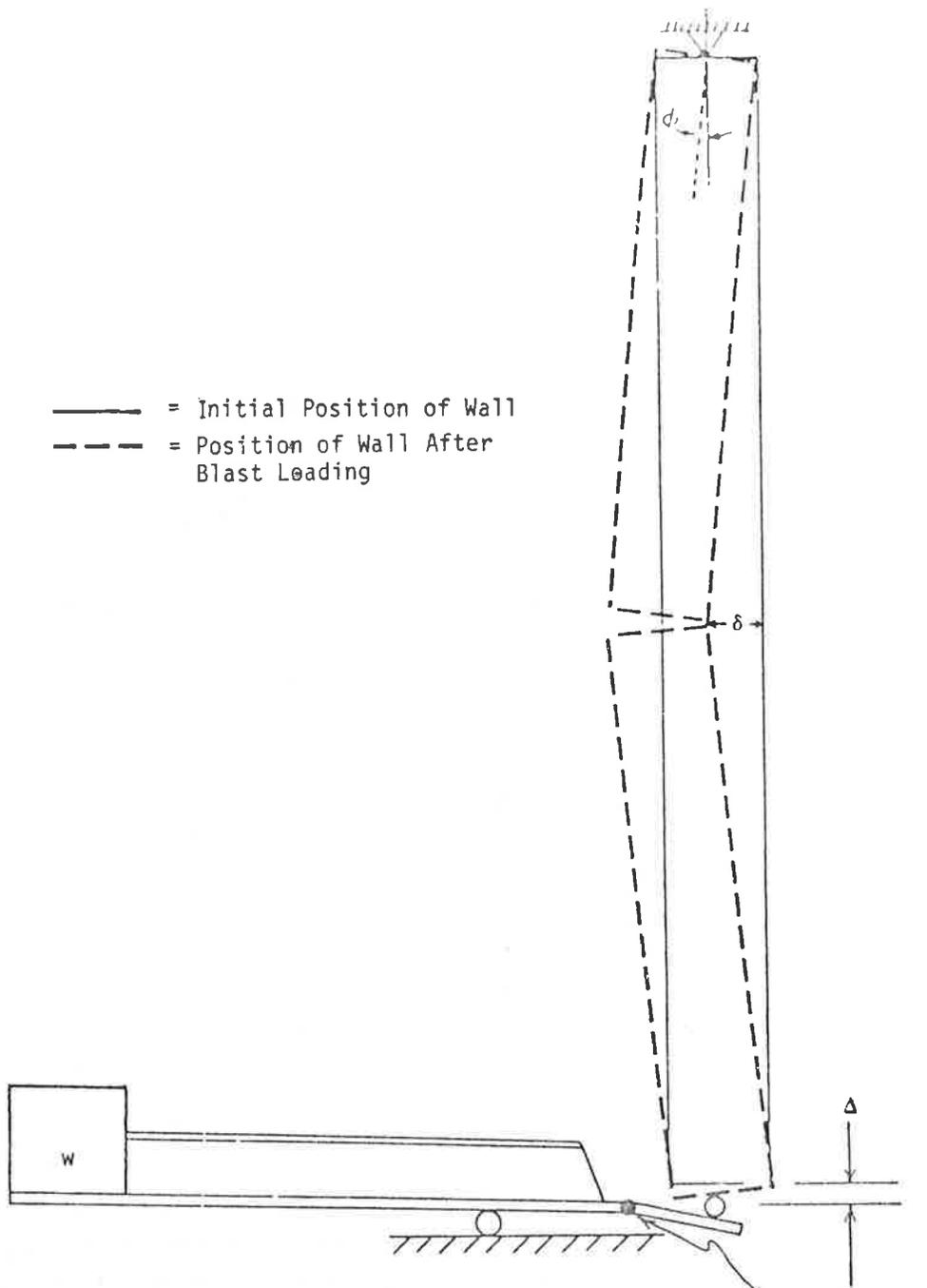
Fig. A-6.   Method Used to Preload Walls in the Shock Tunnel.

A-10
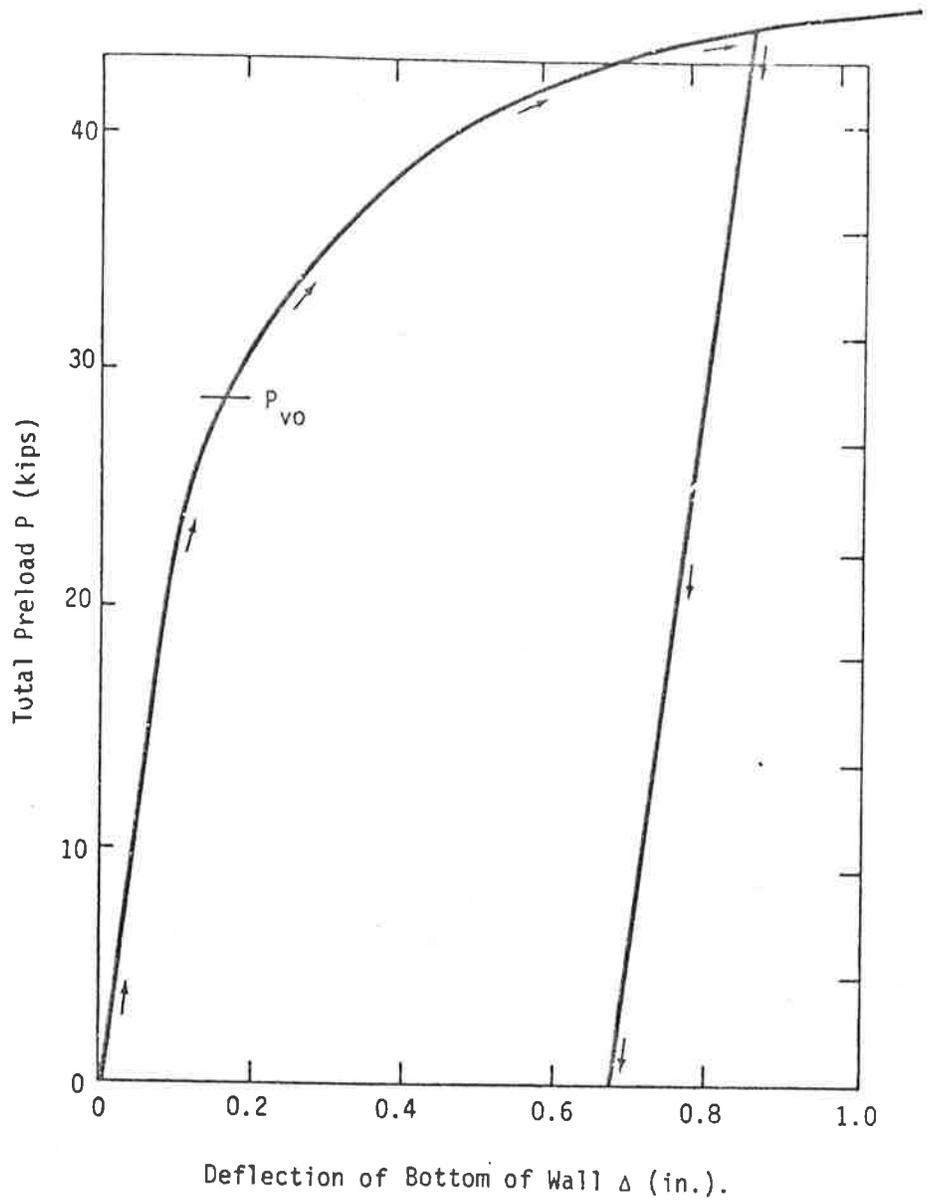
Fig. A-7. Preload vs Deflection from Static Tests of the Plastic Hinge.

Fig. A-8. Photograph of Preload Mechanism.
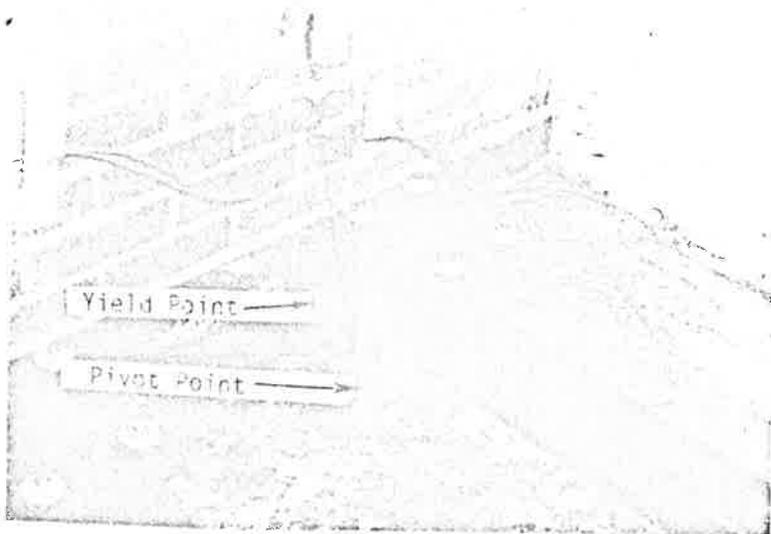
Fig. A-9. Close Up View of Preload Mechanism.

To verify the correct operation of the preload mechanism, load cells were installed between the mechanism and the walls for tests on Walls No. 81 and No. 82 (8-in. thick brick walls) with preloads of 28.5 kips. Records from these load cells are shown in Fig. A-10.

The vertical load that the wall would experience while deflecting after cracking in flexure as derived from Fig. A-7 is shown by the solid line of Fig. A-11A. The other three curves of that figure are measured values, derived from the load cell traces of Fig. A-10 (vertical load vs time) and the displacement gauge traces of Figs. 2-20 and 2-21 (displacement vs time).

In Fig. A-11B, the resistances to horizontal pressure forces, derived from the curves of Fig. A-11A are shown. These "static pressure resistances" are satisfactorily close. The initial dip in the experimental curves of Fig. A-11 are thought to be caused by the initial upward motion at the bottom of the wall caused by the shortening of its neutral axis, due to bending during the elastic phase of the wall's deflection.

Arching Wall Mountings

"Arching" of a masonry wall panel occurs when its supports are "rigid" so that both in-plane motions and rotation at the supports are prevented. When this occurs, even after a wall cracks in flexure, it wedges itself between the supports, forming an arch. Such a wall generates substantial resistance to out-of-plane motions because they can only take place through failure of the wall material itself (e.g., through crushing and spalling).

In the shock tunnel, the floor, walls, and ceiling were all massive enough that arching of a wall panel subject to blast loading would be assured merely by building it into the tunnel directly, in intimate contact (as with a mortar bond) with the floor and ceiling. This would cause the wall panel to undergo so-called one-way arching, that is, arching between two opposite panel edges.*

---

* Even greater resistance to out-of-plane loadings could be developed if the four edges of the panel were fixed so that two-way or plate-type arching could occur. Effort during this program was concentrated on the one-way phenomenon, although on two-way arching walls were tested.
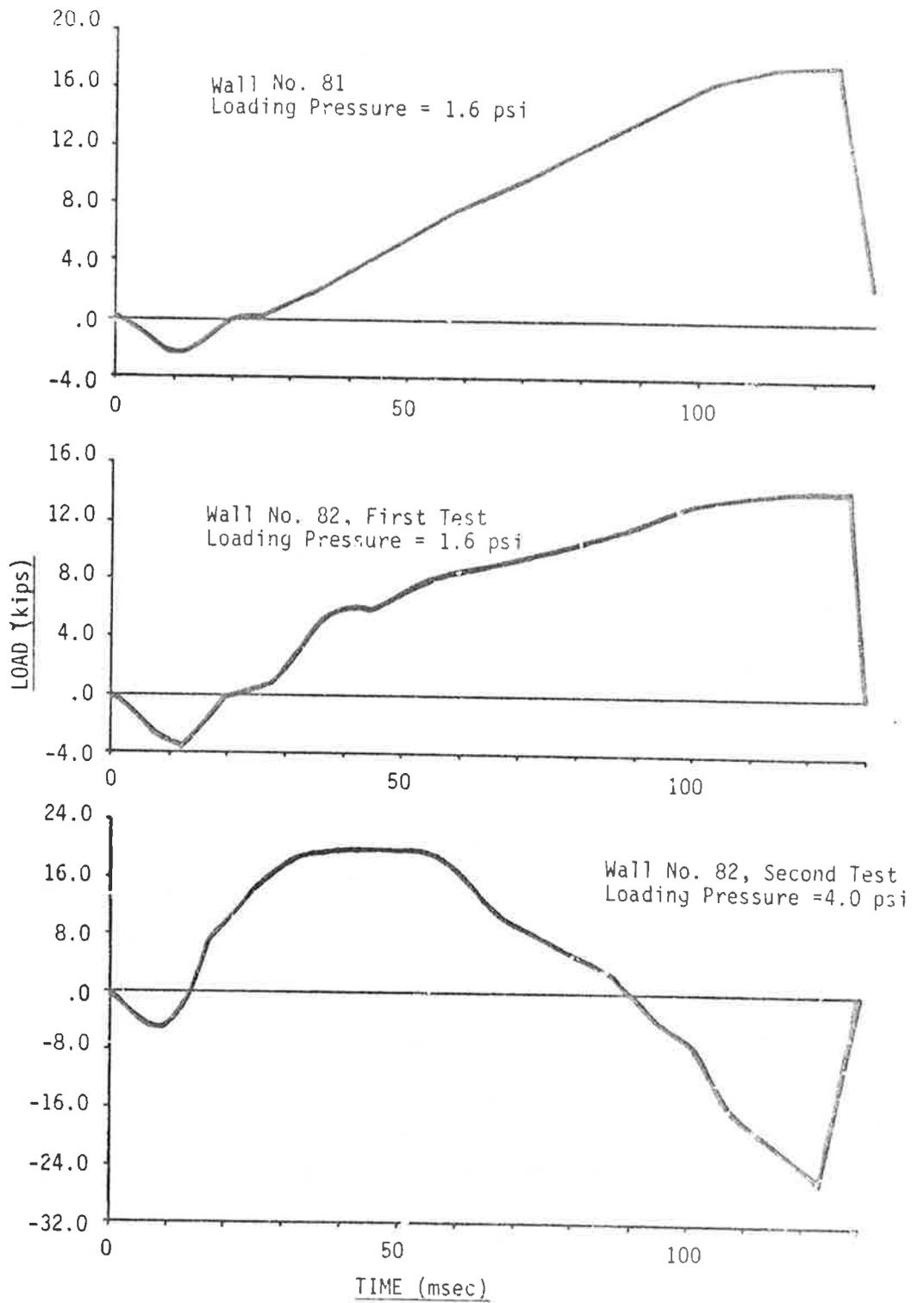
Fig. A-10. Added Vertical Load Imparted to Test Walls No. 81 and 82, with an Initial Preload of 3.5 W (28.5 kips).

A-14
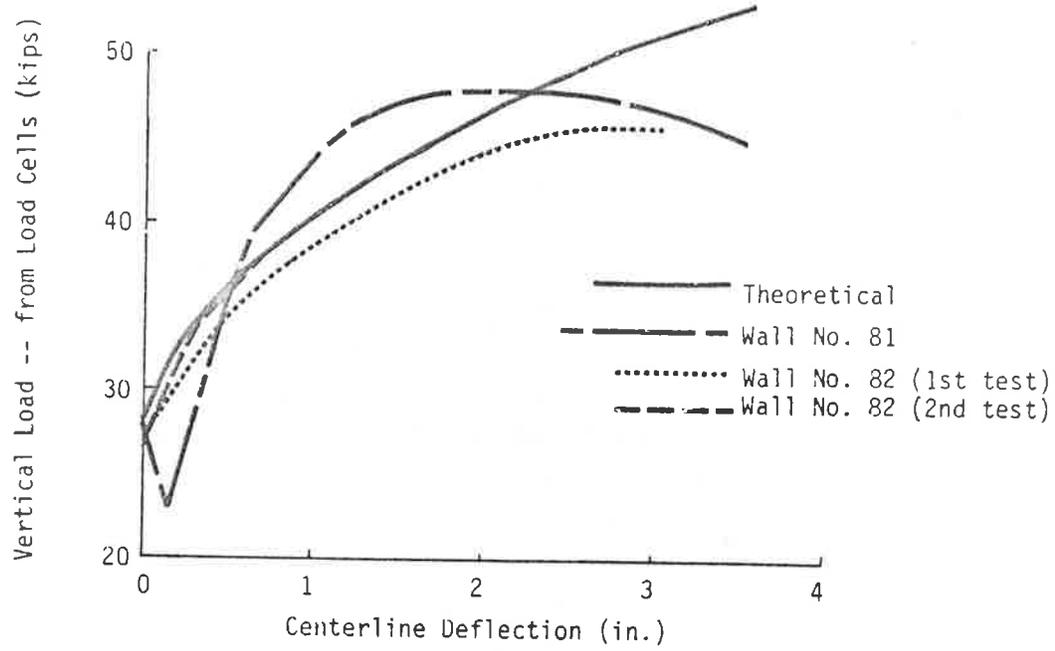
A. Preload vs Centerline Deflection
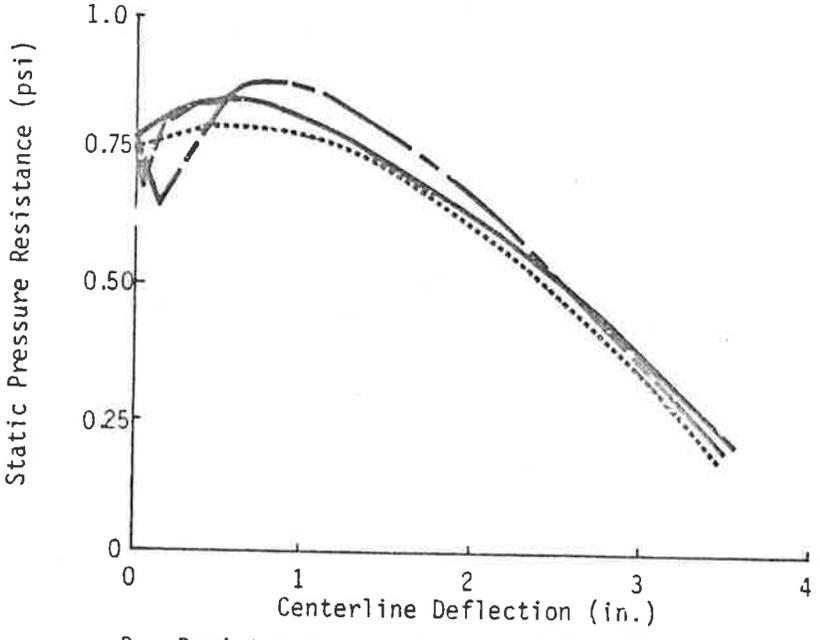
B. Resistance vs Centerline Deflection

Fig. A-11. Preload Mechanism = Predicted and Measured Wall Preload and Associated Static Pressure Resistance.

The first three arching panels tested in the tunnel were constructed in place in the tunnel, each curing a minimum of 28 days before being tested. To allow a faster rate of testing, the remaining panels were built outside the tunnel, stored for curing, and moved into the tunnel.

While the same methods used to transport the simple beam and plate panels into the tunnel were also used with the arching panels, very different methods were used to secure them in the tunnel. The mounting systems used for brick panels and concrete panels is shown in Fig. A-12. The "I" beam portion of the bottom support system (Sketch C) is the lower member of the frame into which the wall was built, and which permitted it to be lifted and transported into the tunnel. Once in the tunnel, the wall was raised, and either the wall itself (Sketch A) or a top frame element (Sketch B) were mortared to the tunnel ceiling. New mortar was then placed at the base as shown in Sketch C. This new mortar had to be wider than the wall itself because thrusts on the lower edge of the wall due to arching were directed at an angle to the plane of the wall face, and a solid load path to the tunnel floor had to be provided. The same consideration led to the use of a wide mortar area at the top of those walls that had a top frame member (Sketch B). Note that the mortar used in the tunnel installation would be more accurately described as a high-early grout.

A similar mounting system was used with composite concrete block and brick walls (Fig. A-13).

Roof of Shock Tunnel

Top Support
System

Bottom Support System

Blast
Direction

Floor of Shock Tunnel
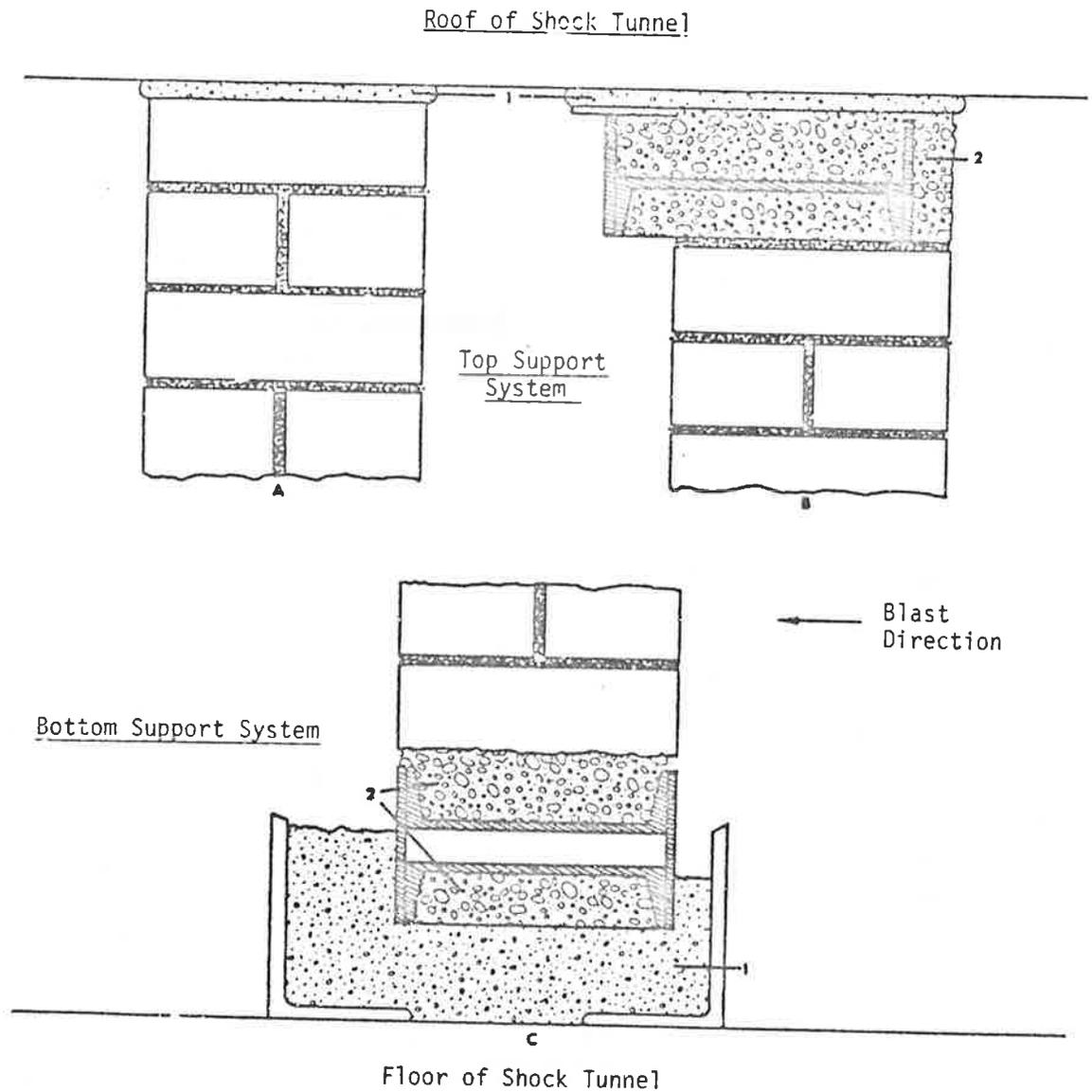
Fig. A-12. Top and Bottom Support Systems for 8-in. Brick Arching Wall Constructed and Cured Outside Shock Tunnel. Top System "A" Used for Walls 75 and 76, System "B" for Walls 77 and 78. Bottom System Used Same for All Tests. Note: 1. Mortar Installed When Wall was Placed in Shock Tunnel. 2. Mortar Installed When Wall Was Constructed.

A-17

Roof of Shock Tunnel

Top Support System

Concrete
Block

Brick
Facing

Blast
Direction

Bottom Support System

Floor of Shock Tunnel
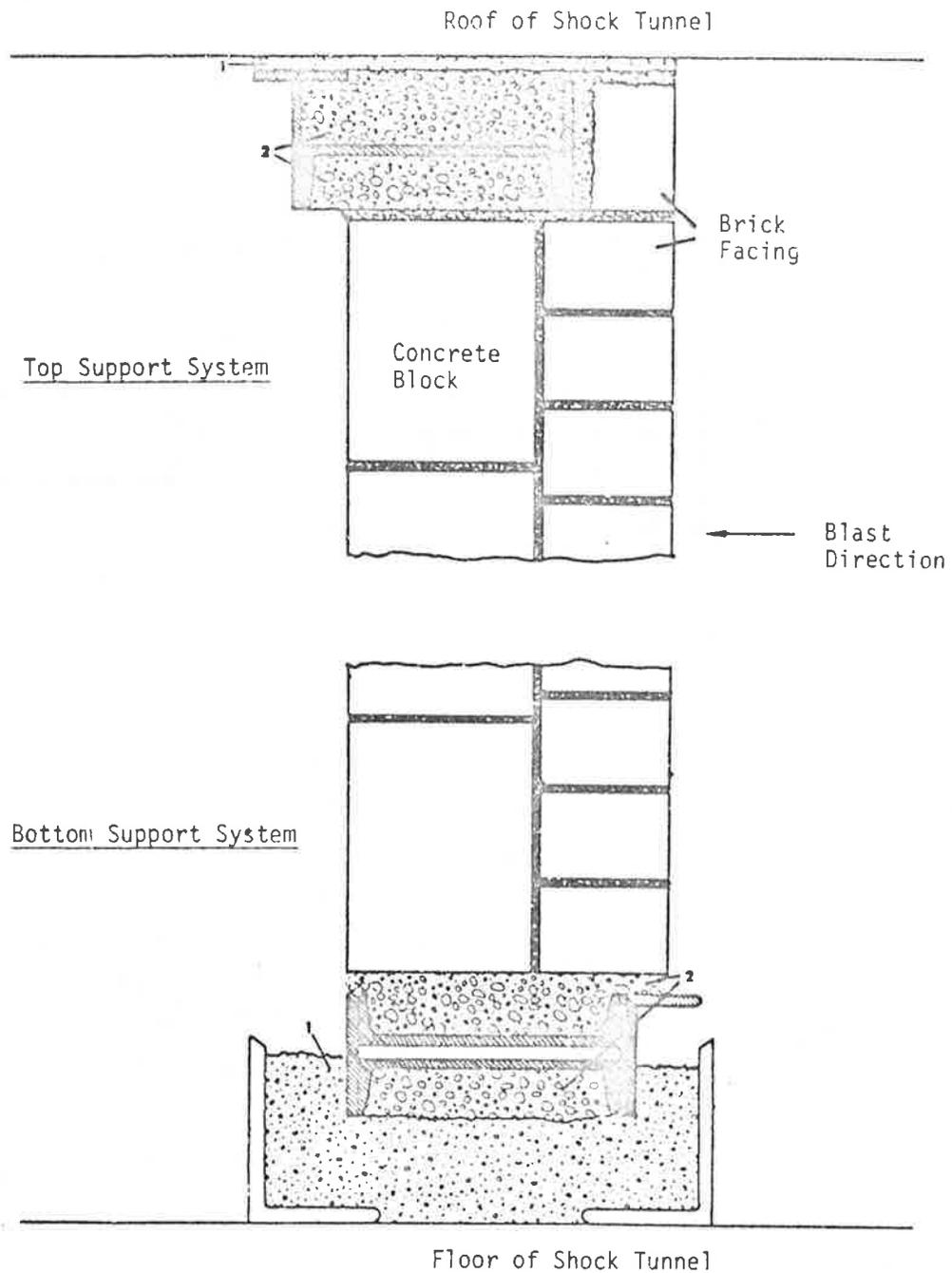
Fig. A-13.   Support Systems for Wall No. 79, 6-in. Concrete Block with
4-in. Brick Facing. Note: 1. Mortar Installed When Wall was
Placed in Shock Tunnel. 2. Mortar Installed When Wall was
Constructed.

APPENDIX B
DESCRIPTION OF COMPUTER CODES USED FOR
PREDICTION OF WALL PANEL RESPONSE

Appendix B

DESCRIPTION OF COMPUTER CODES USED FOR PREDICTION OF WALL PANEL RESPONSE

As noted in Section 1 of this report, three finite element computer codes were use to analyze wall behavior. For all but arching walls, the SAMIS code was used. For arching walls, the MACE code was used initially, and a few calculations were made using the far more powerful STARDYNE code. Descriptions of the codes, and the mathematical models employed with them, follow.

WALL PANELS MOUNTED AS SIMPLE BEAMS AND PLATES -- SAMIS ANALYSES

At the time SAMIS was first employed in this study, it could handle triangular elements (e.g., plates and shells) and line elements (e.g., trusses and frames). (See Ref. 17.)

SAMIS is a segmented or chain program composed of 16 segments or links. The user selects the links to be used to give his desired output, and specifies the order of the selected links by writing a set of instructions called pseudo instructions. A pseudo instruction calls for a set of sub-programs to perform the necessary matrix operations.

The solution of a typical structural progam involves the following steps. First, material tables defining the mechanical properties of all materials of interest are made. Then, a listing of the element data is made defining local geometry (thickness, cross-sectional area, moment of inertia), gridpoints, coordinate systems, temperatures, weight and pressure on each element. Third, boundary and loading conditions in matrix form are put in. And finally, the pseudo instructions are used to direct the operation of SAMIS to achieve the desired results.

Input to SAMIS consisted of: material properties of the wall panels and their supports; the blast loadings to which the walls were to be exposed; and finally, the mathematical models of the walls themselves.

B-1

Material Properties

The material properties used in all the SAMIS calculations are given in Table B-1.

Table B-1
Material Properties Used
for SAMIS Calculations

Property	Material	
	Steel[1]	Brick- Mortar
Young's Modulus, E	30×10^6 psi	1×10^6 psi[2]
Poisson's Ratio	0.3	0.1
Specific Weight	500 lb/ft^3	120 lb/ft^3

Notes - (1) From AISC Manual

(2) From static tests on common brick using ASTM procedures.

Input Loadings

The basic blast pulse generated in the shock tunnel had a sharp front, a flat-topped or constant pressure portion about 40 to 50 msec long, and a portion which decayed to ambient pressure in an additional 50 to 60 msec. In all cases, those walls exposed to these blast pulses that cracked in flexure, did so at times shorter than 30 msec, that is, before the loading pulse started decaying. Since SAMIS operates only in the elastic domain, its use is restricted to time before flexural cracking occurs. The loading pulses used as input to SAMIS, therefore, had to be based on the simple, single-step incident pulses which existed in the tunnel at times before the onset of flexural cracking and pulse decay.

The characteristics of loading pulses generated in the shock tunnel on walls of various geometries (that is, walls with and without doorway and window openings) are discussed in detail in Volume 2 of this series. It was found that loadings on solid walls (walls which completely blocked the tunnel) resembled the single-step incident pulses except that the constant pressure

portion had a value p_r, related to the incident pulse's constant overpressure portion p_i, by

$$p_r = 2p_i \left[(7p_0 + 4p_i) \Big/ (7p_0 + p_i) \right]$$

where p_0 is ambient pressure. A sketch showing the pulse that was used as the basic SAMIS input loading pulse on a solid wall for an incident pressure level of 3.3 psi (which would be generated by the detonation of three 60-ft long strands of Primacord) is shown in Fig. B-1A.

Loading pulses for walls with openings (a window or a doorway) are more complex, since the opening results in decreased pressures on the front, or upstream face of the walls, and permits blast pressure to load the back, or downstream face, thereby reducing the net loadings (the difference between loadings on the upstream and downstream faces) on the wall. It is shown in Volume 2 that the net loading at a point on a wall with a window is initially the same as that on a solid wall, but it rapidly drops in value until it stabilizes at a lower value dependent on the size of the window operning. The same pattern was observed at different points around the window openings so that it was possible to use a single pulse as SAMIS input to load all elements on the wall. The basic pulse used as SAMIS input for the analysis of a wall with a window, derived from an incident step pulse of 3.3 psi, is shown in Fig. B-1B.

The loading pulses used in analyzing walls with doorways were still more complex. Initially, peak reflected pressure occurs across the entire wall. The net loading at a particular location on the wall, however, begins to decrease at a time related to the distance from the doorway. Two factors cause this to happen: First, rarefaction waves start at the doorway and propagate across the upstream face of the wall because initial pressure in the doorway area (incident pressure) is less than that on the wall immediately adjacent to the doorway (peak reflected pressure). Second, a positive pressure pulse propagates across the downstream face of the wall as the shock wave passes through the doorway and expands. The first factor decreases the downstream

B-3
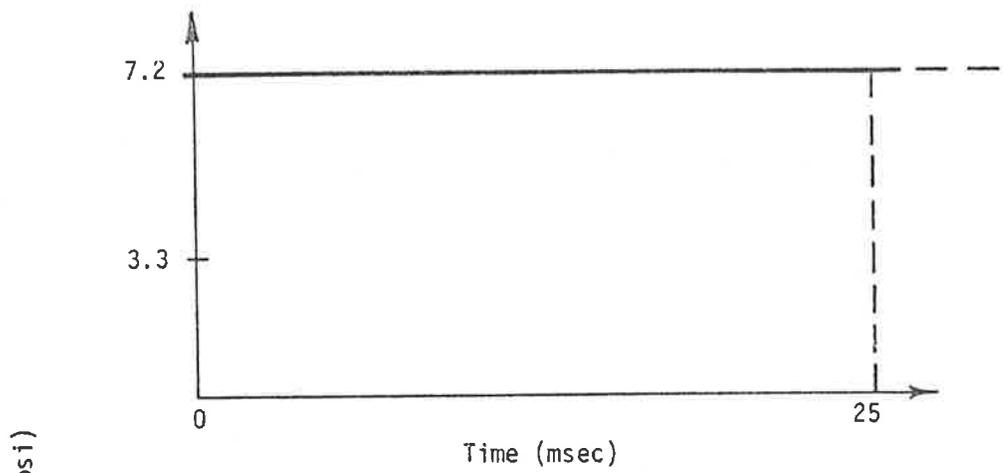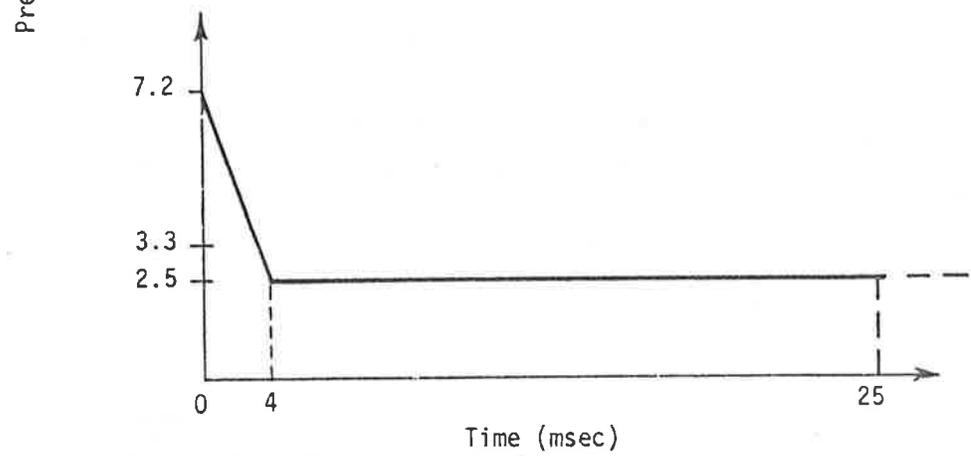
A. Solid Walls.

B. Walls with a Window.

Fig. B-1. Average Input Loadings from an Incident Step Pulse of 3.3 psi Used with SAMIS Calculations for Solid Walls and Walls with a Window.

B-4

directed loading from its peak value; the second causes an upstream-directed
loading that was not present with a solid wall.

In the shock tunnel the two pressure waves which propagated across the
faces of the wall from the doorway eventually encounter the tunnel side wall
and reflect from it. They then travel back across the faces of the wall to
the doorway where another interaction causes additional waves to propagate
toward the tunnel side wall again. The process repeats itself, resulting in
loadings across the face of a wall which are highly non-uniform.

The net loadings generated by an incident step pulse of 3.3 psi measured
at three points on the wall are shown on Fig. B-2A along with lines showing
approximate average values drawn through the high frequency components of the
load. (It was shown in Ref. 9 that these components would have little effect
on wall behavior.) The basic input loadings to SAMIS derived from these
lines are shown in Fig. B-2B.

Computer Models

The basic computer model of walls mounted as beams is shown in Fig. B-3.
Nodal points are identified by numbers in circles, and the discrete elements
by numbers without circles. The wall elements (serially numbered from 1
through 96) are all triangular. The nodes on the wall itself are numbered
in decades from 10 through 610. Only half the nodes and elements are identi-
fied in Fig. B-3 because a beam-mounted wall is geometrically symmetrical
about its horizontal centerline. With uniform loading normal to the face of
the wall, motions at similar points above and below the centerline would be
identical, and the centerline itself could move neither up nor down. This
permitted use of a half-wall mathematical model in which the nodes along
the centerline (numbered by fifties starting at 10) were not allowed to
displace in the y (vertical) direction, nor rotate about an x (horizontal)
axis.

As noted earlier. to minimize deflections along the supported edges,
the test walls supported as beams in the tunnel were mounted on massive
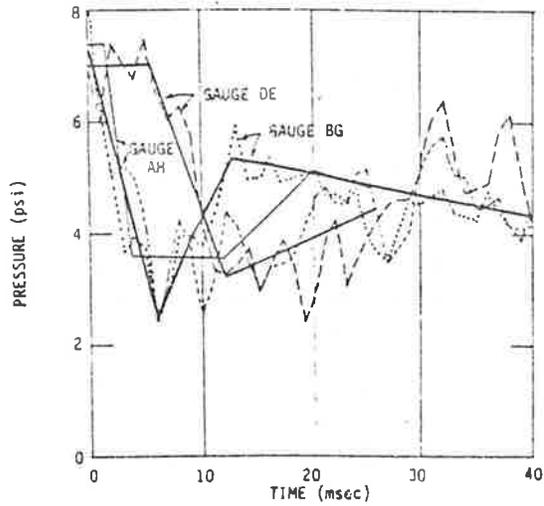
A. MEASURED LOADINGS FROM PAIRED GAUGES ON THE HORIZONTAL
    CENTERLINE OF THE WALL AT THE FOLLOWING LOCATIONS:
    GAUGES BG- 1 ft FROM DOORWAY; GAUGES AH- 3 ft FROM DOORWAY;
    GAUGES DE- 7 ft FROM DOORWAY.
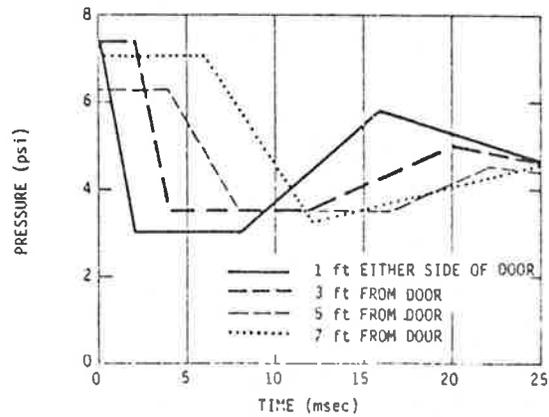
B. AVERAGE LOADING PULSES USED IN SAMIS CALCULATIONS.

Fig. B-2. Net Loadings on a Wall With a Doorway.
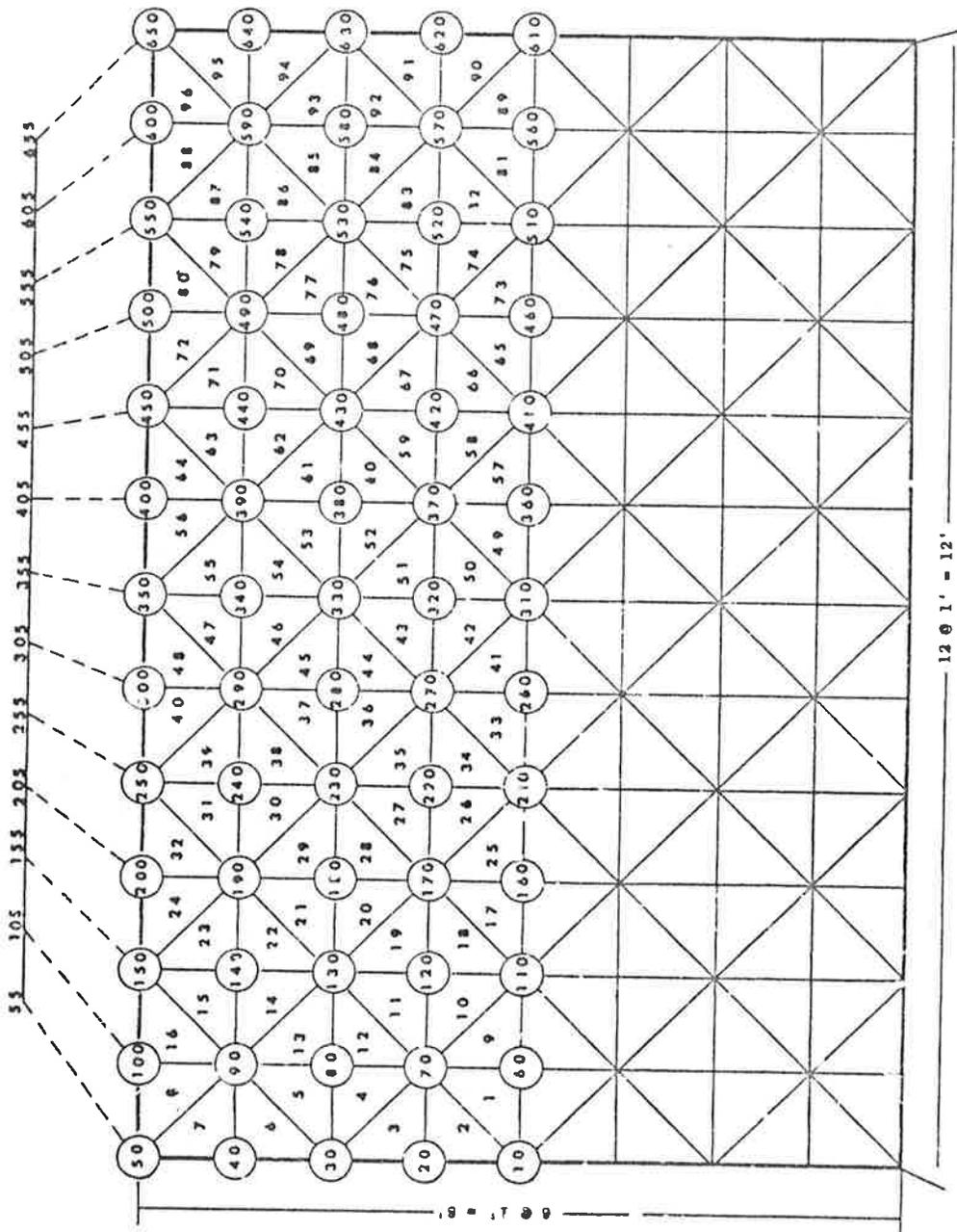
Fig. B-3. Node and Element Locations for Solid Walls.

B-7

horizontal steel girders. In the mathematical model, the upper horizontal girder was replaced by the unnumbered line elements and the connecting nodes (numbered by fifties from 55 to 655) at the top of Fig. B-3. The mass of each girder, which weighed about 2600 lb compared with about 4000 lb for one half of an 8-in. thick brick wall panel, was equally apportioned among these nodes.* Centroids of the model girder and the model wall were connected by nondeformable line elements (shown as dashed lines connecting nodes 50 to 55, 100 to 105, etc.). This arrangement for the girder and wall connections permitted the effects of shear and bending of the girder (essentially a very deep beam) to be included in the system response. The end nodes (55 and 655) were designed to model the restraints of the real girder as offered by a load cell bearing on a steel block affixed to the tunnel wall (see Fig. A-3). The line elements of the model girder represented shear and bending deflections along the girder between these supports.

The nodes at the top of the wall itself (50, 100, 150, etc.) could be restrained from rotating. When they were so restrained, the model represented a moment resisting (virtually a fixed) support condition; when they were free to rotate, the model represented a pinned support condition.

The mathematical model of walls supported as plates in the tunnel is similar to that shown in Fig. B-3, except that line elements and nodes connected to the vertical edge nodes (10, 20, ...50 on the left, and 610, 620, ..650 on the right) were added. These were assigned the same characteristics as were the line elements and nodes at the top of Fig. B-3, which permitted plates with both pinned and fixed supports to be analyzed.

The mathematical models of the wall with a doorway used with SAMIS are very similar to those for the solid walls. Indeed, they are derived from the solid wall models merely by blanking out three vertical columns of elements (65 through 88). The resultant model for a beam-mounted wall is shown in

* SAMIS requires all masses to be lumped at the nodes. For the calculations reported here, preliminary runs on simplified models had indicated that the wall mass could be concentrated at every other nodal point.

Fig. B-4 with the doorway elements shaded.

The computer model of the wall with a window is somewhat more complex than the other two. The model actually consists of only one quarter of the wall instead of one half as in the other two models, a pattern which could be adopted because the wall was symmetrical about both the x and y axes. (This could also have been done with the solid wall, but not the wall with a doorway.) Because it was desired to investigate deflections and stresses in the area immediately adjacent to the window in more detail than was done with either the solid or the doorway wall, additional nodes and elements were used in that area. This was done to allow identification of stress concentration points and predictions of subsequent crack propagation. The model used with SAMIS for a beam-mounted wall with a window is shown in Fig. B-5.
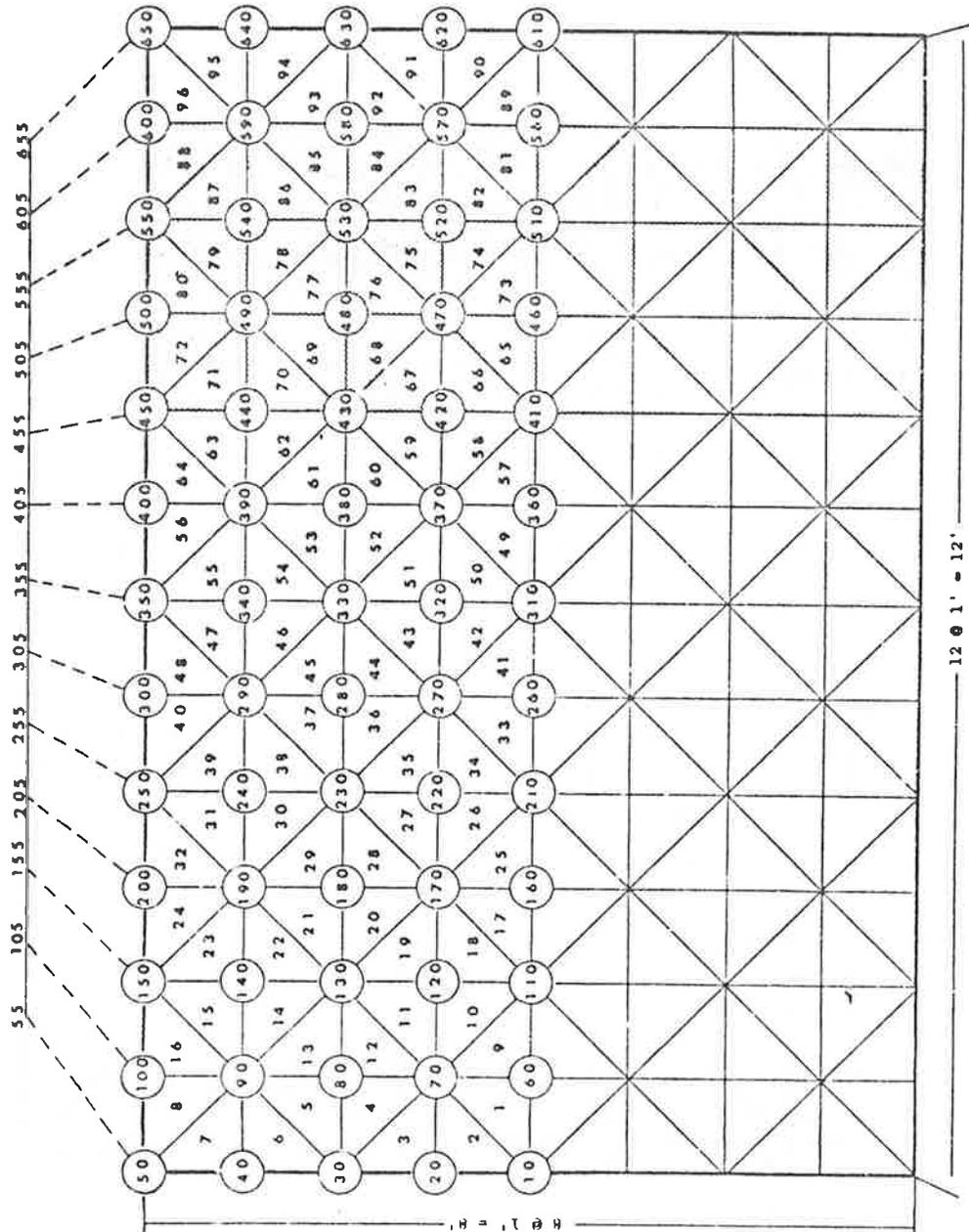
Fig. B-4. Node and Element Locations for Wall with a Doorway.

B-10
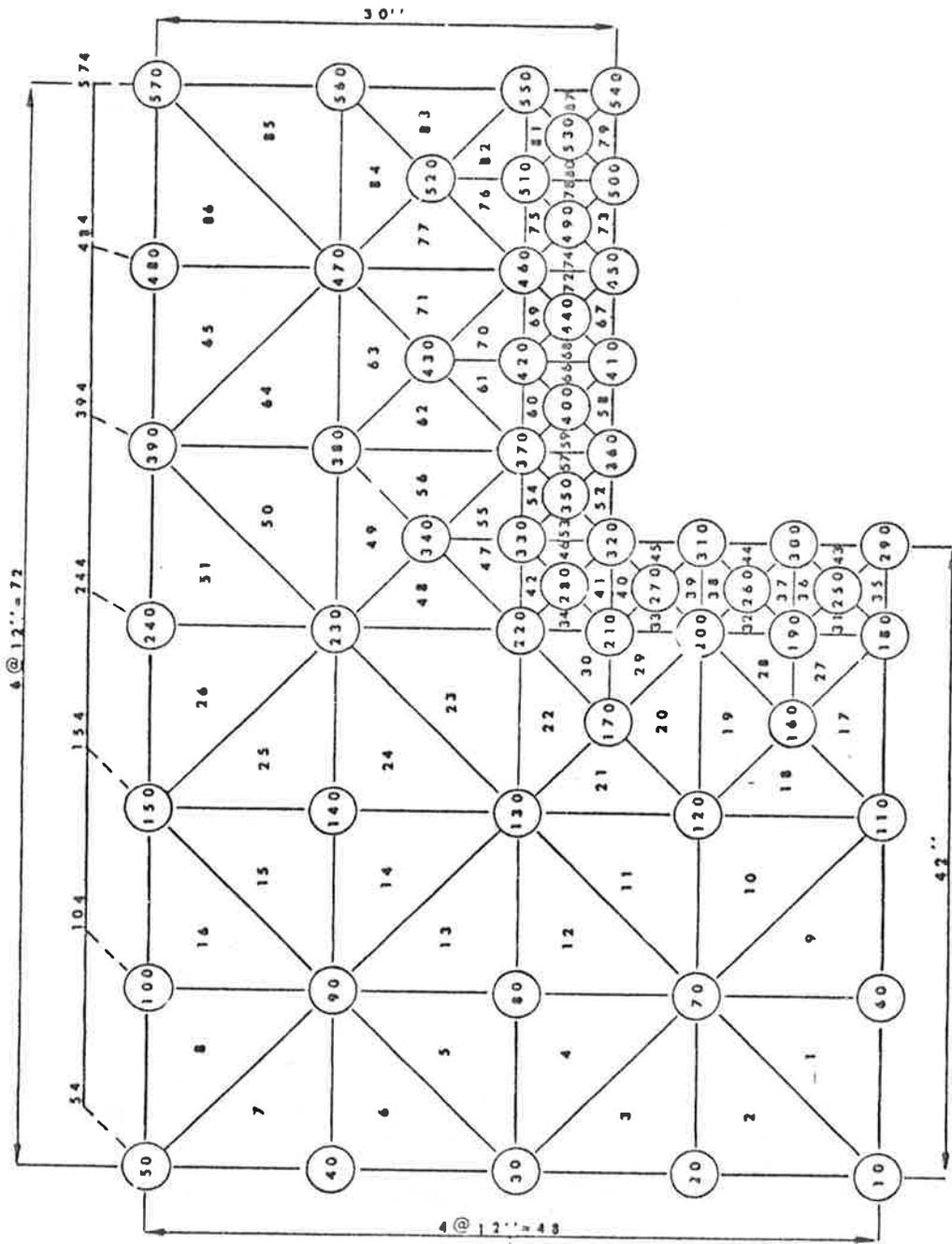
Fig. B-5. Node and Element Locations for Wall with a Window.

B-11

ARCHING WALL PANELS -- MACE ANALYSES

Because of its limited capacity (50 nodes, triangular elements only, static loadings only, and output limited to nodal deflections) relatively little use was made of MACE. As noted earlier, however, it was fast and relatively inexpensive to operate, and did provide insight into both the static material testing program, and the actual blast testing of arching walls.

Two different mathematical models were used. The first resembled the static test configuration used to test brick assemblages under line load. Both the mathematical model and one of the static test configurations (inset) are shown in Fig. B-6. Material properties used in the calculations are the same as those employed with SAMIS.

After the initial work with the model shown in Fig. B-6, a second model, more closely a simulant of the conditions observed to occur in the tunnel, was used. The model for the upper half of a wall is shown in Fig. B-7, along with a sketch of the tunnel condition it was designed to simulate (inset). Crushing and spalling of material along the downstream edge of the top of the wall and the upstream edge of the central crack had been observed in the tunnel. In the model, this was simulated by moving the points of contact in these areas inboard by an inch (the wall being 8 in. thick). Again, the material properties used with this model were the same as those employed with SAMIS.
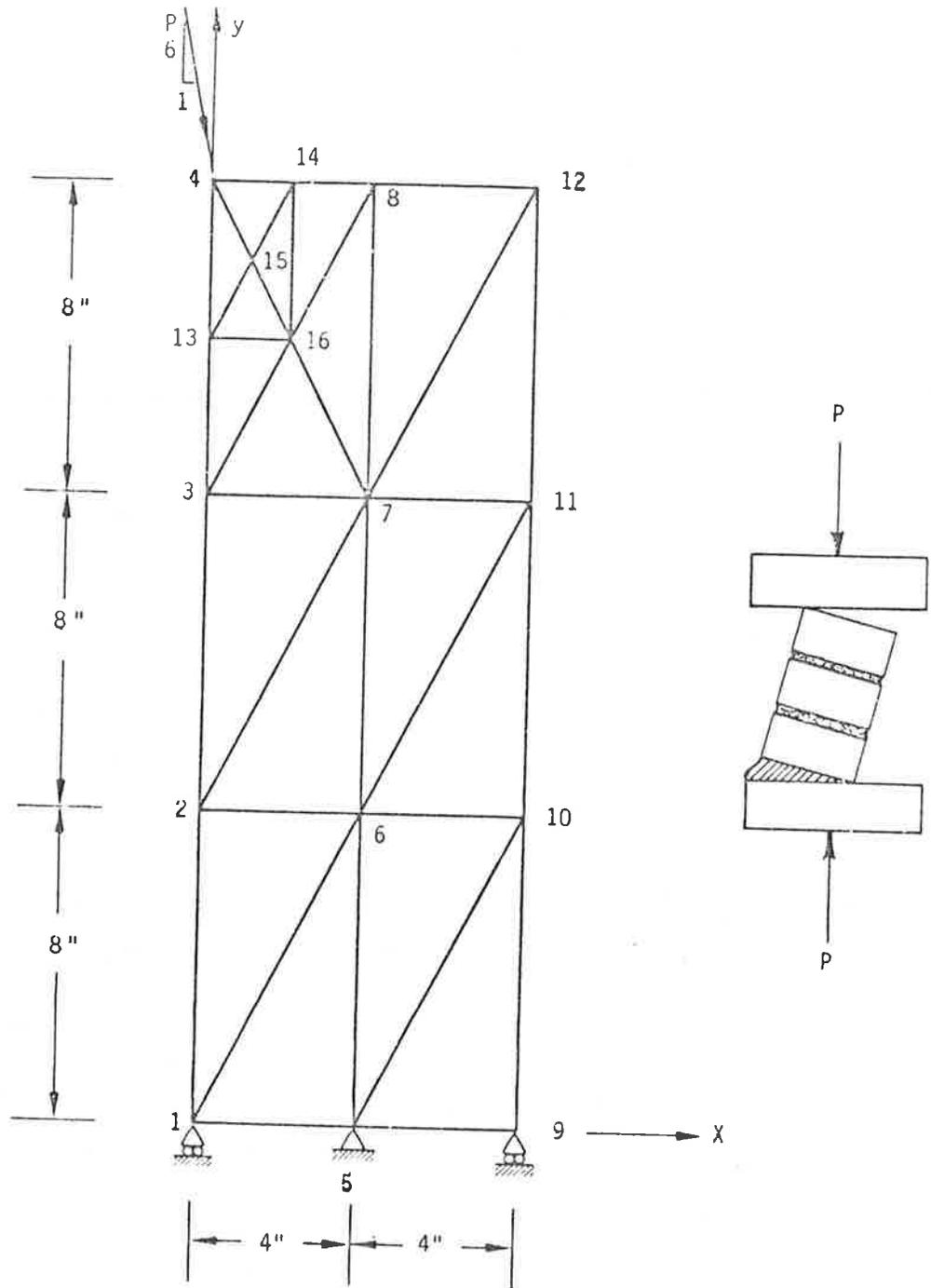
Fig. B-6.   Initial Computer Input Model Used with MACE.
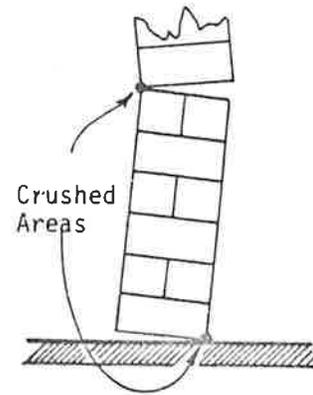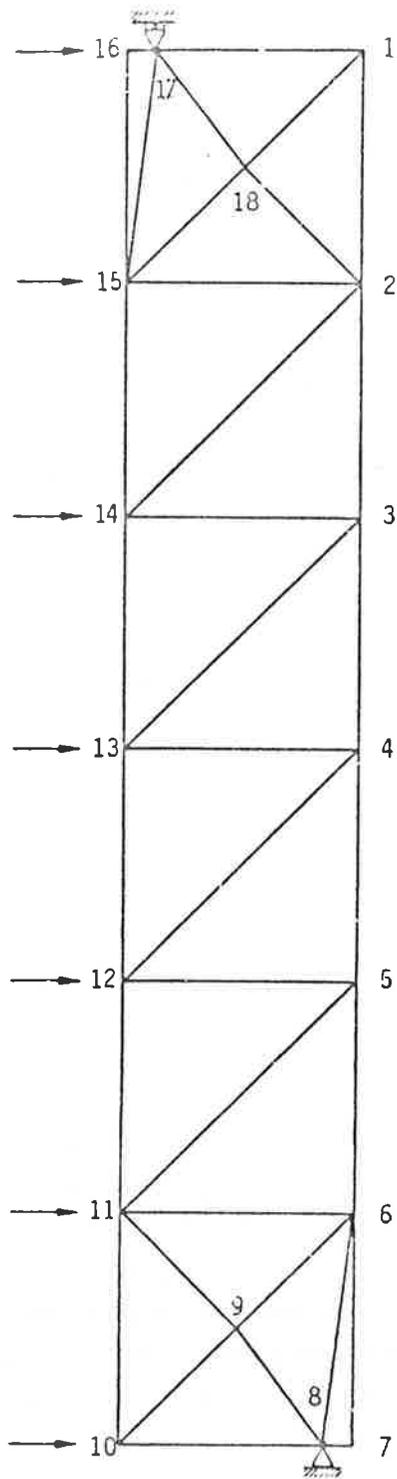
Fig. B-7. Final Computer Model Used with MACE.

ARCHING WALL PANELS -- <u>STARDYNE</u> ANALYSES

The STARDYNE Analysis System consists of a series of compatible digital computer programs designed to analyze linear elastic structural models. The analysis system encompasses the full range of static and dynamic types of analysis and can be used to evaluate a wide variety of problems.

The static capability includes computation of structural deformation and member loads and stresses caused by an arbitrary set of applied loads and/or displacements.

Dynamic response analyses can be performed for transient, steady-state harmonic, random, and shock spectra excitation types. Dynamic response results can be presented as structural deformations (displacements, velocities, and accelerations) and/or internal element loads and stresses.

The computer code is organized and formatted to enable the user to obtain a meaningful solution with a minimal amount of required input data and offers a very wide range of output formats, both numerical and graphical. The mathematical operations contain state-of-the-art innovations in numerical analysis providing the analyst with a sophisticated, cost-effective, structural dynamic analysis system.

Given the physical characteristics of the node and finite elements forming the structural model, the solution procedure consists of the following: first, the stiffness matrix formulation (relating the stiffness of each element); a static analysis solving for either nodal displacements or element internal stresses for a given set of applied nodal forces; an eigenvector determination giving the frequency response of the structure; and finally, the dynamic response analysis using the natural frequencies and normal modes together with the related mass and stiffness characteristics of the structure forming the appropriate equations of motion. The equations are evaluated to determine the structure response to dynamic loading.

B-15

The material properties used with the STARDYNE analysis were the same as those used with SAMIS. Analyses with STARDYNE had just begun when the program ended, and only limited information was developed, for static analyses using a static loading of 1 psi.

Analyses were made with three different STARDYNE mathematical models. The first was for a so-called rigid arching wall, and was essentially an extension of the last work done with the MACE program, with the wall cracked at the center. As with MACE, only a half-wall model, shown in Fig. B-8, was employed. Note that the model grid is far more detailed than is the MACE grid, especially at the top downstream edge, and the center upstream edge, where material crushing was observed to occur. Fig. B-8 also shows some stress directions derived with STARDYNE.

A second set of calculations was carried out with a similar geometry, except that a crack was presumed to exist one quarter the way up the wall instead of at the wall center. This geometry is no longer symmetrical about the centerline, so the mathematical model had to include the entire wall.

Finally, calculations were carried out for gapped arching, in which a gap at the top of the wall permits the top to move far enough that the rear (downstream) edge contacts the rigid frame that causes arching. Walls that undergo this type of arching display less resistance to blast loading than do rigidly arching walls. The upper portion of the mathematical model employed for these calculations is shown in Fig. B-9. The stress directions shown in Fig. B-9 derived with STARDYNE for a gapped arching wall can be compared with those for a rigidly arching wall shown in Fig. B-8.
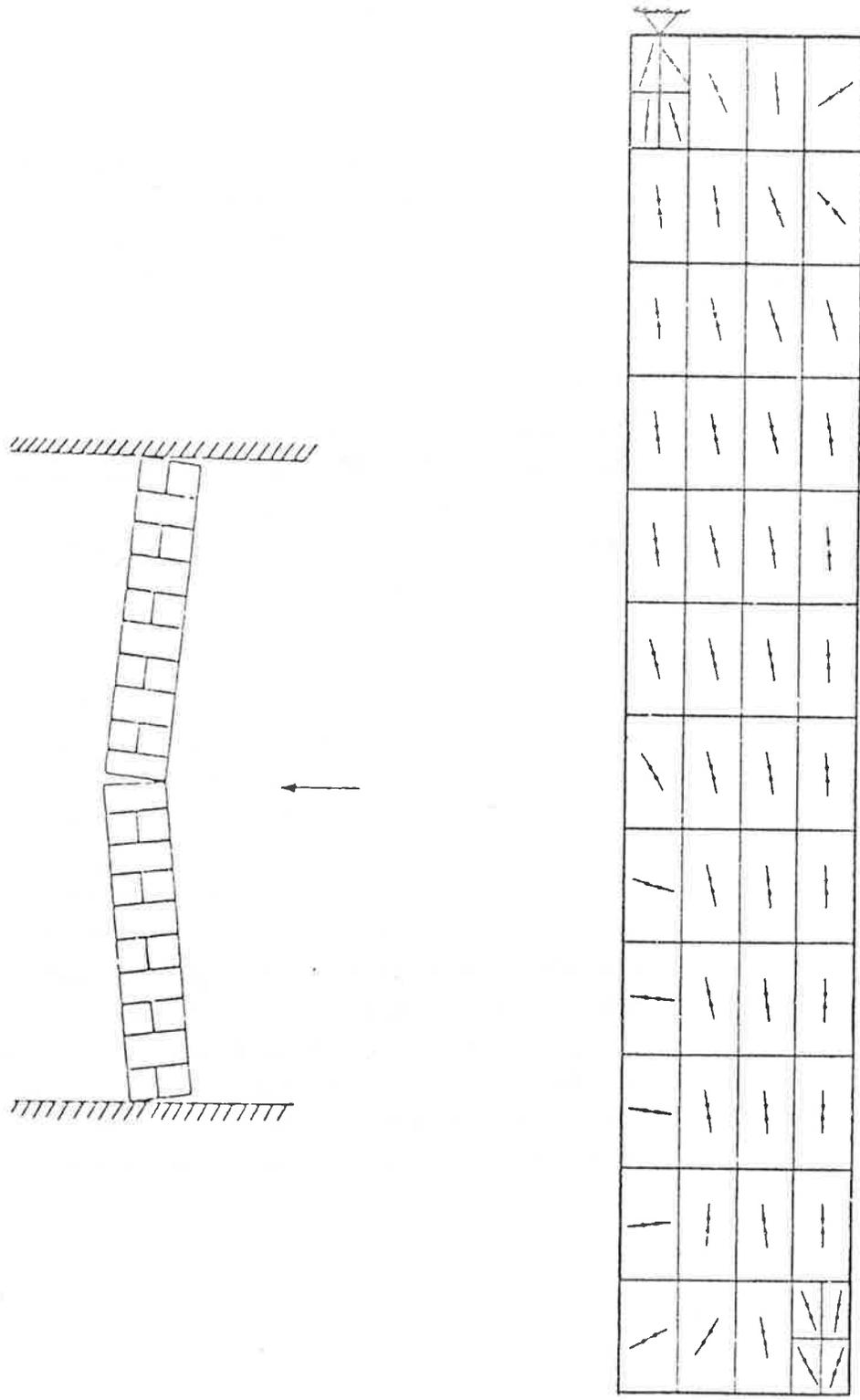
Fig. B-8. Sketch Illustrating Rigid Arching and STARDYNE Model of Upper Half of the Wall Showing Directions of Compressive Stress in the Elements.
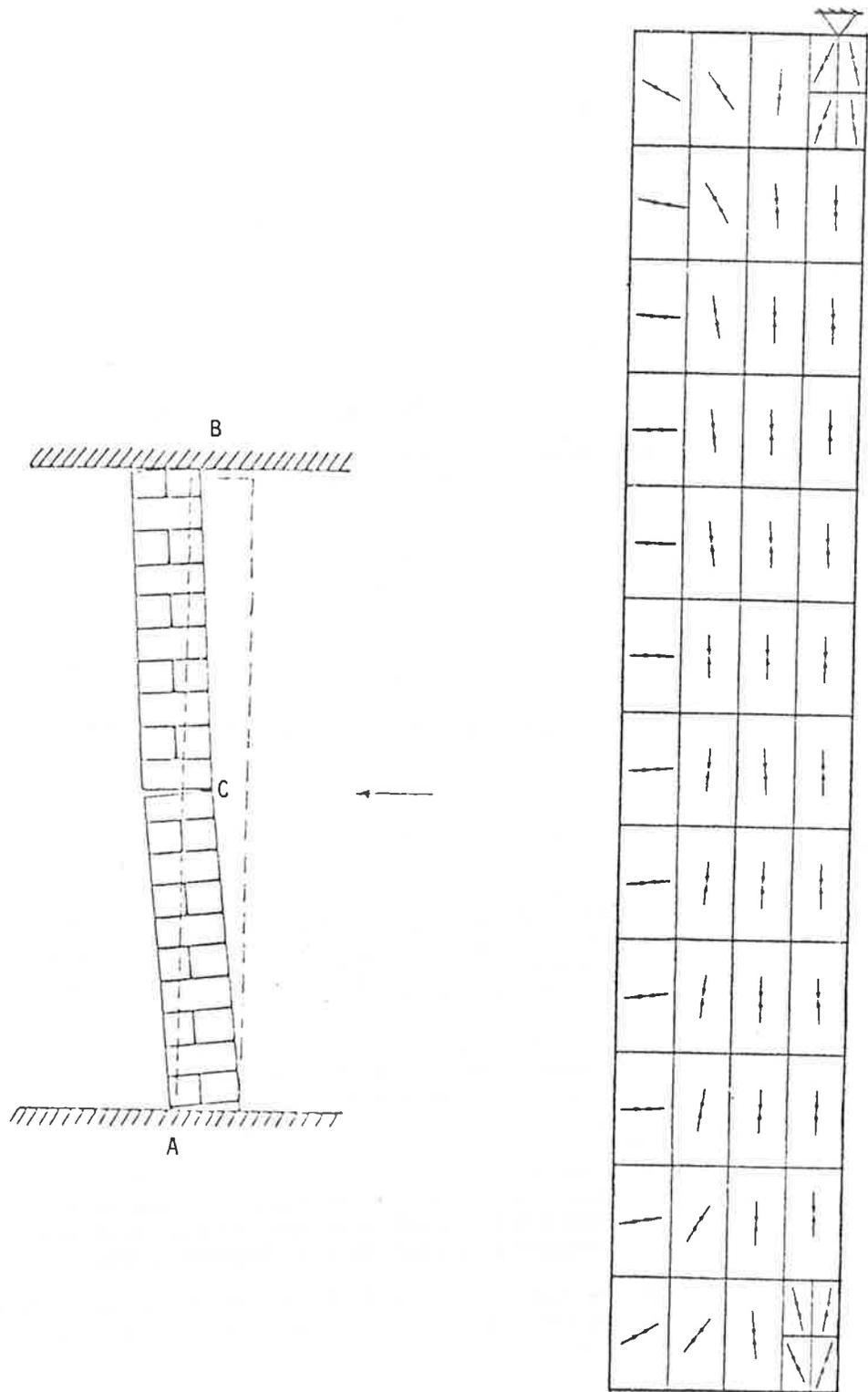
Fig. B-9. Sketch Illustrating Gapped Arching and STARDYNE Model of Upper Half of the Wall Showing Directions of Compressive Stress in the Elements.

B-18

REFERENCES

1. Hill, E.L., et al., "Structural Characteristics of NFSS Buildings", Vols. I-V, Research Triangle Institute, Final Report, OU-237, Durham, North Carolina, February 1976.

2. Lakser, M.E., "User's Guide, Structural Analysis and Matrix Interpretive System (SAMIS)", March 1967.

3. Concrete Masonry Handbook, Portland Cement Association

4. Handbook on Reinforced Grouted Brick Masonry Construction, Brick Institute of California, Los Angeles, California.

5. Wilton, C., B.L. Gabrielsen, J. Edmunds, and S. Bechtel, "Loading and Structural Response of Wall Panels", URS 709-4, URS Research Company, San Mateo, California, November 1969.

6. Wilton, C, and B.L. Gabrielsen, "Shock Tunnel Tests of Preloaded and Arched Wall Panels", URS 7030-10, Final Report, URS Research Company, San Mateo, California, June 1973.

7. Biggs, John M., Introduction to Structural Dynamics, McGraw-Hill Book Company, New York, N.Y.

8. Gabrielsen, B.L., and C. Wilton, "Shock Tunnel Tests of Arched Wall Panels", URS 7030-19, Final Report, URS Research Company, prepared by Scientific Service, Inc., Redwood City, California, December 1974.

9. Willoughby, A.B., C.Wilton, B.L. Gabrielsen, and J.V. Zaccor, "A Study of Loading, Structural Response, and Debris Characteristics of Wall Panels", URS 680-5, Final Report, URS Research Company, San Mateo, California, July 1969.

10. Wilton, C., K. Kaplan, B.L. Gabrielsen, and J.V. Zaccor, "Blast/Fire Interaction, Blast Translation, and Toxic Gases", URS 7239-11, Final Report, URS Research Company, prepared by Scientific Service, Inc., Redwood City, California, July 1976.

11. Gabrielsen, B.L., C. Wilton, and K. Kaplan, "Response of Arching Walls and Debris from Interior Walls Caused by Blast Loading", URS 7030-23, Final Report, URS Research Company, prepared by Scientific Service, Inc., Redwood City, California, February 1975.

12. McDowell, E.L., K.E. McKee, and E. Sevin., "Arching Action Theory of Masonry Walls", ASCE Journal of the Structural Division, Proceedings Paper 915, March 1958.

References (cont.)

13. McKee, K.E., and E. Sevin, "Design of Masonry Walls for Blast Loading", <u>ASCE Transactions</u>, Paper No. 2988, Volume 124, 1959.

14. Gabrielsen, B.L., K. Kaplan, and C. Wilton, "A Study of Arching in Non Reinforced Masonry Walls", Final Report 748-1 for the Veterans Administration, prepared by Scientific Service, Inc., Redwood City, California, March 1975.

15. <u>Building Code Requirements for Reinforced Concrete</u>, ACI 318-71, American Concrete Institute.

16. Wilton, C., and B.L. Gabrielsen, "Shock Tunnel Tests of Wall Panels", URS 7030-7, Technical Report, URS Research Company, San Mateo, California, January 1972.

17. Wilton, C., B.L. Gabrielsen, and P. Morris, "Structural Response and Loading of Wall Panels", URS 709-11, Final Report, URS Research Company, San Mateo, California, July 1971.

THE SHOCK TUNNEL:
HISTORY AND RESULTS
Volume IV
STATIC TEST PROGRAM

ABSTRACT

This is Volume 4 of a five volume report which summarizes the results of a program conducted by the Defense Civil Preparedness Agency to determine blast resistance of wall panels typically found in existing structures. Such information was needed to determine the blast sheltering capability of structures in the National Fallout Shelter Survey inventory and to develop means for upgrading these structures.

This volume describes the static test program conducted to determine the physical properties of the wall panels and to assist in the development of failure theories and test predictions for wall panels.

Volume 1 of this report describes the shock tunnel facility used for the experimental testing of full-scale wall panels. Included is a summary of the capabilities of the shock tunnel for dynamic loading and response studies and brief summaries of various experimental programs conducted in the shock tunnel which were not related to the wall panel test program.

Volume 2 presents the results obtained from the experimental program conducted in the shock tunnel to determine the loadings which are received by wall panels mounted in the test section.

Volume 3 is concerned with the dynamic response and failure of full-scale wall panels. Included are the development of theories of wall panel response and the results obtained from the testing of full-scale wall panels in the shock tunnel.

Volume 5 summarizes the predicted failure pressures for wall panels based on the theoretical and experimental results covered in Volume 3 and the static test data in Volume 4.

Table of Contents

List of Figures

iii

List of Tables

Section 1
INTRODUCTION

An extensive series of static tests was conducted in conjunction with the wall panel test program. The objectives of these tests were:

o to determine the physical properties of the components and composites used in the construction of the wall panels including their statistical distribution.

o to aid in controlling the quality of the full-scale test panel fabrication.

As with the wall panel program the static test program concentrated on non-reinforced masonry and in particular on brick and mortar assemblages. At the time of construction of each full-scale panel, brick and mortar samples were taken and beams, columns, tensile bond test specimens, and shear bond test specimens were constructed. These specimens were stored along with the panels through the 28-day curing time, and were then tested at about the same time as the panels. The types of tests performed are listed below, subdivided into three categories. The first group of tests on individual components was primarily conducted for quality control purposes and the second, on assemblages, for obtaining estimates of values of the physical properties of wall panels. The third series covers tests conducted to study arching and spalling phenomena.

Component quality control tests

Cylinder mortar tests (compression and splitting)
Brick flexural tests (flatwise and edgewise)
Brick and concrete block compressive tests

Test of physical properties of wall panels

Brick and mortar and concrete block and mortar beam tests
Brick and mortar tests (compression)

1-1

Brick and mortar couplet tests (tensile bond)

Brick and mortar tests (shear bond)

Special static tests

Line load tests

Spalling load tests

All tests were performed per ASTM standards where applicable. A brief description of each test type and its purpose are given in Section 2 of this volume, and the results obtained from the tests in Section 3, which also includes a discussion of the statistical method used to correlate the data.

Static test data obtained from other sources which are suitable for comparison with the results of the current program are presented and discussed in Section 4.

A possible approach to the development of a generalized theory of the response of brittle materials is given in Section 5.

Section 2
DESCRIPTION OF STATIC TESTS

In the following material the nature and purpose of each type of static test is summarized. More complete descriptions are given in Refs. 1 and 2.

COMPONENT QUALITY CONTROL TESTS

Cylinder Mortar Tests (Compression and Splitting)

Mortar cylinders, 2 inches in diameter and 4 inches long, were tested in compression and tension as shown below. These tests are standard ASTM tests to determine mortar compressive and tensile strengths.

Tension   Compression

2-1
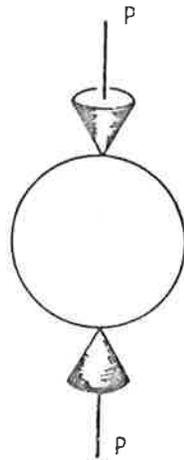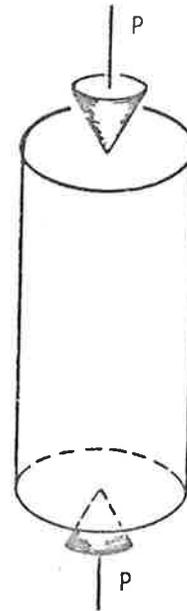
Brick Flexural Tests

In these tests individual bricks were tested in flexure in both the flatwise and edgewise orientations as shown below. This is a standard ASTM test for flexural strength.

Flatwise   Edgewise
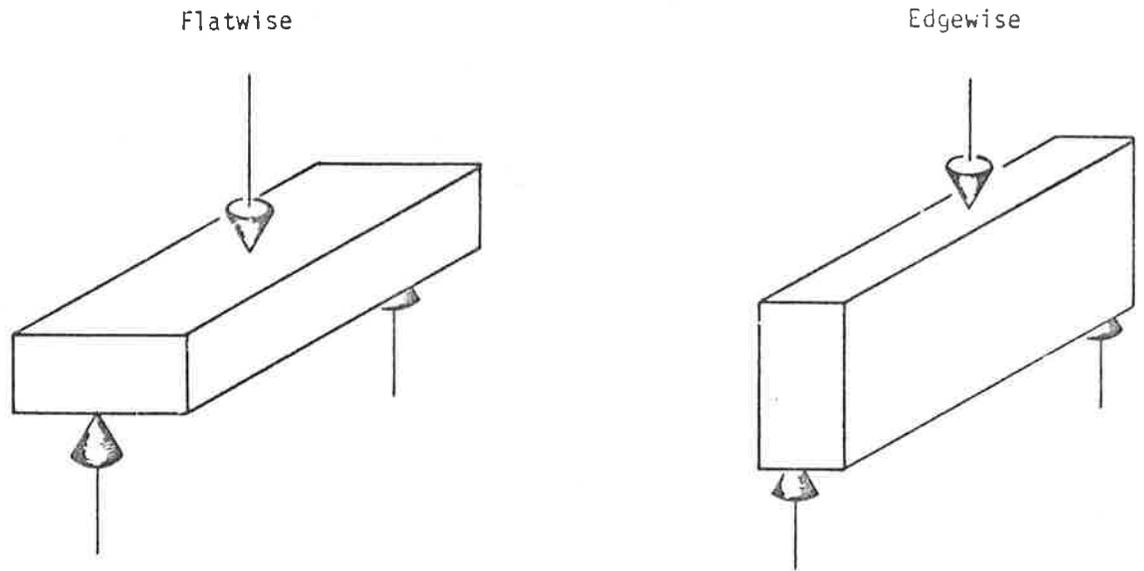
Brick and Concrete Block Tests for Compressive Strength

In this test, 1 x 1 in. squares cut from brick (flatwise) were tested in compression as shown below. The concrete blocks were tested whole. This is a standard ASTM test for compressive strength.

2-2
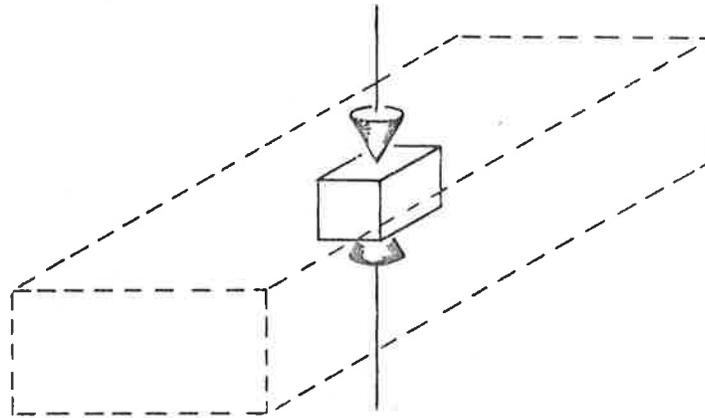
TESTS OF PHYSICAL PROPERTIES OF WALL PANELS

Brick and Mortar and Concrete Block and Mortar Beam Tests

The beams were tested for flexural strength using the arrangement shown below. The test beams for the brick were approximately 26½ in. long, 9 in. high, and 8½ in. wide and were loaded at the one-third points. The test beams for the concrete block were approximately 8 in. x 8 in. x 24 in.
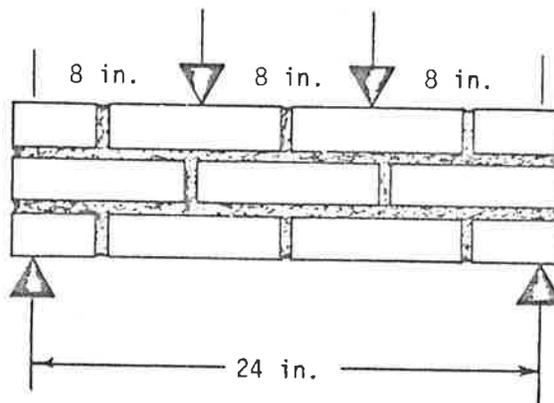
It should be noted that the type of failure obtained in the beam tests with bricks is similar to that of the full-scale wall panels tested in the tunnel except where arching phenomena predominate. Thus, the flexural strengths obtained could be used as a first approximation to predict the behavior of the full-scale brick panels.

Brick and Mortar Tests (Compression)

Brick-mortar assemblages were tested in compression as shown on the next page. This is a standard ASTM test to establish composite compressive strengths and moduli.
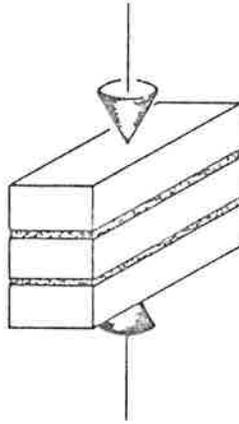
Brick and Mortar Couplets (Tensile Bond)

Brick and mortar couplets were tested in tension as shown below. This is a standard ASTM test to establish the tensile bond of the brick/mortar interface.
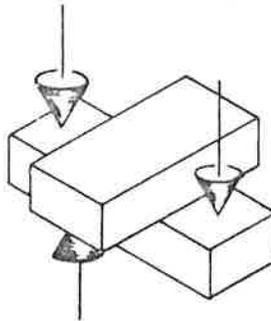
Brick and Mortar Tests (Shear Bond)

Brick-mortar assemblages were tested as shown below to provide a measure of the shear strength of the brick-mortar interface.
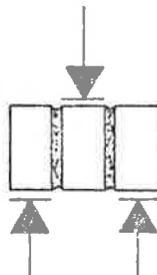
SPECIAL STATIC TESTS

During the course of the program several specialized static tests were developed to assist in understanding rigid and gapped arching phenomena.

Line Load Tests

Tests as illustrated below were used to establish the line load resistance capability of masonry assemblages in rigid arching.
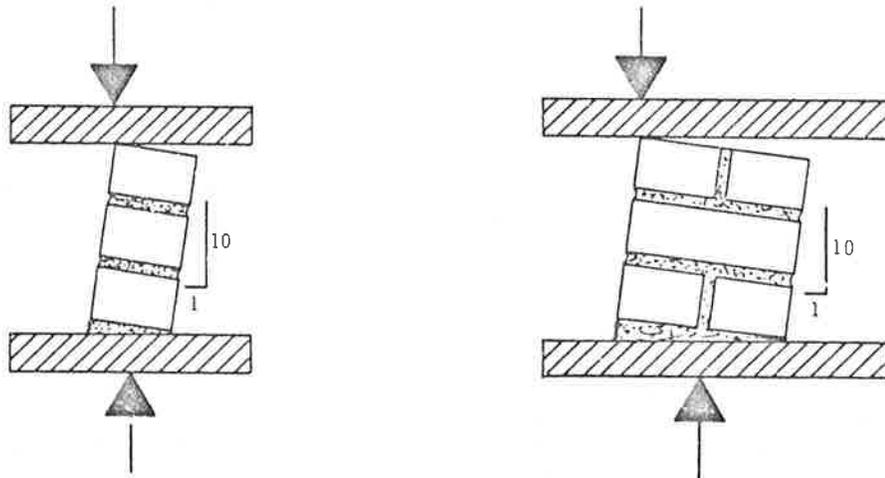
Spalling Load Tests

Load tests as shown below were used to establish masonry assemblages' resistance to spalling load induced during gapped arching.
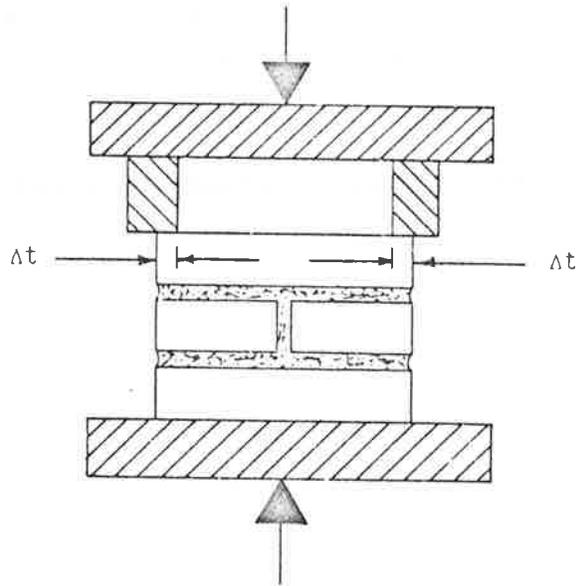
Brick and concrete block beams in rigid arching were tested as shown below to assist in developing arching theory.

Brick Beam
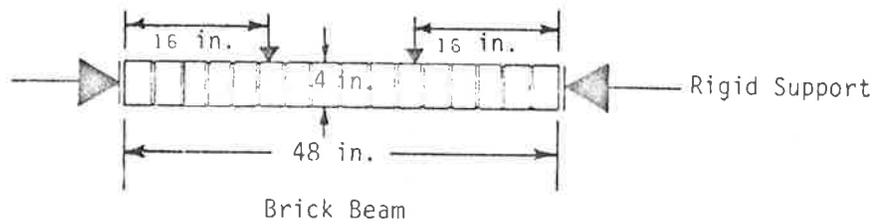
Section 3
STATIC TEST PROGRAM RESULTS*

METHOD OF DATA CORRELATION

To analyze the static test data it was necessary to use statistical techniques because of the inherently large scatter in material properties of brittle materials. An "extreme" type of probability distribution was selected for the data correlation. This procedure was justified by the fact that the experimental data from the static test program fit the extreme type of distribution fairly well and that, in general, the extreme type of performance is typical of brittle materials. Failure is often propagated by flaws and the distribution of flaws is often considered to be extreme (Refs. 3 and 4). The distribution of the "largest flaws" is of interest because it determines the distribution of "smallest strengths", i.e., failure.

A typical sample of test data plotted on extreme probability paper is given in Fig. 3-1 for the flexural strength of brick and mortar beams. The rather nice correlation of data is evident. Shown on the figure are:

the mean value $\bar{x}$ = 176
the modal value μ = 196
the measure of dispersion $1/\alpha$ = 35

obtained from the best fit line through the data. It can be seen that the modal value and the mean value are not the same as they would be for a normal distribution. This is due to the skewed nature of the extreme distribution. It also may be noted that the use of a measure of dispersion (such as one or two standard deviations) measured symmetrically about the mode is less useful than it is with a normal distribution, since it does not include the same probability area on either side.

---

* A detailed listing of all data obtained from the static test program is given in Refs. 1 and 2 and only summary plots and tables are presented here to illustrate significant points.

EXTREME PROBABILITY PAPER

$\bar{x} = 175.9$

$\mu = 196.3$

$1/\alpha = 35.5$

$n = 23$
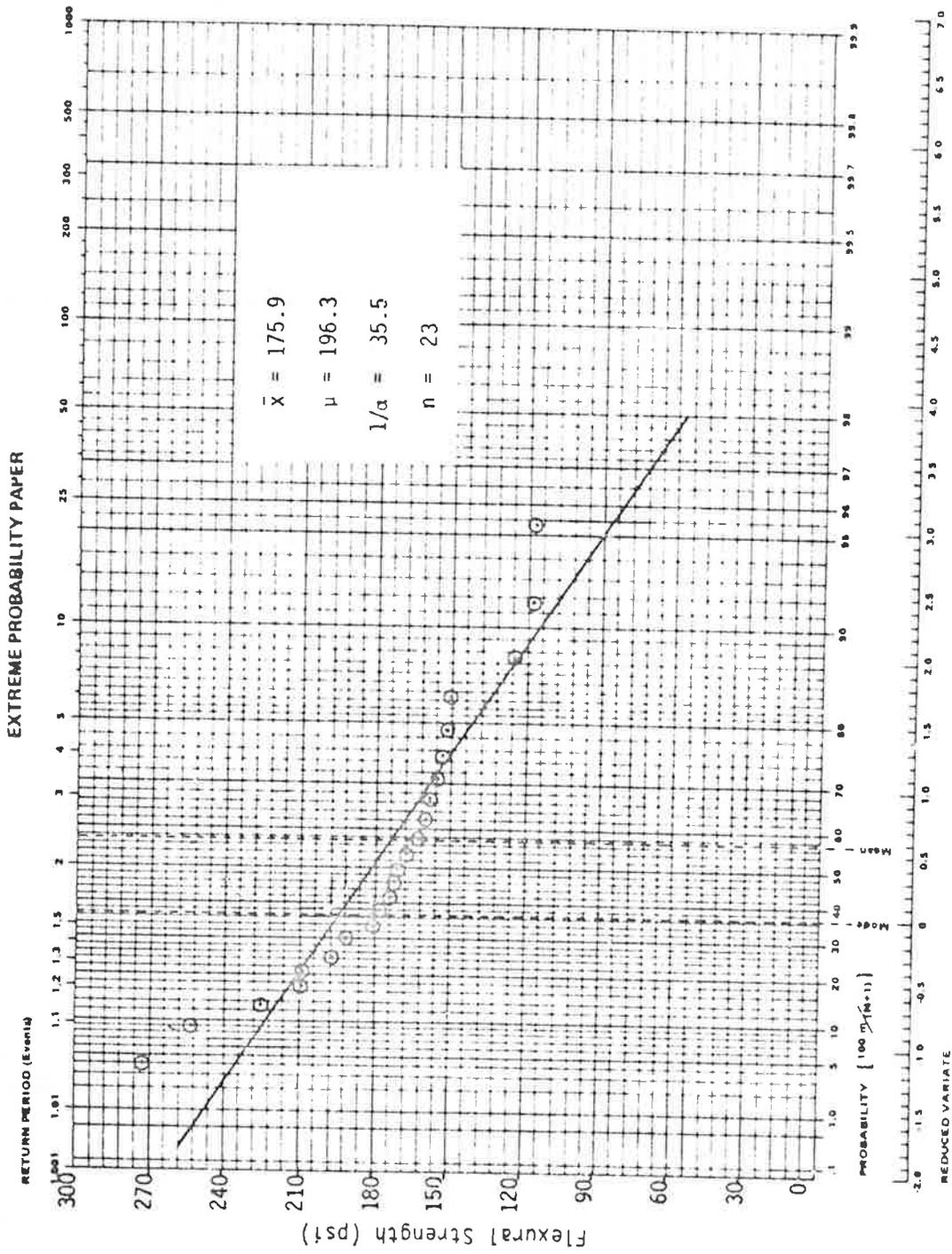
Fig. 3-1 Flexural Strength of Brick and Mortar Beams.

For the purpose of simplifying the presentation of the statistical scatter, a measure of the dispersion from minus one reduced variate to plus two reduced variates about the mode was selected. This included a range from 71 to 88% of the data, is generally symmetric about the mean, and -- for brick beams -- extends over a range of ± 30% about the mean.

Thus, referring to Fig. 3-1 one can say that the flexural strength is 176 ± 53 psi, keeping in mind that approximately 80% of the data lie within these bounds.

RESULTS

Plots of the data on extreme probability paper for the test conditions listed below are given in Figs. 3-1 through 3-6. The spalling load data for brick and mortar specimens are given in Table 3-1, the flexural strength data for composite concrete block-brick beams in Table 3-2, and the compressive strength of 8-in. x 8-in. (nominal) brick and mortar assemblages in Table 3-3, since there was insufficient data for their plotting.

o   Fig. 3-1 - Flexural Strength of Brick and Mortar Beams

o   Fig. 3-2 - Flexural Strength of Concrete Block and Mortar Beams

o   Fig. 3-3 - Line Load Strength of 8-in. x 4-in. x 8-in. (nominal) Brick and Mortar Assemblages*

o   Fig. 3-4 - Line Load Strength of 8-in. x 8-in. x 8-in. (nominal) Brick and Mortar Assemblages*

o   Fig. 3-5 - Brick and Mortar Tensile Bond Strength

o   Fig. 3-6 - Compressive Strength of 8-in. x 4-in. x 8-in. (nominal) Brick and Mortar Assemblages*

o   Table 3-1 - Spalling Load Data of Brick and Mortar Specimens

o   Table 3-2 - Flexural Strength Data of Composite Concrete Block-Brick Beams

o   Table 3-3 - Compressive Strength of 8-in. x 8-in. x 8-in. (nominal) Brick and Mortar Assemblages.*

---

*   The nominal dimensions of the brick and mortar assemblages used in the line load and compressive strength tests refer, in sequence, to: the height of the sample (i.e., the distance between sample faces in the direction of loading -- 8-in. samples are three bricks high); the sample width (in line loading, the length of the sample edge that is not loaded -- a 4-in. sample is one brick wide); and the sample length (in line loading, the length of the sample edge along which load is applied -- an 8-in. sample is one brick long). See sketches in Section 2.
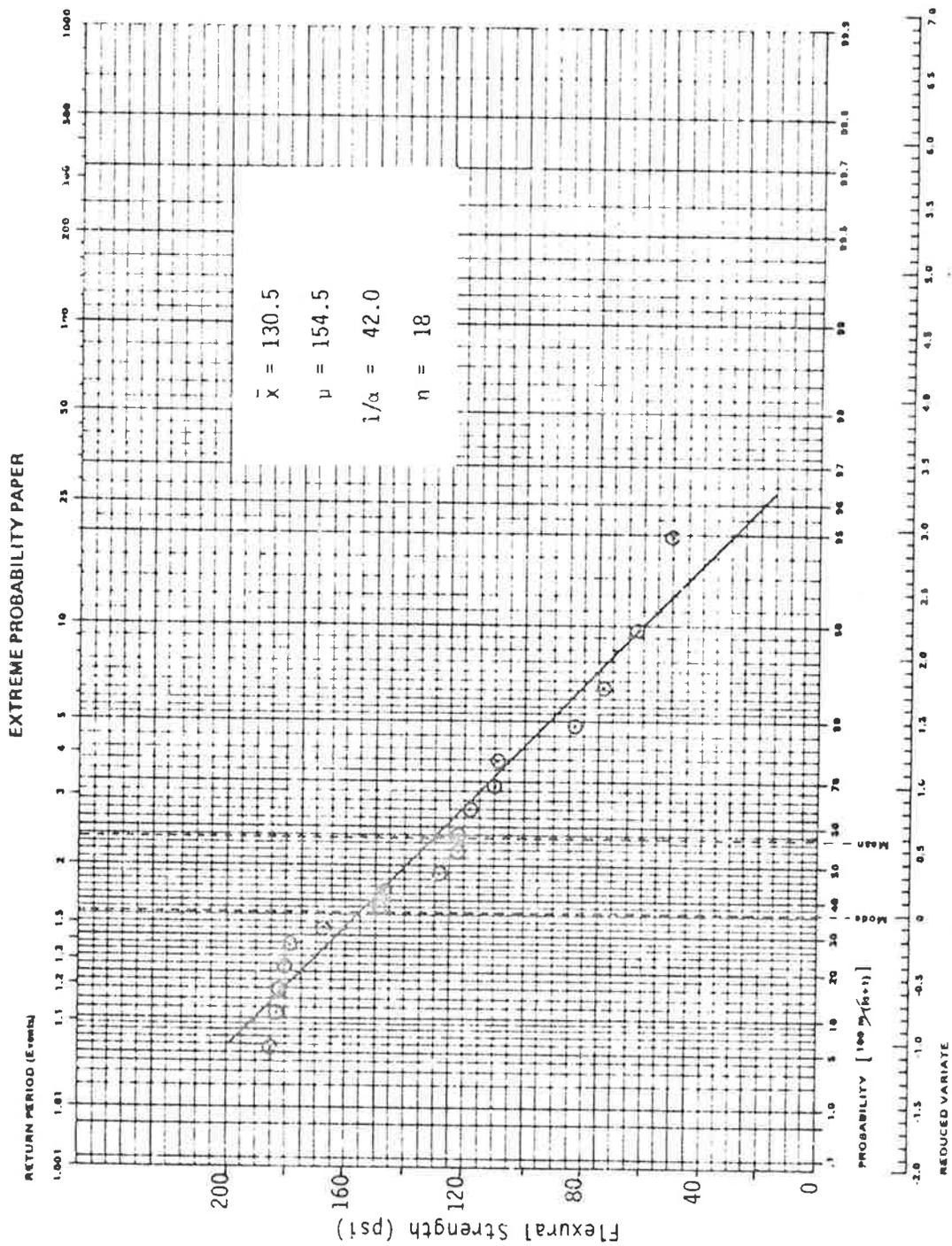
Fig. 3-2. Flexural Strength of Concrete Block and Mortar Beams.
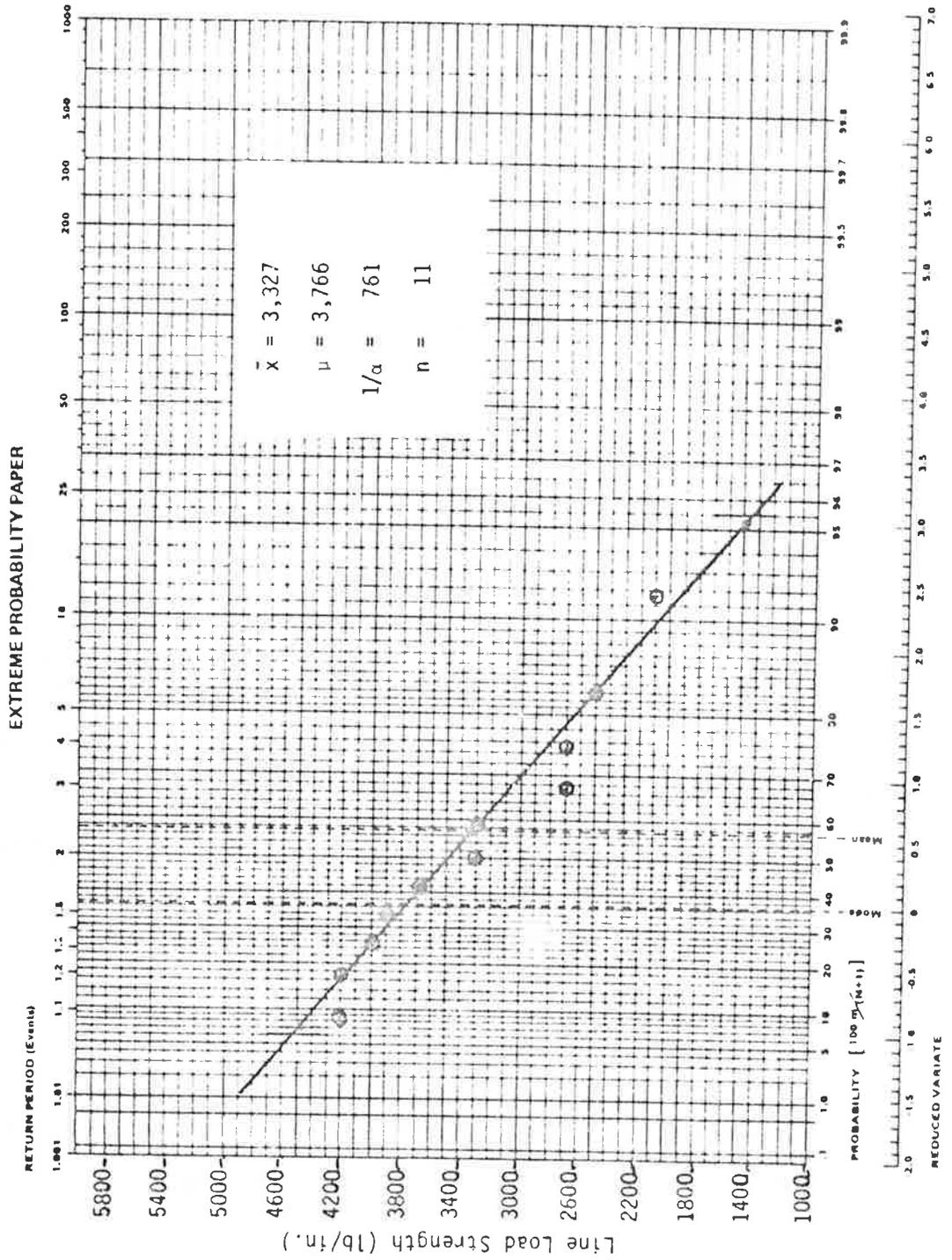
3-5

Fig. 3-3. Line Load Strength of 8-in. x 4-in. x 8-in. (nominal) Brick and Mortar Assemblages.

3-6

Fig. 3-4. Line Load Strength of 8-in. x 8-in. x 8-in. (nominal) Brick and Mortar Assemblages.

3-7

Fig. 3-5. Brick and Mortar Tensile Bond Strength.

3-8

EXTREME PROBABILITY PAPER

$\bar{x}$ = 2,387
μ = 2,676
$1/\alpha$ = 501
n = 15
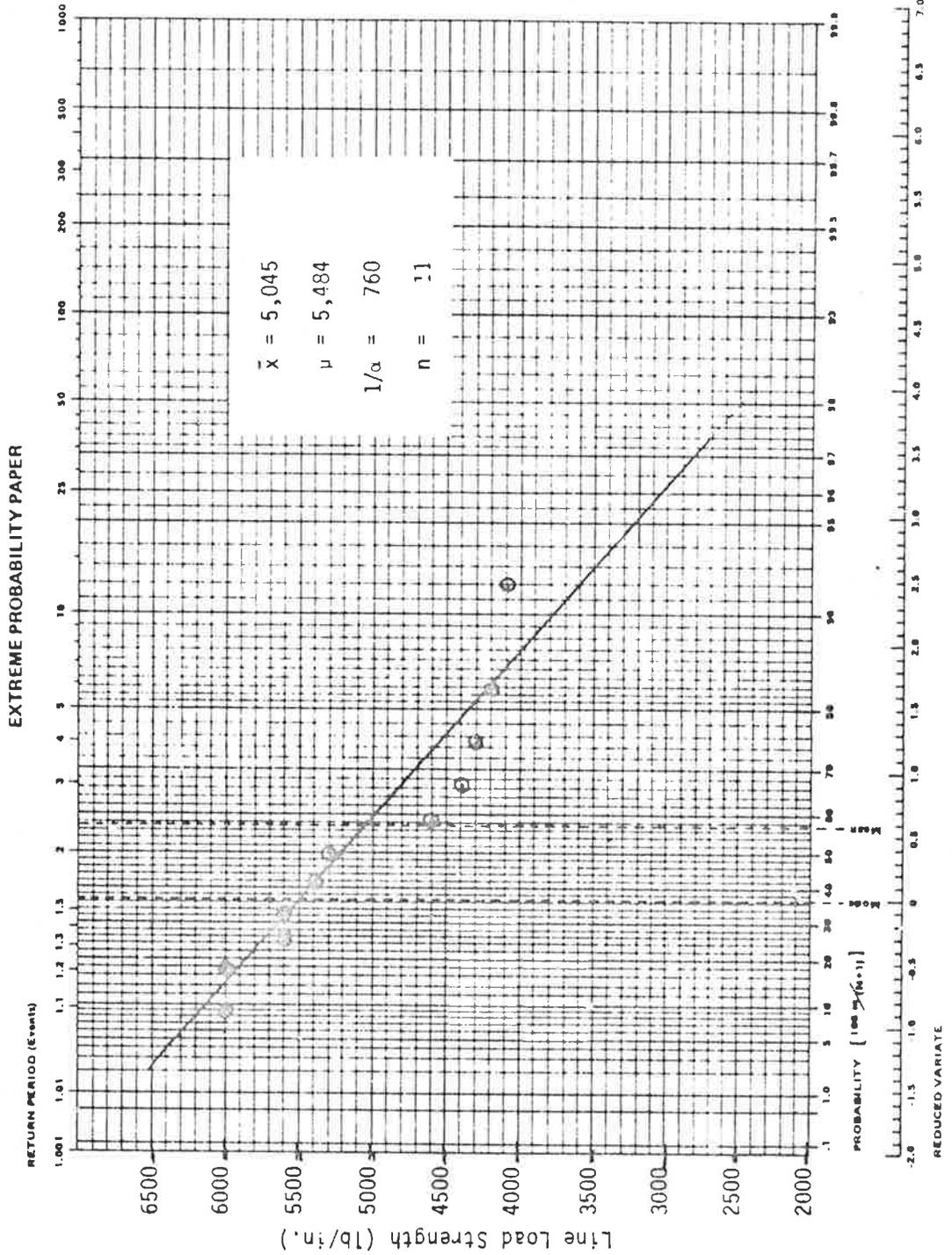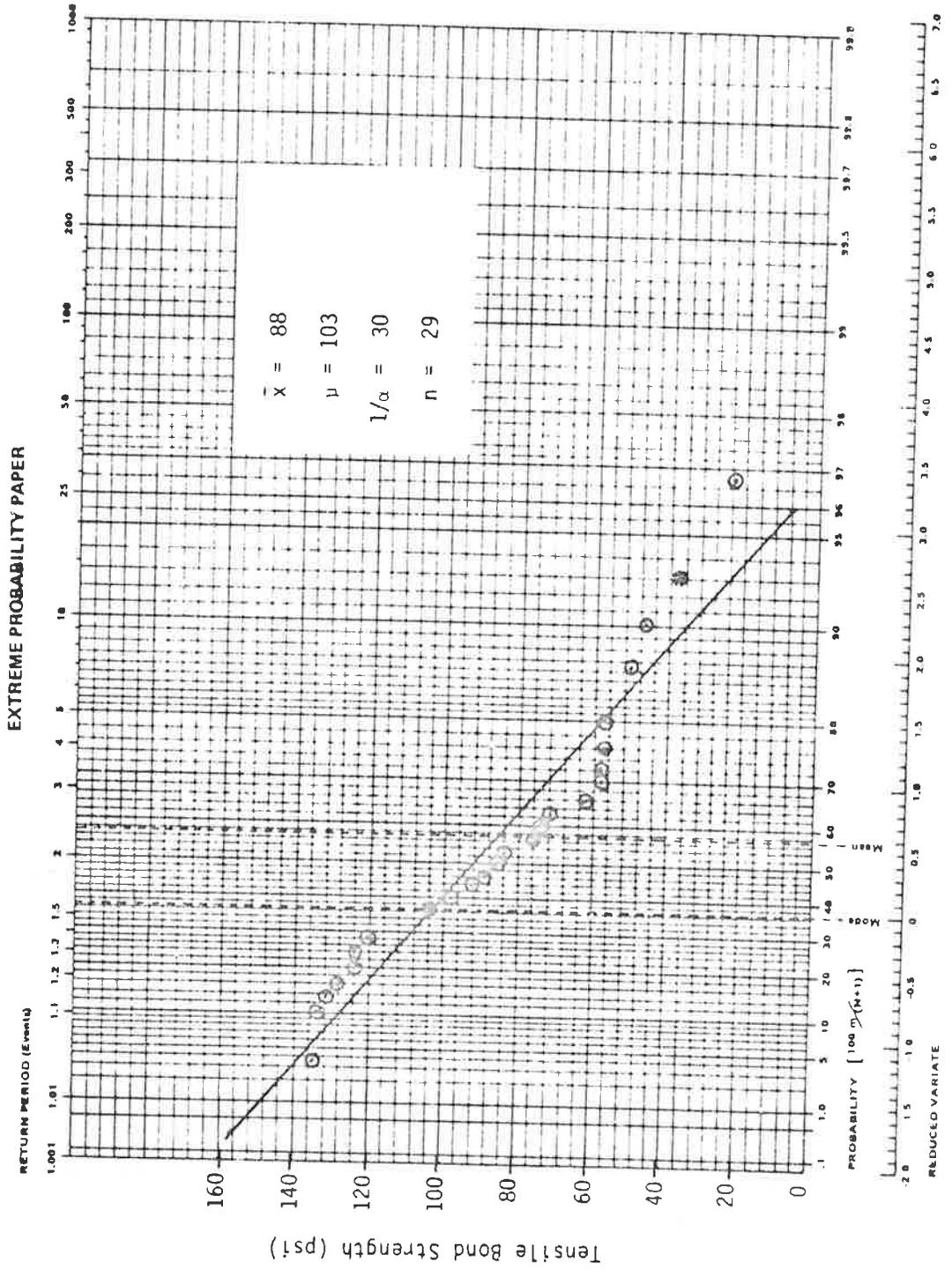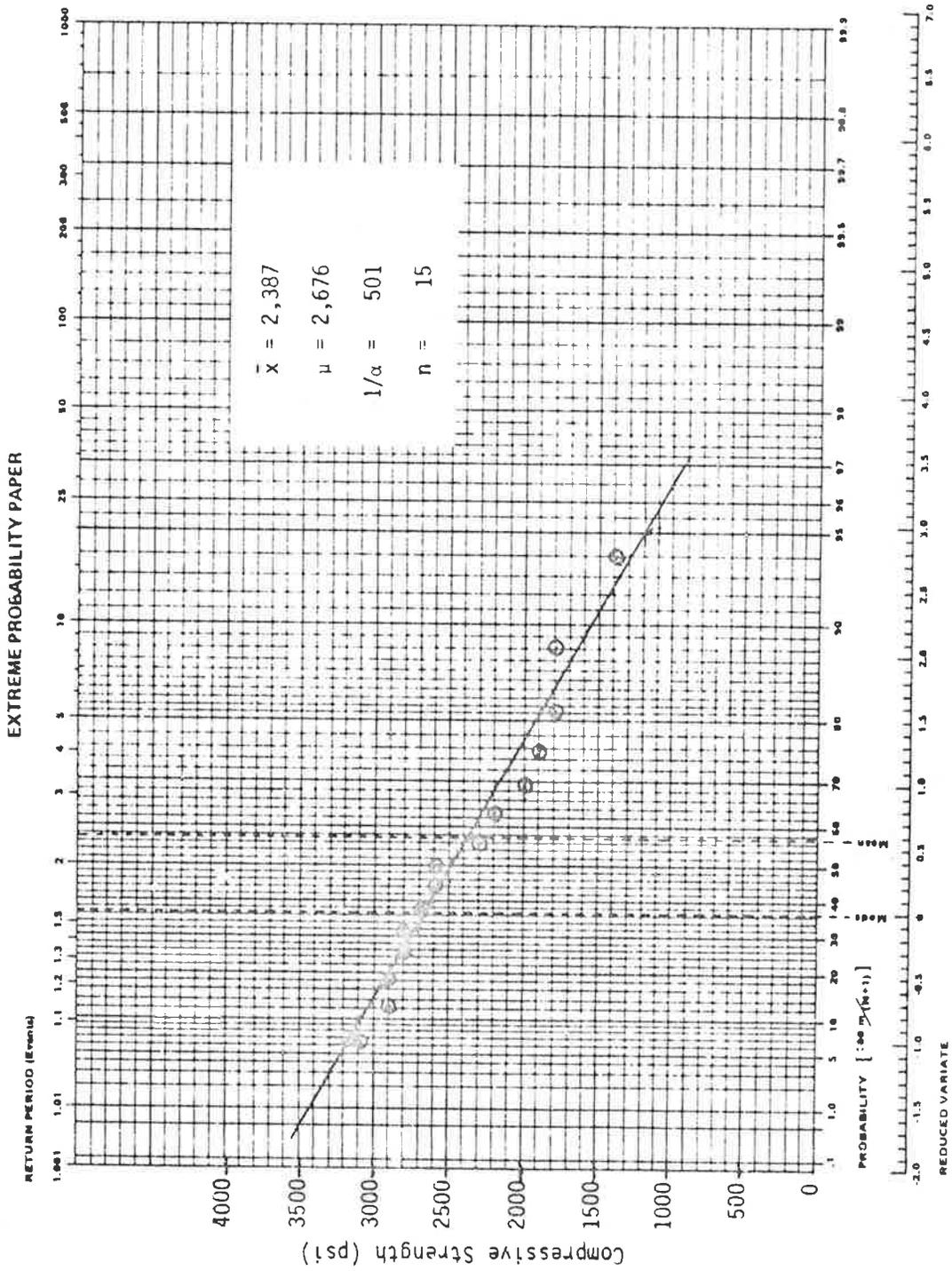
Fig. 3-6. Compressive Strength of 8-in. x 4-in. x 8-in. (nominal) Brick and Mortar Assemblages.

Table 3-1

Test Data for "Spalling" Loads on Brick-Mortar Specimens

Δt (in)	P (lb)	$f_{\ell s}$[1] (lb/in)
1/4	10,900	680
	13,465	840
	13,990	875
	15,200	950
1/2	13,980	875
	33,000	2,070
	34,000	2,160
	19,000	1,191

[1] $f_{\ell s}$ = P divided by total length of loaded edges (8 in. + 8 in.).

3-10
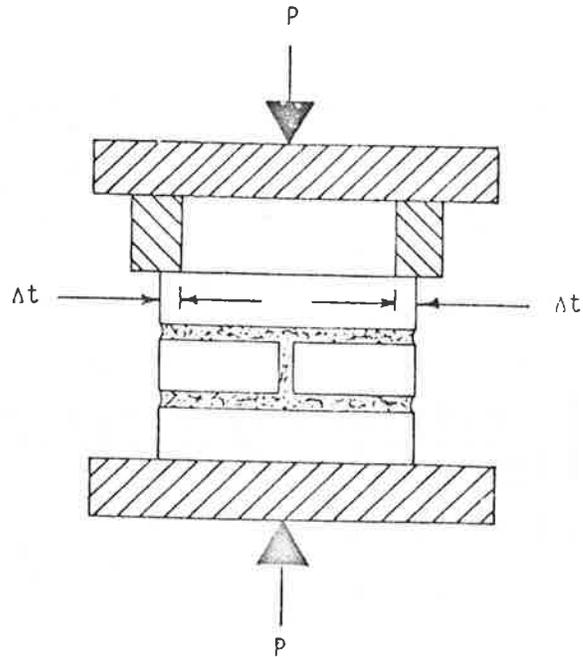
Table 3-2

Results of Tests on Brick-Concrete Block Beams

Test Number	Force, P (lb)
1	9388
2	7731
3	7180
Average:	8100 ... average σ_r = 197 psi
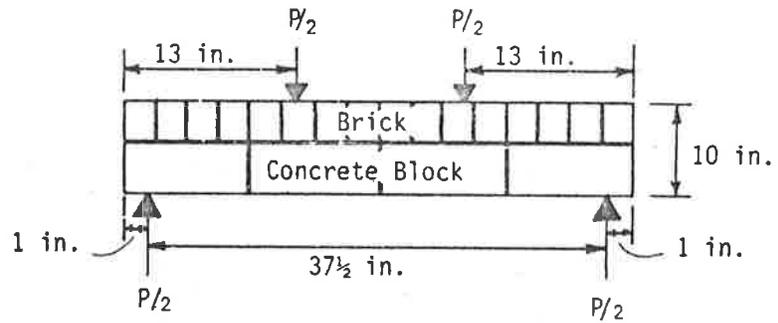
Table 3-3

Compressive Strength of 8-in. x 8-in. x 8-in.

Brick and Mortar Assemblages

Sample Number	Compressive Strength fc' (psi)
1	1900
2	2700
3	2600
4	2300
Average:	2375
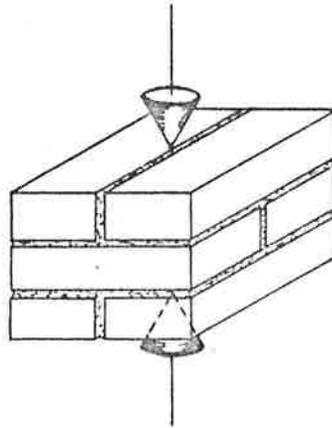
The flexural strength data given in Figs. 3-1 and 3-2 have been included since these data were used with the theoretical calculations to provide first approximations for the failure pressures of simple beam and plate walls (see Volumes 3 and 5). Similarly, the compressive strength for line loads in Figs. 3-3 and 3-4 and the spalling load data in Table 3-1 were used for predictions of failure pressures for arched beams. The remainder of the figures are used in the next section in comparisons with data from other sources.

As noted previously, one of the purposes of the static tests was for quality control. Tests on individual components were made to insure that there were no significant differences in the quality of the materials used in constructing various batches of full-scale wall panels. Statistical analysis of the tests showed that all batches of brick were statistically similar, as were all batches of concrete block, and of mortar.

Section 4
DATA FROM OTHER SOURCES AND COMPARISONS
WITH STATIC PROGRAM RESULTS

In this section, data from other sources are presented and, when possible, compared with static test program data. These comparisons illustrate the degree of similarity of the data from various sources, not only in magnitude but in the degree of scatter.* For this purpose the test data concerning the material properties which are most important in the failure mechanisms were selected.

As is evident from Volume 3 and Volume 5, the flexural strength is the most important property for the failure of beam and plate-mounted walls without arching. Unfortunately, no data exactly comparable to the small test beam data used in this program could be found from other sources. Comparisons with flexural strength data from large walls and very small specimens are given in Fig. 4-1.

However, the flexural strength is related to the brick-mortar tensile strength which was measured in this program by the couplet tests. Such data are available from other sources, and are shown in Fig. 4-2.

For arching walls the line load compression and spalling tests were considered to provide the closest approximation for the wall failure mechanism. For the non-vertical (line load) case no other data are available. There are data available, however, for the vertical load case (standard compression tests) and since there appears to be a direct relation between the non-vertical and vertical results, a comparison between the vertical load data is given in Fig. 4-3.

---

* Note that in the discussions of data scatter all percentages given were calculated as shown on pg. 3-3.

4-1

Finally, Fig. 4-4 shows data from tests on full-scale (story-height) concrete block walls.

COMPARISON OF FLEXURAL STRENGTHS OF BRICK BEAMS

The comparisons of flexural strengths given in Fig. 4-1 show that

o the static test program mean flexural strength is 80% higher
   than Monk's data and 180% higher than Pearson's. It should
   be noted that the comparison with Monk's data is considered
   more significant than that with Pearson's, since Monk's data
   are from 4-ft. x 8-in. x 8-ft. walls while Pearson's are from
   very small specimens. Also note that both of the above were
   based on laboratory construction while the static test program
   data were based on field construction. Monk indicates that
   real, in-place walls appear to have flexural strengths about
   25% higher than his laboratory walls. The static test program
   mean flexural strength would be only 45% higher than that for
   such walls.

o static test program data scatter is ± 30% while that of Pearson's
   data is ± 46% and Monk's, ± 15%. However, Monk indicates that
   real, in-place walls exhibit a scatter 45% greater than for his
   laboratory walls which would lead to a value of ± 21%. It is
   concluded from the above that it is reasonable to apply the
   ± 30% data scatter based on the static test program to full scale
   brick wall panels as is done in Volumes 3 and 5.

o because of the larger data scatter the static test program
   flexural strengths and those from Monk's data tend to converge
   at the high probability (or low flexural strength) end of the
   distribution.

EXTREME PROBABILITY PAPER

RETURN PERIOD (Events)

Flexural Strength (psi)

PROBABILITY $[100 \cdot \frac{m}{(N+1)}]$

REDUCED VARIATE

Fig. 3-1

$\bar{x} = 175.9$
$\mu = 196.3$
$1/\alpha = 35.5$
$n = 23$

Monk (Ref. 5)

$\bar{x} = 96.2$
$\mu = 101$
$1/\alpha = 9.4$
$n = 33$

Pearson (Ref. 6)

$\bar{x} = 62.3$
$\mu = 73.3$
$1/\alpha = 19.2$
$n = 1167$

Fig. 3-1

Monk

Pearson
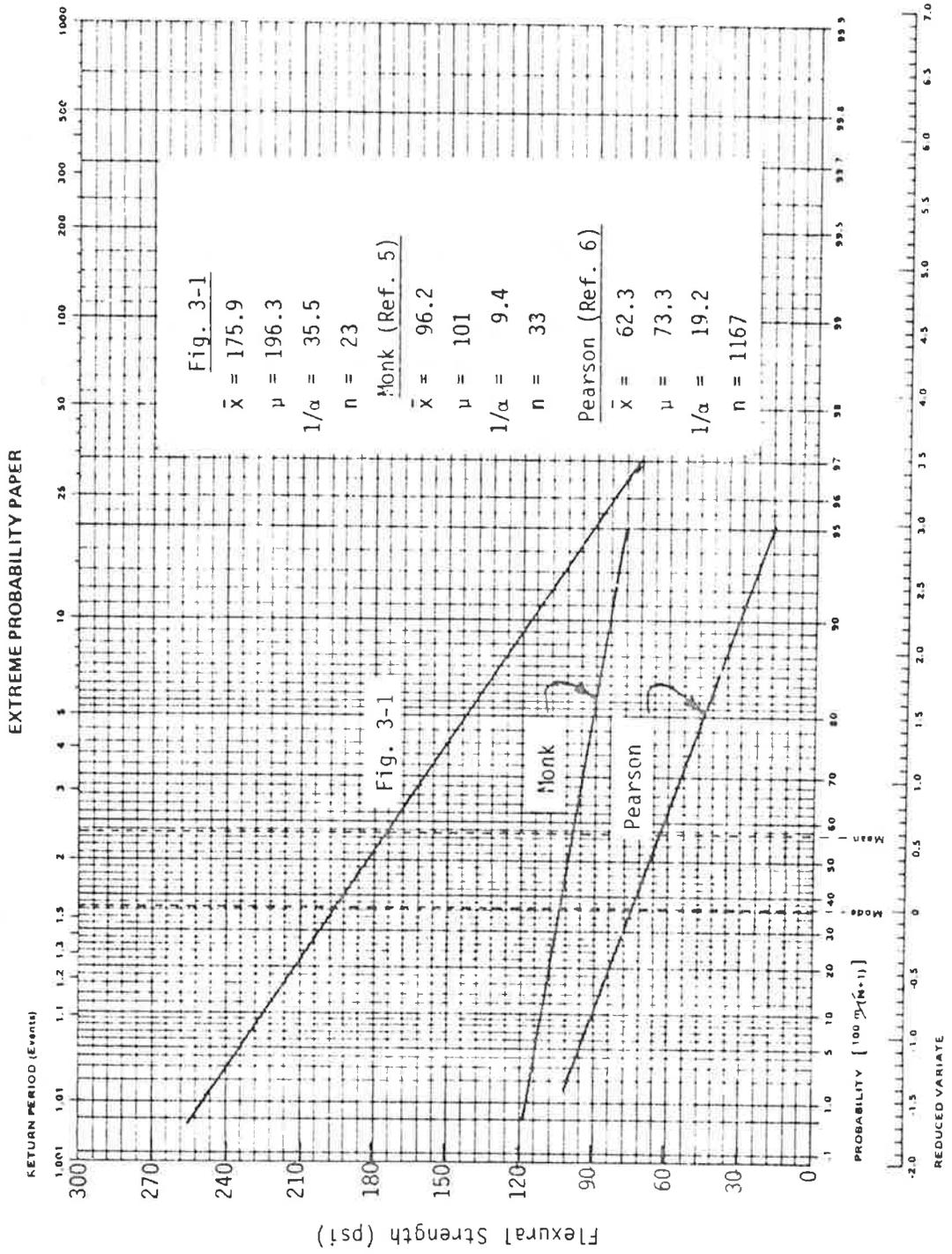
Fig. 4-1. Flexural Strengths of Brick and Mortar Beams from Three Sources.

4-4

COMPARISON OF BRICK-MORTAR TENSILE BOND STRENGTH

The comparisons of tensile strengths given in Fig. 4-2 show that

o the static test program mean tensile bond strength is from
35% to 85% higher than that from the other data.

o the static test program data scatter (on a percentage basis)
is ± 51% while that for Pearson's data is ± 21% and that for
Fishburn's is ± 37%. Note, however, that the static test
program used field construction while the other sources used
laboratory construction.

o because of the larger data scatter, the static test program
tensile strengths at the higher probability end of the distri-
bution tend to match the other data.
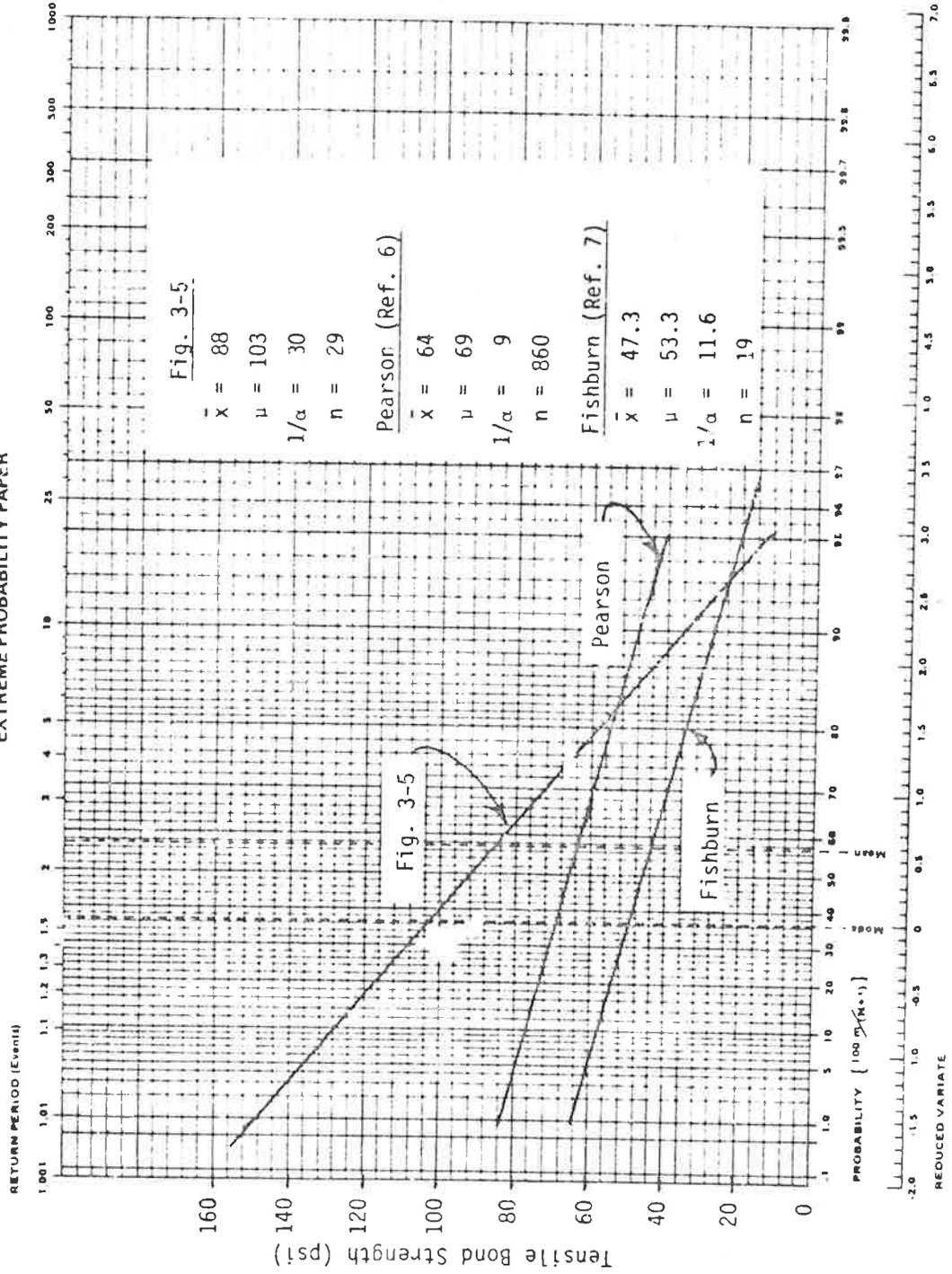
Fig. 4-2. Brick and Mortar Tensile Bond Strengths from Three Sources.

4-6

COMPARISON OF COMPRESSIVE STRENGTHS OF BRICK ASSEMBLAGES

The comparison of compressive strengths given in Fig. 4-3 shows that

o static test program mean compressive strengths are about 20%
   lower than mean strengths from other data. Note, however,
   that the static test program data are from 15 samples three
   bricks high, and only one brick wide, while the other data are
   from 27 samples also three bricks high, but two bricks wide
   (essentially cubes).

o static test program data scatter is ± 31% while that for the
   other sources is ± 13%.

EXTREME PROBABILITY PAPER

Fig. 3-6

$\bar{x}$ = 2,387

μ = 2,676

$1/\alpha$ = 501

n = 15

Astbury & West (Ref. 8)

$\bar{x}$ = 2,974

μ = 3,111

$1/\alpha$ = 256

n = 27

Astbury and West

Fig. 3-6

RETURN PERIOD (Events)

Compressive Strength (psi)

PROBABILITY [100 $\frac{m}{(N+1)}$]

REDUCED VARIATE
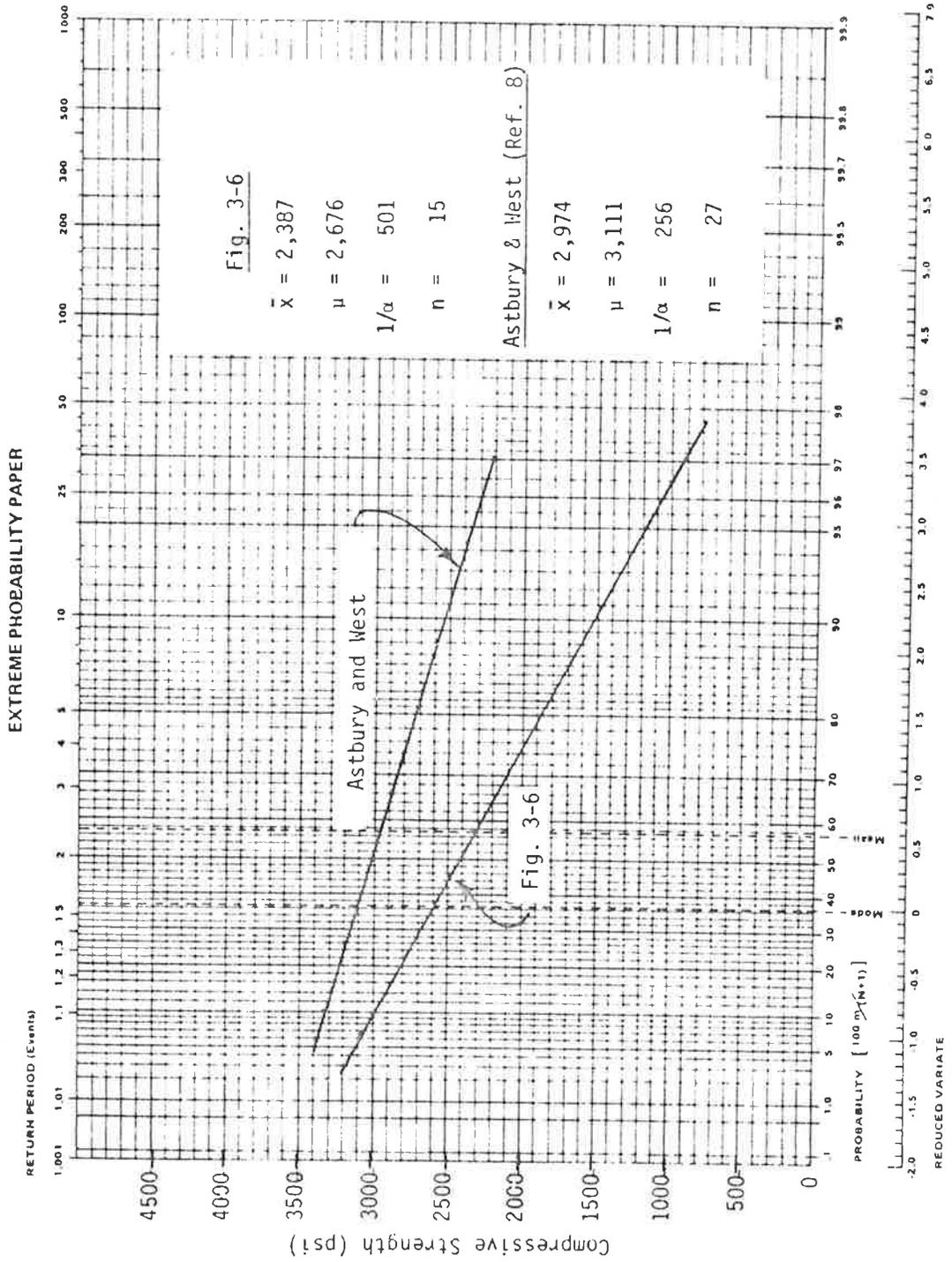
Fig. 4-3. Compressive Strengths of Brick and Mortar Assemblages from Two Sources.

FLEXURAL STRENGTHS OF STORY-HEIGHT CONCRETE BLOCK WALLS

The static test program did not include tests on concrete block beams large enough to be considered representative of full size (story-height) walls. Thus, the results given in Fig. 3-2 from the static test program beams (each of which consisted of only three blocks) are not comparable to results from longer beams or story-height walls.

A number of test programs on story-height concrete block walls have been conducted by other investigators and the results of four groups of such walls are shown in Fig. 4-4. The curves labelled NBS-1 and NBS-2 were derived from Ref. 7 on 27 tests of standard running bond walls (see Fig. 4-5). The 14 NBS-1 walls employed mortars containing about one part of cementing materials to three parts of sand, the cementing materials themselves containing about 50% portland cement or portland cement clinker. The 13 NBS-2 walls employed richer mortars, the ratio of cementing materials to sand being about 1:2.7, with the cementing materials containing about 70% portland cement or portland cement clinker.

The curves labelled PCA-1 and PCA-2 were derived from data in Ref. 9 on 22 sets of walls with the nine different concrete block patterns shown in Fig. 4-5. The 11 PCA-1 walls employed mortars with a ratio of cementing materials to sand of about 1:2.3, the cementing materials containing about 33% portland cement. The 11 PCA-2 walls employed somewhat richer mortars (1:2.1 cementing materials to sand), with the cementing materials containing about 44% portland cement.

Clearly mean strengths increased with mortar richness, the mean strength of the PCA-2 walls being more than four times that of the NBS-1 walls. Data scatter, however, is not greatly different among the walls, with the PCA-1 wall showing the least scatter (± 40%), and the NBS-2 wall, the greatest scatter (± 60%) about the mean.

4-9

The curves labelled PCA-1 and PCA-2 strongly demonstrate the utility of statistical interpretation of static test data with an apparently large dispersion. Examination of the data, which contained flexural strengths ranging from a minimum of 24 psi to a maximum of 103 psi, showed a good correlation for each type of mortar, whatever the wall design,* as can be seen by the data points plotted on the figure.

The average scatter of the four curves on Fig. 4-4 is almost identical to the ± 50% obtained from Fig. 3-2 so that it is reasonable to use this value for full scale concrete block wall panels as is done in Volumes 3 and 5.

* The data from Ref. 9 were interpreted in Ref. 10 to show differences in strength among the different wall designs, but too few tests were run with each wall design (a maximum of four, with six of the wall types being tested only twice) to permit statistically valid interpretations to be made.

EXTREME PROBABILITY PAPER

Fishburn
(Ref. 7)

Hedstrom
(Ref. 9)

NBS-1
x̄ = 15.4
μ = 18.4
1/α = 5.1
n = 14

NBS-2
x̄ = 22.9
μ = 28.2
1/α = 9.1
n = 13

PCA-1
x̄ = 34.4
μ = 39.8
1/α = 9.3
n = 11

PCA-2
x̄ = 65.3
μ = 77.2
1/α = 20.6
n = 11

PCA-2

PCA-1

NBS-2

NBS-1

RETURN PERIOD (Events)

Flexural Strength (psi)

PROBABILITY [100 $\frac{m}{(N+1)}$]

REDUCED VARIATE
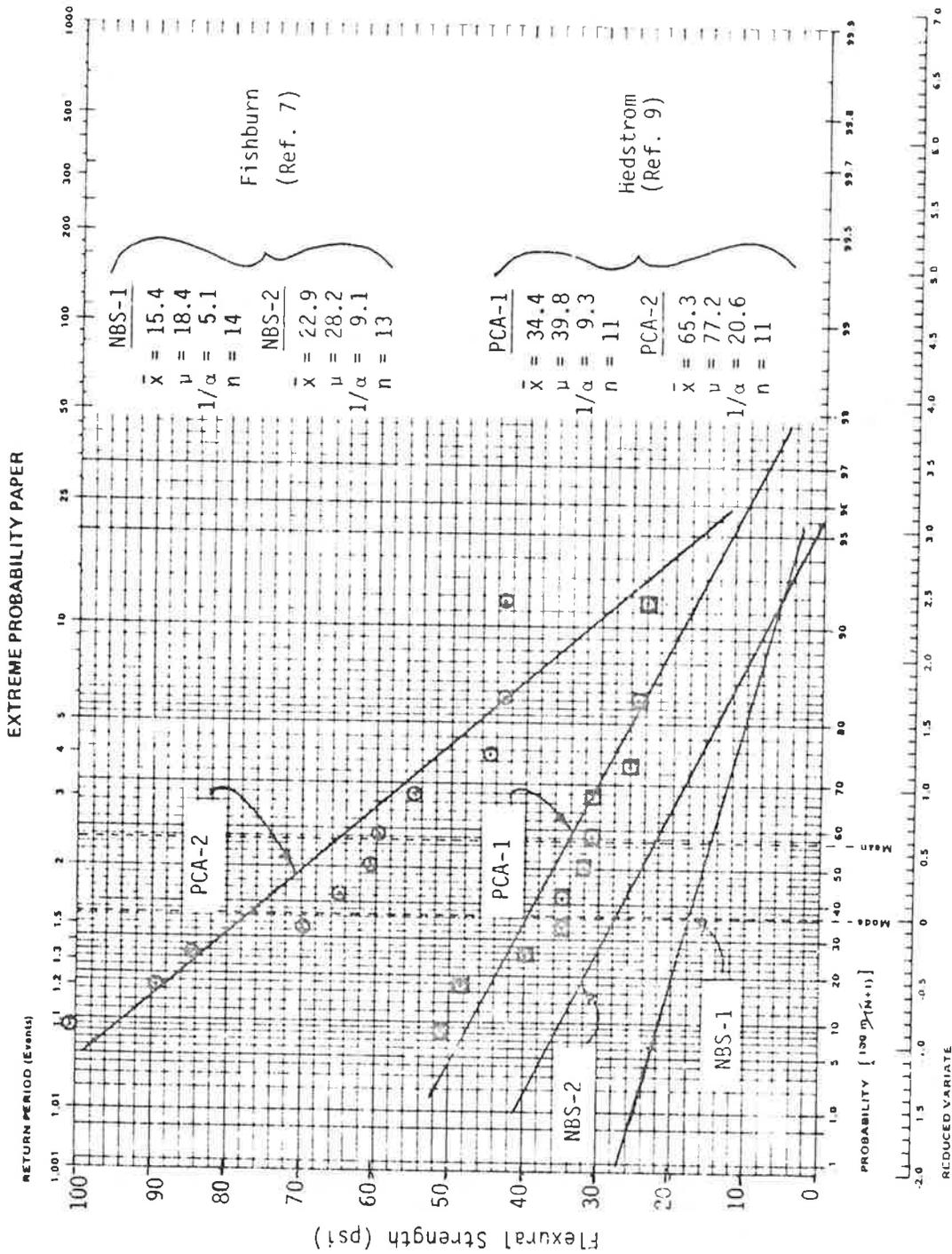
Fig. 4-4. Flexural Strength of Story-Height Walls.

4-11

Running Bond Horizontal Stack Vertical Stack

Diag. Basket Weave Diagonal Bond Basket Weave A

Running Bond
4-in. high units Coursed Ashlar Basket Weave B
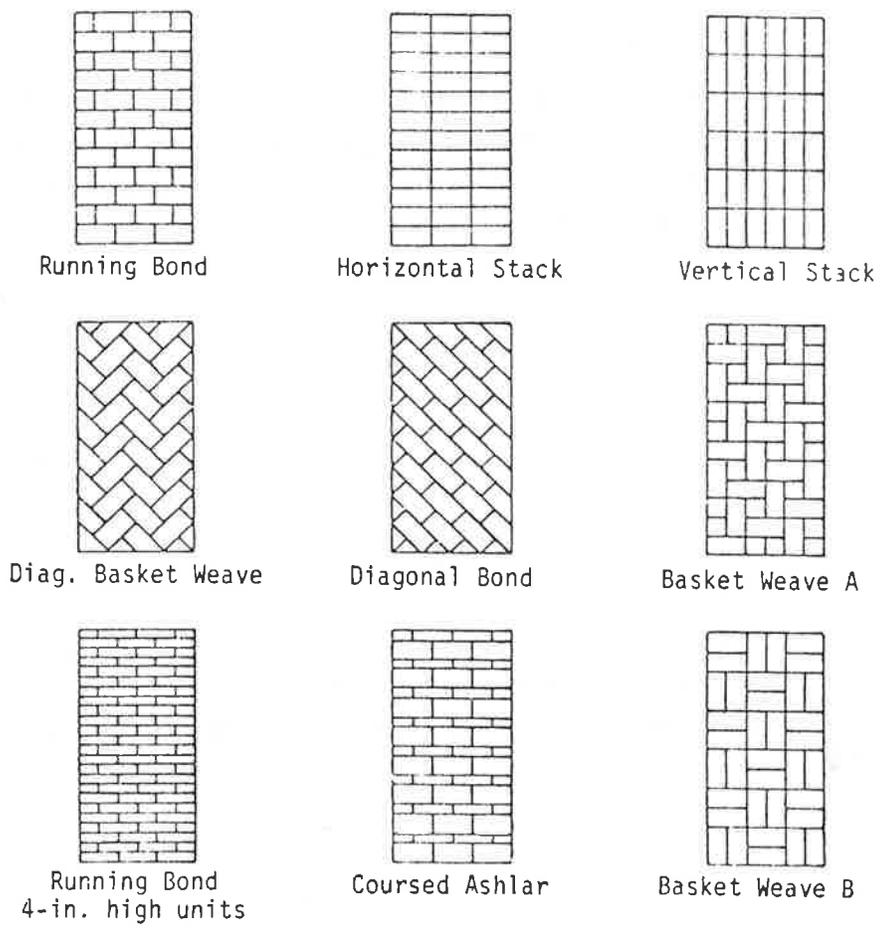
Fig. 4-5. Concrete Masonry Patterns for Structural Tests.

4-12

SUMMARY OF COMPARISONS

Probably the most useful conclusion to be drawn from these various comparisons is that the data scatter of the static test program has the same general type of distribution and is generally consistent with the values obtained from other sources. The importance of this lies in the fact that the inherent variabilitty in material properties of brittle materials is sufficiently great that any comprehensive method for predicting their response under blast loading must take this variability into account. At present there is no adequate brittle failure theory which can be used to predict this variability. Some effort in this program was devoted to such a theory (see Section 5) but it was not sufficiently developed to be used. Thus, the only source for such information is experimental tests. Ideally it would have been desirable to conduct sufficient full scale tests to derive the statistical variation. This, however, was clearly impractical, so it was necessary to resort to the small scale tests used in the static test program. There remains, however, some uncertainty in applying small scale results to full scale. The reasonable agreement in the degree of scatter shown in the foregoing comparisons between the static test program data and data from other sources, particularly those involving full scale walls, certainly helps to justify this approach.

Section 5
DEVELOPMENT OF GENERAL BRITTLE FAILURE THEORY

The analytical work done in regard to the structural response of wall panels is presented in Volume 3 of this report. In these analyses the material properties of the panels were considered to be deterministic and uniform throughout a given panel type. It was clearly recognized that this was only an approximation to the real world of brittle materials because their mechanical properties are in fact expected to be a function of a number of variables including the rate of loading and the specimen size. For this reason, a parallel theoretical analysis was carried out to try to determine the impact of this variability on the above mentioned structural response calculations.

This work consisted of four phases. The first was the development of a low level fatigue model which was intended to shed some light on the apparent strength increases of brittle material under dynamic loading. This model involved simulating the brittle material by a discrete element model. The second phase involved extending this methodology to a crack sensitive continuum. The third phase involved the development of a statistical failure theory for flaw sensitive materials, and the fourth phase consisted of the combination of the first three phases into a general brittle failure theory.

This work has been reported in detail in Ref. 11, so that only a summary of the scope of the effort and of the significant findings will be given here.

LOW LEVEL FATIGUE MODEL

In this development various simple discrete element systems were formulated and their response to dynamic loading investigated using classical dynamics. It was shown that for situations where one of the elements is weaker than the others, loading/strength conditions exist in which

o   the system will stand one application of a step wave dynamic load with failure only of the weaker element and survival of the others, under a situation which would fail no element of the system by purely static considerations.

o   the same system would fail entirely on the application of a second similar loading.

Thus, these simple concepts demonstrate the fatigue phenomenon in dynamic loading of brittle materials. It was also shown that a step wave very much larger than one that would just result in system failure could appear to cause an increase in system strength.

The analysis concluded with the postulation of the relation between the observed resistance of the systems to the static resistance, the maximum possible dynamic resistance, and the ratio of the magnitude of the step wave loading to the fracture force.

CRACK SENSITIVE CONTINUUM MODEL

In this development the concepts developed in the low level fatigue model were extended to the continuum case for the purpose of better defining the nature of the transition domain for dynamic response between the static resistance and an upper bound dynamic resistance. This was done by introducing a measure of crack sensitivity into the mathematical formula in terms of the ratio of the time to complete fracture to the time available to fracture. This formulation is given below:

$$R_o = R_s + (R_D - R_s) \left[1 - \alpha \exp (- \Lambda) \right] \tag{5-1}$$

where

R_o is the observed resistance

R_s is the static resistance, or the dynamic resistance to a step wave just capable of causing failure (the minimum dynamic resistance)

R_D is the apparent dynamic resistance to a step wave infinitely larger (in the limit) than that just capable of causing failure (the maximum dynamic resistance)

Λ $= \beta \left(\dfrac{F_1}{\bar{F}} - 1 \right) \left[\dfrac{L_c/V_c}{(T/2) - t_s} \right]$ for $F_1 > \bar{F}$

Λ $= 0$ for $F_1 \leq \bar{F}$

F_1 is the loading force (applied step load)

$\bar{F}$ is the fracture force (the minimum step load that can cause fracture)

L_c is the length of a crack

V_c is the crack propagation velocity:

$$V_c = \frac{1}{2} \sqrt{E/\rho}$$

E is the modulus of elasticity

ρ is the mass density

T is the period

t_s is the time to failure with $F_1 = F$

α & β are data based constants and assumed to be unity

Note that the term

$$\frac{L_c/V_c}{(T/2) - t_s}$$

consists of the time to completely fracture (L_c/V_c) divided by the time available for fracturing $\left[(T/2) - t_s\right]$. Hence, if $R_s/2 \leq F_1 \leq R_D/2$ and the term

$$\frac{L_c V_c}{(T/2) - t_s} \geq \frac{1}{2}$$

there is a possibility of partial fracture and not complete failure on the first half period of oscillation; however, with the step-like loading, failure will indeed occur on later oscillations and the R_o response computed by the formula is the upper bound value.

Further implications of the above formula are presented in the following material where the statistical loading concepts are included.

STATISTICAL FAILURE THEORY

This effort considers in some detail the problem of material strength variability. Brittle materials inherently have a great deal of scatter in material properties, as has been illustrated earlier in this volume. This random behavior does not preclude the use of these materials or the prediction of their performance, but it does make the problem more complicated. Statistical techniques represent one of the most promising approaches for understanding brittle structural behavior because these methods permit meaningful statements about the expected performance despite the variability.

It should be noted that this variability in material properties is expected to occur not only, for example, from one brick wall panel to the next but also, and more important, from point to point within a given panel. Thus, the development of the statistical theory was based on the assumption that any brick structural element is composed of discrete segments and that the failure of these discrete segments is governed by a probability distribution (spatial process).

It was further assumed that the probability distribution of fracture stresses was governed by the statistical theory of extreme values. This assumption was justified by the fact that the experimental data from the static test program fit the extreme type of distribution fairly well and that, in general, the extreme type of performance is typical of brittle materials. Failure is often propagated by flaws and the distribution of flaws is often considered to be extreme (Refs. 3 and 4). The distribution of the "largest flaws" is of interest because it determines the distribution of "smallest strengths" (i.e., failure which for the purposes of this section is defined as the occurrence of the first crack).

The first case treated was a beam composed of 8 segments and, in accordance with the above, it was assumed that fracture of any segment would cause failure of the beam. In other words the probability of failure of the beam equals the probability of failure of any one of the 8 segments of the beam.

To illustrate the implications of this approach, consider the four typical loading conditions for the beam as shown in Fig. 5-1, and assume that the loading is such that the maximum stress in each case is the same.

From conventional mechanics the same strength would be predicted for each beam since the maximum fiber stress is the same. However, it may be noted that in the uniform moment case all segments are stressed to the maximum stress, while in the other cases certain segments have a much lower stress and thus would have a much lower probability of failure. Thus, even without making any calculations, it is evident that the probability of failure of the beam from uniform moment loading is going to be significantly higher than for any other case -- which in turn means that its expected strength is significantly lower.

With the assumptions given above and standard probability theory, a generalized equation was derived giving the failure distribution for a beam containing n segments in terms of the number of segments, n, the modal value of failure stress, μ, $1/\sigma$ (a measure of dispersion), and the maximum flexural stress, σ.

With this equation and some of the experimental data from the static test program for 24-in. beams, it was possible to derive μ and σ for a unit segment beam, and then with this data the failure distributions for the four different loading conditions given in Fig. 5-1 were derived. These are given in Fig. 5-2.

As expected, these results show that the expected strength for the constant moment case is less than for any other condition. For example,
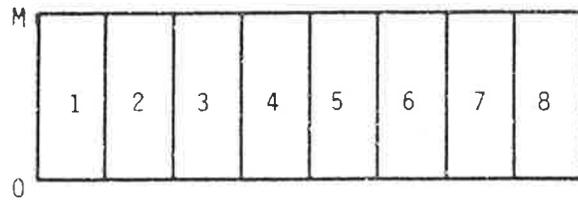
Case 1: Uniform Moment
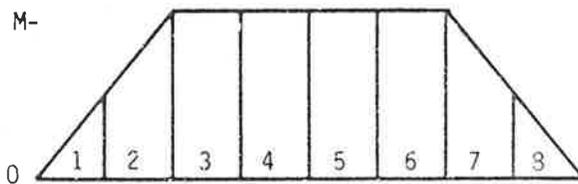
Case 2: 1/4-Point Loading
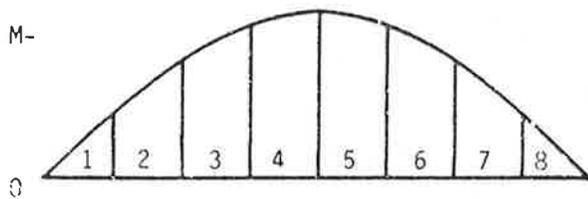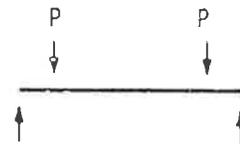
Case 3: Uniform Load
simple
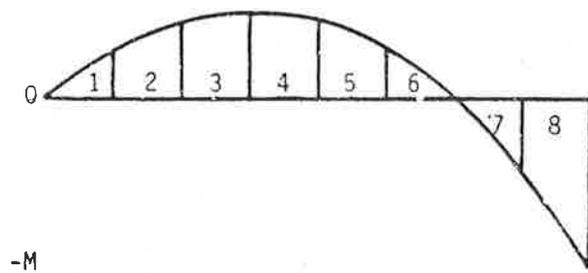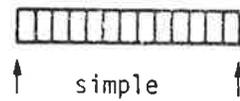
Case 4: Uniform Load
Propped cantilever
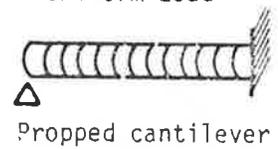
Fig. 5-1. Typical Loading Cases and Moment Diagrams.
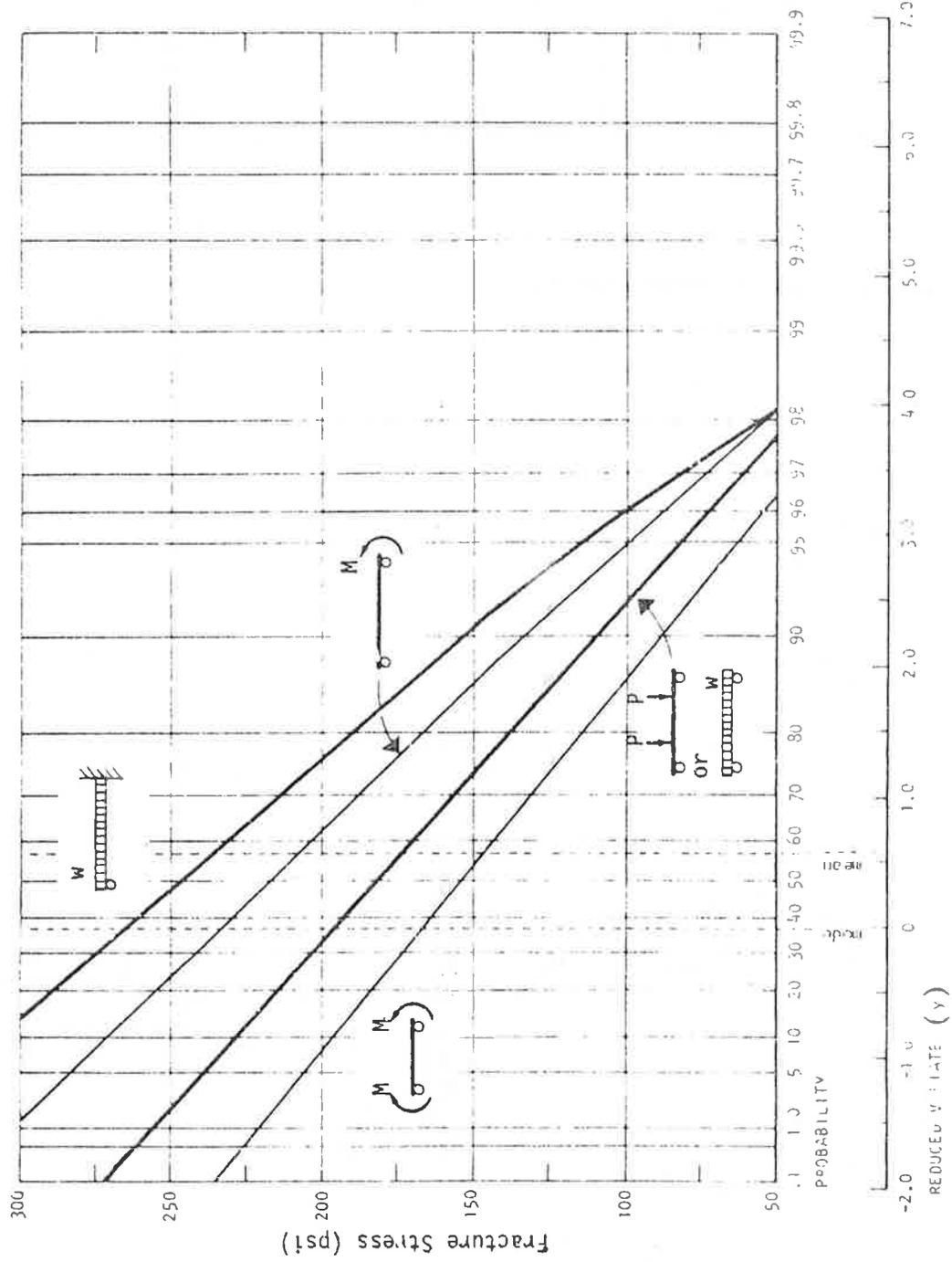
Fig. 5-2. Extreme Probability Plot of Fracture for 24-in. Beams with Various Loadings.

the modal (most frequent) strength for a constant moment beam is 168 psi, while for the propped cantilever or pin-fixed beam it is 270 psi. Similarly, the statistical means are 147 psi vs 235 psi. The pin-fixed case can thus be considered statistically to be about 1.6 times as strong as the constant moment case.

Another important observation is that the distribution for the pin-fixed case differs from that of the constant moment case, that is, no longer is a straight line obtained on the extreme probability paper for the pin-fixed case. From this it can be deduced that a moderately different probability distribution of failures will result from different loadings (moment) of the beam. That is, if a beam is loaded uniformly to a maximum fiber stress of σ_1, or with a concentrated load to a maximum stress of σ_1, different probabilities of failure exist and different statistical laws govern.

In extending this statistical approach to wide beams or plates composed of m parallel rows of beams, two cases were considered. The first, termed the Flaw Theory, assumes that failure in any segment of any row leads to failure of the plate. This implies that a crack at any point will propagate sufficiently throughout the plate to lead to failure. The other assumption, termed the Parallel Theory, is that the m beams are independent of each other (greased joints between) and that failure is caused when the average beam fails. Thus, the expected strength of the average beam is the summation of the expected strengths of the m beams, i.e., of m independent random variables.

For an n-segment long beam, m-segments wide, the Flaw Theory shifts the distribution of failure stress to lower and lower values as m increases in size, but the same variance or scatter is maintained. This is illustrated by the probability distributions on the next page.
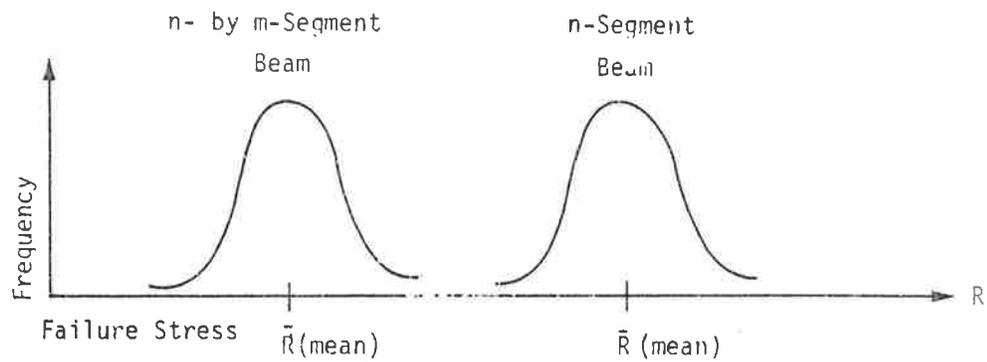
For the same n by m beam, the Parallel Theory leads to the same expect-
ed strength but an increase in variance, as illustrated by the two probability
distributions below,
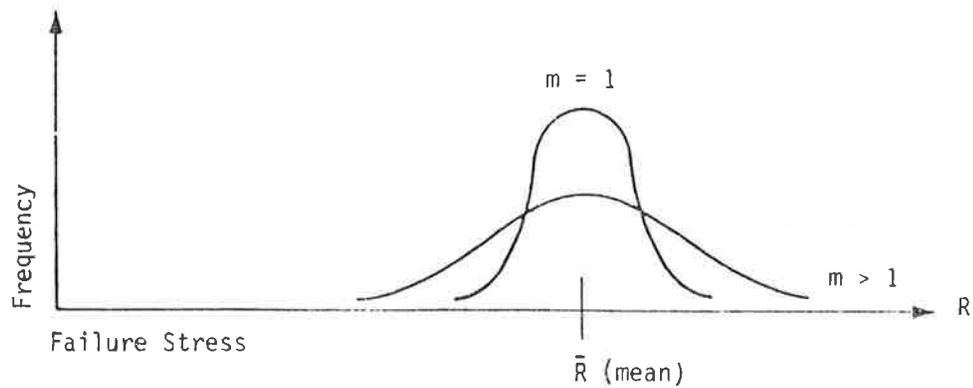
From the preceding work on low level fatigue, one would expect that the
response of a brittle structure to a dynamic load would lie somewhere between
the Flaw Theory and the Parallel Theory. Hence, it was necessary to formulate
a theory or procedure to establish the failure strength between the two
different theories.

Let,

$$\left[p = P\ \text{Complete Failure} \ \middle| \ \text{The } i^{th} \text{ element has failed} \right]$$

and

$$q = 1 - p$$

Then, if $p = 1$, the Flaw Theory prevails; if $p = 0$, the Parallel Theory prevails. Between these domains must lie the "truth", i.e., the distribution that actually applies for the beam m segments wide. As illustrated below, p represents how closely the "truth" approaches the Flaw Theory.
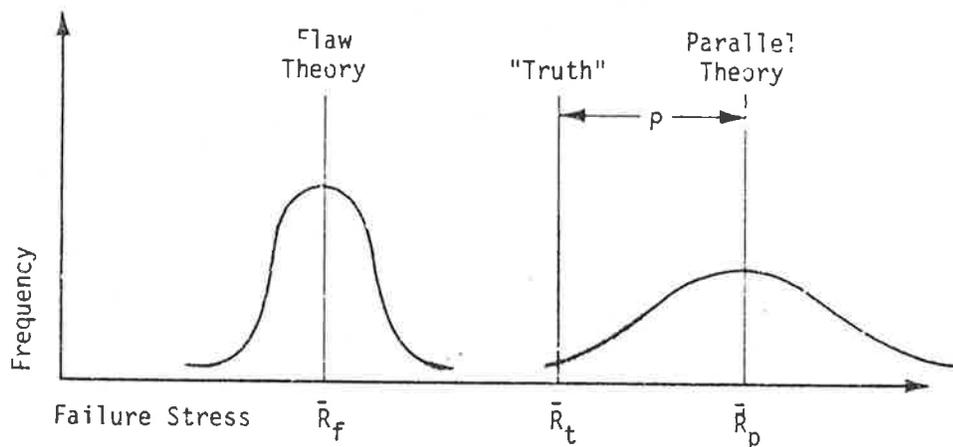
GENERAL BRITTLE FAILURE THEORY

In this formulation, the low level fatigue ideas of the first and second sections were combined with the statistical ideas of the third section to create a reasonably complete failure theory.

The first step was to examine the proposed observed resistance equation (Eq. 5-1), developed in the continuum section, in light of the statistical formulations. For this purpose the equation:

$$R_0 = R_s + (R_D - R_s) \left[1 - \alpha \exp(-\Lambda) \right] \qquad (5\text{-}1)$$

can be rewritten into a more convenient form as

$$R_0 = R_s e^{-\Lambda} + R_D(1 - e^{-\Lambda}): \qquad (5\text{-}1a)$$

then recall that

$$0 \leq e^{-\Lambda} \leq 1.$$

It was readily apparent that there is a close similarity between the Flaw Theory and the case of $\Lambda \rightarrow 0$ since by definition a crack in a basic element leads to total failure. Thus, p was taken as $p = e^{-\Lambda}$ and $q = 1 - e^{-\Lambda}$.

To illustrate the use of these concepts and formulas, calculations were made for the case of the 8-ft x 12-ft brick panels tested in the shock tunnel. First the distribution of R_s (static resistance, or the minimum dynamic resistance) was calculated on the basis of the Flaw Theory (p = 1, q = 0) and using the concepts presented earlier in developing the curves in Fig. 5.2. Similarly, the distribution of R_D (the apparent maximum dynamic resistance) was calculated on the basis of the Parallel Theory (p = 0, q = 1). The basic segment used was 1 in. wide by $8\frac{1}{2}$ in. thick by 24 in. long. Thus, the panel was simulated by a n = 4, m = 144 array of basic elements. The distribution of R_s and R_D are given in Fig. 5-3.

5-12
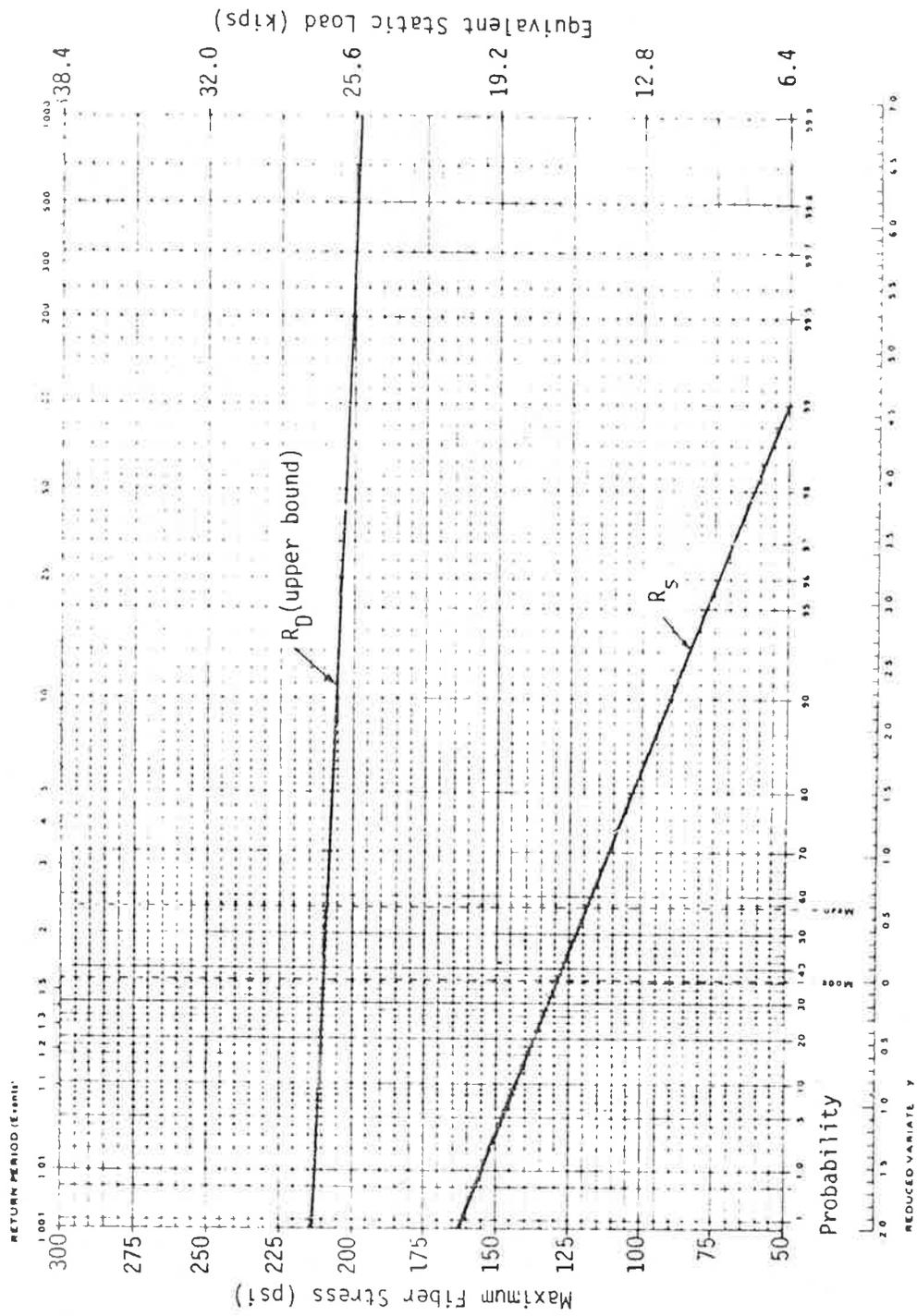
Fig. 5-3. Plot of R_s and R_D of Flaw Theory.

With these distributions and Equation 5-1 the expected values of R_0 and the 95% probability bounds were calculated. The results are given in Fig. 5-4.

The implications of the foregoing work are rather interesting and far-reaching. Perhaps one of the most interesting and intuitively pleasing implications is that there is, indeed, an upper bound dynamic resistance for a particular structure. Further, an upper bound strength distribution is reached, which is more meaningful. Another item that is interesting is the reduction of variability as the dynamic load is reached. One must recall that the plot is of the apparent stress at dynamic failure, and in the derivation the variance of the total load was n times as large as that of a single element. Another thing one must keep in mind is the fact that if we have a large enough number of parallel elements and the failure resistance is the summation of all m resistances, the total resistance will be identically the average for large m.

From the foregoing we can conclude that for flaw sensitive brittle materials subjected to dynamic loads.

1. The smaller the variability under static conditions, the smaller the gap between static and dynamic behavior.

2. The greater the number of possible parallel elements in a system the greater the gap between static and dynamic strength.

3. A large specimen of a flaw sensitive material is going to present the experimenter with a much greater difference in load between static and dynamic cases than smaller specimens. In fact, if a flaw sensitive material is sufficiently homogeneous to make very small specimens, there should be a size where the static and dynamic resistances are identical.

4. On the practical side, the understanding of this phenomenon (if the theory proves correct) will allow the experimenter to infer his upper bound for a particular experiment and plan accordingly.

5-14
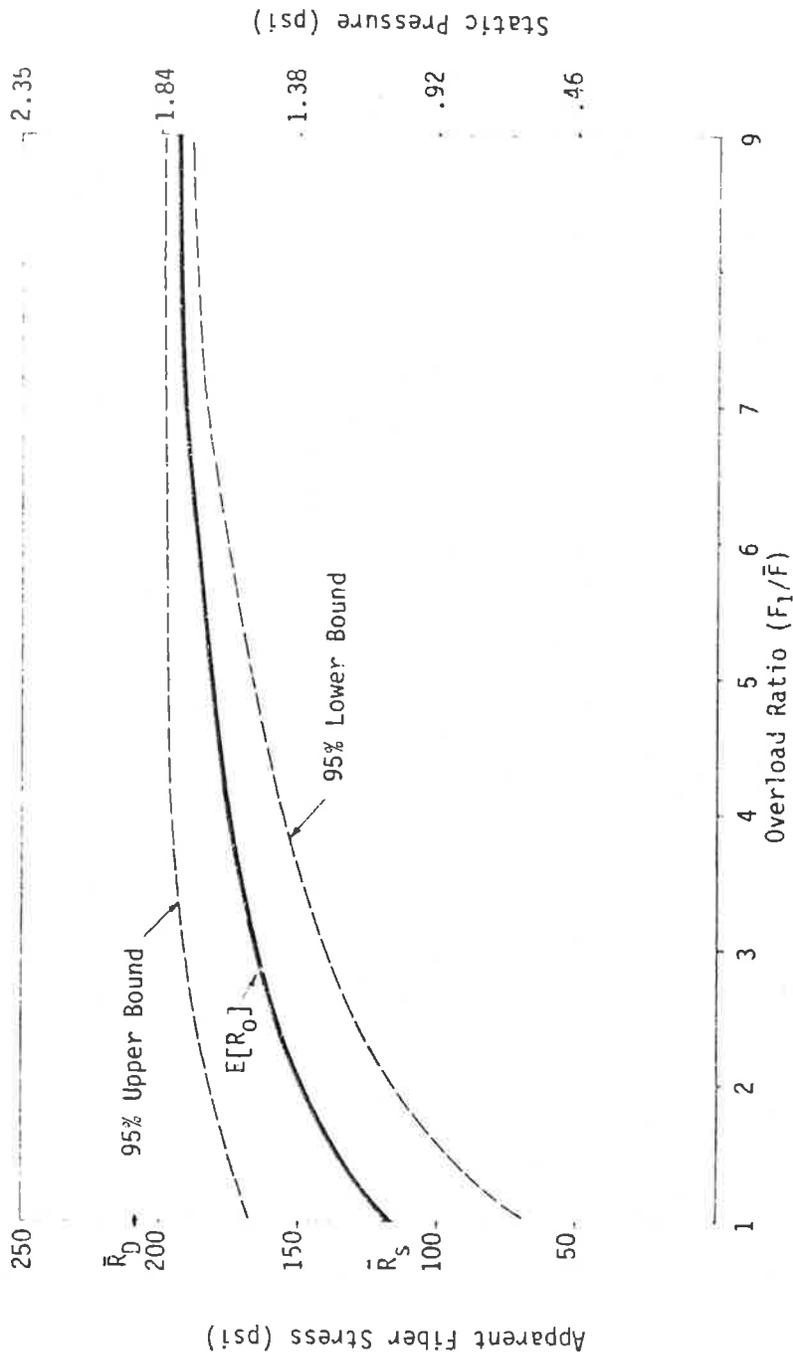
Fig. 5-4. Apparent Fiber Stress vs Overload Ratio.

5. Perhaps the most important overall observation is that the apparent increase in strength is for only a few cycles of loading, and its impact is mainly reflected in measured reactions on building frames or, for example, on the load cells used in testing the 8 by 12 ft wall panels on the shock tunnel.

REFERENCES

1. Wilton, C., B.L. Gabrielsen, J. Edmunds, and S. Bechtel, "Loading and Structural Response of Wall Panels", URS 709-4, URS Research Company, San Mateo, California, November 1969.

2. Gabrielsen, B L., C. Wilton, and K. Kaplan, "Response of Arching Walls and Debris from Interior Walls Caused by Blast Loading", URS 7030-23, Final Report, URS Research Company, prepared by Scientific Service, Inc., Redwood City, California, February 1975.

3. Gumbel, E.J., Theory of Extremes, Columbia University Press, New York, New York, 1958.

4. Weibull, W., A Statistical Theory of the Strength of Materials, Handling No. 151, Engineering Academy, General Lithographic Library, Stockholm, Sweden, 1939.

5. Monk, C.B., "Transverse Tests of Masonry Walls", ASTM Special Technical Publication No. 166, 1954.

6. Pearson, J.C., "Measurement of Bond Between Bricks and Mortar", ASTM Proceedings, Vol. 43, 1943.

7. Fishburn, C.C., "Effect of Mortar Properties on Strength of Masonry", National Bureau of Standards Monograph 36, November 20, 1961.

8. Astbury, N.F., and H.W.H. West, "Tests on Storey-Height Brickwork Panels and Development of Site Control Tests for Brickwork", Chapter 26, Designing, Engineering and Constructing with Masonry Products, Proceedings of The International Conference on Masonry Structural Systems.

9 Hedstrom, R.O., "Load Tests of Patterned Concrete Masonry Walls" American Concrete Institute, June 6, 1960.

10. Portland Cement Association, "Load Tests of Patterned Concrete Masonry Walls", Trowel Talk No. 3, 1963.

11. Wilton, C., B.L. Gabrielsen, and P. Morris, "Structural Response and Loading of Wall Panels", URS 709-11, Final Report, URS Research Company, San Mateo, California, July 1971.

THE SHOCK TUNNEL:
HISTORY AND RESULTS
Volume V
PREDICTION OF FAILURE PRESSURES
FOR WALL PANELS

ABSTRACT

This is Volume 5 of a five volume report which summarizes the results of a program conducted by the Defense Civil Preparedness Agency to determine blast resistance of wall panels typically found in existing structures. Such information was needed to determine the blast sheltering capability of structures in the National Fallout Shelter Survey inventory and to develop means for upgrading these structures.

This volume summarizes the predicted failure pressures for wall panels based on the theoretical and experimental results covered in Volume 3 and the static test data in Volume 4, and provides information on wall survivability.

Volume 1 of this report describes the shock tunnel facility used for the experimental testing of full-scale wall panels. Included is a summary of the capabilities of the shock tunnel for dynamic loading and response studies and brief summaries of various experimental programs conducted in the shock tunnel which were not related to the wall panel test program.

Volume 2 presents the results obtained from the experimental program conducted in the shock tunnel to determine the loadings which are received by wall panels mounted in the test section.

Volume 3 is concerned with the dynamic response and failure of full-scale wall panels. Included are the development of theories of wall panel response and the results obtained from the testing of full-scale wall panels in the shock tunnel.

Volume 4 describes the static test program conducted to determine the physical properties of the wall panels and to assist in the development of failure theories and test predictions for wall panels.

Table of Contents

List of Figures

iii

List of Tables

Section 1
INTRODUCTION

This volume is concerned with the prediction of failure pressures for wall panels subjected to blast loadings based on the theoretical analyses and experimental wall panel test results presented in Volume 3, and results of material property tests given in Volume 4. For this purpose it is convenient to classify the walls into two groups:

Simple Beam and Plate Walls

Arched Walls

For the first group of walls, which are covered in Section 2 of this volume, the controlling failure mechanism is tensile (flexural) failure. That is, when the maximum flexure stress exceeds the flexural strength, the wall will crack, and in general this leads to total failure. Extensive computer calculations based on the SAMIS code were made for this group of walls and it was possible to develop a prediction method based on these calculations that permits ready extrapolation to conditions other than those tested.

For arched walls, which are discussed in Section 3, the controlling failure mechanisms are crushing or spalling of material depending on whether there is rigid or gapped arching. Calculations were made for these cases also, but they were not as extensive as for the first group of walls and primary reliance was placed on the experimental data for prediction of failure pressures.

Section 4 summarizes all predictions in the form of failure pressure and survival pressure matrices and a failure pressure chart.

Section 2
NON-ARCHING BEAM AND PLATE WALLS

As illustrated in Volume 3, it is possible to estimate the incident pressure required to cause each type of wall panel to fail in two ways: First, using only the shock tunnel test results; and second, using the SAMIS computer code with physical properties as determined by small scale static test data.

Table 2-1 gives the estimates of failure pressure based on the shock tunnel data, and Table 2-2 those based on SAMIS and the static test data. It should be noted that in Volume 3 the results were discussed in terms of the loading pressure received by the wall, while in this volume the pressures are presented in terms of the peak incident pressure on the wall, since the latter is more appropriate for prediction purposes.

A comparison of the two methods for estimating failure pressure is given in Fig. 2-1. It can be seen that on an individual basis, with the exception of the brick plate data, the results of the two methods for predicting failure pressures are consistent with each other since the prediction ranges overlap. However, there is a clear trend for the predictions based on the tunnel data to be significantly higher than those based on SAMIS and static test data. This implies that the flexural strength of the full-scale panels (under dynamic loadings) is also significantly greater than the flexural strengths of the small scale test beams (under static loading).*

---

* This tendency had been noted during the course of the program and it was was suspected that the difference might be due to the nature of the loading, i.e., dynamic vs static. For this reason some effort was devoted to the development of generalized theory of the response of brittle materials under dynamic loading to see if any theoretical support could be obtained for this result. Although this work, which is presented in Section 5 of Volume 4, was not completed, certain of the concepts presented do suggest an increase of strength under dynamic loading.

Table 2-1
Prediction of Incident Failure* Pressures
Based on Tunnel Tests

12-in. Brick Simple Beam Wall

Upper Bound - 2.0 psi - Failure

Lower Bound - 0.75 psi - No Damage

No indication of either bound being a threshold value.

Estimated mean value and range: 1.4 ± 0.6 psi

8-in. Brick Simple Beam Wall with Preload

Upper Bound - 0.75 psi - Failure

Lower Bound - No test data but 0.45 psi selected since calculation shows that a single wall of zero flexural strength would fail at this pressure.

Evidence suggests failure pressure near upper bound.

Estimated mean value and range: 0.6 ± 0.2 psi

8-in Brick Simple Beam Wall with Window

Upper Bound - 1.85 psi - Failure

Lower Bound - 0.65 psi - Slight damage but no failure

Evidence suggests failure pressure tends towards lower bound.

Estimated mean value and range: 1.1 ± 0.4 psi

8-in. Brick Simple Beam Wall with Window and Preload

Upper Bound - 2.0 psi - Failure

Lower Bound - 0.8 psi - No Damage

Evidence suggests failure pressure tends towards upper bound

Estimated mean value and range: 1.6 ± 0.6 psi

---

* Failure defined as wall collapse.

Table 2-1 (cont.)

Prediction of Incident Failure Pressures

Based on Tunnel Tests

8-in. Brick Simple Beam Wall with Doorway

    Upper Bound - 1.75 psi - Failure

    Lower Bound - 0.75 psi - No Damage

        No indication of threshold at either limit.

                Estimated mean value and range: 1.2 ± 0.5 psi

8-in. Brick Simple Plate Wall

    Upper Bound - 1.9 psi - Failure

    Lower Bound - No test data

                Estimated mean value and range: 1.5 ± 0.4 psi

8-in. Concrete Block Beam Wall

    Upper Bound - 0.75 psi - Failure

    Lower Bound - No test data

                Estimated mean value and range: 0.4 ± 0.3 psi

8-in. Concrete Block Beam Wall with Window

    Upper Bound - > 0.75 psi

    Lower Bound - < 0.75 psi

        Evidence suggests failure pressure near lower
        bound.

                Estimated mean value and range: 0.7 ± 0.4 psi

8-in. Concrete Block Beam Wall with Window and Preload

    Upper Bound - 2.0 psi - Failure

    Lower Bound - 0.75 psi - Some damage, no failure

        Evidence suggests failure pressure tends towards
        lower bound.

                Estimated mean value and range: 1.2 ± 0.5 psi

2-3

Table 2-2

Prediction of Incident Failure Pressures Based on SAMIS Code

and Static Test Data

Wall Type	Maximum Flexural Stress with Incident Pressure = 1 psi (from SAMIS) σ_s(psi)	Mean Flexural Strength σ_r(psi)	Estimated Incident Failure Pressure* P_f(psi)
12-in. Brick Simple Beam	196	176 ± 30%	0.9 ± 0.3
8-in. Brick Simple Beam with Preload	409	"	0.4 ± 0.1
8-in. Brick Simple Beam with Window	226	"	0.8 ± 0.2
8-in. Brick Simple Beam with Window and Preload	188	"	0.9 ± 0.3
8-in. Brick Simple Beam with Doorway	272	"	0.6 ± 0.2
8-in. Brick Simple Plate	260	"	0.7 ± 0.2
8-in. Concrete Block Simple Beam	440	130 ± 50%	0.3 ± 0.2
8-in. Concrete Block Simple Beam with Window	226	"	0.6 ± 0.3
8-in. Concrete Block Simple Beam with Window and Preload	188	"	0.7 ± 0.4

* $P_f = \sigma_r/\sigma_s$.
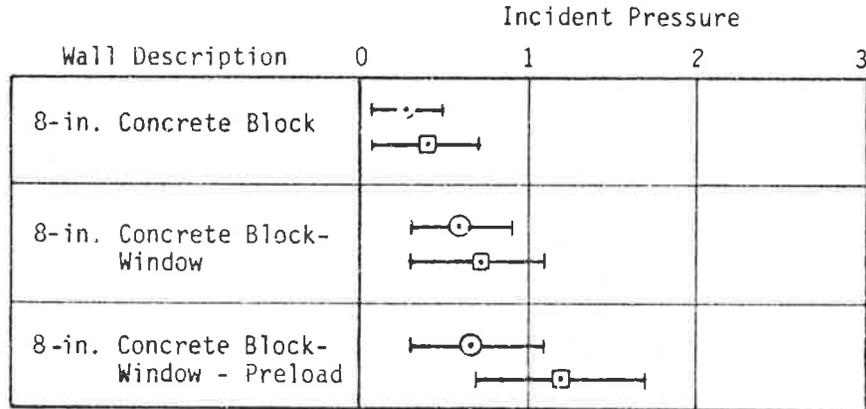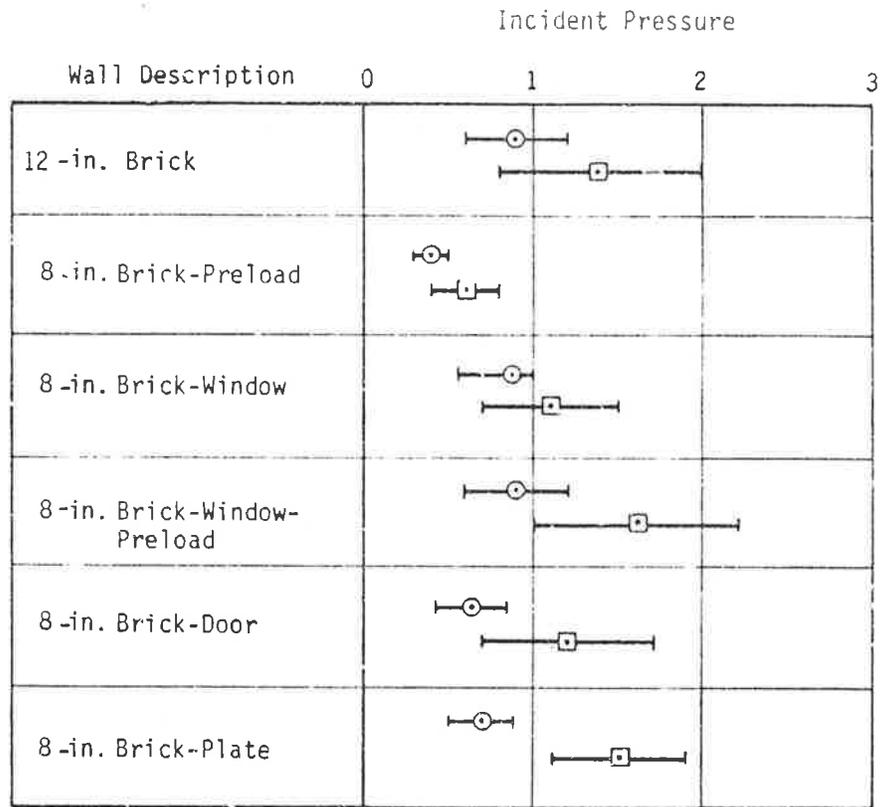
2-4

Fig. 2-1. Comparison of Predicted Incident Failure Pressures.

To estimate the magnitude of the difference in strength the process used to derive Table 2-2 was reversed and a value of mean flexural strength σ_r for each test was calculated from the relationship $\sigma_r = P_f \sigma_s$, where the P_f values are those given in Table 2-1, and the σ_s values are SAMIS values tabulated in Table 2-2. (Actual calculations used P_f values carried to one more significant figure than those tabulated in Table 2-1.) These computed strength values are given in the first column of Table 2-3. It can be seen that the average strength for the brick walls is 310 psi, approximately 75% greater than the 176 psi value from the static tests. Similarly an average strength of 189 psi was obtained for the concrete block walls, about 45% greater than the 130 psi value from the static tests.

Based on the foregoing, it was concluded that the best method of predicting the failure pressures of wall panels would be to use the maximum stress values from the SAMIS code, with the average flexural strengths of the wall panels as computed in Table 2-3, rather than with the strengths from the small scale static tests. Thus, for brick walls a strength of 310 psi replaced 176 psi, and for concrete block walls 189 psi replaced 130 psi.

With these new average values of flexural strengths, the failure pressures were recomputed. The results are given in the second column of Table 2-3 and compared with the experimental values in Fig. 2-2. The uncertainty ranges for these calculations were based on the measured scatter in material properties from the static test program. It can be seen that the agreement is quite good for all cases.

It may also be noted from Fig. 2-2 that the uncertainty ranges for both methods of failure pressure prediction are approximately the same even though they are based on different criteria. While the calculated ranges use information from the static test program, the ranges from the tunnel tests include scatter dependent on the finite pressure steps used in the testing, and the limited number of full-scale tests that could be conducted for any given condition.

2-6

Table 2-3

Revised Incident Failure Pressures

Wall Type	Computed Flexural Strength* σ_r(psi)	Revised Estimated Failure Pressure P_f(psi)
12-in. Brick Simple Beam	284	1.6 ± 0.5
8-in. Brick Simple Beam with Preload	264	0.8 ± 0.2
8-in. Simple Beam with Window	260	1.4 ± 0.4
8-in. Simple Beam with Window and Preload	324	1.6 ± 0.5
8-in. Brick Simple Beam with Doorway	326	1.1 ± ± 0.3
8-in. Brick Plate	403	1.2 ± ± 0.4
Average	310	
8-in. Concrete Block Simple Beam	176	0.4 ± 0.2
8-in. Concrete Block Simple Beam with Window	158	0.8 ± 0.4
8-in. Concrete Block Simple Beam with Window and Preload	234	1.0 ± 0.5
Average	189	

---

* σ_r = P_f (from tests, Table 2-1) times σ_s (from SAMIS, Table 2-2)
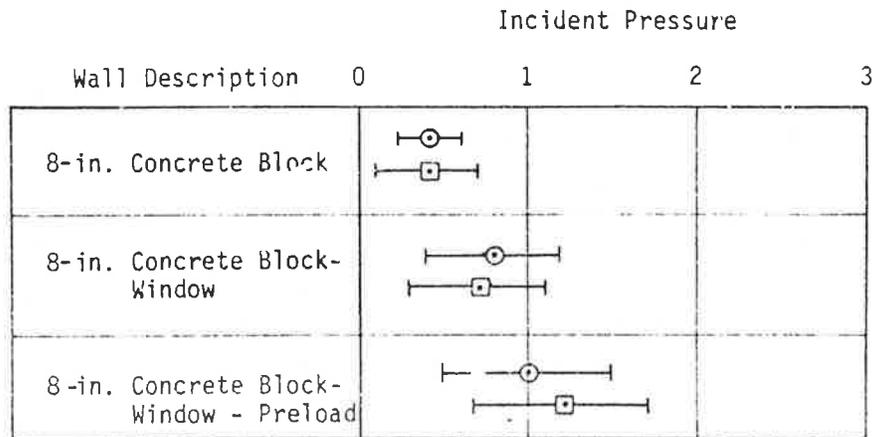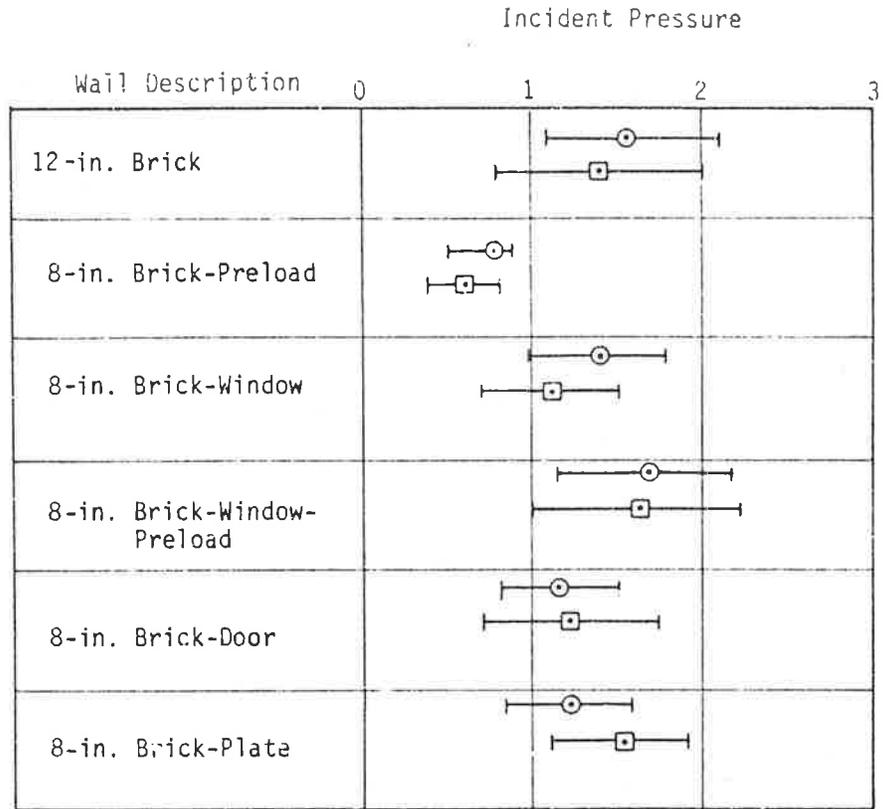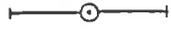
Fig. 2-2.   Comparison of Predicted Incident Failure Pressures, Revised.

For prediction purposes, it is believed that the uncertainty range from the calculation is best to use since it has a firm statistical base and can be extrapolated readily to other conditions. Also, as shown in Volume 4, the same general type of scatter in properties of brittle materials has been obtained by other investigators. Further, if a greater degree of confidence is desired in the prediction, it can be readily derived from the statistical theory described in Volume 4. For example, the range selected for discussion in this report of ± 30% about the mean for the brick walls included 81% of the expected results. If the range is increased to ± 40%, then slightly more than 90% of the expected results would fall within the range.

Another interesting application of the statistically based uncertainty range is in predicting survival probabilities (probability of not having a failure) of walls as a function of incident overpressure. An example of such a determination is given below for the case of a 12-in. solid brick beam wall.

Incident Overpressure (psi)	Fraction of Mean (%)	Survival Probability (%)
1.6	100	57
1.1	70	88
0.8	51	95

The incident overpressure of 1.6 psi is the mean value of the estimated failure pressure. The 1.1 psi value, which gives a survival probability of about 88%, is the lower bound of the ± 30% range selected for general discussion purposes. To achieve a survival probability of 95 it would be necessary to select an incident overpressure of 0.8 psi, about 50% of the mean value.

Included in Section 4 of this report is a matrix for all wall panel types discussed in which incident overpressures for a survival probability of 90% are tabulated. For the 12-in. solid brick beam wall just discussed, this survival pressure would be 63% of the mean value or about 1.0 psi.

2-9

Section 3
ARCHING BEAM AND PLATE WALLS

Table 3-1 gives the estimates of failure pressure based on the shock tunnel data. It should be noted that -- as in Section 2 -- the results are presented in terms of the peak incident pressure on the walls.

For some cases in this table, uncertainty ranges based solely on the data available were not derived because of the limited number of tests conducted. In these cases the uncertainty range was set at ± 30%, a value which is typical of those cases where a larger number of tests were conducted.

The only case for which a theoretical estimate of failure pressure was made is for the 8-in. brick rigid arched one-way wall. This gave a value of 7 psi which compares well with the 6.2 ± 2.0 psi value experimentally determined.

The effects of material type and size are shown in Table 3-2. It can be seen that the 8-in. brick wall withstood about five times the incident pressure that a 4-in. brick wall withstood. This does not imply, however, that the wall strengths are in the ratio of 5 to 1. For a comparision of strengths to be made, it is necessary to use the ratio of loading or reflected pressures (not incident pressures), which in this case, gives a ratio of about 6 to 1. Although predictions of failure pressures under dynamic loadings were not made for the 4-in. wall, a prediction of the maximum static resistance was made. This value, 1.8 psi, can be compared to a similar static resistance prediction for the 8-in. wall, 16 psi. The comparison suggests that the strength of the 8-in. wall would be about 8 times that of the 4-in. wall. considering that only one 4-in. wall was tested, the ratio of 8 is considered to be in satisfactory agreement with the ratio of 6 determined from the test data.

Table 3-1

Prediction of Incident Failure Pressures

Based on Tunnel Data

8-in. Brick One-Way Arched Wall (8 walls)

    Series 1 (4 walls)

        Upper Bound - 5.9 psi - Failure

        Lower Bound - 4.3 psi - No failure

                Estimated mean value and range: 5.1 ± 0.8 psi

    Series 2 (4 walls)

        Upper Bound - 8.2 psi - Failure

        Lower Bound - 6.3 psi - No failure

                Estimated mean value and range: 7.2 ± 1.0 psi

    Average both series

                Estimated mean value and range: 6.2 ± 2.0 psi

8-in. Brick Gapped Arched Wall (2 walls)

    Upper Bound - <2.0 psi - Failure

    Lower Bound - No test data but 1 psi selected based on
                   calculation of maximum static resistance

                Estimated mean value and range: 1.5 ± 0.5 psi

4-in. Brick One-Way Arched Wall (1 wall)

    Upper Bound - 1.7 psi - Failure (second test)

    Lower Bound - 0.75 psi - No failure (first test)

                Estimated mean value and range: 1.2 ± 0.5 psi

4-in. Brick Two-Way Arched Wall (1 wall)

    Upper Bound - >2.2 psi - No failure (first test)

    Lower Bound - <2.1 psi - Failure (second test)

                Estimated mean value and range: 2.1 ± 0.6 psi
                (range set by standard ± 30%)

Table 3-1 (cont.)
Prediction of Incident Failure Pressures
Based on Tunnel Data

8-in. Brick One-Way Arched Wall with Window (3 walls)

    Upper Bound - 9.5 psi - Failure

    Lower Bound - 5.7 psi - No failure

                        Estimated mean value and range: 7.6 ± 1.9 psi

8-in. Brick One-Way Arched Wall with Doorway (1 wall)

    Upper Bound - No test data

    Lower Bound - 8.4 psi - No failure

8-in. Brick One-Way Gapped Arched Wall with Doorway (1 wall)

    Upper Bound - 8.6 psi - Failure (catastrophic)

    Lower Bound - No test data.

10-in. Brick-Concrete Composite One-Way Arched Wall (2 walls)

    Upper Bound - 5.6 psi - Failure

    Lower Bound - 5.0 psi - No failure

                        Estimated mean value and range: 5.3 ± 1.6 psi
                        (range set by standard ± 30%)

8-in. Concrete Block One-Way Arched Wall (2 walls)

    Upper Bound - 4.5 psi - Failure

    Lower Bound - 3.3 psi - No Failure

        Evidence suggests failure threshold near lower bound

                        Estimated mean value and range: 3.7 ± 1.1 psi
                        (range set by standard ± 30%)

8-in. Concrete Block Two-way Arched Wall (2 walls)

    Upper Bound - <4.0 psi - Failure

    Lower Bound - No test data

Table 3-1 (cont.)

Prediction of Incident Failure Pressures

Based on Tunnel Data

8-in. Concrete Block One-Way Gapped Arched Wall (2 walls)

Upper Bound - <1.7 psi - Failure

Lower Bound - No test data

8-in. Concrete Block One-Way Arched Wall with Window (2 walls)

Upper Bound - >3.5 psi - Failure

Lower Bound - <3.5 psi - No failure

Estimated mean value and range: 3.5 + 1.0 psi
(range set by standard ± 30%)

3-4

Table 3-2

Effects of Material Type and Size
on One-Way Rigid Arching for Solid Walls

Wall Thickness, Type, and Number Tested	Estimated Incident Failure Pressure and Uncertainty Range
4-in. Brick: 1 Wall	1.2 ± 0.5 psi
8-in. Brick: 8 Walls	6.2 ± 2.0 psi
8-in. Concrete Block: 2 Walls	3.7 ± 1.1 psi
10-in. Composite Concrete Block and Brick : 2 Walls	5.3 ± 1.6 psi

3-5

Table 3-2 also shows that the 8-in. concrete block wall withstood about one half the incident pressure withstood by the 8-in brick wall, about the same ratio as obtained with simple beams. The 10-in. composite concrete block and brick wall had a slightly lower mean failure pressure than the 8-in. brick wall; however, considering the uncertainty range, this is not deemed significant.

The effects of wall openings for arching conditions are shown in Table 3-3. The most significant comparison is between the solid wall and the wall with a doorway. Their responses should be identical if loadings are identical. However, as discussed in Volume 3, for the same incident loading, the effective loading for the wall with a doorway is much less after the initial peak value. Thus, it is not surpising that the wall with a doorway withstood an incident pressure more than 35% greater than the mean incident pressure on the solid wall (and slightly above its estimated upper bound). It may be noted that, for the simple beam case, the wall with doorway withstood a pressure about 60% greater than the solid wall.

The effect of the window on arching is more complex. Clearly again the net loadings for the window wall are much less than for the solid wall with the same incident pulse. The response of the window wall is expected to be different than the solid wall because the window opening provides a means for relieving the arching on the center section of the wall thus weakening it. The opening, however, allows net loadings on a wall to be smaller so that for the same incident pressure, the wall would appear stronger.

The test data suggest that the combination of these opposite effects still results in the window wall being able to withstand higher incident pressures, however, the differences are not large and are marginally significant in light of the scatter of the data. It may be noted that for the simple beam case the window wall withstood about twice the incident pressure as the solid wall.

The overall affects of arching are given in Table 3-4 which compares the

Table 3-3

Effects of Wall Openings in One-Way Rigid Arching

Wall Thickness, Type and Number Tested	Estimated Incident Failure Pressure and Uncertainty Range
8-in. Brick	
Solid 8 Walls	6.2 ± 2.0 psi
Door 1 Wall	>8.4 psi
Window 3 Walls	7.6 ± 1.9 psi
8-in. Concrete Block	
Solid 2 Walls	3.7 ± 1.1 psi
Window 2 Walls	3.5 ± 1.2 psi

Table 3-4

Effects of Arching

Wall Thickness, Type and Number Tested	Estimated Incident Failure Pressure and Uncertainty Range
8-in. Brick Solid	
Simple Beam	0.7 ± 0.2 psi
Rigid Arching	6.2 ± 2.0 psi
Gapped Arching	1.5 ± 0.5 psi
8-in. Concrete Block Solid	
Simple Beam	0.4 ± 0.2 psi
Rigid Arching One-Way	3.7 ± 1.1 psi
Gapped Arching One-Way	< 1.7 psi
Rigid Arching Two-Way	< 4.0 psi
8-in. Brick with Window	
Simple Beam	1.4 ± 0.4 psi
Rigid Arching One-Way	7.6 ± 1.9 psi
8-in. Brick with Doorway	
Simple Beam	1.1 ± 0.3 psi
Rigid Arching One-Way	> 8.4 psi
Gapped Arching One-Way	< 8.6 psi
4-in. Brick Solid	
Rigid Arching One-Way	1.2 ± 0.5 psi
Rigid Arching Two-Way	2.1 ± 0.6 psi

failure pressures for simple beams, rigid arching beams, gapped arching beams and rigid arched plates for four different wall types. The very large effects of rigid arching can be seen from the table. For 8-in. solid brick and concrete block walls, the one-way arching walls withstood incident pressures nine times those which caused simple beam walls to fail.

For the 8-in. brick wall with a doorway, the upper bound for rigid arching was not determined, but with the data available it could be said that the arching walls were more than eight times as strong as the simple beam walls.

For the reasons described earlier, the window walls were expected to show a significantly smaller effect of arching and the factor of 5 between arching and simple beam walls shown by the data is consistent with this.

Relatively little data are available for the gapped arching case, however, they clearly do show that these walls are much weaker than their rigid arching counterparts. The most complete data are for the 8-in. brick solid walls which show that the rigid arching wall withstood incident pressure four times greater than gapped arching walls. As discussed earlier, strength differences should be calculated by using loading (reflected pressure). This type of calculation implies a strength difference of a factor of about 4.5. It is interesting to note that this factor compares favorably with the ratio of maximum static resistances calculated for these cases of about 5 (see Fig.6-3 of Volume 2).

The data from the 8-in. solid brick walls also show that, as expected, the gapped arching wall was stronger than the simple beam wall.

The other gapped arching data are not inconsistent with the above tendencies but the upper bounds are too broad for the data to be quantitatively useful.

The limited data on two-way rigid arching show somewhat conflicting

3-9

results. The 4-in. brick solid wall data show that the two-way rigid arching walls withstood a 75% greater incident pressure than one-way arching walls (which implies an 80% greater strength). The 8-in. concrete block data, however, suggest little difference between the one-way and two-way arching walls. Although no calculations were made for the two-way arching case, in Volume 3 the effect was estimated to be a factor of 40%.

In summary it can be said that all of the experimental data, with minor exceptions, have been shown to be consistent with each other and with existing theories where comparisons can be made. Thus, they can be used with a reasonable degree of confidence to make predictions of the incident pressure required to cause wall failure. Such predictions are given in the failure matrix and failure chart shown in the next section. Predictions of pressures at which 90% of arching walls survive were derived from the line load strength data given in Volume 4.

Section 4
FAILURE PRESSURE MATRIX AND CHART
AND
SURVIVAL PRESSURE MATRIX

This section contains two matrixes, one showing incident failure pressures, the other, 90% survival pressures, and a chart showing incident failure pressures and ranges. The two matrixes are entered on the side with type of wall mounting, and at the top with wall material and thickness. Each intersection of the failure pressure matrix gives the estimated incident blast overpressure that would result in failure (collapse) of the wall. Each intersection of the survival pressure matrix gives the estimated blast pressure at which 90% of the wall would survive. The failure pressure chart plots incident failure pressures and estimated failure pressure ranges covering 81% of wall subjected to such pressures.

The derivation of the matrixes and chart is described in the material at the end of this section.

FAILURE PRESSURE MATRIX

SOLID WALLS (all tabulated pressures are in psi)

MATERIAL THICKNESS	BRICK			CONCRETE BLOCK	CONCRETE BLOCK-BRICK
	4-in.	8-in.	12-in.	8-in.	10-in.
SIMPLE BEAM	C 0.2	T 0.7	T 1.6	T 0.4	1.1
SIMPLE BEAM W/PRELOAD	C 0.2	T 0.8	C 1.7	C 0.4	1.2
FIXED BEAM	C 0.3	C 1.1	C 2.4	C 0.5	1.7
FIXED BEAM W/PRELOAD	C 0.3	C 1.2	C 2.6	0.5	1.9
SIMPLE PLATE	C 0.3	T 1.2	C 2.7	0.7	1.9
FIXED PLATE	C 0.6	C 2.5	C 5.6	C 1.5	3.9
ARCHED BEAM	T 1.2	T 6.2	11	T 3.7	T 5.3
ARCHED BEAM W/GAP	C 0.3	T 1.5	2.7	T 0.9 (<1.7)	1.3
ARCHED PLATE	T 2.1	11	19	T 3.7 (< 4.0)	5.3
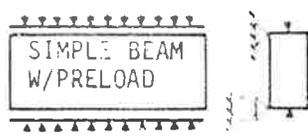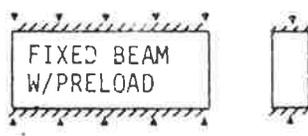
T - Tested   C - Predicted with Confidence

FAILURE PRESSURE MATRIX (cont.)

WALL WITH WINDOWS (all tabulated pressures are in psi)
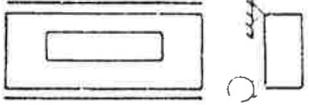
MATERIAL THICKNESS		BRICK			CONCRETE BLOCK	CONCRETE BLOCK-BRICK
		4-in.	8-in.	12-in.	8-in.	10-in.
SIMPLE BEAM		C 0.4	T 1.4	C 3.2	T 0.8	2.2
SIMPLE BEAM W/PRELOAD		C 0.4	T 1.6	C 3.7	T 1.0	2.6
FIXED BEAM		C 0.6	C 2.1	C 4.8	1.2	3.3
FIXED BEAM W/PRELOAD		C 0.7	C 2.3	C 5.3	1.3	3.0
ARCHED BEAM		1.4	T 7.6	14	T 3.5	6.4
ARCHED BEAM W/ GAP		0.4	1.9	3.5	0.9	1.6
ARCHED PLATE		2.4	13	24	3.5	6.4
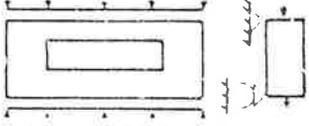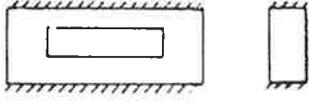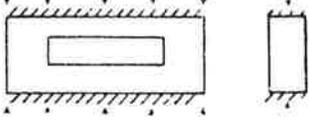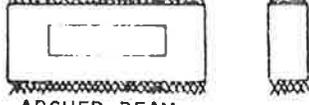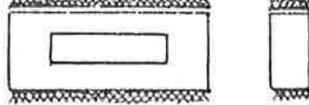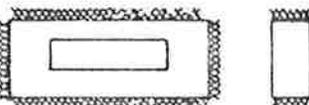
FAILURE PRESSURE MATRIX (cont.)

WALLS WITH DOORWAYS (all tabulated pressures are in psi)

MATERIAL THICKNESS	BRICK			CONCRETE BLOCK	CONCRETE BLOCK-BRICK
	4-in.	8-in.	12-in.	8-in.	10-in.
SIMPLE BEAM	C 0.3	T 1.1	C 2.5	C 0.7	1.7
SIMPLE BEAM W/PRELOAD	C 0.3	C 1.2	C 2.6	0.7	1.8
FIXED BEAM	C 0.5	C 1.7	C 3.8	C 1.1	2.6
FIXED BEAM W/PRELOAD	C 0.6	C 1.9	4.2	1.2	2.9
ARCHED BEAM	2	T 10. (>8.4)	18	6	8.5
ARCHED BEAM W/GAP	0.5	2.5	4.5	1.5	2.2
ARCHED PLATE	2.6	13	24	6.6	9.5

T - Tested   C - Predicted with Confidence

SURVIVAL PRESSURE MATRIX

Incident Overpressures at which 90% of Walls Will Survive
(all tabulated values are in psi)

Wall Material and Thickness / BEAMS	Brick			Concrete Block	Composite Concrete Block/ Brick
	4-in.	8-in.	12-in.	8-in.	10-in.
Solid Walls					
Simple	0.1	0.4	1.0	0.1	0.7
Fixed	0.2	0.7	1.4	0.2	1.0
Rigid Arched	0.8	4.3	7.7	2.6	3.7
Gapped Arched	0.2	1.1	1.9	0.6	0.9
Window Walls					
Simple	0.2	0.8	1.9	0.4	1.3
Fixed	0.4	1.3	2.9	0.5	2.0
Rigid Arched	0.8	5.3	9.8	3.2	4.5
Gapped Arched	0.3	0.6	2.5	0.8	1.3
Doorway Walls					
Simple	0.2	0.7	1.5	0.3	1.0
Fixed	0.3	0.4	2.3	0.5	1.6
Rigid Arched	1.5	7.7	14.0	4.6	6.7
Gapped Arched	0.4	2.0	3.5	1.2	1.7
PLATES					
Solid Walls					
Simple	0.2	0.7	1.6	0.3	1.1
Fixed	0.4	1.5	3.4	0.6	2.3
Rigid Arched	1.5	7.7	13.3	2.6	3.7
Window Walls					
Rigid Arched	1.8	9.3	17.1	3.2	4.5
Doorway Walls					
Rigid Arched	1.8	9.2	16.8	4.6	6.7

FAILURE PRESSURE CHART
Brick Walls

Brick - 12 in.
Incident Pressure (psi)

Brick - 8 in.
Incident Pressure (psi)

Brick - 4 in.
Incident Pressure (psi)

Beams
Solid Walls
  Simple
  Fixed
  Rigid Arched
  Gapped Arched
Window Walls
  Simple
  Fixed
  Rigid Arched
  Gapped Arched
Doorway Walls
  Simple
  Fixed
  Rigid Arched
  Gapped Arched
Plates
Solid Walls
  Simple
  Fixed
  Rigid Arched
Window Walls
  Rigid Arched
Doorway Walls
  Rigid Arched

4-6

FAILURE PRESSURE CHART

Concrete Block and Composite Brick-Concrete Block Walls

Wall Material and   Concrete Block - 8 in.   Concrete Block-Brick - 10 in.
Thickness

Incident Pressure (psi)

Beams		
Solid Walls		
Simple		
Fixed		
Rigid Arched		
Gapped Arched		
Window Walls		
Simple		
Fixed		
Rigid Arched		
Gapped Arched		
Doorway Walls		
Simple		
Fixed		
Rigid Arched		
Gapped Arched		
Plates		
Solid Walls		
Simple		
Fixed		
Rigid Arched		
Window Walls		
Rigid Arched		
Doorway Walls		
Rigid Arched		

0.1 .2   .5 1.0 2   5 10 20

0.1 .2   .5 1.0 2   5 10 20 50 100

4-7

DERIVATION FOR NON-ARCHING WALLS

Failure Pressure Matrix

For all brick walls except those involving arching, the predictions of mean failure pressure were derived directly from the SAMIS results for 8-in. thick walls with flexural strength values obtained from the full-scale tunnel test data. As shown in Section 2, good agreement was obtained for all tested conditions using this approach. The cases predicted in this manner for which no information on failure was derived from tunnel tests are marked with an S on the failure pressure matrix and noted to be predicted with confidence. Also noted are those cases which were tested in the shock tunnel.

The most uncertain case for the non-arching walls is for the 10-in. composite brick-concrete block walls on which no tunnel tests were conducted. The three small-scale composite beams tested in the static program showed a mean modulus of rupture of 197 psi which is only slightly greater than the 176 psi obtained for the 8-in. brick beams. Accordingly, for prediction purposes, the modulus of rupture of the composite concrete block-brick beams was assumed the same as for brick beams.

For wall types which were either not tested or for which direct SAMIS predictions were not made, extrapolations from direct SAMIS predictions were carried out using the following rules:

o Thickness change from 8 in. to "t" in.

$$Pf_t = Pf_8 \ (t/8)^2 = Pf_8 \times F$$

based on SAMIS characteristics

Values of F

wall thickness	F
4 in.	0.25
10 in.	1.563
12 in.	2.25

4-8

o   Effects of Preload

$$Brick: \quad Pf_{preload} = 1.05 \ Pf_{no \ preload}$$

$$Concrete \ Block: \quad Pf_{preload} = 1.10 \ Pf_{no \ preload}$$

based on analysis of effects of preload in Volume 3 and Ref. 1.

o   Change from Brick to Concrete Block

$$Pf_{cb} = \frac{189}{310} \ Pf_b$$

based on Table 2-3 and SAMIS characteristics.

Failure Pressure Chart and Survival Pressure Matrix

The failure pressure chart and survival pressure matrix are both derived directly from the failure pressure matrix, and the statistical analysis of strength derived from static tests discussed in Volume 4. As noted earlier in this report, the firm statistical base of the uncertainty ranges derived from the static tests suggested their use in place of ranges derived from more limited shock tunnel test data.

Plotted on the chart for each wall type and thickness is a point showing the failure pressure from the matrix, and a bar which shows the pressure range which would include about 81% of wall panels subjected to blast. The range for brick walls -- ± 30% of the mean value -- is derived from Fig. 3-1 of Volume 4, the range for concrete block walls -- ± 50% of the mean -- is derived from Fig. 3-2 of Volume 4. Too few static tests were run with composite concrete block-brick beams to provide a firm statistical base, but the behavior of the few that were run suggested that brick beam uncertainty ranges were appropriate to use.

The entries on the survival pressure chart were derived in a similar manner. From the static test data of Figs. 3-1 and 3-2 of Volume 4, flexural strength which would be exceeded 90% of the time was derived and compared

4-9

with the mean strength. The ratio of these strengths was then applied to the mean failure pressure from the failure pressure matrix. For brick walls this 90% survival value was about 63% of the mean; for concrete block walls, about 45% of the mean. Again, composite concrete block-brick walls were assumed to behave like brick walls.

DERIVATION FOR ARCHING WALLS

Failure Pressure Matrix

For arching walls the actual measured failure pressures are entered in the matrix where available. In some cases only upper or lower limits were available from the test data and these are also included along with the best estimate.

For the arching walls predictions of failure pressures for cases not tested were made by extrapolation from cases tested using the following rules:

o Rigid arching thickness change from 8 in. to 12 in.

$$P_{f_{12}} = P_{f_8} \times \left(\frac{12}{8}\right)^{3/2}$$

based on analytical work in Ref. 2.

o Gapped arching thickness change from 8 in. to 12 in.

$$P_{f_{12}} = P_{f_8} \times \frac{12}{8}$$

based on analytical work in Ref. 2.

o Rigid arching brick plates from beams

$$P_{f_{plate}} = P_{f_{beam}} \times 1.75$$

based on 4-in. brick wall data.

o Rigid arching concrete block beams from brick beams

$$P_{f_{cb}} = P_{f_b} \times 0.60$$

based on 8-in. wall data.

4-11

o Rigid arching concrete block and composite concrete block-brick
   plates from beams

$$Pf_p = Pf_{cb/b} = Pf_b$$

based on 8-in. concrete block data which gave 3.7 psi for the
beam and less than 4.0 psi for the plate. Since the plate should
be no weaker than the beam, a value of 3.7 was entered for the
plate rather than the <4.0 actually measured.

o Gapped arching beams from rigid arching beams

$$Pf_G = 0.25 \ Pf_R$$

based on 8-in. brick data.

o Thickness change from 8-in. brick to 4-in. brick

$$Pf_4 = 0.2 \ Pf_8$$

based on 4-in. and 8-in. brick data.

o Wall with window from solid wall

$$Pf_w = 1.2 \ Pf_s$$

based on 8-in. brick

o Wall with doorway from solid wall

$$Pf_d = 1.6 \ Pf_s$$

based on 8-in. brick data.

4-12

o "Two-way" arched brick wall with doorway from "one-way" arched
   brick wall with doorway

$$P_{f_2} = 1.2 \, P_{f_1}$$

based on analysis of effect of fixing single side wall.

Note that in some cases predictions could be made from more than one of
the above rules. Generally the differences were small and the rule selected
was that involving the least extrapolation.

Failure Pressure Chart and Survival Pressure Matrix

Procedures similar to those for non-arching walls were used in the deri-
vation of the entries on the chart and matrix. Mean values on the chart are
shown as dots. For the brick walls, the bars on the chart -- ± 30% of the mean
value -- were derived from the plots of line load strengths of brick samples in
static tests (Figs. 3-3 and 3-4 of Volume 4). This range would include about
81% of expected results. As before, the composite concrete block-brick was
assumed to behave like the brick samples.

Similar data were not available for concrete block walls, nor were enough
tests run with gapped arching line load geometries to provide statistically
valid variance information. Absent any other information, the 30% value was
used for all arching conditions.

Values on the survival pressure matrix were derived in a similar manner.
The 90% probability strengths, again from Figs. 3-3 and 3-4 of Volume 4,
averaged about 69% of the mean. This percentage was then applied to the mean
failure pressure given in the failure pressure matrix.

4-13

REFERENCES

1. Wilton, C., K. Kaplan, B.L. Gabrielsen, and J.V. Zaccor, "Blast/Fire Interaction, Blast Translation, and Toxic Gases", URS 7239-11, Final Report, URS Research Company, prepared by Scientific Service, Inc., Redwood City, California, July 1976.

2. Gabrielsen, B.L., K. Kaplan, and C. Wilton, "A Study of Arching in Non Reinforced Masonry Walls", Final Report 748-1 for the Veterans Administration, prepared by Scientific Service, Inc., Redwood City, California, March 1975.

Appendix A

LISTING OF ALL WALL
TESTS IN SHOCK TUNNEL

Wall Number	Description	Incident Pressure	References	Remarks
1	8-in. brick solid simple beam wall	1.5	1	Wall failed
2	8-in. brick solid simple beam wall	1.7	1	Wall failed
3	"	1.7	1	Wall failed
4	"	4.3	1	"
5	"	1.8	1	"
6	"	4.4	1	"
7	"	1.8	1	"
8	4-in. sheetrock timber stud solid simple beam wall	1.7	2	Wall failed
9	same as Wall No. 8	3.5	2	Wall failed
10	"	1.2	2	"
20	8-in. brick solid simple beam wall	4.6	1	Wall failed
21	"	1.7	1	Wall failed
22	"	3.4	1	"
23	8-in. brick solid simple plate wall	4.0	1	Wall failed
24A	"	1.6	1	Wall did not collapse, but cracked in yield line pattern.
24B	"	1.5	1	Wall failed
25	"	1.5	1	Wall did not fail but a large piece removed.
26	"	9.6	3	Wall failed
27	not tested	-	-	---
28	8-in. brick solid simple plate wall	1.9	3	Wall failed
29A	"	1.9	1	Wall did not collapse but cracked in yield line pattern.

A-2

Wall Number	Description	Incident Pressure	References	Remarks
29B	8-in. brick solid simple plate wall	2.0	1	Wall did not fail
30	" " " " " "	8.3	3	Wall failed
31	" " " " " "	7.5	3	Wall failed
32	" " " " " "	3.9	1	" "
33	" " " " " "	3.9	1	" "
34	not tested		-	---
35	8-in. reinforced concrete solid simple beam wall	no data	-	---
36	same as Wall 35	1.8	3	Wall failed
37	not tested	-	-	---
38	not tested	-	-	---
39	Room with window: non-failing front wall with 33 x 62 in. window; 4-in. sheetrock with timber stud simple beam rear wall. Room length 14.5 ft	0.8	2	Wall failed
40	Same as Wall No. 39	2.7	2	
41	Room with doorway: non-failing front wall with 17.5% open doorway; 4-in. sheetrock with timber stud simple beam rear wall. Room length 14.5 ft	0.8	2	Wall failed
42	same as Wall No. 41	2.7	2	" "
43	Same as Wall No. 41	2.7	2	" "
44	8-in. brick simple beam wall with doorway	4.0	-	Wall failed
45	same as Wall No. 44	1.8	4	Wall failed
46	" " " " "	1.7	2	" "

A-3

Wall Number	Description	Incident Pressure	References	Remarks
47	8-in. brick simple beam wall with doorway	5.0	2	Wall failed
48A	same as Wall No. 47	0.75	4	No visible damage
48B	"	0.75		" " "
48C	"	0.75		" " "
48D	"	1.7		Wall failed
49	not tested		1	---
50	12-in. brick solid simple beam wall	1.9	2	Wall failed
51	" " " "	2.1	2	" "
52A	" " " "	0.75	4	No sign of failure
52B	" " " "	0.75		" " " "
52C	" " " "	0.75		" " " "
53	not tested			---
54	not tested			---
55	not tested			---
56	8-in. brick simple beam wall with 38 x 62 in. window	1.8	4,5	Wall failed
57A	same as Wall No. 56	0.65	4	Wall cracked
57B	"	0.65		Crack enlarged
57C	"	0.65		" "
57D	"	1.9		Wall failed
58A	Room with window: non-failing front wall with 33½ x 62 in window; 8-in. concrete block solid simple beam rear wall. Room length 14.5 ft		4	"Plink" for natural period; wall cracked.

Wall Number	Description	Incident Pressure	References	Remarks
58B	Room with window: non-failing front wall with 33½ x 62 in. window; 8-in. concrete block solid simple beam rear wall. Room length 14.5 ft	0.75	4	Wall failed
59	same as Wall No. 58	0.75	4	Wall failed
60A	8-in. concrete block simple beam wall with 39 x 62 in. window	~	4,5	"Plink" for natural period. Wall cracked.
60B	"	0.75		Wall failed
61A	same as Wall No. 60	--	4,5	"Plink" for natural period. Wall cracked.
61B	"	0.75		Crack enlarged
61C	"	0.75		Wall failed
62	Room with window: non-failing front wall with 33½ x 62 in. window; 6-in. hollow clay tile solid simple beam rear wall	0.75	4	Wall failed
63	same as Wall No. 62	0.75	4	Wall failed
64A	8-in. brick solid simple beam wall with 16,500 lb preload	0.75	4,5	Wall cracked but did not fail.
64B	"	0.75		Wall failed
65	same as Wall No. 64	0.75	4,5	Wall failed
66	8-in. brick solid simple beam wall with 23,500 lbs preload	0.75	4,5	Wall cracked but did not fail
67	same as Wall No. 66	6.1	4,5	Wall failed
68A	4-in. brick solid one-way arched wall	0.75	5	Wall cracked
68B	"	1.7		Wall failed

A-5

Wall Number	Description	Incident Pressure	References	Remarks
69A	8-in. brick simple beam preloaded (22,500 lb) wall with 39 x 62 in. window	0.8	5	No damage
69B	"	2.0		Wall failed
70A	same as Wall No. 69	0.8	5	No damage
70B	"	2.0		Wall failed
71A	8-in. brick solid one-way arched wall	1.9	5	Test for natural period. No apparent damage
71B	"	2.9		Wall cracked
71C	"	4.3		Crack enlarged
71D	"	5.6		Wall failed
72A	8-in. concrete block simple beam preloaded (22,500 lbs) wall with 39 x 62 in. window	0.8	5	Wall cracked
72B	"	2.0		Wall failed
73A	same as Wall No. 72	0.8	5	Wall cracked
73B	"	2.0		Wall failed
74	8-in. brick solid one-way arched wall	5.5	5	Wall failed
75	same as Wall No. 74	5.9	5	Wall failed
76	" " " "	5.6	5	" "
77A	8-in. concrete block solid one-way arched wall	3.3	5	Wall cracked
77B	"	2.0		No additional damage
77C	"	3.4		Wall failed
78	same as Wall No. 77	4.5	5	Wall failed
	10-in. composite brick and concrete block solid one-way arched wall	5.6	5	Wall failed

A-6

Wall Number	Description	Incident Pressure	References	Remarks
80A	8-in. brick one-way arched wall with 38 x 62 in. window	5.7	5	Wall cracked
80B	"	6.3		Wall failed
81	8-in. brick solid simple beam wall with 23,500 lbs preload	0.8	5	Wall cracked
82A	8-in. brick solid simple beam wall with 28,500 lbs preload	0.8	5	Wall cracked
82B		2.0		Wall failed
83A	4-in. brick solid two-way arched wall	2.2	6	Wall cracked
83B	"	2.1		Wall failed
84A	8-in. brick one-way arched wall with 38 x 62 in. window	6.4	6	Wall cracked
84B		7.8		Wall failed
85A	same as Wall No. 84	6.2	6	Wall cracked
85B	"	5.8		Crack enlarged
85C	"	7.5		Slight additional cracking
85D	"	9.5		Wall failed
86A	8-in. brick one-way arched wall with doorway	6.1	6	Wall cracked
86B	"	8.4		Crack enlarged
87A	8-in. brick solid one-way arched wall	5.7	6	Wall cracked
87B	"	6.3		Crack enlarged
87C	"	8.2		Wall failed
88A	same as Wall No. 87	7.8	6	Wall cracked
88B	"	3.6		Crack enlarged

Wall Number	Description	Incident Pressure	References	Remarks
89	8-in. concrete block solid two-way arched wall	5.0	6	Wall failed
90	same as Wall No. 89	4.0	6	Wall failed
91	8-in. concrete block one-way arched wall with 38 x 62 in. window	≈3.5	6	
92A	10-in. composite brick and concrete block solid one-way arched wall	3.5	6	Wall cracked
92B	"	3.5		No additional damage
92C	"	5.0		Crack enlarged
93	8-in. concrete block one-way arched wall with 38 x 62 in. window	≈3	6	Wall cracked
94	8-in. brick solid one-way arched wall	7.8	6	Wall failed
95	8-in. brick solid gapped one-way arched wall	8.6	6	Wall failed
96	8-in. brick solid (pre-split) one-way arched wall	6.7	6	Wall failed
97	8-in. brick solid gapped one-way arched wall	2.3	7	Wall failed
98	same as Wall No. 97	1.9	7	Wall failed
99A	8-in. reinforced brick solid simple beam wall	≈1.0	7	Wall cracked
99B	"	≈2.0		Wall failed
100	same as Wall No. 99	≈2.0	7	Wall failed
101	Room with window: non-failing front wall with 33½ x 62 in. window; 4-in. sheetrock with timber stud solid simple plate rear wall. Room length – 14.5 ft	3.5	7	Wall failed.

Wall Number	Description	Incident Pressure	References	Remarks
102	Room with window: non-failing front wall with 33½ x 62 in. window; 4-in. sheetrock with timber stud simple plate rear wall. Room length - 37.5 ft.	1.7	7	Wall failed
103	Room with window: non-failing front wall with 33½ x 62 in. window; 4-in. sheetrock with metal studs solid simple plate rear wall. Room length - 37.5 ft	1.8	7	Wall failed
104	Room with window: non-failing front wall with 33½ x 62 in. window; 4-in. sheetrock with metal studs solid simple plate rear wall. Room length - 14.5 ft	1.8	7	Wall failed
105	same as Wall No. 104	3.5	7	Wall failed
106	same as Wall No. 102	3.8	7	Wall failed
107	same as Wall No. 103	3.9	7	Wall failed
108	same as Wall No. 103	3.6	7	Wall failed
109	Room with window: non-failing front wall with 33½ x 62 in. window; 8-in. 8-in. concrete block cantilevered beam rear wall. Room length 37.5 ft	4.0	7	Wall failed
110	same as Wall No. 102	3.8	7	"
111	Room with window: non-failing front wall with 33½ x 62 in. window; 4-in. sheetrock with timber stud simple plate rear wall with closed door. Room length 37.5 ft.	3.9	7	"

A-9

Wall Number	Description	Incident Pressure	References	Remarks
112	Room with window: non-failing front wall with 33½ x 62 in. window; 4-in. sheetrock with timber stud simple plate rear wall with open door. Room length - 37.5 ft.	3.8	7	Wall failed
113	Room with window: non-failing front wall with 33½ x 62 in. window; 4-in. sheetrock with metal stud simple plate rear wall with closed door. Room length - 37.5 ft.	1.7	7	Wall failed
114	same as Wall No. 113	3.8	7	Wall failed
115	Room with window: non-failing front wall with 33½ x 62 in. window; 8-in. concrete block one-way gapped arched solid rear wall. Room length - 14.5 ft.	4.1	7	Wall failed
116	same as Wall No. 115	1.7	7	Wall failed
117	Room with window: non-failing front wall with 33½ x 62 in. window; 8-in. concrete block cantilevered beam solid rear wall. Room length - 37.5 ft.	3.8	7	Wall failed
118	Room with window: non-failing front wall with 33½ x 62 in. window; 8-in. concrete block cantilevered beam rear wall with doorway opening. Room length - 37.5 ft.	3.6	7	Wall failed
119	Room with window: non-failing front wall with 33½ x 62 in. window; 6-in. clay tile cantilevered beam solid rear wall. Room length - 37.5 ft.	1.6	7	Wall failed
120	same as Wall No. 119	3.9	7	Wall failed

REFERENCES

1. Willoughby, A.B., C. Wilton, B.L. Gabrielsen, and J.V. Zaccor, "A Study of Loading, Structural Response, and Debris Characteristics of Wall Panels:, URS 680-5, Final Report, URS Research Company, San Mateo, California, July 1969.

2. Wilton, C., B.L. Gabrielsen, and P. Morris, "Structural Response and Loading of Wall Panels", URS 709-11, Final Report, URS Research Company, San Mateo, California, July 1971.

3. Wilton, C., B.L. Gabrielsen, J. Edmunds, and S. Bechtel, "Loading and Structural Response of Wall Panels", URS 709-4, URS Research Company, San Mateo, California, November 1969.

4. Wilton, C. and B.L. Gabrielsen, "Shock Tunnel Tests of Wall Panels", URS 7030-7, Technical Report, URS Research Company, San Mateo, California, January 1972.

5. Wilton, C. and B.L. Gabrielsen, "Shock Tunnel Tests of Preloaded and Arched Wall Panels", URS 7030-10, Final Report, URS Research Company, San Mateo, California, June 1973.

6. Gabrielsen, B.L., and C. Wilton, "Shock Tunnel Tests of Arched Wall Panels", URS 7030-19, Final Report, URS Research Company, prepared by Scientific Service, Inc. Redwood City, California, December 1974.

7. Gabrielsen, B.L., C. Wilton, and K. Kaplan, "Response of Arching Walls and Debris from Interior Walls Caused by Blast Loading", URS 7030-23, Final Report, URS Research Company, prepared by Scientific Service, Inc., Redwood City, California, February 1975.

DISTRIBUTION LIST

(one copy each unless otherwise specified)

Defense Civil Preparedness Agency
Research
Attn: Administrative Officer
Washington, D.C. 20301   (50)

Assistant Secretary of the Army (R&D)
Attn: Assistant for Research
Washington, D.C. 20301

Chief of Naval Research
Washington, D.C. 20360

Commander, Naval Supply Systems
   Command (0421G)
Department of the Navy
Washington, D.C. 20376

Commander
Naval Facilities Engineering Command
Research and Development   (Code 0322C)
Department of the Navy
Washington, D.C. 20390

Defense Documentation Center
Cameron Station
Alexandria, Virginia   (12)

Civil Defense Research Project
Oak Ridge National Laboratory
Attn: Librarian
P.O. Box X
Oak Ridge, Tennessee 37830

Chief of Naval Personnel
(Code Pers M12)
Department of the Navy
Washington, D.C. 20360

U.S. Naval Civil Engineering Lab.
Attn: Document Library
Port Hueneme, CA 93041

Director, Civil Effects Branch
Division of Biology and Medicine
Atomic Energy Commission
Attn: L.J. Deal
Washington, D.C. 20545

Air Force Special Weapons Lab.
Attn: Technical Library
Kirtland Air Force Base
Albuquerque, New Mexico 87117

AFWL/Civil Engineering Division
Kirtland AFB, New Mexico 87117

Civil Engineering Center/AF/PRECET
Tyndall AFB, FL 32401

Chief of Engineers
Department of the Army
Attn: ENGME-RD
Washington, D.C. 20314

Office of Chief of Engineers
Department of the Army
Attn: Mr. Tomasoni
Washington, D.C. 20314

Director, U.S. Army Engineer
   Waterways Experiment Station
P.O. Box 631
Attn: Document Library
Vicksburg, Mississippi 39180

Director, Defense Nuclear Agency
Attn: Technical Library
Washington, D.C. 20305

Director, U.S. Army Engineer
   Waterways Experiment Station
P.O. Box 631
Attn: Nuclear Weapons Effects Branch
Vicksburg, Mississippi 39180

D-1

Director, Defense Nuclear Agency
Attn: Mr. Tom Kennedy
Washington, D.C. 20305

Director, U.S. Army Ballistic
  Research Laboratories
Attn: Document Library
Aberdeen Proving Ground, MD 21005

Director, U.S. Army Ballistic
  Research Laboratories
Attn: Mr. William Taylor
Aberdeen Proving Ground, MD 21005

Dr. F.J. Agardy
c/o URS Research Company
155 Bovet Road
San Mateo, CA 94402

Agbabian Associates
250 N. Nash Street
El Segundo, CA 90245

The Dikewood Corporation
1009 Bradbury Drive, S.E.
University Research Park
Albuquerque, New Mexico 87106

Mr. J.W. Foss
Supervisor, Buildings Studies Group
Bell Telephone Laboratories, Inc.
Whippany Road
Whippany, New Jersey 07981

R & D Associates
4640 Admiralty Way
P.O. Box 9695
Marina Del Rey, CA 90291

Dr. William J. Hall
University of Illinois
111 Talbot Laboratory
Urbana, Illinois 61801

Mr. J.R. Janney
c/o Wiss, Janney, Elstner & Associates
330 Pfingsten Road
Northbrook, Illinois 60062

Mr. Samuel Kramer, Chief
Office of Federal Building Technology
Center for Building Technology
National Bureau of Standards
Washington, D.C. 20234

Mr. Anatole Longinow
IIT Research Institute
10 West 35th Street
Chicago, Illinois 60616

Dr. Stanley B. Martin
Stanford Research Institute
333 Ravenswood Avenue
Menlo Park, CA 94025

Mr. H.L. Murphy
Stanford Research Institute
333 Ravenswood Avenue
Menlo Park, CA 94025

Research Triangle Institute
P.O. Box 12195
Research Triangle Park
North Carolina 27709

Mr. George N. Sisson
Research Directorate
RE(HV)
Defense Civil Preparedness Agency
The Pentagon
Washington, D.C. 20301

Dr. Lewis V. Spencer
National Bureau of Standards
Room C313-Building 245
Washington, D.C. 20234

Mr. Thomas E. Waterman
IIT Research Institute
Technology Center
10 West 35th Street
Chicago, Illinois 60616

Mr. Robert W. Hubenette, P.E.
Senior Associate
Center for Planning and Research, Inc.
750 Welch Road
Palo Alto, CA 94304

D-2

Mr. Carl K. Wiehle
Stanford Research Institute
333 Ravenswood Avenue
Menlo Park, CA 94025

Mr. Eugene F. Witt
Bell Telephone Laboratories, Inc.
Whippany Road
Whippany, New Jersey 07981

Mr. Milton D. Wright
Research Triangle Institute
P.O. Box 12194
Research Triangle Park, No. Carolina 27709

Mr. Paul Zigman
Environmental Science Associates
1291 E. Hillsdale Blvd.
Foster City, CA 94404

Mr. Chuck Wilton
Scientific Service, Inc.
1536 Maple Street
Redwood City, CA 94063

THE SHOCK TUNNEL: HISTORY AND RESULTS
SSI 7618-1
Scientific Service, Inc., Redwood City, California
March 1978   438 pp
Contract No. DCPA01-76-C-0311, Work Unit 1123H

UNCLASSIFIED

This report summarizes the results of a program conducted by the Defense Civil Preparedness Agency to determine blast resistance of wall panels typically found in existing structures. The objective of this program was to determine the blast sheltering capability of structures in the National Fallout Shelter Survey inventory and to obtain information which could be used to upgrade these structures.

Volume I describes the shock tunnel facility used for the experimental testing of full-scale wall panels. Included is a summary of the capabilities of the shock tunnel for dynamic loading and response studies and brief summaries of various experimental programs conducted in the shock tunnel which were not related to the wall panel test program.

Volume II of this report presents the results obtained from the experimental program conducted in the shock tunnel to determine the loadings which are relieved by wall panels mounted in the test section.

Volume III of this report is concerned with the dynamic response and failure of full-scale wall panels. Included are the development of theories of wall panel response and the results obtained from the testing of full-scale wall panels in the shock tunnel.

Volume IV of this report describes the static test program conducted to determine the physical properties of the wall panels and to assist in the development of failure theories and test predictions for wall panels.

Volume V summarizes the predicted failure pressures for wall panels based on the theoretical and experimental results.

END

DATE
FILMED

7-78

DDC